MAINTAINING FIRE-FIGHTER TENABILITY IN UNSPRINKLERED SINGLE-STOREY INDUSTRIAL BUILDINGS USING ROOF VENTING

A thesis submitted in partial fulfilment of the requirements for the

Degree of Master of Engineering in Fire Engineering

at the

University of Canterbury

by

Timothy Myles McDonald

B.For.Sc. (Hons), B.Sc., M.For.Sc. (Hons), M.N.Z.I.F.

College of Engineering

University of Canterbury

2012

ABSTRACT

Roof venting is often utilised in large warehouses to remove smoke in order to reduce damage to a building and its contents, and to maintain access for fire-fighters. In New Zealand, the Compliance Document for the New Zealand Building Code C clauses recommends 15 % opening area for unsprinklered single floor buildings. This opening area is required to be designed for *effective fire venting*. There is no justification for why 15 % is required, and no definition of how fire venting qualifies as being effective.

Fire Dynamics Simulator (FDS) was used to simulate the performance of various roof venting strategies in two different-sized industrial warehouses (both larger than 1,500 m²) with a 50 MW fire with both a rapid and an extreme t^3 growth rate. In particular, roof venting areas of 15 %, 10 %, and 5 % of the floor area were tested with each of the following inlet areas for make-up air: 100 %, 50 %, and 0 % of roof venting area. In each of these cases, the vents were treated as permanently-open holes in the roof.

It was shown that roof venting with 15 % geometric area is ample to provide and maintain tenability for fire-fighters. With sufficient inlet area for make-up air, smaller venting areas could also be employed.

Further simulations were run to test the effect of square-shaped vents that opened simultaneously at 100°C compared with square-shaped vents that opened sequentially at 100°C, 200°C, and 300°C, and strip-shaped vents that opened progressively as each portion of a vent reached activation temperatures of 200°C and 300°C. Vents that opened at 100°C were intended to represent mechanical vents, while vents opening at higher temperatures were intended to represent plastic sky-light or drop-out type vents. The activation temperature proved to be more influential than the opening sequence or shape: there was a significant advantage to be gained by having vents that activated at 100°C as opposed to 200°C or 300°C.

The role of downstands in aiding the effectiveness of roof venting was also investigated, with downstand depths of 10 %, 20 %, and 30 % of the ceiling height being simulated. Downstands were shown to be incredibly useful for exhausting smoke and hot gases, provided their installation was appropriately coordinated with placement of roof venting.

It is concluded that a clear definition of *effective fire venting* must not only include the area of roof venting, but equally important is the definition of required inlet area for make-up air, as it plays a crucial role in the effectiveness of the specified roof venting area. In addition, the clear aerodynamic area should be specified. This could be achieved by use of a discharge coefficient that describes the proportion of the roof venting area that is clear aerodynamic area for a particular material, vent, and geometric area.

Development of a clear definition of *effective fire venting* will help to determine how an economic fire protection system can be continued to be used, while going a long way to ensuring predictable and tenable conditions for fire-fighters in New Zealand.

Key words: *effective fire venting, fire-fighter tenability, unsprinklered, single-storey, FDS, industrial, warehouse, skylight, downstand*

ACKNOWLEDGEMENTS

I would like to thank my supervisors Associate Professor Charley Fleischmann, Ms Carol Caldwell, and Dr. Kai-Yuan Li. You have all provided valuable feedback on methodology, writing and programming, as well as much-needed direction. Thanks to Dennis Pau for your assistance in running the simulations.

Special thanks also to Professor Andy Buchanan, Associate Professor Charley Fleischmann, and Dr. Michael Spearpoint for instigating and running the Master of Engineering in Fire Engineering degree programme. It has been a thoroughly enjoyable learning experience, although it is nice to now have my weekends and holidays back.

I would like to acknowledge the support of the NZ Fire Service Commission. Their support of the M.E.F.E. degree has been essential since the infancy of the programme and continues to be essential for both the lectured courses, and the research & development undertaken within the department.

Thanks also to the administrative staff of the Department of Civil and Natural Resources Engineering, and to Brandon Hutchison, Joost Kroese and Dave van Leeuwen: your assistance with all things computing has been invaluable.

Thank you to Amanda Robbins of BRANZ. Our 5-minute discussion during your coffee break at a conference in Christchurch proved very insightful for my research.

A number of people in the industry took time to answer my questions. I will keep your identities confidential, but really appreciate the starting point you all gave me.

Thanks to my M.E.F.E. class mates: Chee, Marco, Jenny, Di, Kevin, and Peter. I couldn't think of a better group of people to have completed the course requirements with. I think we all quickly learnt the importance of sharing for the collective good. I wish you all well, and I will certainly keep in touch.

Thanks to everyone at Canterbury Rowing Club for providing an escape from campus. The Club has come a long way in the past 3 years – Seniores Priores.

Herzlichen Dank an alle bei Endreß Ingenieurgesellschaft. Ich habe im letzten Jahr viel von Euch gelernt. Meine Fähigkeiten im Thema „Brandschutz“ haben wesentlich verbessert. Ich bin Euch sehr dankbar.

Ein großes Dankeschön an alle Mitruderer der Frankfurter Rudergesellschaft Germania. Wir hatten viel Spaß, und ihr habt mir interessante Sachen gelehrt.

Thanks to Mum for always being there and supporting me every step of the way.

My biggest thank you goes to Kerstin. You have been such a great support throughout this process. Meals-on-wheels services definitely went beyond the call of duty, but were really appreciated on those long evenings in the office. It would have been much more of a struggle to complete the requirements of the degree without your help. Now, we are in Germany and you are commencing your thesis, I hope I can repay the favour in some way. Just imagine the possibilities when neither of us has a thesis to write in the evenings and on weekends!!

TABLE OF CONTENTS

LIST OF FIGURES

LIST OF TABLES

LIST OF ABBREVIATIONS

ABCB	Australian Building Codes Board
CFD	Computational Fluid Dynamics
DBH	Department of Building and Housing
FBIM	Fire Brigade Intervention Model
FMRC	Factory Mutual Research Corporation
FDS	Fire Dynamics Simulator
GRP	Glass-Reinforced Plastic
LES	Large Eddy Simulation
NFPA	National Fire Protection Association
NIST	National Institute of Standards and Technology
NZBC	New Zealand Building Code

1. INTRODUCTION

1.1 General introduction

In large warehouses, roof vents are often used to remove smoke in order to reduce damage and assist fire-fighter's access. Currently the Compliance Document for the C clauses of the New Zealand Building Code (NZBC) recommends 15 % opening area for unsprinklered single floor buildings (D.B.H., 2008a, clause 4.2.4), yet this number has not been justified. Further, the opening area is required to be designed for *effective fire venting*, yet there is no definition of how fire venting qualifies as being effective.

Use of plastic sheeting that is not fire-rated is often used in New Zealand to provide the venting, as it is expected to melt or burn-out sufficiently to reduce elevated temperatures within the building, thereby providing effective fire venting. The NZBC Compliance Document limits maximum firecell floor area (to 1,500 m^2) in an attempt to limit fuel load to 2,000,000 MJ. Use of venting allows construction of larger firecells and, as a consequence, the fuel load in each firecell will be increased. In fact, if at least 15 % of the roof area is designed as fire venting, subdivision of the building is not required as, presumably, it is believed that early venting enables the fire service more time to enter the building, undertake rescue operations, and control or extinguish the fire.

Fires in large industrial buildings can be difficult to control, and there is concern about the performance of plastic roof panels or skylights that are used for fire venting (Edwards *et al.*, 2007; D.B.H., 2008b; Gaskin, 2009). Many plastic materials specified for venting are untested in fire environments: for example, glass-reinforced plastic (GRP) has fibreglass reinforcing that has been found to remain in place during heat-exposure testing (Gaskin, 2009; Robbins and Wade, 2010).

It would be prudent and of practical assistance for the NZBC Compliance Document to include justification for the 15 % rule and to provide guidelines for those in the building industry as to what *effective fire venting* entails.

1.2 Statement of the problem

The NZBC Compliance Document (D.B.H., 2008a, clause 4.2.4) allows firecell floor area to be unlimited if *effective fire venting* is used for 15 % of the roof area in unsprinklered single-storey buildings. However, no definition is provided for *effective fire venting*, and no justification is given as to the appropriateness of the 15 % rule. Concern exists regarding the use of plastic roof panels to provide this fire venting.

1.3 Background

1.3.1 Single-storey industrial buildings

Single-storey industrial buildings are commonly used for manufacturing and storage purposes. The fuel load of such buildings can range from low (e.g. engine parts) to very high (e.g. petroleum products, wood, paper products) (Cosgrove, 1996).

In New Zealand, single-storey industrial buildings have traditionally been constructed using steel portal frames, formed with a rafter spanning between steel columns (Lim, 2000). The portal frames are spaced at 6 to 12 metre centres and the rafters usually have a clear span of between 15 and 30 metres. The steel columns of the portal frames may be fully or partially encased in concrete for fire protection, or alternatively may be constructed with shortened legs on top of concrete columns. Precast concrete wall panels are then attached to the portal frames and thin steel sheeting is used for the roof. More recently, it has been common for industrial walls to comprise precast concrete tilt-panels for external walls, without columns attached, supporting a steel-frame roof (Lim, 2000). This design may also have internal columns. Steel portal frames are available that are up to 70 metres in width, have unlimited lengths, and standard heights of 10 m (although although custom orders can be made taller)[1].

Buildings of the above construction types are considered to have very low fire resistance (Langdon Thomas, 1960). In addition, the large open spaces result in large escape route distances (Cosgrove, 1996). And, it may be necessary for fire-fighter

[1] www.kiwispan.co.nz/pdf/custom-commercial-andIndustrial-Buildings-Brochure.pdf accessed on 16th November 2011 at 5:24pm

entry to occur at considerable distances from the seat of the fire, requiring them to navigate in an environment that is heavily laden with smoke.

Cosgrove (1996) and Edwards *et al.* (2007) note the interest given to fire design of single-storey industrial buildings is mainly due to frequency of construction, high design fire loads, relatively high risk of fire occurring, and peculiar fire behaviour linked to rapid fire growth and probable roof collapse. However, it is pointed out that smoke control systems are only likely to be effective during early stages of a fire, and are not a guarantee for arresting fire spread. Nevertheless, buildings with light non-combustible roof structures, an absence of adequate venting, and no sprinkler protection, have proven in the past to be very vulnerable to the effects of a fire (Sestack, 1957).

Precisely how a fire develops in an industrial building depends upon the size and shape of the building, the wall and roof opening area, the type and arrangement of combustible contents and the nature of the process within the building (Langdon Thomas, 1960). However, the general process involves hot gases rising due to buoyancy, and spreading horizontally beneath the roof until a vertical barrier (e.g. a wall or downstand) is reached (Thomas *et al.*, 1963; Cosgrove, 1996). Once constrained by such barriers, the smoke layer deepens, re-radiating heat to the fire and unburnt combustibles below.

A difficult characteristic often found in single-storey industrial buildings is the development of a stable thermally-stratified environment (Keough, 1972; Fang *et al.*, 2006; Capote *et al.*, 2009). That is, a thick hot-air layer may form beneath the ceiling where the temperature is significantly higher than the ambient air at working level. Such a layer can delay the penetration of hot fire gases to the ceiling, hence delaying activation of vent-opening devices (or any other thermal device such as a sprinkler). This effect will be less pronounced in buildings where some natural air leakage occurs through the roof.

1.3.2 Roof venting

Roof venting can be used to reduce the spread of fire, remove the products of combustion, and maintain temperatures at roof level low enough to prevent distortion and/or collapse of the roof (Langdon Thomas, 1960; Kim, 1992). In a severe fire, the roof cladding system itself may be sufficiently damaged so as to enable the fire to vent (Newman, 1990).

While not extinguishing a fire, a number of studies have shown roof venting to be valuable in limiting fire spread and maintaining conditions that allow the location of the fire to be found more easily (Thomas *et al.*, 1963; Hinkley, 1986; Duong, 1990). A drawback of roof venting is that it may increase the rate of burning (Langdon Thomas, 1960). However, it is also likely to substantially reduce spill-over of combustion products into areas adjoining that of fire origin, particularly where roof divisions are in place.

Thomas *et al.* (1960) have shown in small scale tests that the shape of the vent is not critical for effective smoke and heat removal. However, the distribution of roof vents is an important factor (Kim, 1992). A uniform vent distribution is most efficient as a vent that is directly above the fire is slightly more efficient than one a short distance away (Thomas *et al.*, 1960). But, vent position is only of minor importance where fire gases do not have sufficiently high horizontal velocity to cause them to overshoot the vent(s). Roof slope must also be taken into account when deciding on roof vent distribution. For flat roofs, an even distribution of vents across the roof area is thought to be best, but for steep roofs vents are likely to be more effective if located near the apex (Edwards *et al.*, 2007).

Roof venting may take the form of automatic vents activated by thermal release mechanisms, or it may be formed from plastic sheeting that is expected to melt or burn-out when subject to fire. Both forms appear to have been in existence for at least fifty years (Sestack, 1957). Despite this, there still appears to be major differences in regulation of venting systems within and between the building codes in different parts of the world. Sestack (1957) anecdotally considered a roof venting area of 2.5 % for buildings containing moderate fire load as being very good. For buildings with special

hazards, he suggested venting in the order of 5 % as being desirable. This is considerably less area than the 15 % prescribed in the NZBC Compliance Document.

Like New Zealand, the Building Code in neighbouring Australia allows smoke and heat vents as a means for increasing firecell size in unsprinklered industrial (Class 7 or 8) buildings, but only up to a maximum floor area of 18,000 m^2 and maximum volume of 108,000 m^3 (equivalent to a warehouse 135 m x 135 m x 6 m), where the building has a minimum open space of 18 m around the building (Xin, 2004, specification C2.3a). Vents may also be used to increase firecell area in some other classes (5 and 9a) of unsprinklered single-storey building, although not to the same degree as described above.

The area of effective (aerodynamic) venting required for Australian buildings, up to 6 m high with 1.5-m draught curtains, is 3 % of each compartment in "abnormal fire hazard" occupancies and 2 % otherwise (AS 2665, 2001). For buildings that do not meet these characteristics, a nomogram is used to determine appropriate vent sizes. In contrast to the New Zealand regulations, however, the Building Code of Australia 2009 allows only automatic or permanently-open vents, and these must comply with Australian Standard AS 2665 (Xin, 2004, specification E2.2c).

In the U.S.A., NFPA 204 (Standard for Smoke and Heat Venting) appears mostly directed at mechanical vents or thermoplastic drop-out vents. In fact, vents are required to open fully with the activation of some form of detection device (NFPA 204, 2012, clause 5.2.2). This would appear to rule out the use of plastic skylight-type vents with an expected melting mechanism. In addition, draft curtains are mandatory for large, open areas (NFPA 204, 2012, clause 7.1), and should be a minimum of 20 % of the ceiling height (NFPA 204, 2012, clause 7.3.1).

Required vent area needs to be calculated by equating the mass flow rate in the plume with the mass flow rate through the vent given a design smoke layer height. (By means of comparison to the New Zealand requirements, exemplar calculations for the required roof venting area according to NFPA 204 have been made for warehouses simulated in this study, and included in Appendix A. In this study, two warehouse geometries are investigated: a *small* warehouse with dimensions of 60 m x 30 m x

6.5 m and a *large* warehouse of dimension 100 m x 60 m x 12 m. These warehouses are described in full detail in Section 2.1. A design fire with a maximum fire size of 50 MW was used for both warehouses. The design fire is described in more detail in Section 2.2.)

In the United Kingdom, single-storey industrial buildings are required to either: have a foundation that is designed to allow external walls to continue to provide their structural function in the event of collapse of rafters, purlins, and roof cladding, due to fire; or be fitted with a sprinkler system (U.K. Building Regulations, 2000, section 13.4). Currently, there is no provision for the use of fire venting in new portal frame buildings. However, it is noted that existing buildings with 10 % roof venting are considered acceptable, provided that columns are fitted rigidly to a base that will resist collapse and that columns are protected by concrete, block, or brick. It is understood that the 1985 version of the Approved Documents introduced 10 % fire venting in the form of low melting point plastic material (Edwards *et al.*, 2007). However, this allowance was subsequently removed in the 2000 version.

In the German state of Hessen, industrial buildings without fire extinguishing systems (e.g. sprinklers), and with a floor area greater than 200 m^2, are required to have openings/vents in the walls or roof that are, in total, a minimum of 2 % of the building floor area (ARGEBAU, 2000, Section 5.6). When the floor area exceeds 1,600 m^2, the 2 % minimum still applies, but it must also be demonstrated that a clear layer height of 2.5 m can be maintained. In addition, the vents must be both automatically activated, and able to be activated manually. This standard is also currently applied in the two city-states of Hamburg and Bremen, as well as the thirteen remaining federal states in Germany.

For fire venting to be effective, roof vents must be large enough to expel fire gases at the same rate as gases are produced by the fire plume, while small enough to prevent air from the clear lower-layer from being extracted concurrently with fire gases (Heskestad, 1986). In most instances, the production rate of fire gases is governed by the rate of entrainment of air into the plume (Hinkley, 1986).

Of vital importance in the smoke extraction process is the inflow to the building of cooler make-up or inlet air, to replace the vented fire gases. The required area for inlet air in single-storey unsprinklered buildings in New Zealand is not mentioned explicitly in the NZBC Compliance Document.

Thomas and Hinkley (1964) suggest that opening area for inlet air should be twice as much as fire venting area, with the ratio decreasing to unity as the gas temperature below the ceiling approaches 1,500°F (about 800°C). Inlet openings do not need to have a consistent pattern throughout a building, although a uniform distribution is preferable (Keough, 1972).

It may sometimes be the case for factory-type buildings, that there is sufficient natural leakage area, that special inlet ventilation need not be provided. This was found to be the case in experiments carried out by Keough (1972) in a 94 m by 52 m aircraft hangar. Thomas *et al.* (1963) contend that leaks around windows and doors and in walls are likely to be able to provide sufficient inlet air in the early stages of a fire, however, as more roof vents open the amount of inlet air required will also increase.

1.3.3 Vent materials

Roof venting should be designed to open or melt in the event of a fire. However, there is no guidance in the NZBC Compliance Document on how to assess the effectiveness of venting, nor any specification for venting materials. Langdon Thomas (1960) suggested the use of plastics with low melting points as vent materials.

Gaskin (2009) tested the performance of four plastic materials commonly used for roof panels in New Zealand: polycarbonate, poly-vinyl chloride (PVC), acrylic, and glass fibre-reinforced polyester (GRP). The study intended to investigate the timing of these materials melting and the proportion of area available as venting following application of heat (in an oven). Gaskin (2009) found that at no temperature below 250°C did the entire plastic sample, for any of the plastics, melt from the frame. Hinkley and Theobold (1966) found that, in a 16 m x 5 m brick building with 5 m apex roof, the entire PVC panel would fall out with ceiling jet temperatures in excess of 300°C.

The use of passive fire venting in the form of melting polymer-based roof sheeting in New Zealand appears to be at odds with legislation in some other countries. Further, potential test methods for roof sheeting materials used for fire venting have been, until very recently, non-existent (Robbins and Wade, 2010).

A major problem with reliability of plastic roof panels for fire venting, is that there is no guarantee that installed panels and tested panels have the same chemistry (Robbins and Wade, 2010). In fact, improvements made to plastic roof panels are usually based on provision of natural lighting requirements, so that features such as durability are more important. As an example, the addition of reinforcing fibreglass mesh to the roof panels usually means that no openings will form in the plastic panels during a fire without manual intervention. For this reason, each roof panel product should be tested to an appropriate standard, and have a proprietary rating assigned.

To further complicate the performance of plastic roof panels, Gaskin (2009) noted an interesting anomaly in that buoyancy-driven flow through a vent could be "boosted" by physical deflection. This was observed with those plastics that deformed and sagged at an angle more than 45° from the horizontal.

An additional factor that may need to be taken into consideration for the performance in fire of plastic roof panels, is any possible future requirement (for health and safety purposes) to install a metal safety mesh below each plastic roof panel. Such a requirement could also have an impact on the performance of purpose-designed fire venting panels, depending on how far below the roof a safety mesh is allowed to be, and what the effect is of having the plastic sheeting suspended below the hole, but still intact.

1.3.4 Smoke curtains/downstands

Roof vent efficiency is greatly increased with the use of compartmentation (Sestack, 1957; Thomas *et al.*, 1963; Keough, 1972; Bengston and Hagglund, 1986). This can be achieved using screens that extend downwards from the ceiling. These can be passive fixtures (known as downstands) or can drop down when needed (known as smoke curtains). The screens act to limit the horizontal movement of smoke and limit

excessive cooling of the hot layer, as both of these are potential mechanisms for reducing efficiency (Cosgrove, 1996).

By forming smoke reservoirs, the screens allow the hot layer depth to increase at a higher rate than is possible without screens, hence activating vents and thermal devices sooner (Edwards *et al.*, 2007). Langdon Thomas (1960) points out that a greater "chimney effect" will be produced with deeper barriers. That is, smoke is better channelled to the vents contained between the barriers.

Keough (1972) concluded that smoke curtains were significant only in the initial stages of venting, while the pattern of smoke venting was established. Keough (1972) also noted very little smoke spilling beyond the compartment with 3-m draught curtains and 15 % (63 m^2) roof-venting (or 9 % effective discharge area).

1.3.5 Fire-fighter tenability

Fire-fighters are authorised by law to enter burning buildings for the purposes of fire-fighting and rescue operations. Fire-fighters need burning buildings to behave in a predictable way so they can take appropriate actions and avoid injury. The depth of the hot gas layer is important in terms of facilitating these activities. If the layer is well above head height, fire-fighters will have better visibility and access to the seat of the fire, compared to a gas layer that is approaching floor level (Thomas *et al.*, 1963). In addition, the temperature of the layer of hot gases will determine the likelihood of damage to the roof.

The Fire Brigade Intervention Model (FBIM) contains the only fire-fighter tenability criteria that the New Zealand Fire Service will currently accept for fire engineering design (A.B.C.B., 2009; Claridge, 2009). Young (2004) lists six factors of a fire environment that affect fire-fighters and their equipment including: air temperature, visibility, humidity, incident thermal radiation, air flow past the fire-fighter, and the time for which fire-fighters are exposed. These factors were the basis for the tenability criteria, which need to be met at a height of 1,500 mm above floor level (Table 1). These tenability criteria were adopted, without prejudice, in this project.

The FBIM attempts to quantify time taken for the fire brigade to perform activities during a structure fire, from the moment of notification through to control/extinguishment (Marchant *et al.*, 2001). It was primarily developed for use in fire engineering design in a performance-based regulatory environment, but is applicable to most structural fire scenarios and can be applied to a wide range of brigade types, operating procedures, equipment specifications, crew sizes, and resource limitations.

Table 1 – Tenability criteria for fire-fighters from the Fire Brigade Intervention Model (Adapted from: Young, 2004).

Routine conditions	
Elevated temperatures, but not direct thermal radiation	
Maximum time:	25 minutes
Maximum air temperature:	100°C (in lower layer)
Maximum radiation:	1 kW/m^2
Hazardous conditions	
Expected to operate for short period in high temperatures combined with direct thermal radiation	
Maximum time:	10 minutes
Maximum air temperature:	120°C (in lower layer)
Maximum radiation:	3 kW/m^2
Extreme conditions	
These conditions would be encountered in a snatch rescue situation or a retreat from flashover	
Maximum time:	1 minute
Maximum air temperature:	160°C (in lower layer), 280°C (in upper layer)
Maximum radiation:	4 - 4.5 kW/m^2
Critical conditions	
Firefighters would not be expected to operate in these conditions. Considered to be life-threatening.	
Time:	< 1 minute
Air temperature:	> 235°C (in lower layer)
Radiation	> 10 kW/m^2

These criteria are intended to take into account time, temperature, thermal radiation and humidity (Young, 2004). There is no explicit or implicit criterion for visibility. The practicing engineer is directed by the FBIM to determine visibility requirements in consultation with the relevant fire authority, based on hazards specific to the site concerned and the expectation for what might be required during a fire brigade intervention.

1.4 Objectives

The general objective of this study was to evaluate the effectiveness of roof vents for providing fire-fighter tenability, in order to determine the appropriateness of the 15 % rule in clause 4.2.4 of the Compliance Document for the New Zealand Building Code C clauses (D.B.H., 2008a).

The specific objectives were:

a) Evaluate the percentages of roof vent area and make-up air inlet area required, for unsprinklered single-storey buildings to meet the Fire Brigade Intervention Model fire-fighter tenability criteria;
b) Model the effectiveness of sequential versus simultaneous opening of vents in providing the Fire Brigade Intervention Model fire-fighter tenability criteria; and
c) Evaluate the use of downstands on the effectiveness of roof venting for providing the Fire Brigade Intervention Model fire fighter tenability criteria.

1.5 Intended impact of the research

An understanding of the venting area required to provide fire-fighter tenability will enable a decision to be made about whether or not the 15 % rule is appropriate for aiding the safety of fire-fighters in the event that they enter an unsprinklered single-storey building that is on fire. In addition, it is intended to contribute to the development of a clear definition of *effective fire venting*.

2. METHOD

2.1 Building characteristics

In a study of fire loss estimates for warehouses with rack storage, Porter (2004) points out the variety of single-storey warehouse sizes and configurations. However, he defined a *typical* warehouse as 60 m by 30 m by 6 m. A proposed (by the Department of Building and Housing) framework for demonstrating fire safety for performance-based design describes an example warehouse of similar dimension, but with a ceiling height of 6.5 m. It was decided that a suitable warehouse for this project, was one with dimensions 60 m x 30 m x 6.5 m.

Acknowledging an apparent trend for larger warehouses, or *mega-stores*, it was decided to model a second warehouse of dimensions 100 m x 60 m x 12 m. The floor area of this *large* warehouse well exceeds the maximum floor area (1,500 m^2) allowed by the NZBC Compliance Document for a single firecell, and as such would also be required to have *effective fire venting*. In addition, the roof height reflects a tendency for storage expansion to move in the vertical direction, due to annual land costs being based only on land area occupied.

Zalosh (2003) describes three types of storage that are typical of warehouses: solid-piled, palletised, and rack storage. He adds that the latter is the worst-case in terms of fuel-loading, because the structural stability of the racks allows goods to be stacked to heights in excess of 12 m. In addition, space between racks and space between stored goods allows for a well-ventilated fire. Therefore, rack storage was included in both the small and large warehouses modelled in this project (Figure 1 and Figure 2).

The most common materials for construction of single-storey industrial buildings are concrete and steel, as described in Section 1.3.1. It is shown later in this report (Section 2.5.1) that the choice of construction materials for the buildings have only a small effect on the outcome of the FDS modelling. However, it was decided to model all simulations with adiabatic walls to ensure worst-case temperature conditions 1.5 m above the warehouse floor. Both warehouses were modelled with a leakage area of 4 cm^2/m^2 (Persily, 1998). The influence of a stratified temperature distribution in the

warehouse was not considered here. Instead, an initial ambient temperature of 13°C was chosen to represent an *average* New Zealand outside air temperature.

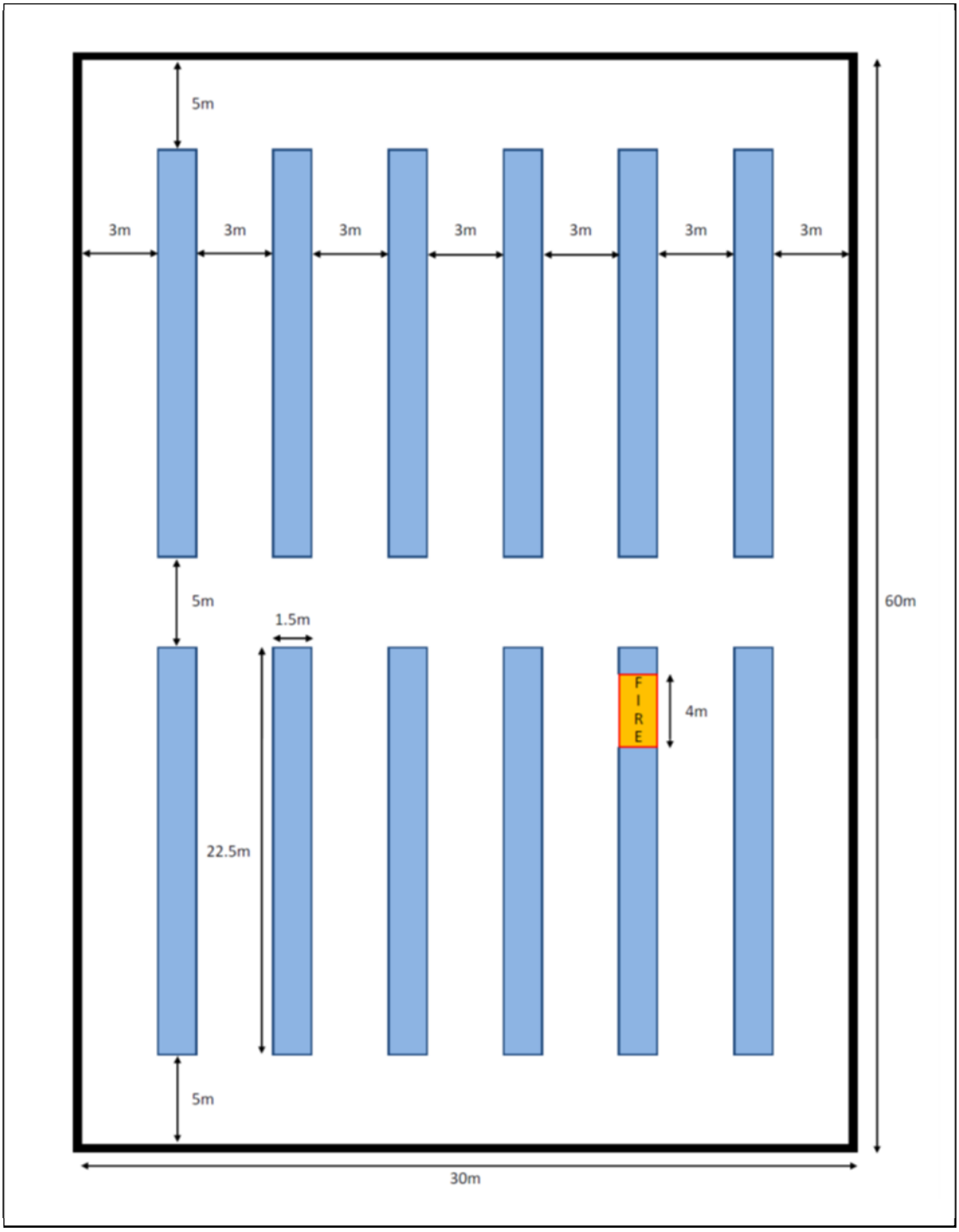

Figure 1: Plan view of small warehouse showing warehouse & rack dimensions, and fire position.

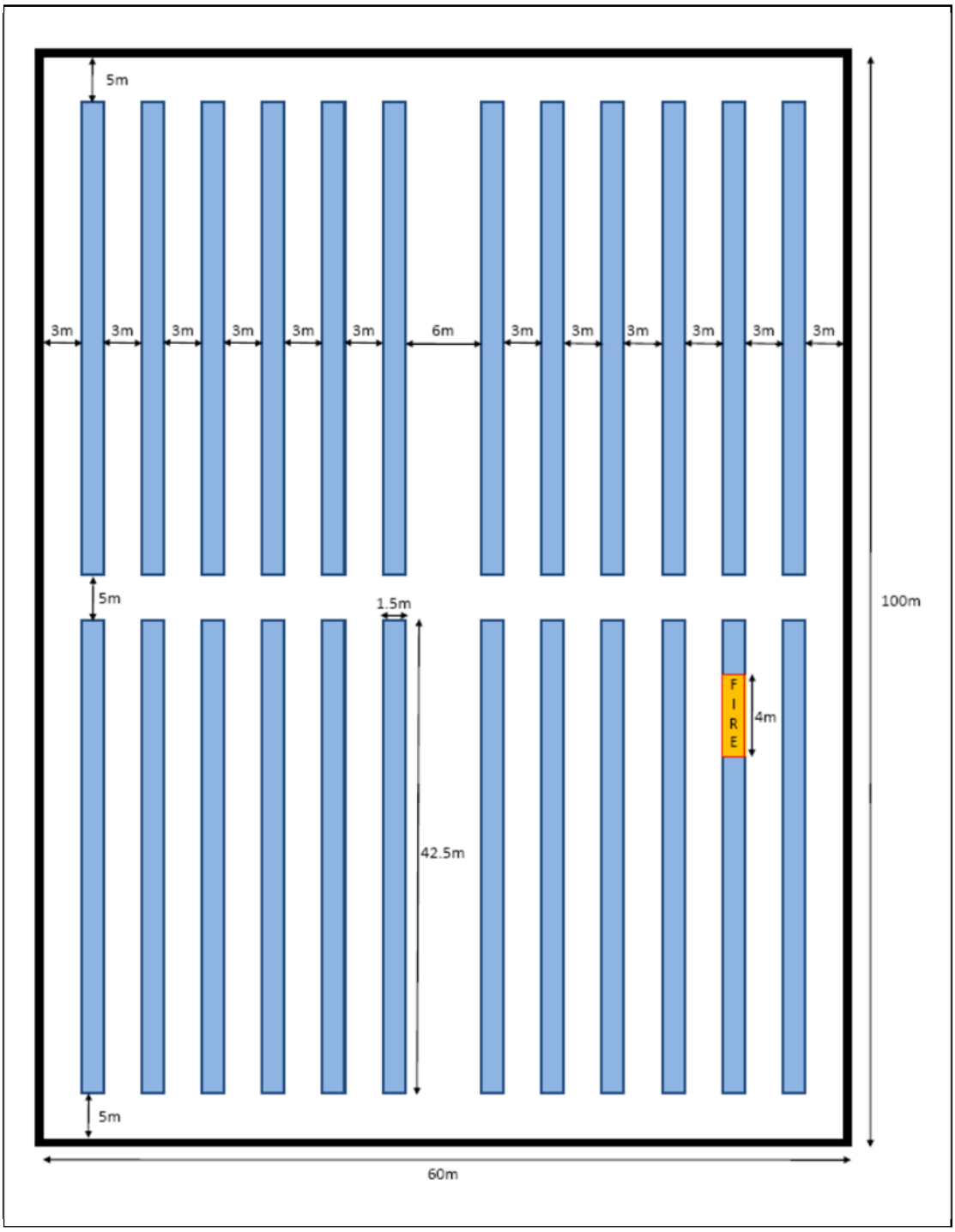

Figure 2: Plan view of large warehouse showing warehouse & rack dimensions, and fire position.

2.2 Design fire

In addition to the ventilation and storage height characteristics of rack storage, the top and sides of racked goods are usually available for flame spread. This allows the fire to spread in three directions simultaneously (Zalosh, 2003). It is, therefore, not

reasonable to apply a (commonly-used) t^2-growth rate to a rack-storage scenario, as this describes growth in only two directions.

A power-law to the third power has been found to describe well the fire growth for rack storage arrays (Yu and Stavrianidis, 1991; Ingason, 2001). Two t^3 fires were chosen for this study. The DBH's proposed framework for demonstrating fire safety for performance-based design describes three t^3 fires, of which the slower and the faster of the three were selected to provide bounds between which future problems can be compared.

The faster t^3 fire, henceforth known as the extreme t^3 fire, is described in Equation 1, and is designed to represent polystyrene in single wall cardboard cartons (a Group 1 Commodity under the Factory Mutual Research Corporation classification). The slower t^3 fire (Equation 2), henceforth known as the rapid t^3 fire, represents a fire involving double triwall cardboard cartons (a Group 3 Commodity under the FMRC classification). Both fires are presented in Figure 3.

$$\dot{Q} = 0.0088t^3H \quad (1)$$

$$\dot{Q} = 0.00068t^3H \quad (2)$$

where H is the height of the rack storage.

Pabich (1998) conducted rack storage fire tests in a 13.7 m x 13.7 m x 16.7 m (45 ft x 45 ft x 55 ft) room under a 7.6 m (25 ft) diameter collection hood for an oxygen consumption calorimeter. Peak heat release rates of up to 19 MW were observed for plastic-type fuels before fire growth was arrested by in-rack sprinklers. Similarly, a peak heat release rate of 17.3 MW was observed by Hasegawa *et al.* (1999) in tests of various computer equipment (packaged with polystyrene, plastic film, cardboard, and wood pallets) under a 5.5 m x 5.5 m collection hood without sprinkler intervention. Karlsson and Quintiere (2000) provide a rough estimation 30-40 MW for polystyrene jars in cartons stacked 4.9 m high. Furthermore, the proposed framework for performance–based design in New Zealand would require that fire-fighter tenability

be demonstrated for a fire size of 50 MW unless the building is sprinklered, ventilation-limited or fuel-limited. It was decided to adopt 50 MW as the peak heat release rate for this project with the aim of providing a worst-case fire size, and in keeping with the requirements of the proposed DBH framework.

The fire was located near, but not exactly at, the middle of the warehouse, where the impact of walls and corners would be reduced (see Figure 1 and Figure 2).

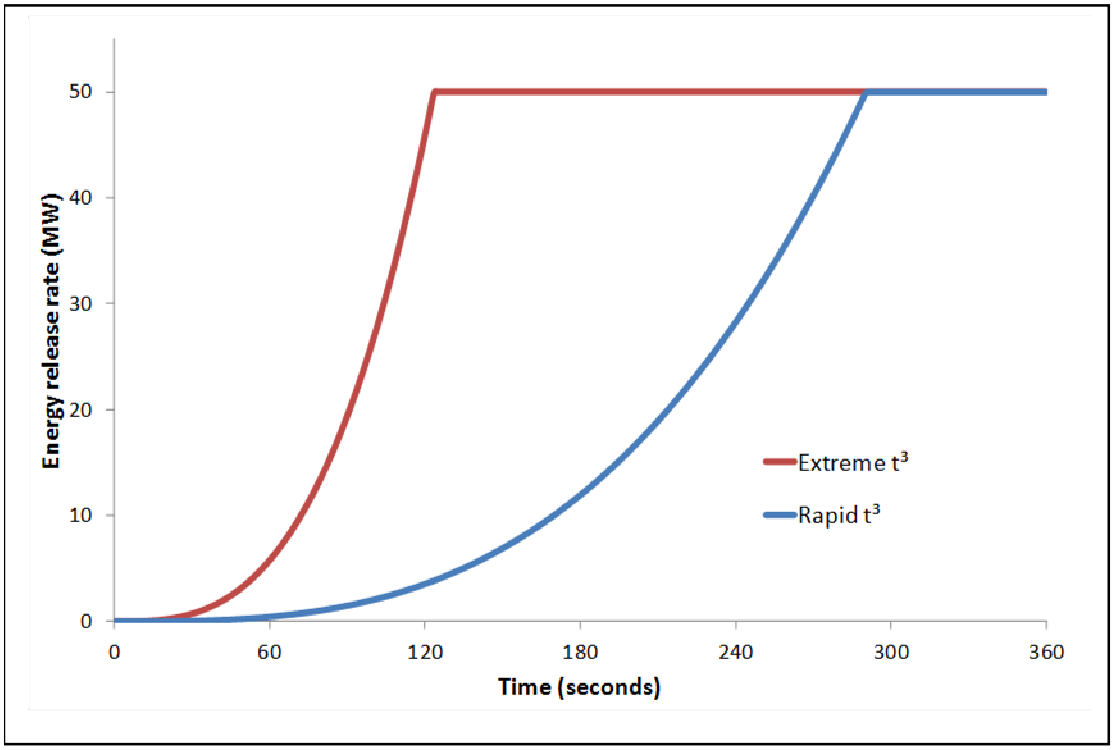

Figure 3: Design fires used in the simulations. The left curve has an extreme t^3 growth rate, and right curve a rapid t^3 growth rate. Both curves have a peak heat release rate of 50 MW.

2.3 Fire-fighter tenability

For this project, the characteristics of the fire reaction were based on those for pre-flashover fires in buildings with rack storage as described in the proposed Verification Method, which includes a soot yield of 0.07 kg/kg of fuel. The production of soot is, along with fire size, of prime importance in determining how visibility is displayed in Smokeview (a program that displays FDS results in a 3-dimensional representation).

In order for radiation to be recorded in FDS, it is necessary to fix the measurement devices to solid obstructions (from henceforth called targets). Nine targets were placed evenly inside each warehouse for this purpose (Figure 4).

Given that for this project the interest is in the tenability of the warehouse for fire-fighting, each target was given the thermal properties of a fire-fighter's jacket, or turnout coat, as described by Mell and Lawson (2000). They describe a turnout coat as having three layers: an outer shell, a moisture barrier and a thermal inner. For the outer shell, Mell and Lawson (2000, Table 1) specify a specific heat of 1.3 kJ/kg °C, a thermal conductivity of 0.047 W/m °C, and a density of 310 kg/m^3; for the moisture barrier they specify a specific heat of 2.01 kJ/kg °C, a thermal conductivity of 0.012 W/m °C, and a density of 800 kg/m^3; and for the thermal inner they specify a specific heat of 0.7 kJ/kg °C, a thermal conductivity of 0.038 W/m °C, and a density of 72 kg/m^3.

Measurements of radiation and temperature at a height of 1.5 m were achieved in FDS by use of radiative heat flux and temperature. Radiative heat flux is that portion of net heat flux that is attributed only to radiation (ignoring the convective component) (McGrattan *et al.*, 2009). The temperature device models the true gas temperature of the cell in which the device is placed. In addition, visibility devices were installed at these same nine positions in order to obtain an estimate of the visibility conditions in the warehouse, to allow relative comparisons between simulations. It was also possible to view both temperature and visibility in slice files and plot3d files in Smokeview. An example FDS script used during this project is provided in Appendix B.

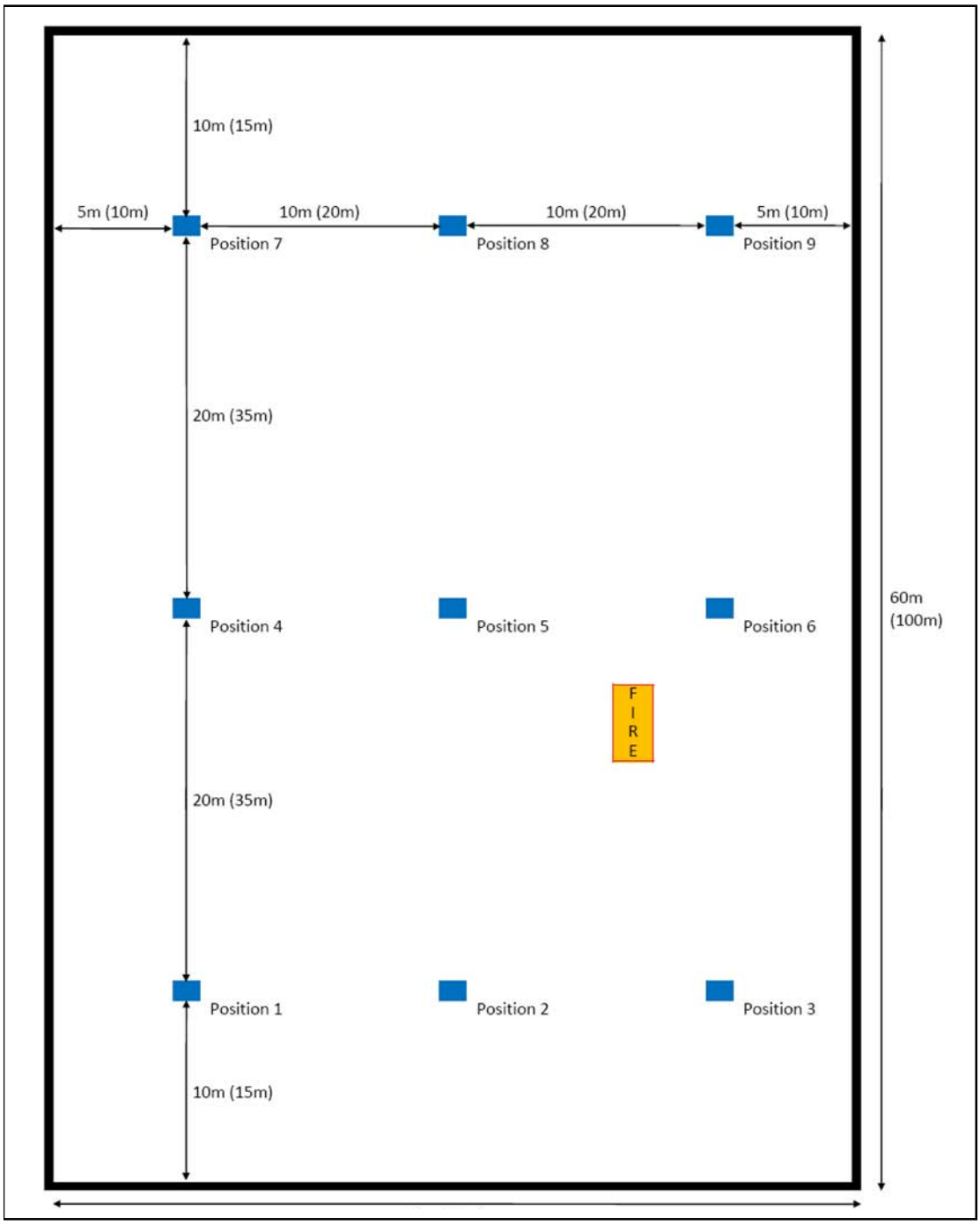

Figure 4: Plan view of warehouse showing position of targets for recording heat flux measurements (distances in brackets are for the large warehouse).

2.4 Modelling in Fire Dynamics Simulator (FDS)

It was decided to use FDS (Version 5.4.3) to determine whether the modelled buildings achieve the fire-fighter tenability criteria outlined above. The Fire Dynamics Simulator (FDS) is a computational fluid dynamics (CFD) model developed by the National Institute of Standards and Technology (NIST). The core of

any CFD model is a set of partial differential equations that describe the conservation of mass, energy, and momentum in each of a very large number of relatively small control volumes (McGrattan and Miles, 2008). FDS solves numerically a form of the Navier-Stokes equations for large scale convective transport, and makes use of Large Eddy Simulation (LES) for turbulence modelling of small-scale diffusive processes (viscosity, thermal conductivity, material diffusivity) in flames and in boundary layers near solid surfaces (McGrattan *et al.*, 2010).

Consideration was given to the use of the multi-compartment zone model, BRANZFIRE, to aid analysis. BRANZFIRE integrates a flame spread and fire growth model with a multi-compartment zone model (Wade, 2004). It is a commonly used zone model in New Zealand. Chow (1994; 1996) noted some success using multiple cells in a zone model to simulate fires in one large enclosure. This might be achieved by including a central room with a significantly higher ceiling than the surrounding rooms (Mills, 2004). The rooms would then be connected by full-height vents, or open walls. However, with such a concept there is potential for results to be confounded by conditions chosen at boundaries connecting one room with another, because a discharge coefficient is applied to flow into the central room from the surrounding rooms. This results in an error of unknown magnitude. A CFD model was thought to be more accurate for larger spaces. In addition, the ease of visualisation via Smokeview was also seen as an advantage.

2.5 Preliminary testing

Four preliminary tests were conducted in an effort to eliminate possible confounding factors due to the simulation set-up in FDS (see Sections 2.5.1 through 2.5.4). Testing, and all following simulations, were carried out on four computers with 64-bit operating systems and Intel® Core™ i7-2600 Processors with 16 GB RAM.

The first three tests considered the influence of different construction materials, grid sizes, and domain heights. The final test considered whether any fire-fighter tenability criteria were exceeded when the warehouse buildings contained no venting. Devices fixed to the nine measurement targets were used as a means of comparison between the different FDS set-ups, as well as investigation of various Smokeview outputs.

2.5.1 Test of wall materials

The first set of test simulations was performed only in the smaller warehouse, with a domain height of 2 metres above the warehouse roof (total domain height of 8.5 m), domain extensions of 3 m on all sides of the warehouse, and inner and outer grid sizes of 0.25 m and 0.5 m, respectively. The warehouse was fitted with the *statu quo* of 15 % roof venting via twenty-seven 3.2 m x 3.2 m holes (the dimension of which was based on the largest mechanical vent size imported amongst a number of local suppliers). Inlet air was provided to match the roof venting area (270 m²), by means of a 1.5 m high gap, extending from the floor, for the entire perimeter of the warehouse (180 m). All simulations were run for 1,500 seconds, with a 300-second linear growth phase to a 50 MW steady-state fire.

Three simulations were carried out to test the influence of wall materials on the fire and other effects pertinent to the FBIM tenability criteria. The first simulation modelled the smaller warehouse with 0.42 mm-thick sheet metal walls[2]. Steel properties used were conductivity of 45.8 W/m K, specific heat of 0.46 kJ/kg K, and density of 7,850 kg/m^3 (Drysdale, 1998, Table 1.2). Concrete walls were used in the second simulation with conductivity of 1.1 W/m K, specific heat of 0.88 kJ/kg K, and density of 2,100 kg/m^3 (Drysdale, 1998, Table 1.2). Concrete walls were given a thickness of 175 mm, based on a conversation with a practising fire engineering consultant who noted that this was currently the most common thickness of precast concrete panels in New Zealand. For the third simulation, the walls were modelled as being adiabatic. This means that there is no net heat transfer (radiative and convective) from the fire (the working fluid) to the walls (the solid) (McGrattan *et al.*, 2009). All simulations used sheet metal (and the steel properties described above) for the roofing material, as would be expected in such a building.

It is noted that all three choices represent non-combustible materials, as is common in industrial warehouses in New Zealand. Should structural components and/or wall linings consist of combustible materials i.e. wood, minimal differences in FDS results would be expected: although less heat transfer from the fire to the walls would occur owing to the lower thermal conductivity of wood compared to those materials tested

[2] http://www.nzsteel.co.nz/files/g550_znal.pdf accessed on 18th January 2010 at 9:42am

here. In reality, combustible linings would serve to increase the fuel load in a warehouse, and increase the potential for fire spread and fire size.

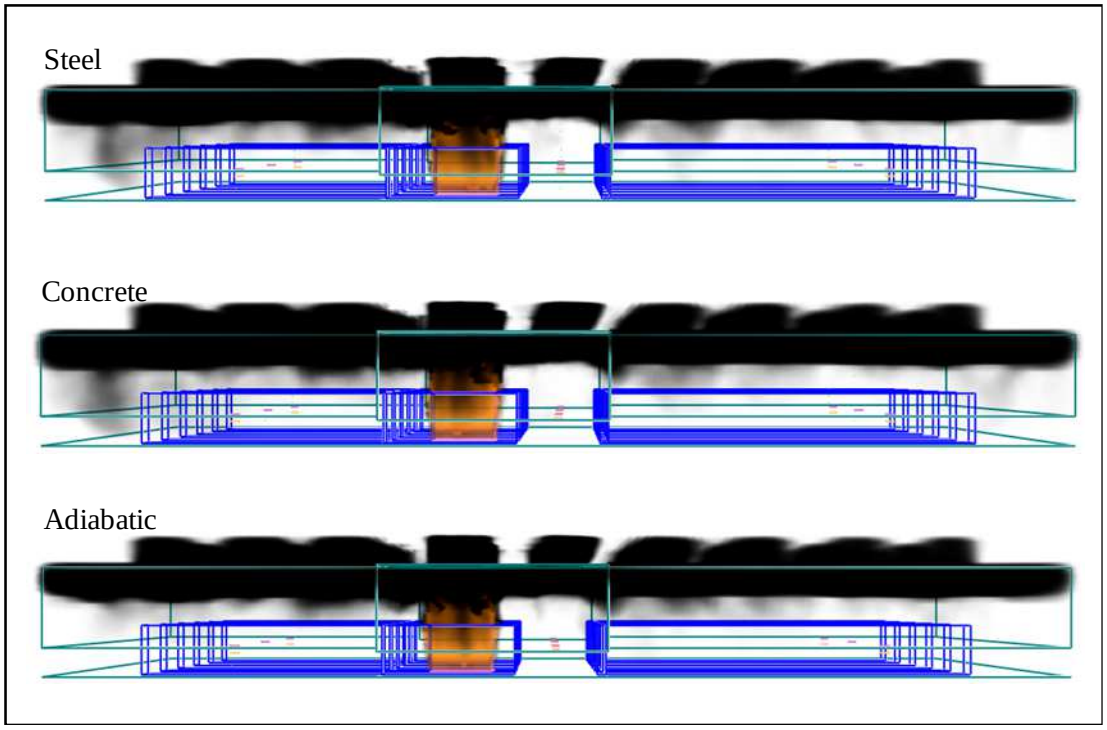

Figure 5: Smokeview depiction of fire and smoke layer after 1,500 seconds in small warehouse with a 300-second linear growth phase to 50 MW. The warehouses have 15 % roof venting area and different wall materials (top – steel, middle – concrete, and bottom – adiabatic).

Smokeview depictions of the fire and smoke conditions in the warehouse with the different wall materials are shown in Figure 5. There were no obvious differences in the appearance of the conditions in the warehouse, due to the use of different wall materials. Both the height of the smoke layer and the utilisation of roof venting were indistinguishable between the three simulations.

In Figure 6, total mass flow out from the roof vents is compared for the three different wall materials. For both steel and concrete, the mass flow out of the domain during the 1,800 seconds simulation was 176.7 kg, and for adiabatic walls, the total mass flow was 178.3 kg. This quantity remained very similar across all three simulations regardless of the wall materials used, indicating that the fire was burning the same regardless of wall material. Mass flow into the warehouse was 0 kg in all three simulations.

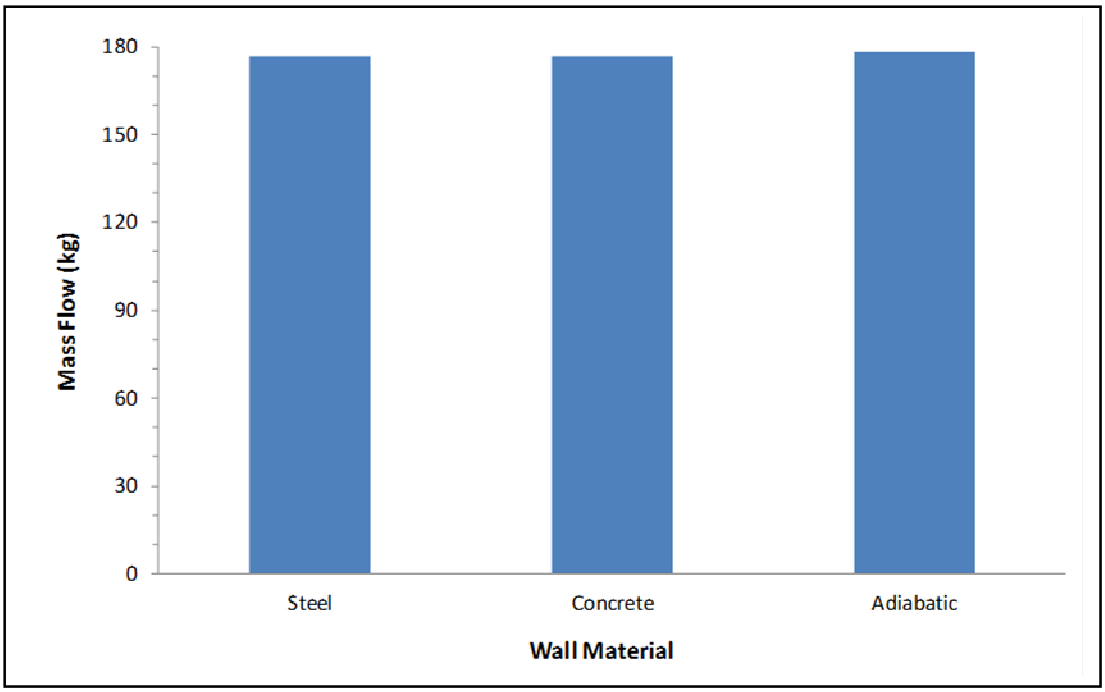

Figure 6: Comparison of total mass flow exiting the warehouse calculated in FDS after 1,500 seconds in the small warehouse with a 300-second linear growth phase to 50 MW.

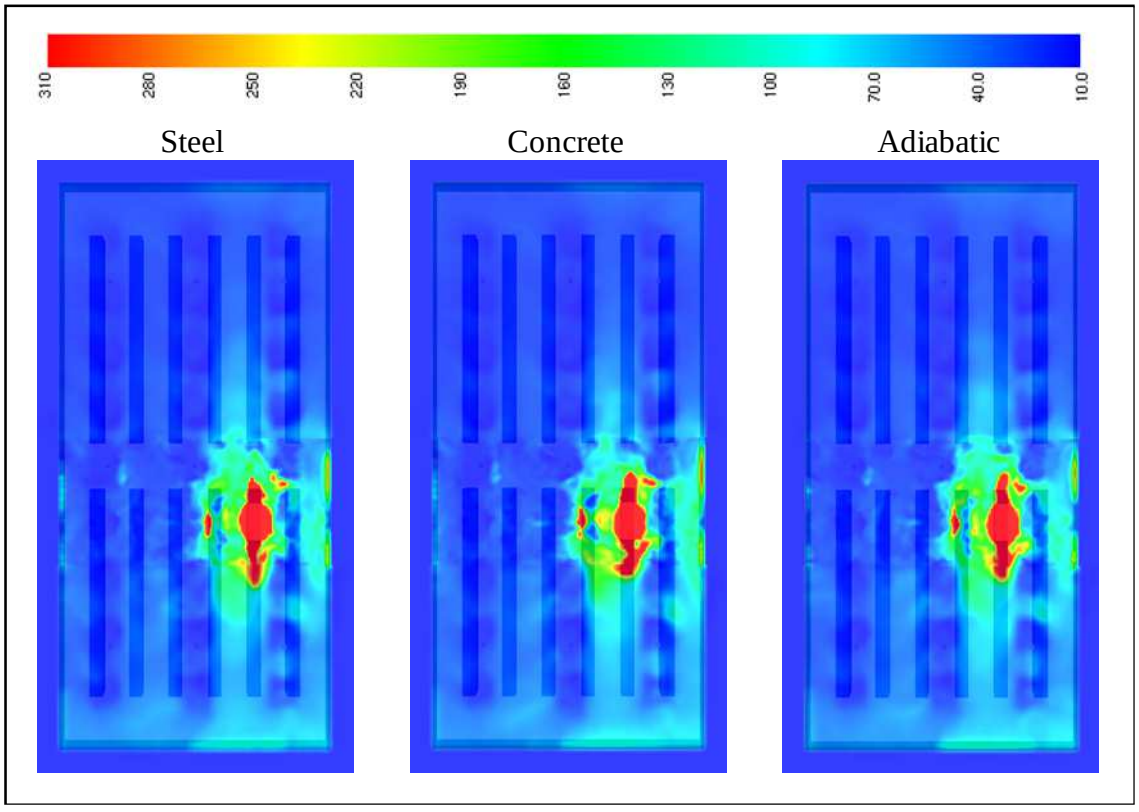

Figure 7: Smokeview depiction of temperature distributions 1.0 m below the ceiling after 1,500 seconds in the small warehouse with a 300-second linear growth phase to 50 MW. The warehouses have 15 % roof venting area and different wall materials (left – steel, middle – concrete, and right – adiabatic).

There were only minor differences in temperature distributions 1 m below the ceiling as a result of modelling different wall materials (Figure 7). Some differences were expected between the simulations, on account of the different properties of the three materials. The fact that these differences were small after 1,500 seconds gives confidence that the choice of wall material would make little difference on the temperature conditions in the warehouse.

Figure 8 compares the radiative heat flux for the three simulations at Positions 4, 5, and 6 in the warehouse (see Figure 4 for a map of heat flux targets). Heat flux data were smoothed using a ninety-second average. Positions 5 and 6 were chosen to display the preliminary test results as they are closest to the fire, and therefore show the most fluctuations. Position 4 was chosen to represent those targets that are not as highly dominated by radiation directly from the fire. The graph does not display any noteworthy effect of the use of different wall materials, although the adiabatic wall simulation produced heat fluxes that were, generally, slightly higher than the simulations with steel or concrete walls.

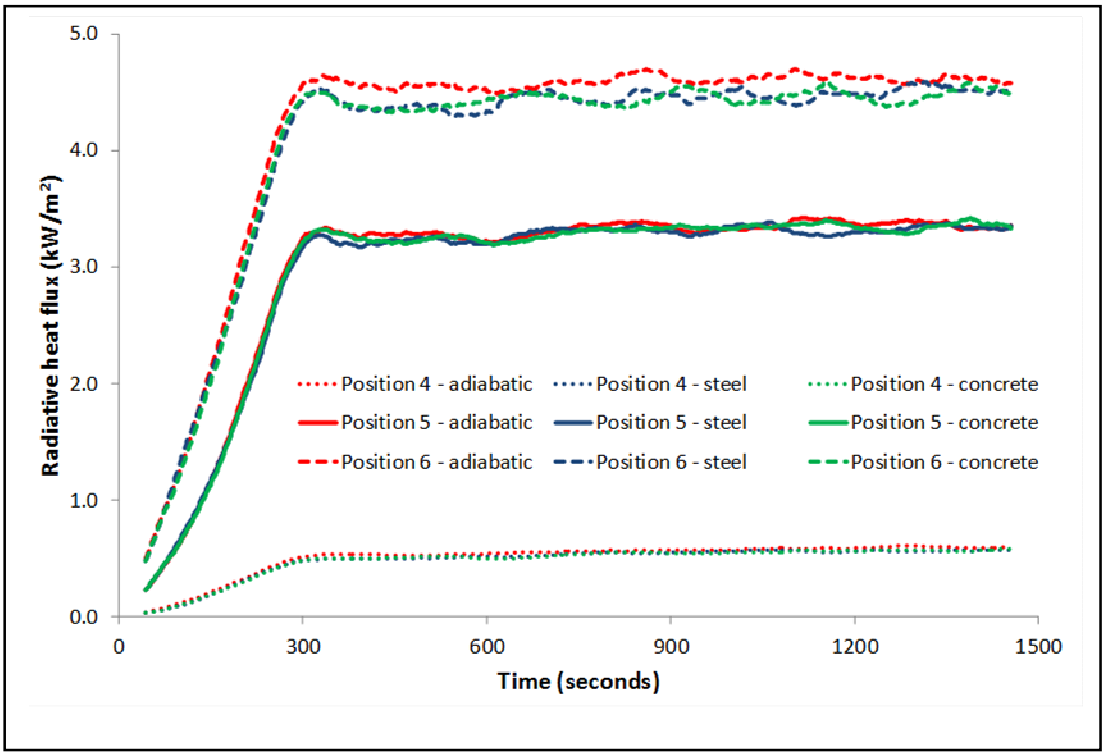

Figure 8: Comparison of smoothed radiative heat flux data from FDS at a height of 1.5 m at Positions 4, 5, and 6 with different wall materials.

Temperature at a height of 1.5 m above the floor is displayed in Figure 9 (Temperature data were smoothed using a ninety-second average, and then further smoothed with a ninety-second average). There are only minor differences in the temperature readings between the three materials and, in all cases, the temperatures fluctuate without any distinct pattern.

From this test of wall materials, it was decided that use of adiabatic walls would not have a detrimental effect on measurements of temperatures and radiative heat fluxes at 1.5 m (important variables in terms of the FBIM criteria). Adiabatic walls were used for all simulations after the preliminary testing stage.

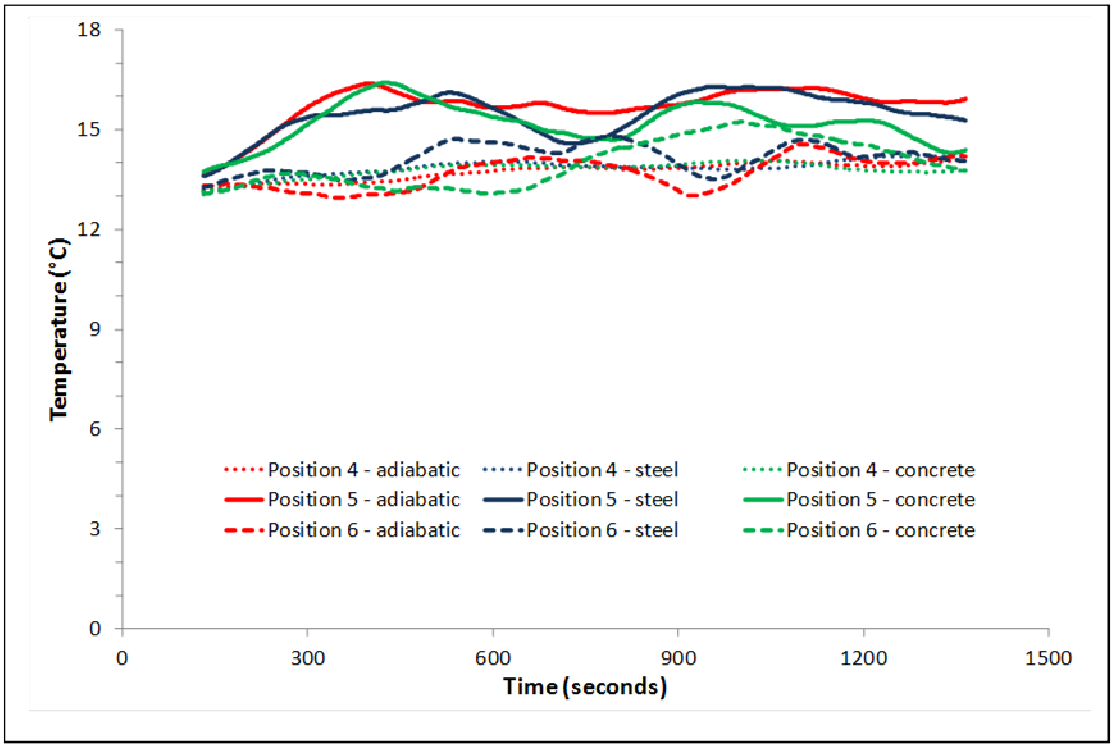

Figure 9: Comparison of smoothed temperature data from FDS at a height of 1.5 m at Positions 4, 5, and 6 with different wall materials.

2.5.2 Test of grid size effect

When modelling in FDS, it is important to take account of grid size effects. Xin (2000, p1) defined the grid size effect as "...the influence on the computational results when different grid sizes are used with all other computational input parameters fixed". For grid-independent results to be achieved, the grid size in the computational

domain needs to be reduced until further reduction has no effect on the results produced (Moinuddin and Thomas, 2007). Ma and Quintiere (2003) proposed that good calculation results can be obtained with grid size $\Delta = 0.05D^*$, where D^* is the characteristic fire length (m) defined in Equation 3 (McGrattan *et al.*, 2009).

$$D^* = \left(\frac{\dot{Q}}{\rho_\infty c_p T_\infty \sqrt{g}}\right)^{2/5} \quad 3$$

where $\dot{Q}$ is the energy release rate (kW), ρ_∞ is the ambient density (kg/m^3), c_p is the specific heat (kJ/kg K), T_∞ is the ambient temperature (K), and g is the acceleration due to gravity which is equal to 9.81 m/s^2.

For this project, with an energy release rate ($\dot{Q}$) of 50,000 kW, an ambient density (ρ_∞) taken as 1.204 kg/m^3, specific heat (c_p) taken as 1.005 kJ/kg K, and ambient temperature (T_∞) of 286 K, the characteristic fire length (D^*) was found to be 4.63 m. Consequently, the method of Ma and Quintiere (2003) would suggest a grid size of 230 mm (0.05 x 4.63 m = 0.23 m).

Another method of selecting grid size is to use the quantity $D^*/\delta x$, where δx is the nominal size of a mesh cell. This ratio describes the number of computational cells spanning the characteristic diameter of the fire. In a study of various fire models, Hill *et al.* (2007) validated the ratio, $D^*/\delta x$, for values from 4 to 16. When set to the finest number of computational cells in this range (*i.e.* 16), the ratio implies a grid size of 290 mm for the characteristic fire length in this study. For the coarsest number of computational cells validated (*i.e.* 4), the ratio-implied grid size is 1160 mm and for a moderate number (*i.e.* 10), 460 mm is the resultant grid size.

For this project, it was decided to divide the computational domain into three meshes: a central mesh containing the central portion of the warehouse with fire and two outer meshes containing the remaining, outer portions of the warehouse. A grid size of 250 mm was selected for the central mesh to ensure appropriate accuracy and 500 mm for the outer meshes an attempt to limit unnecessary processing time. This selection appears to agree well with the two methods of finding grid size described above.

However, two tests of grid size were carried out to confirm this selection. The first set of simulations (run for 1,500 seconds) varied the grid size for the extreme t^3 in the small warehouse, and the second set (run for 1,200 seconds) varied the grid size for the rapid t^3 in the large warehouse.

For the small warehouse, five combinations of grid size were tested (Figure 10). The first three simulations held the inner mesh grid size constant at 250 mm whilst adjusting the outer mesh grid sizes from 500 mm to 750 mm to 1,000 mm. The fourth and fifth simulations combined an inner mesh grid size of 500 mm with outer mesh grid sizes of 500 mm and 1,000 mm, respectively. Due to the selection of 1,000 mm grid sizes, it was necessary to alter the height of the small warehouse roof for all five test simulations from 6.5 m to 6 m in order to allow for meaningful comparisons of the cell size testing results. Without this change, the position of the roof obstacle would be shifted by FDS to match the nearest grid cell boundary. In the case of 1,000 mm grid sizes, the 6.5 m roof obstacle would be moved to 7 m (an exact multiple of 1,000 mm). The domain height remained at 9 m, or 3 m above the warehouse roof for these tests.

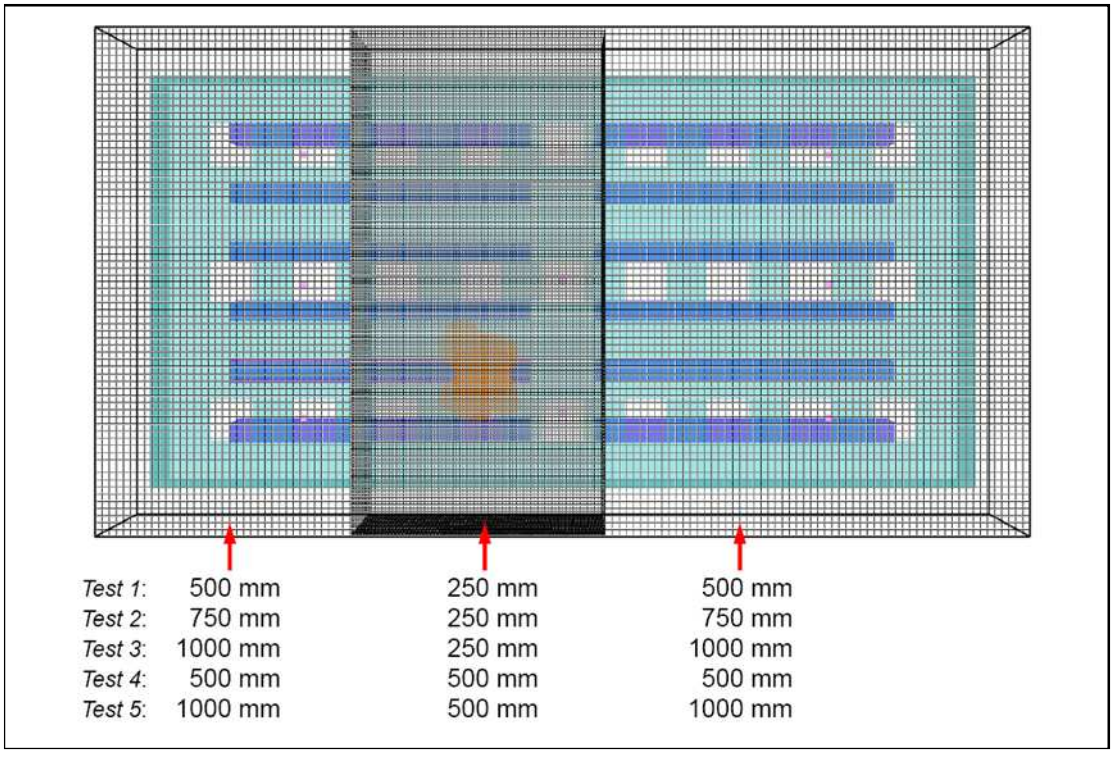

Figure 10: Depiction of small warehouse showing delineation of meshes tested.

For the large warehouse, four combinations of grid size were simulated as shown in Figure 11. The first had an inner mesh grid size of 250 mm and an outer mesh grid size of 500 mm. The second and third simulations held the inner mesh grid size constant at 500 mm whilst adjusting the outer mesh grid size from 500 mm to 1,000 mm. The fourth simulation had a 1,000 mm grid size for both the inner and outer meshes.

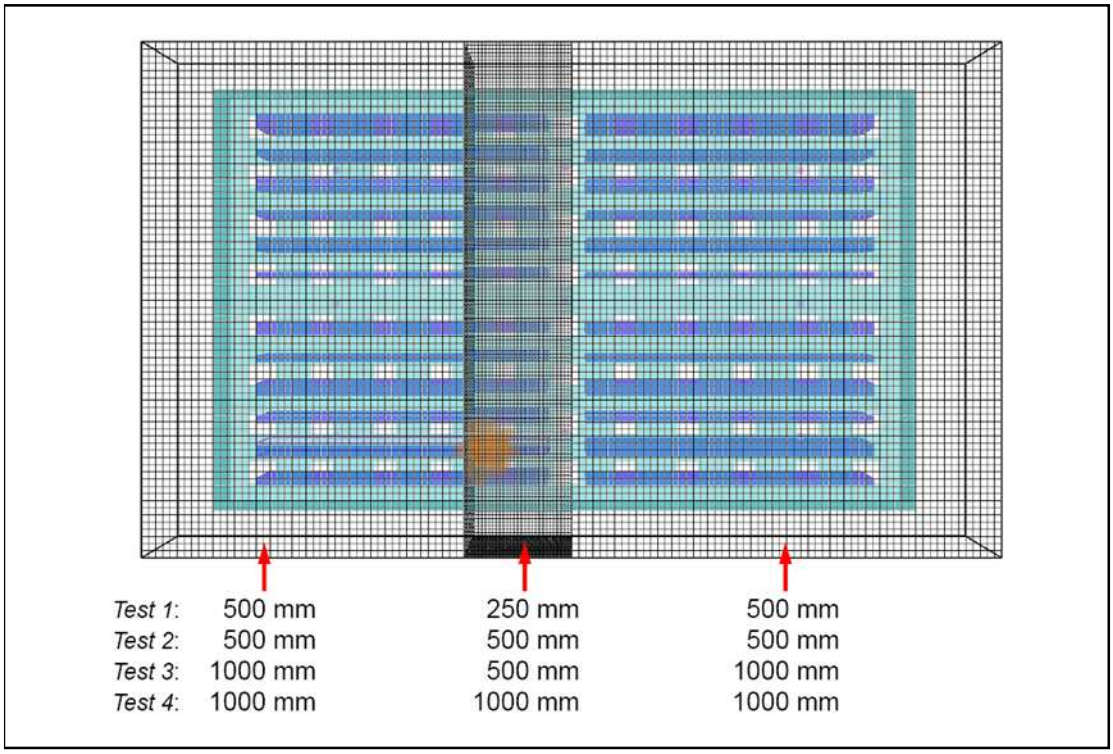

Figure 11: Depiction of large warehouse showing delineation of meshes tested.

Figure 12 shows the effect of different resolutions of grid cell sizes on the depiction of the fire and the smoke layer in Smokeview. There were some differences in the appearance of the smoke layer in particular as the grid size was enlarged. The smoke layer with the finest combination of grid sizes (250 mm/500 mm) extended to the walls of the warehouse, and utilised most vents on the outer perimeter of the warehouse. As grid sizes in became progressively coarser, the smoke layer no longer reached the outer walls in the longest dimension of the warehouse. In addition, flames that were clearly visible above the racks in the warehouse with a 250 mm inner mesh grid size were no longer visible with a 500 mm grid size.

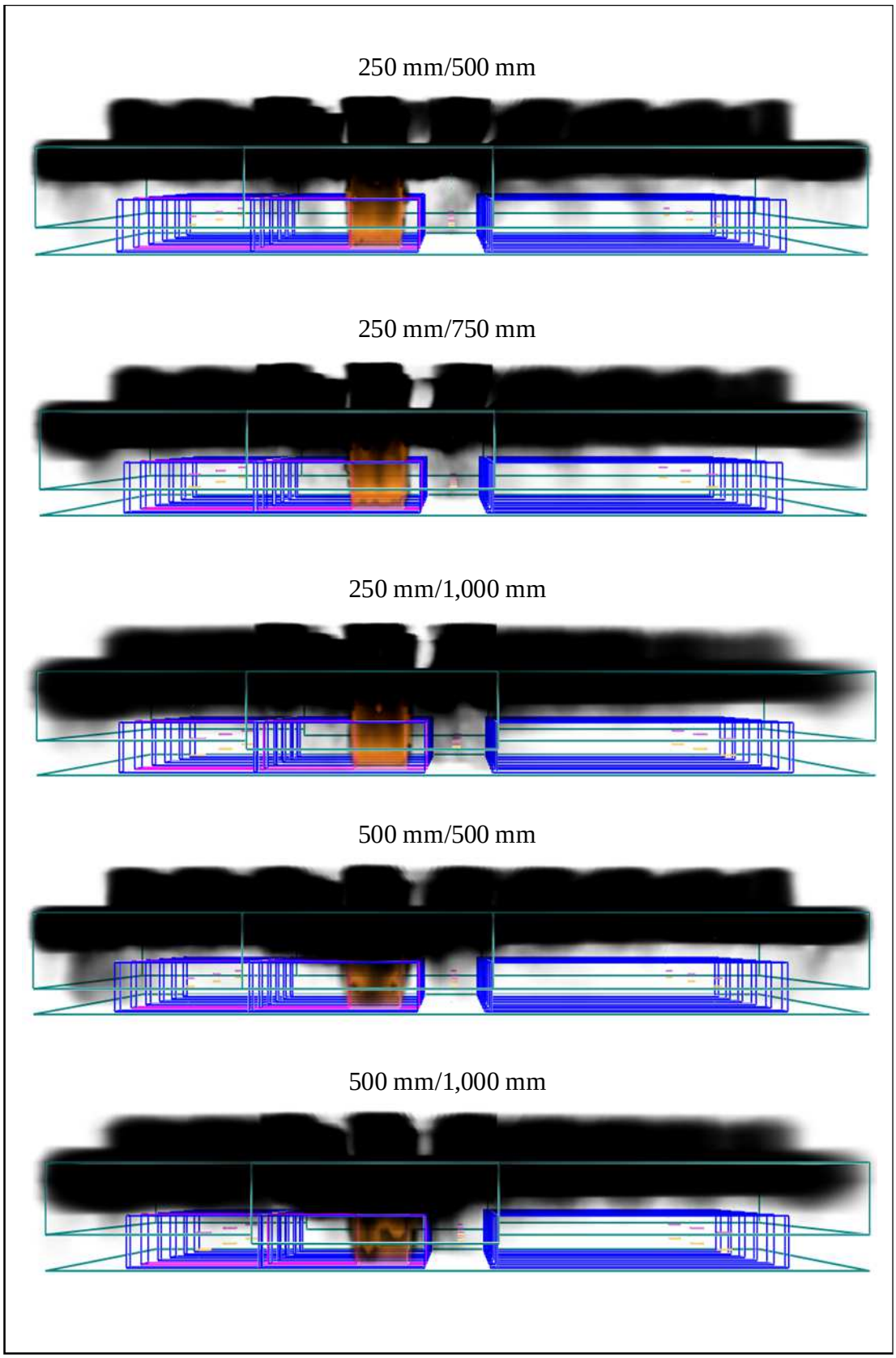

Figure 12: Effect of changing grid cell sizes on Smokeview depictions of fire and smoke layer after 1,500 seconds in small warehouse with extreme t^3 fire growth. The warehouse has 15 % roof venting area and matching inlet area for make-up air.

Total mass flow out of the warehouse from all roof vents is compared for the five tested cell sizes in Figure 13. As the grid sizes became coarser, the total mass flow from the warehouse increased. The combination of 250 mm grid size in the inner mesh and 500 mm grid size in the outer mesh had a total mass flow of 179.9 kg during the 1,500-second simulation. This was the least of the five cell size combinations, and substantially less than the 296.7 kg observed for the coarsest cell size. Of importance here is the convergence of the mass flows as grid cell sizes became finer: the selection of the 250 mm/500 mm combination being the better selection of the five. Mass flow into the warehouse was 0 kg in all five simulations.

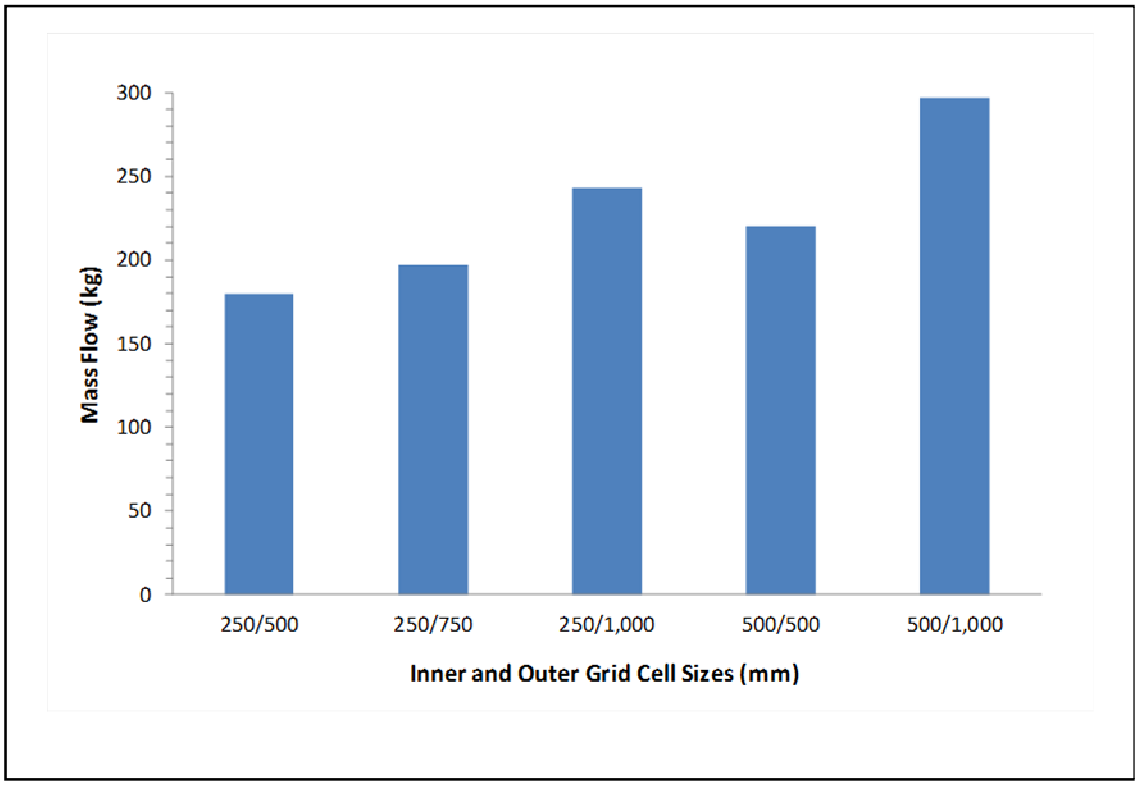

Figure 13: Comparison of total mass flow exiting the warehouse calculated in FDS after 1,500 seconds in the small warehouse with extreme t^3 fire growth. The warehouses have 15 % roof venting area and different grid cell sizes. The grid cell size for the inner mesh is listed first, followed by the grid cell size for the two outer meshes.

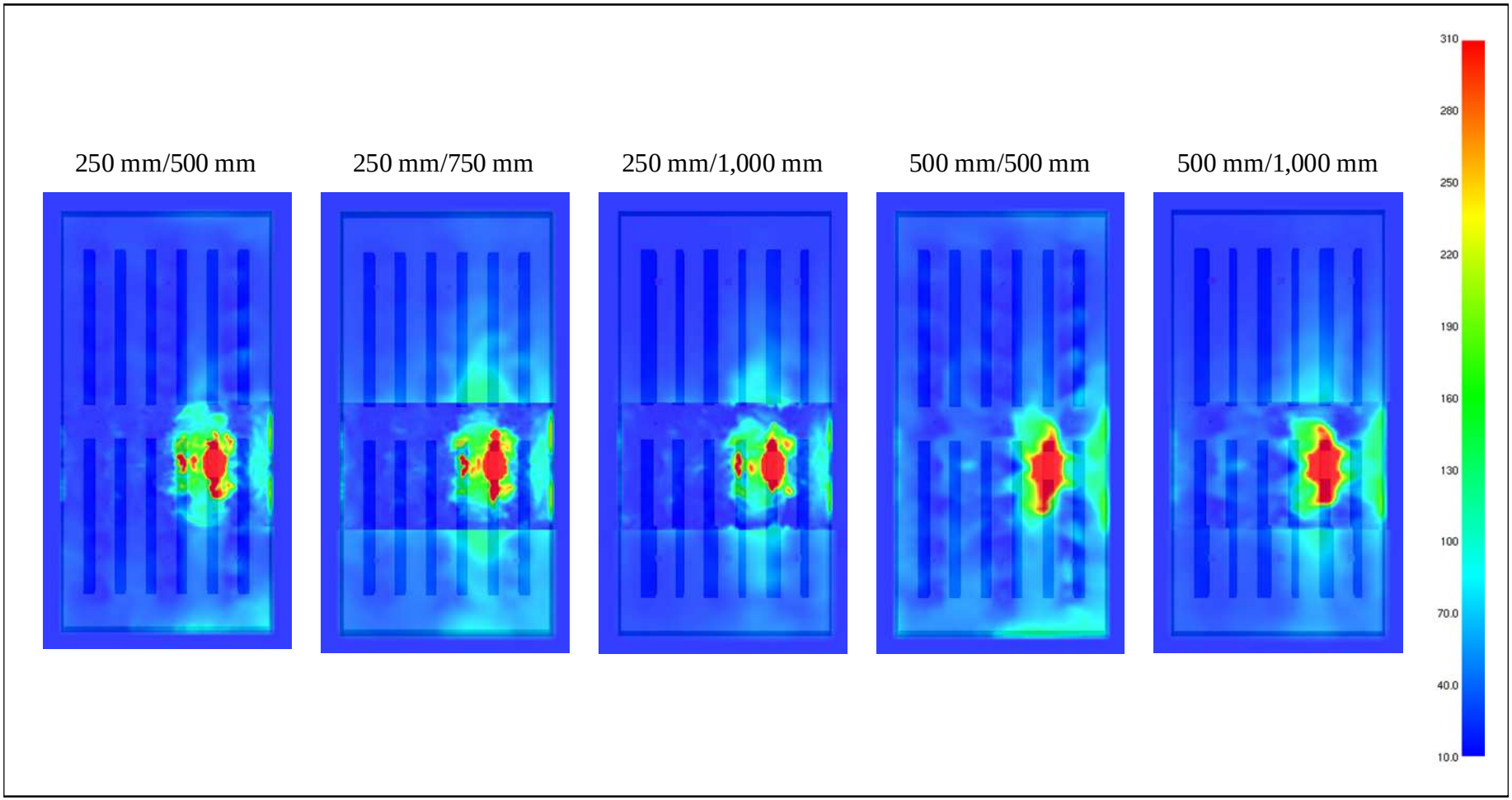

Figure 14: Smokeview depiction of temperature distributions 1.0 m below the ceiling after 1,500 seconds in the small warehouse with extreme t^3 fire growth. The warehouse has 15 % roof venting area and different grid cell sizes. The grid cell size for the inner mesh is listed first, followed by the grid cell size for the two outer meshes.

Figure 14 shows temperature distributions in the small warehouse with different grid cell sizes. For the same size grid cells in the inner mesh, changing the size of the grid cells in the outer meshes had an effect on temperature distributions in the outer meshes: more turquoise colours were observed in the outer mesh as the grid cell size was increased, which indicates warmer temperatures than were be predicted with finer cell sizes. In addition, changes to the outer mesh grid resolution also had an impact on temperature distributions in the inner mesh: more turquoise and red colours were observed under with coarser outer mesh cell sizes, again indicating a warmer distribution of temperatures in the upper layer of the warehouse.

The choice of grid cell size clearly had an impact on the simulations in the small warehouse. To better identify a good choice of mesh resolution for the simulations, radiative heat flux and temperature data were assessed graphically. As with the test of wall materials in Section 2.5.1, heat flux data for the two sets of simulations were smoothed over ninety seconds, and the temperature data required smoothing over one hundred and eighty seconds followed by further smoothing over ninety seconds.

In Figure 15, it can be seen that for the three simulations with a 250 mm inner mesh grid cell size, the choice of outer mesh grid cell size made very little difference to the heat flux measurement in the small warehouse. At the three selected measurement positions, the three curves with a 250 mm inner mesh grid cell size track together relatively closely for the duration of the simulations. Similarly, for the 500 mm inner mesh grid cell size, the curves for the two outer mesh grid cell sizes of 500 mm and 1,000 mm track together, below the curves for the 250 mm inner mesh grid size.

Temperatures did not increase much above the ambient temperature at any of the nine targets regardless of grid cell size. In Figure 16, temperatures at a height of 1.5 m are presented for Positions 4, 5, and 6. At Position 4, temperatures were particularly benign. There was no clear pattern at the remaining two positions, with temperatures at Position 5 higher with the grid size combinations with an inner mesh cell size of 250 mm and temperatures at Position 6 higher with those combinations where the inner mesh cell size was 500 mm.

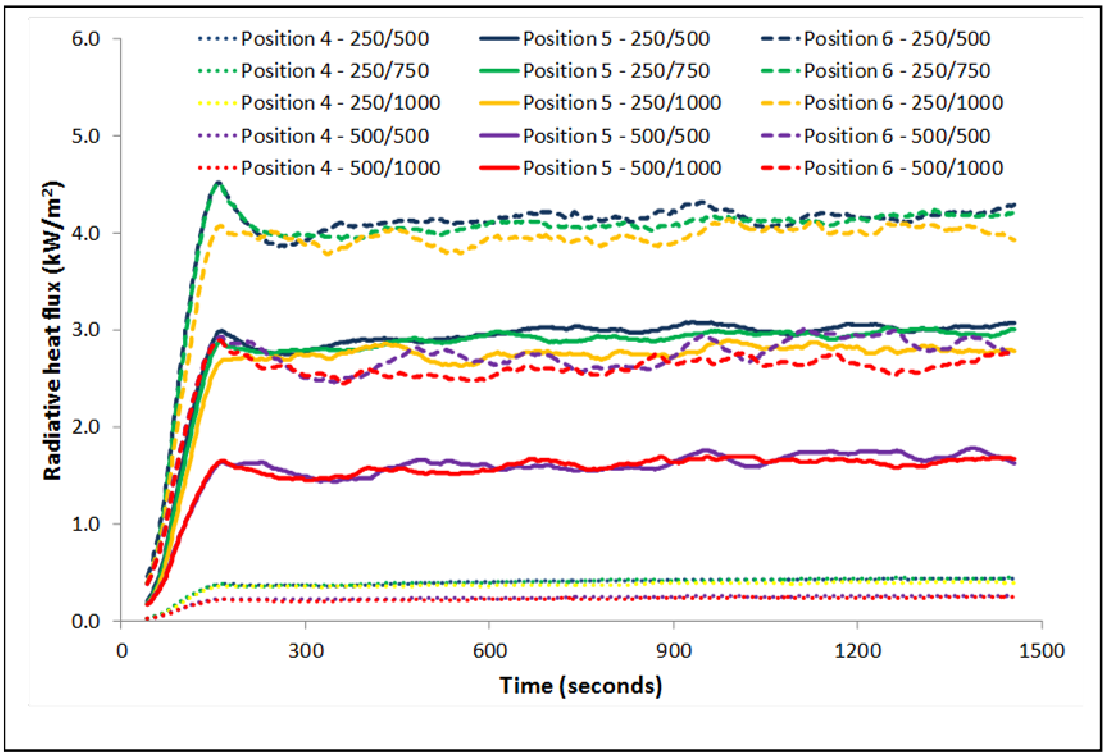

Figure 15: Comparison of smoothed radiative heat flux data from FDS at a height of 1.5 m at Positions 4, 5, and 6 with different grid cell sizes (mm) for the fire with extreme t^3 growth in the small warehouse.

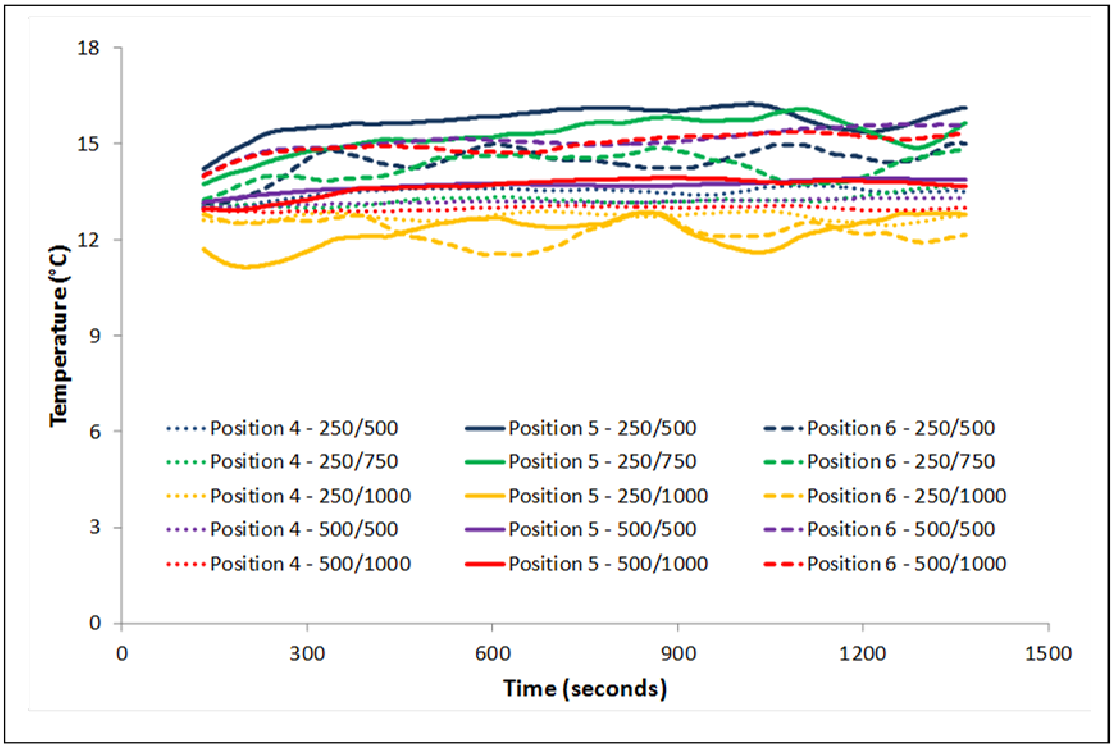

Figure 16: Comparison of smoothed temperature data from FDS at a height of 1.5 m at Positions 4, 5, and 6 with different grid cell sizes (mm) for the fire with extreme t^3 growth in the small warehouse.

It was attempted to run further tests with an inner mesh grid size of 125 mm and outer mesh grid sizes 250 mm and 500 mm in order to judge whether grid independence had been achieved. However, these simulations were both interrupted after approximately 100 seconds by a segmentation fault. This issue could not be solved, however, and it was decided to proceed with a grid size combination of 250 mm for the inner mesh and 500 mm for the outer meshes, owing to the convergence of radiative heat fluxes in Figure 15 and the minimal difference in temperatures at 1.5 m between the five simulations shown in Figure 16.

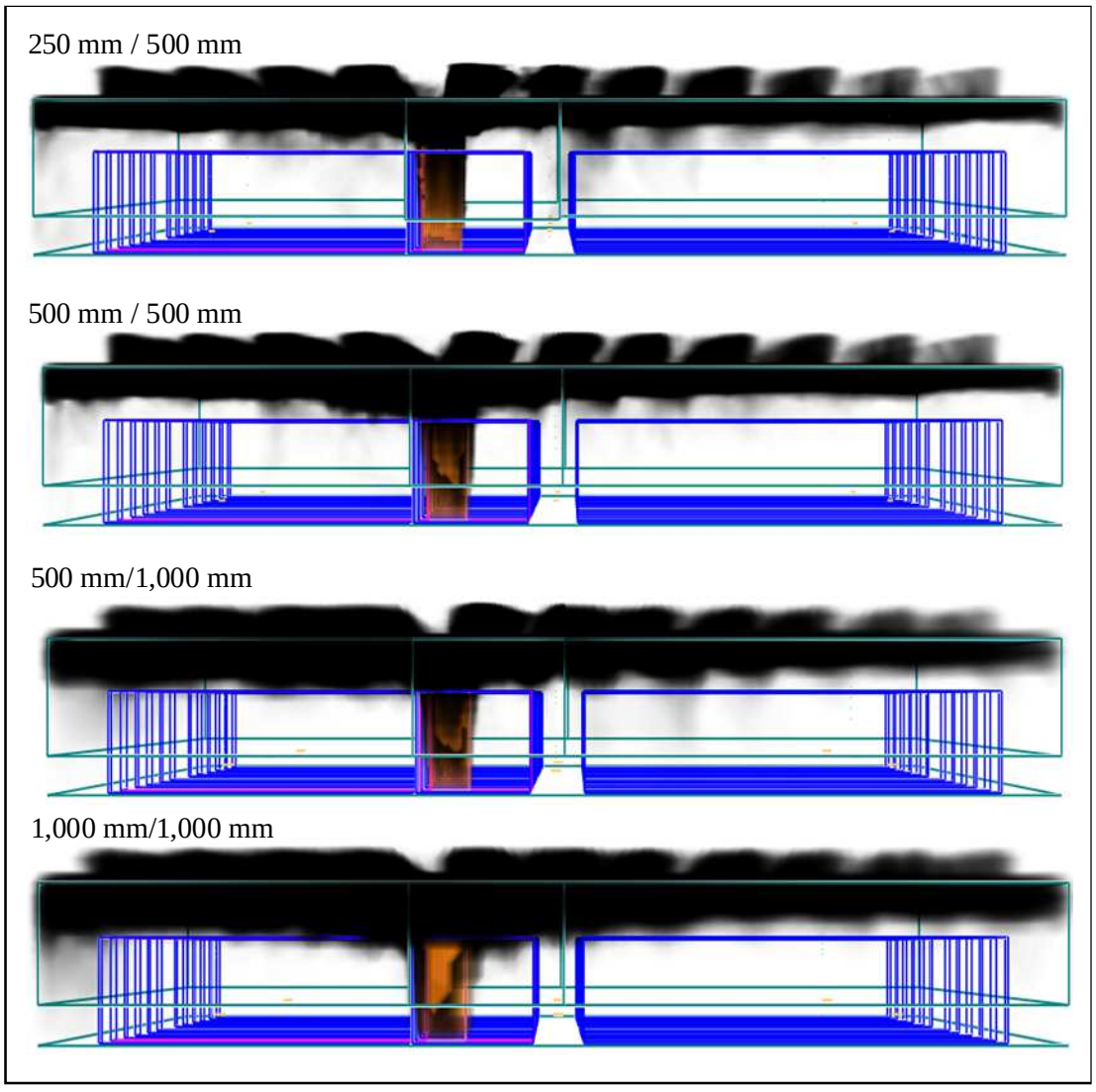

Figure 17: Effect of changing grid cell sizes on Smokeview depictions of fire and smoke layer after 1,200 seconds in large warehouse with rapid t^3 fire growth. The warehouse has 15 % roof venting area and matching inlet area for make-up air.

For the large warehouse, the results were much more easily interpreted. There was very little effect of the rapid t^3 fire on the ambient environment in the warehouse after 1,200 seconds. Figure 17 shows the depiction of the fire and smoke layer from Smokeview for each of the four grid cell size combinations tested in the large warehouse. There are only trivial differences between the four images. In each simulation the smoke layer was only faint or non-existent along the wall (along the short side of the warehouse) which is furthest from the fire. The fire itself was very similar in the first three simulations, but not as well-defined in the final simulation with the 1,000 mm/1,000 mm grid cell size combination.

Total mass flow out of the warehouse from all roof vents is compared for the four tested cell sizes in Figure 18. All four simulations had very similar mass flows: 291.7 kg for cells sizes of 250 mm/500 , 291.6 kg for cell sizes of 500 mm/500 mm, 291.9 kg for cell sizes of 500/1,000 mm, and 292.2 kg for cell sizes of 1,000/1,000 mm. Mass flow into the warehouse was 0 kg in all four simulations.

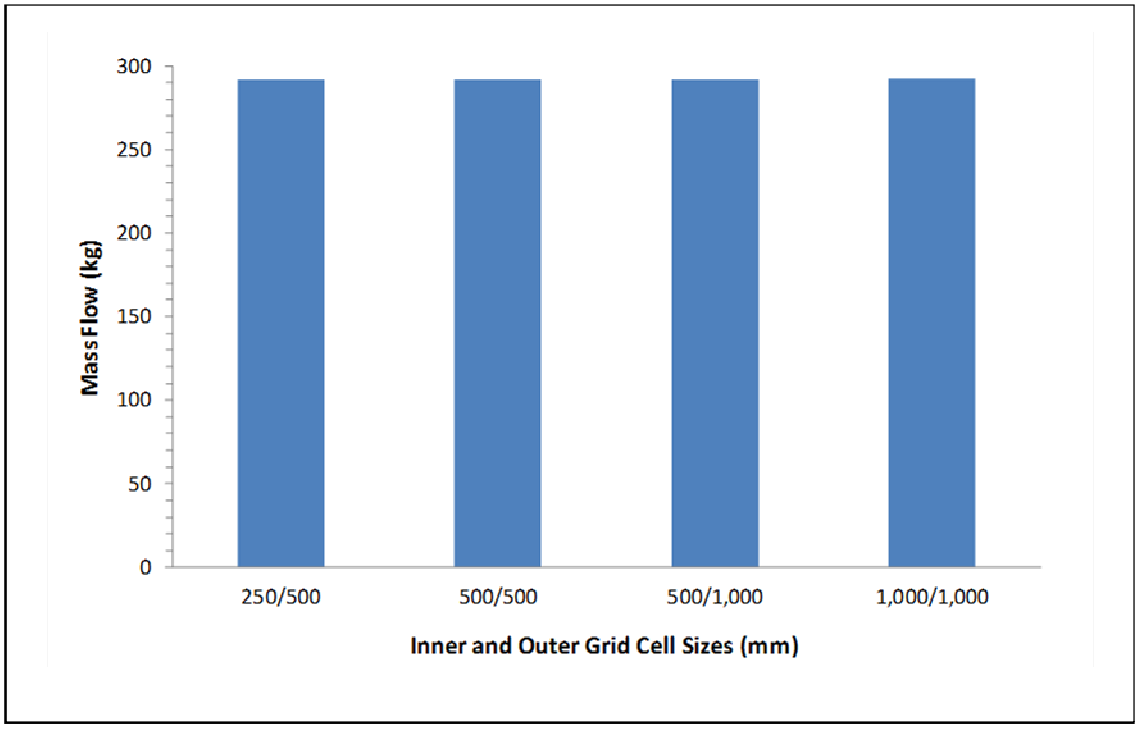

Figure 18: Comparison of total mass flow exiting the warehouse calculated in FDS after 1,200 seconds in the large warehouse with rapid t^3 fire growth. The warehouses have 15 % roof venting area and different grid cell sizes. The grid cell size for the inner mesh is listed first, followed by the grid cell size for the two outer meshes.

Differences in temperatures 1 m below the ceiling were also similar among the four simulations (Figure 19). A large proportion of the upper layer temperatures at this height remained ambient, while increases occurred only in the immediate vicinity of the fire.

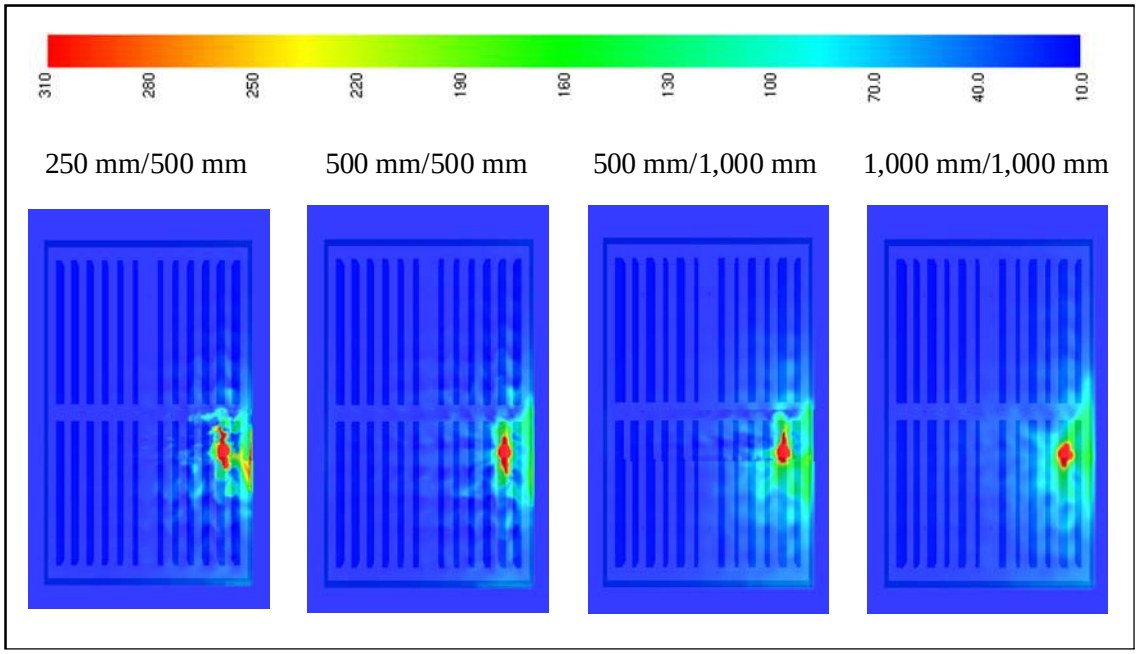

Figure 19: Smokeview depiction of temperature distributions 1.0 m below the ceiling after 1,200 seconds in the large warehouse with rapid t^3 fire growth. The warehouse has 15 % roof venting area and different grid cell sizes. The grid cell size for the inner mesh is listed first, followed by the grid cell size for the two outer meshes.

Figure 20 shows the radiative heat fluxes recorded at a height of 1.5 m. At both Position 4 and Position 5, radiative heat fluxes only increased a small amount above zero by the end of the simulation. Larger increases in radiation were observed at the targets located at Position 6 in each of the simulations. However, the heat flux for the 1,000 mm/1,000 mm grid size combination was the only curve to not to track not to track closely with the other curves.

The choice of mesh resolution had no substantial effect on lower layer temperatures in the large warehouse. Temperatures at a height of 1.5 m are not shown here, but did not increase significantly above the ambient in any of the four simulations.

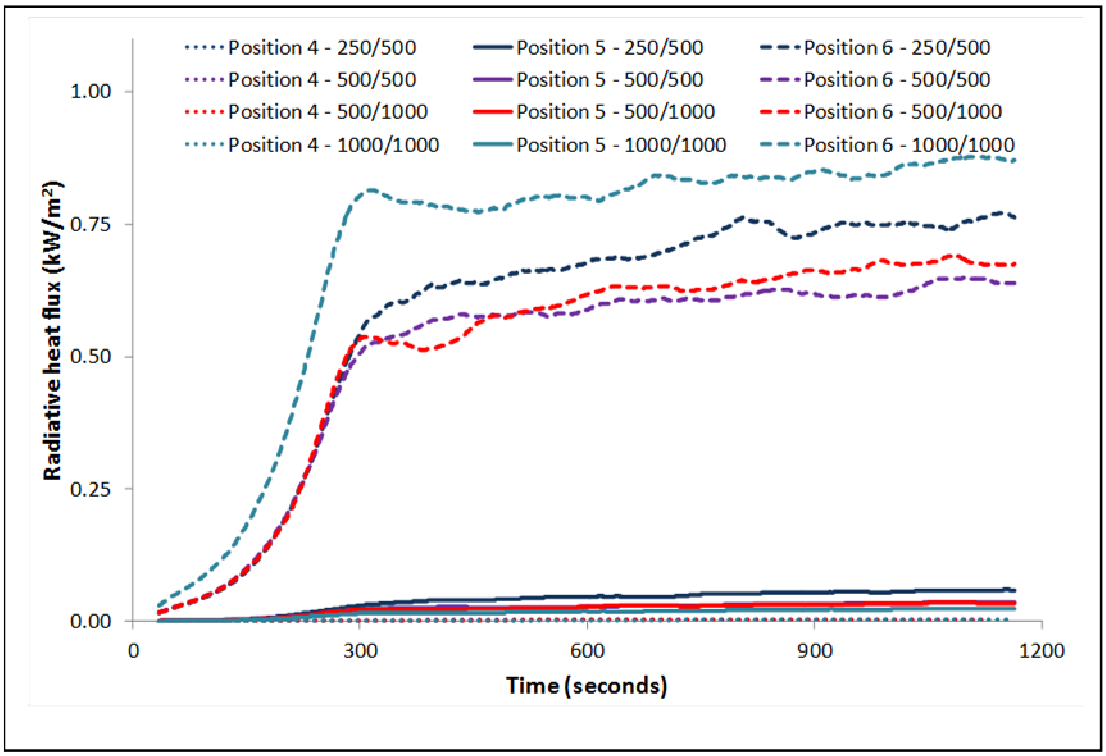

Figure 20: Comparison of smoothed radiative heat flux data from FDS at a height of 1.5 m in positions 4, 5, and 6 with different grid sizes for the fire with rapid t^3 growth in the large warehouse.

From this test of grid size effects, there was no reason to believe that use of a 250 mm grid size for the inner mesh and a 500 mm grid size for the outer mesh would confound results for the small warehouse: this selection implies a $D^*/\delta x$ ratio of 9.3 for the outer meshes and 18.5 for the inner mesh, which is slightly outside that validated by Hill *et al.* (2007). For the large warehouse, a grid size combination of 500 mm/1,000 mm was believed to be the most time-efficient of the four combinations tested, while still producing grid-independent results: here, implied $D^*/\delta x$ ratios are 9.3 and 4.6 for the inner and outer meshes, respectively, both of which are inside the range validated by Hill *et al.* (2007).

2.5.3 Test of domain height above warehouse roof

Similar to grid size effects, the domain size can have an influence on computational results (Xin, 2004; He *et al.*, 2008; Zhang *et al.*, 2010). In particular, the height of the domain above the warehouse was considered to be of importance for this project, in order to account for interactions between the flow field external to the warehouse

vents and the flow inside the warehouse. That is, when hot air flows out of the warehouse, a plume is formed outside each vent. By placing the boundary of the computational domain immediately adjacent to the warehouse, any orifice effect is truncated and pressure distributions immediately outside vents are neglected. The modeller cannot be sure whether or not this truncation has had an effect on the conditions inside the warehouse. By expanding the computational domain beyond the dimensions of the warehouse, these interactions can be taken into account. However, by extending the domain, computational times are also extended. The purpose of this test was to determine how far the domain should be extended for each warehouse, without adding undue processing time.

Using a small compartment, measuring 3 m x 3 m x 3 m, Zhang *et al.* (2010) tested domain extensions of size 0.0 m, 0.5 m, 1.0 m, 2.0 m, and 4.0 m for fire sizes between 62.9 kW and 6 MW. They only tested with vertical vents, but found domain extension to be effective and necessary perpendicular to the vertical vent. Zhang *et al.* (2010) concluded that heat release rate and hydraulic diameter of vertical vent openings could be used to find effective domain extensions. Further, they suggested that it is generally sufficient to extend the computational domain beyond the vertical vent opening by one hydraulic diameter of the vent.

Prior to this, He *et al.* (2008) conducted a parametric study that indicated hydraulic vent diameter could be correlated to required domain extension. After many simulations involving a room of size 4 m x 4 m x 2.5 m with one vertical opening, they concluded that computational domains should be extended by one half the hydraulic diameter of the opening for fuel-controlled cases[3]. He *et al.* (2008) invited further numerical investigation for wider computational domains, more openings and other fire scenarios. Unfortunately, Zhang *et al.* (2010) used just one compartment size in their study. In the case of larger compartments with multiple horizontal openings, there appears to be little guidance on an appropriate domain extension. It is noted that the hydraulic diameter of a single vent in this study is 3.2 m (for the larger *mechanical* vent modelled).

[3] Hydraulic diameter, $D_H = \frac{4A}{P}$, where A is area of the opening and P is perimeter of the opening.

For the present study, it was decided to test the effect on temperature and radiation by adjusting the domain height. For both the small and the large warehouse, the domain height was extended by 1 m, 2 m, 3 m, and 4 m above the warehouse roof. In addition, for the small warehouse, an extension of 2.5m was tested. This extension would allow a more efficient use of the Poisson solver used in the FDS calculation than the 2 m extension (McGrattan *et al.*, 2009). The solver makes use of a Fast Fourier Transform, and as such, multiples of the form $2^l 3^m 5^n$ are best (where l, m, and n are integers).

Figure 21 depicts the fire and smoke layer as they appear in Smokeview for the five simulations in the small warehouse after 1,500 seconds. As the domain height increases, the development of the vent plumes and the flame region outside of the warehouse becomes visually clearer. However, the appearance of the smoke and flame inside the warehouse remains the same regardless of the height of the domain above the warehouse roof.

Temperature distributions at a height of 1.5 m above floor level and 1.0 m below the ceiling are shown in Figure 22. The choice of domain height had only a minimal effect on temperature distributions at both heights in the small warehouse. Temperatures did not increase significantly above the ambient throughout the warehouse in any of the five simulations, except in the immediate vicinity of the fire. Further, there were no substantial differences visible between the five choices of domain height.

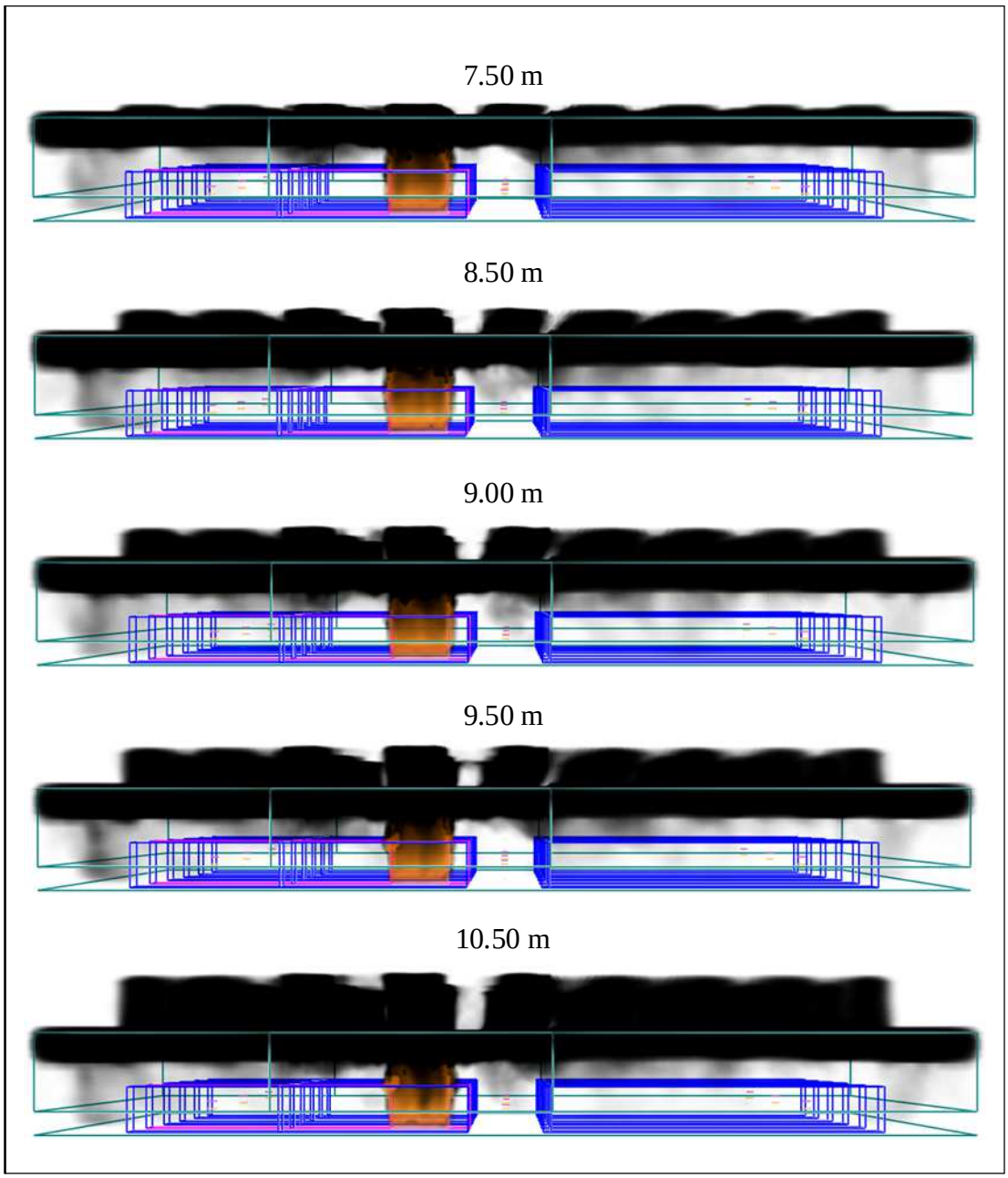

Figure 21: Effect of changing domain height on Smokeview depictions of fire and smoke layer after 1,500 seconds in small warehouse with extreme t^3 fire growth. The warehouse has 15 % roof venting area and matching inlet area for make-up air.

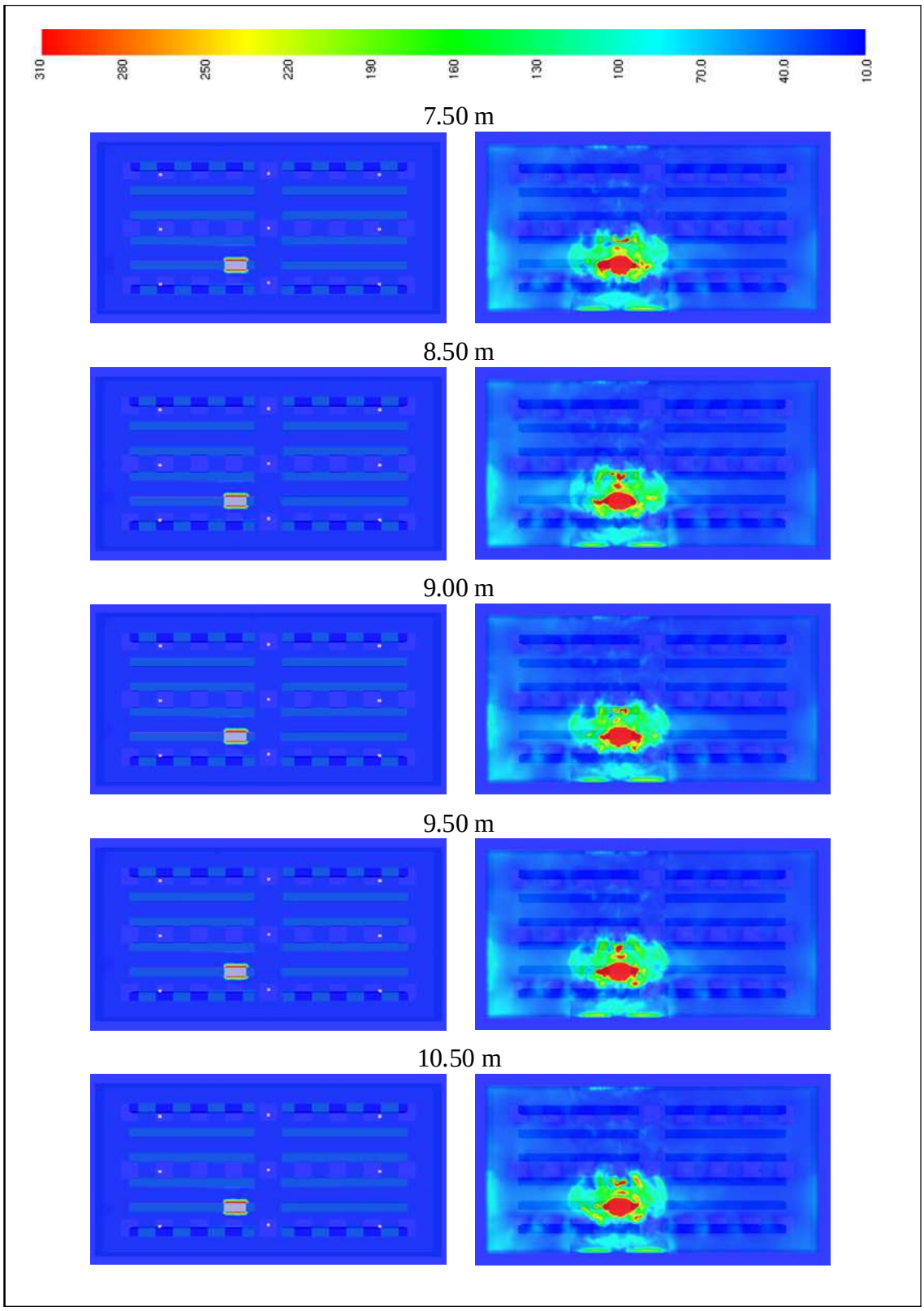

Figure 22: Smokeview depiction of temperature distributions 1.5 m above floor level (left) and 1.0 m below the ceiling (right) after 1,500 seconds in the small warehouse with extreme t^3 fire growth. The warehouses have 15 % roof venting area and different domain heights.

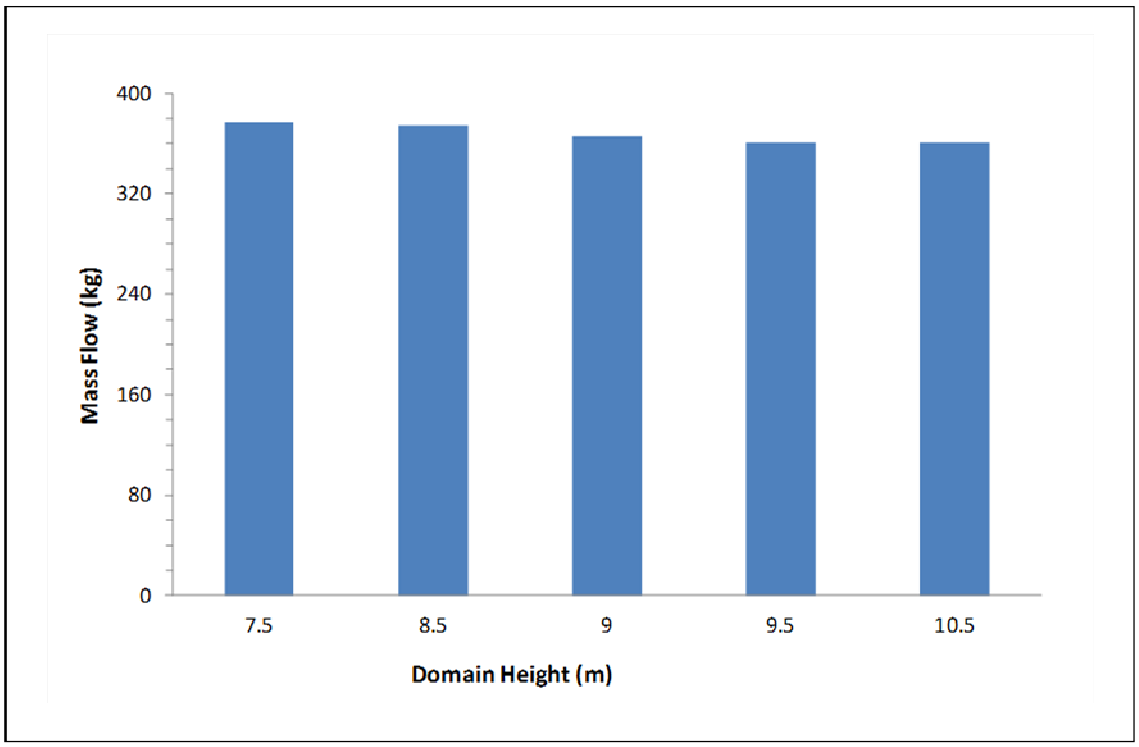

Figure 23: Comparison of total mass flow exiting the warehouse calculated in FDS after 1,500 seconds in the small warehouse with different domain heights.

In Figure 23, total mass flow out from the roof vents is compared for the five different domain heights. For the five simulations, the total mass flow was between 360.8 kg and 377.1 kg, indicating no significant difference in fire behaviour among the simulations. Mass flow into the warehouse was 0 kg in all five simulations.

Figure 24 displays the radiative heat flux measurements for the small warehouse at three representative targets: Positions 3, 5, and 6. There was almost no effect of adjusting the height of the domain on the heat flux at 1.5 m above floor level. At all targets in the small warehouse the curves for the radiative heat flux tracked together for the entire simulation, so that provided the domain was extended by at least 1 m, there was no effect in radiative heat flux inside the warehouse.

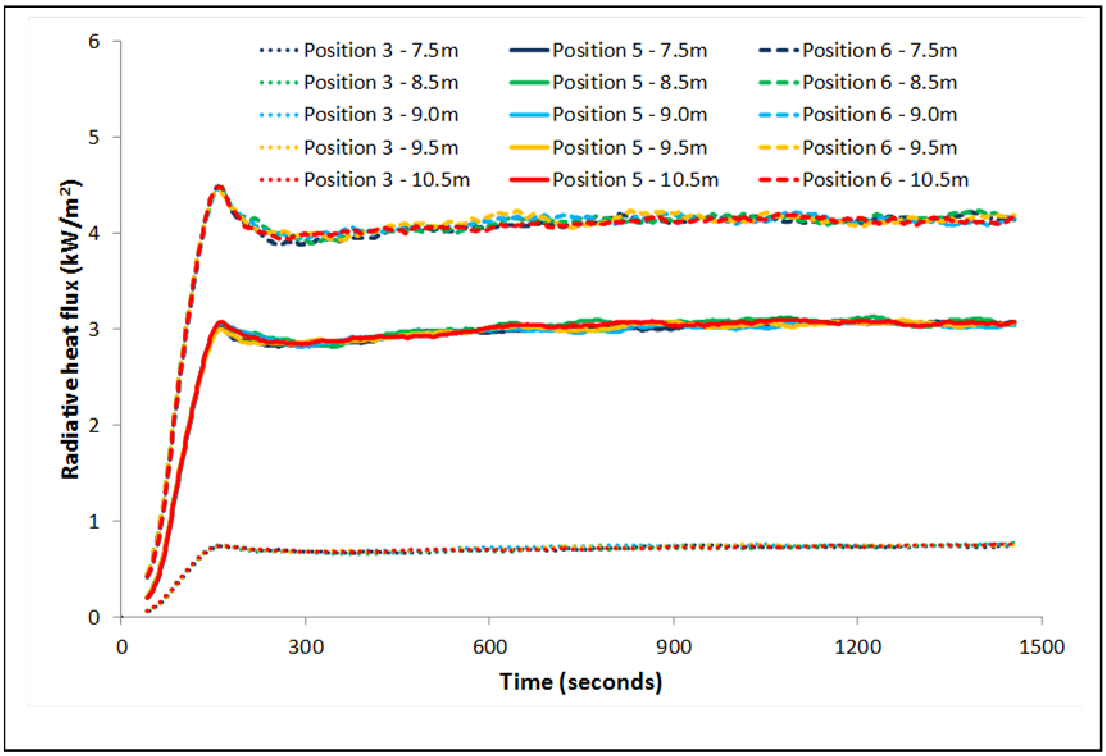

Figure 24: Comparison of smoothed radiative heat flux data from FDS at a height of 1.5 m at Positions 3, 5, and 6 with different domain heights for the small warehouse simulations.

It was decided to use a 9 m domain height (2.5m extension) for the small warehouse, as this would give confidence that there would be no detrimental effect on vent flows or on radiation and temperature conditions inside the warehouse. In addition, it was thought to be a more computationally efficient selection than the 8.5 m domain height due to more efficient use of the Fast Fourier Transform's Poisson solver in FDS.

The fire and smoke layer inside the large warehouse have the same appearance in Smokeview for all four simulations after 1,200 seconds (Figure 25). However, as seen in the small warehouse, development of vent plumes and the flame region outside of the warehouse becomes visually clearer as the domain height is progressively increased. Behaviour of smoke and flame inside the large warehouse remains the same regardless of the height of the domain above the warehouse roof.

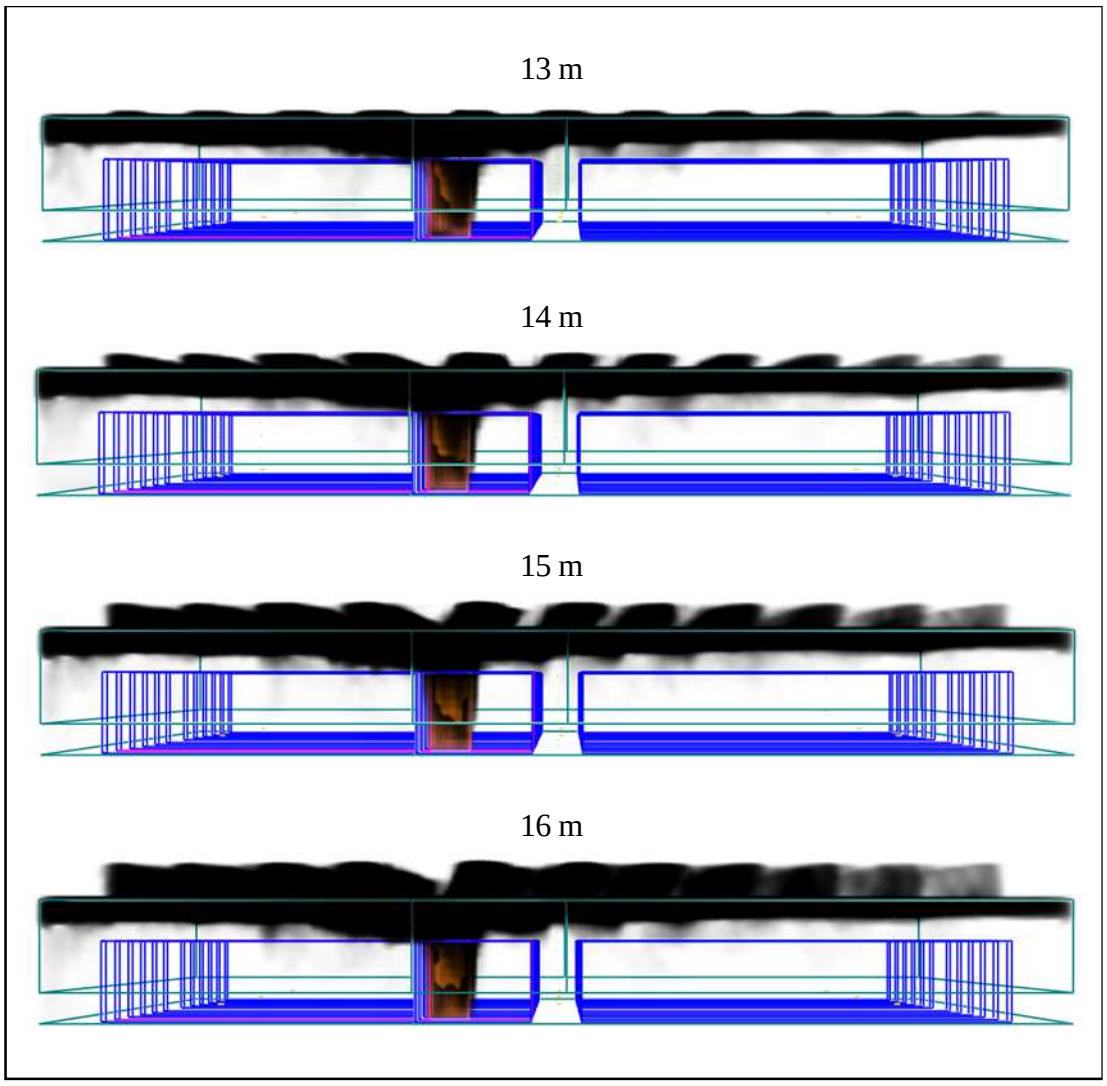

Figure 25: Effect of changing domain height on Smokeview depictions of fire and smoke layer after 1,200 seconds in large warehouse with rapid t^3 fire growth. The warehouse has 15 % roof venting area and matching inlet area for make-up air.

Temperature distributions at a height of 1.5 m above floor level and 1.0 m below the ceiling are shown in Figure 26. The choice of domain height had only a minimal effect on temperature distributions at both heights in the large warehouse. Temperatures did not increase significantly above the ambient throughout the warehouse in any of the four simulations, except in the immediate vicinity of the fire.

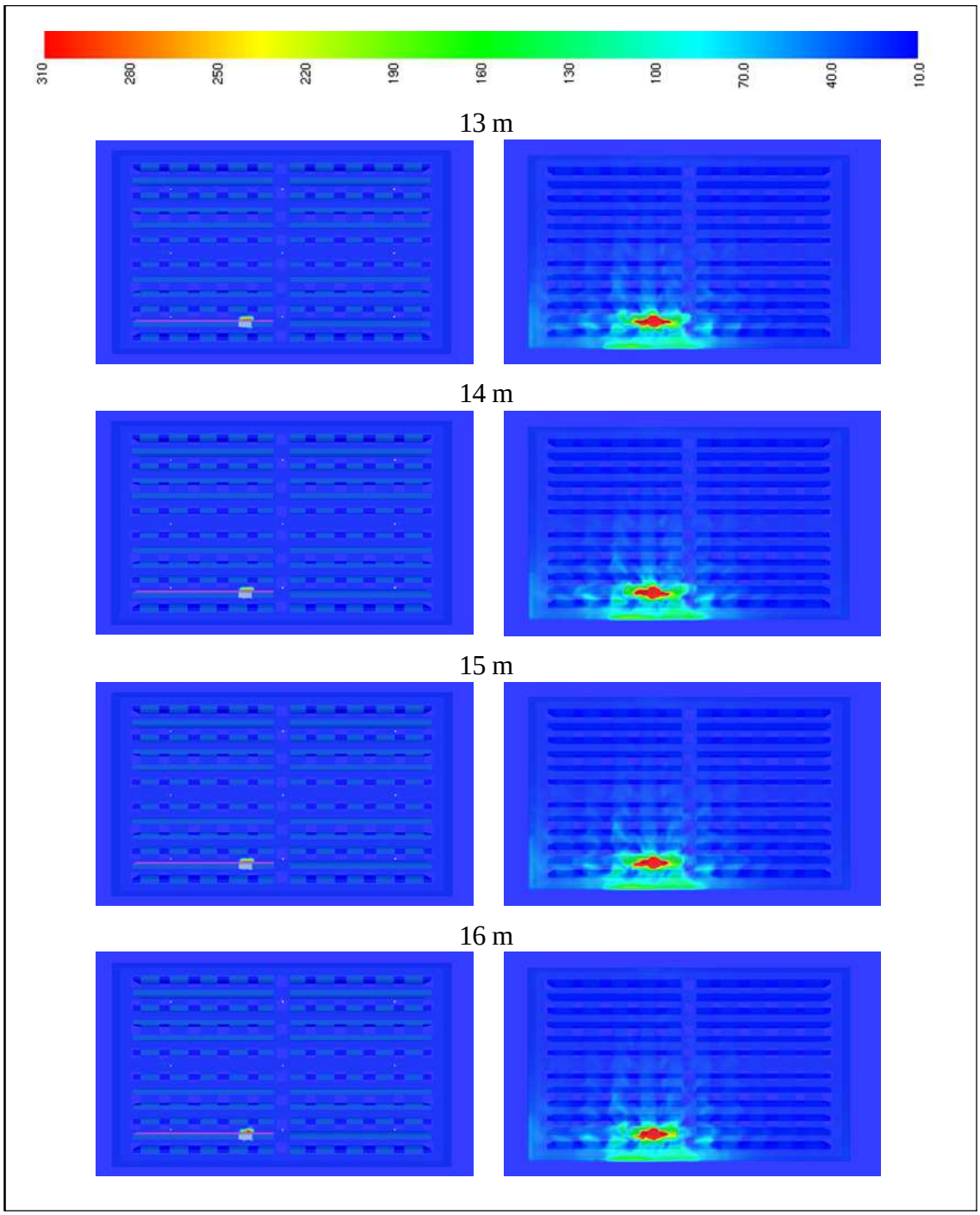

Figure 26: Smokeview depiction of temperature distributions 1.5 m above floor level (left) and 1.0 m below the ceiling (right) after 1,200 seconds in the large warehouse with rapid t^3 fire growth. The warehouses have 15 % roof venting area and different domain heights.

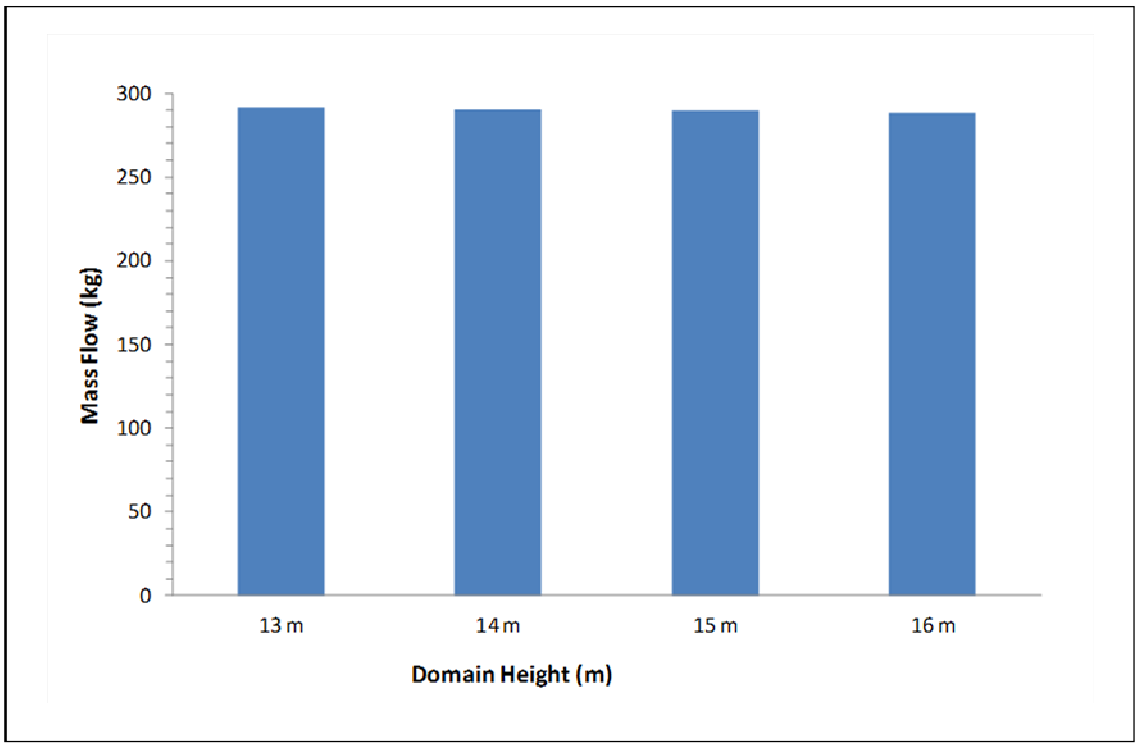

Figure 27: Comparison of total mass flow exiting the warehouse calculated in FDS after 1,200 seconds in the large warehouse with different domain heights.

In Figure 27, total mass flow out from the roof vents is compared for the four different domain heights. For the four simulations, the total mass flow was between 288.8 kg and 291.5 kg, indicating no significant difference in fire behaviour among the simulations. Mass flow into the warehouse was 0 kg in all four simulations.

As seen in Figure 28, altering domain height had minimal effect on radiative heat flux measurements: the measurement curves in the figure track very closely to each other for the entirety of the simulations.

Any of the four domain extensions are acceptable for grid-independent modelling in this project. However, it was decided to use a 15 m domain height (3 m extension) for the simulations involving the large warehouse, as this would provide more computational efficiency for the Fast Fourier Transform (used in the Poisson solver of FDS) than the 13 m and 14 m domain heights.

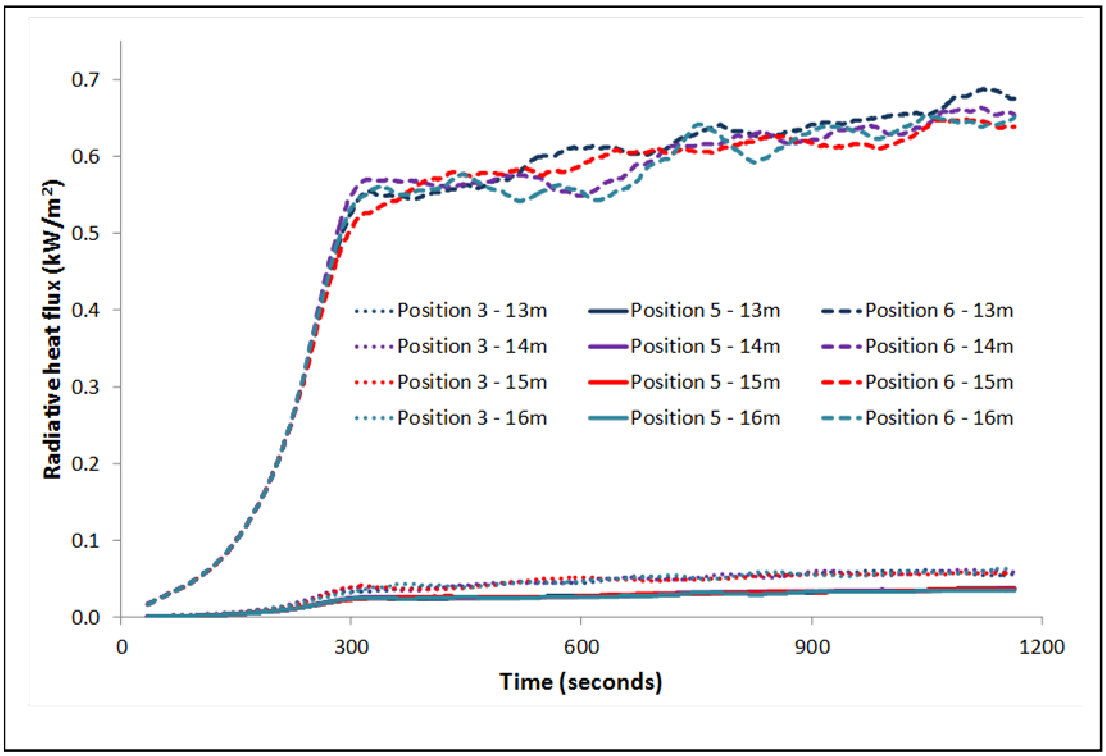

Figure 28: Comparison of smoothed radiative heat flux data from FDS at a height of 1.5 m at Positions 3, 5, and 6 with different domain heights for the large warehouse simulations.

There is little guidance in the literature for appropriate domain extensions for buildings with dimensions of the magnitudes represented by the two warehouse geometries in this study (He *et al.*, 2008; Zhang *et al.*, 2010). However, with a largest hydraulic diameter of 3.2 m for the square-shaped vents in this project, a domain extension of 1.6 m is implied by the work of He *et al.* (2008) for a fuel-controlled fire: the 2.5 m domain extension in the small warehouse and the 3 m extension in the large warehouse both well-exceed this suggested margin.

Similar calculations for the use of strip-venting or for the make-up air inlets were not performed, due to the limited dimensions tested in recent grid-independence studies (He *et al.*, 2008; Zhang *et al.*, 2010). The dimensions of the strip vents and the make-up air vents used in this study were considerably larger than any of the openings considered in the literature, and therefore domain extensions of at least a similar magnitude to those used above the square-shaped vents were used for make-up air inlets on the sides of the warehouse, as well above the warehouse in the strip-venting simulations (see Section 2.5.5).

2.5.4 Test with no vents

Two simulations were carried out for the small warehouse and two simulations for the large warehouse to illustrate the effect of not having roof venting. The first simulation for each warehouse was fully enclosed, that is, no inlet air was provided other than the aforementioned leakage area. And for the second simulation for each warehouse, area for inlet air equal to 15 % of the floor area was provided. These simulations produced some interesting phenomena, particularly for the small warehouse.

In Figure 29, the heat release rate recorded in the small warehouse is presented. The heat release rate is seen to oscillate dramatically either side of the target heat release rate of 50 MW. The oscillations are particularly pronounced for the fully-enclosed warehouse, and less so for the warehouse with inlet air provided. These results are not realistic. However, it can be concluded that beyond 300 seconds the conditions inside the warehouse are very unstable, and fire-fighter entry would not occur in such a situation.

These oscillations are an effect of the gas-phase combustion modelling in FDS and can be further visualised with the aid of Smokeview (Figure 30). For the first 180 seconds, the fire grows at a steady rate, to the targeted 50 MW. From this point on, there is a short period of steady heat release of 50 MW. However, as the time approaches 330 seconds, the fire reduces in size. Between this point and 380 seconds the Smokeview representation of the flame appears to *wander* and the fire size substantially increases. At 420 seconds, the flame returns to a fire size of around 20 MW, from which point the pattern repeats at approximately 120 seconds intervals. A similar pattern is seen in the case where the small warehouse was provided with inlet air, although the amplitude is much lower than in the fully-enclosed case.

Wang (2009) also observed such oscillations in a numerical study of a medium-scale ventilation-limited enclosure. He suggested the *pulsating flame* and *wandering flame* phenomena were due to the entrainment and consumption of the oxidiser. In the simulations conducted here, the anomaly is due to the availability of oxidiser and fuel at different locations at different points in time: if both oxidiser and fuel are present in sufficient quantities in FDS, they will mix and burn.

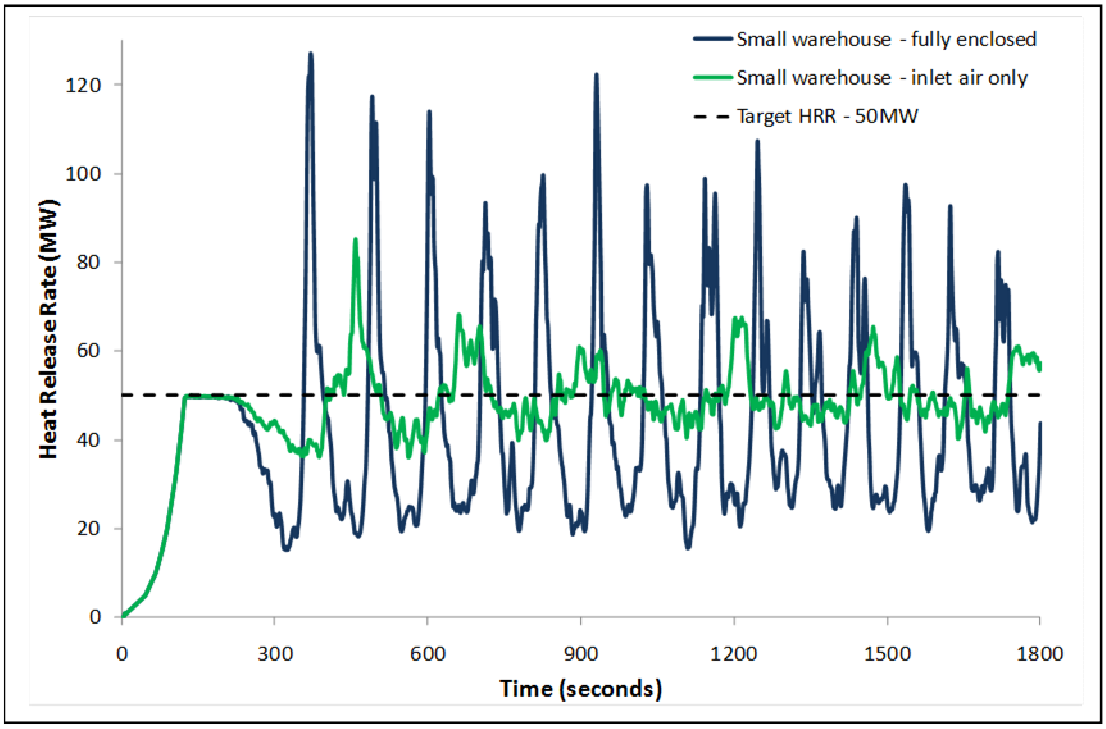

Figure 29: Comparison of heat release rate from FDS with no roof venting in the small warehouse, when it is fully-enclosed versus when it is provided with area for inlet air equal to 15 % of roof area.

The heat release rate recorded in the large warehouse is presented in Figure 31. In this case, where there was significantly more oxygen available, the fire size was seen to be steady at 50 MW for the first 1,000 seconds. At this point, the conditions inside the warehouse became unstable. As with the small warehouse, the behaviour of the fire is unrealistic: it is an artefact of the gas-phase combustion modelling in FDS.

The instabilities in both the large and small warehouse point to the need for effective roof venting in unsprinklered single-storey buildings, if only to make the fire environment more predictable.

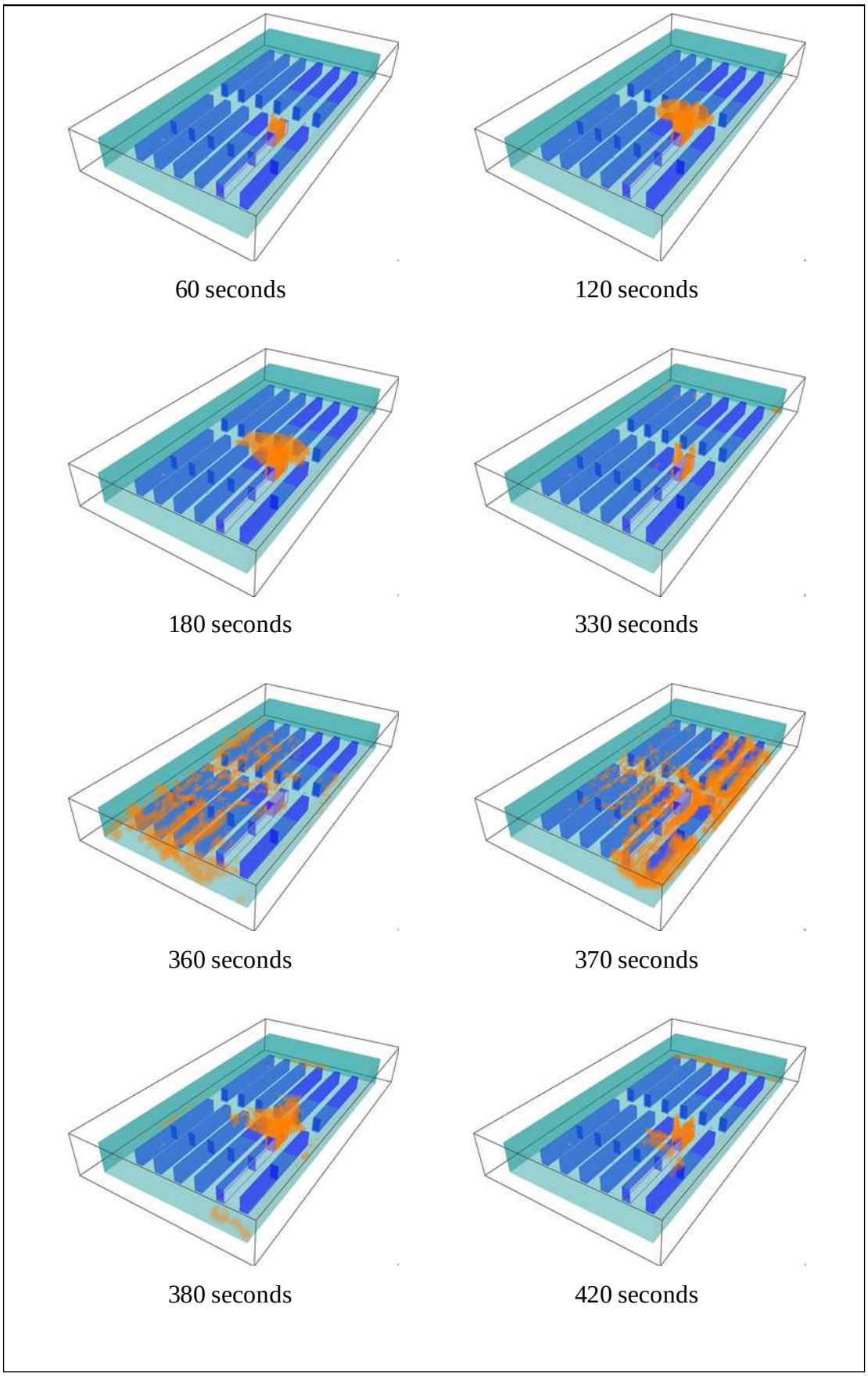

Figure 30: Smokeview representation of a gas-phase combustion modelling anomaly in FDS: if the fuel and oxidiser can mix, they will burn.

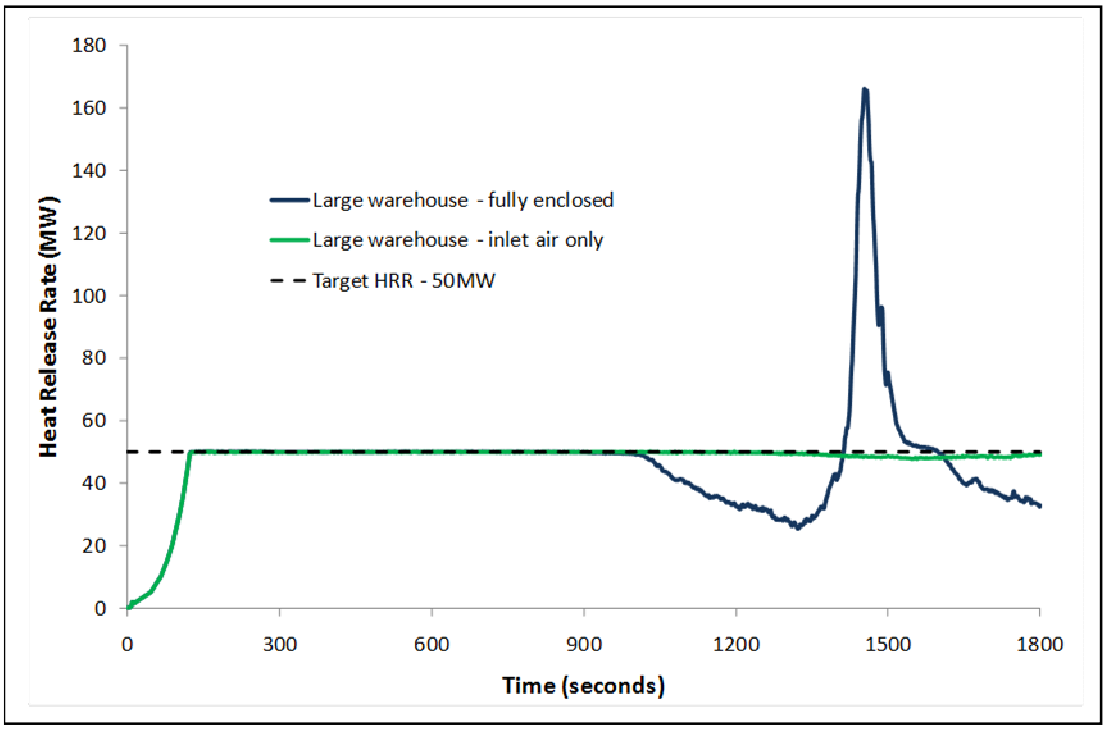

Figure 31: Comparison of heat release rate from FDS with no roof venting in the large warehouse, when it fully-enclosed versus when it is provided with area for inlet air equal to 15 % of roof area.

2.5.5 Summary of preliminary testing

A summary of the results of the preliminary testing are laid out in Table 2. These variables were held constant and applied to all following simulations.

Table 2 – Summary of preliminary testing results applied to following simulations.

Variable	Small Warehouse	Large Warehouse
Warehouse dimensions	60 m x 30 m x 6.5 m	100 m x 60 m x 12 m
Domain dimensions	66 m x 36 m x 9 m	120 m x 72 m x 15 m
Grid size – inner mesh	250 mm	500 mm
Grid size – outer mesh	500 mm	1,000 mm
Wall material	Adiabatic	Adiabatic

2.6 Matrices of modelling phases

It was decided to model the problem in three phases to reflect the three objectives of the project. The first phase investigated appropriate area of roof venting and make-up air required to provide or maintain fire-fighter tenability (Table 3). The second phase modelled the effectiveness of venting if the appropriate roof venting area is opened simultaneously versus sequentially (Table 4). Finally, use of downstands was investigated (Table 5).

In the first phase of testing, vents were open for the entirety of the simulation. The vent areas simulated corresponded to the current 15 % recommended in the NZBC Compliance Document, as well as two smaller vent areas of 10 % and 5 %. No vent area larger than 15 % was chosen, as requirements in other countries tend to be significantly smaller than the requirement in New Zealand. To achieve 15 % roof venting, twenty-seven evenly-spaced vents (in the small warehouse) of dimension 3.2 m x 3.2 m were installed as three rows of nine vents (Figure 32). Vent positions were maintained for 10 % and 5 % roof venting area, however, vent dimensions were reduced to 2.6 m x 2.6 m and 1.9 m x 1.9 m, respectively. In the large warehouse, eight rows of 11 vents were installed (Figure 33), with the same vent dimensions as for the small warehouse.

Inlet areas were chosen to be percentages of vent areas in order to cover a range of possible realistic situations. More specifically, a warehouse that relies on entrances to the warehouse to provide make-up air may not have any inlet areas during hours of non-operation (*i.e.* during the night), hence the selection of 0 % of vent area as inlet area. A warehouse that uses entrances to provide part of the make-up air may have permanent vents still in operation during evenings or cold days, although entrances are likely to be closed (hence selection of 50 % of vent area as inlet area). Finally, a warehouse is quite likely to have been designed to have inlet area equal to venting area (hence selection of 100 % of vent area as inlet area).

Table 3 – Phase one of modelling: tests of required vent and inlet area.

		Vent area (% of floor area)		
		15%	10%	5%
Inlet area (% of vent area)	100%	✓	✓	✓
	50%	✓	✓	✓
	0%	✓	✓	✓

Table 4 – Phase two of modelling: tests of simultaneous opening versus sequential opening.

		Vent opening temperature		
		100°C	200°C	300°C
Opening progression and shape	Simultaneous, squares	✓		
	Sequential, squares	✓	✓	✓
	Sequential, strips		✓	✓

Table 5 – Phase three of modelling: tests of the use of downstands.

		Downstand depth (% of roof height)		
		10%	20%	30%
Opening progression, shape, and opening temperature	Simultaneous, squares, 100°C	✓	✓	✓
	Sequential, squares, 100°C	✓	✓	✓
	Sequential, squares, 300°C	✓	✓	✓
	Sequential, strips, 300°C	✓	✓	✓

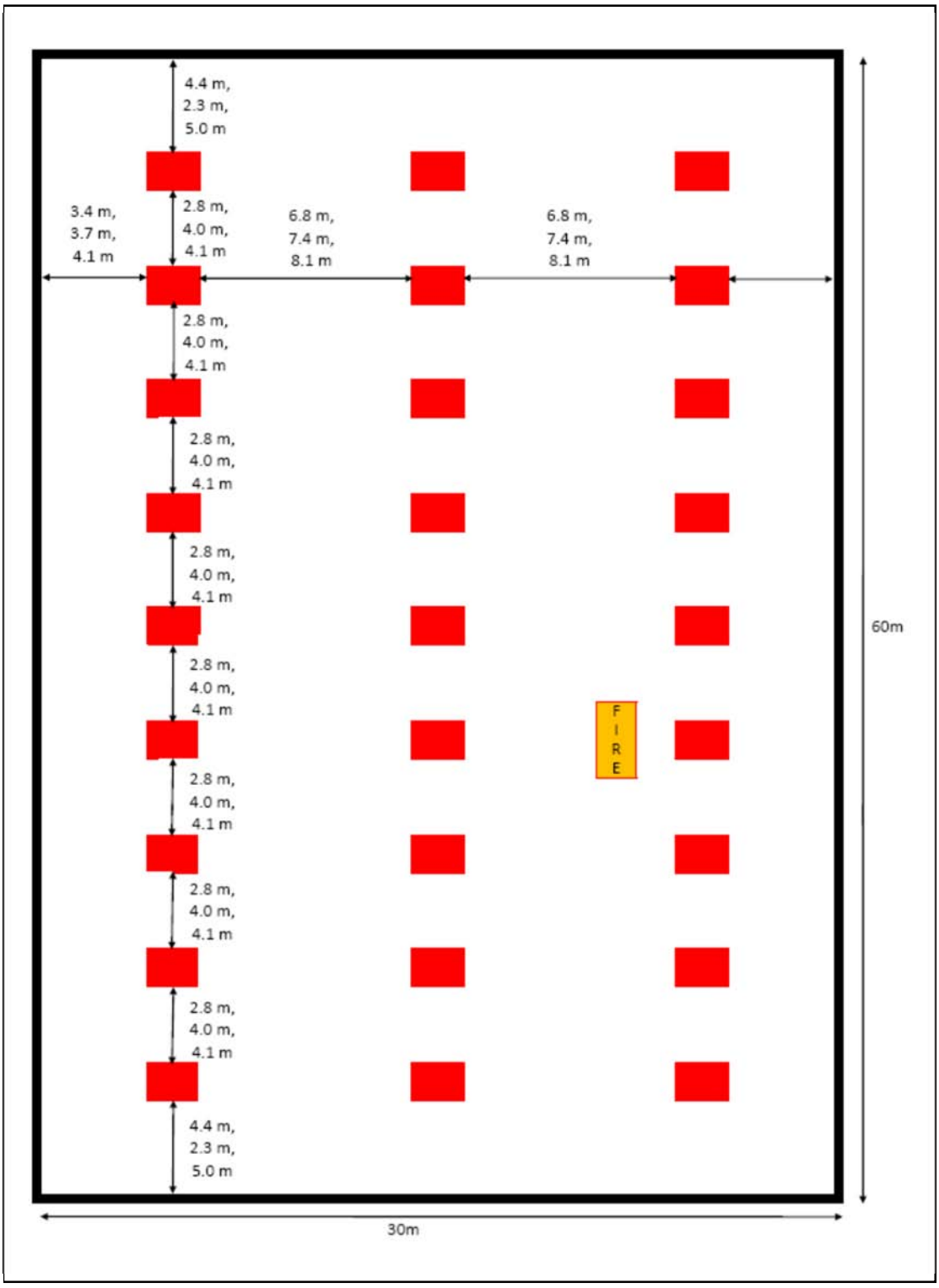

Figure 32: Plan view of warehouse showing position of square-shaped vents in the small warehouse. Measurements are for 15 % venting, 10 % venting, and 5 % venting.

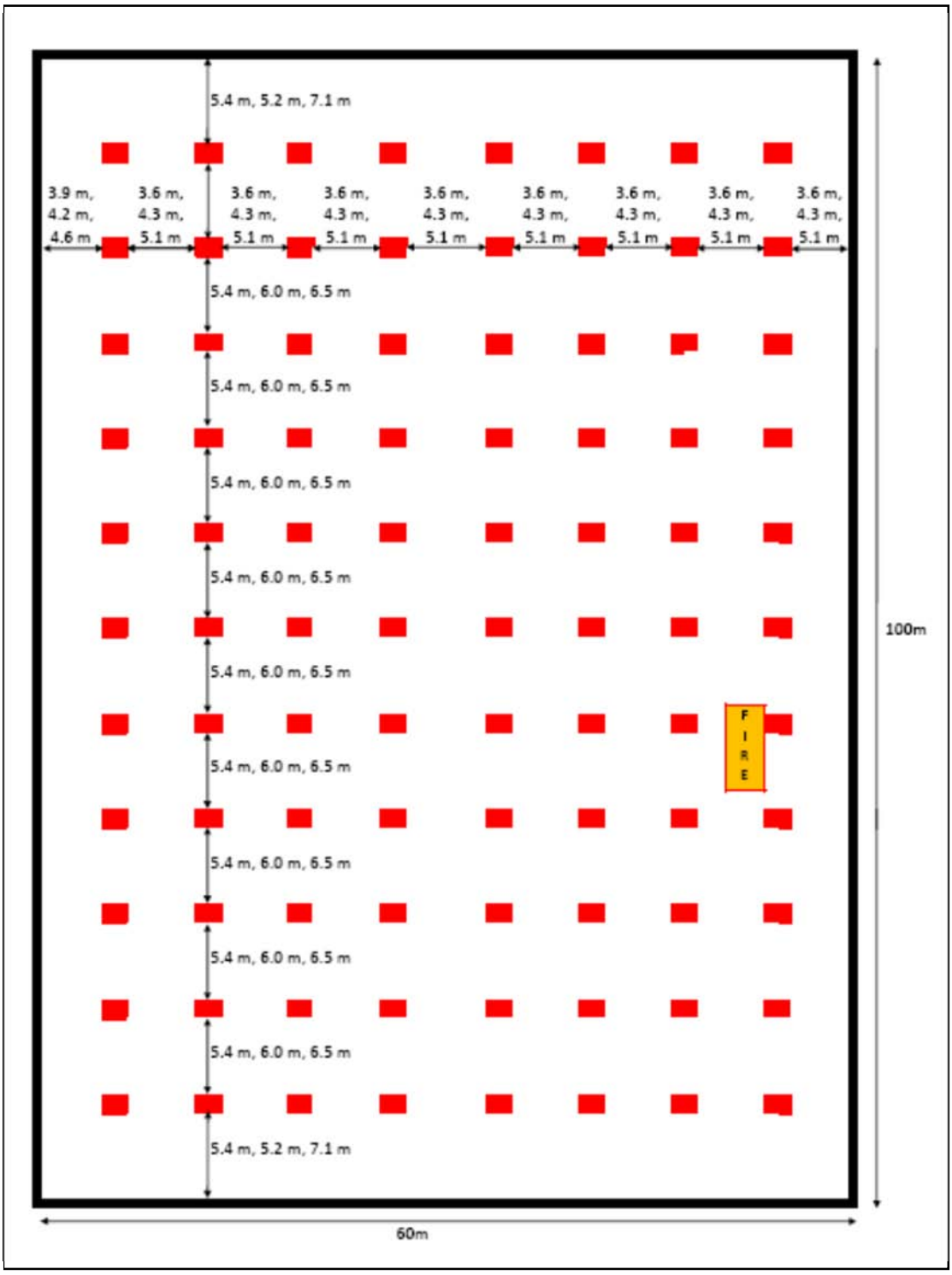

Figure 33: Plan view of warehouse showing position of square-shaped vents in the large warehouse. Measurements are for 15 % venting, 10 % venting, and 5 % venting.

Rapid and extreme t^3 growth phases (Equations 1 and 2, respectively) were applied to each vent area-inlet area combination. The fire in both cases peaked at 50 MW, where the heat release rate remained for the remainder of the simulations. Each vent area-inlet area combination and each fire growth rate were run in both in the small and the large warehouse. This gave a total of 36 simulations (two building sizes x two fire growth rates x nine vent area-inlet area combinations) in modelling phase one.

After analysis of phase one results, a roof venting area (and associated inlet area) was selected and applied in the second phase: the selected area was required to meet the FBIM routine criterion, whilst simultaneously minimising roof venting area (see Section 3.2). In addition, it was desired that an apparent layer of clear air was maintained in the Smokeview depiction of the warehouse. Vents were then modelled as being closed at the beginning of the simulation and were opened according to warehouse conditions.

Temperatures for vent opening were chosen based on consultation with a number of local suppliers of roof venting products. Specifically designed fire vents are available in New Zealand where panel fixings are expected to melt, with the panel dropping out at 104°C. A similar product is available that is activated with a thermal release mechanism at 93°C (or 68°C). Therefore, it was decided to model mechanical vents as operating at 100°C, as either simultaneously opening vents (*i.e.* all opened after activation of the first vent), or sequentially opening vents (*i.e.* a vent only opened when temperature at that particular vent reached 100°C). All vents were of dimension 2.6 m x 2.6 m. No attempt was made to account for the effect of the open position of the vent. A vent opening was simply modelled as a hole appearing in the roof.

Modelling of plastic skylights was based on the thermal properties of polycarbonate. Polycarbonate has a melting temperature between 280-320°C (Harper, 2006, Table 1.7). It was not thought necessary to model higher than 300°C due to the FBIM fire-fighter tenability criteria describing upper layer temperatures exceeding 280°C as critical conditions. Consequently, vents modelled as plastic skylights were opened at 200°C and 300°C. These vents were only opened as sequential vents. However, the vent arrangements included longer strips of width 0.80 m (Figure 34), representative of such skylight arrangements that are common in industrial warehouses, as well as

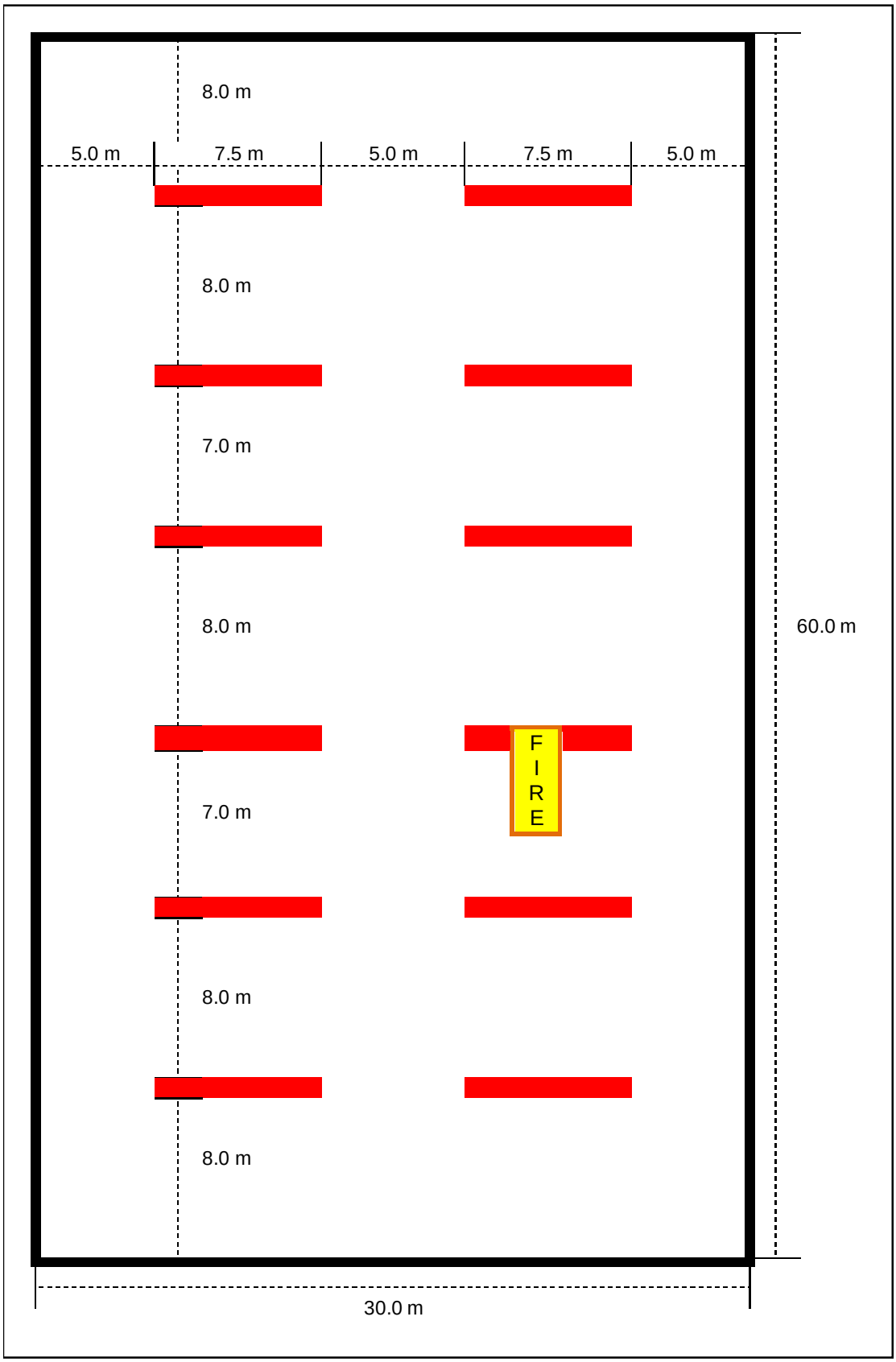

Figure 34: Plan view of small warehouse showing position of strip-shaped vents.

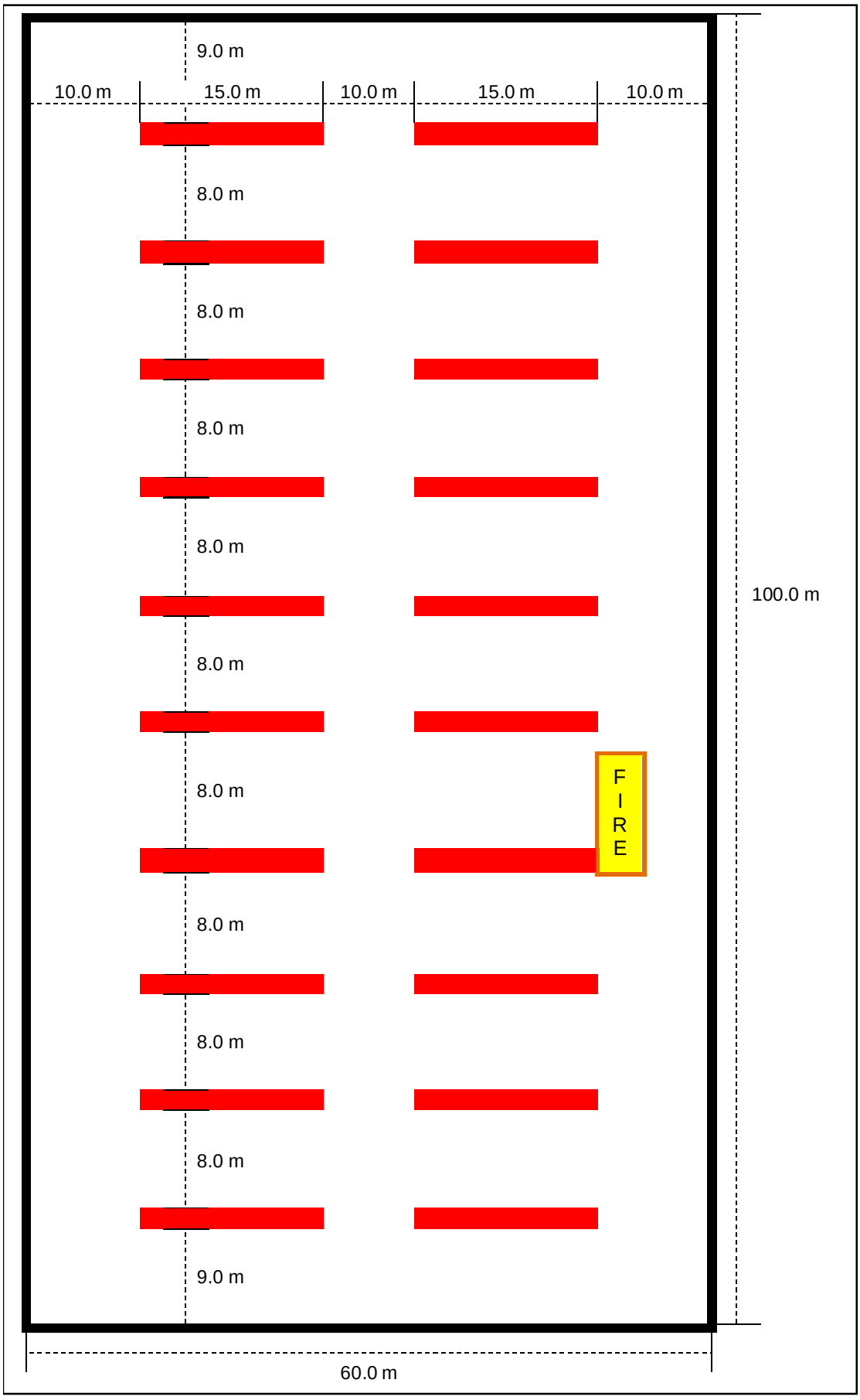

Figure 35: Plan view of large warehouse showing position of strip-shaped vents.

the individual square-shaped vents with dimensions based on those dimensions used for the mechanical vents. In the small warehouse, twelve strips vents were employed with sufficient length to achieve the required roof venting area. In the large warehouse, twenty strip vents were employed to achieve the same roof venting area (Figure 35). Again, no attempt was made to account for any part of the skylight that remained in a hanging or erect position after opening. The vent opening was simply modelled as a hole appearing in the roof, and in the case of the strip venting, each vent divided into 2-metre sections that opened as the "activation temperature" was achieved, in an effort to represent the melting of such vents.

The second phase of testing totalled 24 simulations, consisting of two building sizes, two fire growth rates, and six opening shape-progression and opening (or activation) temperature combinations.

For the final phase of modelling, downstand depths of 10 %, 20 %, and 30 % of the distance between the floor and the ceiling were tested (based on recommended 20 % in Edwards *et al.*, 2007). All downstand depths were simulated for four of the six opening shape-progression combinations from Phase 2, for both warehouse sizes and both fire growth rates, giving a total of 48 simulations.

Clause 6.22.9 of the Compliance Document for the NZBC specifies smoke reservoir restrictions in area and maximum dimension for *limited area atrium firecells* of 1,000 m² and 60 m, respectively. However, there does not appear to be guidance for downstand spacing for other types of building. For guidance in these cases, the practitioner might turn to the Australian Standard for Smoke/heat venting systems (AS 2665, 2001) or the National Fire Protection Association (NFPA) Standard for Smoke and Heat Venting (NFPA 204, 2012).

The Australian standard requires that the horizontal area of smoke reservoirs does not exceed 1,500 m² (AS 2665, 2001; clause 2.3.1). The clause also specifies that for areas of abnormal fire hazard that the horizontal distance between parallel smoke curtains is not to exceed 30 m. According to Appendix B of the standard, warehouses of the type studied here could often be classified as areas of abnormal hazard.

Application of the Australian standard would require that the small warehouse simulated here contained just one downstand dividing the warehouse into two 900 m² smoke reservoirs. For the large warehouse, three downstands dividing the 100 m side into four 1,500 m² smoke reservoirs would meet the requirements.

The NFPA standard requires for the 10 % and 20 % downstand depths that neither the length nor the width of the smoke reservoirs exceed the ceiling height (NFPA 204, 2012; clause 7.4.2). For the small warehouse, it would be required to have a distance no greater than 6.5 m between downstands in both the *x-direction* and *y-direction*. For the simulations in this study, a minimum of three downstands would be needed to divide the 30 m side into reservoirs, and nine downstands for the 60 m side. For the large warehouse, this distance would increase to 12 m (due to the higher ceiling height), meaning four downstands along the 60 m side and eight downstands for the 100 m side.

For the 30 % downstand depth, the distance between downstands can be eight-times greater (NFPA 204, 2012; clause 7.4.1): 52 m for the small warehouse and 96 m for the large warehouse. Both of these cases would require just one downstand dividing the warehouse ceiling space in the middle.

It was decided to apply the more stringent of the two standards in determining downstand spacing. Therefore, NFPA 204 was used, with the exception that the increased distance between downstands allowed for the 30 % depth simulations, was not taken advantage of. That is, in the 30 % downstand depth simulations, as in the 10 % and 20 % downstand depth simulations, the spacing between downstands was a maximum of one ceiling height. This decision was made to allow ease of comparison between all simulations. The layouts of the downstands for the small and large warehouses are shown in Figure 36 and Figure 37, respectively.

A roof venting area was selected from the Phase One results, and applied to the third phase (see Section 3.3). It was not considered necessary for this roof venting area to have met the FBIM criteria: in fact for routine conditions, the usefulness of downstands would be evident if a previously untenable situation could be made to meet the FBIM criteria for routine conditions.

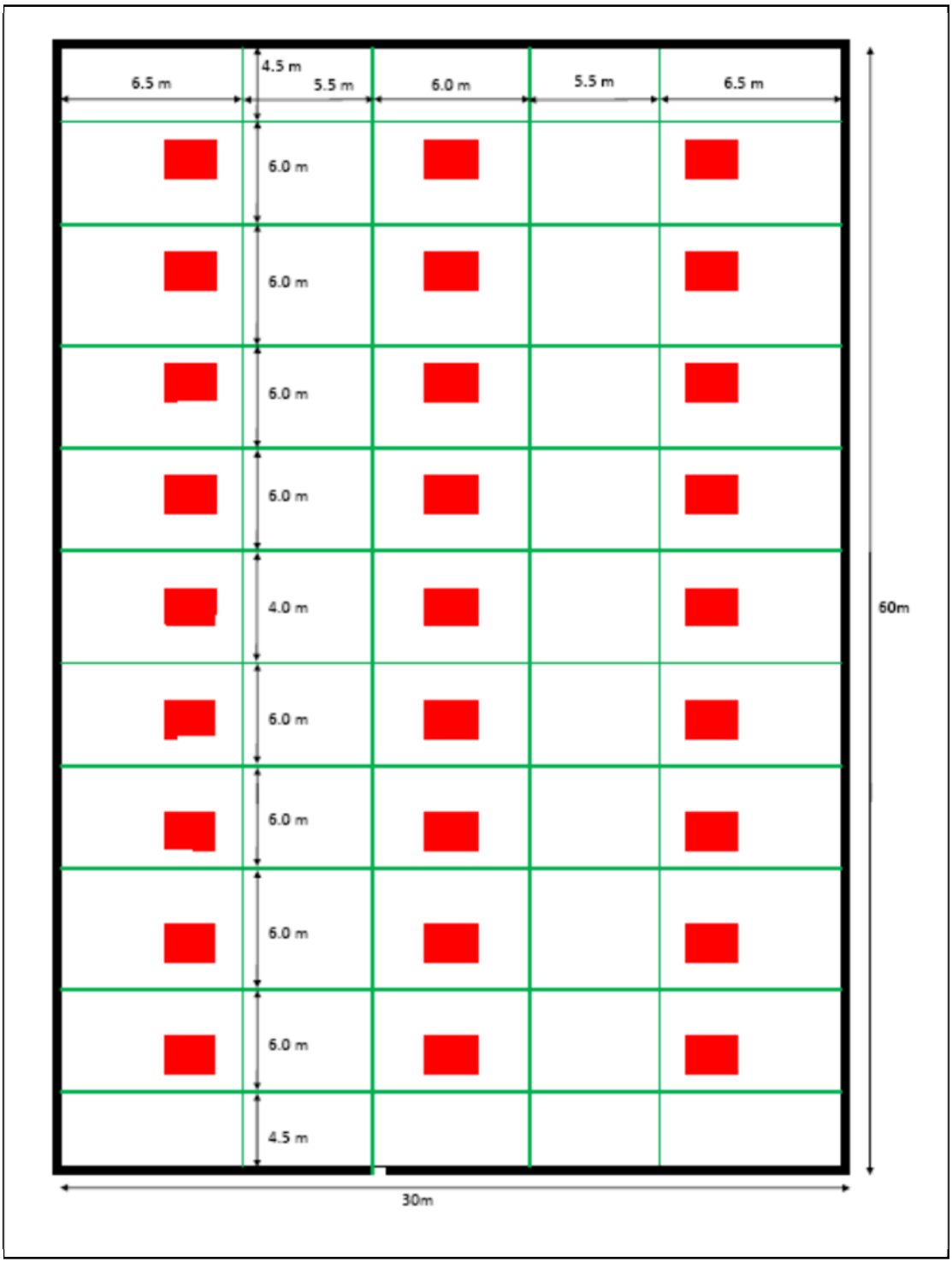

Figure 36: Plan view of small warehouse showing position of downstands.

It should be noted that for all simulations, the areas of roof venting and inlets are nominal values. Due to computing limitations inherent in a grid-based simulation as in FDS, obstacles and holes will be resized to fit the nearest grid cell size. Nominal

dimensions are used synonymously in this report with actual dimensions used by FDS for items such as vent and inlets areas.

Figure 37: Plan view of large warehouse showing position of downstands.

3. RESULTS

3.1 Phase One: Required vent and inlet areas

3.1.1 Phases 1a & 1b: Simulations in the small warehouse

Presented in Table 6 are the summary results from the first phase of testing in the small warehouse concerning the area of roof venting and make-up air inlets required to fulfil the FBIM criteria. With the base case of 15 % roof venting area and a matching area of inlets for make-up air (*i.e.* 100 % of roof venting area), maximum radiative heat fluxes near the fire (*i.e.* at Positions 5 and 6) 1.5 m above floor level were worse than extreme, reaching a peak value of 4.6 kW/m². In contrast, radiative heat fluxes on the outer edges of the warehouse remained within the Routine Conditions criterion of the FBIM, with a peak of 0.8 kW/m² recorded. Temperatures at 1.5 m above floor level also remained routine, both near the fire and away from the fire, where peak temperatures of 16.1°C and 14.7°C were recorded, respectively.

Reducing the area of inlets for make-up air resulted in less radiation reaching the targets at all positions in the warehouse with rapid t^3 fire growth. The highest radiative heat flux value recorded near the fire was 4.4 kW/m² with an inlet area for make-up air of 50 % of the roof venting area and just 2.2 kW/m² with an inlet area of 0 % of roof venting area: the former heat flux value is considered worse than extreme, and the latter value is well-inside the Hazardous Conditions criterion. Radiative heat fluxes recorded away from the fire also reduced as the inlet area was restricted, with maximums of 0.8 kW/m² with 50 % inlet area and 0.5 kW/m² with 0 % inlet area.

In contrast, the reduction in inlet area led to increased temperatures both near and away from the fire. With 50 % inlet area, temperatures rose to a maximum of 16.8°C near the fire and 16.0°C away from the fire. With 0 % inlet area, maximum temperatures were 47.0°C near the fire, and 45.9°C away from the fire. However, in all cases with 15 % roof venting area, temperatures at 1.5 m above floor level were considered routine.

As roof venting area was reduced to 10 % of the warehouse floor area, radiative heat

Table 6 – Summary of maximum results for Phase 1 simulations in small warehouse.

Fire growth	Vent area (% of floor area)	Inlet area (% of vent area)	Radiation near fire[1] (kW/m^2 - Criterion)	Radiation away from fire (kW/m^2 - Criterion)	Temperature near fire[1] (°C - Criterion)	Temperature away from fire (°C - Criterion)
Rapid	15 %	100 %	4.6 - Extreme$^+$	0.8 - Routine	16.1 - Routine	14.7 - Routine
Rapid	15 %	50 %	4.4 - Extreme$^+$	0.8 - Routine	16.8 - Routine	16.0 - Routine
Rapid	15 %	0 %	2.2 - Hazardous	0.5 - Routine	47.0 - Routine	45.9 - Routine
Rapid	10 %	100 %	4.9 - Extreme$^+$	0.8 - Routine	17.3 - Routine	15.6 - Routine
Rapid	10 %	50 %	4.9 - Extreme$^+$	0.8 - Routine	20.3 - Routine	18.2 - Routine
Rapid	10 %	0 %	2.2 - Hazardous	0.5 - Routine	62.0 - Routine	57.7 - Routine
Rapid	5 %	100 %	5.0 - Extreme$^+$	0.9 - Routine	19.0 - Routine	19.1 - Routine
Rapid	5 %	50 %	4.8 - Extreme$^+$	0.9 - Routine	20.1 - Routine	19.3 - Routine
Rapid	5 %	0 %	1.6 - Hazardous	0.6 - Routine	111.4 - Hazardous	117.8 - Hazardous
Extreme	15 %	100 %	4.7 - Extreme$^+$	0.8 - Routine	16.7 - Routine	14.7 - Routine
Extreme	15 %	50 %	4.5 - Extreme$^+$	0.8 - Routine	17.0 - Routine	16.2 - Routine
Extreme	15 %	0 %	2.7 - Hazardous	0.6 - Routine	47.5 - Routine	46.6 - Routine
Extreme	10 %	100 %	4.9 - Extreme$^+$	0.9 - Routine	17.7 - Routine	15.8 - Routine
Extreme	10 %	50 %	4.9 - Extreme$^+$	0.8 - Routine	19.7 - Routine	18.7 - Routine
Extreme	10 %	0 %	2.9 - Hazardous	0.6 - Routine	61.4 - Routine	56.2 - Routine
Extreme	5 %	100 %	5.0 - Extreme$^+$	0.9 - Routine	19.1 - Routine	19.3 - Routine
Extreme	5 %	50 %	5.1 - Extreme$^+$	0.9 - Routine	20.2 - Routine	19.4 - Routine
Extreme	5 %	0 %	2.2 - Hazardous	0.7 - Routine	112.6 - Hazardous	115.9 - Hazardous

[1] Indicates Positions 5 and 6 only.

[+] Indicates that conditions exceeded the extreme criterion, but were not severe enough to be classed as critical.

fluxes remained very similar to the case with 15 % roof venting, with conditions exceeding the Extreme Conditions criterion close to the fire for inlet area of 100 % and 50 % of roof venting area, being hazardous close to the fire for the case of 0 % inlet area, and remaining routine at positions away from the fire under all three inlet area scenarios. Further reduction of roof venting area to 5 % produced similar values of radiative heat flux where inlet air was present, and lower values when not present.

The effect on temperature of reduced roof venting area was pronounced. Each reduction in roof venting area resulted in increases in temperature at a height of 1.5 m. With 10 % roof venting area, temperatures near the fire increased to 17.3°C for the 100 % inlet area case, 20.3°C with 50 % inlet area, and 62.0°C with 0 % inlet area. With 5 % roof venting area, the corresponding temperatures increased to 19.0°C, 20.1°C, and 111.4°C. Similarly, temperatures away from the fire increased to 15.6°C, 18.2°C, and 57.7°C for the three inlet areas in combination with 10 % roof venting, and increased further to 19.1°C, 19.3°C, and 117.8°C for the three scenarios with 5 % roof venting. These results indicate a trend for the atmosphere inside warehouse to become substantially hotter as roof venting area and/or inlet area is reduced.

The trends described above were similar for the measurements of the extreme t^3 fire growth in the small warehouse which are displayed in the lower half of Table 6: radiative heat fluxes recorded at 1.5 m above floor level remained the same away from the fire, but increased slightly near the fire as roof venting area was reduced. Radiation declined at all positions as inlet area was reduced. In contrast, temperatures recorded at the same height increased substantially at all positions as both roof venting area and inlet area were reduced.

3.1.2 Phase 1a: Small warehouse - rapid t^3 fire growth & 15 % venting

The individual simulations were examined more closely with the aid of Smokeview. In the small warehouse with rapid t^3 fire growth and 15 % roof venting area, reduction of make-up air area from 100 % to 50 % made only a small difference to Smokeview depictions of the smoke layer (Figure 38). In both situations, a distinct clear layer remained below the smoke layer. In contrast, reducing area of make-up air from 50 % to 0 % impacted conditions greatly with total smoke-logging occurring.

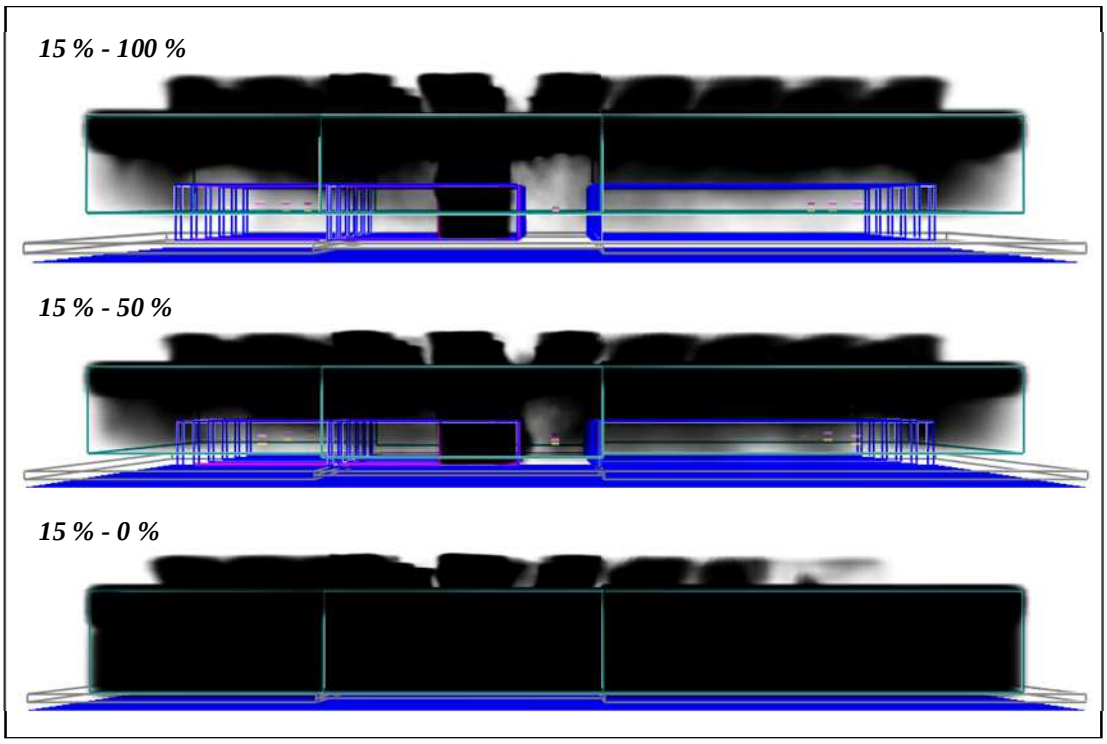

Figure 38: Smokeview depiction of smoke layer after 1,800 seconds in small warehouse with rapid t^3 fire growth and 15 % roof venting area (top – 100 % inlet area, middle – 50 % inlet area, and bottom – 0 % inlet area).

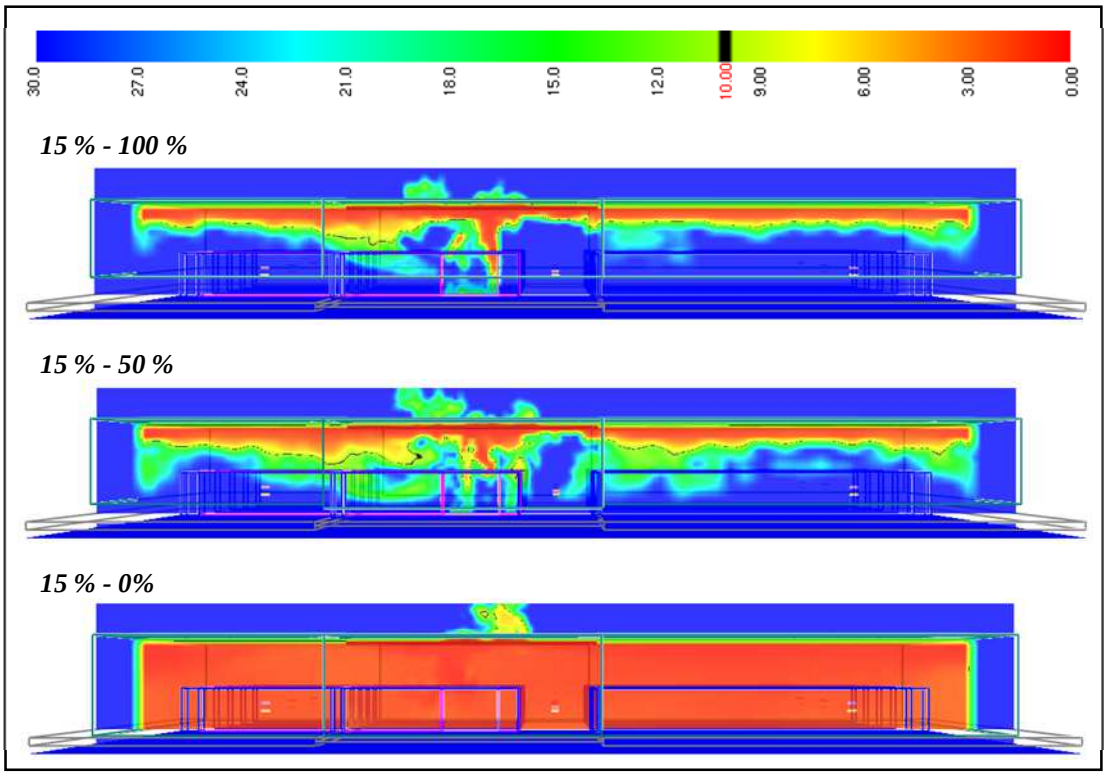

Figure 39: Visibility (m) after 1,800 seconds in small warehouse with rapid t^3 fire growth and 15 % roof venting area (top – 100 % inlet area, middle – 50 % inlet area, and bottom – 0 % inlet area). Slice is taken through long axis of warehouse, 10 m inside nearest warehouse wall.

This result is better visualised using slice files of visibility through the long axis of the warehouse (Figure 39). With area of make-up inlets equivalent to roof venting area, there is a well-defined smoke layer above the storage racks. Reduction of the inlet area induces an increase in the depth of the smoke layer, but visibility in the lower layer remains greater than 10 m. Total removal of make-up air inlets causes visibility to reduce to close to 0 m throughout the entire warehouse.

Shown in Figure 40 are the radiative heat flux measurements 1.5 m above the floor at three selected targets with 15 % roof venting area in the small warehouse with rapid t^3 fire growth. Radiative heat fluxes reached more than 3 kW/m^2 and 4 kW/m^2 at Positions 5 and 6, respectively, with both 100 % and 50 % make-up air inlet area. These two positions are the closest of the nine positions to the fire origin. It is therefore not unreasonable to expect significant radiation at these points from a 50 MW fire. With inlet area set to 0 % of roof venting area, radiative heat fluxes were hazardous (*i.e.* above 1 kW/m^2) for most of the simulation. In contrast, radiation remained within the Routine Conditions criterion of the FBIM model at all positions further removed from the fire. These measurements are represented in the figure by the results at Position 1. Results for all positions can be found in Appendix C1.

Temperatures at a height of 1.5 m above floor level remained near ambient at all positions in the simulations with 100 % and 50 % inlet area (Figure 41). Therefore, temperatures remained within the Routine Conditions criterion. Lower layer temperatures increased markedly at all positions in the simulation with 0 % inlet area for make-up air. However, at the positions closer to the fire, temperatures were still considered routine according to the FBIM model, with a maximum value of 47.0°C recorded at Position 6. At the other points, temperatures were above or approaching 40°C after 1,800 seconds: represented here by Position 1 (see also Appendix C1).

Temperature distributions at heights of 1.5 m above the floor and 5.5 m above the floor (1 m below the ceiling) can be viewed with the aid of Smokeview slice files (Figure 42). Temperatures for the first two simulations remained below ~70°C in the upper layer, except directly above the fire. With just 0 % inlet area for make-up air, temperatures increased substantially. However, maximum temperature in the upper layer was ~190°C: not enough to make conditions extreme according to the FBIM.

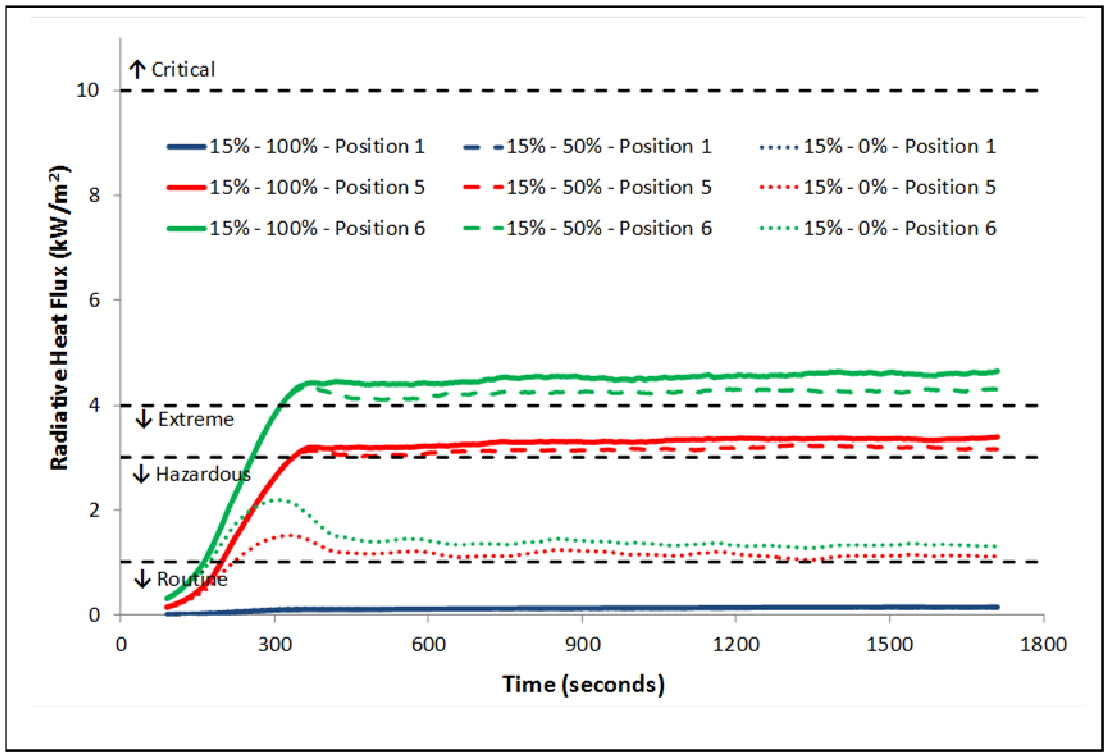

Figure 40: Comparison of smoothed radiative heat flux data from FDS at a height of 1.5 m in small warehouse with rapid t^3 fire growth and 15 % roof venting area.

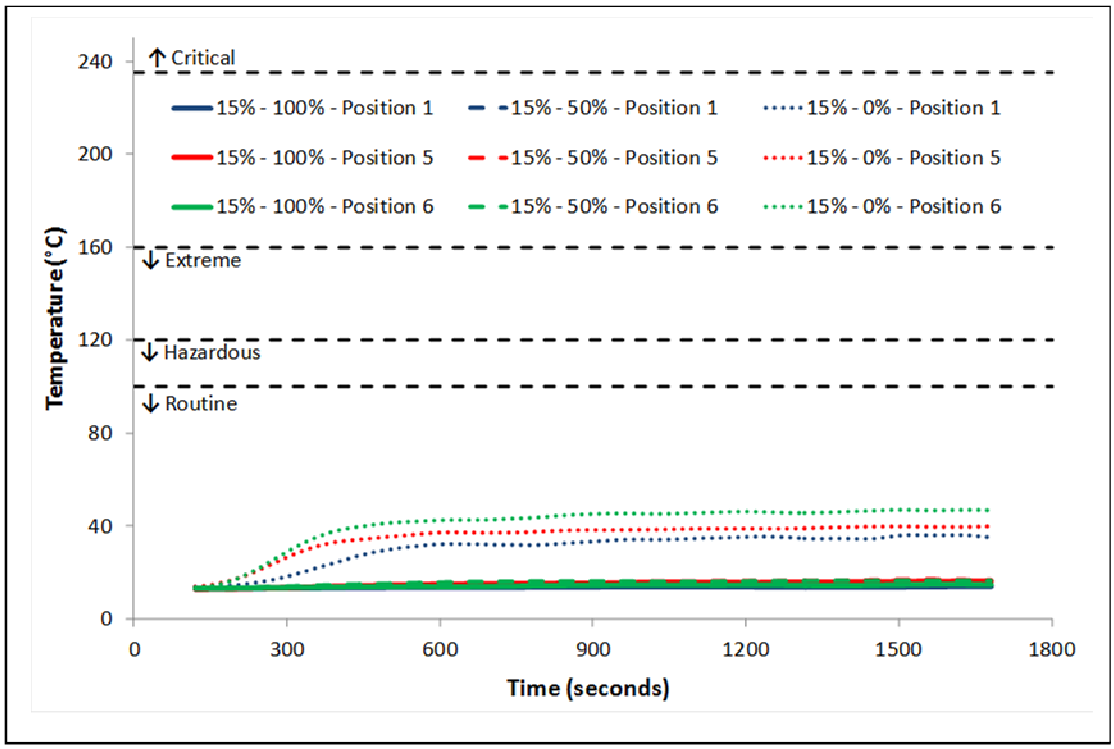

Figure 41: Comparison of smoothed temperature data from FDS at a height of 1.5 m in small warehouse with rapid t^3 fire growth and 15 % roof venting area.

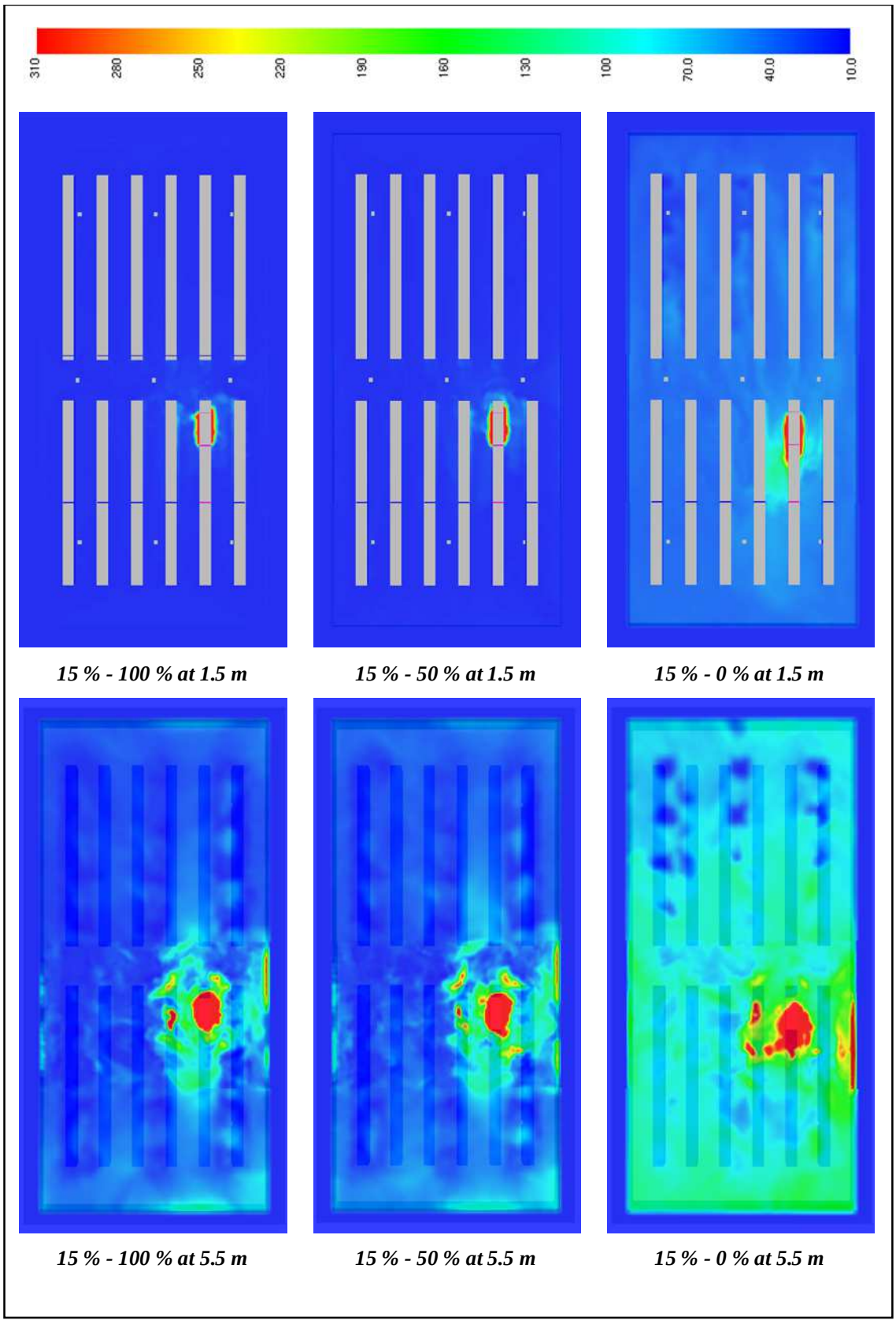

Figure 42: Comparison of temperature distributions after 1,800 seconds in small warehouse with rapid t^3 fire growth, 15 % roof venting area and inlet areas of 100 %, 50 %, and 0 % of roof venting area.

3.1.3 Phase 1a: Small warehouse – rapid t³ fire growth & 10 % venting

A similar result was observed for the Smokeview depictions of the smoke layer when 10 % roof venting was applied in the small warehouse (Figure 43). With both 100 % and 50 % make-up air area, a layer of clear air remained visible beneath the smoke layer (see also Figure 44). As was the case in Section 3.1.2, with 0 % make-up air area, the warehouse became totally inundated with smoke with visibility reducing to 0 m.

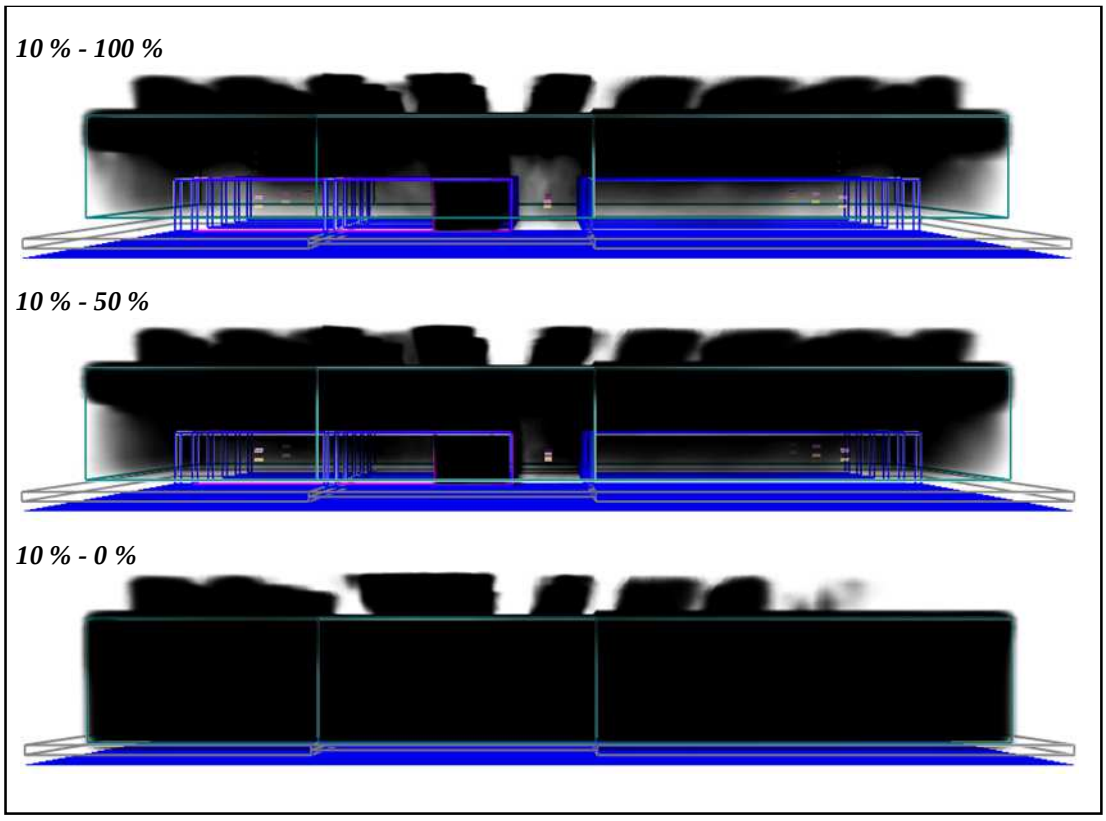

Figure 43: Smokeview depiction of smoke layer after 1,800 seconds in small warehouse with rapid t³ fire growth and 10 % roof venting area (top – 100 % inlet area, middle – 50 % inlet area, and bottom – 0 % inlet area).

Radiative heat fluxes and temperatures measured at 1.5 m above the floor were very little changed in the simulations with 10 % roof venting area than was seen in the simulations with 15 % roof venting area. These results are not described here, but are presented in Appendix C2.

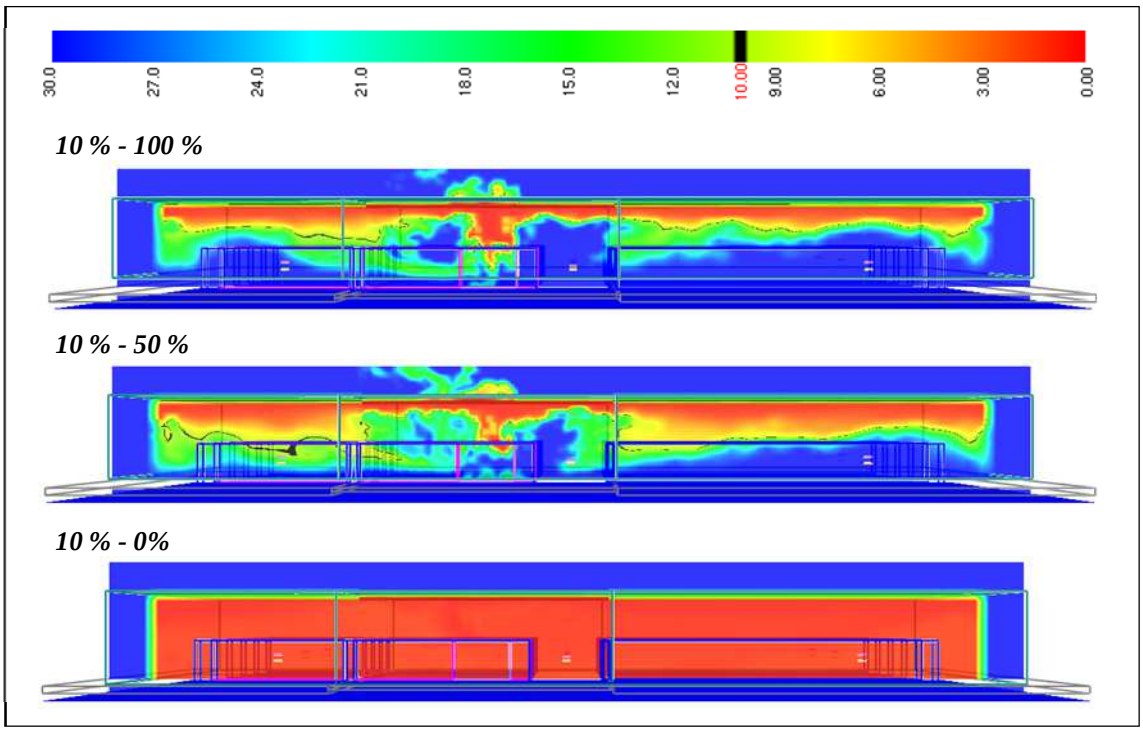

Figure 44: Visibility (m) after 1,800 seconds in small warehouse with rapid t^3 fire growth and 10 % roof venting area (top – 100 % inlet area, middle – 50 % inlet area, and bottom – 0 % inlet area). Slice is taken through long axis of warehouse, 10 m inside nearest warehouse wall.

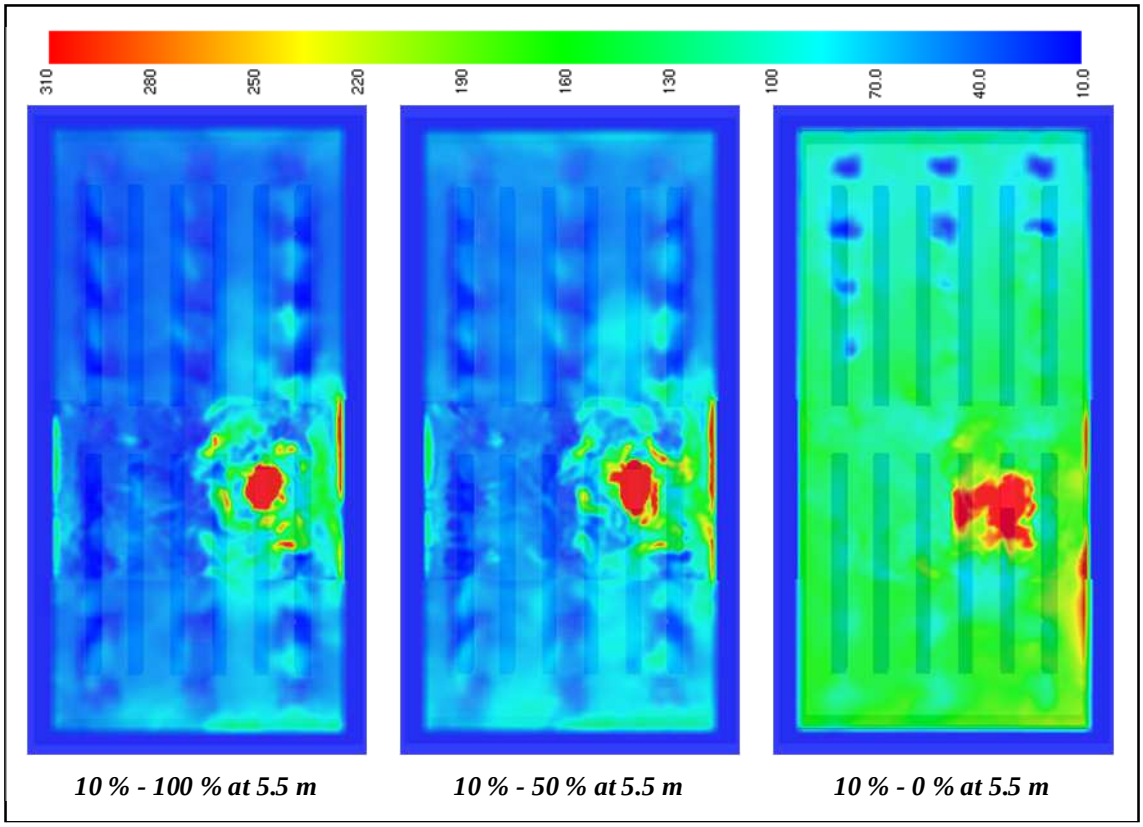

Figure 45: Comparison of temperature distributions after 1,800 seconds in small warehouse with rapid t^3 fire growth, 10 % roof venting area and inlet areas of 100 %, 50 %, and 0 %.

In contrast, temperatures in the upper layer were noticeably hotter after 1,800 seconds with just 10 % roof venting area. The slice file images of temperature distribution 1 m below the ceiling, seen in Figure 45, display more turquoise and green tones which indicate temperatures of up to ~190°C were reached. In addition, vents far from the fire began to lose efficiency: blue colourations at eight of the vent openings remote from the fire indicate that cool air was drawn into the warehouse through these vents, rather than hot air being expelled through them.

3.1.4 Phase 1a: Small warehouse - rapid t³ fire growth & 5 % venting

When 5 % roof venting was applied in the small warehouse, smoke layer depth reduced further than in the previous simulations with a concomitant decline in visibility (Figure 46 and Figure 47). With 100 % and 50 % inlet area for make-up air, *fingers* of low visibility were observed protruding into the lower layer and reaching towards the fire: a combined effect of the presence of rack storage and the ceiling jet tumbling off the warehouse walls. Removal of inlet area resulted in visibility of 0 m.

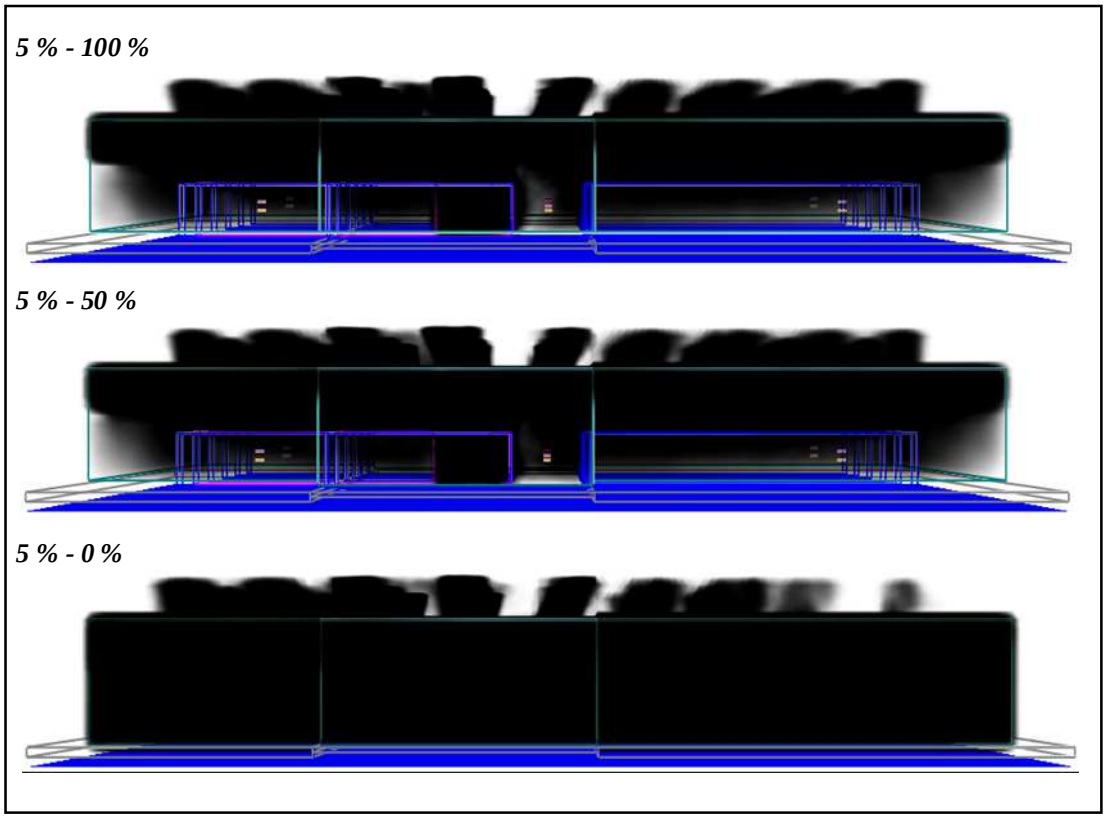

Figure 46: Smokeview depiction of smoke layer after 1,800 seconds in small warehouse with rapid t^3 fire growth and 5 % roof venting area (top – 100 % inlet area, middle – 50 % inlet area, and bottom – 0 % inlet area).

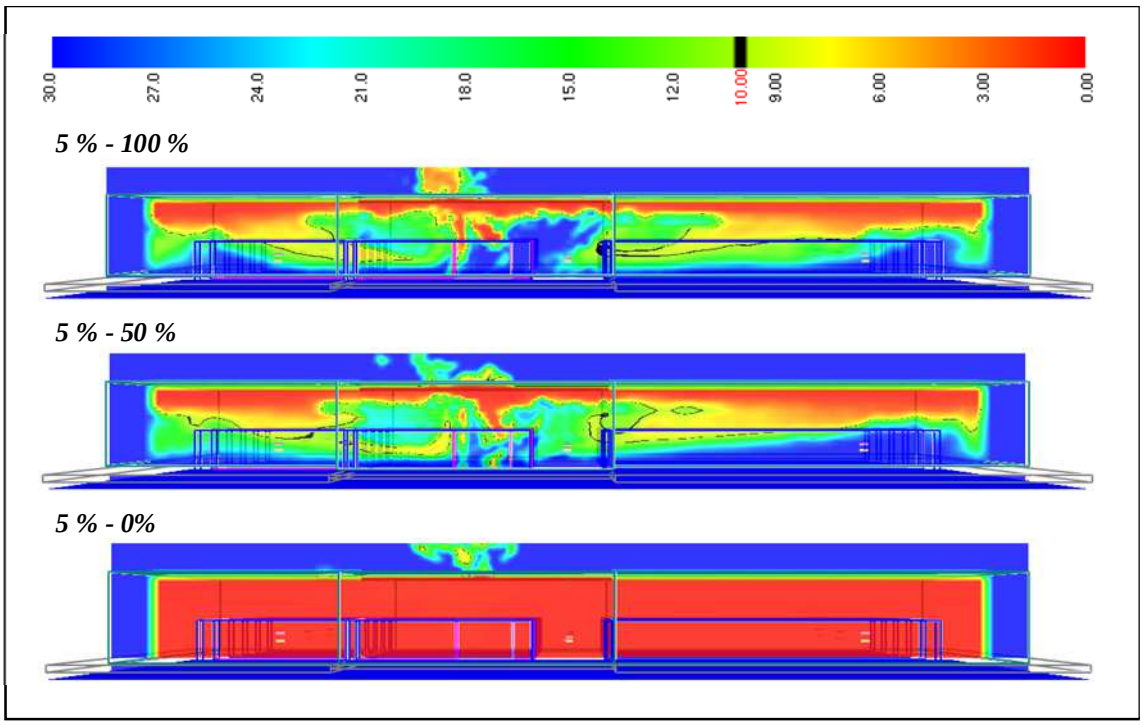

Figure 47: Visibility (m) after 1,800 seconds in small warehouse with rapid t^3 fire growth and 5 % roof venting area (top – 100 % inlet area, middle – 50 % inlet area, and bottom – 0 % inlet area). Slice is taken through long axis of warehouse, 10 m inside nearest warehouse wall.

Radiative heat fluxes for the simulations with 5 % roof venting area displayed minimal differences to those recorded in the warehouses with 10 % and 15 % roof venting (Figure 48). Only with 0 % inlet area was a significant change observed, with the radiative heat fluxes near the fire reducing to below 1 kW/m² for the majority of the simulation. Apart from a short-lived peak in radiative heat flux at Position 6 at 255 seconds, this had the effect of making radiation conditions routine at positions near the fire. In previous cases, radiative heat fluxes near the fire were hazardous for the entire simulation. Heat fluxes for all positions can be seen in Appendix C3.

Temperatures recorded 1.5 m above the warehouse floor were also significantly affected by the reduction in inlet area for make-up air (represented by Positions 3, 4, and 6 in Figure 49). In contrast to the previous scenarios, with 5 % roof venting and 0 % inlet area for make-up air, temperatures rose to above 90°C at all targets and to above 100°C (Hazardous Conditions criterion) at four of the nine targets. This would have a practical effect of reducing time available for a fire-fighter inside the warehouse from 25 minutes to 10 minutes. Temperature results at all positions can be found in Appendix C3.

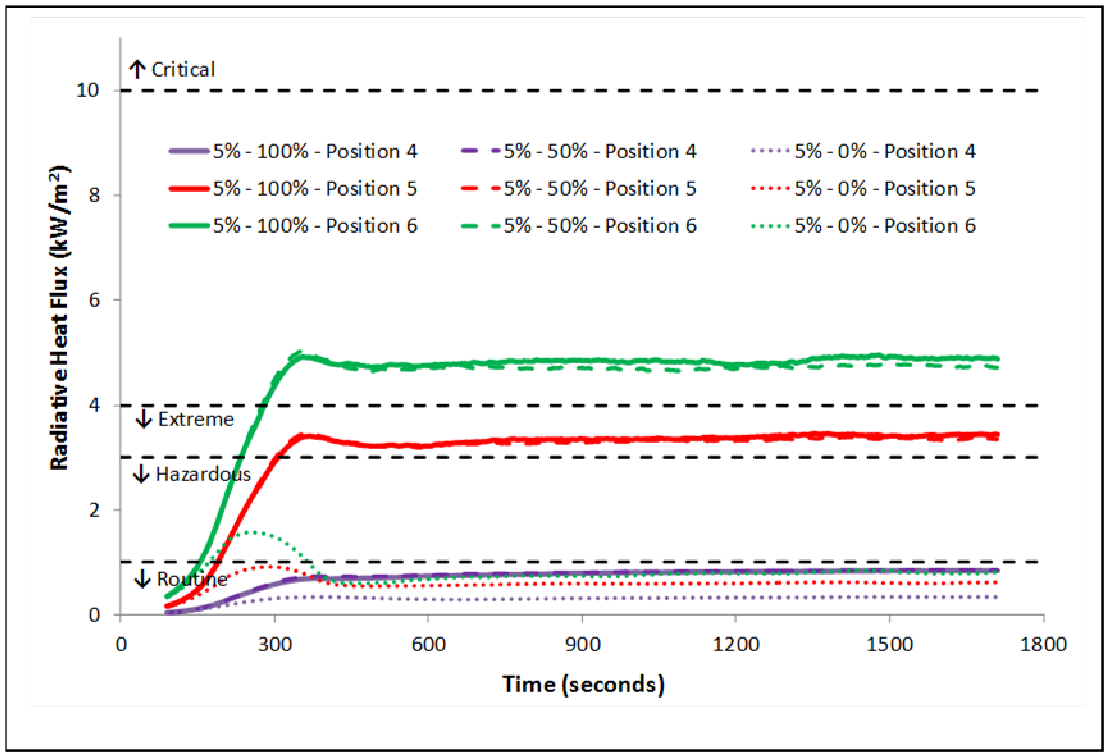

Figure 48: Comparison of smoothed radiative heat flux data from FDS at a height of 1.5 m in small warehouse with rapid t^3 fire growth and 5 % roof venting area.

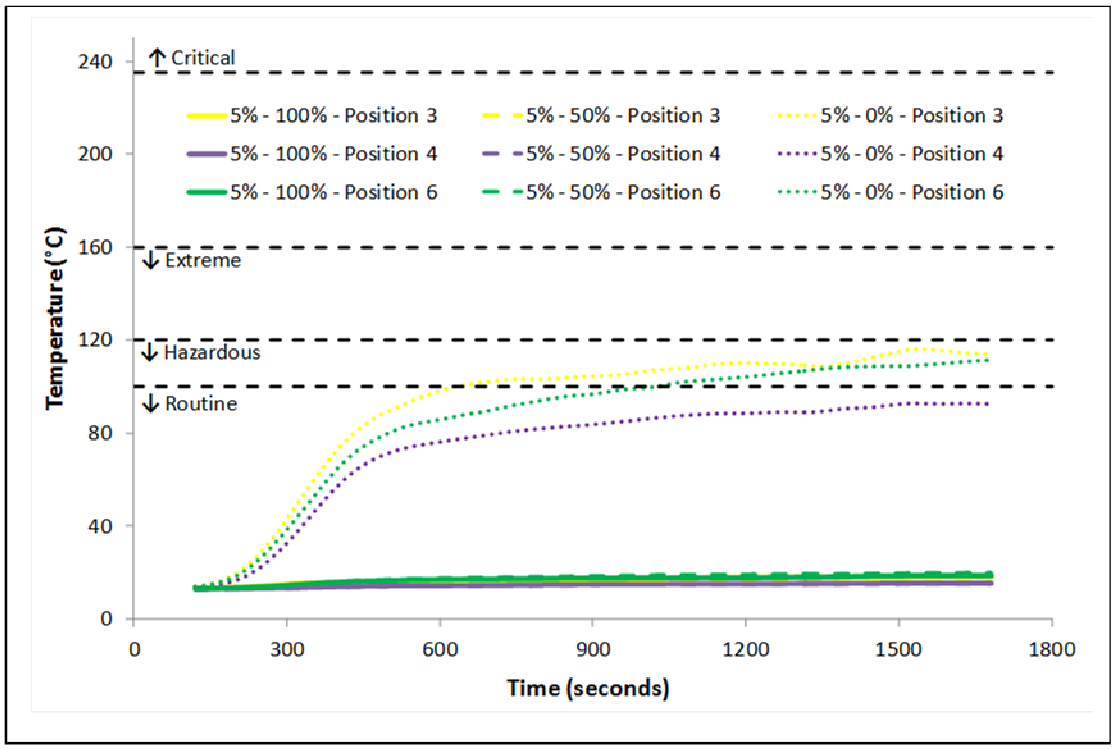

Figure 49: Comparison of smoothed temperature data from FDS at a height of 1.5 m in small warehouse with rapid t^3 fire growth and 5 % roof venting area.

3.1.5 Phase 1b: Small warehouse - extreme t^3 fire growth & 15 % venting

Figure 50 and Figure 51 depict the smoke layer and the visibility in the small warehouse with 15 % roof venting after 1,800 seconds under an extreme t^3 fire growth rate for all inlet area scenarios, respectively. Smoke layer and visibility development in each case was almost identical to the simulations with a rapid t^3 fire growth rate (*cf*. Figure 38 and Figure 39, respectively). Reduction of area of make-up air inlets from 100 % to 50 % made only a small difference to depth of the smoke layer, with a layer of clear air remaining. In these two simulations visibility in the lower layer remained greater than 10 m. As was seen in previous small warehouse simulations, reduction of inlet area for make-up air from 50 % to 0 % resulted in smoke-logging occurring, and as a result, visibility was reduced to close to 0 m.

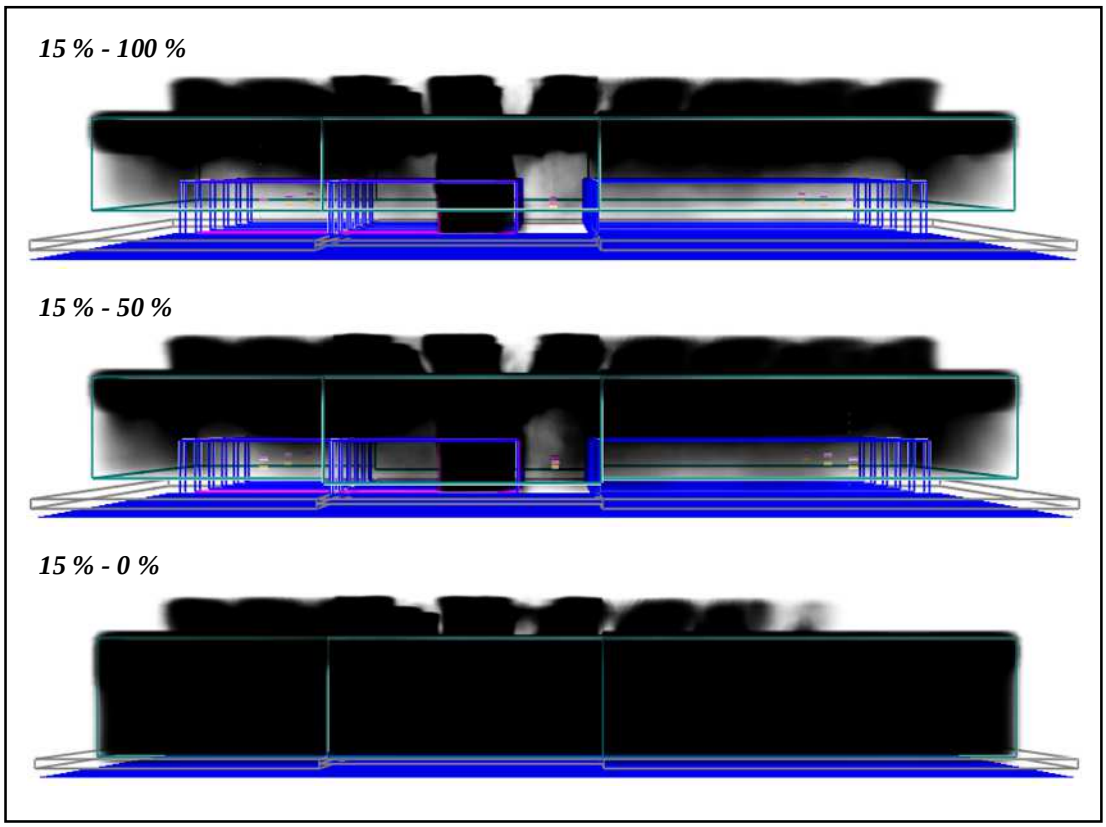

Figure 50: Smokeview depiction of smoke layer after 1,800 seconds in small warehouse with extreme t^3 fire growth and 15 % roof venting area (top – 100 % inlet area, middle – 50 % inlet area, and bottom – 0 % inlet area).

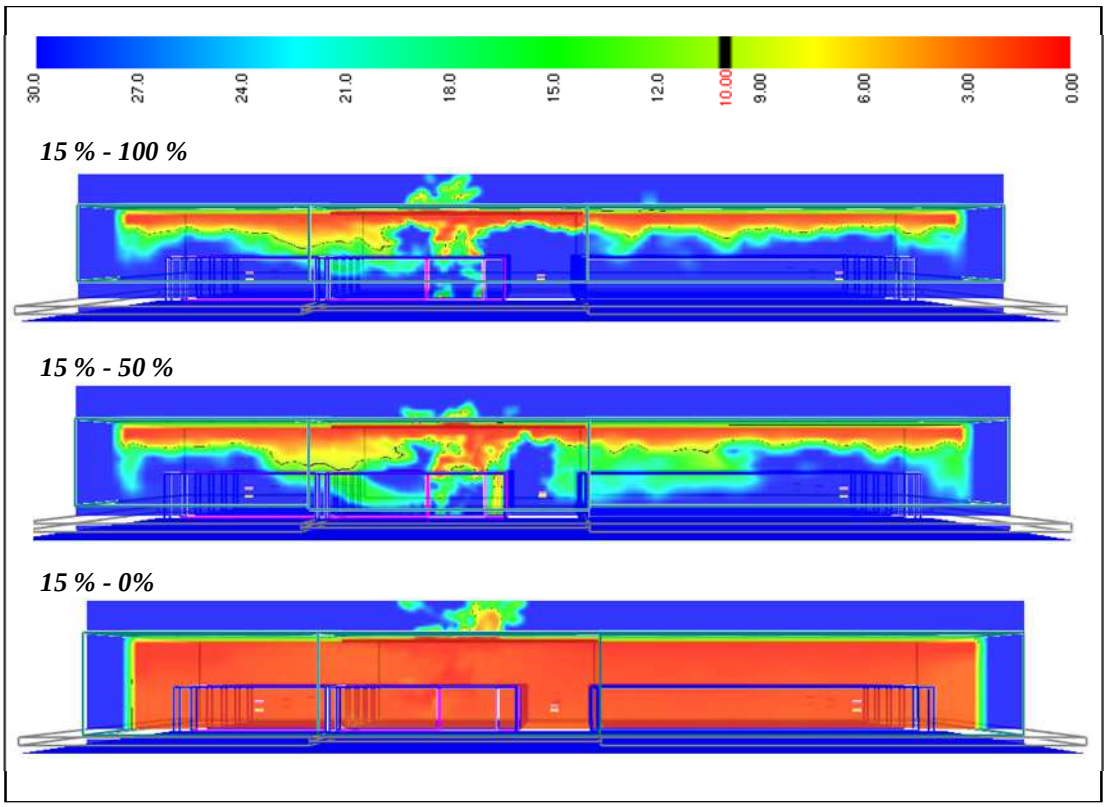

Figure 51: Visibility (m) after 1,800 seconds in small warehouse with extreme t^3 fire growth and 15 % roof venting area (top – 100 % inlet area, middle – 50 % inlet area, and bottom – 0 % inlet area). Slice is taken through long axis of warehouse, 10 m inside nearest warehouse wall.

Radiative heat flux measurements 1.5 m above floor level at three selected targets in the small warehouse (with 15 % roof venting area and extreme t^3 fire growth) are shown in Figure 52. As was observed with the rapid t^3 fire growth rate in Section 3.1.2, radiative heat flux reached a plateau of more than 3 kW/m^2 and 4 kW/m^2 at Positions 5 and 6, respectively, with both 100 % and 50 % make-up air inlet area The extreme fire growth rate had the effect of bringing the onset of this plateau forward in time from ~360 seconds to ~200 seconds. Similarly, with inlet area set to 0 % of roof venting area, radiative heat fluxes remained within the Hazardous Conditions criterion of the FBIM model near the fire, with maximum radiative heat flux being recorded ~25 seconds sooner than with the rapid fire. Radiative heat fluxes remained within the Routine Conditions criterion at all positions away from the fire. These measurements are represented in the figure by heat fluxes at Position 1. Temperatures at a height of 1.5 m above floor level remained routine at all positions for all three combinations of inlet area with 15 % roof venting area (Figure 53). Radiative heat flux and temperature results for all positions can be found in Appendix D1.

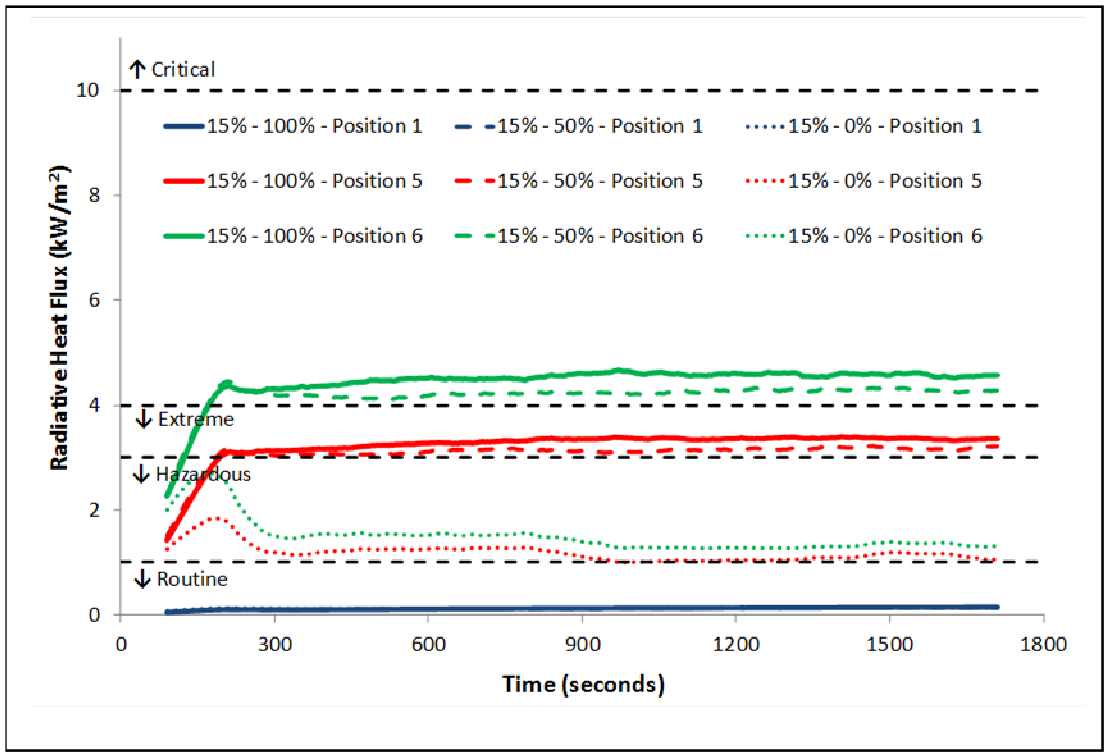

Figure 52: Comparison of smoothed radiative heat flux data from FDS at a height of 1.5 m in small warehouse with extreme t^3 fire growth and 15 % roof venting area.

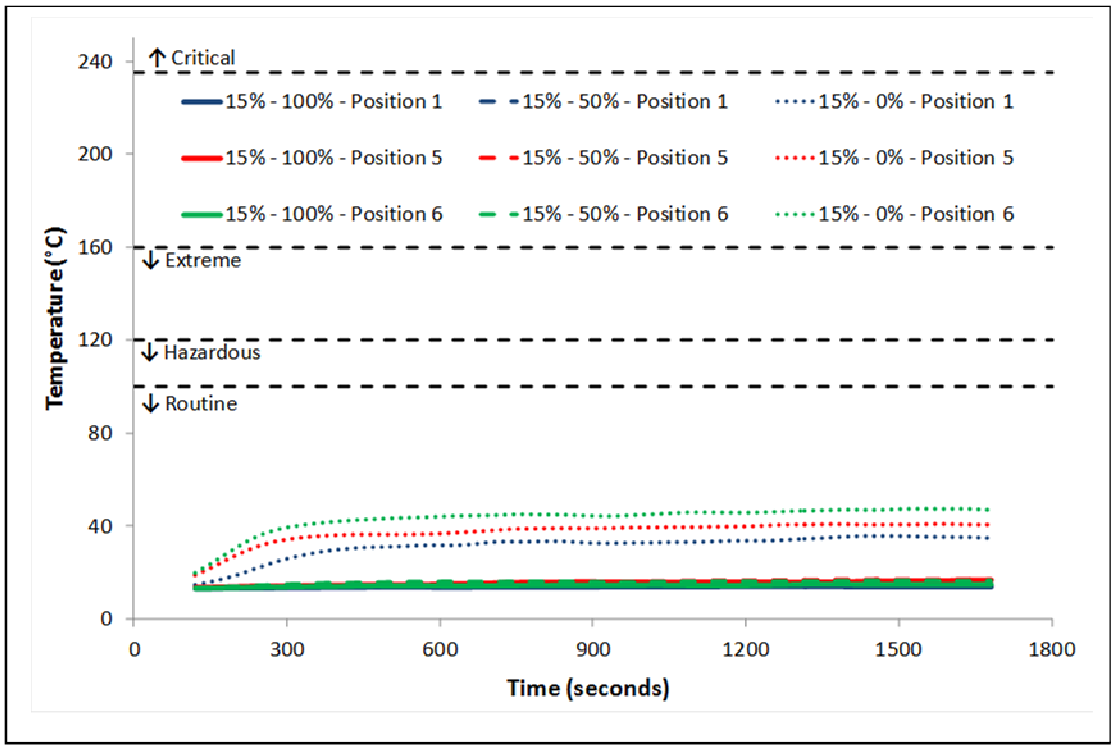

Figure 53: Comparison of smoothed temperature data from FDS at a height of 1.5 m in small warehouse with extreme t^3 fire growth and 15 % roof venting area.

3.1.6 Phase 1b: Small warehouse – extreme t^3 fire growth & 10 % venting

Smokeview depictions of the smoke layer revealed a similar result for the 10 % roof venting scenarios as was observed with 15 % roof venting area in Section 3.1.2 (Figure 54 *cf*. Figure 38). With both 100 % and 50 % make-up air area, a layer of clear air remained visible beneath the smoke layer, but the warehouse became smoke-logged with 0 % inlet area for make-up air. The increase in smoke layer depth had a corresponding decrease in visibility, as can be seen in Figure 55. With make-up air supplied to the lower region of the warehouse, visibility remains above 10 m in most of the area below the rack storage. However, total removal of the make-up air supply reduces visibility throughout the warehouse to 0 m.

Radiative heat fluxes and temperatures in the lower layer with the extreme t^3 fire were similar to the cases with the rapid t^3 fire and can be found in Appendix D2.

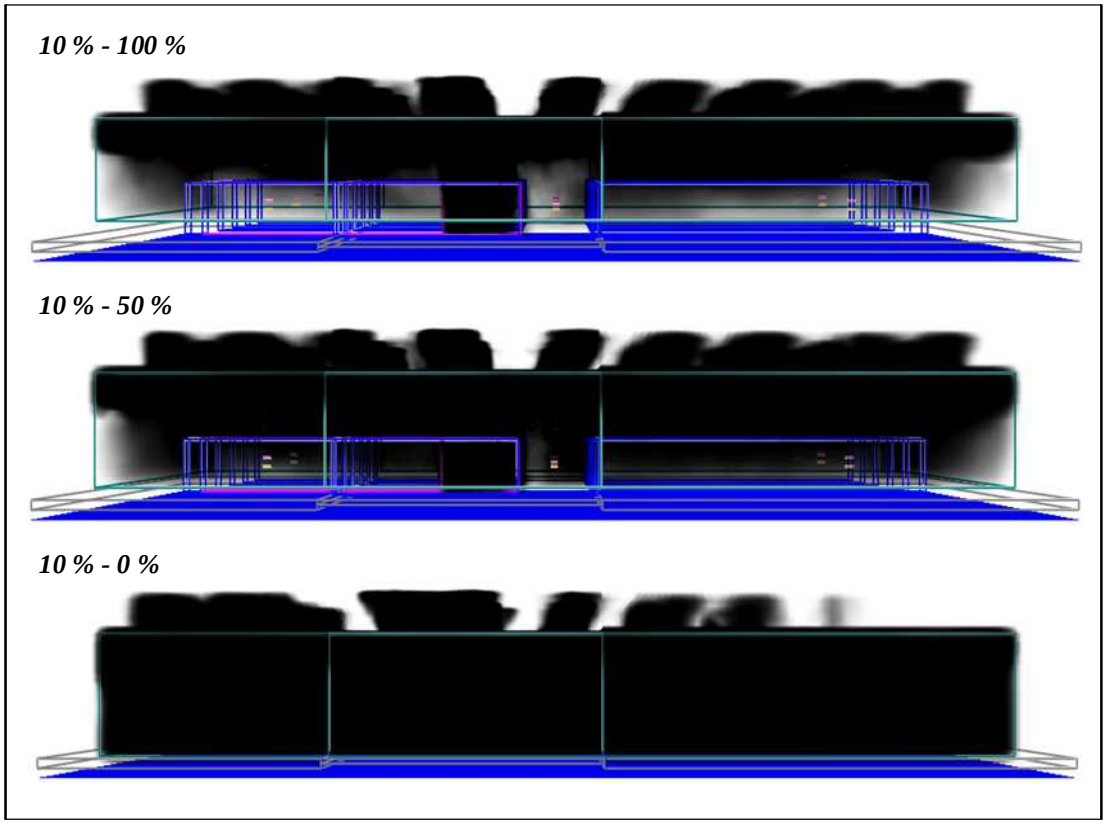

Figure 54: Smokeview depiction of smoke layer after 1,800 seconds in small warehouse with extreme t^3 fire growth and 10 % roof venting area (top – 100 % inlet area, middle – 50 % inlet area, and bottom – 0 % inlet area).

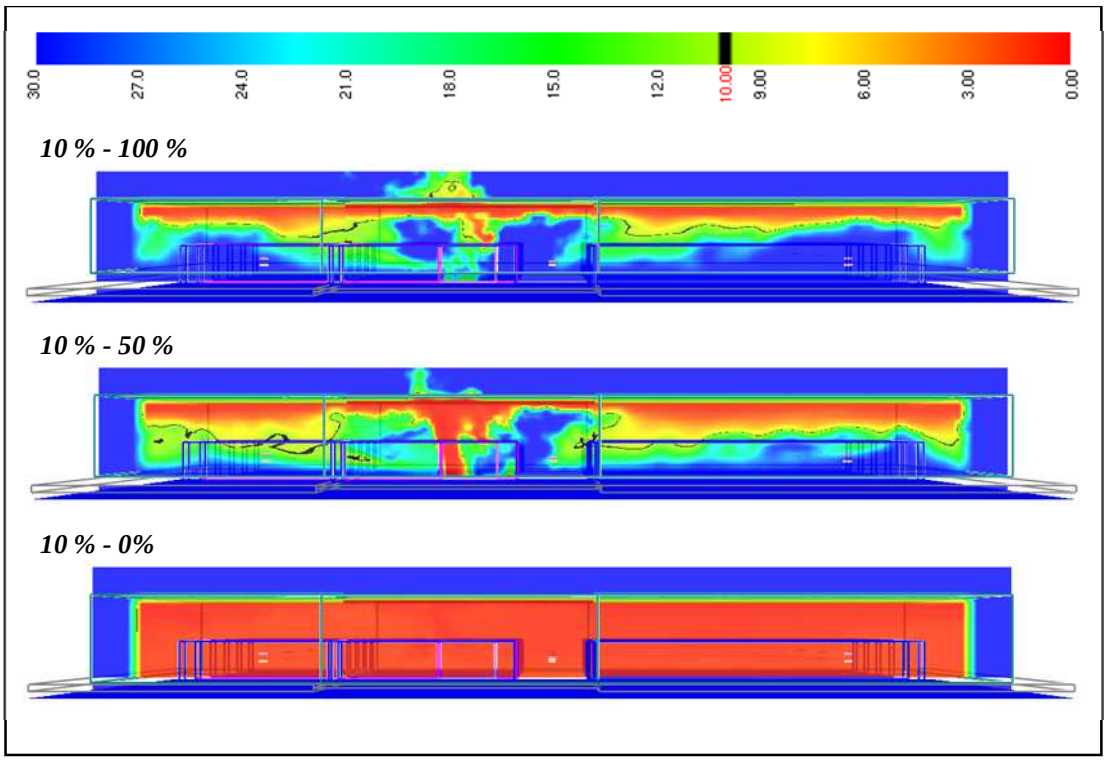

Figure 55: Visibility (m) after 1,800 seconds in small warehouse with extreme t^3 fire growth and 10 % roof venting area (top – 100 % inlet area, middle – 50 % inlet area, and bottom – 0 % inlet area). Slice is taken through long axis of warehouse, 10 m inside nearest warehouse wall.

3.1.7 Phase 1b: Small warehouse - extreme t^3 fire growth & 5 % venting

Smoke layer depth with an extreme t^3 fire growth rate reduced even further with just 5 % roof venting area compared to the cases with 15 % and 10 % roof venting area (Figure 56). This trend corresponds to that seen in the simulations with a rapid t^3 fire growth rate (Sections 3.1.2 to 3.1.4). The deeper smoke layer was also matched by decreased visibility, as compared to the cases with more roof venting area (Figure 57 *cf.* Figure 51 and Figure 55). For the two simulations with some inlet area for make-up air, *fingers* of low visibility protruded into the lower layer between the storage racks. Removal of all inlet area resulted in visibility of 0 m.

Radiative heat fluxes for the simulations with 5 % roof venting area displayed minimal differences to those recorded in the warehouses with 10 % and 15 % roof venting (Figure 58). Only with 0 % inlet area was a significant change observed, with the radiative heat fluxes near the fire reducing to below 1 kW/m² for the majority of the simulation. This had the effect of making radiation conditions routine at positions near the fire, with the exception of a short-lived peak in heat fluxes at Position 6 after

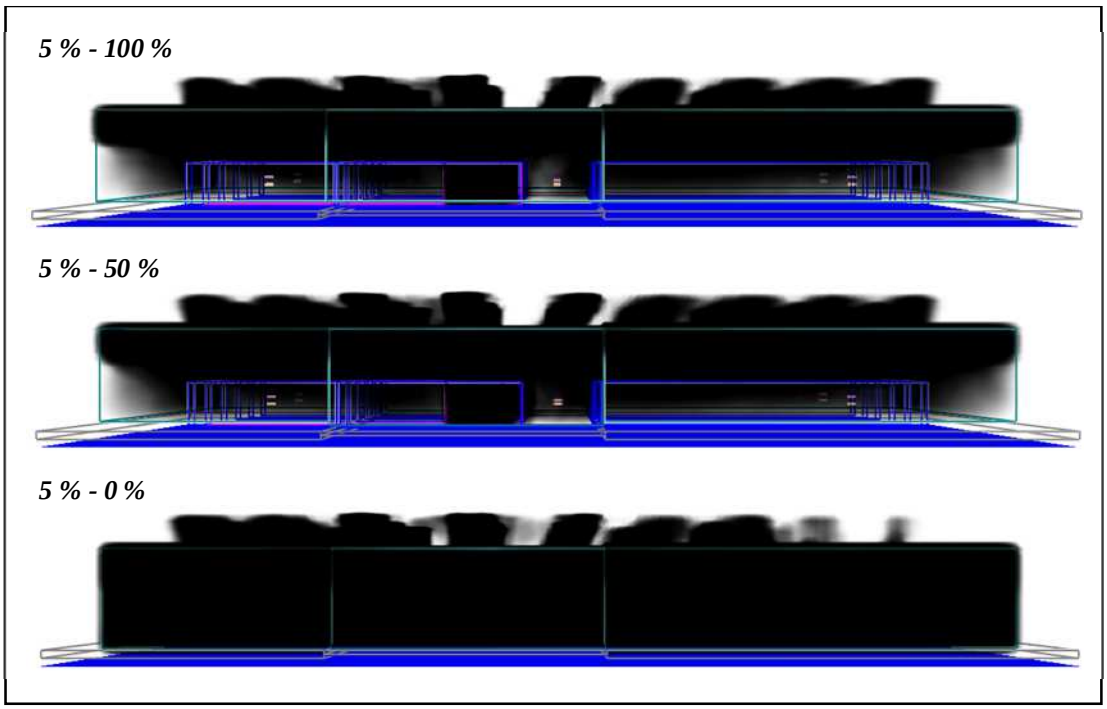

Figure 56: Smokeview depiction of smoke layer after 1,800 seconds in small warehouse with extreme t^3 fire growth and 5 % roof venting area (top – 100 % inlet area, middle – 50 % inlet area, and bottom – 0 % inlet area).

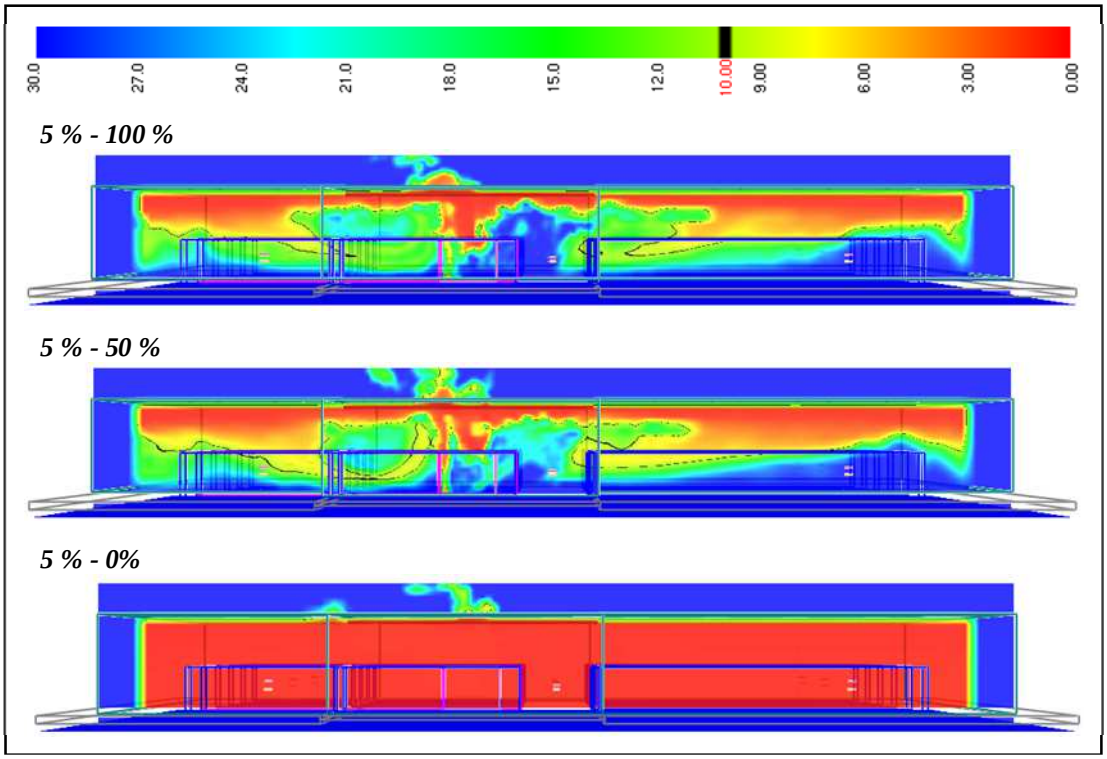

Figure 57: Visibility (m) after 1,800 seconds in small warehouse with extreme t^3 fire growth and 5 % roof venting area (top – 100 % inlet area, middle – 50 % inlet area, and bottom – 0 % inlet area). Slice is taken through long axis of warehouse, 10 m inside nearest warehouse wall.

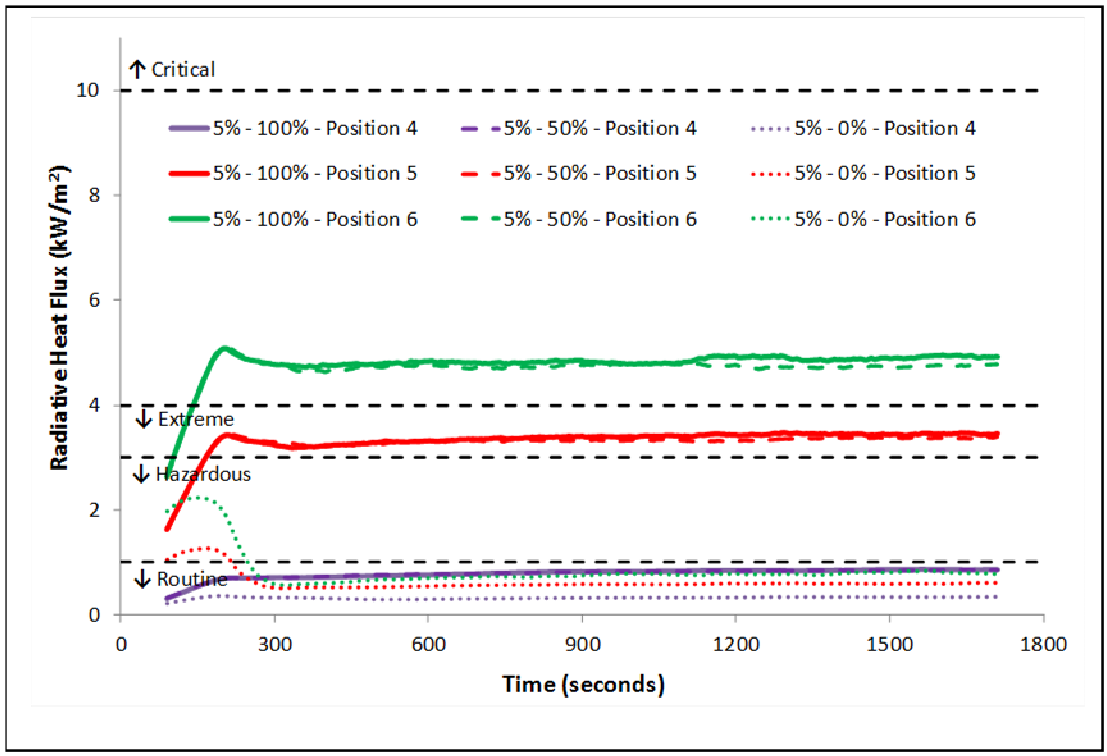

Figure 58: Comparison of smoothed radiative heat flux data from FDS at a height of 1.5 m in small warehouse with extreme t^3 fire growth and 5 % roof venting area.

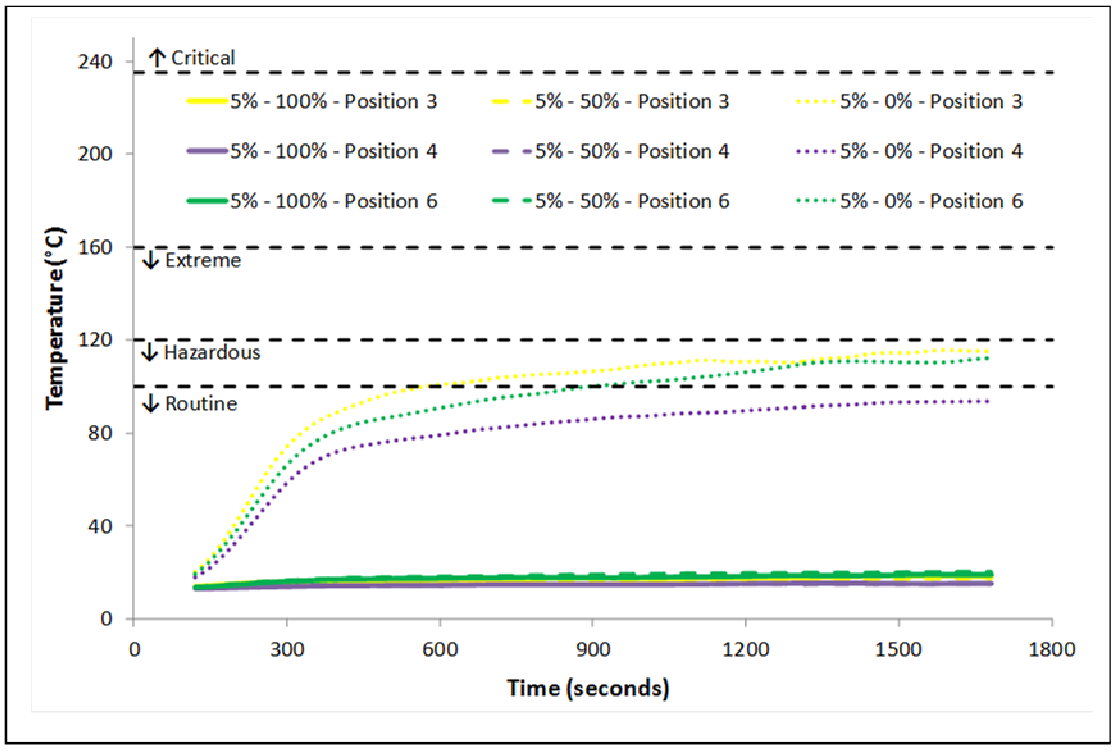

Figure 59: Comparison of smoothed temperature data from FDS at a height of 1.5 m in small warehouse with extreme t^3 fire growth and 5 % roof venting area.

255 seconds. In previous cases, radiative heat fluxes near the fire were hazardous for the entire simulation. Heat fluxes for all positions can be seen in Appendix D3.

Temperatures recorded 1.5 m above the warehouse floor were significantly affected by the reduction in inlet area for make-up air (represented by Positions 3, 4, and 6 in Figure 59). Temperatures increased to above 90°C at all targets and to above 100°C (Hazardous Conditions criterion) at five of the nine targets: hence, reducing the time available for a fire fighter inside the warehouse from 25 minutes to 10 minutes. Temperature results at all positions can be found in Appendix D3.

3.1.8 Phases 1c & 1d: Simulations in the large warehouse

Summary results from the first phase of testing in the large warehouse, to determine the area of roof venting and make-up air inlets required to fulfil the FBIM criteria, are presented in Table 7. Under the current requirement of 15 % roof venting area, with a matching area of inlets for make-up air, conditions were routine at all positions in the warehouse with rapid t^3 fire growth, in regards to both radiative heat flux and temperature. Near the fire (*i.e.* at Positions 5 and 6), maximum radiative heat flux recorded 1.5 m above floor level was just 0.6 kW/m². At the same height, a maximum temperature of 13.6°C was recorded. At the remaining targets, located further from the fire, radiative heat flux peaked at 0.1 kW/m² and temperature at 13.2°C.

Neither a reduction of the area of inlets for make-up air to 50 % of the roof venting area, nor a subsequent reduction of inlet area to 0 % of the roof venting area, had any meaningful effect on radiative heat fluxes recorded in the lower layer: in both cases, radiative heat fluxes remained the same as observed with 100 % inlet area. This result differs from that seen in the small warehouse, where radiative heat fluxes reduced with each successive reduction in inlet area. There was, however, a small effect on lower layer temperatures as make-up air was reduced in the large warehouse. Near the fire, maximum temperatures recorded 1.5 m above the ground increased to 13.8°C with 50 % inlet area, and further to 15.5°C with 0 % inlet area. Similarly, temperatures away from the fire increased to 13.4°C and 14.8°C, respectively, as inlet area for make-up air was reduced. This follows a similar, albeit more subtle, trend than was observed in the small warehouse.

A reduction of roof venting area to 10 % of the warehouse floor area had little impact on radiative heat fluxes recorded in the large warehouse. At all positions, radiative heat flux conditions remained routine. In the cases with inlet areas of 100 % and 50 % of the roof venting area, maximum recorded radiative heat fluxes were 0.7 kW/m²; this is, in both cases, a 0.1 kW/m² increase over peak radiative heat fluxes recorded in the simulations with 15 % roof venting area. In the case with 0 % inlet area for make-up air, peak radiative heat flux decreased by 0.1 kW/m² to 0.5 kW/m². Temperatures recorded at the same positions increased marginally over those observed with 15 %

Table 7 – Summary of maximum results for Phase 1 simulations in large warehouse.

Fire growth	Vent area (% of floor area)	Inlet area (% of vent area)	Radiation near fire[1] (kW/m^2 - Criterion)	Radiation away from fire (kW/m^2 - Criterion)	Temperature near fire[1] (°C - Criterion)	Temperature away from fire (°C - Criterion)
Rapid	15 %	100 %	0.6 - Routine	0.1 - Routine	13.6 - Routine	13.2 - Routine
Rapid	15 %	50 %	0.6 - Routine	0.1 - Routine	13.8 - Routine	13.4 - Routine
Rapid	15 %	0 %	0.6 - Routine	0.1 - Routine	15.5 - Routine	14.8 - Routine
Rapid	10 %	100 %	0.7 - Routine	0.1 - Routine	13.7 - Routine	13.3 - Routine
Rapid	10 %	50 %	0.7 - Routine	0.1 - Routine	13.8 - Routine	13.7 - Routine
Rapid	10 %	0 %	0.5 - Routine	0.1 - Routine	17.4 - Routine	16.7 - Routine
Rapid	5 %	100 %	0.8 - Routine	0.1 - Routine	14.4 - Routine	13.3 - Routine
Rapid	5 %	50 %	1.2 - Hazardous	0.1 - Routine	14.6 - Routine	14.3 - Routine
Rapid	5 %	0 %	0.5 - Routine	0.1 - Routine	40.2 - Routine	36.7 - Routine
Extreme	15 %	100 %	0.6 - Routine	0.1 - Routine	13.7 - Routine	13.3 - Routine
Extreme	15 %	50 %	0.6 - Routine	0.1 - Routine	13.8 - Routine	13.5 - Routine
Extreme	15 %	0 %	0.6 - Routine	0.1 - Routine	15.5 - Routine	14.6 - Routine
Extreme	10 %	100 %	0.6 - Routine	0.1 - Routine	13.7 - Routine	13.3 - Routine
Extreme	10 %	50 %	0.7 - Routine	0.1 - Routine	13.8 - Routine	13.6 - Routine
Extreme	10 %	0 %	0.5 - Routine	0.1 - Routine	17.3 - Routine	16.8 - Routine
Extreme	5 %	100 %	0.9 - Routine	0.1 - Routine	14.4 - Routine	13.4 - Routine
Extreme	5 %	50 %	1.2 - Hazardous	0.1 - Routine	14.7 - Routine	14.4 - Routine
Extreme	5 %	0 %	0.5 - Routine	0.1 - Routine	40.4 - Routine	37.7 - Routine

[1] Indicates Positions 5 and 6 only.

[+] Indicates that conditions exceeded the extreme criterion, but were not severe enough to be classed as critical.

roof venting, but remained within the Routine Conditions criterion. Near the fire, temperatures were 13.7°C, 13.8°C, and 17.4°C with inlet areas of 100 %, 50 %, and 0 %, respectively. And, away from the fire, temperatures were 13.3°C, 13.7°C, and 16.7°C, respectively, for the same inlet area percentages.

When roof venting area was further reduced to 5 % of the warehouse floor area, the impact on radiative heat fluxes was mixed. Near the fire, the maximum radiative heat flux of 0.8 kW/m² was just 0.2 kW/m² higher than was observed for the base case with 15 % roof venting area and 100 % inlet area. Reduction of inlet area to 50 %, resulted in an increased peak radiative heat flux near the fire of 1.2 kW/m²; this is hazardous according to the FBIM. The maximum radiative heat flux recorded with 0 % inlet area was 0.5 kW/m². A much larger effect on the lower layer temperatures was observed in this simulation than seen in the simulations with larger roof venting areas. Near the fire, maximum temperatures at the target positions were 14.4°C, 14.6°C, and 40.2°C for inlet areas of 100 %, 50 %, and 0 %, respectively. Away from the fire, the peak temperatures were 13.3°C, 14.3°C, and 36.7°C, respectively.

The trends described above were similar for measurements with extreme t^3 fire growth in the large warehouse which are displayed in the lower half of Table 7: Radiative heat fluxes recorded at 1.5 m above the ground remained nearly identical to those recorded with rapid t^3 fire growth, both near and away from the fire. Temperatures increased at all positions as both roof venting area and inlet area were reduced. Absolute values tended to be the same or slightly larger in the extreme t^3 fire growth case with just 5 % roof venting area when compared to the corresponding case with rapid t^3 fire growth.

3.1.9 Phase 1c: Large warehouse - rapid t^3 fire growth & 15 % venting

Reduction of inlet area for make-up air from 100 % to 50 % of the roof venting area in the large warehouse (with rapid t^3 fire growth and 15 % roof venting area) made only a small difference to Smokeview depictions of the smoke layer (Figure 60). In both cases, a distinct clear layer remained below the smoke layer. However, the effect of further reduction of inlet area to 0 % was a more noticeable impact on conditions inside the warehouse, with total smoke-logging occurring.

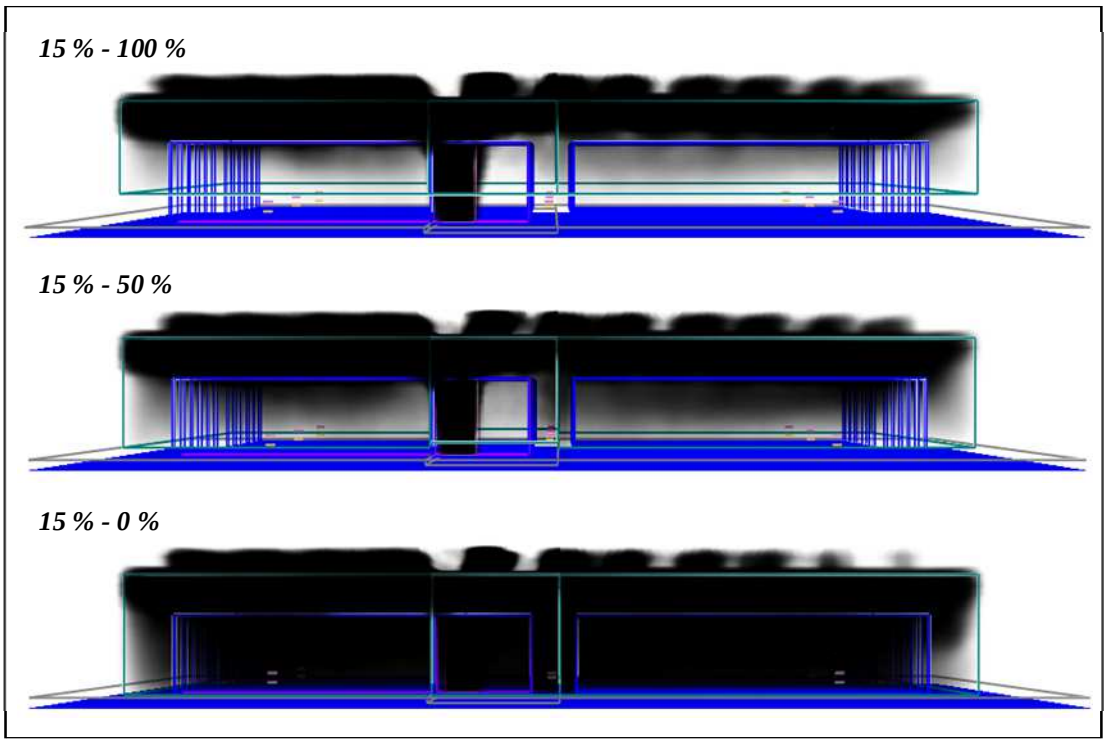

Figure 60: Smokeview depiction of smoke layer after 1,800 seconds in large warehouse with rapid t^3 fire growth and 15 % roof venting area (top – 100 % inlet area, middle – 50 % inlet area, and bottom – 0 % inlet area).

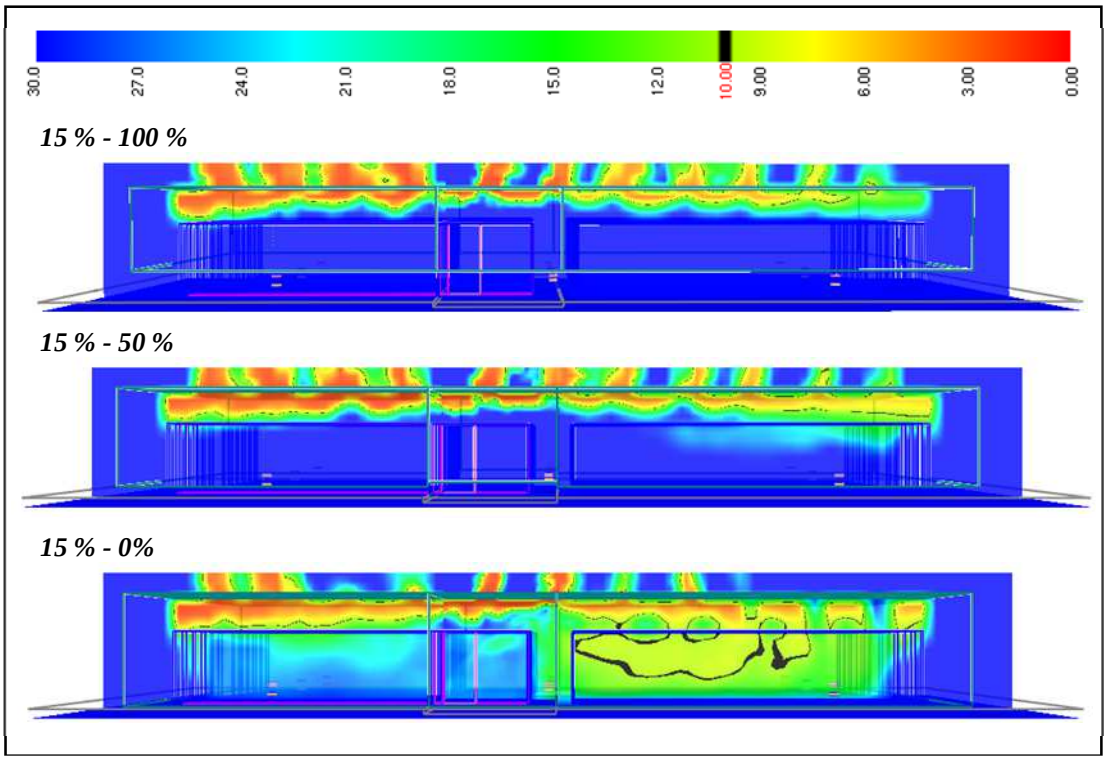

Figure 61: Visibility (m) after 1,800 seconds in large warehouse with rapid t^3 fire growth and 15 % roof venting area (top – 100 % inlet area, middle – 50 % inlet area, and bottom – 0 % inlet area). Slice is taken through long axis of warehouse, 20 m inside nearest warehouse wall.

Visibility slice files through the long axis of the warehouse allow this result to be well-visualised (Figure 61). With both 100 % and 50 % inlet area there is a well-defined clear layer extending up to the tops of the storage racks. Total removal of make-up air inlets interferes with this clear layer, and the smoke layer penetrates to the floor. On the right hand side of the bottom image in Figure 61, a large pocket of low visibility, enclosed by the black 10-metre visibility line, can be observed. Total removal of the inlet vents required that those roof vents further from the fire acted as inlets for make-up air. This can be seen by the disappearance of the smoke plumes above this section of the roof, and the appearance of cool air (blue colourations) being drawn into the warehouse.

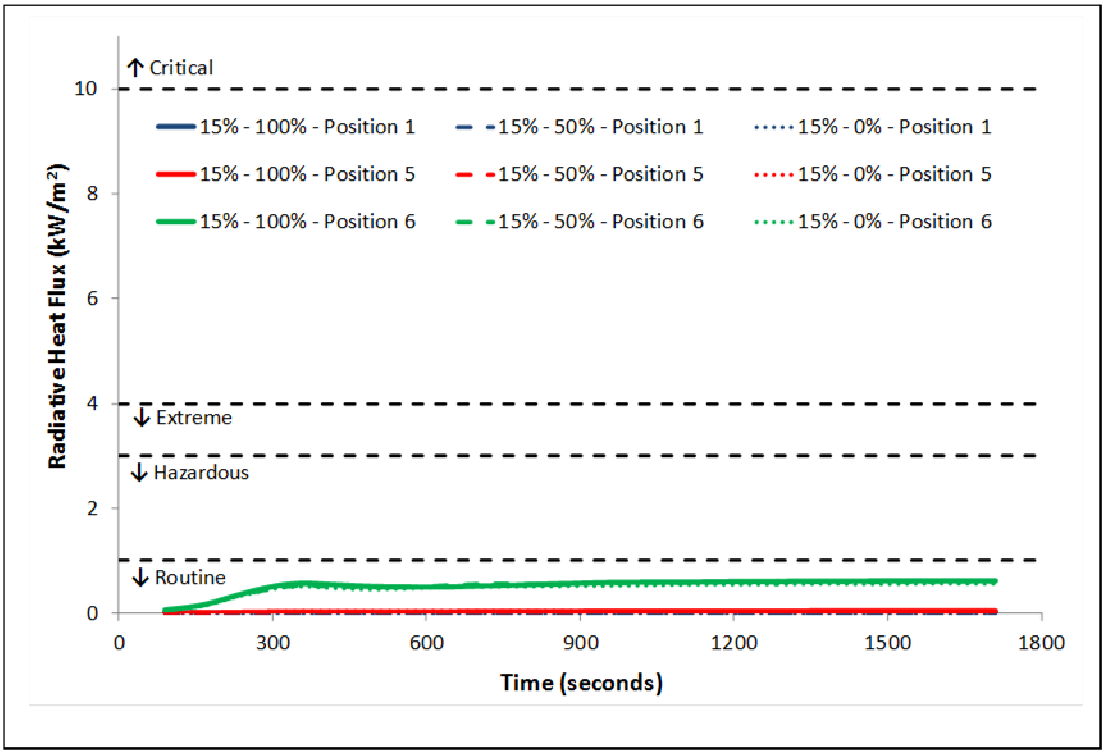

Figure 62: Comparison of smoothed radiative heat flux data from FDS at a height of 1.5 m in large warehouse with rapid t^3 fire growth and 15 % roof venting area.

In Figure 62, radiative heat flux measurements 1.5 m above floor level are presented for three selected targets in the large warehouse. At all positions in the warehouse, maximum radiative heat fluxes remained routine (*i.e.* less than 1 kW/m²) for all three inlet area sizes. Measurements at positions away from the fire are represented in the figure by the results at Position 1. Results for all positions can be found in Appendix E1. For all three inlet area scenarios, temperature measurements at a height

of 1.5 m above floor level were similarly benign (Figure 63). Temperatures remained near ambient, and therefore routine, at all positions for the entirety of the three simulations (see Appendix E1).

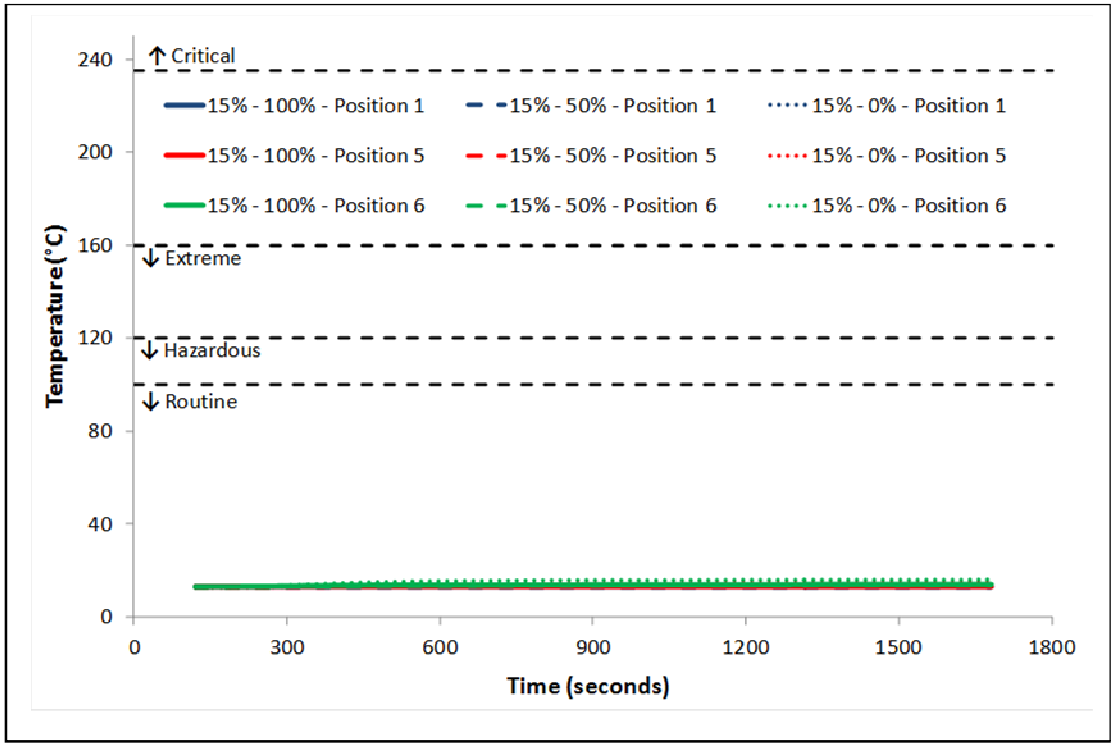

Figure 63: Comparison of smoothed temperature data from FDS at a height of 1.5 m in large warehouse with rapid t^3 fire growth and 15 % roof venting area.

Temperature distributions at heights of 1.5 m above the floor and 11.0 m above the floor (1 m below the ceiling) can be viewed with the aid of Smokeview slice files (Figure 64). For all simulations, temperatures showed only moderate increases in a defined area, regardless of the percentage of inlet area applied to the warehouse. However, with the exception of the area immediately above the fire, maximum temperatures in the upper layer did not exceed ~100°C.

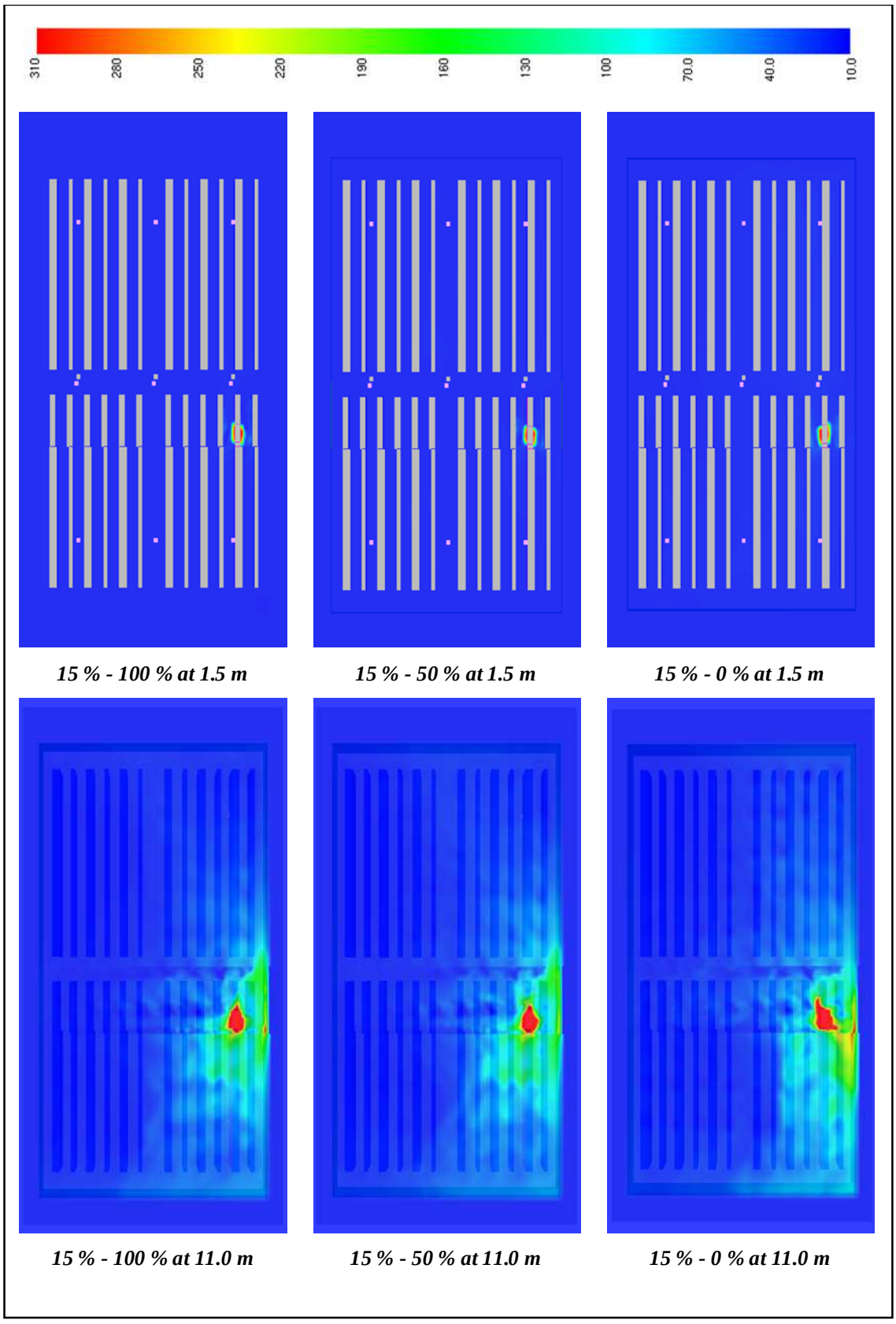

Figure 64: Comparison of temperature distributions after 1,800 seconds in large warehouse with rapid t^3 fire growth, 15 % roof venting area and inlet areas of 100 %, 50 %, and 0 % of roof venting area.

3.1.10 Phase 1c: Large warehouse - rapid t^3 fire growth & 10 % venting

With a reduction in roof venting area to 10 % of the warehouse floor area, a similar result was seen to that observed in Section 3.1.9 with the base case of 15 % roof venting (Figure 65). When inlet area for make-up air was equivalent to the roof venting area, a layer of clear air remained below the smoke layer. When inlet area was reduced to 50 % of the roof venting area, a clear layer remained although the smoke layer became deeper. And, with no inlet area provided, the smoke layer extended to the floor.

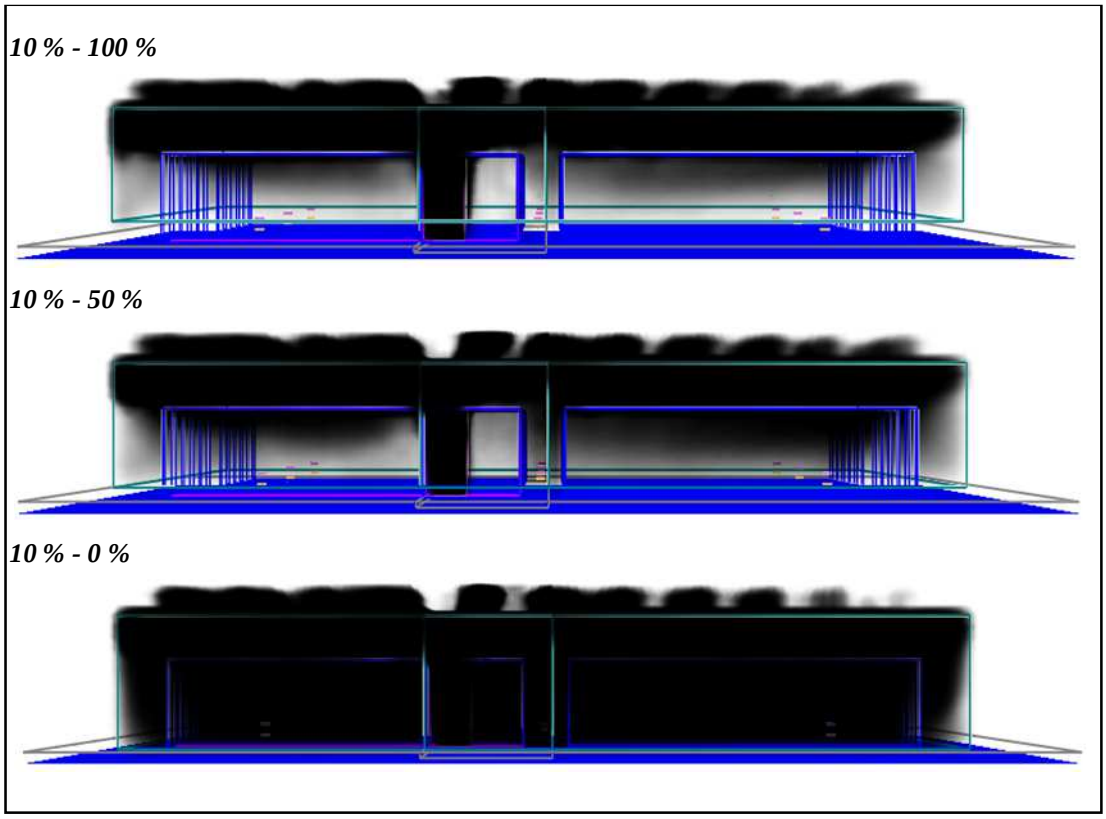

Figure 65: Smokeview depiction of smoke layer after 1,800 seconds in large warehouse with rapid t^3 fire growth and 10 % roof venting area (top – 100 % inlet area, middle – 50 % inlet area, and bottom – 0 % inlet area).

In Figure 66, this smoke layer development is depicted with the use of slice file images of visibility. In the upper-most image, with 100 % inlet area, the bottom of the smoke layer coincides with the top of the rack storage. The middle image shows the penetration of the smoke layer into the aisles between the rack storage when the area of make-up air inlets was reduced to 50 % of roof venting area. And finally, the

lower-most image depicts the smoke layer extending to floor level for more than half of the length of the warehouse when no inlet area for make-up air was provided. The black colouration in the images demarcates the 10-metre visibility boundary: below the line, visibility is better than 10 m, and above the line, visibility is less than 10 m.

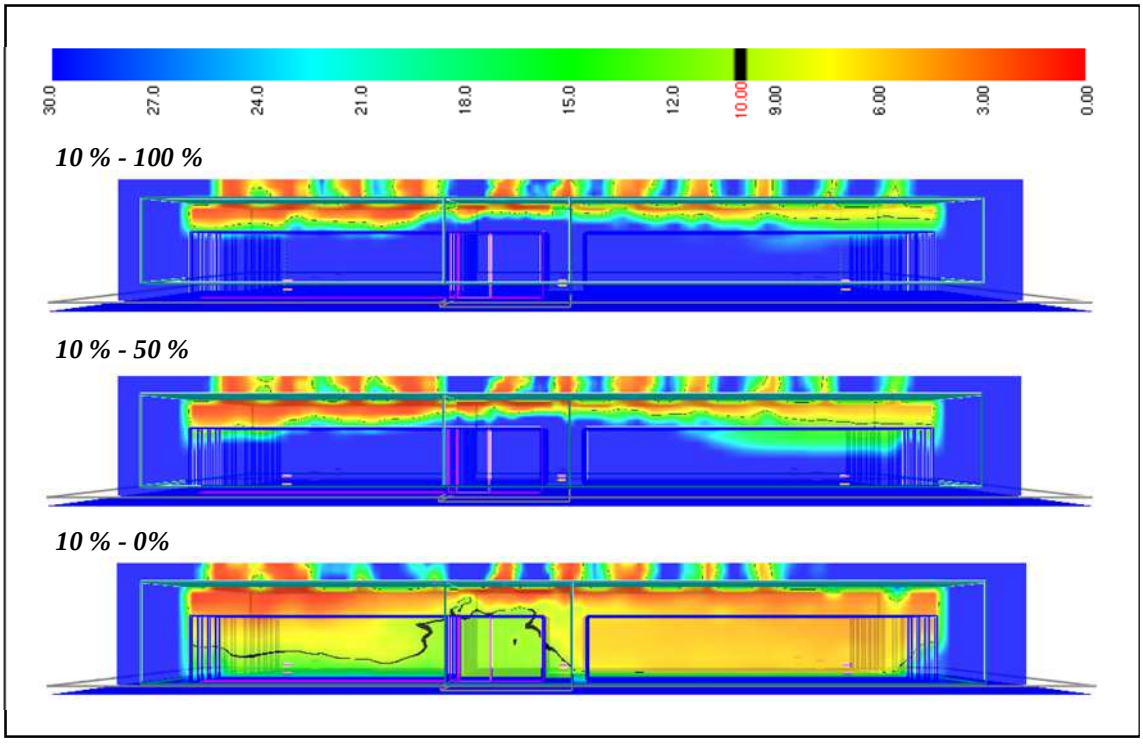

Figure 66: Visibility (m) after 1,800 seconds in large warehouse with rapid t^3 fire growth and 10 % roof venting area (top – 100 % inlet area, middle – 50 % inlet area, and bottom – 0 % inlet area). Slice is taken through long axis of warehouse, 20 m inside nearest warehouse wall.

Radiative heat fluxes and temperatures measured at 1.5 m above the floor were very little changed in the simulations with 10 % roof venting area than was seen in the simulations with 15 % roof venting area. These results are not described here, but are presented in Appendix E2. Upper layer temperature distributions were not substantially different to the case with 15 % venting and are not presented here.

3.1.11 Phase 1c: Large warehouse - rapid t^3 fire growth & 5 % venting

The application of just 5 % roof venting in the large warehouse had the effect of further thickening the smoke layer (Figure 67 *cf*. Figure 65). As in previous simulations, a layer of clear air remained below the smoke layer for both the 100 % and 50 % inlet area cases, and in the simulation with 0 % inlet area for make-up air, a

clear layer was unable to be maintained. This result is confirmed in the slice files of visibility taken through the long axis of the warehouse (Figure 68). In both the upper-most and middle images in the figure, the bottom of the smoke layer is clearly delineated at about the same height as the top of the storage racks, as seen in previous sections. In the lower-most image, visibility reduced to 0 m within 10 minutes following the outbreak of fire, and remained this way to the end of the simulation.

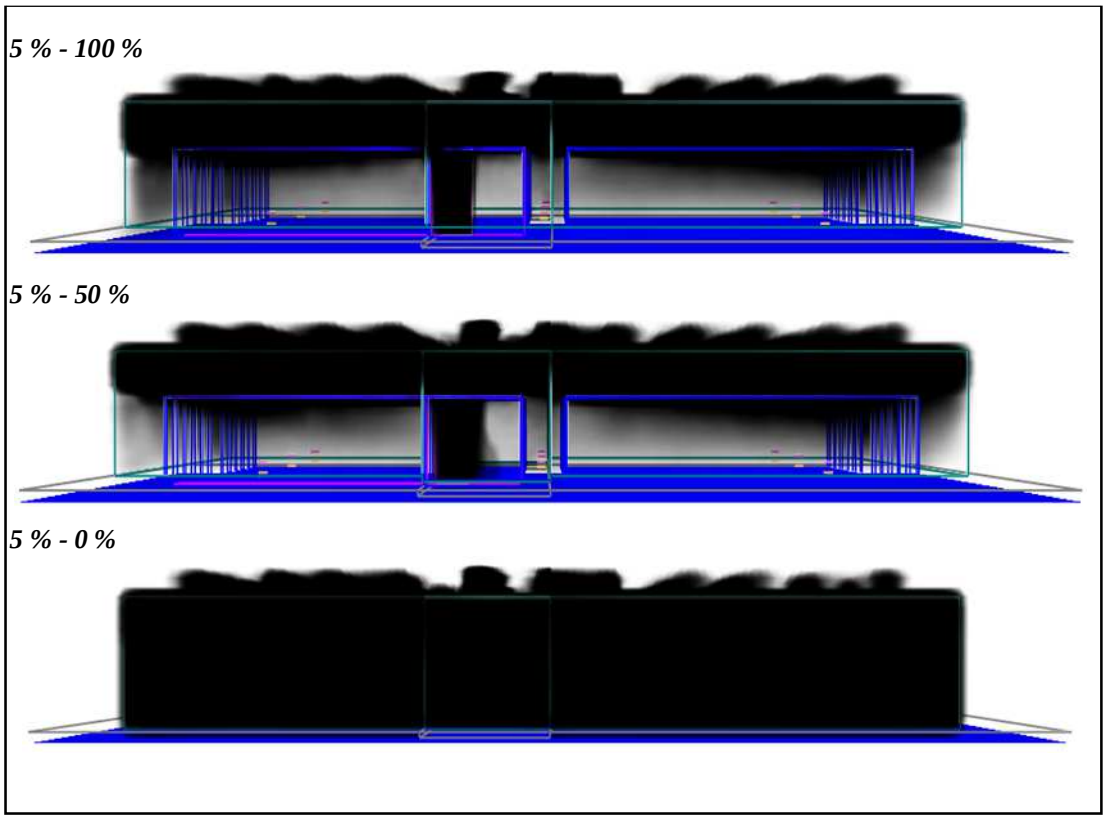

Figure 67: Smokeview depiction of smoke layer after 1,800 seconds in large warehouse with rapid t^3 fire growth and 5 % roof venting area (top – 100 % inlet area, middle – 50 % inlet area, and bottom – 0 % inlet area).

Minimal differences were observed for radiative heat flux measurements in the simulations with 5 % roof venting area. The results for all positions can be seen in Appendix E3. In contrast, there was a notable effect on temperatures recorded at 1.5 m above the floor. With just 5 % roof venting area and 0 % inlet area for make-up air, lower layer temperatures were well above the ambient at all positions (Figure 69). However, the highest temperature achieved among the nine targets was 40.2°C; this is well inside the Routine Conditions criterion of the FBIM. Temperature results at all positions and for all three simulations can also be found in Appendix E3.

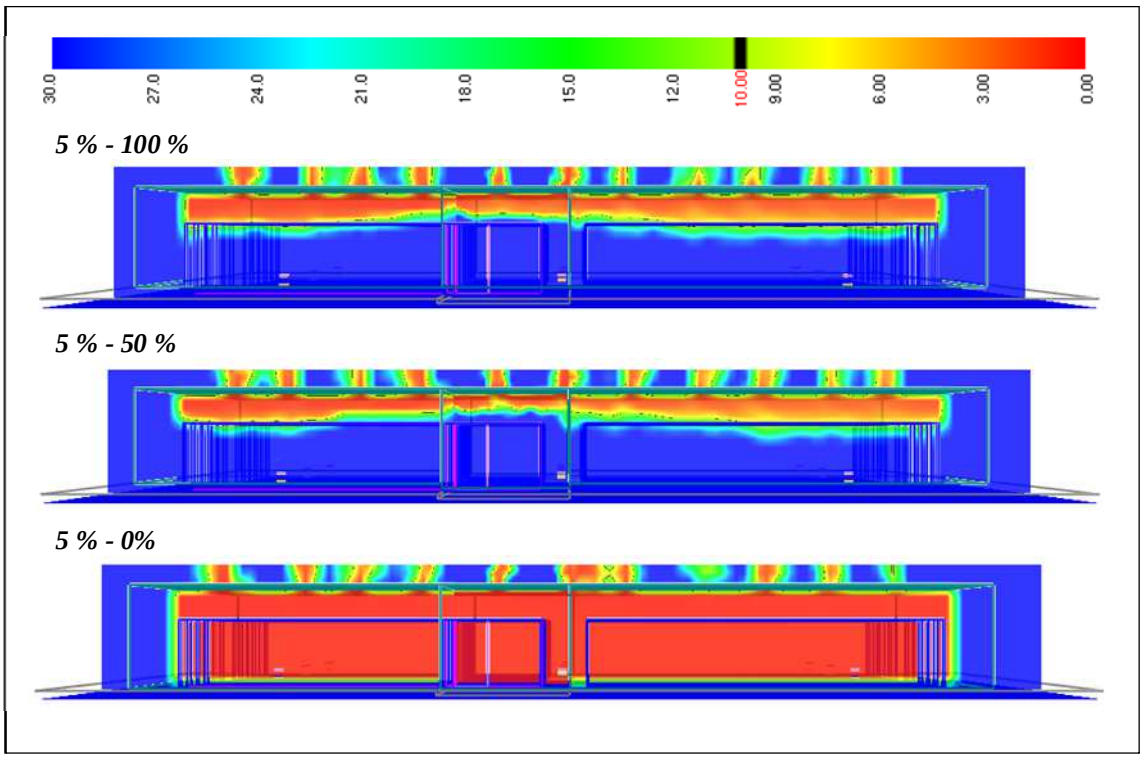

Figure 68: Visibility (m) after 1,800 seconds in large warehouse with rapid t^3 fire growth and 5 % roof venting area (top – 100 % inlet area, middle – 50 % inlet area, and bottom – 0 % inlet area). Slice is taken through long axis of warehouse, 20 m inside nearest warehouse wall.

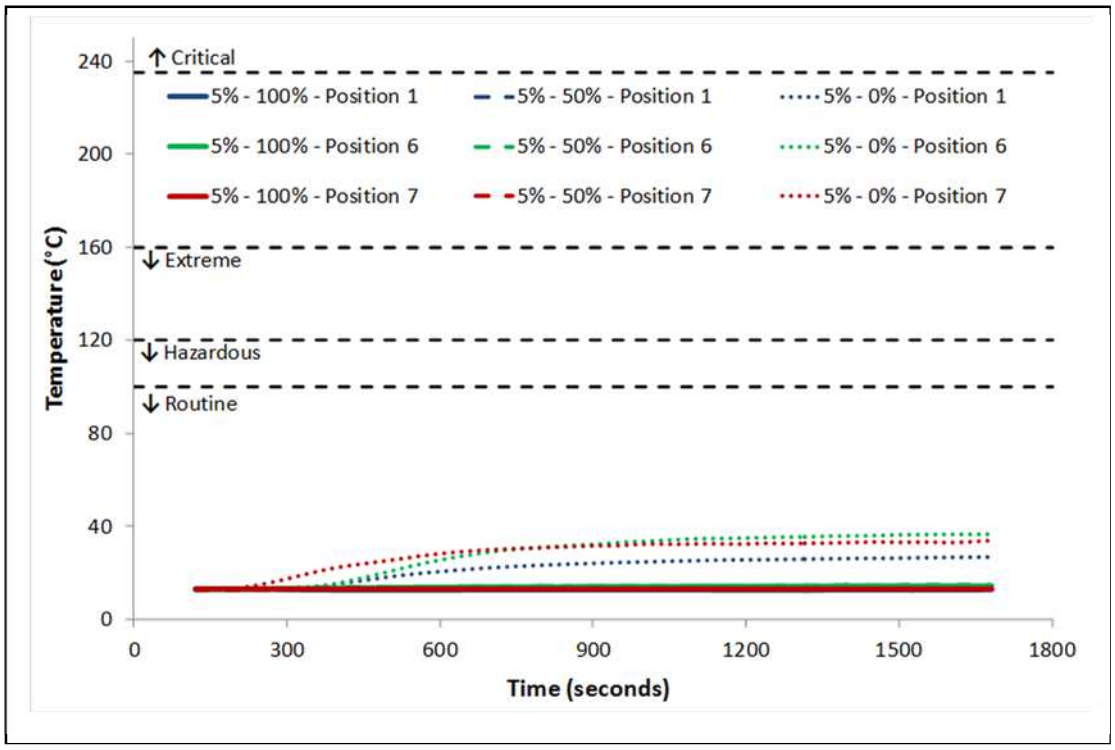

Figure 69: Comparison of smoothed temperature data from FDS at a height of 1.5 m in large warehouse with rapid t^3 fire growth and 5 % roof venting area.

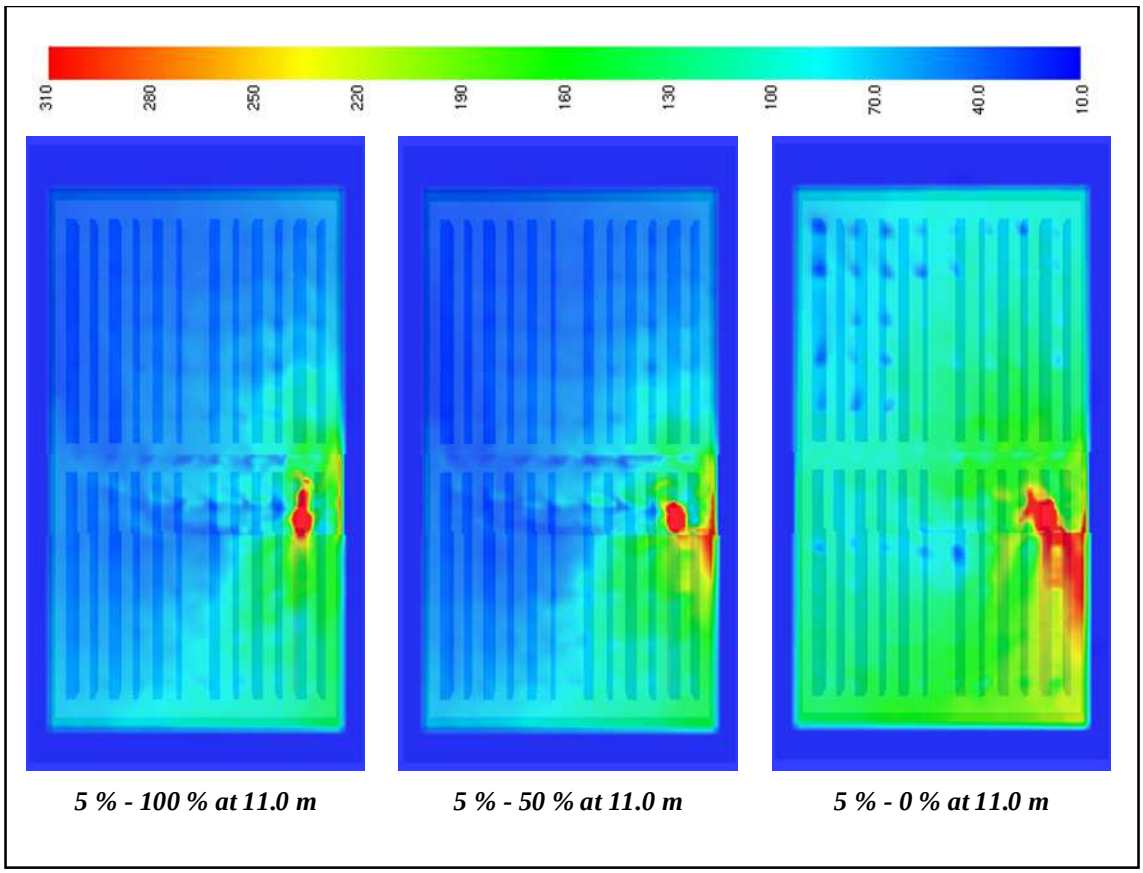

Figure 70: Comparison of temperature distributions after 1,800 seconds in large warehouse with rapid t^3 fire growth, 5 % roof venting area and inlet areas of 100 %, 50 %, and 0 %.

Figure 70 displays the temperature distributions 1 m below the ceiling in the large warehouse with 5 % roof venting area. While in previous large warehouse simulations with large roof venting areas, upper layer temperatures remained below ~100°C (*cf.* Figure 62), in the latter simulation, with 0 % inlet area, upper layer temperatures approached, and in places exceeded ~220°C. Such temperatures are close to the maximum air temperature of 280°C in the upper layer under the Extreme Conditions criterion of the FBIM. IF such a temperature were to be reached, it would shorten the time allowed for fire-fighters in the warehouse from 25 minutes with routine conditions to 1 minute: enough time to conduct a snatch rescue or to make a retreat from more threatening conditions.

3.1.12 Phase 1d: Large warehouse - extreme t^3 fire growth & 15 % venting

Introduction of an extreme t^3 fire growth rate in the large warehouse made very little difference to smoke layer development during the 1,800-second simulation than was

observed with rapid t^3 fire growth (Figure 71 *cf*. Figure 60). With inlet areas of both 100 % and 50 % of the roof venting area, the smoke layer remained at or just below the top of the storage racks. Further reduction of inlets for make-up air to 0 % of the roof venting area, resulted in the smoke layer descending to the floor. However, as was observed with rapid t^3 fire growth in the large warehouse (refer to Figure 61), slice files of visibility indicate that depth of the smoke layer is inconsistent along the length of the warehouse (Figure 72): there is a pocket of low visibility (*i.e*. less than 10 m) between the storage racks, on the right-hand side of the lower-most image in the figure, but visibility is acceptable for fully-equipped fire-fighters in the left-hand side of the same image.

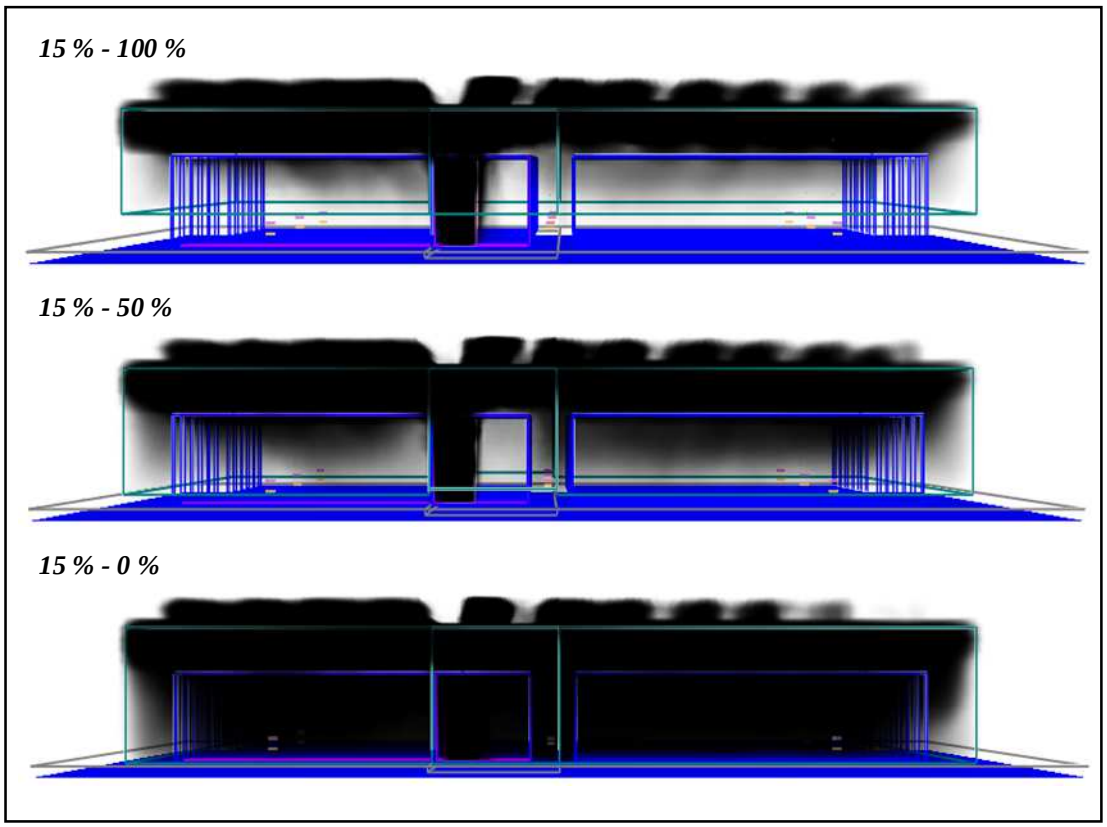

Figure 71: Smokeview depiction of smoke layer after 1,800 seconds in large warehouse with extreme t^3 fire growth and 15 % roof venting area (top – 100 % inlet area, middle – 50 % inlet area, and bottom – 0 % inlet area).

Figure 73 shows radiative heat flux measurements at three selected targets in the large warehouse. At all positions, and for all three sizes of inlets for make-up air, maximum radiative heat fluxes remained routine (*i.e*. less than 1 kW/m²). Results for all positions can be found in Appendix F1.

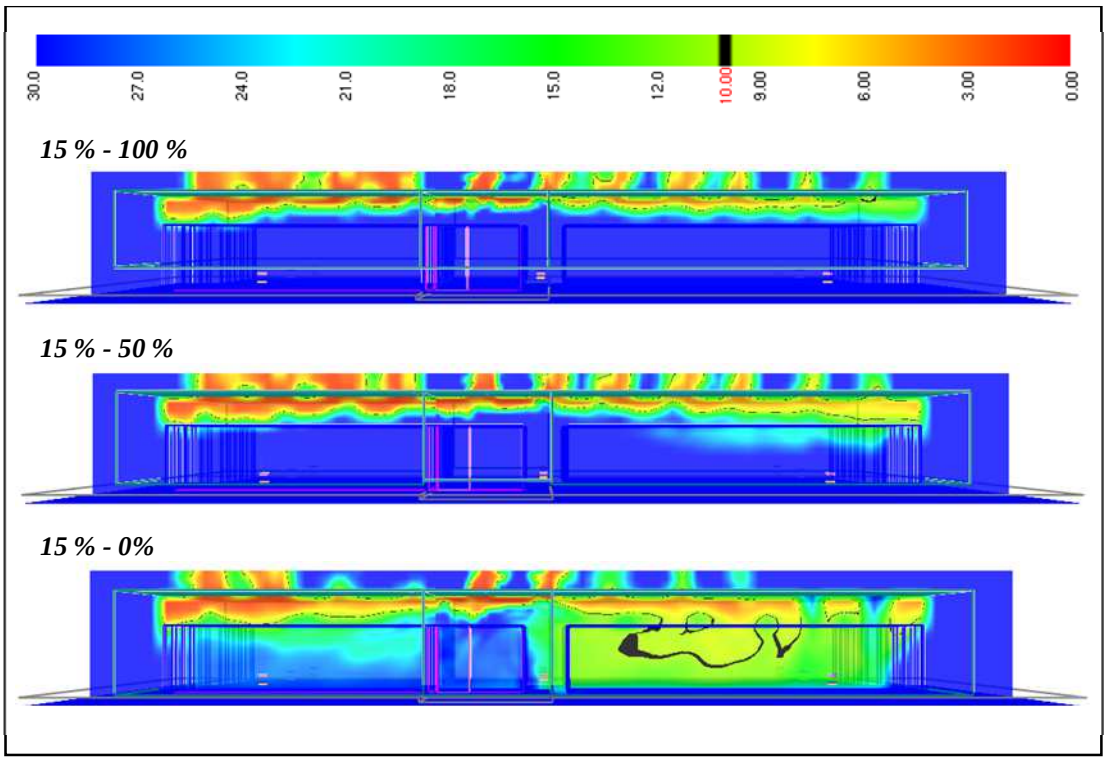

Figure 72: Visibility (m) after 1,800 seconds in large warehouse with extreme t^3 fire growth and 15 % roof venting area (top – 100 % inlet area, middle – 50 % inlet area, and bottom – 0 % inlet area). Slice is taken through long axis of warehouse, 20 m inside nearest warehouse wall.

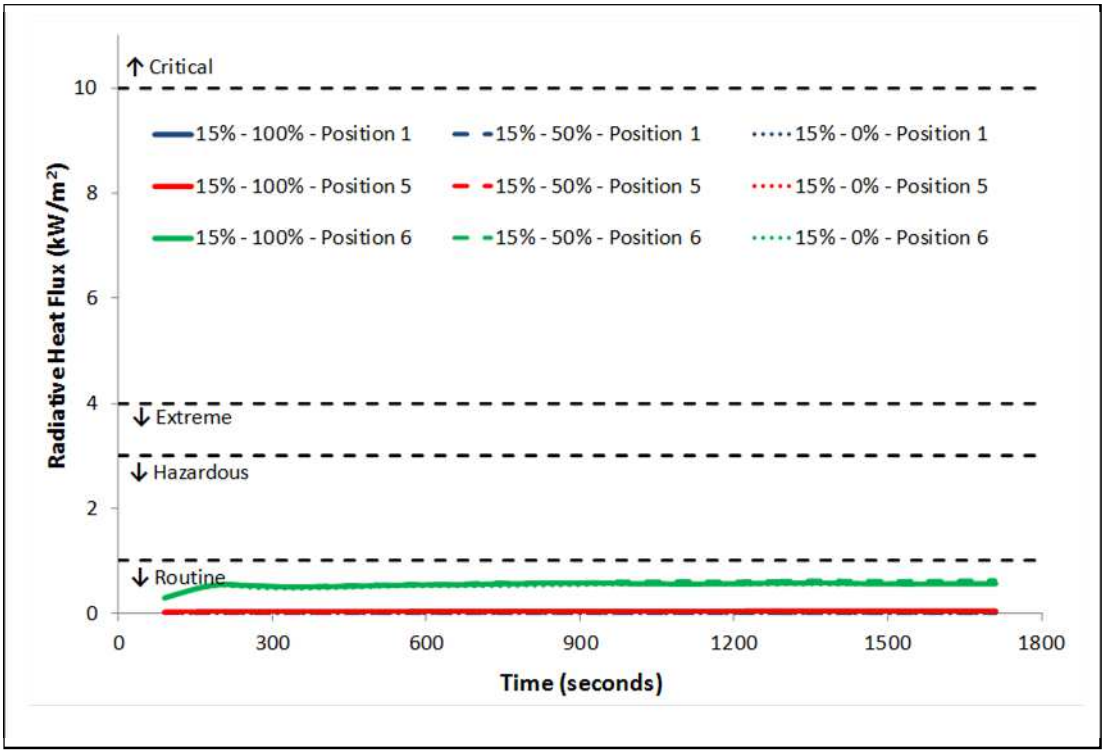

Figure 73: Comparison of smoothed radiative heat flux data from FDS at a height of 1.5 m in large warehouse with extreme t^3 fire growth and 15 % roof venting area.

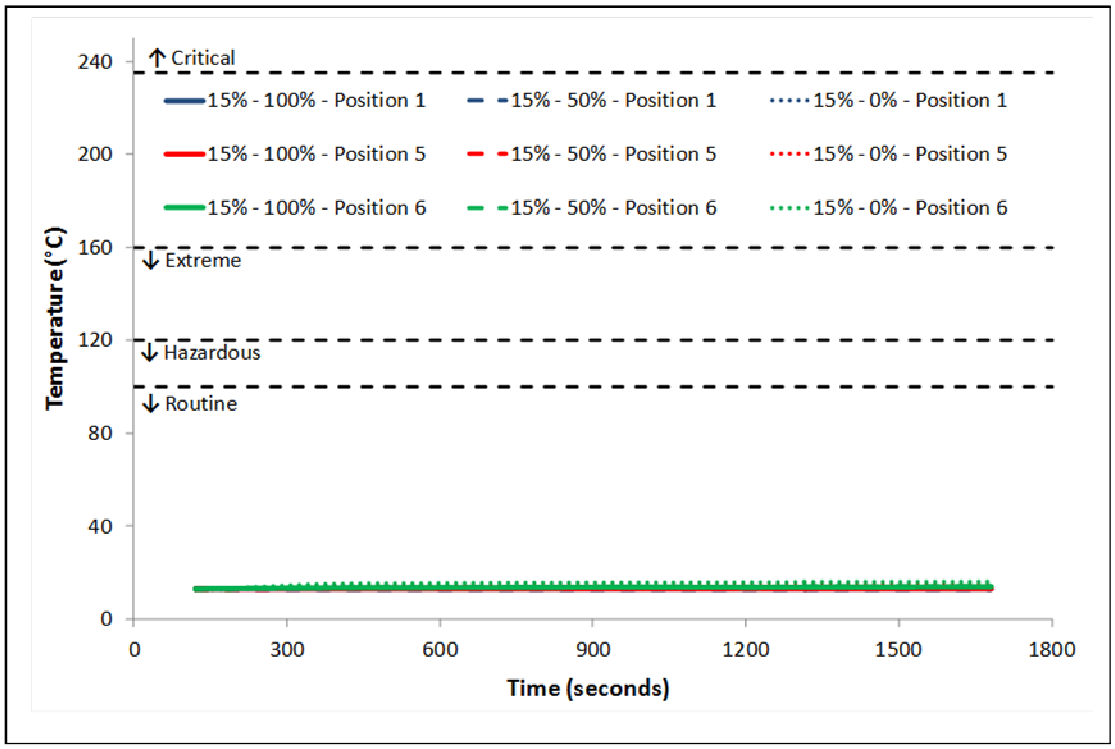

Figure 74: Comparison of smoothed temperature data from FDS at a height of 1.5 m in large warehouse with extreme t^3 fire growth and 15 % roof venting area.

For all three inlet area scenarios, temperature measurements at a height of 1.5 m above floor level remained almost ambient (Figure 74). Results for all positions can be found in Appendix F1.

3.1.13 Phase 1d: Large warehouse – extreme t^3 fire growth & 10 % venting

Smokeview depictions of the smoke layer revealed a similar result for the 10 % roof venting scenarios as was observed with 15 % roof venting area in Section 3.1.12 (Figure 75 *cf*. Figure 71). For inlet areas of 100 % and 50 % of the roof venting area, a layer of clear air remained visible beneath the smoke layer. The warehouse became smoke-logged when inlet area was removed totally. A corresponding decrease in visibility resulted from this increase in smoke layer depth (Figure 76): visibility remained close to 30 m at head height when make-up air was supplied to the lower region of the warehouse, but total removal of the make-up air supply reduced visibility throughout the warehouse to less than 10 m at the same height.

Radiative heat fluxes and temperatures in the lower layer with extreme t^3 fire growth were similar to the cases with rapid t^3 fire growth, and can be found in Appendix F2.

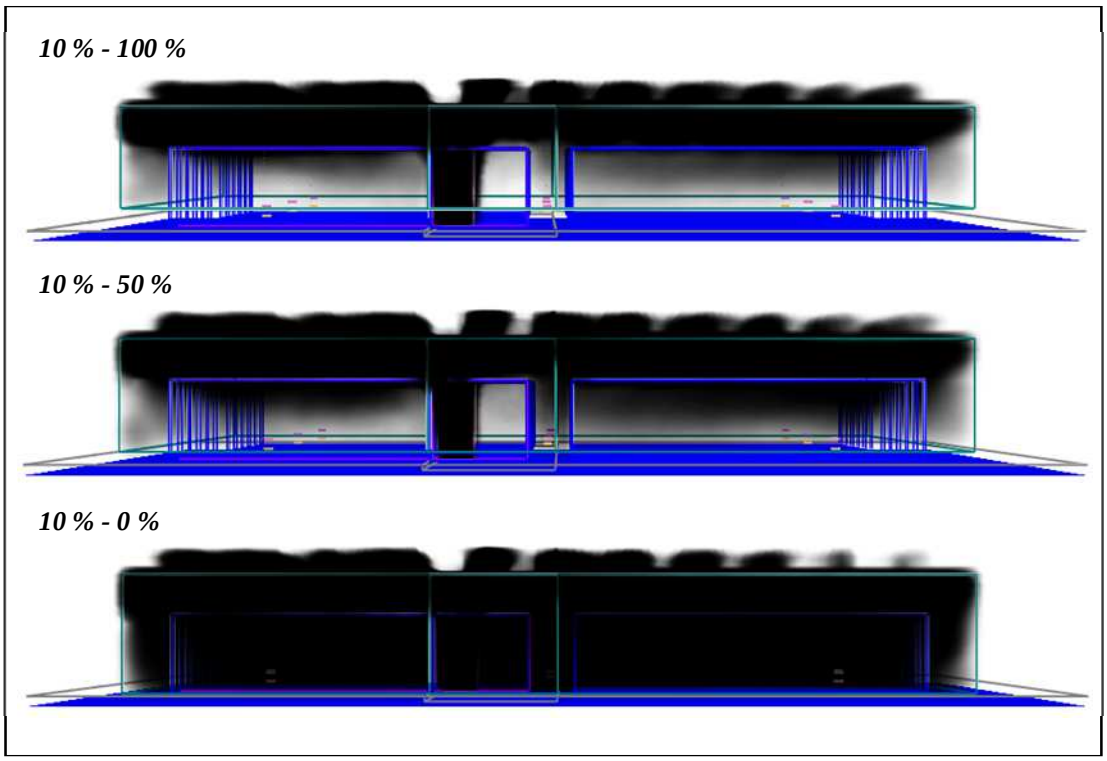

Figure 75: Smokeview depiction of smoke layer after 1,800 seconds in large warehouse with extreme t^3 fire growth and 10 % roof venting area (top – 100 % inlet area, middle – 50 % inlet area, and bottom – 0 % inlet area).

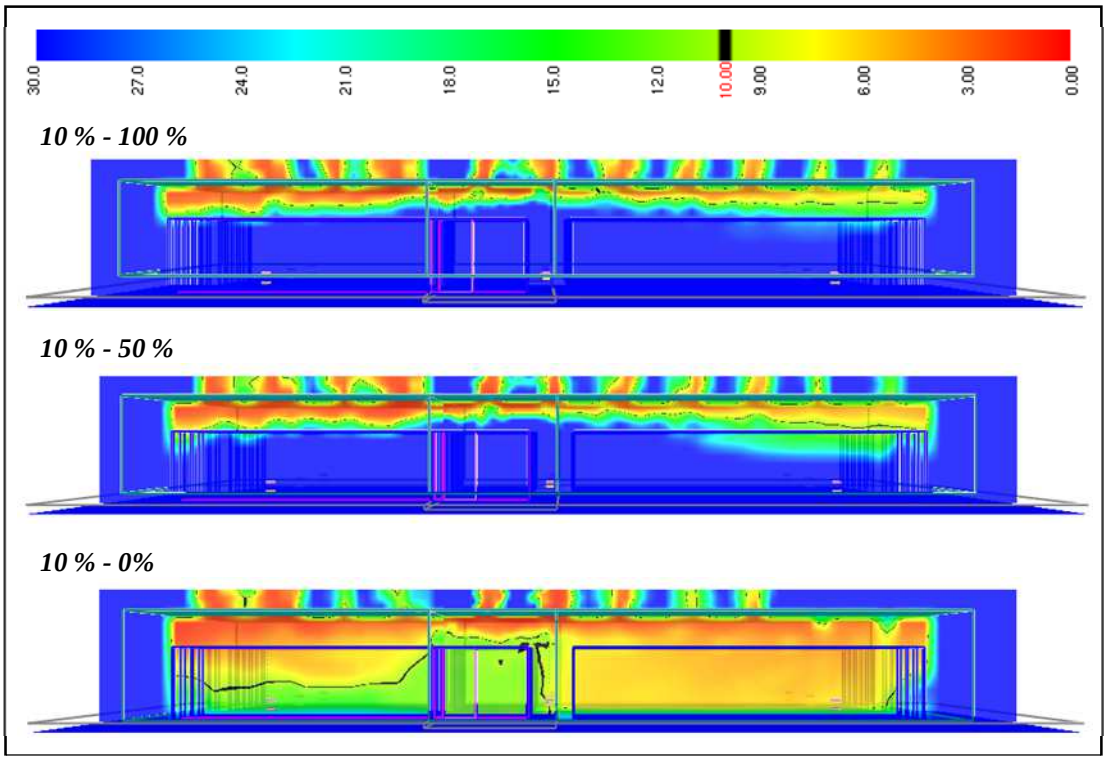

Figure 76: Visibility (m) after 1,800 seconds in large warehouse with extreme t^3 fire growth and 10 % roof venting area (top – 100 % inlet area, middle – 50 % inlet area, and bottom – 0 % inlet area). Slice is taken through long axis of warehouse, 20 m inside nearest warehouse wall.

3.1.14 Phase 1d: Large warehouse - extreme t^3 fire growth & 5 % venting

With just 5 % roof venting area, smoke layer depth reduced even further compared to the cases with 15 % and 10 % roof venting (Figure 77). This trend corresponds to that seen in the simulations with a rapid t^3 fire growth rate (Sections 3.1.9 to 3.1.11). The deeper smoke layer was matched by decreased visibility, as compared to the cases with more roof venting area (Figure 78 *cf.* Figure 72 and Figure 76). With both 100 % and 50 % inlet area for make-up air, a layer of clear air remained below the storage racks, as seen for all previous simulations with corresponding inlet areas. However, the reduction of inlet area to 0 % of roof venting area removed all visibility in the warehouse within 10 minutes.

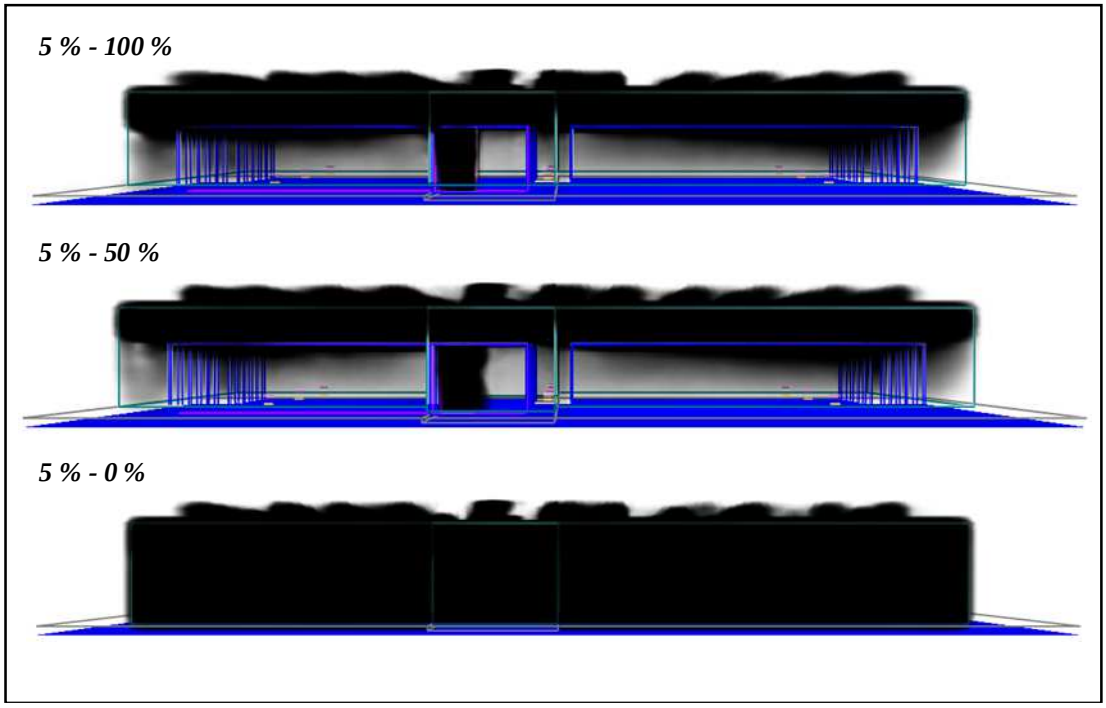

Figure 77: Smokeview depiction of smoke layer after 1,800 seconds in large warehouse with extreme t^3 fire growth and 5 % roof venting area (top – 100 % inlet area, middle – 50 % inlet area, and bottom – 0 % inlet area).

In Figure 79, lower layer temperatures in the large warehouse are represented by measurements at three targets. Removal of inlet area produced an increase in temperatures to be at or above 30°C at all positions. Temperatures, however, remained well-within the Routine Conditions criterion. Appendix F3 displays results for temperatures and radiative heat fluxes at all positions.

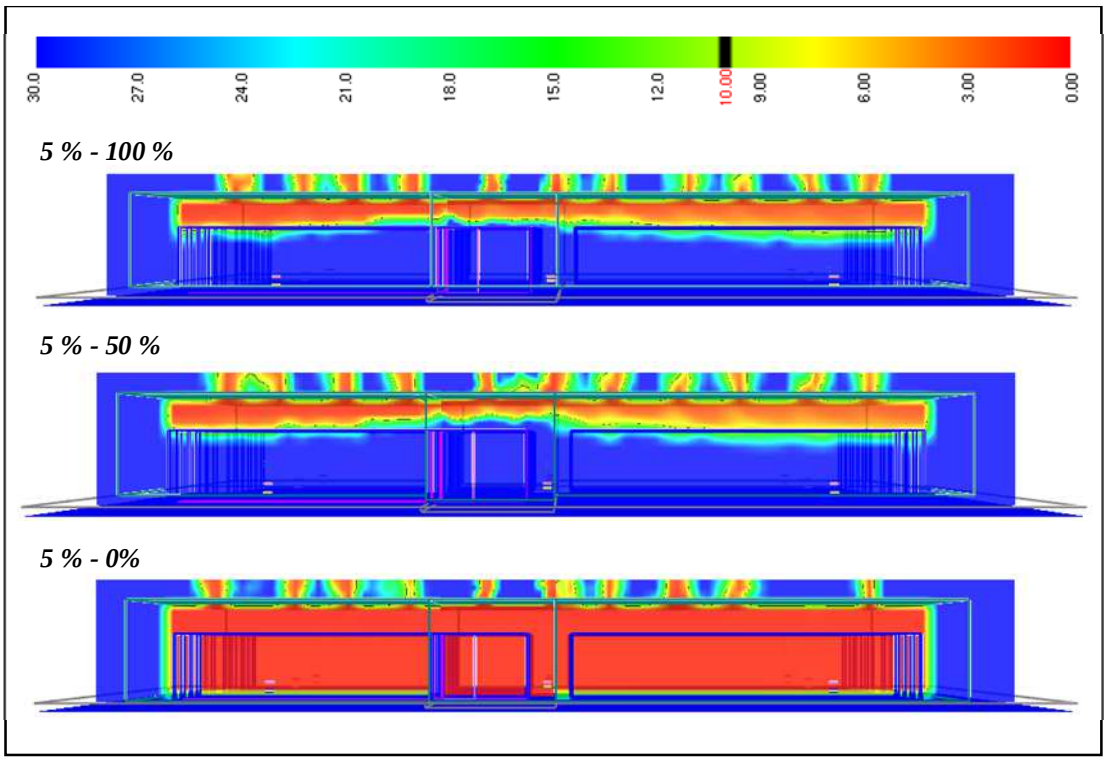

Figure 78: Visibility (m) after 1,800 seconds in large warehouse with extreme t^3 fire growth and 5 % roof venting area (top – 100 % inlet area, middle – 50 % inlet area, and bottom – 0 % inlet area). Slice is taken through long axis of warehouse, 20 m inside nearest warehouse wall.

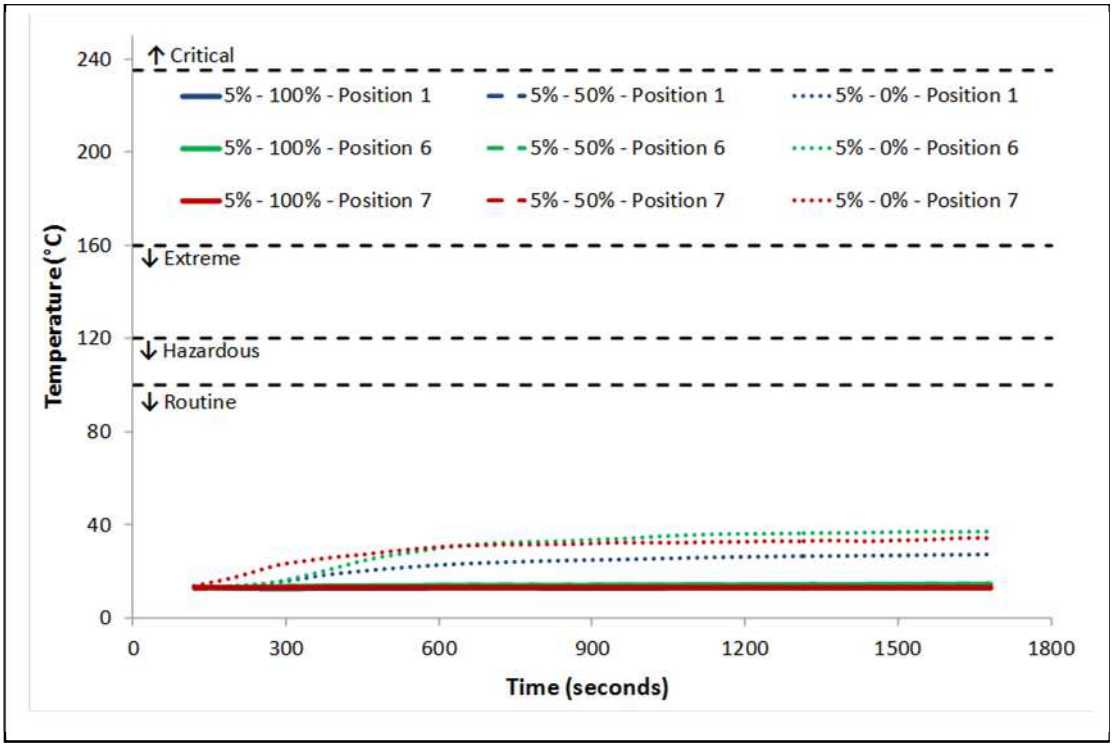

Figure 79: Comparison of smoothed temperature data from FDS at a height of 1.5 m in large warehouse with extreme t^3 fire growth and 5 % roof venting area.

3.2 Phase Two: Vent Design and Timing of Vent Opening

3.2.1 Phase 2: Simulations in the small & large warehouses

Roof venting area of 5 % of floor area, along with 50 % make-up air area, was selected for use in further simulations for Phases Two and Three of this project. In Phase One simulations in both the small and the large warehouse, this combination of roof venting and inlets for make-up air minimized the area a building owner would need to set-aside for fire venting purposes, while maintaining routine conditions at positions away from the fire, on the outer edges of the warehouse. Further reduction of inlet area to 0 % was considered disadvantageous due to the reduction of visibility to 0 m within a 10-minute timeframe: meaning that fire-fighter entry would already not be possible upon arrival.

Presented in Table 8 are the summary results from the second phase of testing in both the small and the large warehouses. For each warehouse size and fire growth rate, six combinations of vent shape, vent opening progression and vent activation temperature were tested, with the stated objective from Section 1.4 being to model the effectiveness of sequential versus simultaneous opening of vents in providing the Fire Brigade Intervention Model fire-fighter tenability criteria.

With a rapid t^3 fire growth rate in the small warehouse, with 5 % permanently-open roof venting area and an inlet area for make-up air of 50 % of the roof venting area, maximum radiative heat flux was 4.8 kW/m² close to the fire and 0.9 kW/m² away from the fire. Maximum temperature was 20.1°C close to the fire and 19.3°C away from the fire (see Table 6). Introduction of vents that were closed at the start of the simulation and opened simultaneously when the temperature at any one vent exceeded 100°C had no practical effect on radiation or temperature conditions in the warehouse: maximum recorded radiative heat flux was 5.1 kW/m² near the fire and 0.9 kW/m² away from the fire, and maximum recorded temperature was 20.1°C near the fire and 19.3°C away from the fire (Table 8).

Table 8 – Summary of maximum results for Phase 2 simulations in small and large warehouses.

Warehouse	Fire growth	Vent shape	Opening Sequence	Opening Temperature	Radiation near fire[1] (kW/m^2 - Criterion)	Radiation away from fire (kW/m^2 - Criterion)	Temperature near fire[1] (°C - Criterion)	Temperature away from fire (°C - Criterion)
Small	Rapid	Square	Simultaneous	100°C	5.1 - Extreme$^+$	0.9 - Routine	20.3 - Routine	19.4 - Routine
Small	Rapid	Square	Sequential	100°C	5.0 - Extreme$^+$	0.9 - Routine	20.1 - Routine	19.3 - Routine
Small	Rapid	Square	Sequential	200°C	4.9 - Extreme$^+$	0.9 - Routine	20.2 - Routine	20.3 - Routine
Small	Rapid	Square	Sequential	300°C	4.8 - Extreme$^+$	1.1 - Hazardous	24.3 - Routine	24.3 - Routine
Small	Rapid	Strips	Sequential	200°C	3.5 - Extreme	1.1 - Hazardous	19.3 - Routine	19.7 - Routine
Small	Rapid	Strips	Sequential	300°C	3.4 - Extreme	1.0 - Hazardous	20.3 - Routine	29.9 - Routine
Small	Extreme	Square	Simultaneous	100°C	5.1 - Extreme$^+$	0.9 - Routine	20.4 - Routine	19.5 - Routine
Small	Extreme	Square	Sequential	100°C	5.0 - Extreme$^+$	0.9 - Routine	20.3 - Routine	19.5 - Routine
Small	Extreme	Square	Sequential	200°C	4.9 - Extreme$^+$	0.9 - Routine	19.8 - Routine	20.3 - Routine
Small	Extreme	Square	Sequential	300°C	4.9 - Extreme$^+$	1.0 - Hazardous	24.8 - Routine	24.2 - Routine
Small	Extreme	Strips	Sequential	200°C	3.4 - Extreme	1.1 - Hazardous	19.2 - Routine	20.9 - Routine
Small	Extreme	Strips	Sequential	300°C	3.5 - Extreme	1.0 - Hazardous	20.8 - Routine	28.0 - Routine
Large	Rapid	Square	Simultaneous	100°C	1.2 - Hazardous	0.1 - Routine	14.6 - Routine	14.3 - Routine
Large	Rapid	Square	Sequential	100°C	1.0 - Hazardous	0.2 - Routine	15.1 - Routine	14.4 - Routine
Large	Rapid	Square	Sequential	200°C	0.7 - Routine	0.1 - Routine	14.7 - Routine	17.1 - Routine
Large	Rapid	Square	Sequential	300°C	0.4 - Routine	0.2 - Routine	16.0 - Routine	20.5 - Routine
Large	Rapid	Strips	Sequential	200°C	1.2 - Hazardous	0.2 - Routine	15.4 - Routine	17.0 - Routine
Large	Rapid	Strips	Sequential	300°C	0.4 - Routine	0.2 - Routine	21.5 - Routine	22.0 - Routine
Large	Extreme	Square	Simultaneous	100°C	1.2 - Hazardous	0.1 - Routine	18.9 - Routine	14.6 - Routine
Large	Extreme	Square	Sequential	100°C	1.0 - Hazardous	0.2 - Routine	18.9 - Routine	14.8 - Routine
Large	Extreme	Square	Sequential	200°C	0.6 - Routine	0.1 - Routine	17.7 - Routine	18.4 - Routine
Large	Extreme	Square	Sequential	300°C	0.6 - Routine	0.2 - Routine	16.2 - Routine	20.1 - Routine
Large	Extreme	Strips	Sequential	200°C	0.6 - Routine	0.1 - Routine	19.1 - Routine	14.6 - Routine
Large	Extreme	Strips	Sequential	300°C	0.5 - Routine	0.1 - Routine	23.3 - Routine	23.2 - Routine

[1] Indicates Positions 5 and 6 only.
[+] Indicates that conditions exceeded the extreme criterion, but were not severe enough to be classed as critical.

Introduction of vents that opened sequentially as the temperature at each individual vent exceeded 100°C produced similar results: maximum radiative heat flux was 5.0 kW/m² near the fire and 0.9 kW/m² away from the fire, and maximum temperature was 20.2°C near the fire and 19.3°C away from the fire.

Increasing vent activation temperature for sequentially-opening roof venting to 200°C produced only minor changes to radiation and temperature conditions in the small warehouse. A subsequent increase of activation temperature to 300°C effected a change in FBIM criterion for radiative heat flux away from the fire from the Routine to the Hazardous Conditions criterion. However, near the fire, the tendency was for radiative heat fluxes to decrease slightly as activation temperature increased. In addition, maximum temperatures both near and away from the fire increased by ~4°C, but remained routine.

Utilisation of strip-shaped vents instead of square-shaped vents brought about large reductions in maximum radiative heat fluxes near the fire with 3.5 kW/m² recorded with a vent activation temperature of 200°C and 3.4 kW/m² with activation at 300°C. Away from the fire, radiative heat fluxes remained almost the same as in the simulations with square-shaped vents; they did not exceed 1.1 kW/m². Temperatures were also similar to the cases with square-shaped vents, except for those recorded away from the fire under strip-shaped vents that activated at 300°C, where the maximum increased to 29.9°C.

Maximum values for extreme t^3 fire growth in the small warehouse were almost identical to those described above for rapid t^3 fire growth and do not warrant further discussion.

In the large warehouse, the largest effect of changed vent-opening mechanism came with the increase of activation temperature from 100°C to 200°C. In the case of the lower activation temperature, radiative heat fluxes were considered hazardous under the FBIM, reaching values of 1.2 kW/m² and 1.0 kW/m² with simultaneous opening- and sequential opening, respectively, under both fire growth rate scenarios. With activation temperatures of 200°C and 300°C, maximum radiative heat fluxes reduced

substantially with both the rapid and extreme fire growth rates, to lie within the Routine Conditions criterion of the FBIM. The same was true strip-shaped vents.
An anomaly was observed in the case of the rapid fire growth rate in the large warehouse with strip vents opening at an activation temperature of 200°C, where the maximum radiative heat flux increased to 1.2 kW/m². This increase occurred in the final seconds of simulation, leaving insufficient time for the next unactivated sensor to react. Prior to this, radiative heat fluxes had also remained within the Routine Conditions criterion.

Maximum temperatures in the lower layer of the large warehouse did not differ substantially among the twelve simulations, and in all cases remained routine, with a maximum temperature of 23.3°C recorded.

3.2.2 Phase 2a: Small warehouse – rapid t^3 fire growth & square-shaped roof vents opening simultaneously at an activation temperature of 100°C

Depictions of the smoke layer from Smokeview show that there is very little effect of delayed vent opening times to be seen in the small warehouse (Figure 80 *cf.* Figure 46 and Figure 47). The activation temperature of 100°C was reached after 50 seconds, and all 27 vents opened. As was seen with roof venting that was permanently open from the start of the simulation, visibility remained higher than 10 m in the majority of the lower layer; the exception being *fingers* of low visibility between the rack storage units.

Radiative heat fluxes were also similar at all positions in the warehouse (Figure 81 *cf.* Figure 48): near the fire, radiative heat fluxes reached well into and beyond the Extreme Conditions criterion of the FBIM; away from the fire, conditions stayed routine. Similarly, temperatures 1.5 m above floor level were little changed from the case with permanently-open vents examined in Section 3.1.4 (Figure 82 *cf.* Figure 49): temperatures remained routine for the duration of the simulation, with 20.3°C being the maximum temperature recorded at this height (*cf.* 20.1°C with permanently-open vents).

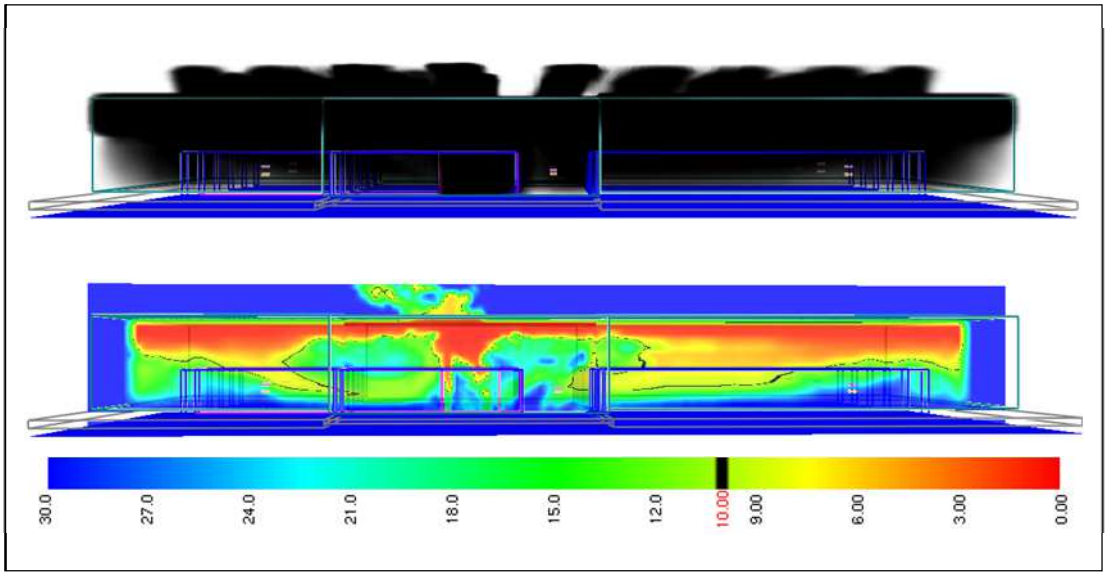

Figure 80: Smokeview depiction of smoke layer after 1,800 seconds (top) and visibility in metres (bottom) in small warehouse with rapid t^3 fire growth and square-shaped roof vents opening simultaneously at an activation temperature of 100°C. Visibility slice is taken through long axis of warehouse, 10 m inside nearest warehouse wall.

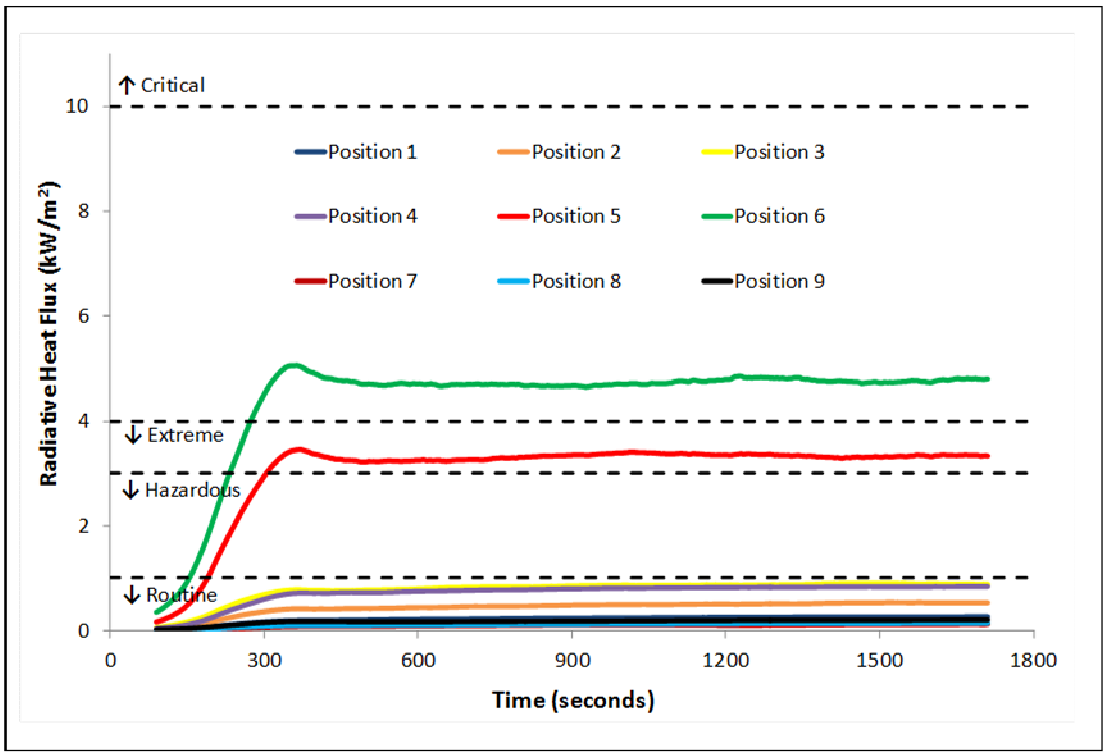

Figure 81: Comparison of smoothed radiative heat flux data from FDS at a height of 1.5 m in small warehouse with rapid t^3 fire growth and square-shaped roof vents opening simultaneously at an activation temperature of 100°C.

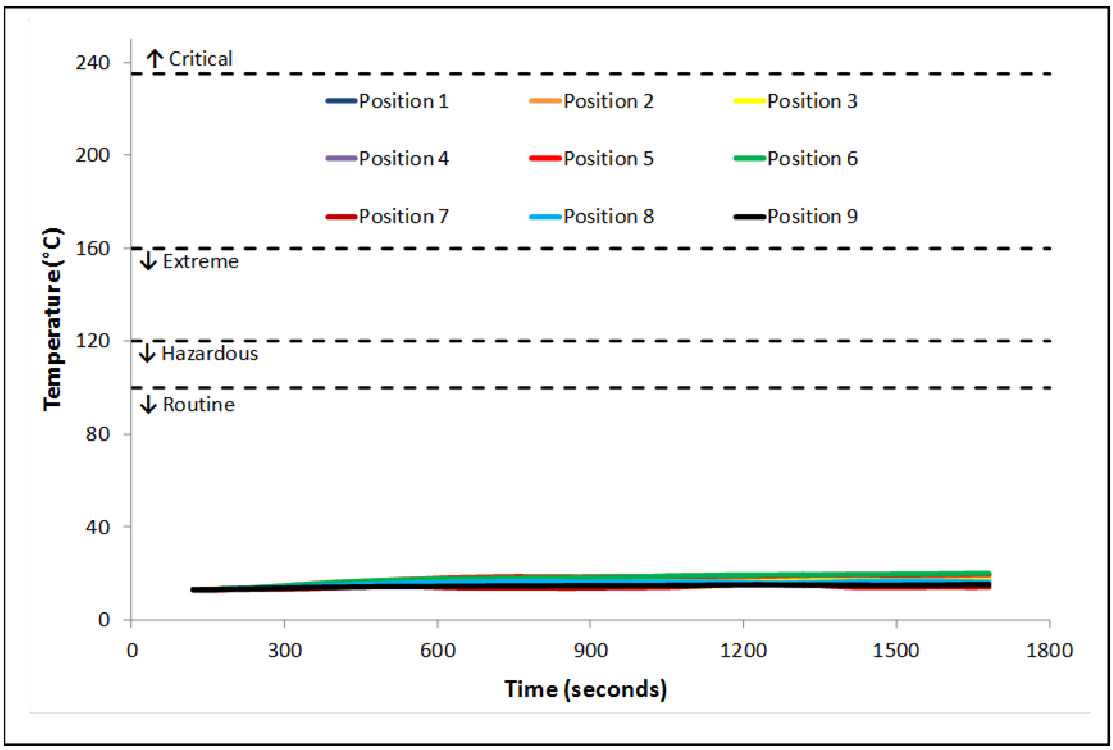

Figure 82: Comparison of smoothed temperature data from FDS at a height of 1.5 m in small warehouse with rapid t^3 fire growth and square-shaped roof vents opening simultaneously at an activation temperature of 100°C.

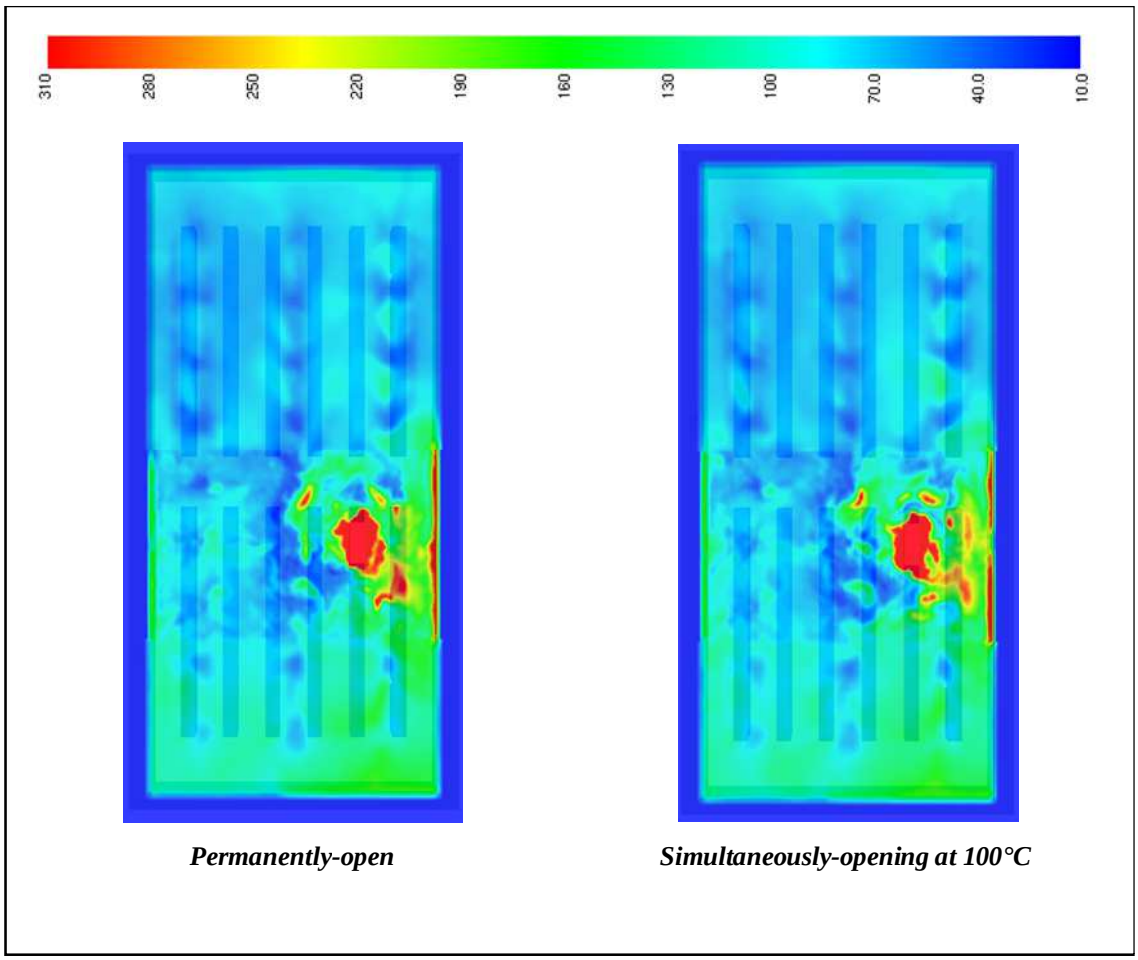

Figure 83: Comparison of temperature distributions at a height of 5.5 m after 1,800 seconds in small warehouse with rapid t^3 fire growth: permanently-open square-shaped roof vents versus square-shaped roof vents opening simultaneously at an activation temperature of 100°C.

Temperature distributions in the upper layer were almost identical to those observed in the case with permanently-open vents (Figure 83). In both cases, temperatures were generally no higher than ~130°C, apart from the area in the immediate vicinity of the fire plume.

3.2.3 Phase 2a: Small warehouse – rapid t^3 fire growth & square-shaped roof vents opening sequentially at three different activation temperatures

A Smokeview image of the smoke layer in the small warehouse, with sequentially-opening roof vents and an activation temperature of 100°C, looks almost identical to those with permanently-open roof vents (Figure 84 *cf*. Figure 46) and also to those with simultaneous opening of all vents at the 100°C activation temperature (Figure 84 *cf*. Figure 80).

Visibility in the small warehouse with sequentially-opening roof vents and activation temperature of 100°C was indistinguishable from the case with simultaneously-opening vents (Figure 85 *cf*. Figure 80). Increasing vent activation temperature to 200°C and further to 300°C created a deeper and thicker smoke layer.

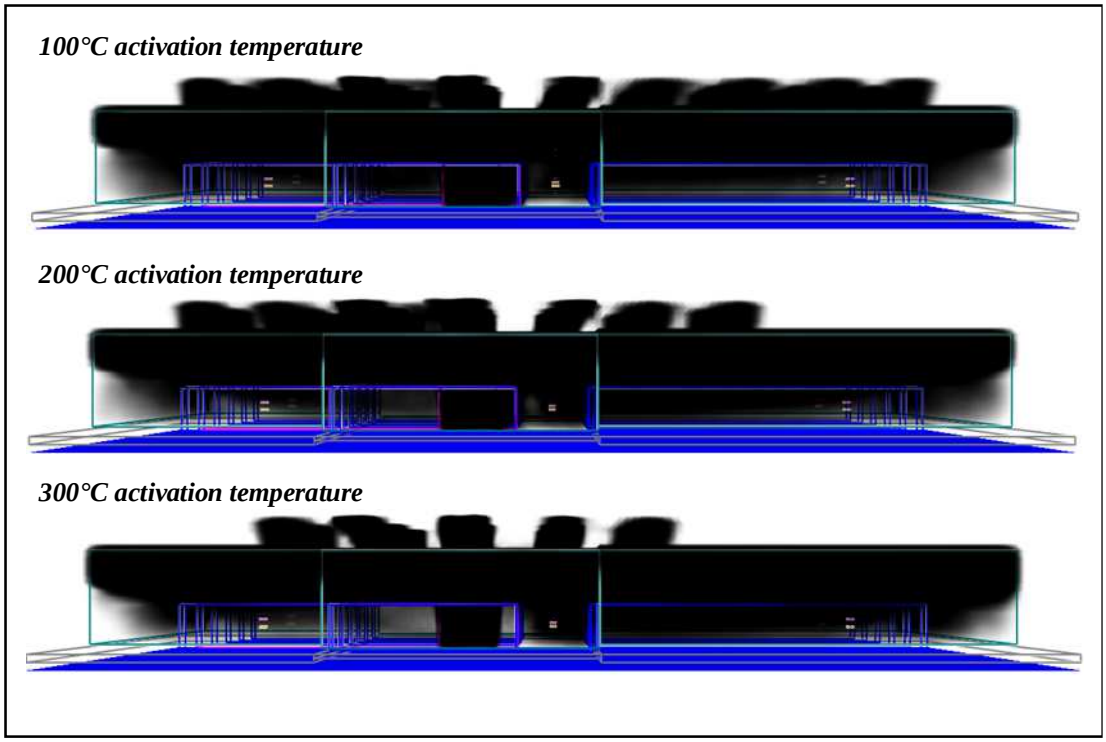

Figure 84: Smokeview depiction of smoke layer after 1,800 seconds in small warehouse with rapid t^3 fire growth and square-shaped roof vents opening sequentially at three different activation temperatures (top – 100°C, middle – 200°C, and bottom – 300°C).

The most notable effect of increasing activation temperature to 200°C, and further to 300°C, was the diminishing utilisation of roof venting area. This can be clearly seen in Figure 84 by viewing the reduction in the number of smoke plumes above the warehouse in each successive Smokeview image, and is easily visualized by viewing the warehouse from above as in Figure 86. In the first scenario with sequentially-opening roof vents, the 100°C activation temperature was first reached after 50 seconds: as expected, initial activation time was equal to that observed in Section 3.2.2 for the simultaneous-opening case. Eventually all 27 vents in the warehouse roof opened, with the last (and furthest removed from the fire) opening after nearly 15 minutes (887 seconds), indicating a continual worsening of temperature conditions in the upper layer of the warehouse. With a 200°C activation temperature, 19 of the

27 vents had opened at the end of the 30-minute simulation, with the first vent activated after nearly 2 minutes (100 seconds) and the last vent after more than 13 minutes (806 seconds). The 12th and final vent to open in the scenario with a 300°C activation temperature activated after nearly 10 minutes (599 seconds); the first vent had opened after more than 2 minutes (138 seconds).

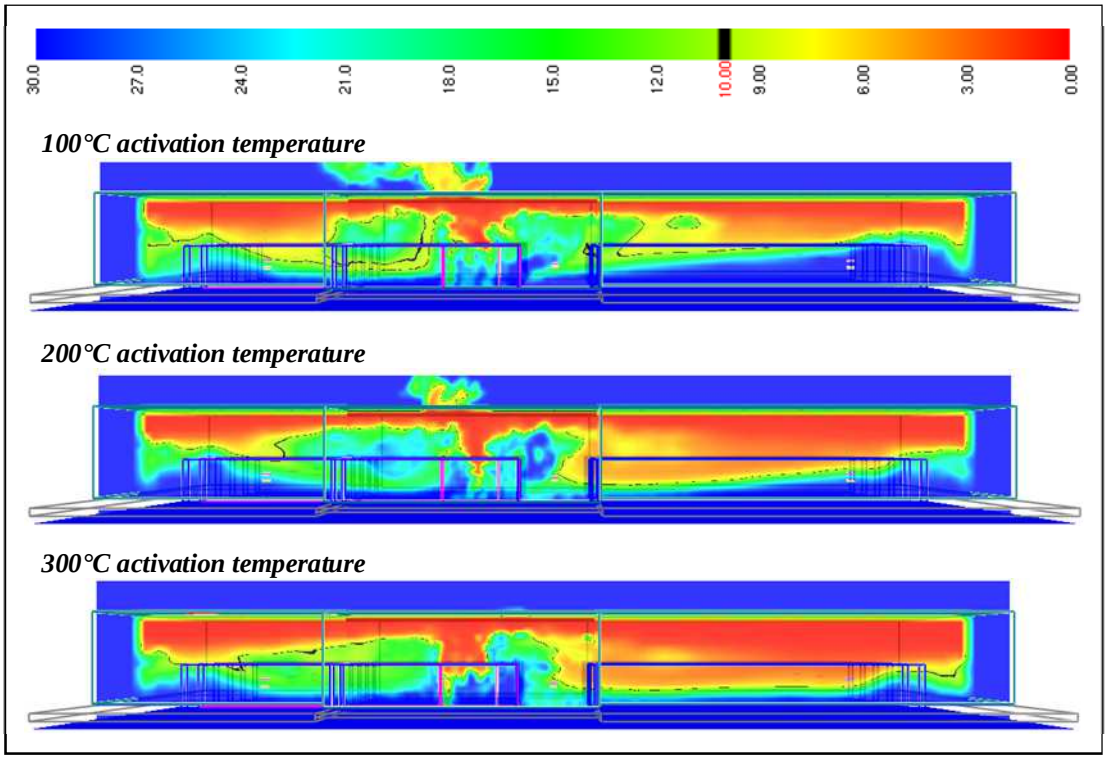

Figure 85: Visibility (m) after 1,800 seconds in small warehouse with rapid t^3 fire growth and square-shaped roof vents opening sequentially at three different activation temperatures (top – 100°C, middle – 200°C, and bottom – 300°C).

Radiative heat fluxes for the three simulations with sequentially-opening roof vents are represented by data from four targets displayed in Figure 87. (Results for the remaining positions can be viewed in Appendix G1.) The results are identical to the case with permanently-open vents seen in Figure 48: worse than extreme conditions at Position 6, extreme conditions at Position 5, and routine conditions at all other positions except in the 300°C activation temperature scenario, where conditions are considered hazardous by the FBIM.

Temperature trends at 1.5 m were also nearly unchanged from the permanently-open venting scenario; conditions were routine at all positions (Figure 88 *cf.* Figure 49).

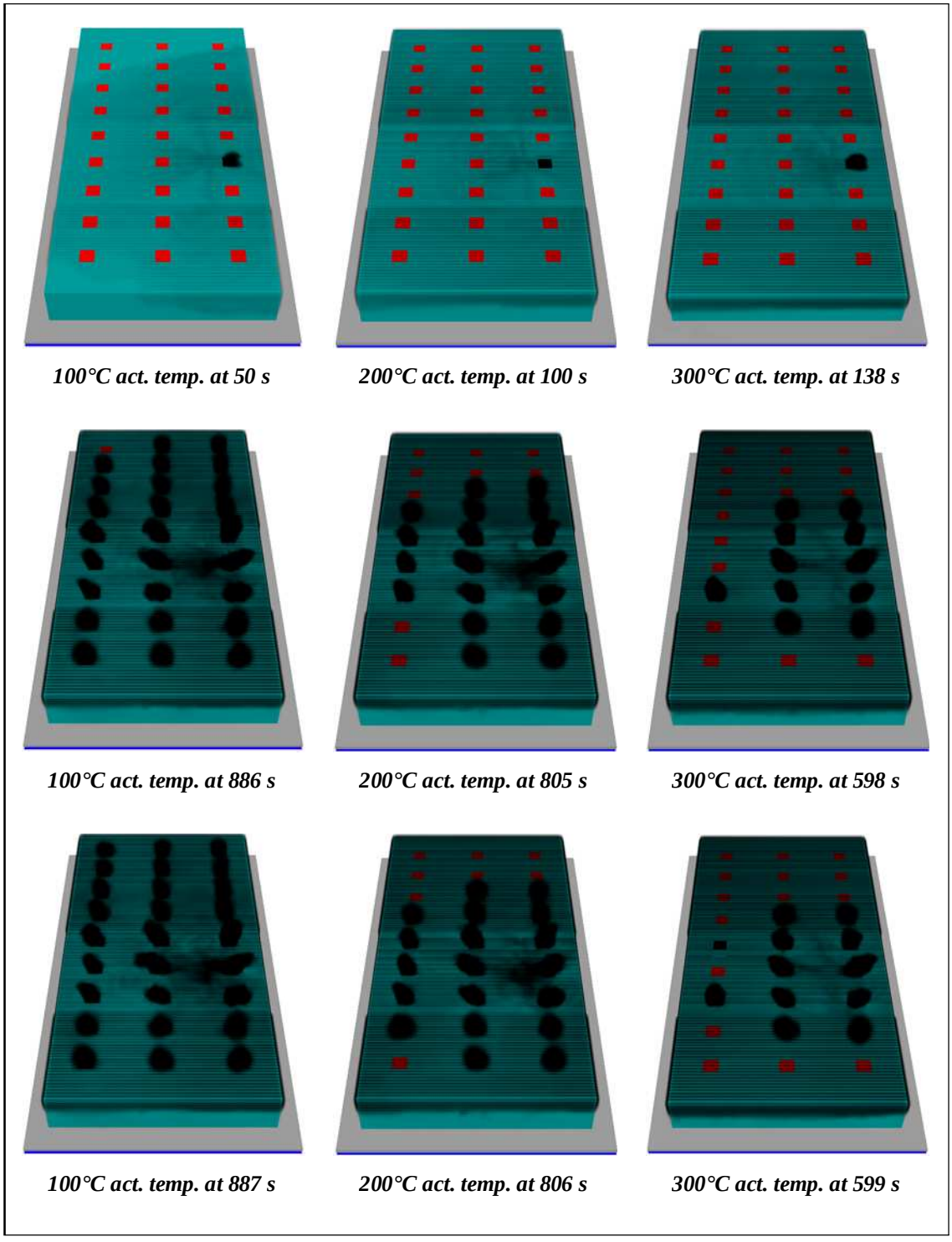

Figure 86: Comparison of vent opening area and timing in small warehouse with rapid t^3 fire growth and square-shaped roof vents opening sequentially at three different activation temperatures (left – 100°C activation temperature, centre – 200°C activation temperature, and right – 300°C activation temperature). The top row of images shows activation of the first vent; the middle row shows the situation 1 second before activation of the final vent; and the bottom row shows activation of the final vent during the specified simulation time of 1,800 seconds.

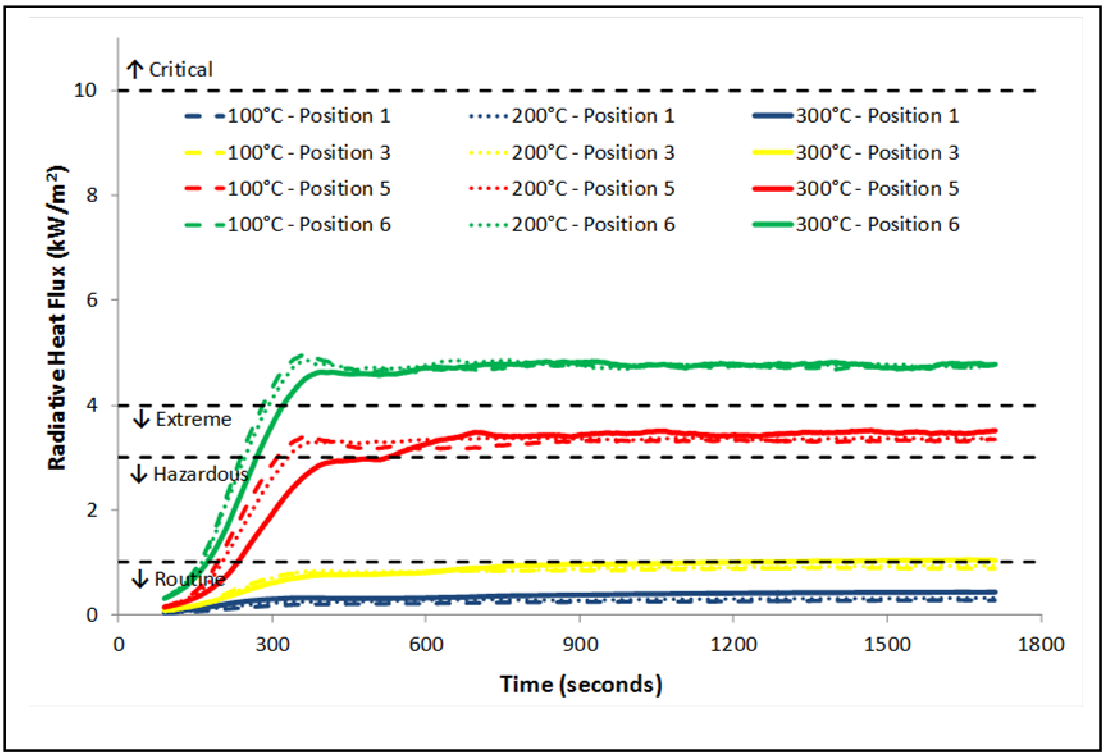

Figure 87: Comparison of smoothed radiative heat flux data from FDS at a height of 1.5 m in small warehouse with rapid t^3 fire growth and square-shaped roof vents opening sequentially at three different activation temperatures.

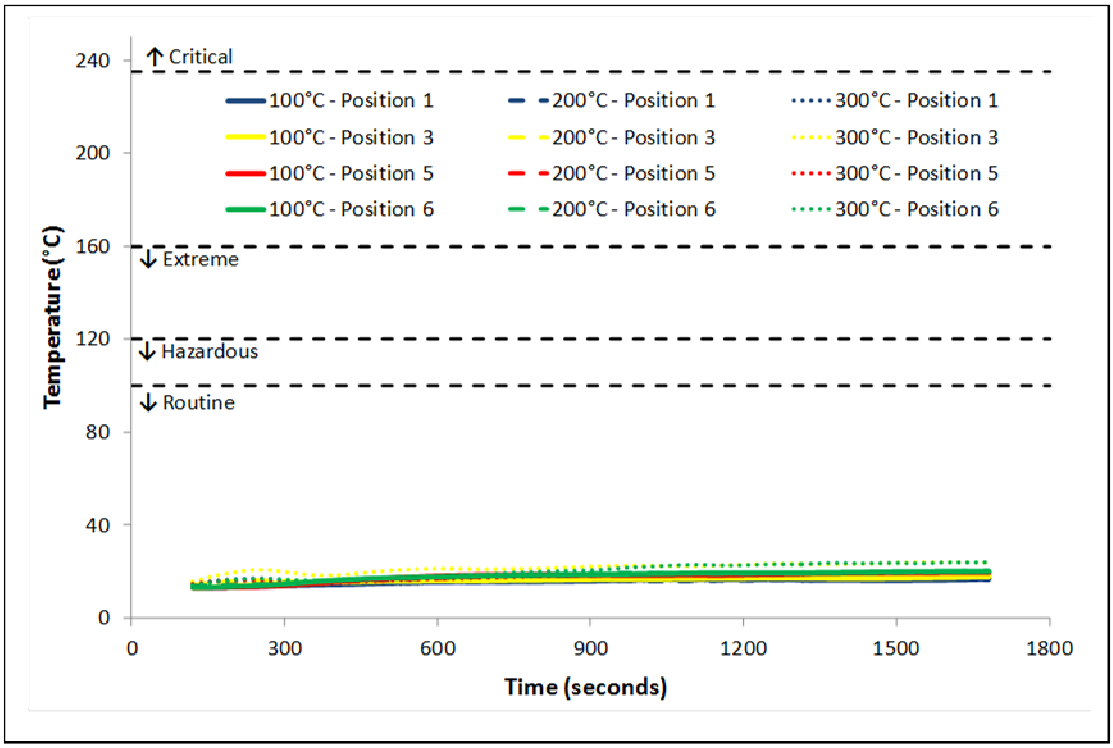

Figure 88: Comparison of smoothed temperature data from FDS at a height of 1.5 m in small warehouse with rapid t^3 fire growth and square-shaped roof vents opening sequentially at three different activation temperatures.

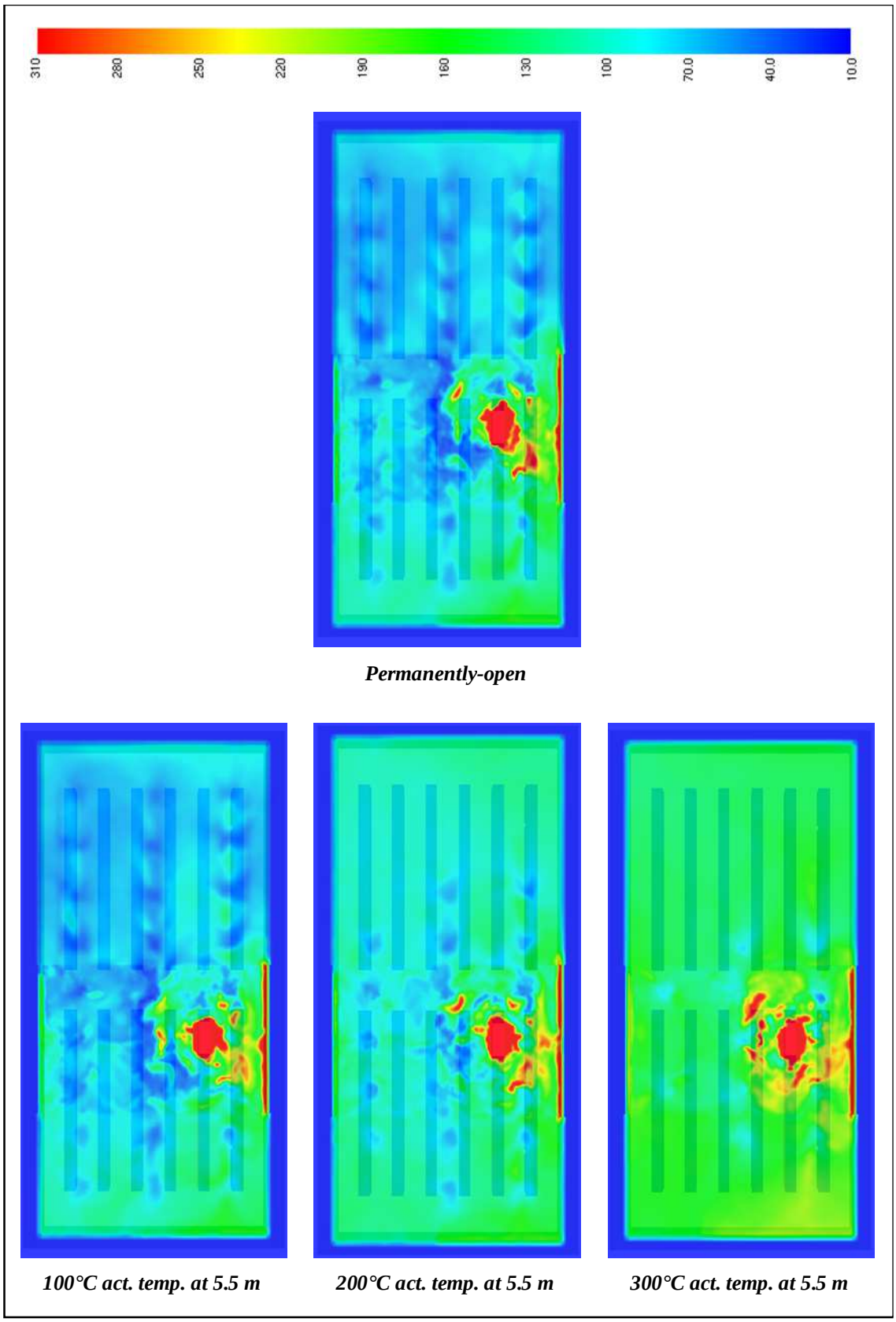

Figure 89: Comparison of temperature distributions at a height of 5.5 m after 1,800 seconds in small warehouse with rapid t^3 fire growth: square-shaped roof vents that are permanently-open (top) versus square-shaped roof vents that open sequentially at three different activation temperatures (bottom left – 100°C, bottom centre – 200°C, and bottom right – 300°C).

In Figure 89, upper layer temperature distributions for the three scenarios with sequentially-opening square-shaped roof vents are compared to the case with permanently-open roof vents from Section 3.1.4. Temperatures are almost identical for the case with a 100°C activation temperature when compared to the base case with permanently-open vents. Increasing vent-activation temperature resulted in higher temperatures throughout the warehouse.

3.2.4 Phase 2a: Small warehouse – rapid t³ fire growth & strip-shaped roof vents opening sequentially at two different activation temperatures

Examination of Smokeview showed that use of strip-shaped roof vents was able to alleviate the effect of the smoke layer slightly when compared to all simulations with square-shaped vents (Figure 90). This effect is highlighted on the left-hand side of the images of visibility in Figure 91: as the fire is located left-of-centre in the images, it is the vents in this section of the warehouse that activate earliest and allow the clear layer to remain for longer. In contrast, on the right-hand side of the visibility images, the smoke layer can be seen to descend deeper than it had with square-shaped vents: strip-shaped vents in this part of the warehouse were not activated, as sufficient roof venting area was provided by the vents that had already activated on the left-hand side of the image to ensure activation temperature was not achieved away from the fire.

The area and timing of vent activation for the strip-shaped roof venting simulations is displayed in Figure 92. For an activation temperature of 200°C, the first segment of a strip-shaped vent opens after nearly 2 minutes (102 seconds). After nearly 20 minutes (1,193 seconds), the final segment to achieve the activation temperature opened. By this stage, 7 of the 12 strip-vents had opened, although one of the strip vents was only 70 % open and another 90 % open. With a 300°C activation temperature, the first vent segment was activated more than 2 minutes (126 seconds) after the outbreak of fire. The final segment to open in this simulation did so after nearly 24 minutes (1,426 seconds). In this simulation, segments from just 6 of the 12 vents were activated to open: two of which were completely open, one was 90 % open, one was 70 % open, and two were 30 % open. Each strip vent has an area of 7.5 m², meaning the *utilised roof-venting area* equates to 50 m² (6.6 strip vents) and 32 m² (4.2 strip vents) for the 200°C and 300°C activation temperatures, respectively. The equivalent

utilised roof venting area for the square-shaped vents in Section 3.2.3 are 90 m² (27 vents of 3.33 m²), 63 m² (19 vents of 3.33 m²), and 40 m² (12 vents of 3.33 m²) for the 100°C, 200°C, and 300°C activation temperatures, respectively. Given that other warehouse conditions were identical among all simulations, this result indicates an advantage of strip-shaped vents over square-shaped vents of the same total area.

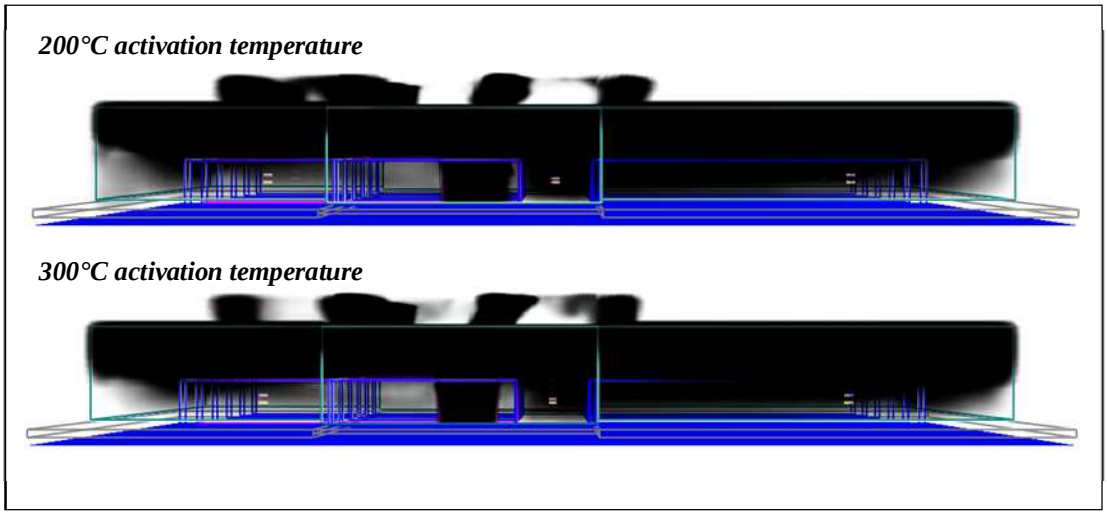

Figure 90: Smokeview depiction of smoke layer after 1,800 seconds in small warehouse with rapid t^3 fire growth and strip-shaped roof vents opening sequentially at two different activation temperatures (top – 200° and bottom – 300°).

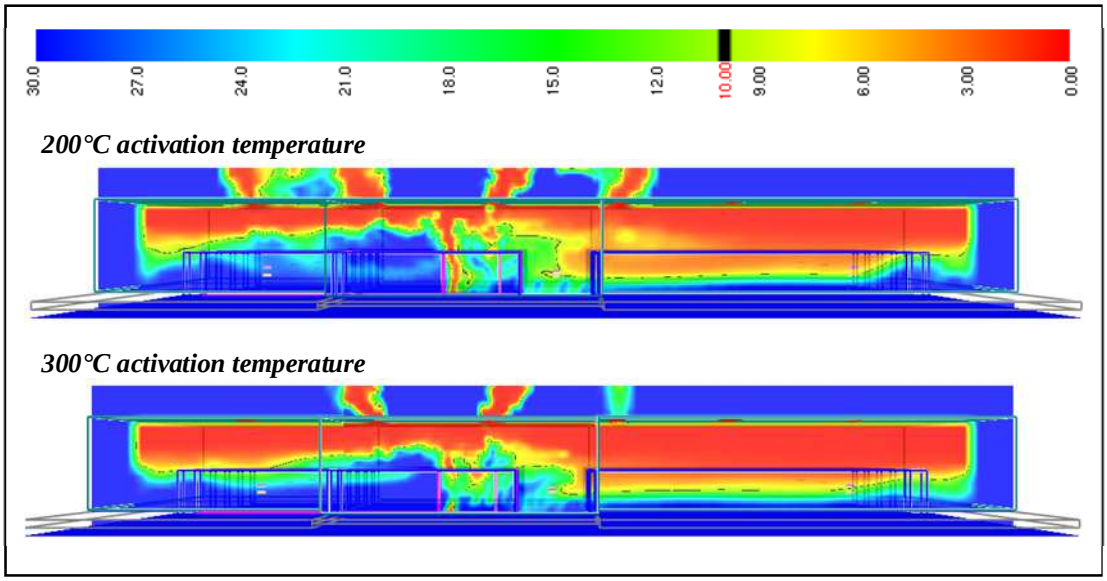

Figure 91: Visibility (m) after 1,800 seconds in small warehouse with rapid t^3 fire growth and strip-shaped roof vents opening sequentially at two different activation temperatures (top – 200°C and bottom – 300°C). Slice is taken through long axis of warehouse, 10 m inside nearest warehouse wall.

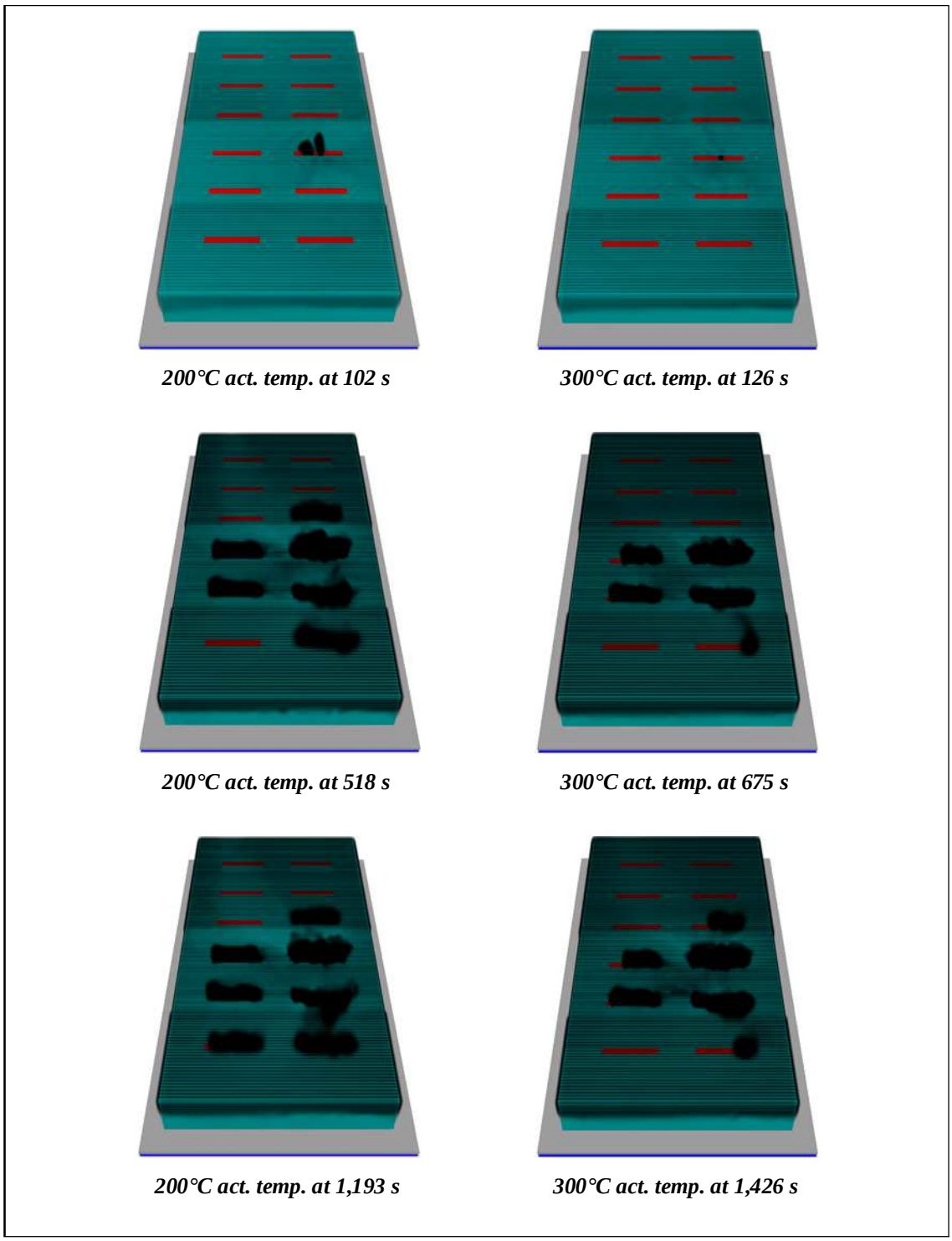

Figure 92: Comparison of vent opening area and timing in small warehouse with rapid t^3 fire growth and strip-shaped roof vents opening sequentially at two different activation temperatures (left – 200°C activation temperature and right – 300°C activation temperature). The top row of images shows activation of the first vent segment; the middle row shows the situation 1 second before activation of the first segment of the final vent; and the bottom row shows activation of the final vent segment during the specified simulation time of 1,800 seconds.

There was a clear advantage of using strip-shaped vents in terms of radiative heat flux (Figure 93 *cf*. Figure 48 and Figure 87). In all previous simulations with square-shaped vents, radiative heat flux at Position 6 exceeded the Extreme Conditions criterion of the FBIM within 5 minutes. With strip vents, the Extreme Conditions criterion was met at Position 6, but never exceeded. Further, in the case of the 300°C activation temperature, conditions were considered only hazardous for the first 15 minutes. Assuming arrival 10 minutes after the outbreak of fire, this would allow the fire fighter 5 minutes inside the warehouse (according to the FBIM), compared to less than 1 minute when arriving to find extreme conditions, as was the case with square-shaped vents.

Temperatures at Position 3 were several degrees higher in the simulations with strip-shaped venting as compared to the simulations with square-shaped venting (Figure 94). However, temperatures at all positions remained routine. Temperatures in the upper layer were similar to previous simulations and are presented in Figure 95 for comparison.

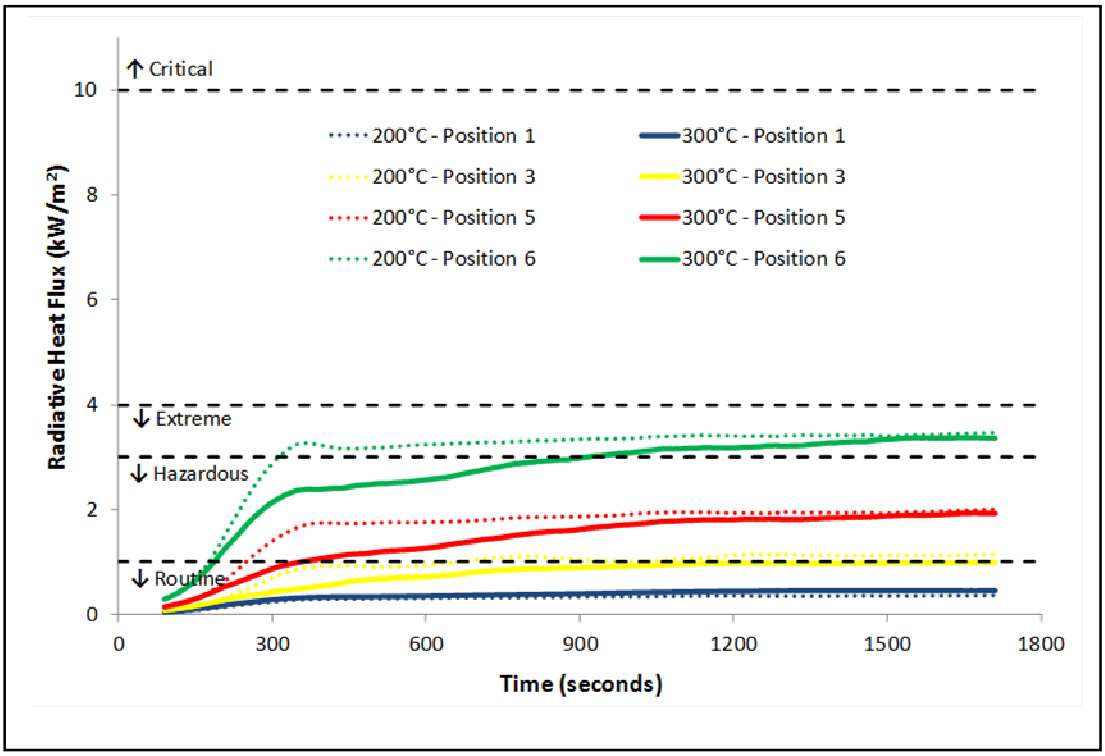

Figure 93: Comparison of smoothed radiative heat flux data from FDS at a height of 1.5 m in small warehouse with rapid t^3 fire growth and strip-shaped roof vents opening sequentially at two different activation temperatures.

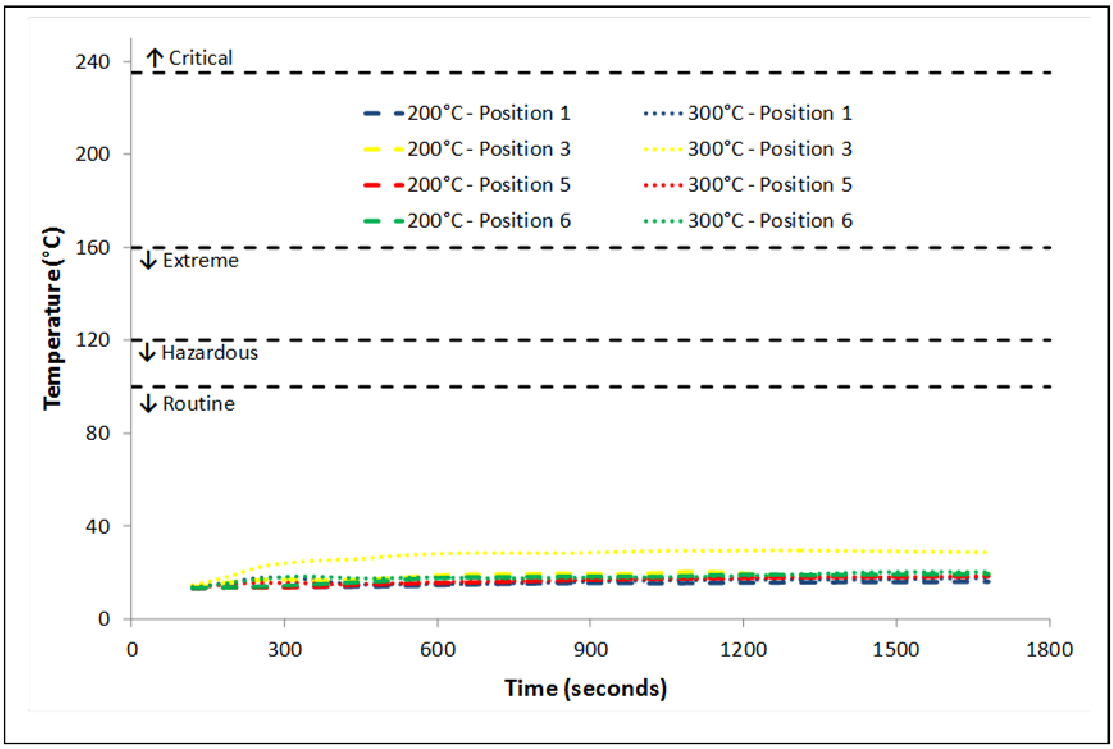

Figure 94: Comparison of smoothed temperature data from FDS at a height of 1.5 m in small warehouse with rapid t^3 fire growth and strip-shaped roof vents opening sequentially at two different activation temperatures.

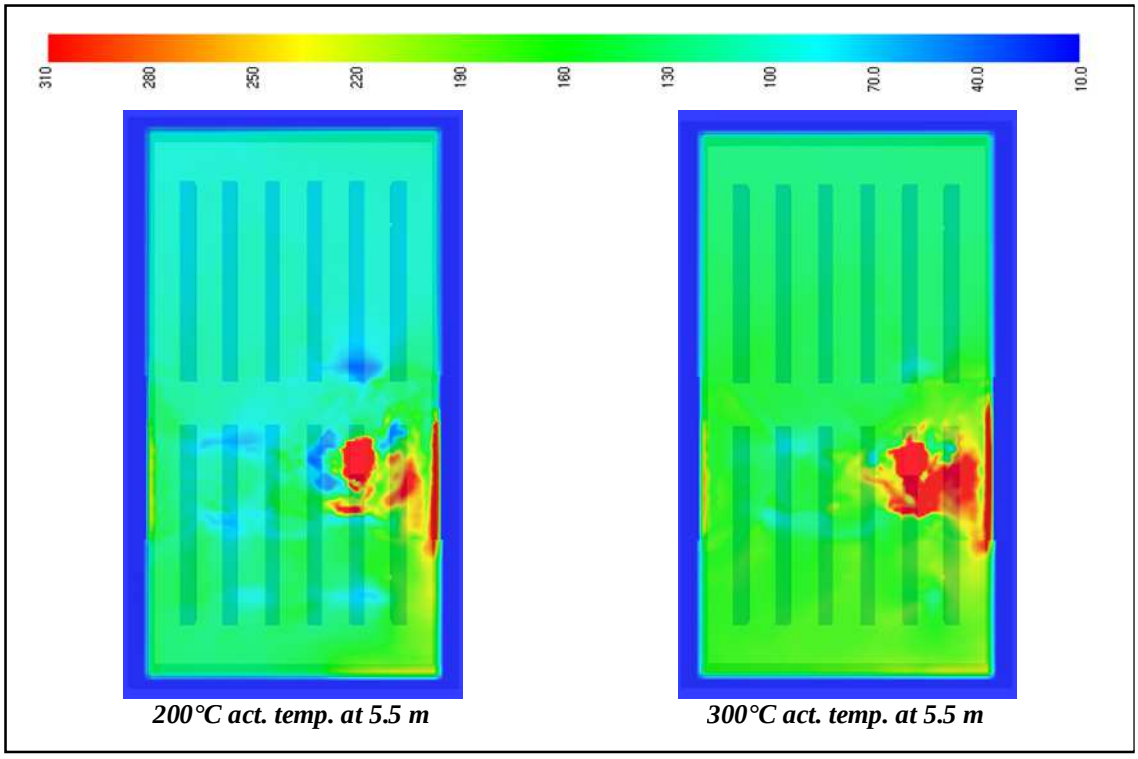

Figure 95: Comparison of temperature distributions after 1,800 seconds in small warehouse with rapid t^3 fire growth and strip-shaped roof vents opening sequentially at two different activation temperatures (left – 200°C and right – 300°C).

3.2.5 *Phase 2b: Small warehouse – extreme t^3 fire growth & square-shaped roof vents opening simultaneously at an activation temperature of 100°C*

Compared to the case of permanently-open roof venting from Section 3.1.7, the smoke layer and visibility conditions in the small warehouse with an extreme t^3 fire growth rate are little changed when a temperature-dependent opening of roof vents is applied (Figure 96 *cf*. Figure 56 and Figure 57). All 27 vents opened after 25 seconds when the first vent achieved the activation temperature of 100°C. Visibility was better than 10 m in most of the lower layer, with the exception of *fingers* of low visibility between the rack storage units.

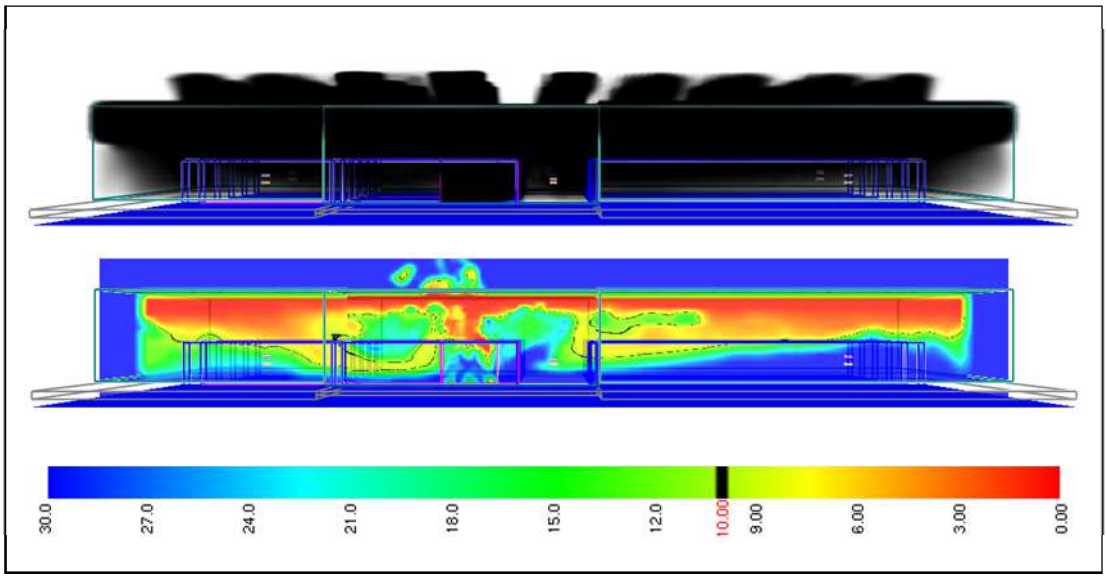

Figure 96: Smokeview depiction of smoke layer after 1,800 seconds (top) and visibility in metres (bottom) in small warehouse with extreme t^3 fire growth and square-shaped roof vents opening simultaneously at an activation temperature of 100°C. Visibility slice is taken through long axis of warehouse, 10 m inside nearest warehouse wall.

Radiative heat fluxes and temperatures at all positions were practically identical to the permanently-open case, and can be found in Appendix H1.

3.2.6 *Phase 2b: Small warehouse – extreme t^3 fire growth & square-shaped roof vents opening sequentially at three different activation temperatures*

An image of the smoke layer from Smokeview, for the small warehouse with sequentially-opening roof vents and an activation temperature of 100°C, is almost identical to both the case with permanently-open vents and that with simultaneously-opening vents (Figure 97 *cf.* Figure 56 and Figure 96).

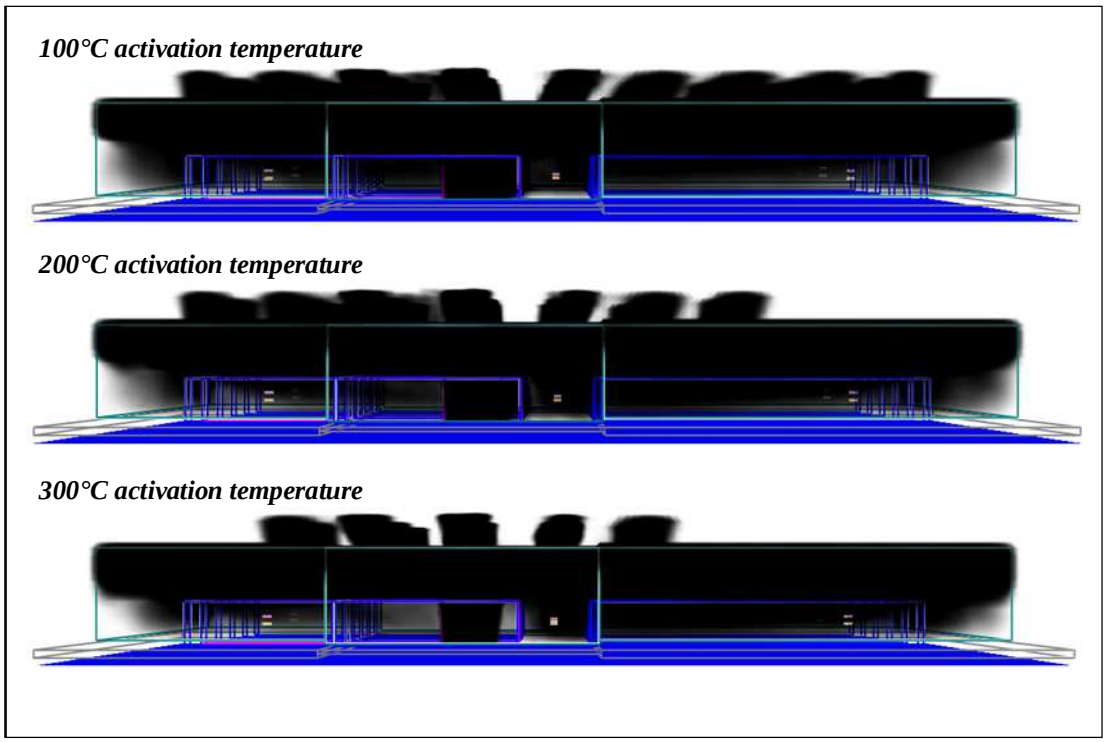

Figure 97: Smokeview depiction of smoke layer after 1,800 seconds in small warehouse with extreme t^3 fire growth and square-shaped roof vents opening sequentially at three different activation temperatures (top – 100°C, middle – 200°C, and bottom – 300°C).

As was seen with the rapid t^3 fire growth rate in Section 3.2.3, increasing activation temperatures in the simulations with extreme t^3 fire growth resulted in diminished use of roof venting area. In Figure 98, the reduction of utilised vents is well-visualized: with an activation temperature of 100°C, all vents were eventually activated; with an activation temperature of 200°C, just 19 of the 27 vents were activated; and, with activation at 300°C, only 12 of the 27 vents opened during the 30 minute simulation. The numbers of activated vents in these scenarios match exactly those from Section 3.2.3.

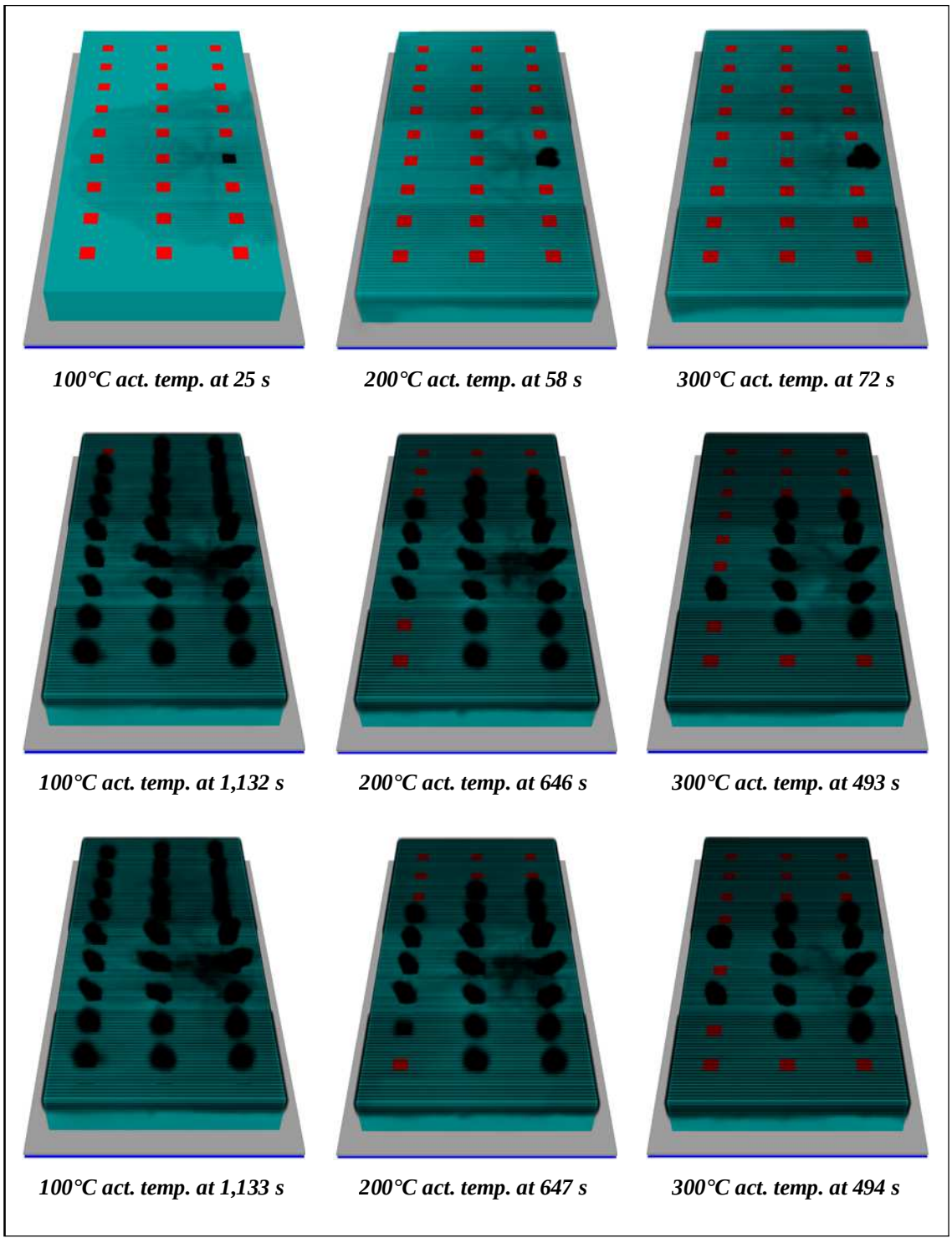

Figure 98: Comparison of vent opening area and timing in small warehouse with extreme t^3 fire growth and square-shaped roof vents opening sequentially at three different activation temperatures (left – 100°C activation temperature, centre – 200°C activation temperature, and right – 300°C activation temperature). The top row of images shows activation of the first vent; the middle row shows the situation 1 second before activation of the final vent; and the bottom row shows activation of the final vent during the specified simulation time of 1,800 seconds.

Visibility with extreme t^3 fire growth in the small warehouse with sequentially-opening roof vents and an activation temperature of 100°C was indistinguishable from the case with simultaneously-opening vents (Figure 99 *cf*. Figure 96). Increasing vent activation temperature to 200°C, and further to 300°C, brought about a deepening and thickening of the smoke layer.

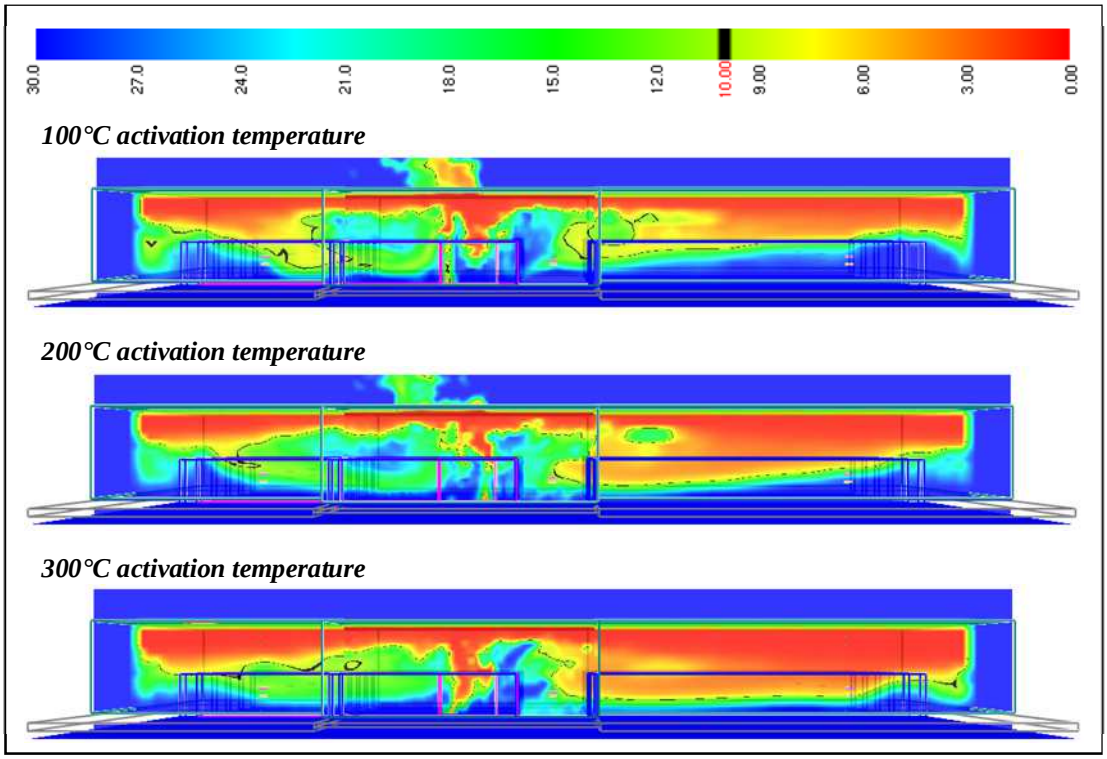

Figure 99: Visibility (m) after 1,800 seconds in small warehouse with extreme t^3 fire growth and square-shaped roof vents opening sequentially at three different activation temperatures (top – 100°C, middle – 200°C, and bottom – 300°C). Visibility slice is taken through long axis of warehouse, 10 m inside nearest warehouse wall.

Radiative heat fluxes and temperatures measured at the nine targets at 1.5 m above floor level remained almost unchanged from the simultaneous vent-opening scenario, and can be viewed in Appendix H2. Upper layer temperatures displayed no major differences to those recorded in the small warehouse with rapid t^3 fire growth, and are not reported here.

3.2.7 Phase 2b: Small warehouse – extreme t^3 fire growth & strip-shaped roof vents opening sequentially at two different activation temperatures

Depth of the smoke layer was alleviated at one end of the small warehouse by the use of strip-shaped vents (Figure 100): on the left-hand side of the images the dark black smoke layer remained above the storage racks, while below this height only some, lighter-coloured smoke was present. In contrast, the smoke layer had descended to close to floor level on the right-hand side of the warehouse, further removed from the fire, where activation of strip-shaped vents was not widespread.

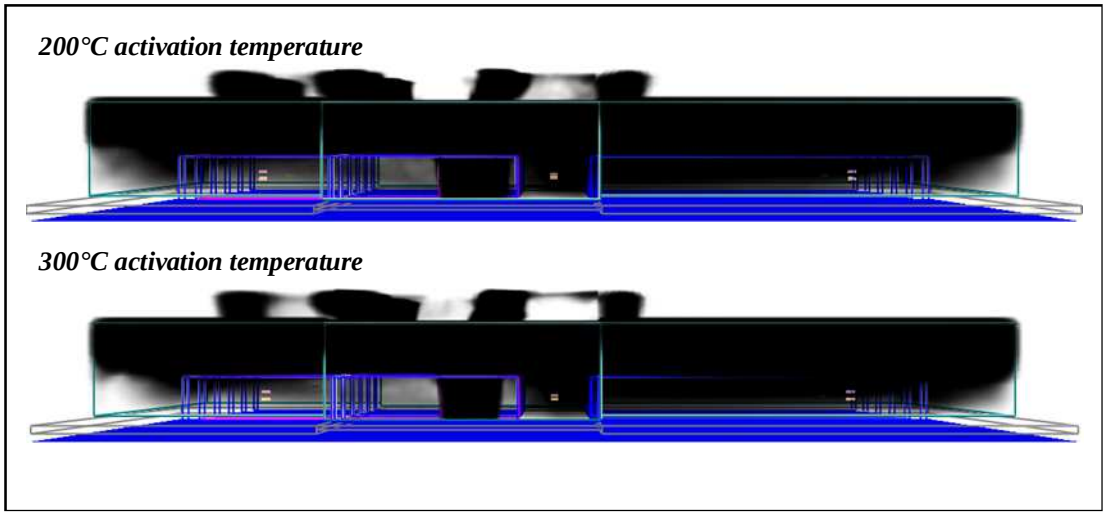

Figure 100: Smokeview depiction of smoke layer after 1,800 seconds in small warehouse with extreme t^3 fire growth and strip-shaped roof vents opening sequentially at two different activation temperatures (top – 200° and bottom – 300°).

This same effect can also be seen in the slice files of visibility shown in Figure 101: the area of the smoke above the black-coloured boundary line, indicating a visibility of less than 10 m, remained well-above the rack storage on the left-hand side of the warehouse, but dropped well below the tops of the storage racks on the right-hand side of the warehouse.

The area and timing of vent activation for the strip-shaped roof venting simulations is displayed in Figure 102.With an activation temperature of 200°C, the first segment of the first strip-shaped vent to open was activated after less than 1 minute (47 seconds) and the last segment to open did so after 25 minutes (1,497 seconds). In total, 8 of the 12 vents contained segments that achieved the activation temperature: one vent was

just 10 % open, one vent was 70 % open, one vent was 90 % open and five vents were fully open (equating to 6.7 vents or 50 m²). This is only a fraction more *utilised roof venting area* than was with the rapid t^3 fire growth rate. It is also substantially less than the 63 m² that was observed for the simulation with square-shaped vents (with 200°C activation temperature) and extreme t^3 fire growth. With a 300°C activation temperature, the first vent segment was activated after nearly 1 minute (55 seconds), and the last vent segment after nearly 13 minutes (775 seconds). The *utilised roof venting area* was 35 m² (or 4.6 vents), made up of one vent that was 30 % open, one vent that was 60 % open, one vent that was 70 % open, and three vents that were 100 % open. This area compares favourably with the equivalent *utilised roof venting area* of 40 m² in the square-shaped roof venting scenario (with a 300°C activation temperature) presented in Section 3.2.6. These results further suggest an advantage of strip-shaped vents over square-shaped vents of the same total area.

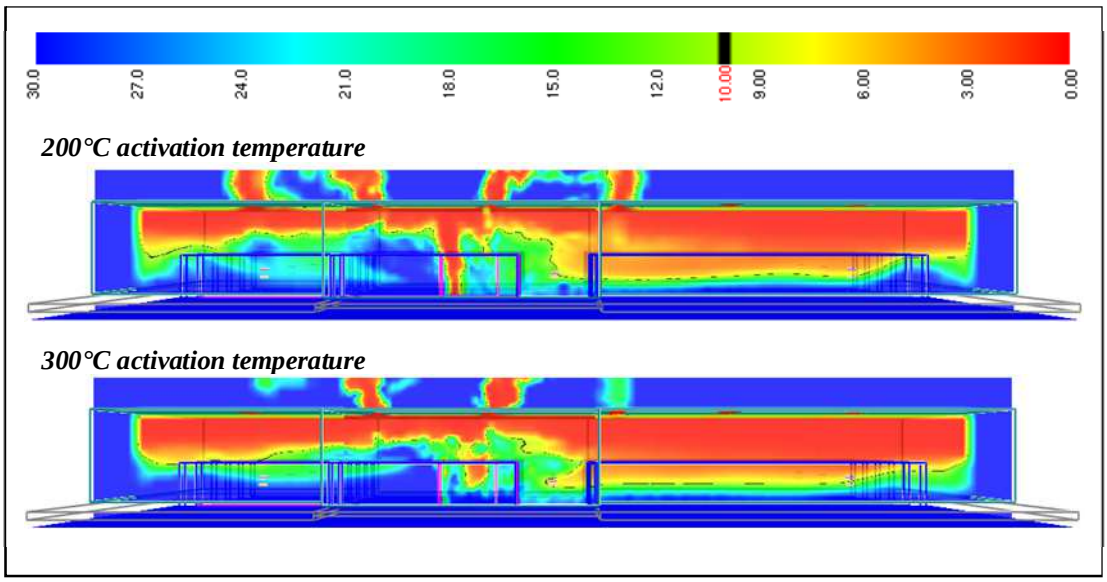

Figure 101: Visibility (m) after 1,800 seconds in small warehouse with extreme t^3 fire growth and strip-shaped roof vents opening sequentially at two different activation temperatures (top – 200°C and bottom – 300°C). Slice is taken through long axis of warehouse, 10 m inside nearest warehouse wall.

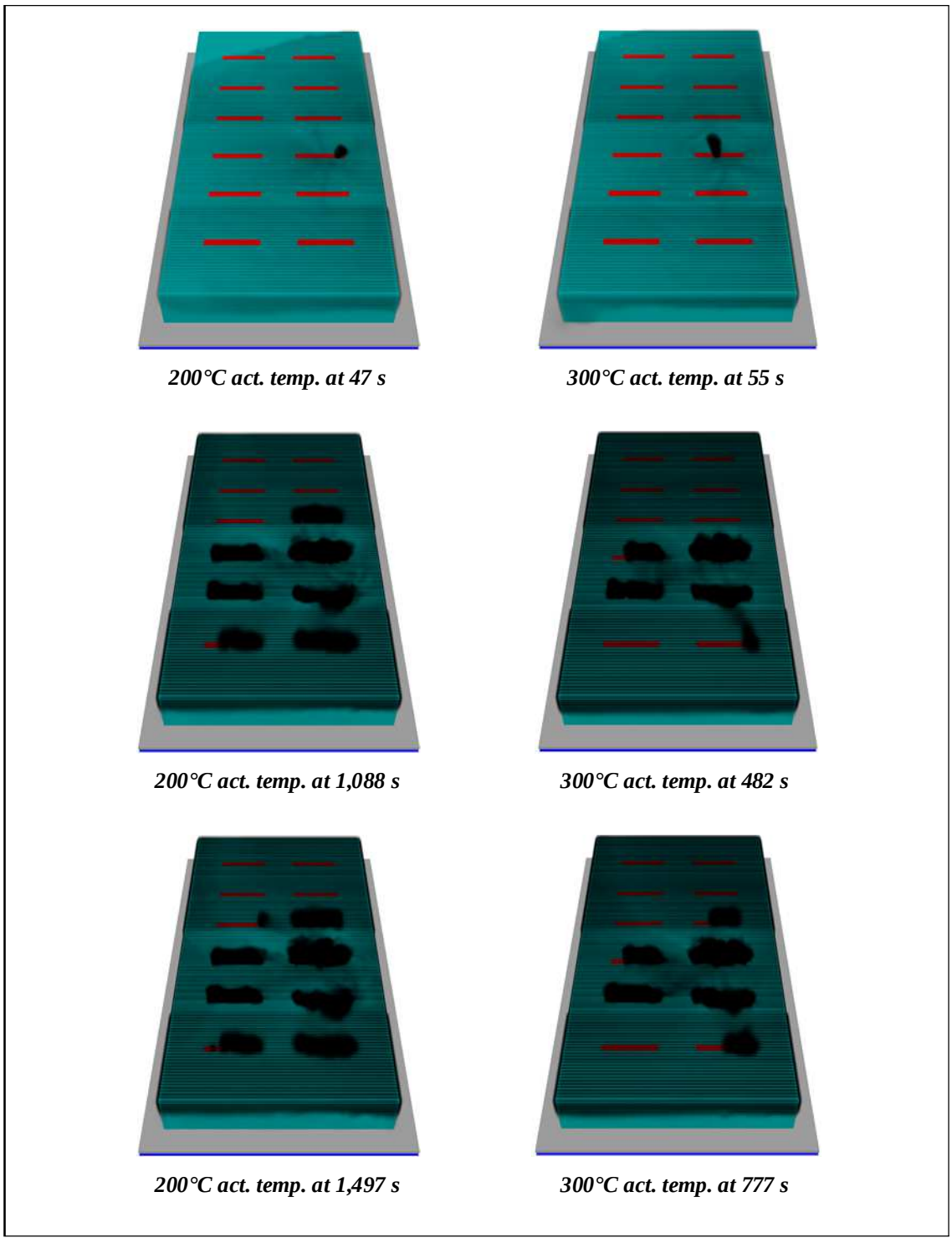

Figure 102: Comparison of vent opening area and timing in small warehouse with extreme t^3 fire growth and strip-shaped roof vents opening sequentially at two different activation temperatures (left – 200°C activation temperature and right – 300°C activation temperature). The top row of images shows activation of the first vent segment; the middle row shows the situation 1 second before activation of the first segment of the final vent; and the bottom row shows activation of the final vent segment during the specified simulation time of 1,800 seconds.

Use of strip-shaped vents was also advantageous in terms of radiative heat flux in the lower layer (Figure 103 *cf.* Figure 58 and Appendix H2). With strip-shaped vents, radiative heat flux at Position 6 remained in the Extreme Conditions criterion of the FBIM, whereas with square-shaped vents it had exceeded this criterion. Similarly, radiative heat flux at Position 5 reduced to remain within the Hazardous Conditions criterion, in contrast to the extreme conditions observed with square-shaped vents. At all other positions, conditions were routine. (Full results can be found in Appendix H3.)

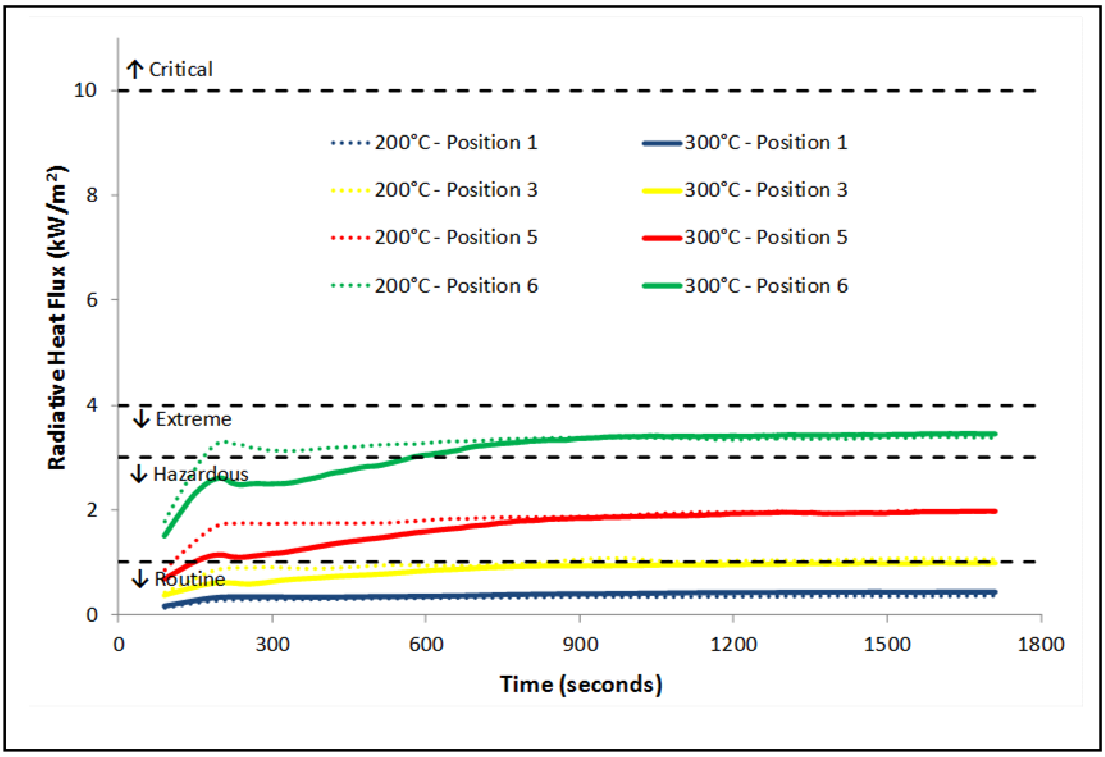

Figure 103: Comparison of smoothed radiative heat flux data from FDS at a height of 1.5 m in small warehouse with extreme t^3 fire growth and strip-shaped roof vents opening sequentially at two different activation temperatures.

As seen for rapid fire growth in Section 3.2.4, temperatures in the lower layer remained routine with extreme fire growth and can be found in Appendix H3.

3.2.8 *Phase 2c: Large warehouse – rapid t^3 fire growth & square-shaped roof vents opening simultaneously at an activation temperature of 100°C*

Depictions of the smoke layer from Smokeview show that there is very little effect of delaying individual vent opening times (through a sequential opening mechanism) to be seen in the large warehouse (Figure 104 *cf*. Figure 67 and Figure 68). The activation temperature of 100°C was reached after 140 seconds, and all 88 vents opened. Visibility remained above 30 m in the large warehouse for the duration of the simulation, as was seen when roof venting was permanently open from the start of the simulation.

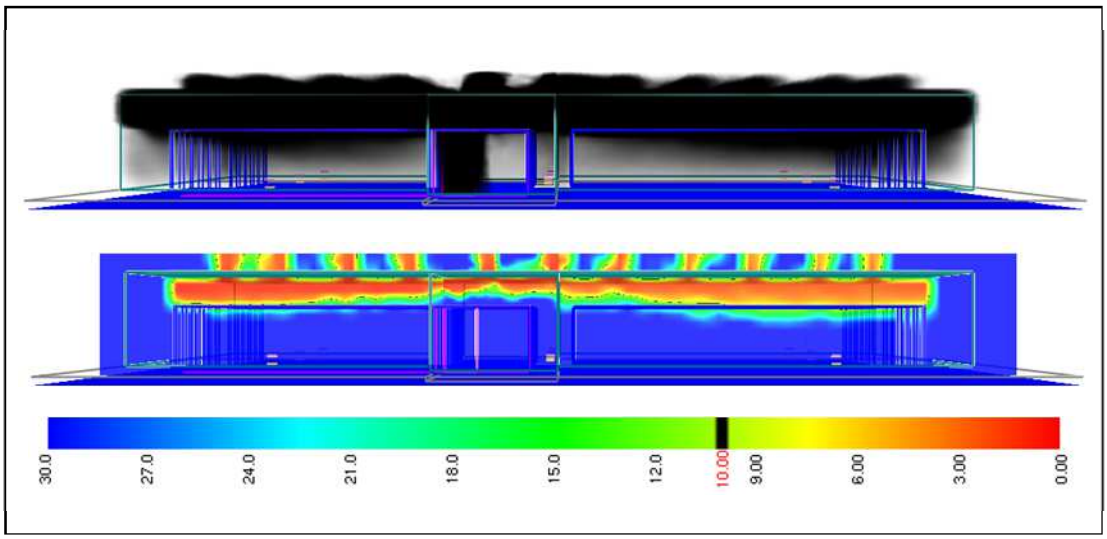

Figure 104: Smokeview depiction of smoke layer after 1,800 seconds (top) and visibility in metres (bottom) in large warehouse with rapid t^3 fire growth and square-shaped roof vents opening simultaneously at an activation temperature of 100°C. Visibility slice is taken through long axis of warehouse, 20 m inside nearest warehouse wall.

Radiative heat fluxes were also similar at all positions in the warehouse to the case with permanently-open vents (Figure 105 *cf*. Appendix E3): only at Position 6 were conditions worse than routine.

Similarly, temperatures 1.5 m above floor level were little changed from the case with permanently-open vents examined in Section 3.1.11 (Figure 106 *cf*. Figure 69): temperatures remained routine for the duration of the simulation, and were almost unaltered from the ambient temperature of 13°C.

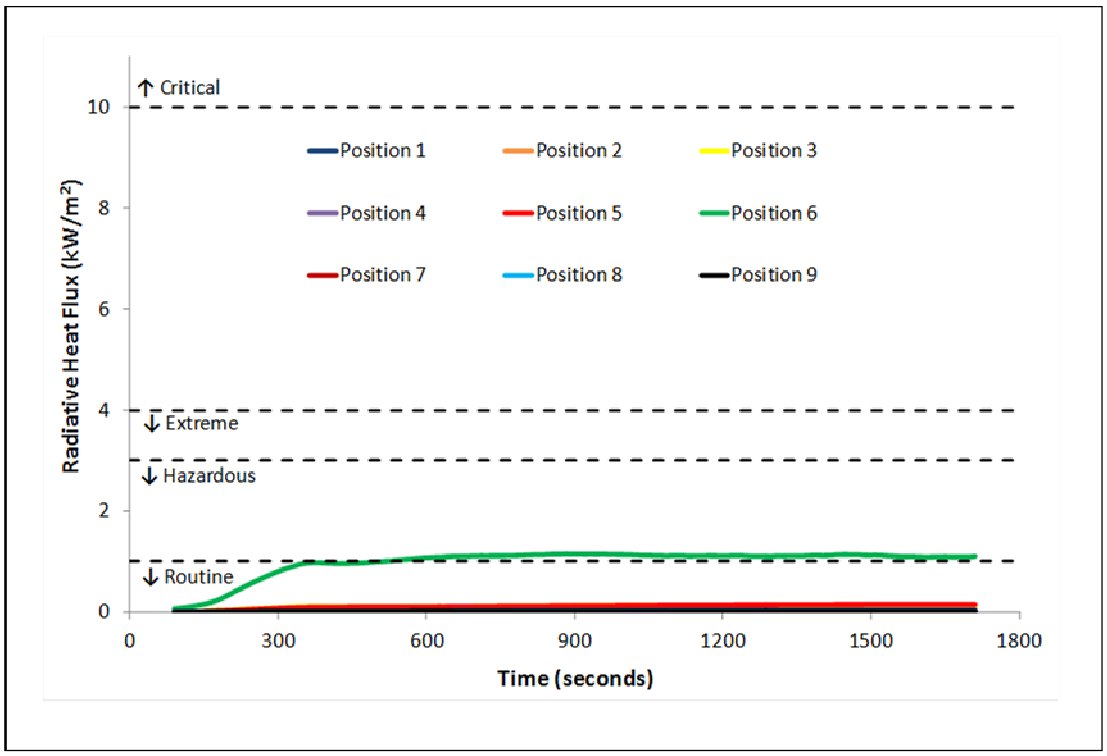

Figure 105: Comparison of smoothed radiative heat flux data from FDS at a height of 1.5 m in large warehouse with rapid t^3 fire growth and square-shaped roof vents opening simultaneously at an activation temperature of 100°C.

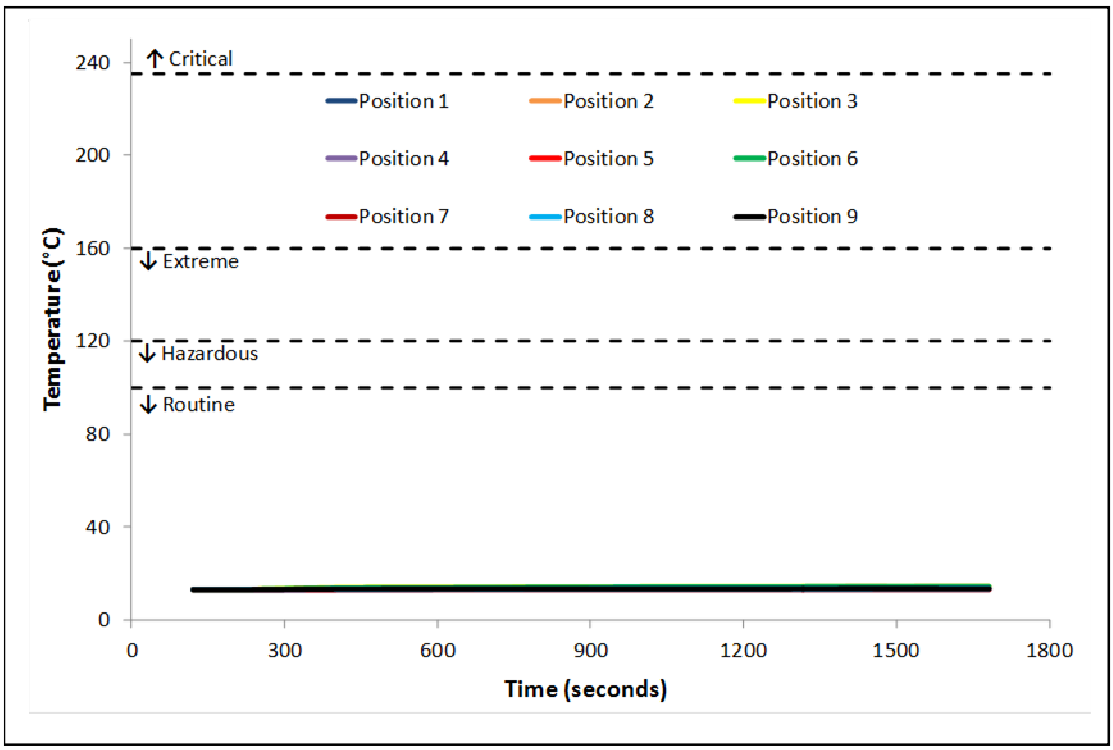

Figure 106: Comparison of smoothed temperature data from FDS at a height of 1.5 m in large warehouse with rapid t^3 fire growth and square-shaped roof vents opening simultaneously at an activation temperature of 100°C.

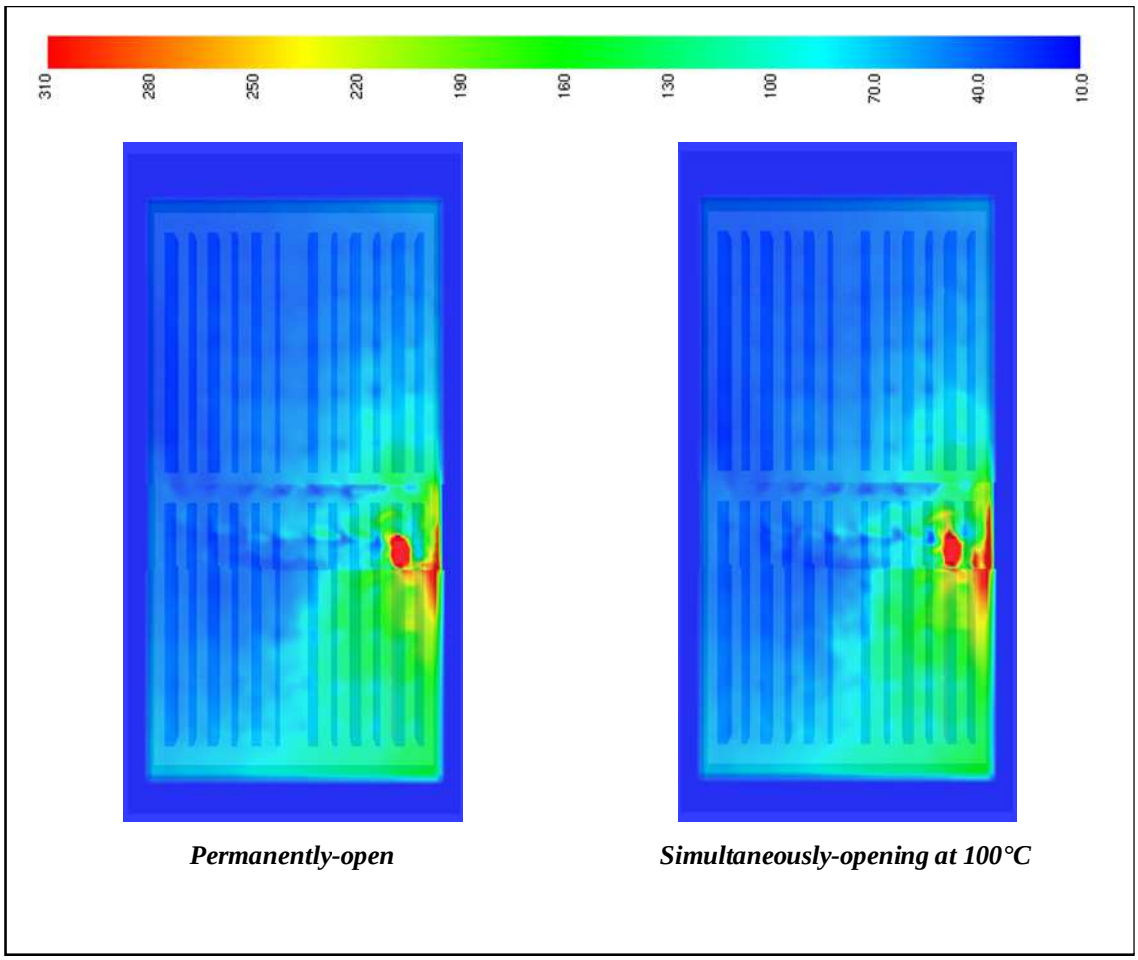

Figure 107: Comparison of temperature distributions at a height of 11.0 m after 1,800 seconds in large warehouse with rapid t^3 fire growth: permanently-open square-shaped roof vents versus square-shaped roof vents opening simultaneously at an activation temperature of 100°C.

Temperature distributions in the upper layer were almost identical to those observed in the case with permanently-open vents (Figure 107). In both cases, temperatures were generally no higher than ~160°C, apart from the area in the immediate vicinity of the fire plume.

3.2.9 Phase 2c: Large warehouse – rapid t^3 fire growth & square-shaped roof vents opening sequentially at three different activation temperatures

The Smokeview image in Figure 108 of the smoke layer in the large warehouse with an activation temperature of 100°C for sequentially-opening roof vents is similar to the image from Figure 67 of the smoke layer in the large warehouse with permanently-open roof vents, and from Figure 104 with simultaneous opening of all vents at an activation temperature of 100°C. There was also minimal difference when

activation temperature was increased to 200°C. However, a significant deepening of the smoke layer was seen when the activation temperature was increased to 300°C.

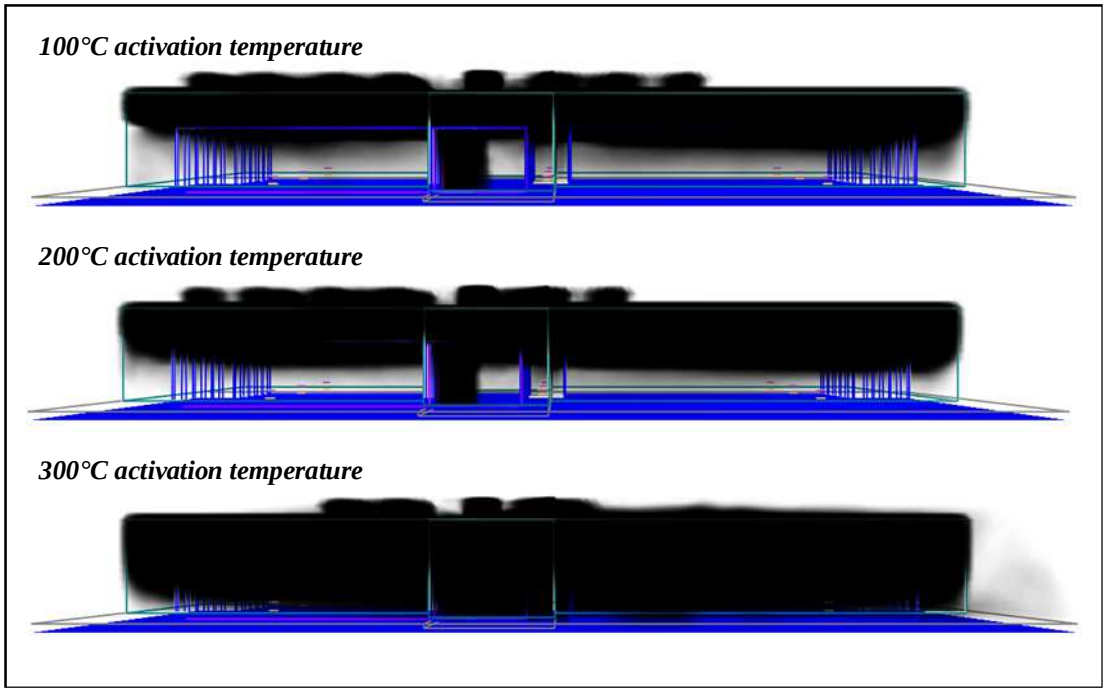

Figure 108: Smokeview depiction of smoke layer after 1,800 seconds in large warehouse with rapid t^3 fire growth and square-shaped roof vents opening sequentially at three different activation temperatures (top – 100°C, middle – 200°C, and bottom – 300°C).

An increase in activation temperature also had an effect on the area of venting utilised for fire venting. In Figure 109, the area of open roof venting and activation timing is compared for each of the three activation temperatures (100°C, 200°C, and 300°C). The first vent to open, in the 100°C activation temperature scenario, did so after 140 seconds. A short time before 19 minutes (1,120 seconds) the 33rd roof vent had opened, giving a *utilised roof venting area* of 112 m² (33 x 3.41 m²). With an increased activation temperature of 200°C, the first roof vent was activated after more than 3 minutes (193 seconds) and the 18th, and final, vent after more than 23 minutes (1,407 seconds); this equates to a *utilised roof venting area* of 61 m². The 9th and final vent to open in the scenario with a 300°C activation temperature activated after just over 7 minutes (431 seconds) to give a *utilised roof venting area* of 31 m²; the first vent had opened after nearly 4 minutes (232 seconds).

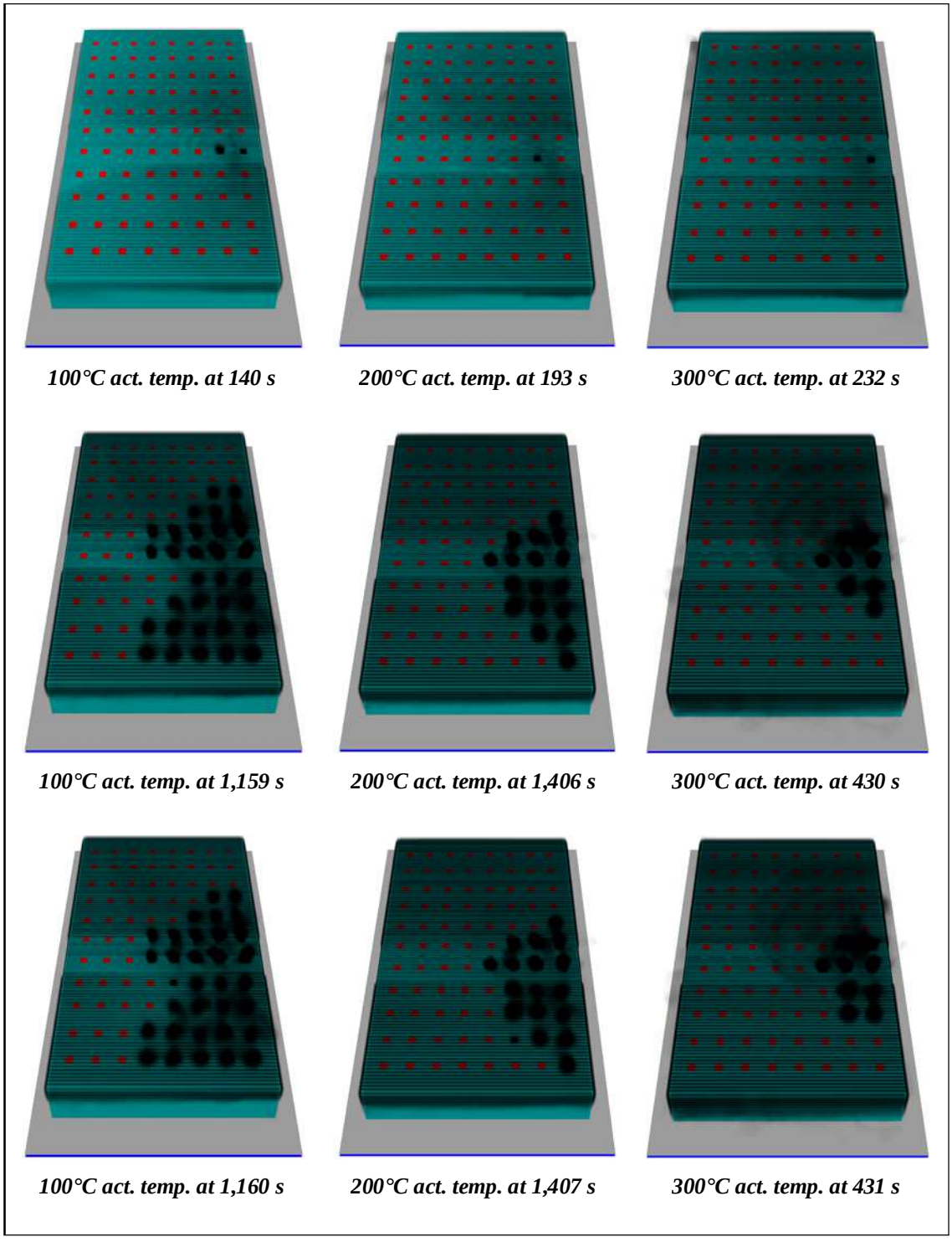

Figure 109: Comparison of vent opening area and timing in large warehouse with rapid t^3 fire growth and square-shaped roof vents opening sequentially at three different activation temperatures (left – 100°C activation temperature, centre – 200°C activation temperature, and right – 300°C activation temperature). The top row of images shows activation of the first vent; the middle row shows the situation 1 second before activation of the final vent; and the bottom row shows activation of the final vent during the specified simulation time of 1,800 seconds.

Visibility in the large warehouse with sequentially-opening roof vents and an activation temperature of 100°C was similar to the case with simultaneously-opening vents (Figure 110 *cf*. Figure 104). However, delaying the activation temperature resulted in a deepening of the smoke layer to below the top of the rack storage by the end of the simulation in the cases of 200°C and 300°C activation temperatures. In all scenarios, however, visibility remained very good below 1.5 m, with only temporary reductions in visibility to about 12 m during the first 10 minutes in the case with 300°C activation temperatures.

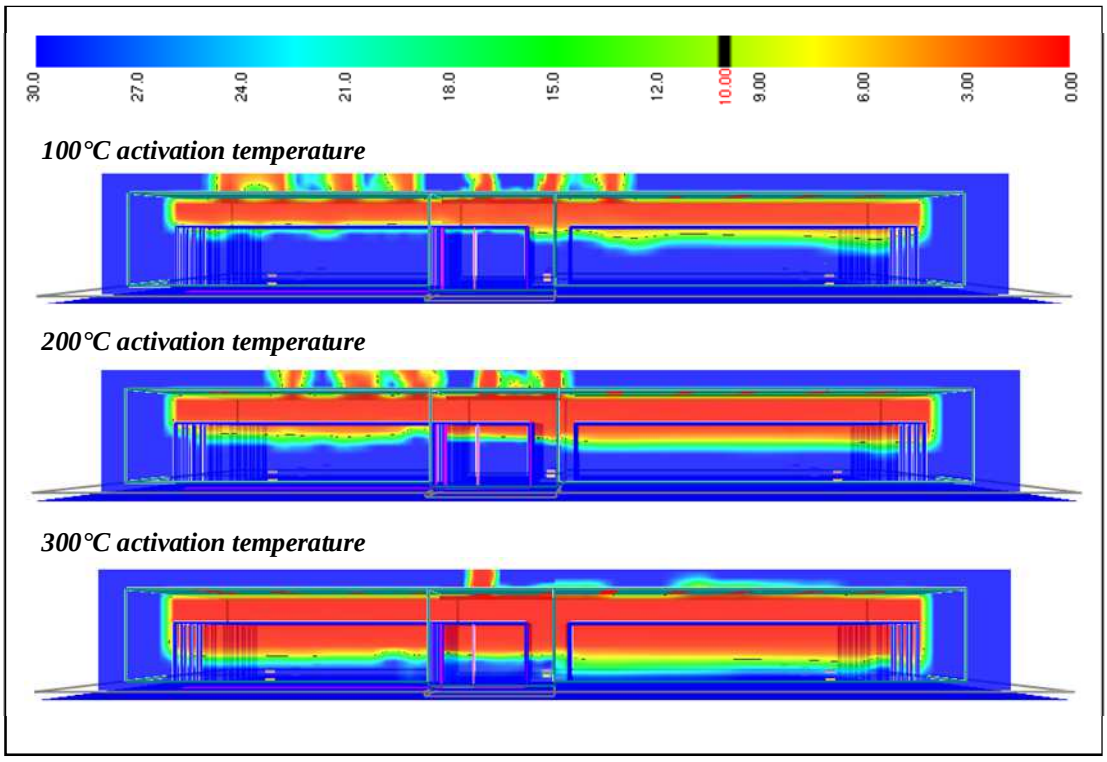

Figure 110: Visibility (m) after 1,800 seconds in large warehouse with rapid t^3 fire growth and square-shaped roof vents opening sequentially at three different activation temperatures (top – 100°C, middle – 200°C, and bottom – 300°C). Visibility slice is taken through long axis of warehouse, 20 m inside nearest warehouse wall.

Activation temperatures of 200°C and 300°C effected significant reductions to radiative heat fluxes in the lower layer: in the simulation with permanently-open vents, and both simulations with 100°C activation temperature, radiative heat flux conditions were hazardous. In the simulations with increased activation temperatures, radiative heat fluxes were routine only. These results are represented in Figure 111 by three selected positions. Results for other positions can be found in Appendix I1.

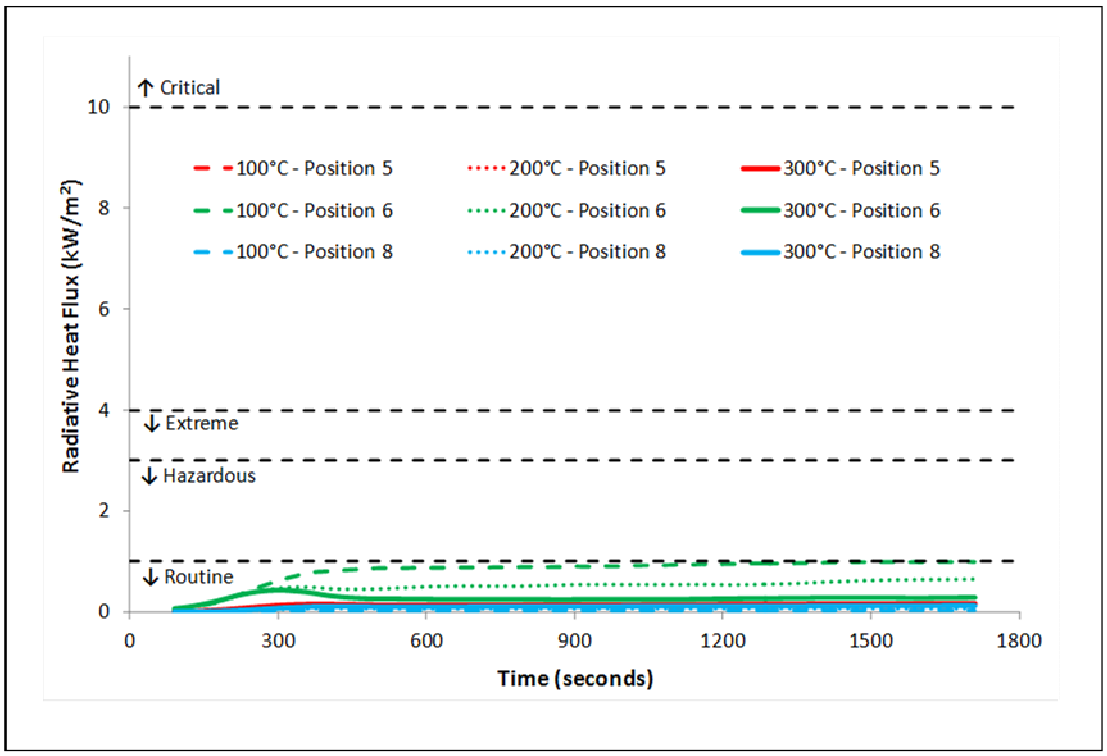

Figure 111: Comparison of smoothed radiative heat flux data from FDS at a height of 1.5 m in large warehouse with rapid t^3 fire growth and square-shaped roof vents opening sequentially at three different activation temperatures.

Temperatures measured at 1.5 m above floor level were not significantly changed from either the permanently-open or simultaneously opening roof venting scenarios. These results can be found in Appendix I1. Upper layer temperature distributions were practically unchanged among all three scenarios and are not discussed further.

3.2.10 Phase 2c: Large warehouse – rapid t^3 fire growth & strip-shaped roof vents opening sequentially at two different activation temperatures

Use of strip-shaped roof vents was not able to alleviate the effect of the smoke layer in the large warehouse when compared to those simulations in the large warehouse with square-shaped vents (Figure 112 *cf*. Figure 108): as was seen in Section 3.2.9, with an activation temperature of 200°C a clear layer remained available for the duration of the simulation, but when the activation temperature was increased to 300°C the smoke layer increased in depth, reaching floor level by the end of the simulation. In Figure 113 it can be seen that the visibility in the lower layer remained acceptable below a height of ~6 m, but visibility reduced to close to 0 m at floor level

by the end of the simulation with a 300°C activation temperature. The visibility conditions are worse than was observed in the case with simultaneously-opening vents in Section 3.2.8, where the bottom of the smoke layer remained above the top of the storage racks.

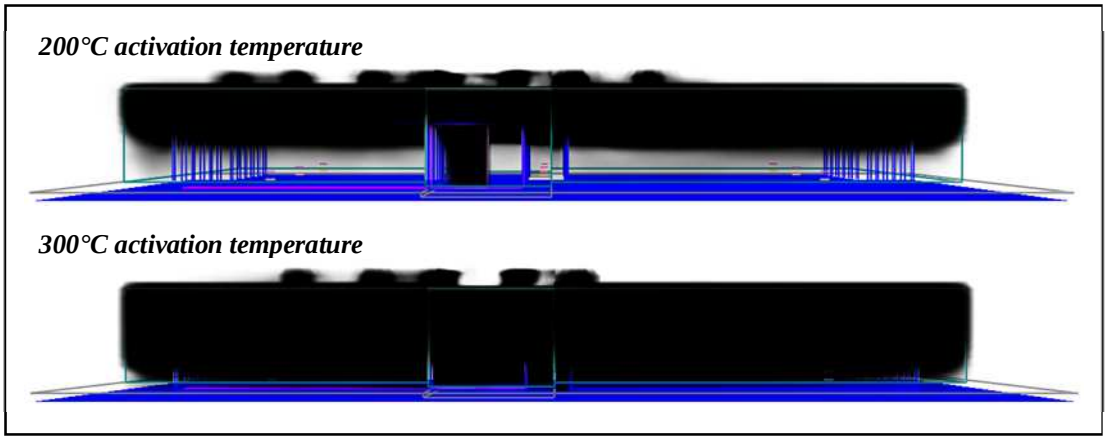

Figure 112: Smokeview depiction of smoke layer after 1,800 seconds in large warehouse with rapid t^3 fire growth and strip-shaped roof vents opening sequentially at two different activation temperatures (top – 200° and bottom – 300°).

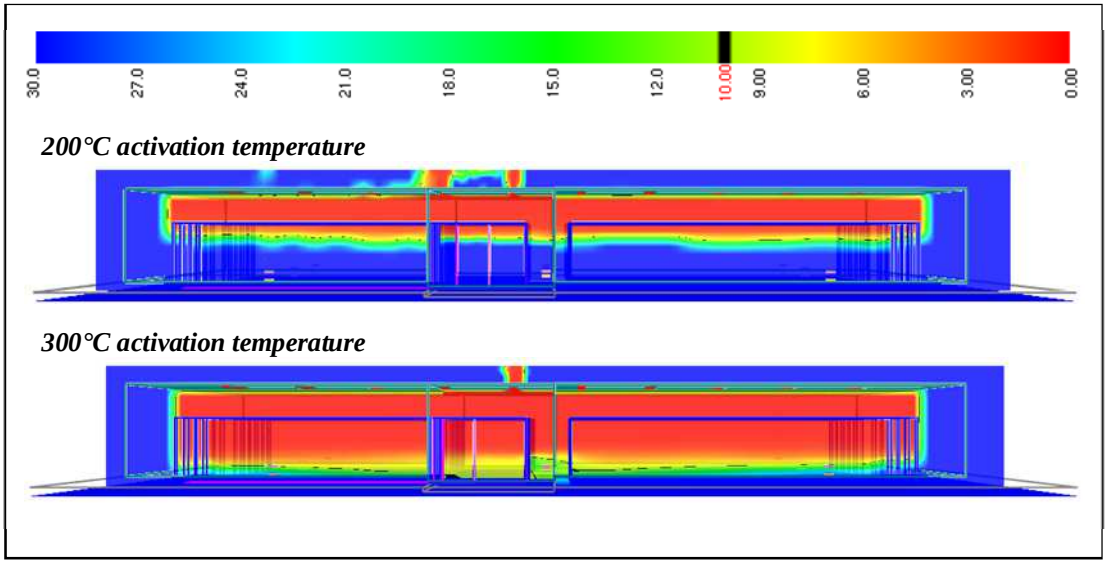

Figure 113: Visibility (m) after 1,800 seconds in large warehouse with rapid t^3 fire growth and strip-shaped roof vents opening sequentially at two different activation temperatures (top – 200°C and bottom – 300°C). Slice is taken through long axis of warehouse, 20 m inside nearest warehouse wall.

In Figure 114, the area and timing of vent activation for the strip-shaped roof venting simulations is compared. The first segment of a strip-shaped vent to achieve the

200°C activation temperature does so after nearly 3 minutes (172 seconds). After nearly 26 minutes (1,552 seconds), the final segment to achieve the activation temperature opened. By this stage, 7 of the 20 strip vents had fully or partially opened, in effect, the equivalent of 3.7 strip-shaped vents. Each strip vent has an area of 15 m², meaning the *utilised roof venting area* equates to 56 m². In the 300°C activation temperature scenario, 5 of the 20 strip vents had opened to some degree, translating to 1.8 strip vents or 27 m² *utilised roof venting area*. The roof venting area utilised in both of these scenarios is substantially less than was required in the corresponding square-venting scenarios. In the square-venting scenario with 200°C activation temperature, 61 m² was required to vent the warehouse: significantly more than with strip-shaped vents. In the case with a 300°C activation temperature, the 27 m² required with strip-shaped vents also compares favourably to the 31 m² required with square-shaped vents, however, this venting area proved insufficient, as visibility worsened when compared to both the permanently-open case and the two cases with activation of the roof vents at a temperature of 100°C.

Radiative heat fluxes and temperatures measured at 1.5 m above floor level were not significantly changed from either the permanently-open or simultaneously opening roof venting scenarios. These results can be found in Appendix I2. Upper layer temperature distributions were practically unchanged between the two scenarios and are not discussed further.

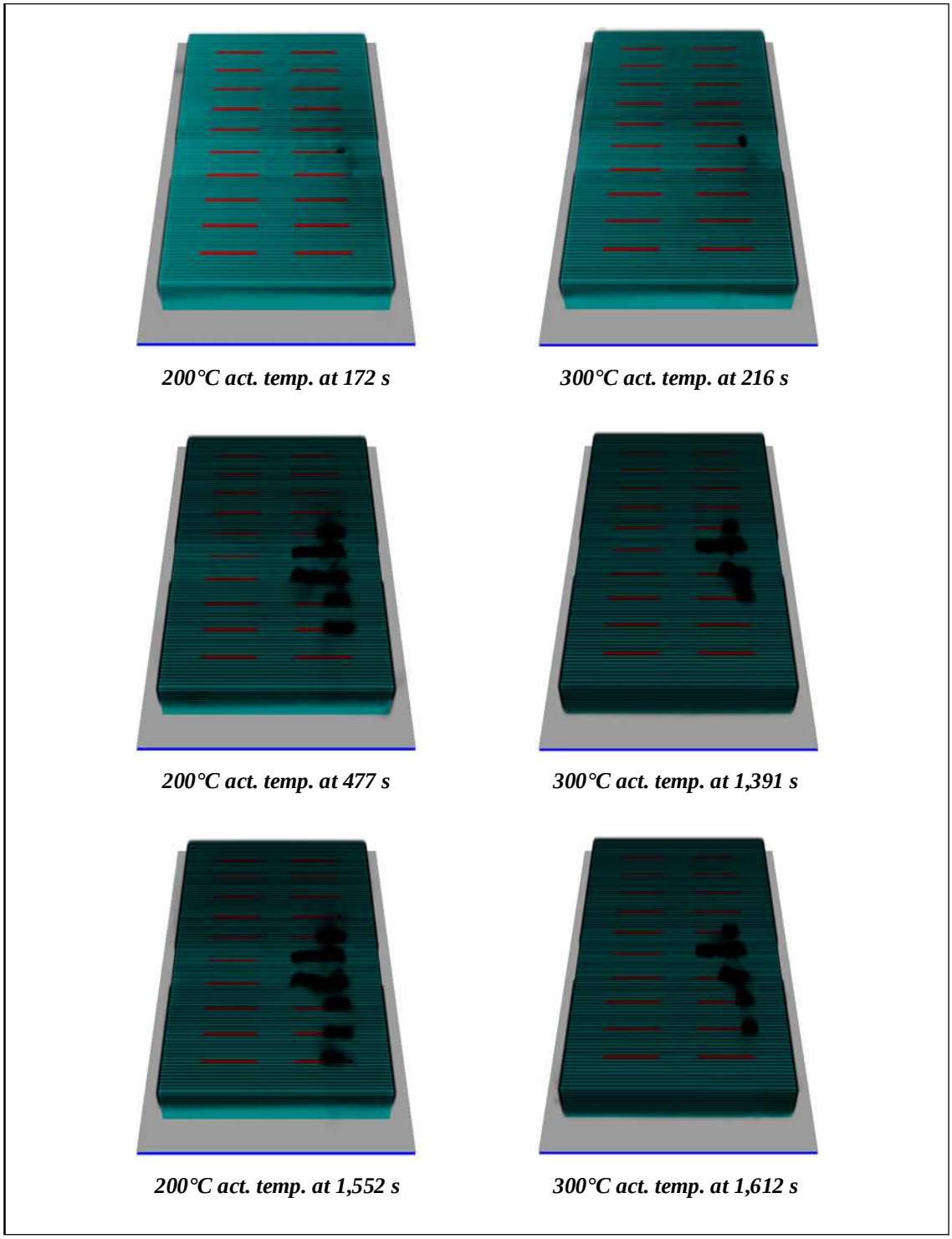

Figure 114: Comparison of vent opening area and timing in large warehouse with rapid t^3 fire growth and strip-shaped roof vents opening sequentially at two different activation temperatures (left – 200°C activation temperature and right – 300°C activation temperature). The top row of images shows activation of the first vent segment; the middle row shows the situation 1 second before activation of the first segment of the final vent; and the bottom row shows activation of the final vent segment during the specified simulation time of 1,800 seconds.

3.2.11 Phase 2d: Large warehouse – extreme t^3 fire growth & square-shaped roof vents opening simultaneously at an activation temperature of 100°C

Compared to the case of permanently-open roof venting from Section 3.1.14, the smoke layer and visibility conditions in the large warehouse with an extreme t^3 fire growth rate are little changed when temperature-dependent opening of roof vents is applied (Figure 115 *cf*. Figure 77 and Figure 78). All 88 vents opened after just over 1 minute (65 seconds) when the first vent achieved the activation temperature of 100°C. Visibility was remained very good for the entire simulation, with the smoke layer remaining at or above the top of the rack storage.

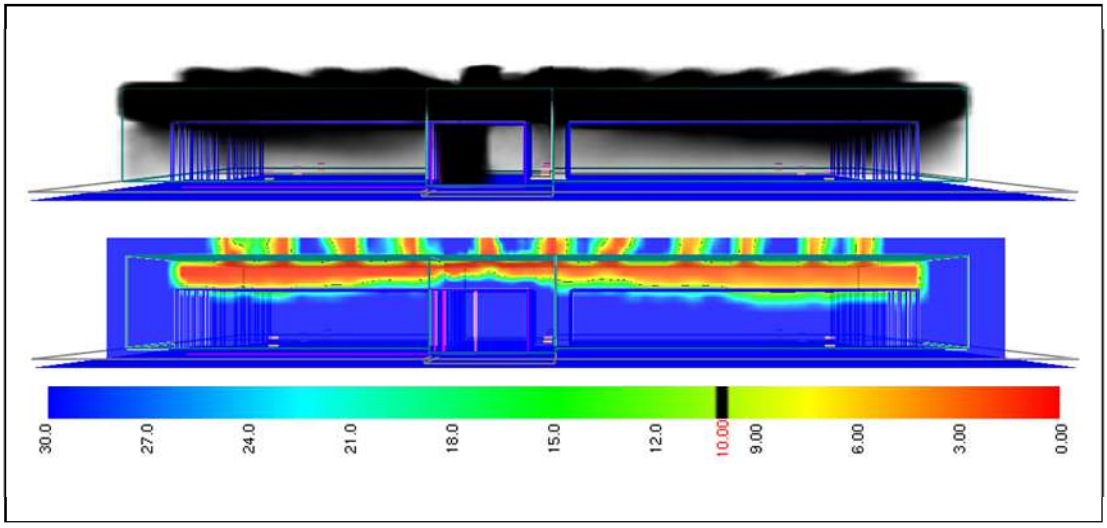

Figure 115: Smokeview depiction of smoke layer after 1,800 seconds (top) and visibility in metres (bottom) in large warehouse with extreme t^3 fire growth and square-shaped roof vents opening simultaneously at an activation temperature of 100°C. Visibility slice is taken through long axis of warehouse, 20 m inside nearest warehouse wall.

Radiative heat fluxes and temperatures at all positions were practically identical to the case with permanently-open vents, and can be found in Appendix J1.

3.2.12 Phase 2d: Large warehouse – extreme t^3 fire growth & square-shaped roof vents opening sequentially at three different activation temperatures

Smokeview images of the smoke layer in the large warehouse with sequentially-opening roof vents at an activation temperatures of 100°C looks almost identical to both the case with permanently-open vents and that with simultaneously-opening vents (Figure 116 *cf*. Figure 77 and Figure 115). As the activation temperature was increased to 200°C and 300°C, the smoke layer became progressively deeper. Further, in the case of activation at 300°C, visibility at the end of the 30-minute simulation had reduced to 0 m almost to floor level throughout the warehouse (Figure 117).

In Figure 118, the reduction of utilised vents is well-visualized: with an activation temperature of 100°C, 35 vents were eventually activated; with an activation temperature of 200°C, just 17 of the 88 vents were activated; and, with activation at 300°C, only 10 of the 88 vents opened during the 30 minute simulation. The numbers of activated vents in these scenarios match very closely with those from Section 3.2.9.

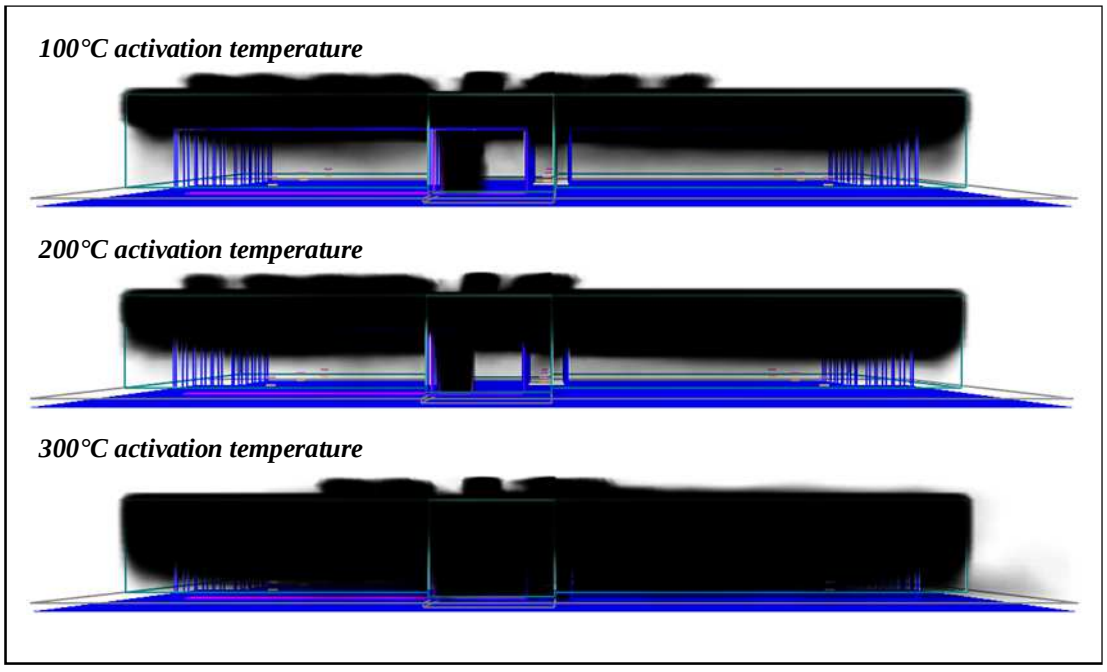

Figure 116: Smokeview depiction of smoke layer after 1,800 seconds in large warehouse with extreme t^3 fire growth and square-shaped roof vents opening sequentially at three different activation temperatures (top – 100°C, middle – 200°C, and bottom – 300°C).

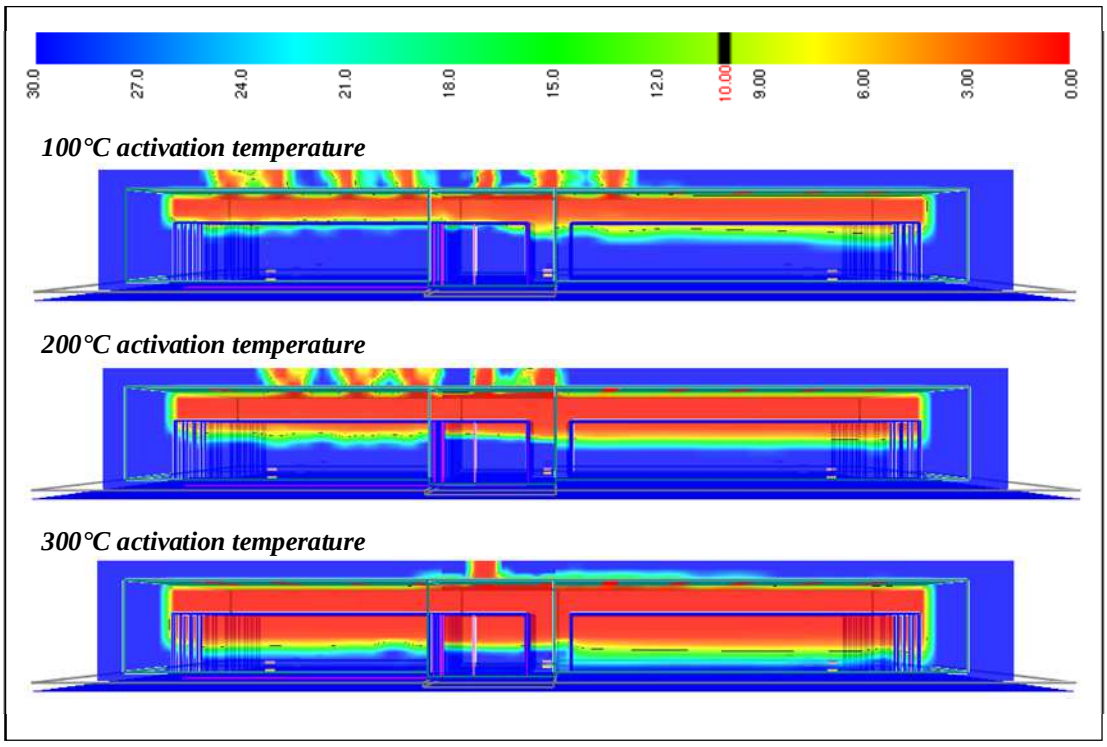

Figure 117: Visibility (m) after 1,800 seconds in large warehouse with extreme t^3 fire growth and square-shaped roof vents opening sequentially at three different activation temperatures (top – 100°C, middle – 200°C, and bottom – 300°C). Visibility slice is taken through long axis of warehouse, 20 m inside nearest warehouse wall.

Radiative heat fluxes and temperatures measured at the nine targets at 1.5 m above floor level remained almost unchanged from the simultaneous vent-opening scenario, and can be viewed in Appendix J2. Upper layer temperatures displayed no major differences to those recorded in the large warehouse with rapid t^3 fire growth, and are not reported here.

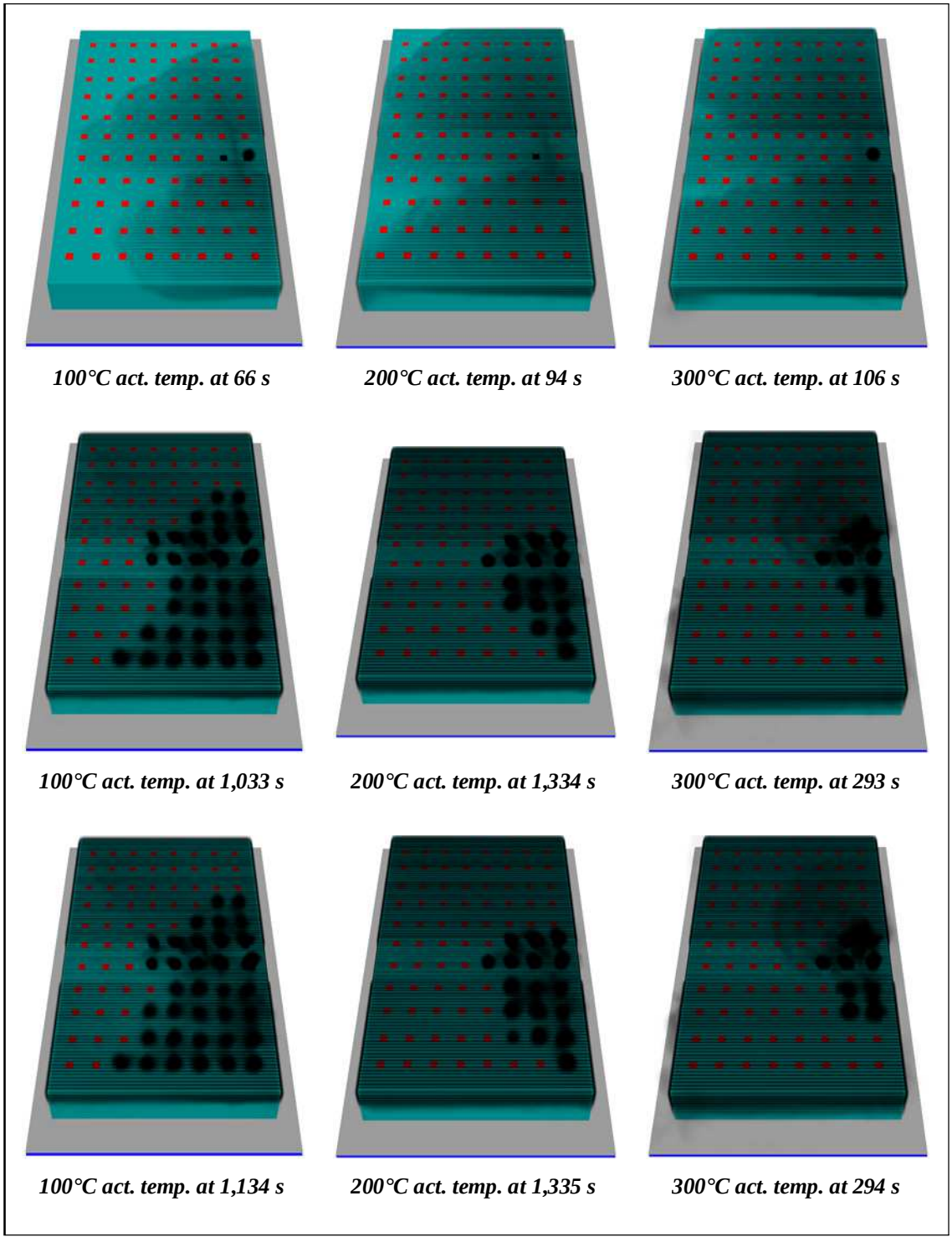

Figure 118: Comparison of vent opening area and timing in large warehouse with extreme t^3 fire growth and square-shaped roof vents opening sequentially at three different activation temperatures (left – 100°C activation temperature, centre – 200°C activation temperature, and right – 300°C activation temperature). The top row of images shows activation of the first vent; the middle row shows the situation 1 second before activation of the final vent; and the bottom row shows activation of the final vent during the specified simulation time of 1,800 seconds.

3.2.13 Phase 2d: Large warehouse – extreme t^3 fire growth & strip-shaped roof vents opening sequentially at two different activation temperatures

Depth of the smoke layer was not alleviated in the large warehouse (with extreme t^3 fire growth) by the use of strip-shaped vents (Figure 119). Visibility was, for the 200°C and 300°C activation temperatures, very similar to that observed for square-shaped vents with the same activation temperatures (Figure 120 *cf*. Figure 117).

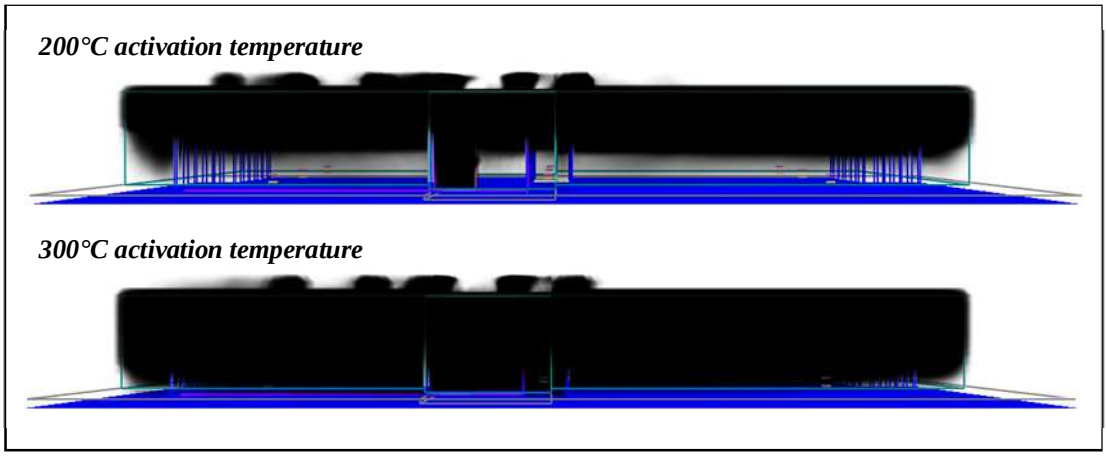

Figure 119: Smokeview depiction of smoke layer after 1,800 seconds in large warehouse with extreme t^3 fire growth and strip-shaped roof vents opening sequentially at two different activation temperatures (top – 200° and bottom – 300°).

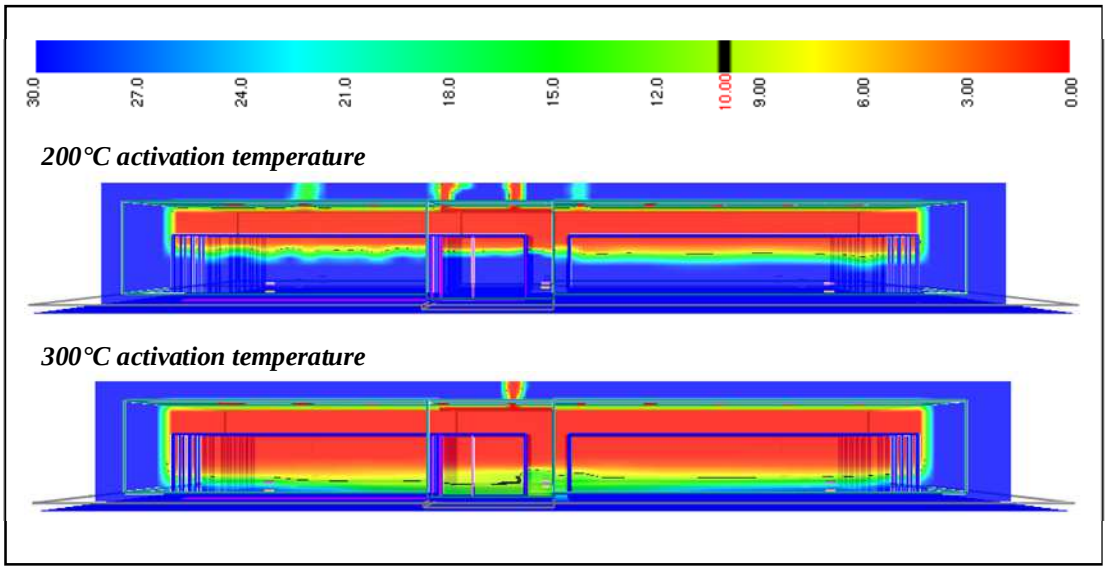

Figure 120: Visibility (m) after 1,800 seconds in large warehouse with extreme t^3 fire growth and strip-shaped roof vents opening sequentially at two different activation temperatures (top – 200°C and bottom – 300°C). Slice is taken through long axis of warehouse, 20 m inside nearest warehouse wall.

Activated vent area and timing of vent activation for the strip-shaped roof venting simulations is displayed in Figure 121. The first segment of the first strip-shaped vent opened after one and a half minutes (90 seconds) for the scenario with an activation temperature of 200°C. The last segment to open in this scenario did so after nearly 27 minutes (1,598 seconds). Of the 20 strip-shaped vents, 7 had opened, at least partially, by the end of the simulation, equating to 3.7 strip vents (or 55 m² of *utilised roof venting area*): this is less than was utilised with the corresponding square-venting scenario (58 m²). With a 300°C activation temperature, the first vent segment was activated after nearly 2 minutes (106 seconds), and the last vent segment after nearly 24 minutes (1,426 seconds). The *utilised roof venting area* was 29 m² (or 1.9 vents): this area compares favourably with the equivalent *utilised roof venting area* of 34 m² in the square-shaped roof venting scenario (with a 300°C activation temperature) presented in Section 3.2.12.

Radiative heat fluxes and temperatures at 1.5 m above floor level in the case of strip-shaped roof venting were not substantially different from those seen in the simulations with square-shaped vents, and can be viewed in Appendix J3.

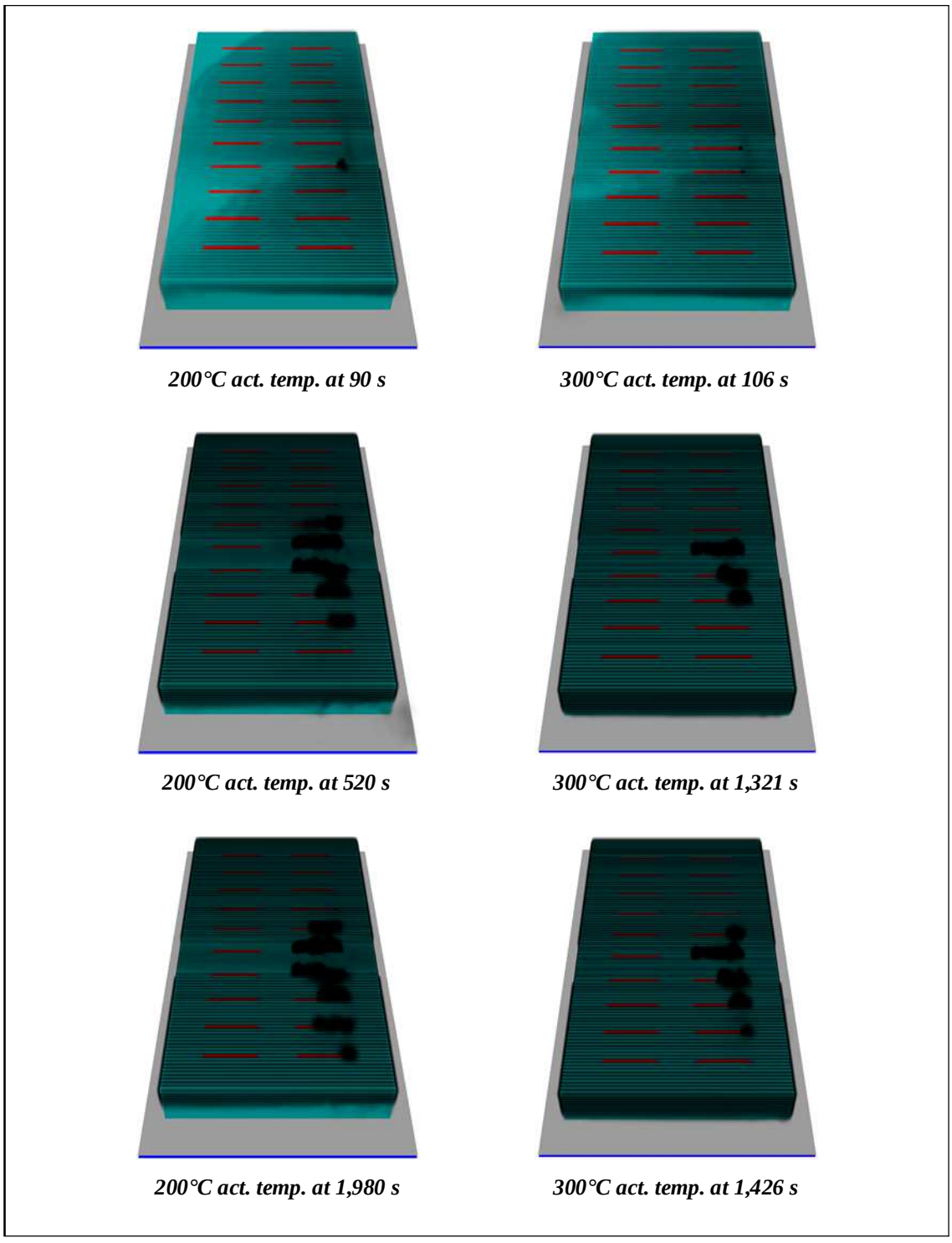

Figure 121: Comparison of vent opening area and timing in large warehouse with extreme t^3 fire growth and strip-shaped roof vents opening sequentially at two different activation temperatures (left – 200°C activation temperature and right – 300°C activation temperature). The top row of images shows activation of the first vent segment; the middle row shows the situation 1 second before activation of the first segment of the final vent; and the bottom row shows activation of the final vent segment during the specified simulation time of 1,800 seconds.

3.3 Phase Three: Use of Downstands

Presented in Table 9 are the summary results from the third phase of testing in the small warehouse. Results for the large warehouse are presented later in this chapter in Table 10. For each warehouse size and fire growth rate, four combinations of vent shape, vent opening progression and vent activation temperature from Phase Two were tested in combination with three downstand depths: 10 %, 20 %, and 30 % of the warehouse height. The stated objective from Section 1.4 was to evaluate the use of downstands on the effectiveness of roof venting for providing the Fire Brigade Intervention Model fire fighter tenability criteria. All simulations in Phase Three included 5 % roof venting area and an inlet area for make-up air of 50 % of the roof venting area.

3.3.1 Phases 3a & 3b: Simulations in the small warehouse

In the small warehouse containing a rapid t^3 fire growth rate, a simultaneous vent-opening sequence, and a downstand depth of 10 %, maximum radiative heat fluxes were 4.2 kW/m² close to the fire and 0.7 kW/m² away from the fire. Maximum temperature was 20.1°C close to the fire and 18.7°C away from the fire (see Table 9). Deeper downstands effected a decrease in radiative heat fluxes both near and away from the fire to 3.9 kW/m² and 0.6 kW/m² with downstand depth of 20 %, and 3.5 kW/m² and 0.4 kW/m² with downstand depth of 30 %, respectively. This trend of reducing radiative heat fluxes with increased depth of downstands was observed for all forms of vent shape and opening sequence: simultaneous opening of square-shaped vents at a 100°C activation temperature, sequential opening of square-shaped vents at 100°C activation temperatures, sequential opening of square-shaped vents at 300°C activation temperatures and sequential opening of strip-shaped vents at 300°C. As was seen in Phase Two, the simulations containing strip venting exhibited much lower radiative heat fluxes and higher temperatures than those with square-shaped venting.

Overall, conditions were considerably more favourable in the small warehouse with the use of downstands, although with the exception of the strip-venting case, this did not usually lead to a reclassification of the conditions according to the FBIM criteria (Table 9). It was evident that the installation of downstands had a significant effect on

Table 9 – Summary of maximum results for Phase 3 simulations in small warehouse.

Fire growth	Vent shape	Opening Sequence	Opening Temperature	Downstand Depth	Radiation near fire[1] (kW/m^2 - Criterion)	Radiation away from fire (kW/m^2 - Criterion)	Temperature near fire[1] (°C - Criterion)	Temperature away from fire (°C - Criterion)
Rapid	Square	Simultaneous	100°C	10 %	4.2 - Extreme$^+$	0.7 - Routine	20.1 - Routine	18.7 - Routine
Rapid	Square	Simultaneous	100°C	20 %	3.9 - Extreme	0.6 - Routine	18.7 - Routine	18.5 - Routine
Rapid	Square	Simultaneous	100°C	30 %	3.5 - Extreme	0.4 - Routine	17.8 - Routine	17.5 - Routine
Rapid	Square	Sequential	100°C	10 %	4.2 - Extreme$^+$	0.7 - Routine	21.3 - Routine	18.8 - Routine
Rapid	Square	Sequential	100°C	20 %	4.0 - Extreme$^+$	0.5 - Routine	20.5 - Routine	19.4 - Routine
Rapid	Square	Sequential	100°C	30 %	3.3 - Extreme	0.4 - Routine	22.6 - Routine	20.5 - Routine
Rapid	Square	Sequential	300°C	10 %	4.1 - Extreme$^+$	0.5 - Routine	27.0 - Routine	31.3 - Routine
Rapid	Square	Sequential	300°C	20 %	3.5 - Extreme	0.3 - Routine	35.0 - Routine	36.5 - Routine
Rapid	Square	Sequential	300°C	30 %	3.1 - Extreme	0.2 - Routine	31.6 - Routine	38.8 - Routine
Rapid	Strip	Sequential	300°C	10 %	2.1 - Hazardous	0.3 - Routine	27.2 - Routine	42.1 - Routine
Rapid	Strip	Sequential	300°C	20 %	2.0 - Hazardous	0.2 - Routine	31.1 - Routine	43.7 - Routine
Rapid	Strip	Sequential	300°C	30 %	1.5 - Hazardous	0.1 - Routine	32.0 - Routine	42.3 - Routine
Extreme	Square	Simultaneous	100°C	10 %	4.5 - Extreme$^+$	0.7 - Routine	20.0 - Routine	18.8 - Routine
Extreme	Square	Simultaneous	100°C	20 %	4.0 - Extreme$^+$	0.6 - Routine	19.3 - Routine	18.4 - Routine
Extreme	Square	Simultaneous	100°C	30 %	3.4 - Extreme	0.4 - Routine	17.8 - Routine	17.5 - Routine
Extreme	Square	Sequential	100°C	10 %	4.5 - Extreme$^+$	0.7 - Routine	21.2 - Routine	19.0 - Routine
Extreme	Square	Sequential	100°C	20 %	4.1 - Extreme$^+$	0.6 - Routine	22.7 - Routine	19.6 - Routine
Extreme	Square	Sequential	100°C	30 %	3.9 - Extreme	0.3 - Routine	22.8 - Routine	20.5 - Routine
Extreme	Square	Sequential	300°C	10 %	4.2 - Extreme$^+$	0.5 - Routine	23.4 - Routine	32.4 - Routine
Extreme	Square	Sequential	300°C	20 %	3.8 - Extreme	0.4 - Routine	36.0 - Routine	39.4 - Routine
Extreme	Square	Sequential	300°C	30 %	3.2 - Extreme	0.2 - Routine	32.1 - Routine	38.2 - Routine
Extreme	Strip	Sequential	300°C	10 %	2.5 - Hazardous	0.4 - Routine	26.5 - Routine	38.3 - Routine
Extreme	Strip	Sequential	300°C	20 %	2.0 - Hazardous	0.2 - Routine	31.1 - Routine	43.7 - Routine
Extreme	Strip	Sequential	300°C	30 %	1.8 - Hazardous	0.2 - Routine	32.1 - Routine	43.3 - Routine

[1] Indicates Positions 5 and 6 only.
[+] Indicates that conditions exceeded the extreme criterion, but were not severe enough to be classed as critical.

the radiative heat fluxes. For the case with simultaneous vent opening at an activation temperature of 100°C, the maximum radiative heat flux recorded near the fire in Phase Two (without downstands) was 5.1 kW/m² (see Table 8). With downstands measuring 10 % of the height of the warehouse, this value reduced to 4.2 kW/m². Further increases of downstand depth to 20 % and 30 % of the height of the warehouse, reduced the maximum radiative heat flux even further to 3.9 kW/m² and 3.5 kW/m², respectively. This effect was also true away from the fire, and for all vent shapes and opening mechanisms. In contrast, temperatures tended to increase following the installation of downstands. However, temperatures remained routine for all simulations.

Maximum values for extreme t^3 fire growth in the small warehouse tended to be slightly higher than to those described above for rapid t^3 fire growth, but otherwise do not present further points of interest.

3.3.2 Phase 3a: Small warehouse - rapid growth fire & square roof vents activating simultaneously at 100°C

Smokeview representations of the smoke layer and visibility in the small warehouse with the rapid growth t^3 fire, simultaneously–activating roof vents, and three different depth of downstand are shown in Figure 122 and Figure 123, respectively. In the case of 10 % downstand depth, regions of very low visibility (6-7 m) were present between the storage racks for almost the entire length of the warehouse. Increases to downstand depth made visibility worse either side of the fire origin, but promoted visibility away from the fire.

Visibility at a height of 1.5 m for all three downstand depths is compared to the case without downstands in Figure 124. Installation of downstands did not improve visibility in the small warehouse, at least not for the 10 % and 20 % downstands depths. At these downstand depths, the smoke reservoirs were too shallow to effectively restrict smoke movement: instead the downstands created a turbulent environment, which pushed the smoke layer deeper. With a 30 % downstand depth, improvement in visibility was seen in the north-west corner of the warehouse, but any advantage of the downstands over the case without downstands is debatable.

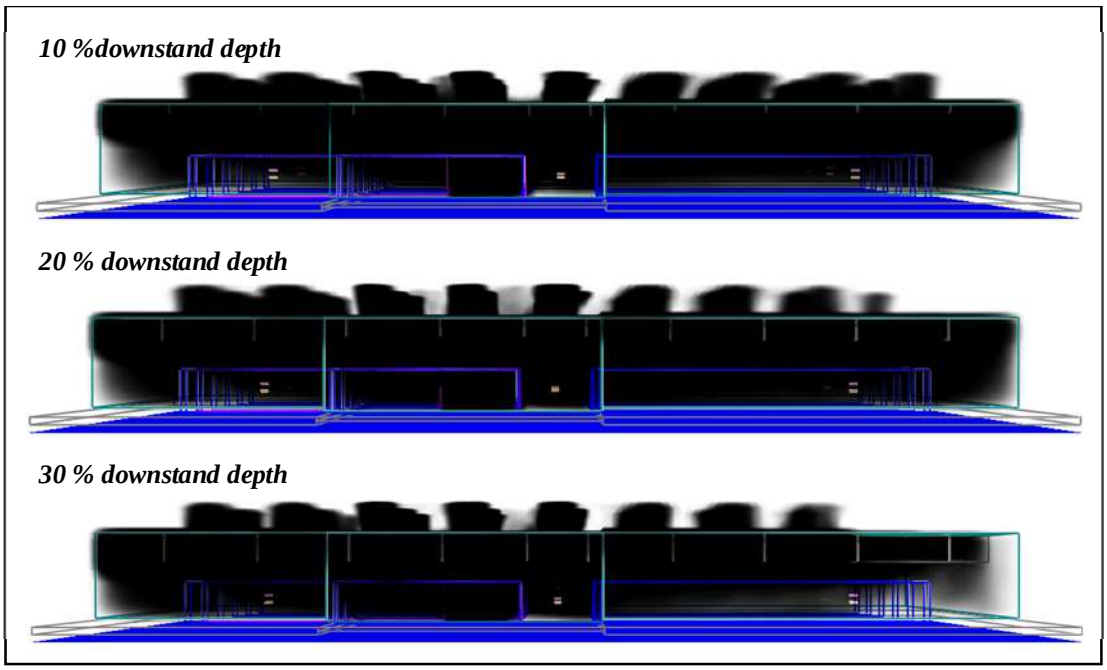

Figure 122: Smokeview depiction of smoke layer after 1,800 seconds in small warehouse with rapid t^3 fire growth and square-shaped roof vents opening simultaneously at 100 °C with three different downstand depths (top – 10 %, middle – 20 %, and bottom – 30 %).

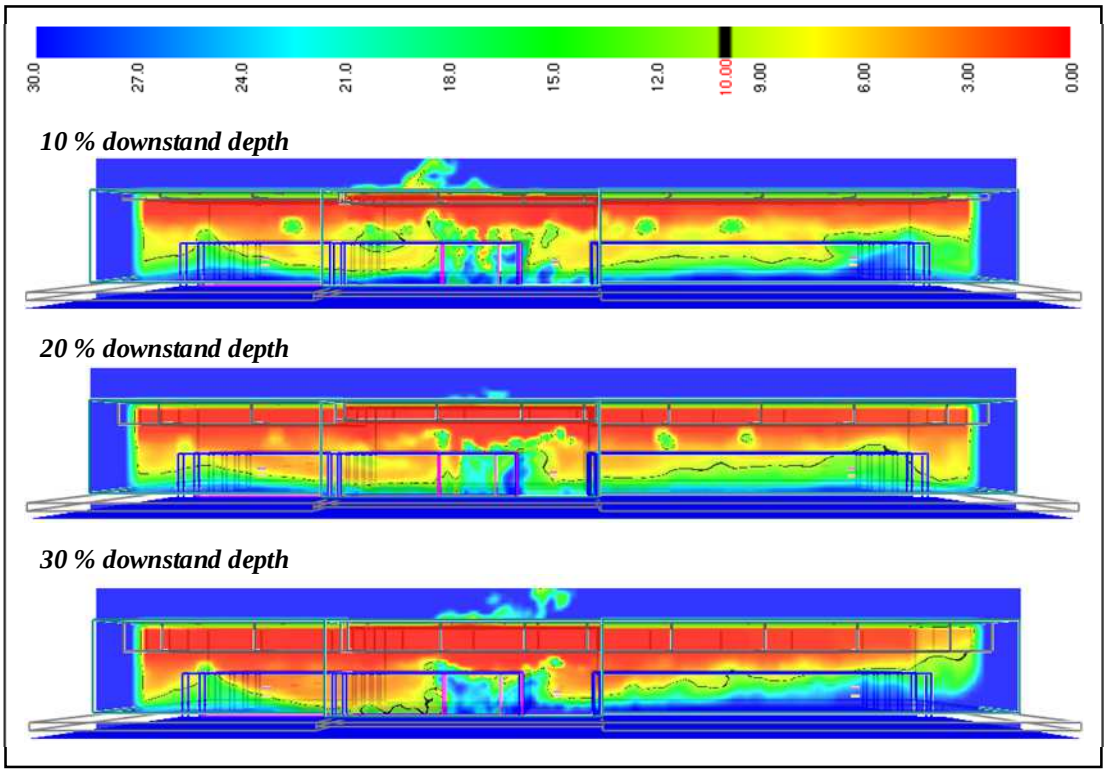

Figure 123: Visibility (m) after 1,800 seconds in small warehouse with rapid t^3 fire growth and square-shaped roof vents opening simultaneously at 100 °C with three different downstand depths (top – 10 %, middle – 20 %, and bottom – 30 %). Visibility slice is taken through long axis of warehouse, 20 m inside nearest warehouse wall.

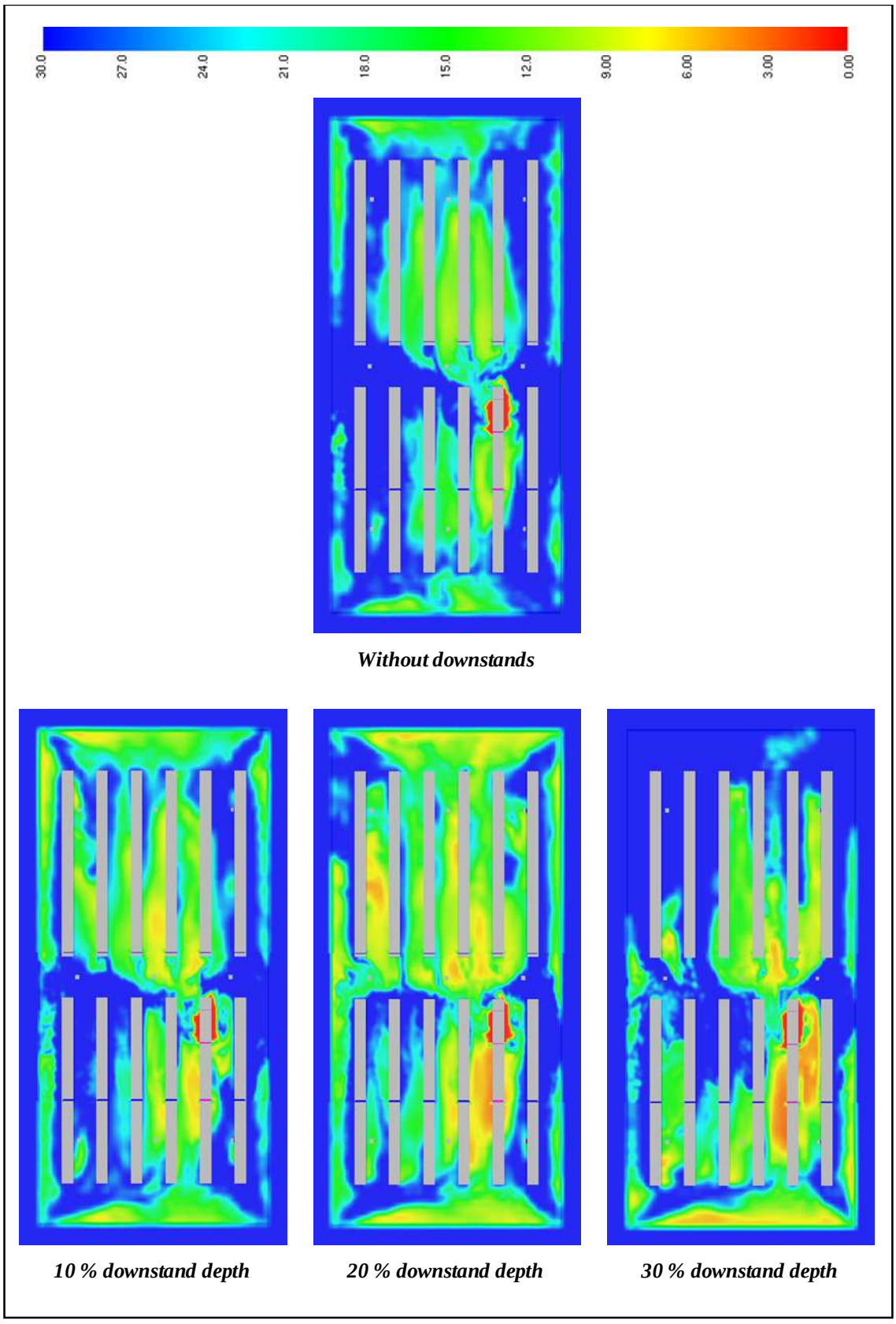

Figure 124: Comparison of visibility (m) at a height of 1.5 m after 1,800 seconds in small warehouse with rapid t^3 fire growth and simultaneously-opening square-shaped vents with 100°C activation: without downstands versus three different downstand depths (top – without, bottom left – 10 % depth , bottom centre – 20 % depth, and bottom right – 30 % depth).

Vent activation temperature of 100°C was reached after slightly more than 1 minute (64 seconds) with a 10 % downstand depth. This time was 14 seconds slower than without downstands (*cf.* Section 3.2.2) due to the downstands acting to delay vent activation by blocking movement of the ceiling jet towards the nearest temperature sensor. That is, the geometry of the downstands created 55 smoke reservoirs under the warehouse ceiling. With only 27 vents required, not every smoke reservoir contained a vent with an associated temperature sensor. This effect was more pronounced with 20 % and 30 % downstand depths: activation occurred after 69 seconds and 70 seconds, respectively.

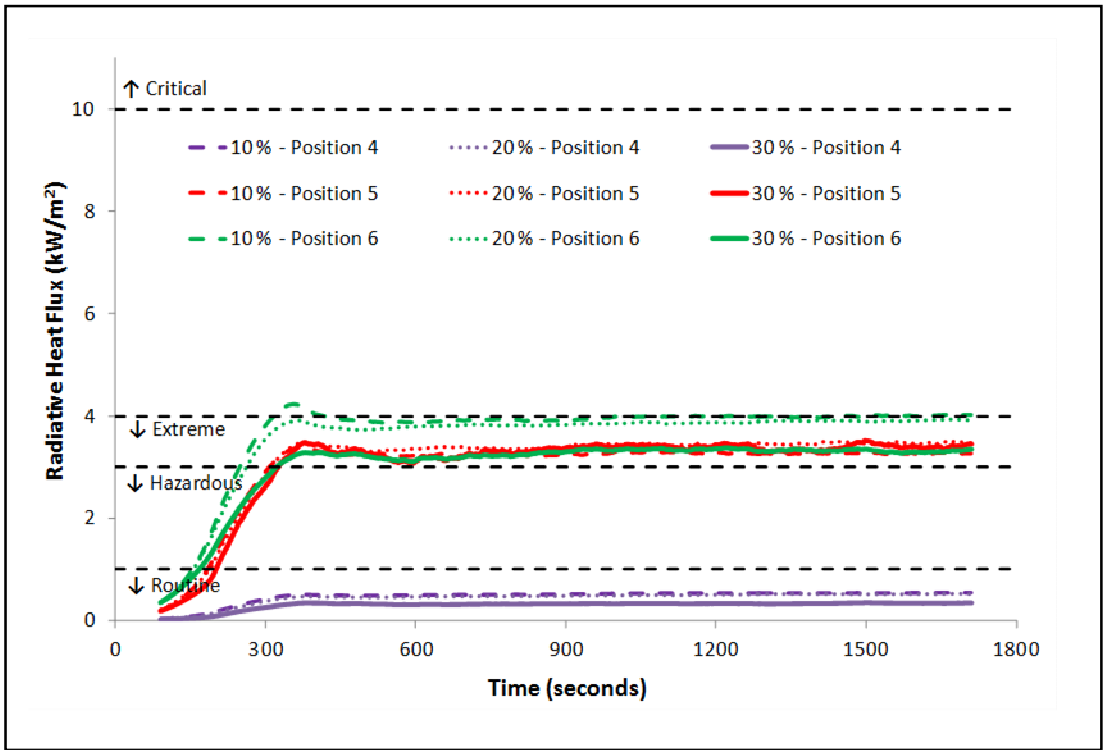

Figure 125: Comparison of smoothed radiative heat flux data from FDS at a height of 1.5 m in small warehouse with rapid t^3 fire growth and square-shaped roof vents opening simultaneously at an activation temperature of 100°C for three different downstand depths.

At a height of 1.5 m above floor level, there was a significant reduction in radiative heat fluxes at Position 6 (Figure 125 *cf.* Figure 81). In the simulation without downstands, radiative heat fluxes at Position 6 were worse than extreme within 300 seconds. The Extreme Conditions criterion was only briefly exceeded with 10 % downstands, but otherwise radiative heat fluxes for all three downstand depths remained within the Extreme Conditions criterion. There was minimal difference at

Position 5 with or without downstands. At all other positions radiative heat fluxes were reduced with the use of downstands, and with each successive reduction in downstand depth. These results are represented by Position 4 in Figure 125: full results, as well as those for temperature at 1.5 m can be found in Appendix K1.

The impact of the downstands on the temperature distributions in the upper layer of the warehouse is highlighted in Figure 126. As the downstands increased in depth, the area that remained at ambient temperature (dark blue) increased substantially. This advantageous trend was accompanied by the contrary trend of increasing area of temperatures exceeding 280°C, *i.e.* temperatures exceeding the Extreme Conditions criterion of the FBIM, making conditions *less tenable* than the case without downstands. However, this does not imply that use of downstands should be avoided. The area of extreme temperatures was all contained in smoke reservoirs in the region near the fire, many of which did not contain a roof vent. The mismatch between downstand placement and roof venting distribution meant that many smoke reservoirs were not able to exhaust hot smoke and gases. Should these two factors be more closely aligned, then the inclusion of downstands would be expected to display at least equally advantageous upper layer temperatures as the case without downstands.

3.3.3 Phase 3a: Small warehouse - rapid growth fire & square roof vents activating sequentially at 100°C

When vent opening sequence was changed from simultaneous to sequential opening, the smoke layer depend and the visibility became worse (Figure 127 and Figure 128). As downstand depth increased, fewer vents opened due to fewer sensors achieving the required 100°C activation temperature. In the case with 10 % downstand depth, 20 vents had activated by the end of the simulation compared to all 27 vents in the simulation with simultaneous activation. As downstand depth increased to 20 %, the total number of vents to activate decreased to 14. And, with downstand depth of 30 %, just 11 vents opened. In the simulations with downstands, as the smoke spread from further from the fire, it cooled and sank into the lower regions of the warehouse rather than remaining above the rack storage, as it had done in the simulation without downstands (*cf*. Figure 85).

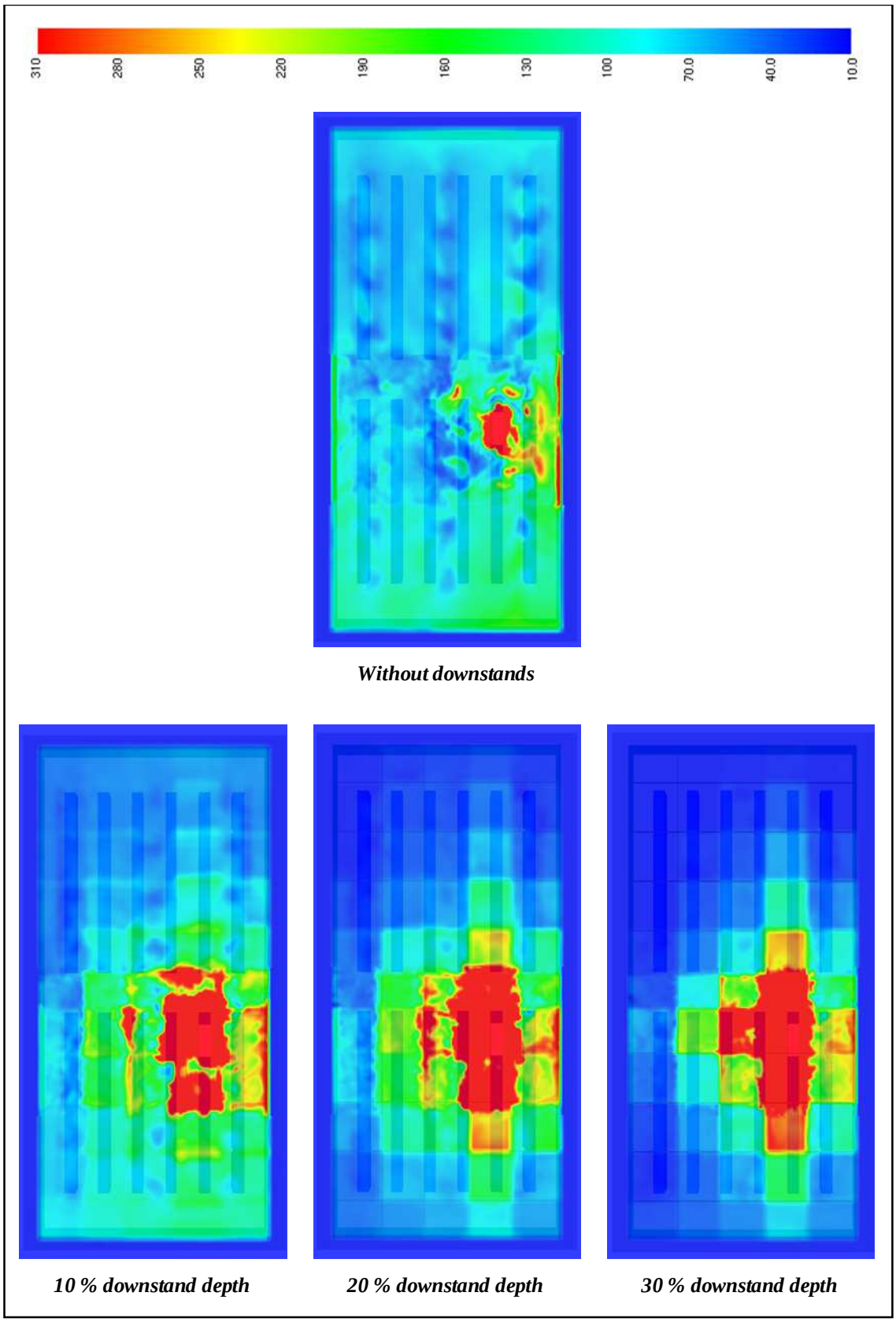

Figure 126: Comparison of temperature distributions at a height of 5.5 m after 1,800 seconds in small warehouse with rapid t^3 fire growth and simultaneously-opening square-shaped vents with 100°C activation: without downstands versus three different downstand depths (top – without, bottom left – 10 % depth , bottom centre – 20 % depth, and bottom right – 30 % depth).

Figure 127: Smokeview depiction of smoke layer after 1,800 seconds in small warehouse with rapid t^3 fire growth and square-shaped roof vents opening sequentially at 100 °C with three different downstand depths (top – 10 %, middle – 20 %, and bottom – 30 %).

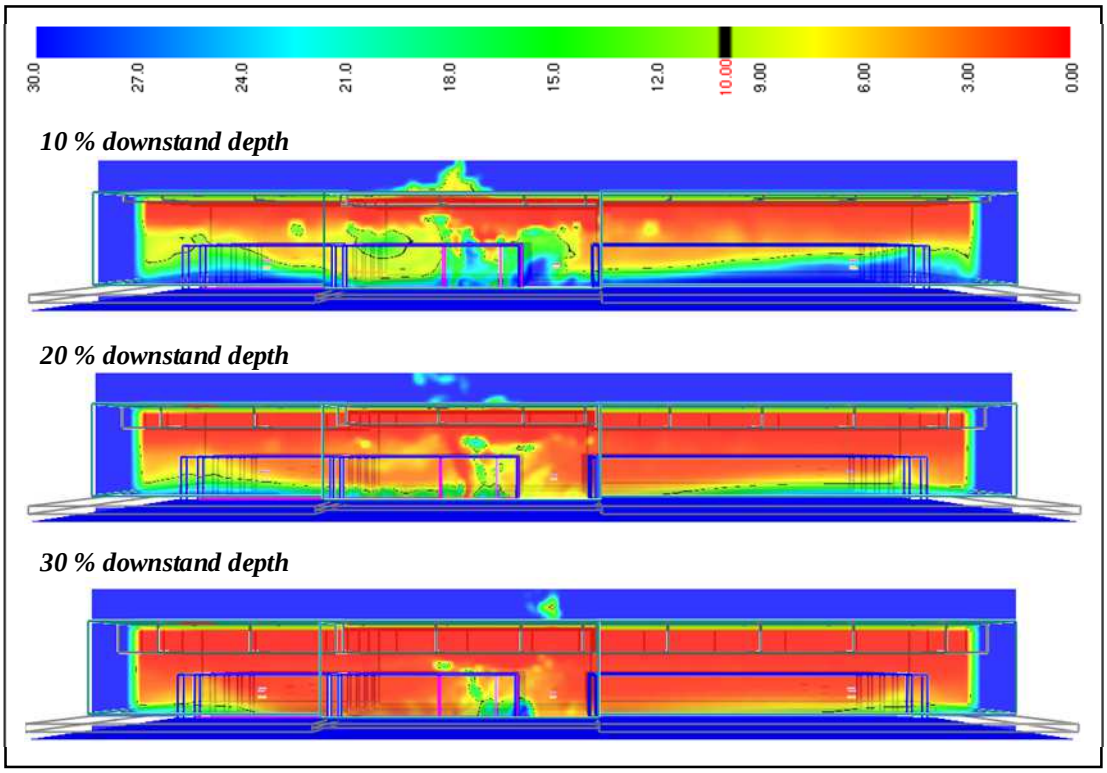

Figure 128: Visibility (m) after 1,800 seconds in small warehouse with rapid t^3 fire growth and square-shaped roof vents opening sequentially at 100 °C with three different downstand depths (top – 10 %, middle – 20 %, and bottom – 30 %). Visibility slice is taken through long axis of warehouse, 20 m inside nearest warehouse wall.

Radiative heat fluxes were much improved through the use of downstands (Figure 129 *cf.* Figure 87). From 10 minutes after the outbreak of fire, about the time the fire service might be expected to arrive, radiative heat fluxes at all positions remained almost entirely below the 4 kW/m² upper limit of the Extreme Conditions criterion. With a downstand depth of 30 %, conditions were almost entirely within the Hazardous Conditions criterion for the same time period. At positions further from the fire, represented by Position 4 in Figure 129, conditions were routine for the entirety of all simulations. Radiative heat flux results, and those for temperature at 1.5 m above floor level, can be found for all positions in Appendix K2.

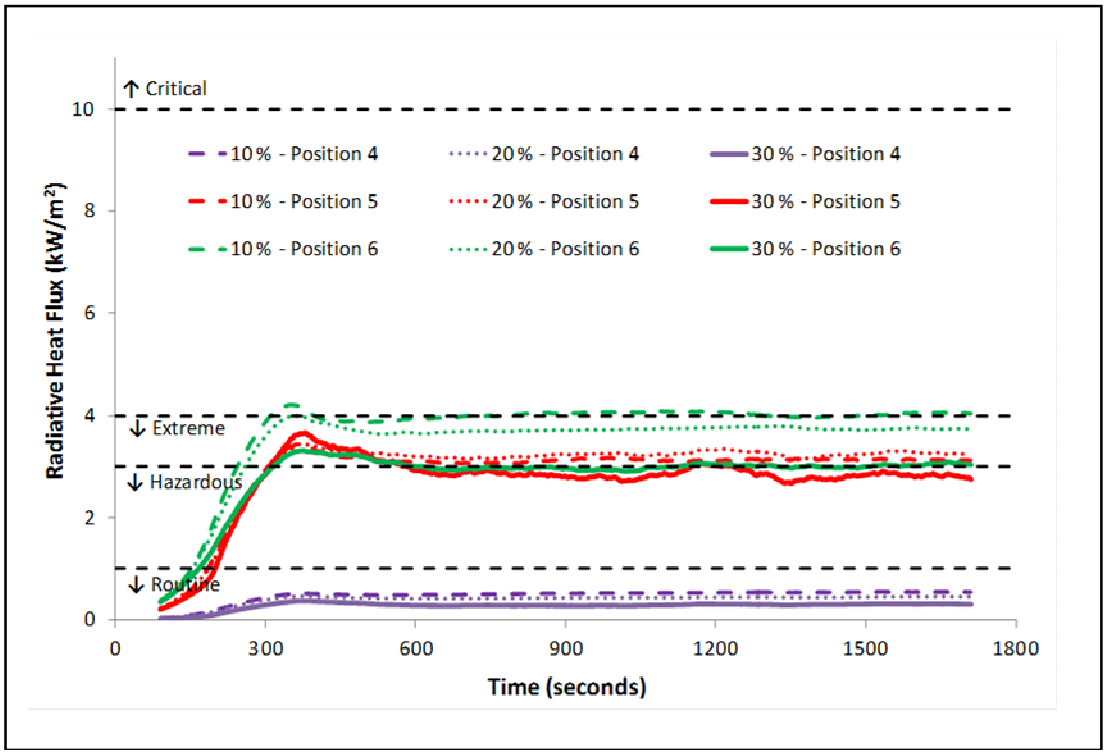

Figure 129: Comparison of smoothed radiative heat flux data from FDS at a height of 1.5 m in small warehouse with rapid t^3 fire growth and square-shaped roof vents opening sequentially at an activation temperature of 100°C for three different downstand depths.

Temperature distributions in the upper layer were very similar to those observed in the simulations with simultaneously-opening vents (Figure 130 *cf.* Figure 126). However, in the simulations with sequentially-opening vents, upper layer temperatures were hotter in the smoke reservoirs further from the fire, due to the smoke and gases in these regions having cooled to below the activation temperature.

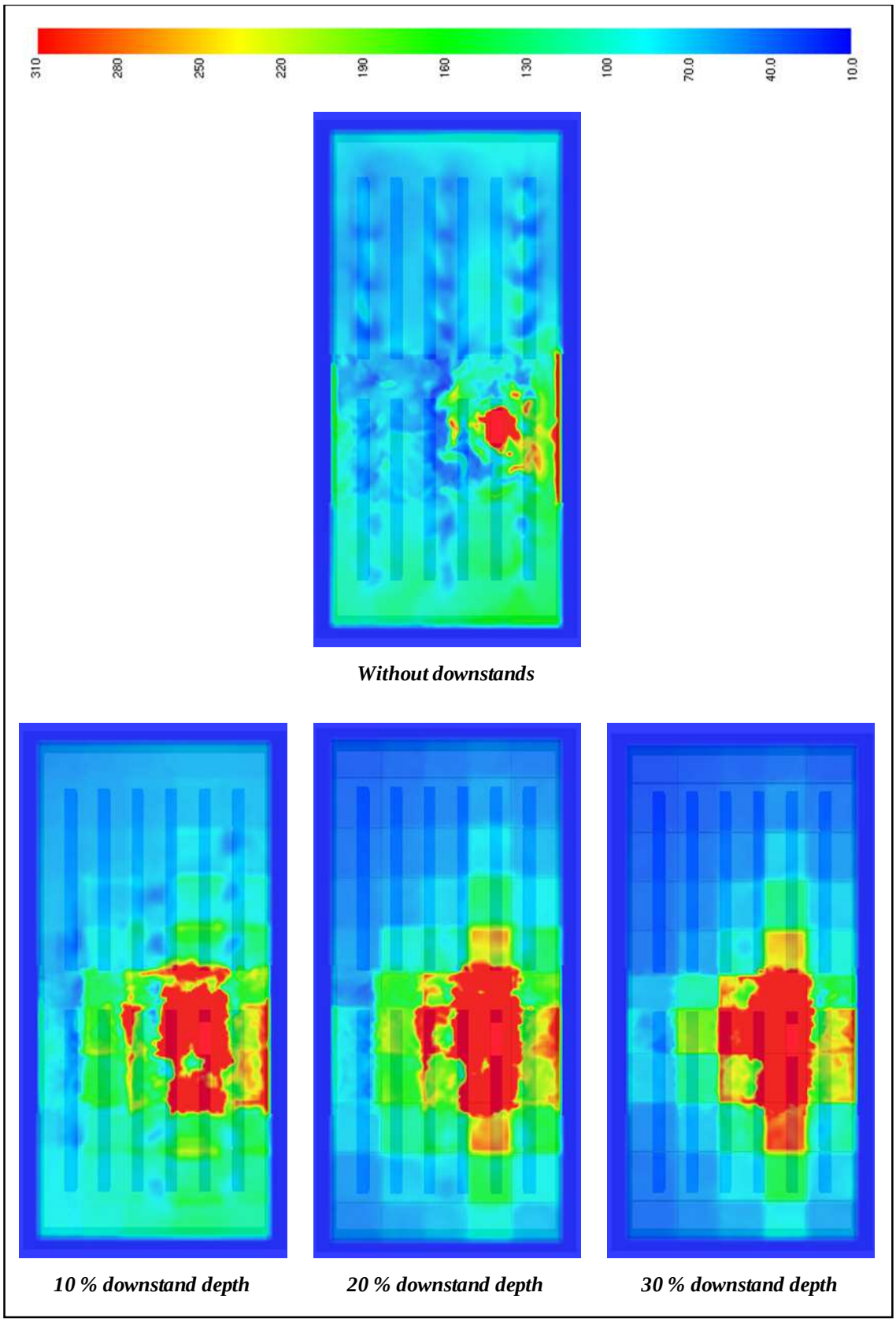

Figure 130: Comparison of temperature distributions at a height of 5.5 m after 1,800 seconds in small warehouse with rapid t^3 fire growth and sequentially-opening square-shaped vents with 100°C activation: without downstands versus three different downstand depths (top – without, bottom left – 10 % depth , bottom centre – 20 % depth, and bottom right – 30 % depth).

3.3.4 *Phase 3a: Small warehouse - rapid growth fire & square roof vents activating sequentially at 300°C*

The effect of delaying vent opening time, through an increase in activation temperature, is to deepen and thicken the smoke layer even further than in previous simulations with downstands, and thereby reduce visibility to 0 m for the length of the warehouse (Figure 131 and Figure 132). The activation temperature of 300°C was first reached after nearly three minutes (161 seconds) in the case with 10 % downstand depth, before a total of 9 vents eventually opened. In the cases with downstand depths of 20 % and 30 %, just 6 vents had opened by the end of the simulation.

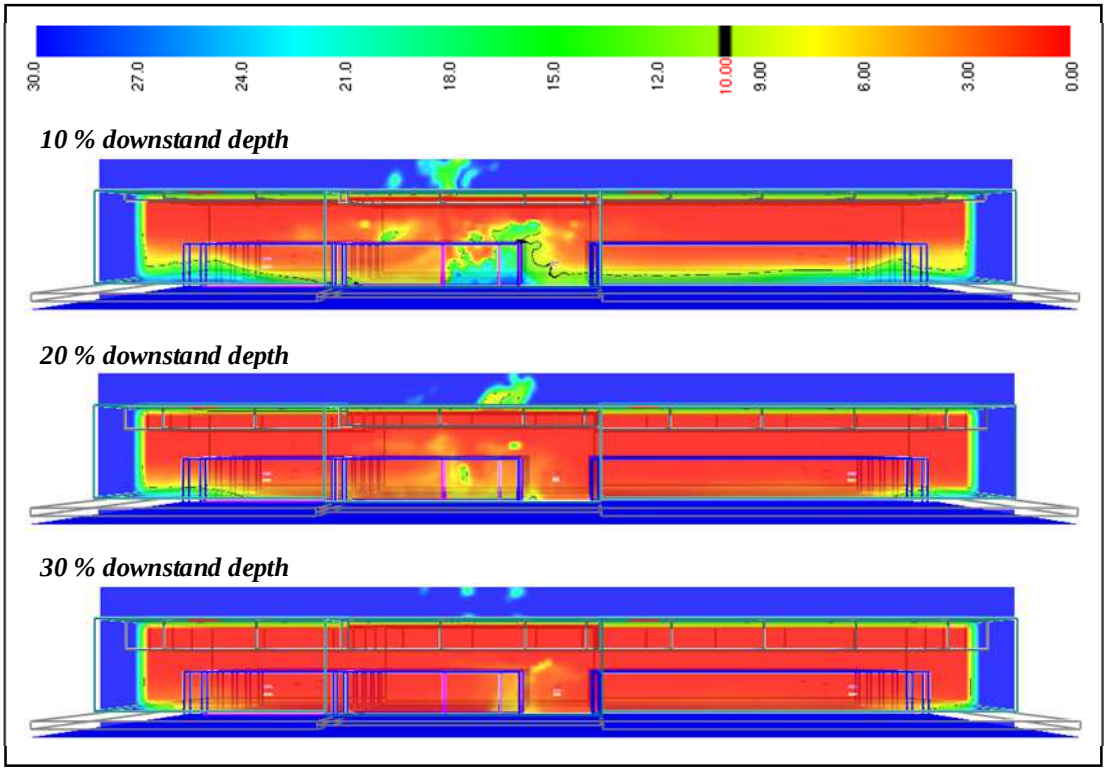

Figure 131: Visibility (m) after 1,800 seconds in small warehouse with rapid t^3 fire growth and square-shaped roof vents opening sequentially at 300 °C with three different downstand depths (top – 10 %, middle – 20 %, and bottom – 30 %). Visibility slice is taken through long axis of warehouse, 20 m inside nearest warehouse wall.

Radiative heat fluxes and temperatures at a height of 1.5 m above floor level were similar to those for the case with a 100°C activation temperature, and can be found in Appendix K3.

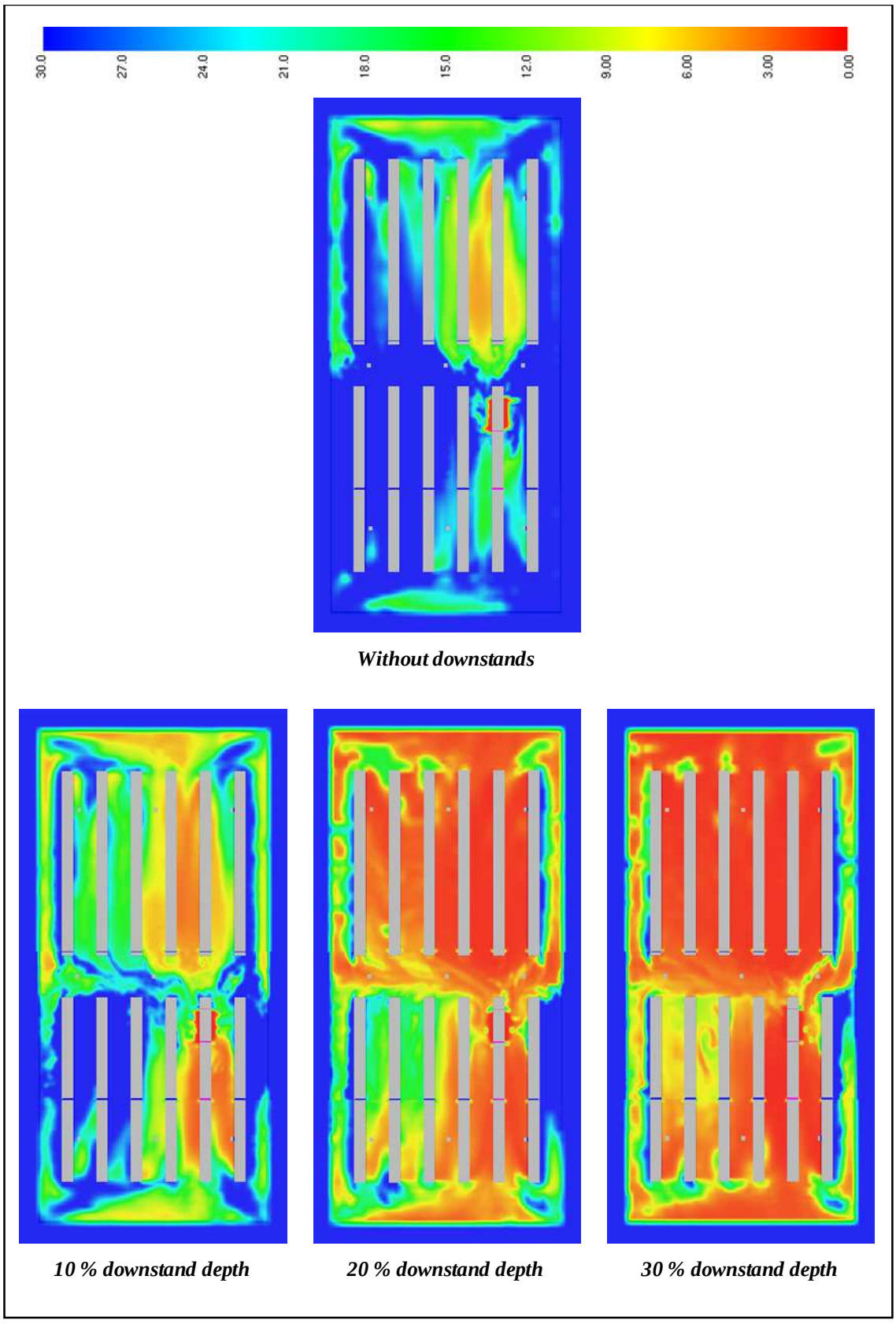

Figure 132: Comparison of visibility (m) at a height of 1.5 m after 1,800 seconds in small warehouse with rapid t^3 fire growth and sequentially-opening square-shaped vents with 300°C activation: without downstands versus three different downstand depths (top – without, bottom left – 10 % depth , bottom centre – 20 % depth, and bottom right – 30 % depth).

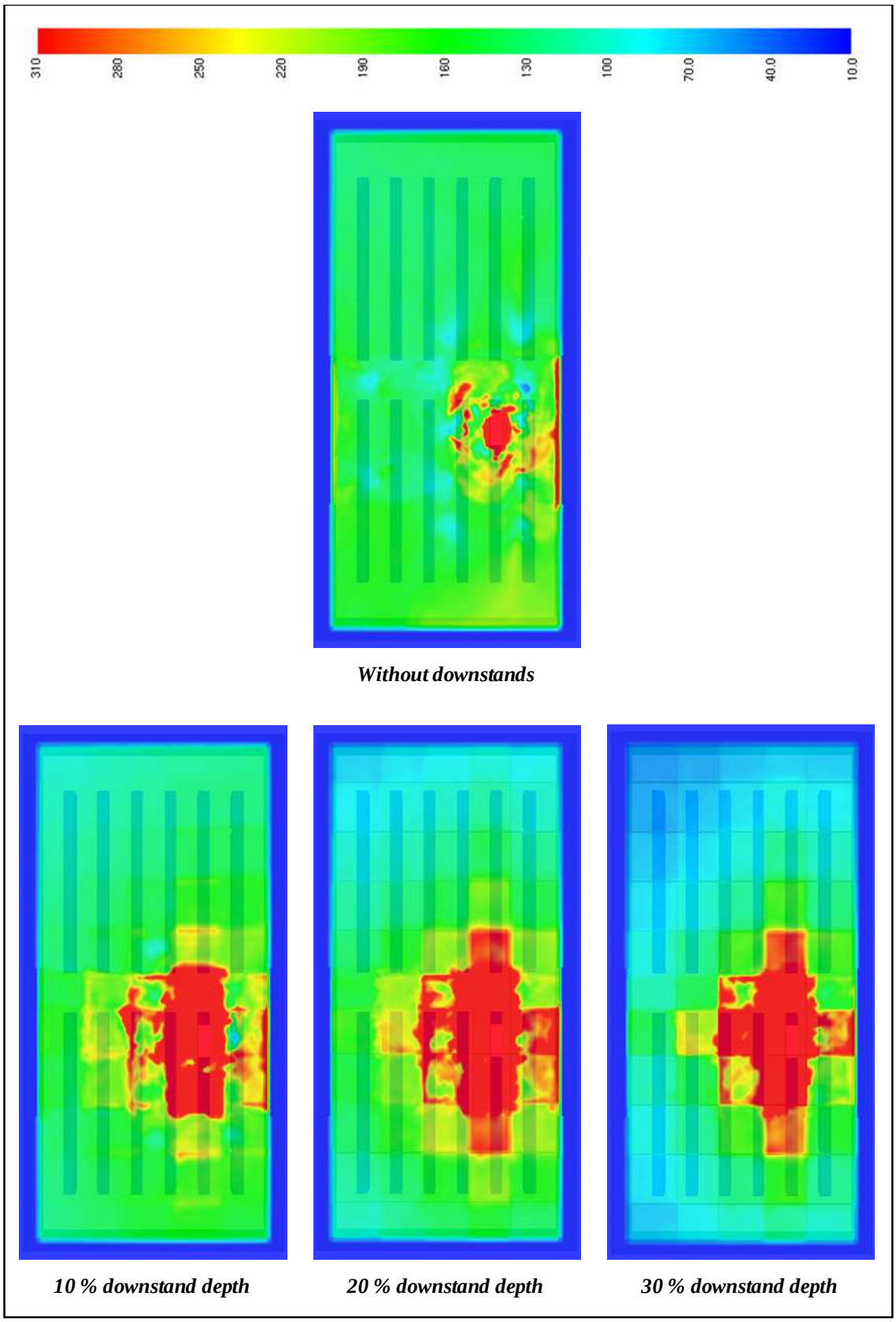

Figure 133: Comparison of temperature distributions at a height of 5.5 m after 1,800 seconds in small warehouse with rapid t^3 fire growth and sequentially-opening square-shaped vents with 300°C activation: without downstands versus three different downstand depths (top – without, bottom left – 10 % depth , bottom centre – 20 % depth, and bottom right – 30 % depth).

With the higher activation temperature of 300°C, upper layer temperatures were substantially hotter than for the simulations with 100°C activation temperatures (Figure 133 *cf*. Figure 126 and Figure 130). However, the same trends were apparent: as downstand depth was increased, temperatures in smoke reservoirs further from the fire decreased, while temperatures in smoke reservoirs close to the fire increased.

3.3.5 Phase 3a: Small warehouse - rapid growth fire & strip-shaped roof vents activating sequentially at 300°C

Use of downstands was not able to alleviate the effect of the smoke layer when used in conjunction with strip-shaped roof vents (Figure 134 *cf*. Figure 91). In fact, visibility in the lower layer was considerably less with downstands, sinking to close to 0 m visibility at 1.5 m above floor level throughout the warehouse in the cases of 20 % and 30 % downstand depths, and to between about 6 m and 12 m in the case with 10 % downstand depth (Figure 135).

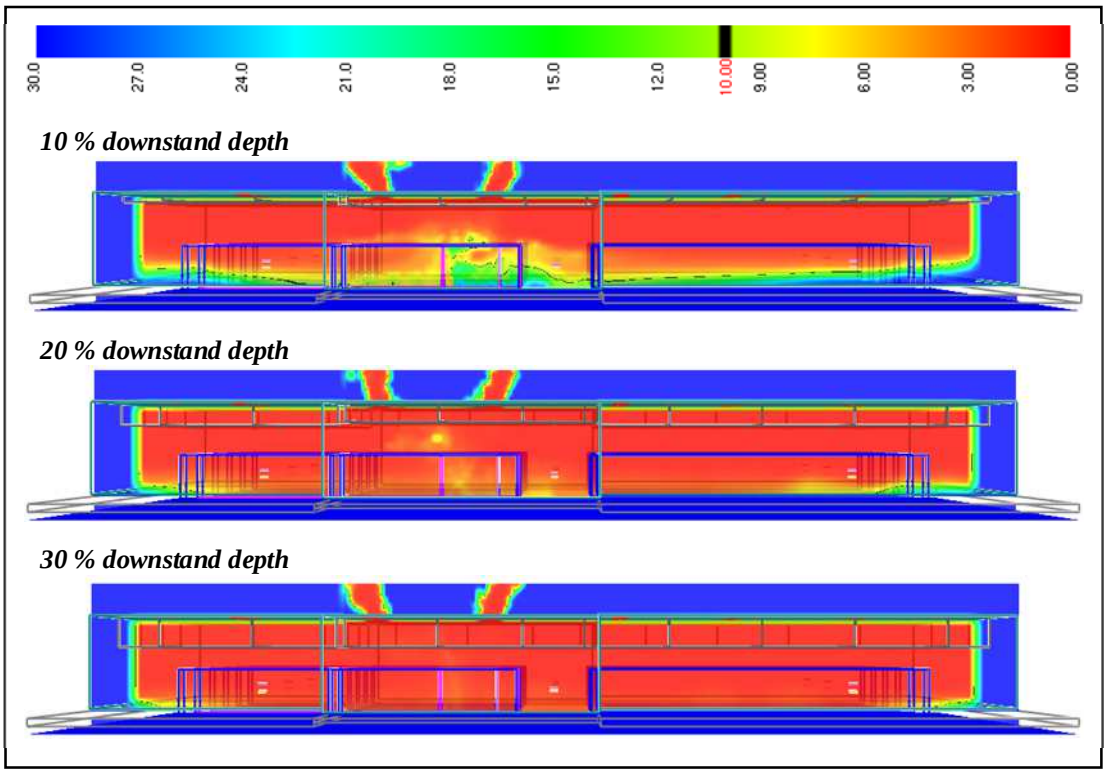

Figure 134: Visibility (m) after 1,800 seconds in small warehouse with rapid t^3 fire growth and strip-shaped roof vents opening sequentially at 300 °C with three different downstand depths (top – 10 %, middle – 20 %, and bottom – 30 %). Visibility slice is taken through long axis of warehouse, 20 m inside nearest warehouse wall.

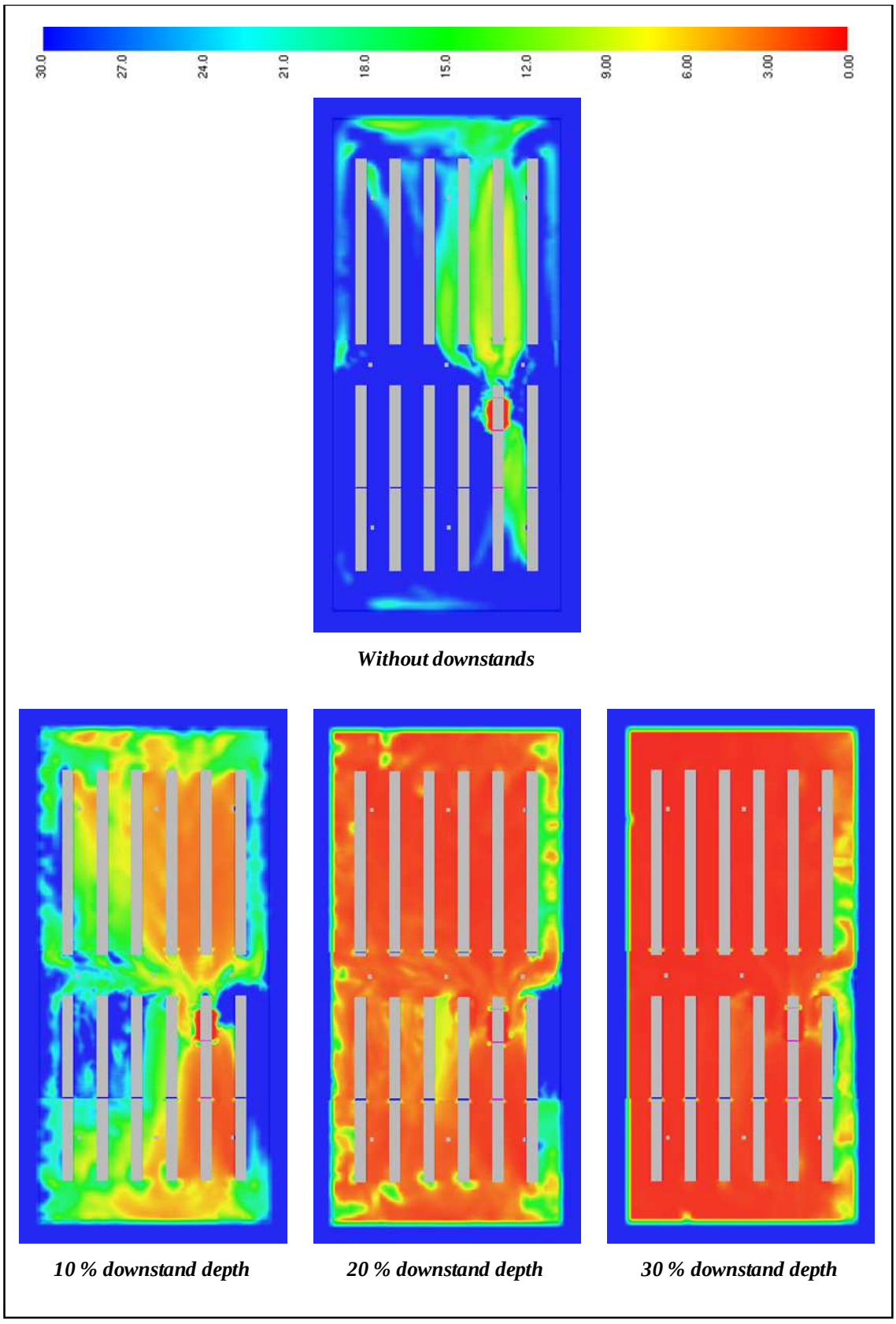

Figure 135: Comparison of visibility (m) at a height of 1.5 m after 1,800 seconds in small warehouse with rapid t^3 fire growth and sequentially-opening strip-shaped vents with 300°C activation: without downstands versus three different downstand depths (top – without, bottom left – 10 % depth , bottom centre – 20 % depth, and bottom right – 30 % depth).

In terms of radiative heat flux, there was an advantage of using downstands in combination with strip-shaped vents as opposed to using strip-shaped vents alone (Figure 136 *cf*. Figure 93). At Position 6, radiative heat fluxes reduced from extreme to hazardous with the addition of downstands of 10 % depth, and further to routine for most of the simulation time when the downstand depths were 20 % and 30 % of the warehouse height. At Position 5 and all positions further from the fire (represented in the figure by Position 4), radiative heat fluxes were routine for the entirety of the simulation regardless of the downstand depth tested. Results for all positions, as well as results for temperature can be found in Appendix K4.

As seen with the simulations involving square-shaped vents, use of downstands was able to restrict the spread of the hottest gases in the upper layer (Figure 137). Downstands of increasing depth were able to reduce upper layer temperatures from up to 180°C in the case without downstands to less than ~100°C with 30 % downstand depth. Near the fire, upper layer temperatures were also held in-check owing to better placement of the strip vent nearest the fire.

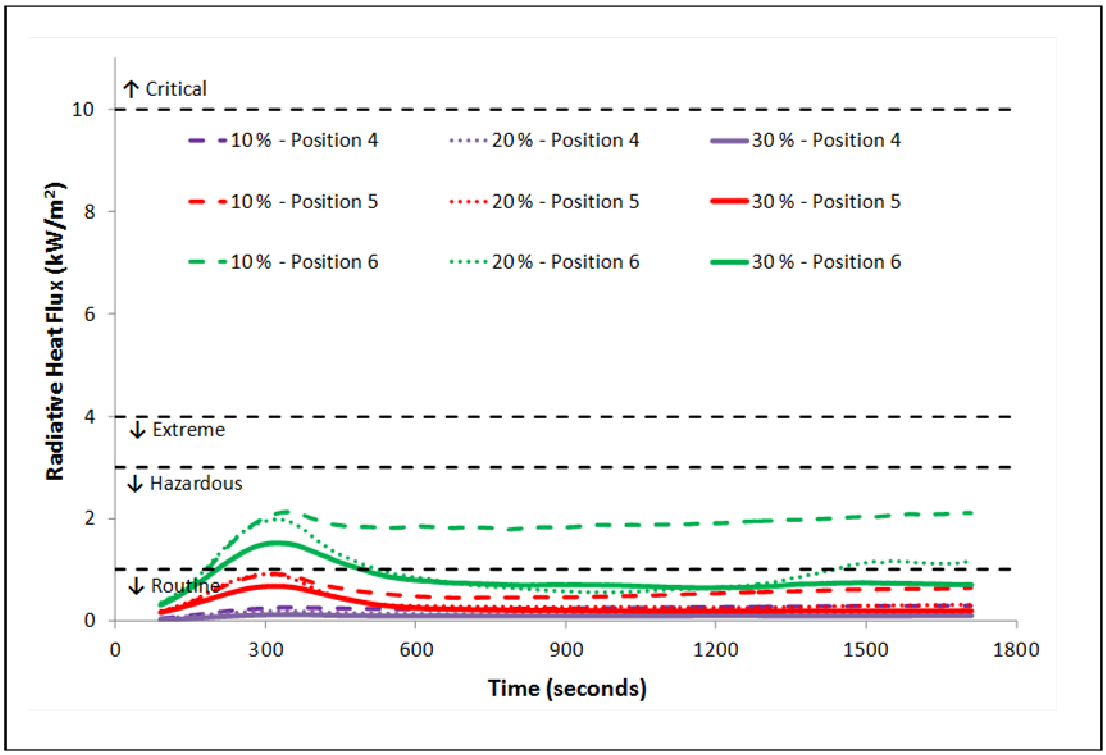

Figure 136: Comparison of smoothed radiative heat flux data from FDS at a height of 1.5 m in small warehouse with rapid t^3 fire growth and strip-shaped roof vents opening sequentially at an activation temperature of 300°C for three different downstand depths.

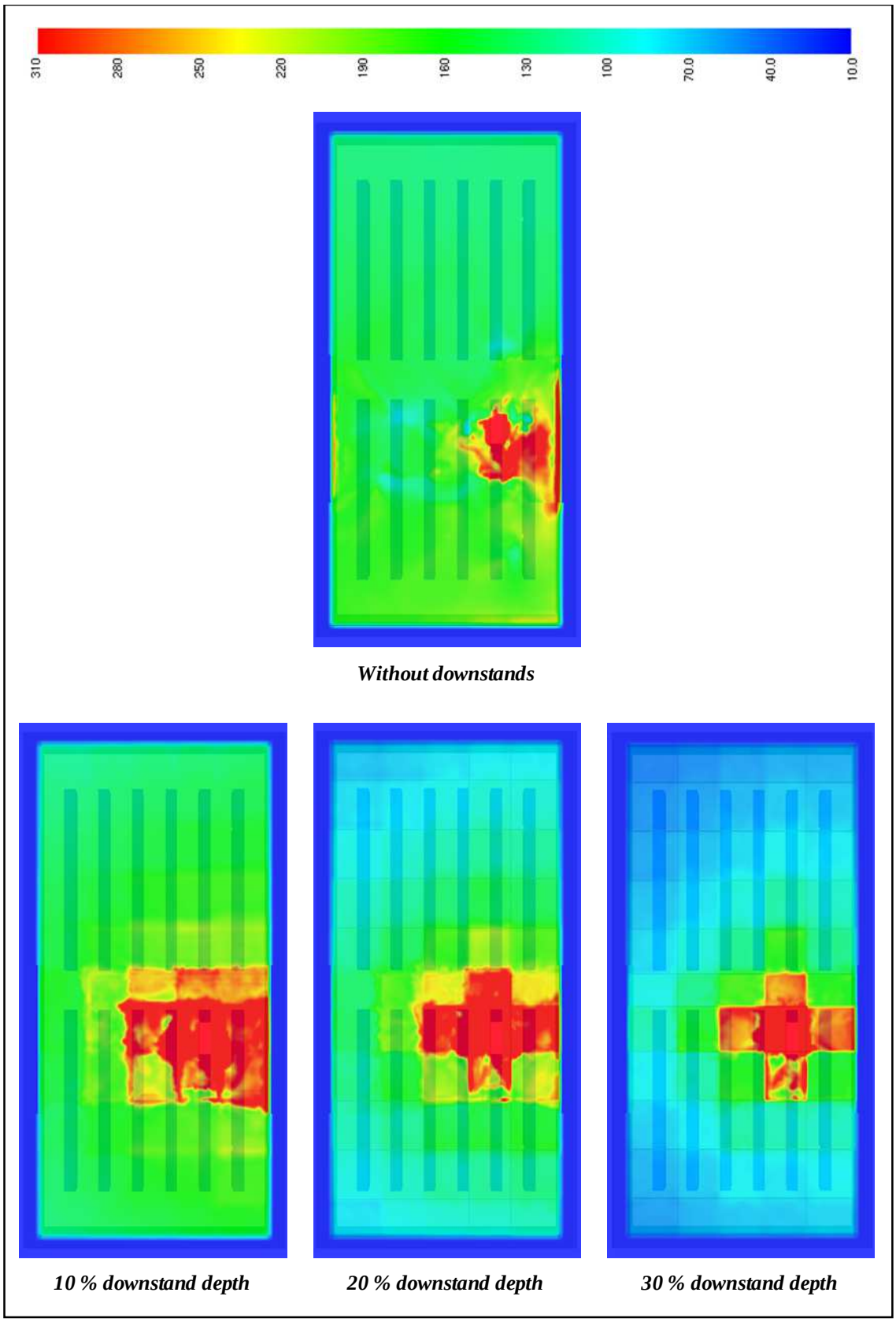

Figure 137: Comparison of temperature distributions at a height of 5.5 m after 1,800 seconds in small warehouse with rapid t^3 fire growth and sequentially-opening strip-shaped vents with 300°C activations: without downstands versus three different downstand depths (top – without, bottom left – 10 % depth , bottom centre – 20 % depth, and bottom right – 30 % depth).

3.3.6 Phase 3b: Small warehouse - extreme growth fire

Results for the small warehouse with downstands and an extreme t^3 fire growth rate were almost identical to those covered in Sections 3.3.2 through 3.3.5. For this reason, Smokeview images for these simulations are not presented here, but the radiative heat flux and temperature data can be found in: Appendix L1 for the case of square-shaped vents opening simultaneously at an activation temperature of 100°C, Appendix L2 for the case of square-shaped vents opening sequentially at an activation temperature of 100°C, Appendix K3 for the case of square-shaped vents opening sequentially at an activation temperature of 300°C and Appendix L4 for the case of strip-shaped vents opening sequentially at an activation temperature of 300°C.

3.3.7 Phases 3c & 3d: Simulations in the large warehouse

Presented in Table 10 are the summary results from the third phase simulations, run for the large warehouse. In the large warehouse containing a rapid t^3 fire growth rate, a simultaneous vent-opening sequence, and a downstand depth of 10 %, maximum radiative heat fluxes were 1.0 kW/m² close to the fire and 0.1 kW/m² away from the fire. Maximum temperatures were 14.4°C close to the fire and 13.4°C away from the fire. These measurements are all slightly lower than was observed without downstands in Section 3.2.8. As downstand depth increased to 20 % and 30 % of the warehouse height, both radiative heat fluxes and temperatures exhibited slight decreases: this change was, however, significant in terms of the FBIM criteria, reducing radiative heat flux conditions near the fire from routine to hazardous, compared to the cases with permanently-open vents and simultaneously-opening vents without downstands (*cf.* Table 7 and Table 8). These results also match the trend that was observed for the small warehouse.

The use of sequentially-activated vents reflected the same pattern of decreasing radiative heat fluxes with increasing downstand depth. In contrast, temperatures showed an increasing trend recording a maximum of 15.1°C with 30 % downstand depth: the same as was recorded in the corresponding case without downstands. In all cases, however, changes were small, and conditions remained routine.

Table 10 – Summary of maximum results for Phase 3 simulations in large warehouse.

Fire growth	Vent shape	Opening Sequence	Opening Temperature	Downstand Depth	Radiation near fire[1] (kW/m^2 - Criterion)	Radiation away from fire (kW/m^2 - Criterion)	Temperature near fire[1] (°C - Criterion)	Temperature away from fire (°C - Criterion)
Rapid	Square	Simultaneous	100°C	10 %	1.0 - Hazardous	0.1 - Routine	14.4 - Routine	13.4 - Routine
Rapid	Square	Simultaneous	100°C	20 %	0.8 - Routine	0.1 - Routine	14.1 - Routine	13.1 - Routine
Rapid	Square	Simultaneous	100°C	30 %	0.8 - Routine	0.0 - Routine	13.7 - Routine	13.1 - Routine
Rapid	Square	Sequential	100°C	10 %	0.9 - Routine	0.1 - Routine	14.5 - Routine	13.5 - Routine
Rapid	Square	Sequential	100°C	20 %	0.7 - Routine	0.1 - Routine	14.7 - Routine	13.8 - Routine
Rapid	Square	Sequential	100°C	30 %	0.8 - Routine	0.0 - Routine	15.1 - Routine	14.0 - Routine
Rapid	Square	Sequential	300°C	10 %	0.6 - Routine	0.1 - Routine	21.0 - Routine	23.1 - Routine
Rapid	Square	Sequential	300°C	20 %	0.6 - Routine	0.1 - Routine	23.3 - Routine	28.9 - Routine
Rapid	Square	Sequential	300°C	30 %	0.6 - Routine	0.0 - Routine	16.8 - Routine	18.1 - Routine
Rapid	Strip	Sequential	300°C	10 %	0.7 - Routine	0.1 - Routine	27.4 - Routine	31.5 - Routine
Rapid	Strip	Sequential	300°C	20 %	0.7 - Routine	0.1 - Routine	31.4 - Routine	40.5 - Routine
Rapid	Strip	Sequential	300°C	30 %	0.8 - Routine	0.1 - Routine	23.1 - Routine	27.0 - Routine
Extreme	Square	Simultaneous	100°C	10 %	1.0 - Hazardous	0.1 - Routine	14.4 - Routine	13.4 - Routine
Extreme	Square	Simultaneous	100°C	20 %	0.8 - Routine	0.1 - Routine	14.1 - Routine	13.1 - Routine
Extreme	Square	Simultaneous	100°C	30 %	0.8 - Routine	0.0 - Routine	13.6 - Routine	13.1 - Routine
Extreme	Square	Sequential	100°C	10 %	0.9 - Routine	0.1 - Routine	14.6 - Routine	13.3 - Routine
Extreme	Square	Sequential	100°C	20 %	0.8 - Routine	0.1 - Routine	14.9 - Routine	13.4 - Routine
Extreme	Square	Sequential	100°C	30 %	0.8 - Routine	0.0 - Routine	14.7 - Routine	13.8 - Routine
Extreme	Square	Sequential	300°C	10 %	0.7 - Routine	0.1 - Routine	22.0 - Routine	23.4 - Routine
Extreme	Square	Sequential	300°C	20 %	0.7 - Routine	0.1 - Routine	22.2 - Routine	28.0 - Routine
Extreme	Square	Sequential	300°C	30 %	0.7 - Routine	0.1 - Routine	16.9 - Routine	18.2 - Routine
Extreme	Strip	Sequential	300°C	10 %	0.8 - Routine	0.1 - Routine	26.3 - Routine	30.8 - Routine
Extreme	Strip	Sequential	300°C	20 %	0.9 - Routine	0.1 - Routine	30.3 - Routine	39.5 - Routine
Extreme	Strip	Sequential	300°C	30 %	0.9 - Routine	0.1 - Routine	24.0 - Routine	27.9 - Routine

[1] Indicates Positions 5 and 6 only.
[+] Indicates that conditions exceeded the extreme criterion, but were not severe enough to be classed as critical.

Increasing the activation temperature of each vent from 100°C to 300°C, in combination with the use of downstands, reduced maximum radiative heat fluxes further to 0.6 kW/m² for all downstand depths. Conversely, temperatures increased with the higher activation temperature, particularly for the 20 % downstand case. There was no trend for the effect of downstand depth on this roof venting mechanism, but the case with 30 % downstand depth displayed the lowest radiative heat fluxes and temperatures of the three. In all three simulations, radiative heat flux and temperatures conditions remained within the Routine Conditions criterion of the FBIM.

As was seen in Phase Two, and for the small warehouse in Phase Three, the simulations containing strip venting exhibited higher temperatures than the corresponding simulations with square-shaped venting. A clear trend, in terms of downstand depth was not clear, but the 30 % downstand depth case produced the lower temperatures of the three simulations, while having minimal effect on radiative heat fluxes.

In the large warehouse, conditions were more favourable with the use of downstands only when the activation temperature was 100°C. With this earlier activation, both maximum radiative heat fluxes and maximum temperatures were lower than was seen for the corresponding simulations without downstands. With the higher activation temperature, and hence later vent opening, maximum radiative heat fluxes were substantially higher with the use of downstands compared to those recorded without the use of downstands. In general, temperatures were also higher.

Maximum values for extreme t^3 fire growth in the large warehouse were nearly identical to those described above for rapid t^3 fire growth and do not present further points of interest.

3.3.8 Phase 3c: Large warehouse - rapid growth fire & square roof vents activating simultaneously at 100°C

Smokeview representations of the smoke layer in the large warehouse with the rapid growth t^3 fire, simultaneously-activating roof vents, and three different depth of downstand are shown in Figure 138. The depicted smoke layer in the case of the 10 % downstand depth looks almost unchanged from the case without downstands (*cf.* Figure 104). Increasing downstand depth restricted the spread of the smoke layer considerably, so that in the case of 30 % downstand depth, the smoke layer did not extend to the walls of the warehouse on three sides. As a consequence, visibility conditions were excellent in the case of 10 % downstand depth, and continued to improve with increasing downstand depth (Figure 139).

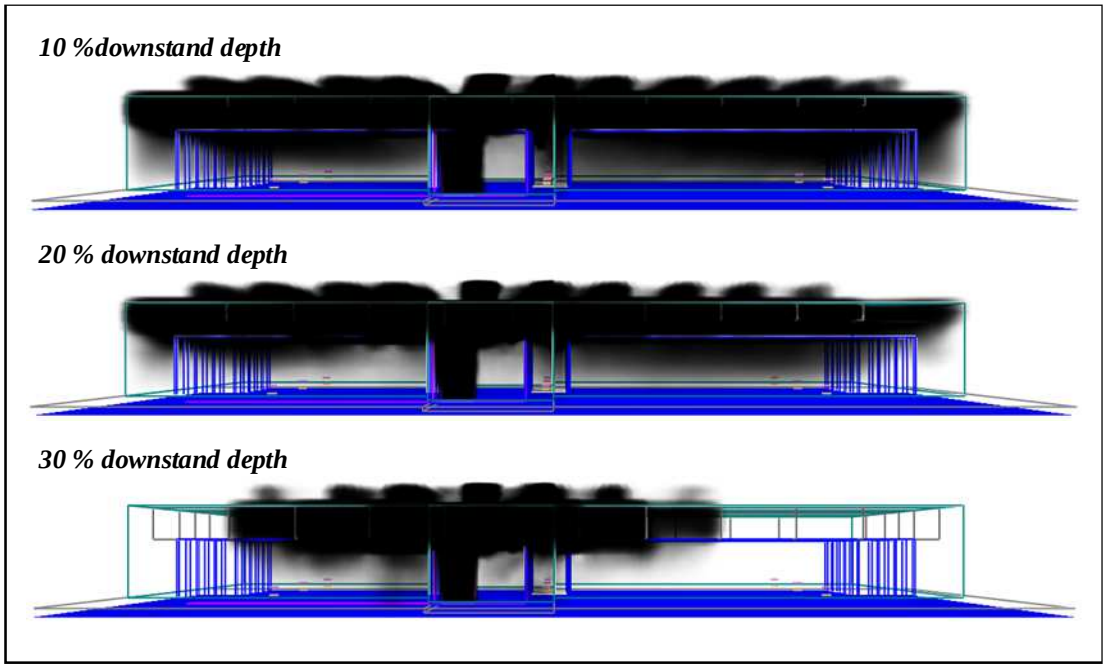

Figure 138: Smokeview depiction of smoke layer after 1,800 seconds in large warehouse with rapid t^3 fire growth and square-shaped roof vents opening simultaneously at 100 °C with three different downstand depths (top – 10 %, middle – 20 %, and bottom – 30 %).

This result is in contrast to that found in the small warehouse, where increasing downstand depths hampered visibility. The reason for this is that the allocation of roof vents to downstands in the case of the large warehouse was considerably more effective: the geometry of the downstands created 66 smoke reservoirs (*cf.* 55 smoke reservoirs in the small warehouse) under the warehouse ceiling, among which

88 vents were distributed (*cf.* 27 vents in the small warehouse). In the large warehouse, therefore, a minimum of one vent was present in each smoke reservoir, allowing downstands to be more effective and vents to be more efficient.

It is also a significant result in that a venting strategy in a *large* warehouse incorporating both simultaneously-opening square-shaped vents (at an activation temperature of 100°C) and downstands of a depth at least 20 % of the roof height can provide conditions that are at least as tenable for fire-fighters than strategies with much larger areas for roof venting and make-up air.

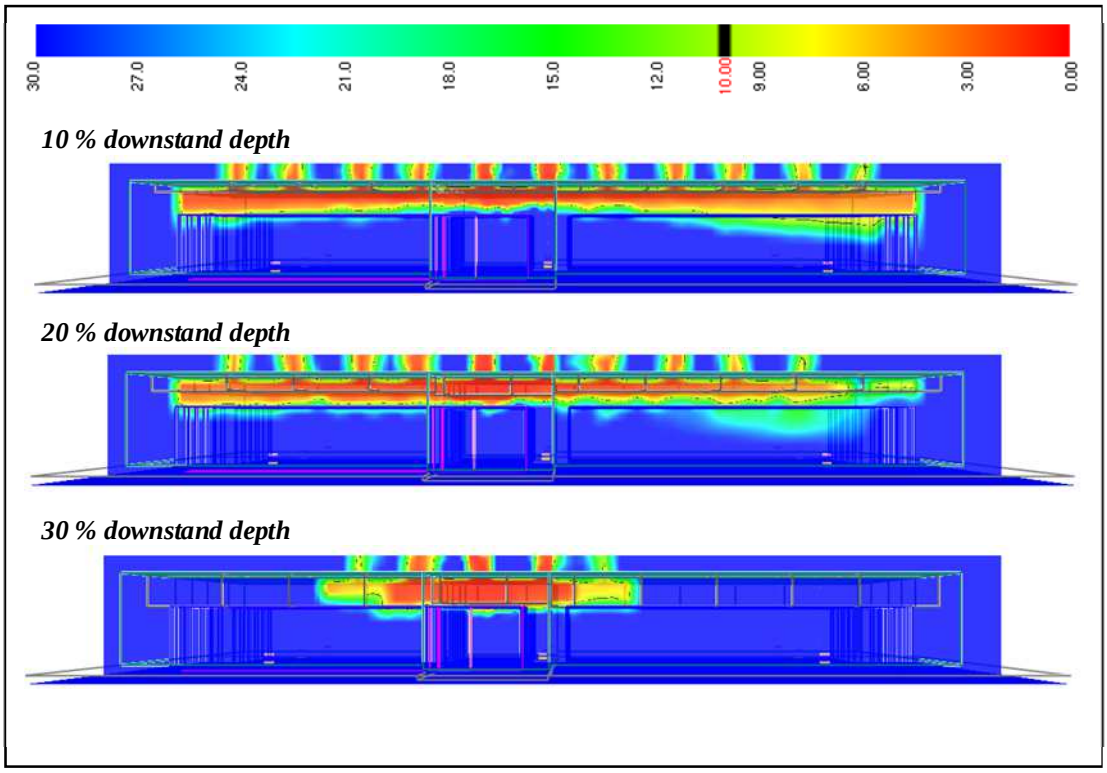

Figure 139: Visibility (m) after 1,800 seconds in large warehouse with rapid t^3 fire growth and square-shaped roof vents opening simultaneously at 100 °C with three different downstand depths (top – 10 %, middle – 20 %, and bottom – 30 %). Visibility slice is taken through long axis of warehouse, 20 m inside nearest warehouse wall.

The impact of downstand on the temperature distributions in the upper layer are highlighted in Figure 140. As seen for the small warehouse, increased downstand depth restricted substantially the area under the ceiling with elevated temperature and increased the number of smoke reservoirs that maintained the ambient temperature (dark blue).

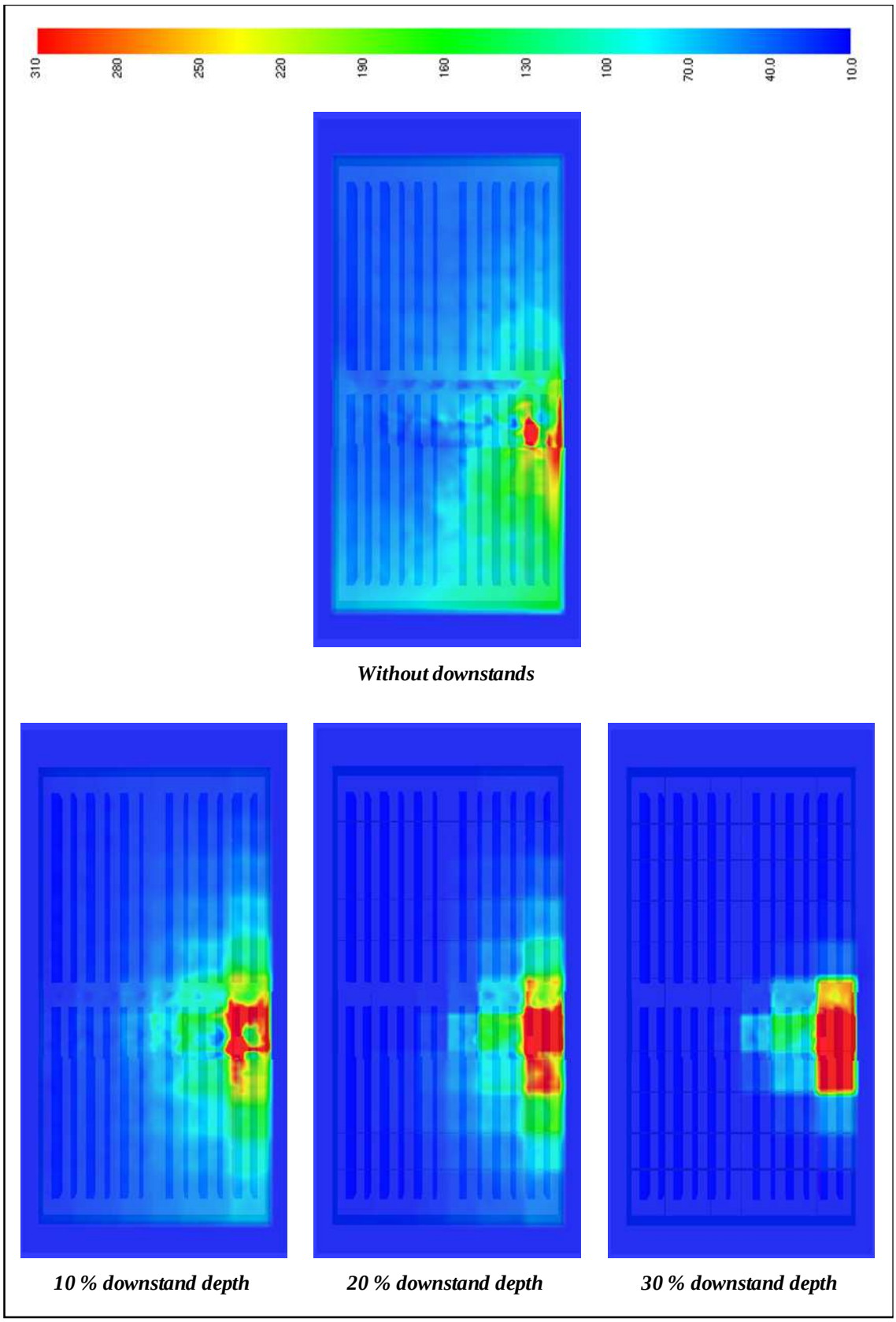

Figure 140: Comparison of temperature distributions at a height of 11.0 m after 1,800 seconds in large warehouse with rapid t^3 fire growth and simultaneously-opening square-shaped vents with 100°C activation: without downstands versus three different downstand depths (top – without, bottom left – 10 % depth , bottom centre – 20 % depth, and bottom right – 30 % depth).

Radiative heat fluxes and temperatures in the lower layer remained relatively benign: this data can be found in Appendix M1.

3.3.9 Phase 3c: Large warehouse - rapid growth fire & square roof vents activating sequentially at 100°C

When vent opening sequence was changed from simultaneous to sequential opening, the smoke layer depend and the visibility became considerably worse (Figure 141 and Figure 142). As downstand depth increased, fewer vents opened vents that had opened were unable to cope with mass flow from the plume. As a consequence, the smoke layer was allowed to cool to a temperature below that required for further vent activation, before eventually sinking towards the lower regions of the warehouse. Despite this effect, visibility at 1.5 m and below remained very good for all three simulations, although towards the end of the simulation with 30 % downstand depths, there was some decline in visibility in parts of the warehouse (Figure 143).

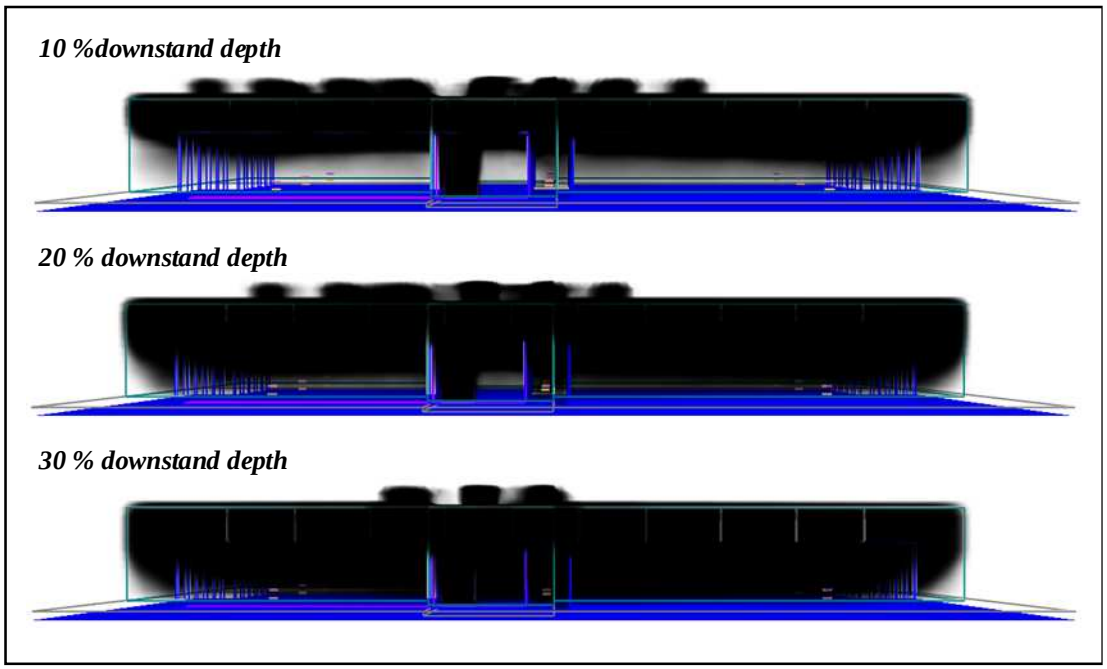

Figure 141: Smokeview depiction of smoke layer after 1,800 seconds in large warehouse with rapid t^3 fire growth and square-shaped roof vents opening sequentially at 100 °C with three different downstand depths (top – 10 %, middle – 20 %, and bottom – 30 %).

Radiative heat fluxes and temperatures at 1.5 m above floor level did no show any significant changes from the ambient and can be found in Appendix M2.

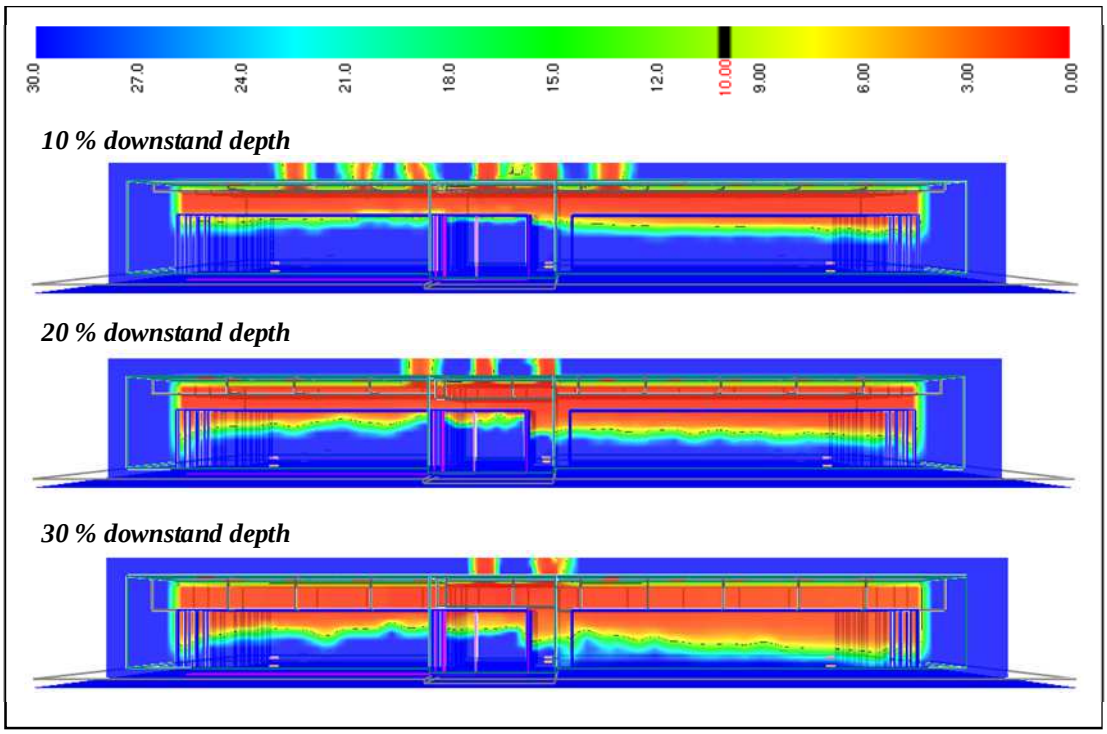

Figure 142: Visibility (m) after 1,800 seconds in large warehouse with rapid t^3 fire growth and square-shaped roof vents opening sequentially at 100°C with three different downstand depths (top – 10 %, middle – 20 %, and bottom – 30 %).

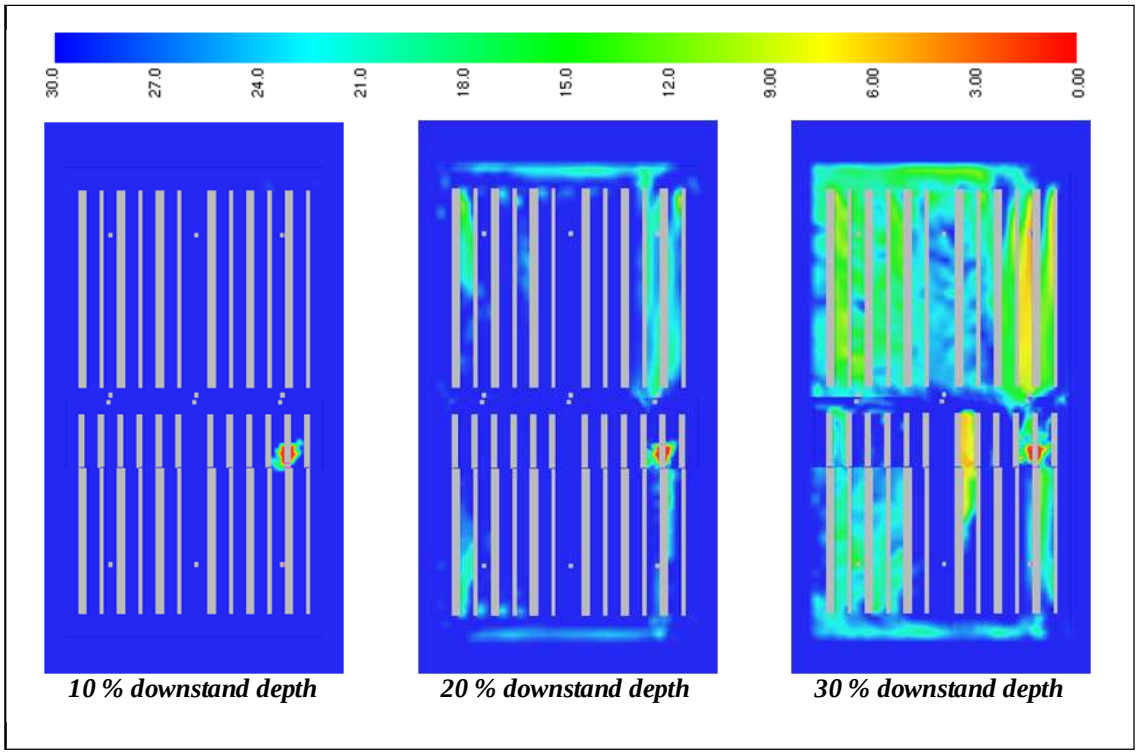

Figure 143: Comparison of visibility (m) at a height of 1.5 m after 1,800 seconds in large warehouse with rapid t^3 fire growth and sequentially-opening square-shaped vents with 100°C activation for three downstand depths (left – 10 % , centre – 20 %, and right – 30 % depth).

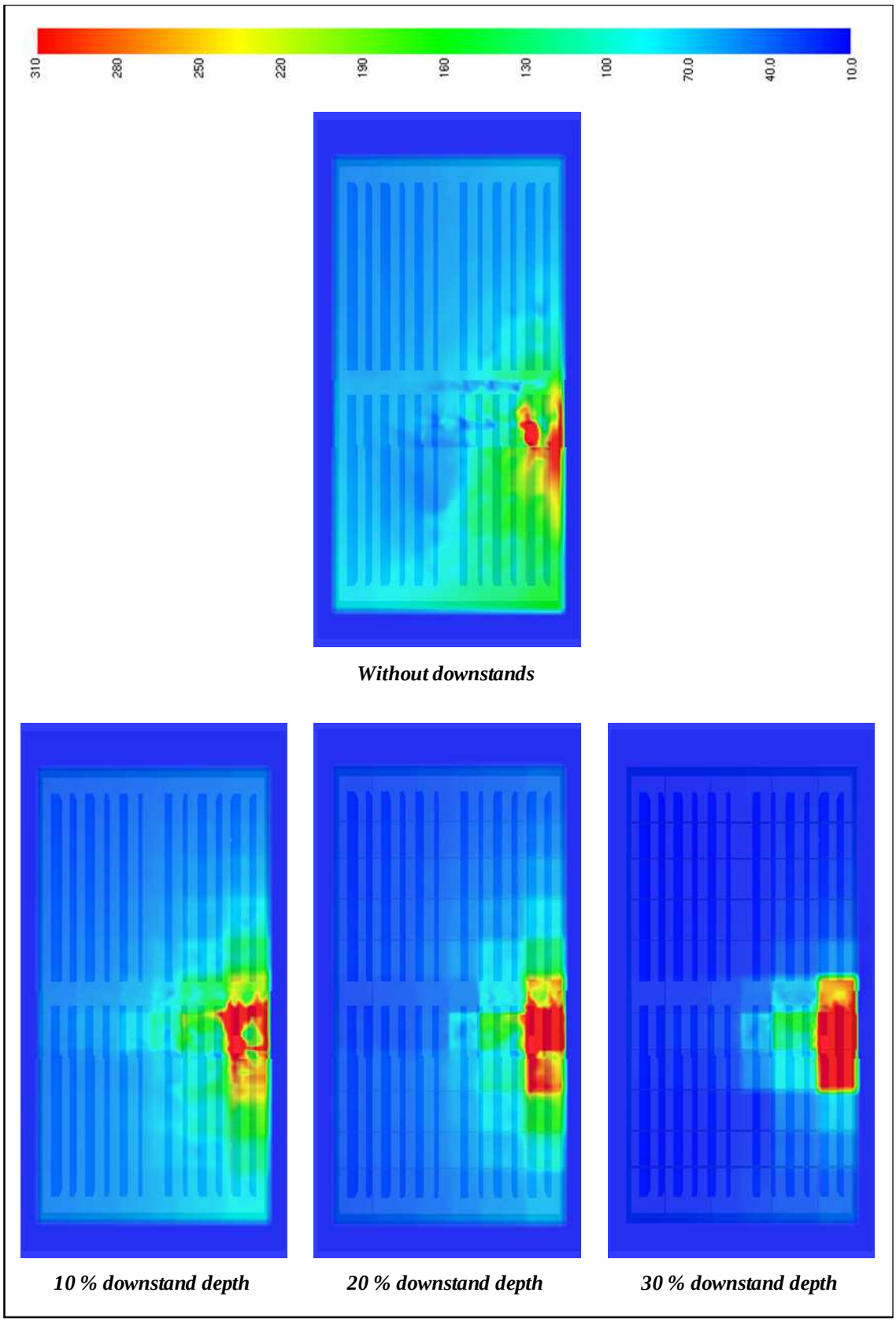

Figure 144: Comparison of temperature distributions at a height of 11.0 m after 1,800 seconds in large warehouse with rapid t^3 fire growth and sequentially-opening square-shaped vents with 100°C activation: without downstands versus three different downstand depths (top – without, bottom left – 10 % depth , bottom centre – 20 % depth, and bottom right – 30 % depth).

Temperature distributions in the upper layer were very similar to those observed in the simulations with simultaneously-opening vents (Figure 144 *cf*. Figure 140). However, upper layer temperatures were slightly higher in the smoke reservoirs further from the fire for the simulations with sequentially-opening vents, due to smoke in these regions having cooled to below the activation temperature and being unable to be exhausted from the warehouse.

3.3.10 Phase 3c: Large warehouse - rapid growth fire & square roof vents activating sequentially at 300°C

As seen with the small warehouse, delaying activation time, through an increase in activation temperature to 300°C, had the effect of deepening and thickening the smoke layer so that visibility was reduced to 0 m (Figure 145). For all downstand depths, this reduction in visibility occurred within 10 minutes.

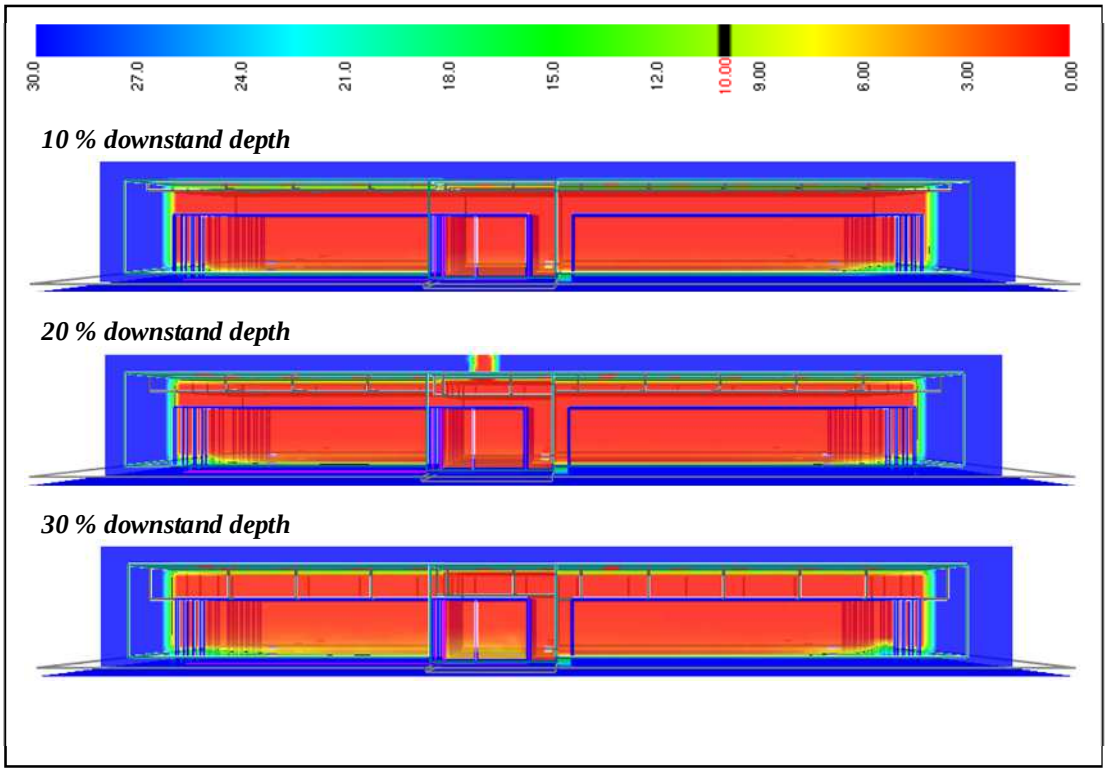

Figure 145: Visibility (m) after 1,800 seconds in large warehouse with rapid t^3 fire growth and square-shaped roof vents opening sequentially at 300 °C with three different downstand depths (top – 10 %, middle – 20 %, and bottom – 30 %). Visibility slice is taken through long axis of warehouse, 20 m inside nearest warehouse wall.

The three simulations were the first of the simulations for the large warehouse, when fitted with downstands, in which the lower layer temperatures moved more than 2°C above the ambient for any significant period to time: this is represented in Figure 146 by the results at three positions in the warehouse. Radiative heat fluxes and temperatures for all positions can be seen in Appendix M3.

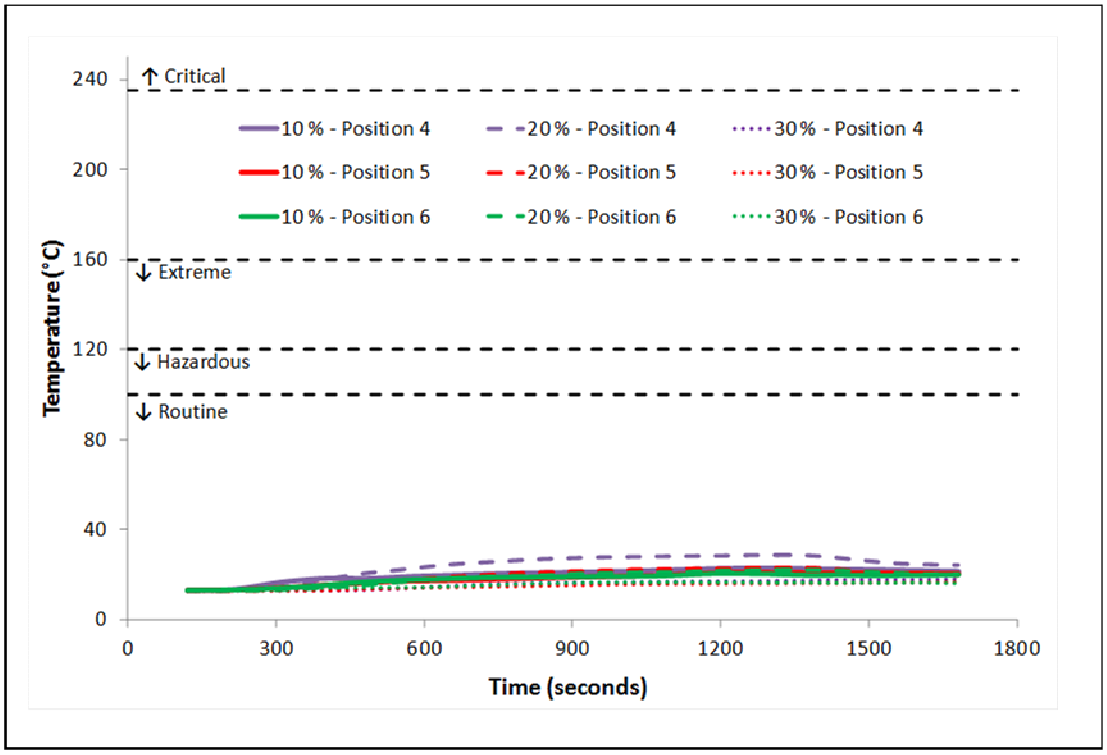

Figure 146: Comparison of smoothed temperature data from FDS at a height of 1.5 m in large warehouse with rapid t^3 fire growth and square-shaped roof vents opening sequentially at an activation temperature of 300°C for three different downstand depths.

As was also observed for the simulations in the small warehouse, the higher vent activation temperature of 300°C brought about much hotter temperatures in the , upper than for the simulations with 100°C activation temperatures (Figure 147 *cf.* Figure 140 and Figure 144). However, the same trends were apparent: as downstand depth was increased, temperatures in smoke reservoirs further from the fire decreased, while temperatures in smoke reservoirs close to the fire increased. In comparison to the case without downstands, all three depth of downstand were able to effect an improvement to upper layer temperature conditions.

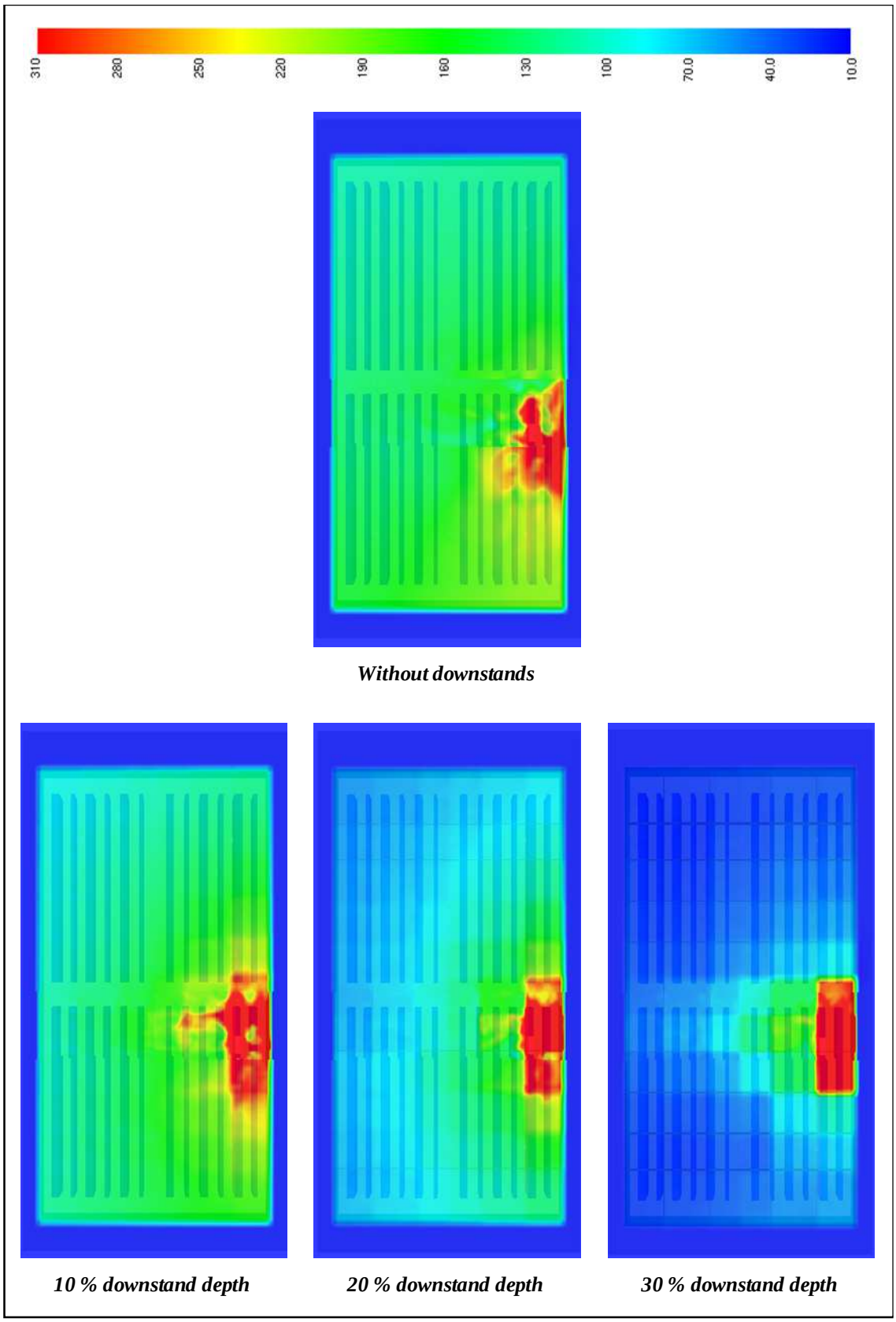

Figure 147: Comparison of temperature distributions at a height of 11.0 m after 1,800 seconds in large warehouse with rapid t^3 fire growth and sequentially-opening square-shaped vents with 300°C activation: without downstands versus three different downstand depths (top – without, bottom left – 10 % depth , bottom centre – 20 % depth, and bottom right – 30 % depth).

3.3.11 Phase 3c: Large warehouse - rapid growth fire & strip-shaped roof vents activating sequentially at 300°C

The depth and thickness of the smoke layer was not able to be alleviated with the use of a combination of strip-shaped vents and downstands (Figure 148 *cf*. Figure 120). Visibility in the lower layer decreased even further, sinking to 0 m visibility at floor level throughout the entire warehouse for all downstand depths.

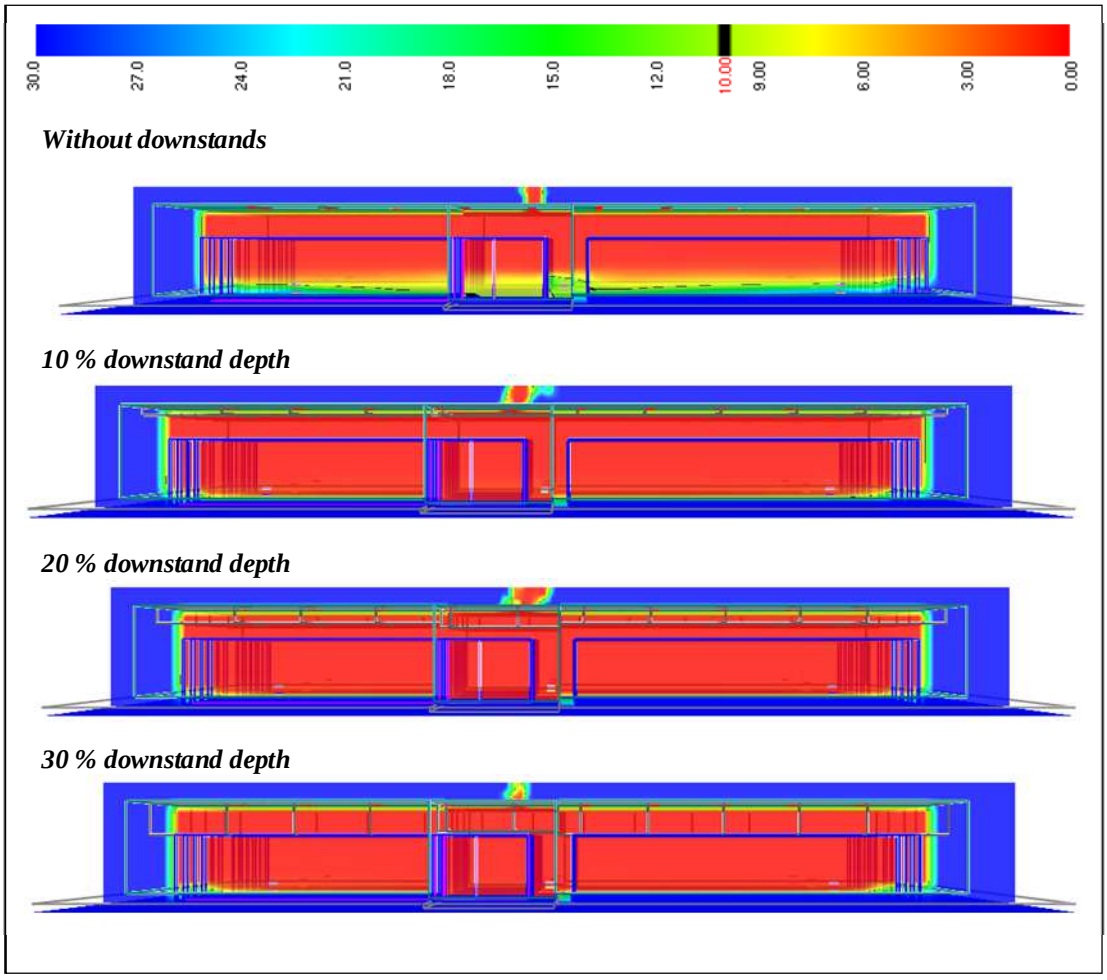

Figure 148: Visibility (m) after 1,800 seconds in large warehouse with rapid t^3 fire growth and strip-shaped roof vents opening sequentially at 300 °C with three different downstand depths (top – 10 %, middle – 20 %, and bottom – 30 %). Visibility slice is taken through long axis of warehouse, 20 m inside nearest warehouse wall.

Temperatures in the lower layer were elevated after the introduction of downstands into the large warehouse using strip-shaped vents (Figure 149). Lower layer temperatures were higher than when using strip-shaped vents alone. There was no clear trend of the effect of changing downstand depth on the temperature in the lower

layer: however, the highest temperature achieved of 40.5°C (with downstand depths of 20 %) was still well-within the Routine conditions criterion of the FBIM. Radiative heat fluxes were 0.4 kW/m² higher than the corresponding case without downstands, but do not present any interesting trends with changing downstand depth. Radiative heat fluxes and temperature results for all positions can be found in Appendix M4.

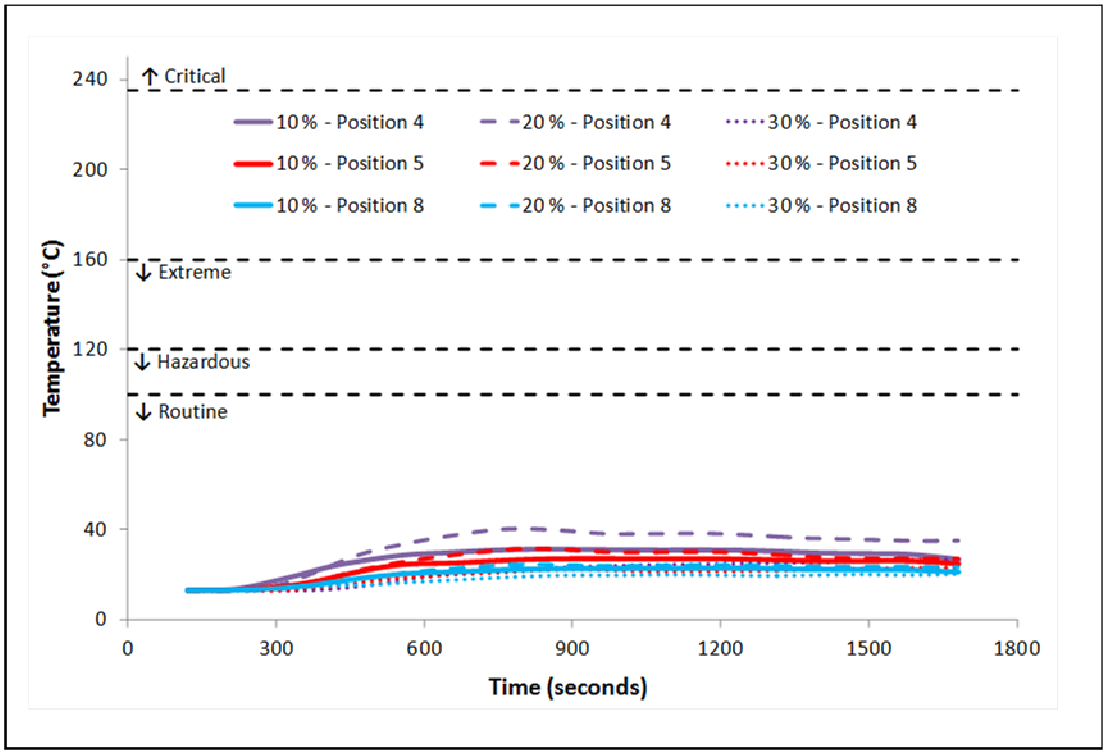

Figure 149: Comparison of smoothed temperature data from FDS at a height of 1.5 m in large warehouse with rapid t^3 fire growth and strip-shaped roof vents opening sequentially at an activation temperature of 300°C for three different downstand depths.

As seen with the simulations involving square-shaped vents, use of downstands was able to restrict the spread of the hottest gases in the upper layer (Figure 150). Downstands of increasing depth were able to reduce upper layer temperatures from up to 180°C in the case without downstands to less than ~100°C with 30 % downstand depth.

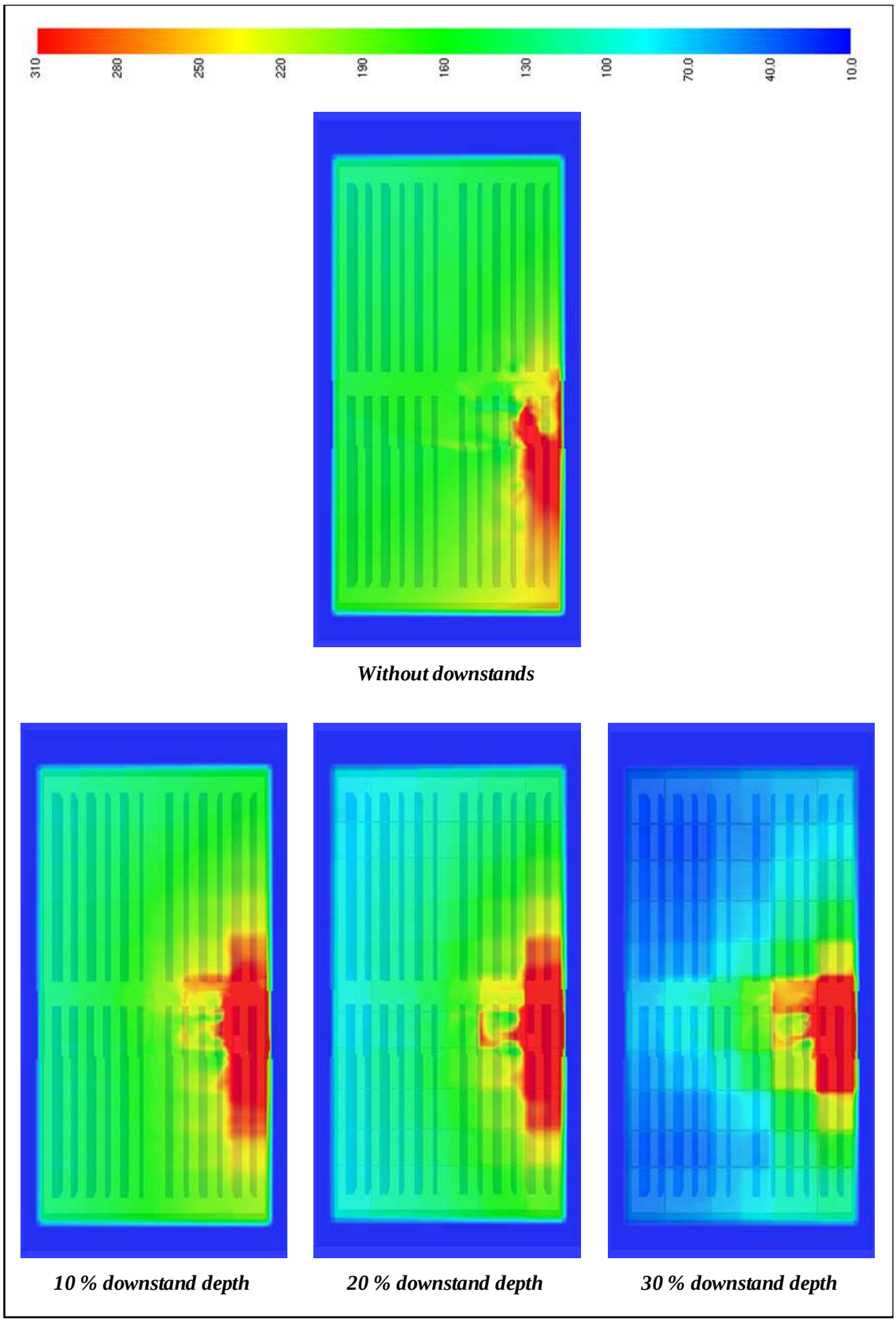

Figure 150: Comparison of temperature distributions at a height of 11.0 m after 1,800 seconds in large warehouse with rapid t^3 fire growth and sequentially-opening strip-shaped vents with 300°C activations: without downstands versus three different downstand depths (top – without, bottom left – 10 % depth , bottom centre – 20 % depth, and bottom right – 30 % depth).

3.3.12 Phase 3d: Large warehouse - extreme growth fire

Results for the large warehouse with downstands and an extreme t^3 fire growth rate were almost identical to those covered in Sections 3.3.8 through 3.3.11 for the cases with a rapid t^3 fire growth rate. For this reason, Smokeview images for these simulations are not presented here, but the radiative heat flux and temperature data can be found in: Appendix N1 for the case of square-shaped vents opening simultaneously at an activation temperature of 100°C, Appendix N2 for the case of square-shaped vents opening sequentially at an activation temperature of 100°C, Appendix N3 for the case of square-shaped vents opening sequentially at an activation temperature of 300°C and Appendix n4 for the case of strip-shaped vents opening sequentially at an activation temperature of 300°C.

4. DISCUSSION

The first simulation conducted in the small warehouse was intended to represent an idealistic situation for an industrial warehouse in New Zealand: that is, 15 % of the roof area used as a fire protection measure, in the form of roof venting, as required by the NZBC. The building was given an equivalent area of inlets for make-up air. Therefore, this simulated warehouse was fitted with an inlet area that was also sized to be 15 % of the roof area.

Results of this first simulation allowed foresight to be gained into possible conditions a fire-fighter could expect to encounter when confronted with a warehouse fire scenario: radiative heat fluxes 1.5 m above the ground, on the outer edges and corners of the warehouse, were below 0.8 kW/m² for the entire 30 minute simulation; lower layer temperatures were only slightly higher than the ambient of 13°C; and, upper layer temperatures were well below the limiting value described within the FBIM model. Fully-equipped fire-fighters would have sufficient tenability to carry out fire-fighting and rescue operations for up to 25 minutes (assuming simulated conditions held from the time of fire-fighter arrival until 25 minutes later, which could be later than the end of the 30-minute simulation time).

Conditions in the immediate vicinity of the fire were considerably worse. This is an expected result and does not contradict the above assertions: entry to the warehouse would be expected to occur at one of the edges or corners of the warehouse, and presumably, at some distance from the area suspected to contain the worst conditions.

Reduction of inlet area for make-up air to 50 % of roof area, and further to 0 % of roof area, did not have a significantly detrimental effect on conditions in the small warehouse. In fact, radiative heat fluxes reduced at all positions in the warehouse and temperatures both in the vicinity of the fire and further from the fire remained within the Routine Conditions criterion of the FBIM. An examination of temperature slice files (and Plot3d files not shown here) from Smokeview revealed vents further from the fire compensated for the loss of make-up air by drawing-in cool air from the outside, while hot gases were expelled through those vents nearer the fire. Despite the

reduction of inlet area, there was no practical difference in terms of conditions that would be faced by a fire-fighter upon entry into the warehouse.

This first set of simulations contained the slower of the two design fires chosen in this project. When the design fire with extreme growth was used, the results were identical in terms of tenability: conditions were routine at positions further from the fire, and allowed for fire-fighter entry for up to 25 minutes.

Roof venting area in the small warehouse was then reduced to 10 %, for both the rapid and extreme fire growth scenarios, and simulated with the three levels of inlet area. Conditions for the warehouse with reduced roof venting area were nearly identical compared to the warehouse with the currently required 15 % roof venting. Temperatures were, however, generally higher in the reduced roof venting simulations. But, overall, there was no deviation from tenable conditions at the outskirts of the warehouse under both fire growth scenarios.

Further reduction of roof venting area made a significant difference to warehouse tenability regardless of which design fire was applied, but only when inlet area for make-up air was totally removed. That is, with just 5 % of the roof area used as venting, conditions for fire-fighting were still considered routine at all outer positions, as long as area for make-up air was greater than or equal to half of the roof venting area. With no area provided for make-up air, routine conditions were only held for the first 600-650 seconds (depending on the fire growth rate), before lower layer temperatures exceeded the 100°C maximum of the Routine Conditions criterion. Practising fire protection engineers often use 10 minutes as a guideline for the arrival of the fire service at a fire incident; upon arrival to a warehouse, constructed as described here, a fire-fighter would find conditions already precarious for entry. In addition, upper layer temperatures were approaching, and in places exceeding, 280°C: such conditions are considered to be extreme, and would only allow a fire-fighter to be inside the warehouse for a maximum of 1 minute.

For the large warehouse, conditions at positions remote from the fire were substantially better than for the small warehouse with both the rapid and the extreme t^3 growth rate fires: absolute values were lower for lower layer radiation and

temperatures, as well as for upper layer temperatures. In addition, conditions at positions closer to the fire origin were less extreme.

However, this is not to say that larger warehouses should be subject to more lenient regulations than smaller warehouses. There still remains the expectation of increased fire loads in larger building spaces, as well as the possibility of fire spread. In this project, both warehouse sizes were subject to equivalent-sized, and localised, fires. In reality, a larger warehouse would be expected to have a larger fire load than a smaller warehouse containing the same fuel type. Therefore a larger warehouse would also be expected to facilitate a larger fire. While it would be possible to create simulations with a larger fire size, it is currently difficult to accurately model fire spread in FDS, so this fuel load effect is in turn difficult to account for. In this project, the larger warehouse simply benefitted from its larger volume (compared to the small warehouse) by being able to disperse heat and radiation more readily.

One point that was evident in this simulation phase was that inlet area for make-up air was a major influencing factor on fire conditions. While in many of the simulations the effect of decreased make-up air did not warrant a reclassification of conditions according to the FBIM criteria, conditions inside the warehouse became very sensitive to the amount of make-up air available in simulations with reduced roof venting. In fact, roof vents were often used to draw outside air into the warehouse in these reduced-ventilation conditions.

In deciding the area of roof venting and inlet area for use in subsequent simulations, temperature and radiation predictions were not looked at in isolation. This project has been undertaken with a view to enabling fire-fighting and rescue to take place in environments that are more predictable and accessible than might be the case in the absence of well-designed fire protection measures. It was for this reason that the depiction of the smoke layer in Smokeview was utilised to help distinguish between conditions that aided fire-fighting and rescue from conditions that unnecessarily hindered these operations.

It is acknowledged that use of such depictions from Smokeview carries with it its own risks: images in Smokeview are merely abstractions that are based on research in the

fire protection field. As such, they cannot be relied upon to perfectly portray a real fire situation. However, the soot yield factor of 0.07 kg/kg-fuel used in this project was taken from a proposed Verification Method for that could soon be the *de facto* method for proving compliance with the 'C' Clauses of the New Zealand Building Code.

If the Smokeview depictions of smoke layer and visibility were to be disregarded, one could argue that for a 50 MW fire, tenability (*i.e.* routine conditions as defined in the FBIM model) would be sufficient for fire-fighters in warehouses with at least 10 % roof venting area, regardless of inlet area for make-up air. Tenable conditions would also be available for fire-fighters on the outer regions of warehouses with 5 % roof venting area, on the proviso that inlet area of at least half the roof venting area is provided for make-up air.

These results refine the advice of Langdon Thomas and Hinkley (1965, p8) who warned that: "Where possible the area of air inlets should not be less than the total area of roof vents". For the same design fire, there is an interaction-effect of warehouse size and roof venting area on the required ratio of roof venting area to inlet area. A larger warehouse will allow less inlet area for a given roof venting area, and more roof venting area will allow less inlet area for a given warehouse.

If the Smokeview depictions of smoke layer and visibility are used as a form of guidance, and it is desired that a layer of clear air remained below the smoke layer allowing easier orientation for fire-fighting, then the roof venting and inlet area guidelines would change: inlet area for make-up air must be provided for all chosen roof venting areas, which must be at least 5 % of the warehouse floor area; and, the area of inlets provided for make-up air should be at least half of the area used for roof venting.

The above guidelines stem from investigations of temperatures, radiative heat fluxes, and apparent smoke layer developments in warehouses with permanently-open vents. However, permanently-open vents are not the concern in New Zealand, and unlikely to be the norm. Therefore, Phase Two of this project focussed on investigating vents

that are normally closed, and only open when activated (either through automatic opening or melting) due to excessive temperatures being reached.

It must again be noted that no attempt was made here to take into account thermal stratification existing in the warehouse prior to fire ignition. Stratification of the air temperatures in the warehouse could lead to differences in initial vent activation time, or, in length of time periods between initial activation and subsequent activations. It is possible to model thermal stratification in a computational fluid dynamics programme, such as FDS, and this is something that should be investigated in future studies.

Vents that activated at 100°C were selected to represent mechanical-type vents, that either opened simultaneously or sequentially; and, vents that activated at 200°C or 300°C were chosen to represent plastic skylight-type vents, which either burn-out or melt. In general, conditions at the perimeter of the warehouse remained routine regardless of vent design and activation temperature: exceptions were for radiative heat flux in the small warehouse with square-shaped vents that activated at 300°C, and with strip-shaped vents at both the 200°C and 300°C activation temperatures. In the cases where conditions on the outer edges of the warehouse were not routine, the Routine Conditions criterion had been exceeded by a maximum of 0.1 kW/m². The Routine Conditions criterion of the FBIM was also exceeded for radiative heat flux in the immediate vicinity of the fire for both the small and the large warehouse.

When absolute values were considered, radiative heat flux and temperature results were almost identical for simultaneous and sequential vent activation at 100°C, both in comparison to each other, and when compared to the case with permanently-open vents. This finding agrees with that found by Keough (1972, p113) who observed that "… during the study of how the opening of all roof vents simultaneously might adversely affect the normal venting pattern … shows that the smoke and hot gases were discharged principally through the vents immediately above the fire, and the fact that vents further along the roof were open did not significantly alter the pattern …". In addition, visibility in the lower layer remained excellent for the duration of these simulations.

An increased activation temperature led to higher radiative heat fluxes at positions on the perimeter of the warehouse, and lower heat fluxes near the fire. In addition, less vents opened during the 30-minute simulation, leading to increased depth and thickness of the smoke layer. In the large warehouse, visibility at a height of 1.5 m was able to be kept above 12 m in the worst cases, and in many cases visibility remained at or above 30 m. In the small warehouse, however, the descent of the smoke layer interface meant that visibility often reduced to 0 m at floor level.

With strip-shaped venting, radiative heat fluxes near the fire tended to reduce substantially compared to the corresponding cases with square-shaped venting. In contrast, lower layer temperatures tended to be higher.

With the chosen roof venting and inlet area combination, strip venting, and square vents with higher activation temperatures, hindered the maintenance of tenability in both the small and the large warehouse. The favoured mechanism among those simulated for providing fire-fighter tenability was the earlier activating square-shaped vents, regardless of the whether the activation occurs simultaneously or sequentially.

Whichever, venting system is considered the best selection from those tested, it is important to remember that the area modelled assumes the vent is totally unobstructed. This may not always be in the case in a real warehouse. For example, a warehouse relying on strip-venting in the form of plastic skylights may have 15 % roof venting area, but it is likely that only some of this area will melt to leave clear aerodynamic venting area, and that some of this area will remain in place, potentially blocking the removal of hot gases and smoke. For mechanical vents (*i.e.* square-shaped vents activating at 100°C), which showed good promise in both the small and the large warehouse, the results here are readily transferred to a design situation (although the position of the open vent would still need to be taken into account).

Further large-scale experimental work still needs to be done to determine the ability of plastic skylights to melt away during a realistic fire scenario, and to establish what percentage of clear aerodynamic area remains. Some guidance is provided in the American standard for roof venting, where a discharge coefficient of 0.6 is considered reasonable for vents that open to at least 45° (NFPA 204, 2012, A.9.2.4.2). However,

whether such a number can be readily applied in New Zealand remains to be seen, but could imply that a 15 % roof venting system will in reality have less than 10 % clear aerodynamic area. A similar coefficient should also be applied to the area of inlet air. It is unlikely that this coefficient would be equal to the discharge coefficient of the roof vents, with the same standard suggesting values of 0.1 to 0.4 where louvers are utilised.

The principle of increased efficiency of roof venting with higher gas temperatures led naturally to the simulations in Phase Three, where downstands were implemented in the warehouses. With the implementation of downstands, the results of Phase Two were supported: roof venting is more effective with early activation. In both the small and the large warehouse, the addition of downstands to the two sets of simulations with square-shaped roof vents and an activation temperature of 100°C, in general, brought about further reductions in radiative heat fluxes and temperatures. However, due to a mismatch between vent and downstand placement, this improvement was accompanied by a decline in visibility in the small warehouse. Roof vents and downstands were much better aligned in the large warehouse, and the roof vents exhibited much greater efficiency where simultaneous activation was in-place. This was particularly evident in the simulation with 30 % downstand depths and simultaneous opening of all roof vents, where the combined roof venting strategy was able to prevent the smoke layer from reaching three of the four walls in the warehouse: the only simulation to achieve such a result. After activation of each vent in the affected smoke reservoirs, smoke was exhausted from the warehouse due to its temperature and buoyancy.

An important point was highlighted in the small warehouse is the danger of misaligning downstands and roof venting. A smoke reservoir created by downstands is of little use if the smoke reservoir does not contain at least one roof vent. The current guidance in the NZBC Compliance Document does not protect against this possibility occurring in practice. Instead, it is left for the fire engineering consultant to design according to either an overseas document or his/her own experience and judgement. This presents a risk for both the building owner and the fire engineering consultant. It also gives rise to an opportunity to include appropriate specifications for

downstands in the Compliance Document, as part of a definition of *effective fire venting*.

In the simulations with higher activation temperatures, conditions worsened considerably in both the small and the large warehouse. In particular, visibility reduced to 0 m at or close to floor level. As the temperature of the smoke layer was insufficient to activate the vents, the smoke layer spread throughout the upper region of the warehouse, spilling out of each smoke reservoir. As it did so, and the temperature of the smoke cooled further from the fire, the smoke layer began to descend, having lost much of its buoyancy. This is quite the opposite of the desired effect.

The depth of downstand required is directly related to fire size (Langdon Thomas and Hinkley, 1965). Downstands of just 10 % of ceiling height had minimal influence on smoke spread in the upper layer, even for the most ideal simulation carried out here. The 50 MW design fire used for these simulations was chosen to represent a worst-case scenario. Such a fire size can be considered too large for downstands of 10 % depth to be effective in warehouse of similar sizes modelled in this study.

Added benefits of downstand use will be seen, with better consideration given to optimal placement of the downstand and vent positions. In the above simulation downstands and vents were placed in the warehouse in positions that would satisfy building code requirements while not upsetting calculation protocols in FDS. An experienced fire engineering consultant would align roof vents and downstands for better optimisation of the venting system.

One must also not lose sight of the fact that this study was undertaken with a view to safety for fire-fighting in industrial warehouses. Other considerations, such as life safety of the building occupants, will necessarily take priority. Roof venting cannot take the place of clear, well-designed escape routes, detection & notification systems, or systems designed for controlling fires such as sprinklers. In the past, mention has been made of the trend for increased floor area in single-storey industrial buildings, and unpopularity of sub-divisions such as fire barrier walls from a productivity perspective (Langdon Thomas and Hinkley, 1965). Today, the focus has shifted

slightly, in that not only are floor areas larger, but single-storey industrial buildings are extending vertically, increasing the potential for high fire loads, and rapid fire spread in such buildings. But, the dislike of sub-divisions remains. The use of an effective fire venting system is, therefore, still an important strategy for aiding fire-fighting efforts. Such a system will not only aid in maintaining tenability, but will also help to provide predictability of conditions.

5. CONCLUSIONS

An objective of this study was to evaluate the percentage of roof vent area required to meet the FBIM tenability criteria. The current Compliance Document for the New Zealand Building Code 'C' Clauses has a 15 % rule regarding the opening area for unsprinklered single floor buildings. It was shown in this study, with the use of FDS, that roof venting with 15 % geometric area is ample to maintain tenability for fire-fighting in each of two buildings with 50 MW a fire. Further, it was shown that the area of inlets for providing make-up air is also an important factor in determining the effectiveness of a roof venting system. When sufficient make-up air is available, it could be possible to reduce the roof venting area to just 5 % geometric area.

A second objective was to compare the effects of sequential and simultaneous vent opening designs. The intention with this objective was to determine whether there was an obvious difference in the performance of plastic skylight-type vents as compared to mechanical vents that have a more assured activation mechanism. The most conclusive result to arise from this phase was that early activation of roof venting is the key for promoting tenability for fire fighters. More often than not, the mechanical venting design (*i.e.* activation of roof venting at 100°C) provided more tenable conditions than did the non-mechanical option (*i.e.* activation of roof venting at 200°C or 300°C).

The final objective was to evaluate the use of downstands for promoting vent efficiency. When downstands and roof venting were astutely aligned, and vent activation occurred while the smoke layer was still relatively buoyant, the ability to maintain tenability was profound. When downstands and roof venting were not well-matched to each other and/or the activation temperature of the vents was set too high for the smoke layer to maintain buoyancy, the results were detrimental to maintaining tenable conditions.

Underpinning this study was the goal to contribute to the development of a clear definition of *effective fire venting*. It has been demonstrated here that geometric area of 15 % is sufficient roof venting area to provide fire-fighter tenability. But, it has

also been demonstrated that a complete definition of *effective fire venting* requires more than just a specification of how much area of roof venting should be installed. A clear definition of *effective fire venting* must include a specification of required inlet area for make-up air. The results discussed here showed conclusively that the absence of inlet area for make-up air will relegate to meaningless the installation of roof venting, at least up to an area of 15 %. The Compliance Document for the New Zealand Building Code 'C' Clauses should also include direction on the combined use of fire venting and downstands, as the misalignment of these two features can be of great detriment to the ability venting strategy to perform. A clear definition of *effective fire venting* must discern between clear aerodynamic area and geometric area (area of roof venting to be installed). This could be practically achieved by the use of a discharge coefficient for roof venting types, and a similar coefficient for inlets. Such coefficients will vary depending on the mechanisms used for venting (and for inlets). Therefore, it would also be prudent for products utilised in New Zealand to be tested under a uniform test method or certification scheme that assigns discharge coefficients or some other form of fire performance rating.

Use of plastic panels that melt in order to vent hot gases and smoke from a fire are an economic solution to providing fire-fighter tenability. A clear definition of *effective fire venting* can determine if their continued use in New Zealand is appropriate, by ensuring sufficient roof venting area is provided for the expected, but unwanted, fire.

During the course of this study, a number of potential future investigations have been highlighted that will enhance the knowledge base with regard to fires in warehouse-type buildings and use of roof venting. These research shortfalls are listed here for ease of reference: A parametric study is required that relates appropriate computation domain extensions to hydraulic vent diameters for a range of building geometries, fire sizes and opening frequency; A parametric study is required that investigates the effect of stratified temperature layers in tall compartments on the activation of roof venting; Large-scale experimental work needs to be done to determine the ability of plastic skylights to melt away during a realistic fire scenario, to establish what percentage of clear aerodynamic area remains, and to potentially instigate a discharge coefficient for describing the effectiveness of roof venting products.

6. REFERENCES

A.B.C.B. (2009). *Building Code of Australia*. Australian Building Codes Board. Canberra, Australia.

ARGEBAU (2000). *Muster-Richtlinie über den baulichen Brandschutz im Industriebau, März 2000*, Fachkommission Bauaufsicht der ARGEBAU, Germany.

AS 2665 (2001). *Smoke/heat venting systems - Design, installation, and commissioning*. Council of Standards Australia. Sydney, NSW, Australia, Standards Australia International Ltd.

Bengston, S. and B. Hagglund (1986). *A Smoke-Filling Simulation Model and Its Engineering Applications*. Fire Technology 22(2): 92-103.

Capote, J. A., D. Alvear, O. V. Abreu, M. Lazaro and P. Espina (2009). *Scale Tests of Smoke Filling in Large Atria*. Fire Technology 45: 201-220.

Chow, W. K. (1994). *A Short Note on the Simulation of the Atrium Smoke Filling Process Using Fire Zone Models*. Journal of Fire Sciences 12: 516-528.

Chow, W. K. (1996). *Multi-cell concept for simulating fires in big enclosures using a zone model*. Journal of Fire Sciences 14(3): 186-198.

Claridge, E. (2009). *Personal communication to New Zealand Fire Service Design Review Unit concerning email entitled: MEFE thesis - firefighter tenability criteria, 28 September 2009*.

Cosgrove, B. W. (1996). *Fire Design of Single Storey Industrial Buildings*. Christchurch, New Zealand, University of Canterbury.

D.B.H. (2008a). *Compliance Document for New Zealand Building Code: Clauses C1, C2, C3, C4 - Fire Safety*, Department of Building and Housing, Wellington, New Zealand: 227.

D.B.H. (2008b). *Effective Venting for Single Storey Buildings*. Codewords 25.

Drysdale, D. (1998). *An Introduction to Fire Dynamics*. Chichester, U.K., John Wiley & Sons.

Duong, D. Q. (1990). *The Accuracy of Computer Fire Models: Some Comparisons with Experimental Data from Australia*. Fire Safety Journal 16: 415-431.

Edwards, A. P. R., E. Soja and C. A. Wade (2007). *Effective Passive Roof Venting in the Event of a Fire - Literature Review*. BRANZ Study Report SR 165. Judgeford, New Zealand, BRANZ Ltd.

Fang, J., J. Jie, Y. Hong-Yong and Z. Yong-Ming (2006). *Early fire smoke movements and detection in high large volume spaces*. Building and Environment 41: 1482-1493.

Gaskin, J. (2009). *The Efficiency of Plastic Skylight Panels as Smoke Vents in the Event of Fire*. College of Engineering, Christchurch, New Zealand, University of Canterbury. A thesis submitted in partial fulfillment of the requirements for the degree of Master of Engineering in Fire Engineering: 238.

Harper, C. A., Ed. (2006). Handbook of Plastics Technologies: the complete guide to properties and performance. Materials Science and Engineering Series. New York, McGraw-Hill.

Hasegawa, H. K., N. J. Alvares and J. A. White (1999). *Fire tests of packaged and palletized computer products*. Fire Technology 34(4): 291-307.

He, Y., C. Jamieson, A. Jeary and J. Wang (2008). *Effect of Computation Domain on Simulation of Small Compartment Fires*. 9th International Symposium on Fire Safety Science. Karlsruhe, Germany, International Association for Fire Safety Science.

Heskestad, G. (1983). *Luminous Heights of Turbulent Diffusion Flames*. Fire Safety Journal 5(2): 103-108.

Heskestad, G. (1983). *Virtual Origins of Fire Plumes*. Fire Safety Journal 5(2): 109-114.

Heskestad, G. (1986). *Smoke movement and venting*. Fire Safety Journal 11(1-2): 77-83.

Hill, K., J. Dreisbach, F. Joglar, B. Najafi, K. B. McGrattan, R. Peacock and A. Hamins (2007). *Verification and Validation of Selected Fire Models for Nuclear Power Plant Applications*, United States Nuclear Regulatory Commission, Office of Nuclear Regulatory Research (RES), Rockville, MD, and Electric Power Research Institute (EPRI), Palo Alto, CA, NUREG-1824 and EPRI 1011999. Volume 1: Main Report.

Hinkley, P. L. (1986). *Rates of 'Production' of Hot Gases in Roof Venting Experiments*. Fire Safety Journal 10: 57-65.

Hinkley, P. L. and C. R. Theobold (1966). *P.V.C. rooflights for venting fires in single-storey buildings*. Fire Research Technical Paper No.14. London, Her Majesty's Stationery Office.

Ingason, H. (2001). *Heat Release Rate of Rack Storage Fires*. Interflam 2001. SP Swedish National Testing and Research Institute, Sweden.

Karlsson, B. and J. G. Quintiere (2000). *Enclosure Fire Dynamics*. Boca Raton, FL., CRC Press LLC.

Keough, J. J. (1972). *Venting Fires Through Roofs: Experimental Fires in an Aircraft Hangar*. North Ryde, N.S.W., Australia, Commonwealth Experimental Building Station,. Report No. UP 344.

Kim, A. K. (1992). *A Review of Venting of Compartment Fires to Aid Firefighting*. National Research Council Canada, Institute for Research in Construction, Internal Report No. 627: 7.

Langdon Thomas, G. J. (1960). *Fire Protection in Large Single-Storey Factory Buildings*. F. R. Station. F.R. Note No. 427, Fire Research Station, Boreham Wood, Hertfordshire.

Langdon Thomas, G. J. and P. L. Hinkley (1965). *Fire Venting in Single-storey Buildings*. Fire Note No. 5, J.F.R.O.

Lim, L. C. S. (2000). *Stability of Precast Concrete Tilt Panels in Fire*. Department of Civil and Natural Resources Engineering, Christchurch, New Zealand, University of Canterbury. A report submitted in partial fulfilment of the requirements for the Degree of Master of Engineering in Fire Engineering.

Ma, T. G. and J. G. Quintiere (2003). *Numerical simulation of axi-symmetric plumes: accuracy and limitations*. Fire Safety Journal 38(5): 467-492.

Marchant, R., N. Kurban and S. Wise (2001). *Development and Application of the Fire Brigade Intervention Model**. Fire Technology 37(3): 263.

McGrattan, K. B., S. Hostikka and J. E. Floyd (2009). *Fire Dynamics Simulator (Version 5) User's Guide*. NIST Special Publication 1019-5, National Institute of Standards and Technology.

McGrattan, K. B., S. Hostikka, J. E. Floyd, H. R. Baum, R. G. Rehm, W. E. Mell and R. McDermott (2010). *Fire Dynamics Simulator (Version 5) Technical Reference Guide*. NIST Special Publication 1018-5, National Institute of Standards and Technology. Volume 1: Mathematical Model.

McGrattan, K. B. and S. Miles (2008). *Modeling Enclosure Fires Using Computational Fluid Dynamics (CFD)*. The SFPE Handbook of Fire Protection Engineering, 4th Edition. P. J. DiNenno, D. Drysdale, C. L. Beyleret al. Quincy, Massachusetts, National Fire Protection Association.

Mell, W. E. and J. R. Lawson (2000). *A Heat Transfer Model for Firefighters' Protective Clothing*. Fire Technology 36(1): 39-68.

Mills, C. K. (2004). *Comparison of Flow Predictions Made by BRANZFIRE and Fire Dynamics Simulator for Shallow Horizontal Ceiling Vents*. Department of Civil Engineering, Christchurch, New Zealand, University of Canterbury. Submitted as partial fulfillment of a Masters Degree in Fire Engineering: 75.

Moinuddin, K. A. M. and I. R. Thomas (2007). *Factors Affecting Grid-Independent Results for Compartment Fire Modelling*. 16th Australasian Fluid Mechanics Conference. Crown Plaza, Gold Coast, Australia: 1254-1257.

Newman, G. M. (1990). *Fire and Steel Construction: The behaviour of steel portal frames in boundary conditions*. Berkshire.

NFPA 204 (2012). *Standard for Smoke and Heat Venting*. NFPA 204. National Fire Protection Association (N.F.P.A.) National Fire Codes.

Pabich, M. J. (1998). *Report of In-rack Sprinkler Comparison Fire Tests*. Underwriter's Laboratories Inc.

Persily, A. K. (1998). *Airtightness of Commercial and Industrial Buildings: Blowing Holes in the Myth of Tight Buildings*. Thermal Envelopes VII Conference. DOE/ASHRAE/ORNL/BETEC/NRCC/CIBSE. Clearwater, FL.

Porter, T. M. (2004). *Determining Realistic Loss Estimates for Rack Storage Warehouse Fires*. Department of Civil Engineering, Christchurch, University of Canterbury. A thesis submitted in partial fulfillment of the requirements for the degree of Master of Engineering in Fire Engineering: 235.

Robbins, A. P. and C. A. Wade (2010). *Test method for roof panels to be used for passive fire roof venting*. Fire Safety Journal 45(2): 142-148.

Sestack (1957). *Roof Venting for Fire Safety*. Quarterly of the National Fire Protection Association 50: 212-215.

Thomas, P. H. and P. L. Hinkley (1964). *Design of roof-venting systems for single-storey buildings*. Fire Research Technical Paper No.10. London, Her Majesty's Stationary Office.

Thomas, P. H., P. L. Hinkley, C. R. Theobold and D. L. Simms (1963). *Investigations into the flow of hot gases in roof venting*. Fire Research Technical Paper No.7. London, Her Majesty's Stationery Office.

Thomas, P. H., D. L. Simms, P. L. Hinkley and C. R. Theobold (1960). *Roof Venting of Burning Enclosures: Part III. Venting Fires of Constant Heat Output*. Fire Research Note #419. Borehamwood, England, Fire Research Station.

U.K. Building Regulations (2000). *Approved Document B of the UK Building Regulations: Fire Safety*. Office of the Deputy Prime Minister.

Wade, C.A. (2004). BRANZFIRE Technical Reference Guide 2004. BRANZ Study Report 92 (revised). Building Research Association of New Zealand. Judgeford, Porirua City, New Zealand.

Wang, H. Y. (2009). *Numerical study of under-ventilated fire in medium-scale enclosure*. Building and Environment 44: 1215-1227.

Xin, Y. (2004). *Assessment of Fire Dynamics Simulation for Engineering Applications: Grid and Domain Size Effects*. Fire Suppression and Detection Research Application Symposium. Orlando, Florida: 30.

Young, S. A. (2004). *Fire Brigade Intervention Model V2.2 October 2004*. FBIM Computer Program (Version 1.01 Beta). Australasian Fire Authorities Council (A.F.A.C.) Developed by Warrington Fire Research, Australia.

Yu, H.-Z. and P. Stavrianidis (1991). *The Transient Ceiling Flows of Growing Rack Storage Fires*. Fire Safety Science - Proceedings of the Third International Symposium: 281-290.

Zalosh, R. G. (2003). *Industrial Fire Protection Engineering*. New York, John Wiley & Sons.

Zhang, X., M. Yang, J. Wang and Y. He (2010). *Effects of Computational Domain on Numerical Simulation of Building Fires*. Journal of Fire Protection Engineering 20.

APPENDIX A – ROOF VENTING AREA REQUIRED BY NFPA 204

By means of comparison to the New Zealand requirements, exemplar calculations for the required roof venting area in the small and large warehouses simulated in this study can be made according for NFPA 204.

The mean flame height above the base of the fire, *L*, is given by (Heskestad, 1983):

$$L = -1.02D + 0.235Q^{2/5} \qquad 4$$

where *Q* is the total energy release rate (kW) and *D* is the base diameter of the fire (m). For both the small and large warehouse in this study, the fire has a base area, *A*, of 6 m^2 (width 1.5 m and length 4 m). This can be converted to an equivalent circular (or base) diameter using the equation:

$$D = \sqrt{\frac{4 \cdot A}{\pi}} = \sqrt{\frac{4 \cdot 6}{\pi}} = 2.8\ m \qquad 5$$

From Equation 4, with an energy heat release rate of 50,000 kW, the mean flame height, *L*, is then 14.1 m.

The virtual origin, z_0, is the effective point source of the fire plume, and is calculated to be 3.5 m, using the equation (Heskestad, 1983):

$$z_0 = 0.083Q^{2/5} - 1.02D \qquad 6$$

The mass flow rate in the plume (kg/s), $\dot{m}_p$, is given by (NFPA 204, 2012, Equation 9.2.3.7):

$$\dot{m}_p = (0.0056Q_c)\frac{z_s}{L} \qquad 7$$

where z_s is the height of the smoke layer above the base of the fire, and Q_c is the convective energy release rate (taken here as 35,000 kW). Given that the smoke layer height should be above the bottom of the draft curtains (NFPA 204, 2012, clause 9.2.2.2), the height of the smoke layer in the small warehouse (height of 6.5 m) can be assumed to be 5.2 m, and in the large warehouse (height of 12 m), 9.6 m (both figures based on the 20 % rule discussed earlier). The mass flow rate in the plume in the small warehouse is then 72.2 kg/s, and in the large warehouse it is 133.3 kg/s.

The smoke layer temperature is given by (NFPA 204, 2012, Equation 9.2.4.3):

$$T = T_0 + \frac{KQ_c}{c_p \dot{m}_p} \qquad 8$$

where T is the smoke layer temperature (K), T_0 is the ambient temperature (286 K), K is the fraction of convected energy contained in the smoke layer gases (assumed to be 0.5, in accordance with NFPA 204, 2012, clause 9.2.4.4), Q_c is the convective heat release rate defined above as 35,000 kW, c_p is the specific heat of the smoke layer gases (assumed to be 1 kJ/kg K), and $\dot{m}_p$ is the plume mass flow rate (kg/s) as calculated in Equation 7. The smoke layer temperature in the small warehouse is then 528 K, and in the large warehouse it is 417 K.

The mass flow rate through the vents is then calculated as (NFPA 204, 2012, Equation 9.2.4.1):

$$\dot{m}_v = \frac{C_{d,v} A_v}{\sqrt{1 + \frac{C_{d,v}^2 A_v^2}{C_{d,i}^2 A_i^2}\left(\frac{T}{T_0}\right)}} \sqrt{(2\rho_0^2 g d)} \sqrt{\frac{T_0 (T - T_0)}{T^2}} \qquad 9$$

where $\dot{m}_v$ is the mass flow through the vent (kg/s), $C_{d,v}$ is the vent discharge co-efficient (assumed to be 0.7), $C_{d,i}$ is the inlet discharge co-efficient (assumed to be 0.7), A_v is the vent area (m^2) found by equating 7 with 9, A_i is the inlet area (m^2) here set to be equal to the vent area, T_0 is the ambient temperature (286 K), T is the smoke layer temperature from Equation 8 (528 K for the small warehouse and 417 K for the large warehouse), ρ_0 is the ambient density (1.204 kg/m^3), g is the acceleration due to gravity (9.81 m/s^2), and d is the smoke layer depth (taken as 20 % of height of ceiling, m).

Setting $\dot{m}_v$ equal to 72.2 kg/s gives a required venting area of 42.3 m^2 (or 2.3 %) in the small warehouse. And, setting $\dot{m}_v$ equal to 133.3 kg/s gives a required venting area of 56.9 m^2 (or 0.9 %) in the large warehouse.

APPENDIX B – EXAMPLE FDS SCRIPT

```
&HEAD CHID = 'P3_Sim10', TITLE = 'MEFE Thesis - Venting, Phase 3, Simulation 10' /

/-----------------------------------------------------------------------------------------------------------------------------------------
/ The main variables of this programme are:

/ Domain height above roof:     2.5 m
/ Warehouse dimensions:         30 m x 60 m x 6.5 m
/ Walls made of:                adiabatic
/ Roof made of:                 steel sheeting
/ Adiabatic condition:          false
/ Fire growth:                  rapid t-cubed
/ Venting area:                 5 %
/ Make-up air area:             50 %
/ Vent type:                    Spots
/ Opening sequence:             Sequential
/ Opening temperature:          100°C
/ Vent size:                    1.9 m x 1.9 m
/ Central mesh size:            250 mm
/ Outer mesh sizes:             500 mm
/ Downstand depth:              30 %

/-----------------------------------------------------------------------------------------------------------------------------------------

&MESH ID = 'mesh1', IJK = 144,72,40, XB = -3.0,33.0,15.0,33.0,-1.0,9.0 / Finest mesh of 250 mm
&MESH ID = 'mesh2', IJK =  72,36,20, XB = -3.0,33.0, -3.0,15.0,-1.0,9.0 / Coarse mesh of 500 mm
&MESH ID = 'mesh3', IJK =  72,60,20, XB = -3.0,33.0,33.0,63.0,-1.0,9.0 / Coarse mesh of 500 mm

&TIME T_END = 1800., SYNCHRONIZE = .TRUE. /

&VENT MB = 'XMIN', SURF_ID = 'OPEN' /
&VENT MB = 'XMAX', SURF_ID = 'OPEN' /
&VENT MB = 'YMIN', SURF_ID = 'OPEN' /
&VENT MB = 'YMAX', SURF_ID = 'OPEN' /
&VENT MB = 'ZMAX', SURF_ID = 'OPEN' /

/-----------------------------------------------------------------------------------------------------------------------------------------
/ Defining the building materials and properties and rack storage and fire-fighter protective clothing.

&MISC SURF_DEFAULT = 'SHELVES', TMPA = 13. /

&MATL ID = 'SHEET_METAL'
      CONDUCTIVITY = 45.8
      SPECIFIC_HEAT = 0.46
      DENSITY = 7850 / From Buchanan 2002, p49

&MATL ID = 'CONCRETE'
      CONDUCTIVITY = 1.1
      SPECIFIC_HEAT = 0.88
      DENSITY = 2100 / From Buchanan 2002, p49

&MATL ID = 'SHELL'
    CONDUCTIVITY = 0.047
    SPECIFIC_HEAT = 1.3
    DENSITY = 310. / From Mell and Lawson 2000, p55

&MATL ID = 'MOISTURE_BARRIER'
```

```
      CONDUCTIVITY = 0.012
      SPECIFIC_HEAT = 2.01
      DENSITY = 800. / From Mell and Lawson 2000, p55

&MATL ID = 'THERMAL_LINER'
      CONDUCTIVITY = 0.038
      SPECIFIC_HEAT = 0.7
      DENSITY = 72. / From Mell and Lawson 2000, p55

&SURF ID = 'WALL'
            COLOR = 'TEAL'
            ADIABATIC = .TRUE.
            TRANSPARENCY = 0.4 /

&SURF ID = 'ROOF'
            MATL_ID = 'SHEET_METAL'
            COLOR = 'TEAL'
            ADIABATIC = .FALSE.
            THICKNESS = 0.0042
            BACKING = VOID
            TRANSPARENCY = 0.4 / thickness from Zincalume G550 steel, www.nzsteel.co.nz

&SURF ID = 'FLOOR'
            MATL_ID = 'CONCRETE'
            COLOR = 'GRAY'
            ADIABATIC = .FALSE.
            THICKNESS = 0.30
            TRANSPARENCY = 1.0 /

&SURF ID = 'SHELVES'
            MATL_ID = 'SHEET_METAL'
            COLOR = 'BLUE'
            THICKNESS = 0.0042
            TRANSPARENCY = 1.0 /

&SURF ID = 'TARGET'
            FYI = 'TURNOUT_COAT'
            MATL_ID = 'SHELL', 'MOISTURE_BARRIER', 'THERMAL_LINER'
            COLOR = 'ORCHID'
            THICKNESS = 0.00082, 0.00055, 0.0035 / Turnout Coat properties from Mell and Lawson

/-----------------------------------------------------------------------------------------------------------------------------
/ Creating the building and rack storage units.

&OBST XB = 00.00, 30.00, 00.00, 00.05, 00.00, 06.50, SURF_ID = 'WALL' / Front wall
&OBST XB = 00.00, 00.05, 00.00, 60.00, 00.00, 06.50, SURF_ID = 'WALL' / Left-hand side wall
&OBST XB = 29.95, 30.00, 00.00, 60.00, 00.00, 06.50, SURF_ID = 'WALL' / Right-hand side wall
&OBST XB = 00.00, 30.00, 59.95, 60.00, 00.00, 06.50, SURF_ID = 'WALL' / Rear wall
&OBST XB = 00.00, 30.00, 00.00, 60.00, 06.45, 06.50, SURF_ID = 'ROOF' / Ceiling
&OBST XB = -3.00, 33.00, -3.00, 63.00, -0.30, 00.00, SURF_ID = 'FLOOR' / Floor

&OBST XB = 03.00, 04.50, 05.00, 27.50, 00.00, 03.00, SURF_IDS = 'SHELVES','SHELVES','INERT' /
&OBST XB = 07.50, 09.00, 05.00, 27.50, 00.00, 03.00, SURF_IDS = 'SHELVES','SHELVES','INERT' /
&OBST XB = 12.00, 13.50, 05.00, 27.50, 00.00, 03.00, SURF_IDS = 'SHELVES','SHELVES','INERT' /
&OBST XB = 16.50, 18.00, 05.00, 27.50, 00.00, 03.00, SURF_IDS = 'SHELVES','SHELVES','INERT' /
&OBST XB = 21.00, 22.50, 05.00, 22.00, 00.00, 03.00, SURF_ID6 =
            'OPEN','OPEN','SHELVES','OPEN','INERT','SHELVES' /
```

```
&OBST XB = 21.00, 22.50, 22.00, 26.00, 00.00, 03.00, SURF_ID6 =
        'FIRE','FIRE','FIRE','FIRE','INERT','FIRE' /
&OBST XB = 21.00, 22.50, 26.00, 27.50, 00.00, 03.00, SURF_ID6 =
        'OPEN','OPEN','OPEN','SHELVES','INERT','SHELVES' /
&OBST XB = 25.50, 27.00, 05.00, 27.50, 00.00, 03.00, SURF_IDS = 'SHELVES','SHELVES','INERT' /
&OBST XB = 03.00, 04.50, 32.50, 55.00, 00.00, 03.00, SURF_IDS = 'SHELVES','SHELVES','INERT' /
&OBST XB = 07.50, 09.00, 32.50, 55.00, 00.00, 03.00, SURF_IDS = 'SHELVES','SHELVES','INERT' /
&OBST XB = 12.00, 13.50, 32.50, 55.00, 00.00, 03.00, SURF_IDS = 'SHELVES','SHELVES','INERT' /
&OBST XB = 16.50, 18.00, 32.50, 55.00, 00.00, 03.00, SURF_IDS = 'SHELVES','SHELVES','INERT' /
&OBST XB = 21.00, 22.50, 32.50, 55.00, 00.00, 03.00, SURF_IDS = 'SHELVES','SHELVES','INERT' /
&OBST XB = 25.50, 27.00, 32.50, 55.00, 00.00, 03.00, SURF_IDS = 'SHELVES','SHELVES','INERT' /

/----------------------------------------------------------------------------------------------------------------------------
/ Adding leakage 4 cm²/m² (25 m³/h.m² x 0.16) from Persily 1998 or 0.0004 m²/m².

&HOLE XB = 15.00, 15.026, 00.00, 00.05, 01.50, 04.50 /
&HOLE XB = 00.00, 00.05, 30.00, 30.0312, 01.50, 06.50 /
&HOLE XB = 29.95, 30.00, 30.00, 30.0312, 01.50, 06.50 /
&HOLE XB = 15.00, 15.026, 59.95, 60.00, 01.50, 04.50 /

/----------------------------------------------------------------------------------------------------------------------------
/ Adding downstands that are 30 % of roof height, which is 6.5 m.

&OBST XB = 06.50, 06.50, 00.00, 60.00, 04.55, 06.50, RGB = 92,92,92, THICKEN = .FALSE. /
&OBST XB = 12.00, 12.00, 00.00, 60.00, 04.55, 06.50, RGB = 92,92,92, THICKEN = .FALSE. /
&OBST XB = 18.00, 18.00, 00.00, 60.00, 04.55, 06.50, RGB = 92,92,92, THICKEN = .FALSE. /
&OBST XB = 23.50, 23.50, 00.00, 60.00, 04.55, 06.50, RGB = 92,92,92, THICKEN = .FALSE. /

&OBST XB = 00.00, 30.00, 04.50, 04.50, 04.55, 06.50, RGB = 92,92,92, THICKEN = .FALSE. /
&OBST XB = 00.00, 30.00, 10.50, 10.50, 04.55, 06.50, RGB = 92,92,92, THICKEN = .FALSE. /
&OBST XB = 00.00, 30.00, 16.50, 16.50, 04.55, 06.50, RGB = 92,92,92, THICKEN = .FALSE. /
&OBST XB = 00.00, 30.00, 22.50, 22.50, 04.55, 06.50, RGB = 92,92,92, THICKEN = .FALSE. /
&OBST XB = 00.00, 30.00, 28.00, 28.00, 04.55, 06.50, RGB = 92,92,92, THICKEN = .FALSE. /
&OBST XB = 00.00, 30.00, 32.00, 32.00, 04.55, 06.50, RGB = 92,92,92, THICKEN = .FALSE. /
&OBST XB = 00.00, 30.00, 37.50, 37.50, 04.55, 06.50, RGB = 92,92,92, THICKEN = .FALSE. /
&OBST XB = 00.00, 30.00, 43.50, 43.50, 04.55, 06.50, RGB = 92,92,92, THICKEN = .FALSE. /
&OBST XB = 00.00, 30.00, 49.50, 49.50, 04.55, 06.50, RGB = 92,92,92, THICKEN = .FALSE. /
&OBST XB = 00.00, 30.00, 55.50, 55.50, 04.55, 06.50, RGB = 92,92,92, THICKEN = .FALSE. /

/----------------------------------------------------------------------------------------------------------------------------
/ Creating 5 % venting of 90 m² for 1800 m² roof – 27 x 1.9 m x 1.9 m  (fictitious dimension) vents.

&HOLE XB = 04.05, 05.95, 05.00, 06.90, 06.45, 06.55, COLOR = 'RED', DEVC_ID = 'DETECT_01' /
&HOLE XB = 04.05, 05.95, 11.00, 12.90, 06.45, 06.55, COLOR = 'RED', DEVC_ID = 'DETECT_02' /
&HOLE XB = 04.05, 05.95, 17.00, 18.90, 06.45, 06.55, COLOR = 'RED', DEVC_ID = 'DETECT_03' /
&HOLE XB = 04.05, 05.95, 23.00, 24.90, 06.45, 06.55, COLOR = 'RED', DEVC_ID = 'DETECT_04' /
&HOLE XB = 04.05, 05.95, 29.00, 30.90, 06.45, 06.55, COLOR = 'RED', DEVC_ID = 'DETECT_05' /
&HOLE XB = 04.05, 05.95, 35.00, 36.90, 06.45, 06.55, COLOR = 'RED', DEVC_ID = 'DETECT_06' /
&HOLE XB = 04.05, 05.95, 41.00, 42.90, 06.45, 06.55, COLOR = 'RED', DEVC_ID = 'DETECT_07' /
&HOLE XB = 04.05, 05.95, 47.00, 48.90, 06.45, 06.55, COLOR = 'RED', DEVC_ID = 'DETECT_08' /
&HOLE XB = 04.05, 05.95, 53.00, 54.90, 06.45, 06.55, COLOR = 'RED', DEVC_ID = 'DETECT_09' /

&HOLE XB = 14.05, 15.95, 05.00, 06.90, 06.45, 06.55, COLOR = 'RED', DEVC_ID = 'DETECT_10' /
&HOLE XB = 14.05, 15.95, 11.00, 12.90, 06.45, 06.55, COLOR = 'RED', DEVC_ID = 'DETECT_11' /
&HOLE XB = 14.05, 15.95, 17.00, 18.90, 06.45, 06.55, COLOR = 'RED', DEVC_ID = 'DETECT_12' /
&HOLE XB = 14.05, 15.95, 23.00, 24.90, 06.45, 06.55, COLOR = 'RED', DEVC_ID = 'DETECT_13' /
&HOLE XB = 14.05, 15.95, 29.00, 30.90, 06.45, 06.55, COLOR = 'RED', DEVC_ID = 'DETECT_14' /
```

```
&HOLE XB = 14.05, 15.95, 35.00, 36.90, 06.45, 06.55, COLOR = 'RED', DEVC_ID = 'DETECT_15' /
&HOLE XB = 14.05, 15.95, 41.00, 42.90, 06.45, 06.55, COLOR = 'RED', DEVC_ID = 'DETECT_16' /
&HOLE XB = 14.05, 15.95, 47.00, 48.90, 06.45, 06.55, COLOR = 'RED', DEVC_ID = 'DETECT_17' /
&HOLE XB = 14.05, 15.95, 53.00, 54.90, 06.45, 06.55, COLOR = 'RED', DEVC_ID = 'DETECT_18' /

&HOLE XB = 24.05, 25.95, 05.00, 06.90, 06.45, 06.55, COLOR = 'RED', DEVC_ID = 'DETECT_19' /
&HOLE XB = 24.05, 25.95, 11.00, 12.90, 06.45, 06.55, COLOR = 'RED', DEVC_ID = 'DETECT_20' /
&HOLE XB = 24.05, 25.95, 17.00, 18.90, 06.45, 06.55, COLOR = 'RED', DEVC_ID = 'DETECT_21' /
&HOLE XB = 24.05, 25.95, 23.00, 24.90, 06.45, 06.55, COLOR = 'RED', DEVC_ID = 'DETECT_22' /
&HOLE XB = 24.05, 25.95, 29.00, 30.90, 06.45, 06.55, COLOR = 'RED', DEVC_ID = 'DETECT_23' /
&HOLE XB = 24.05, 25.95, 35.00, 36.90, 06.45, 06.55, COLOR = 'RED', DEVC_ID = 'DETECT_24' /
&HOLE XB = 24.05, 25.95, 41.00, 42.90, 06.45, 06.55, COLOR = 'RED', DEVC_ID = 'DETECT_25' /
&HOLE XB = 24.05, 25.95, 47.00, 48.90, 06.45, 06.55, COLOR = 'RED', DEVC_ID = 'DETECT_26' /
&HOLE XB = 24.05, 25.95, 53.00, 54.90, 06.45, 06.55, COLOR = 'RED', DEVC_ID = 'DETECT_27' /

&DEVC XYZ = 05.00, 05.95, 6.35, ID = 'DETECT_01', QUANTITY = 'TEMPERATURE', SETPOINT = 100,
      INITIAL_STATE = .FALSE. /
&DEVC XYZ = 05.00, 11.95, 6.35, ID = 'DETECT_02', QUANTITY = 'TEMPERATURE', SETPOINT = 100,
      INITIAL_STATE = .FALSE. /
&DEVC XYZ = 05.00, 17.95, 6.35, ID = 'DETECT_03', QUANTITY = 'TEMPERATURE', SETPOINT = 100,
      INITIAL_STATE = .FALSE. /
&DEVC XYZ = 05.00, 23.95, 6.35, ID = 'DETECT_04', QUANTITY = 'TEMPERATURE', SETPOINT = 100,
      INITIAL_STATE = .FALSE. /
&DEVC XYZ = 05.00, 29.95, 6.35, ID = 'DETECT_05', QUANTITY = 'TEMPERATURE', SETPOINT = 100,
      INITIAL_STATE = .FALSE. /
&DEVC XYZ = 05.00, 35.95, 6.35, ID = 'DETECT_06', QUANTITY = 'TEMPERATURE', SETPOINT = 100,
      INITIAL_STATE = .FALSE. /
&DEVC XYZ = 05.00, 41.95, 6.35, ID = 'DETECT_07', QUANTITY = 'TEMPERATURE', SETPOINT = 100,
      INITIAL_STATE = .FALSE. /
&DEVC XYZ = 05.00, 47.95, 6.35, ID = 'DETECT_08', QUANTITY = 'TEMPERATURE', SETPOINT = 100,
      INITIAL_STATE = .FALSE. /
&DEVC XYZ = 05.00, 53.95, 6.35, ID = 'DETECT_09', QUANTITY = 'TEMPERATURE', SETPOINT = 100,
      INITIAL_STATE = .FALSE. /
&DEVC XYZ = 15.00, 05.95, 6.35, ID = 'DETECT_10', QUANTITY = 'TEMPERATURE', SETPOINT = 100,
      INITIAL_STATE = .FALSE. /
&DEVC XYZ = 15.00, 11.95, 6.35, ID = 'DETECT_11', QUANTITY = 'TEMPERATURE', SETPOINT = 100,
      INITIAL_STATE = .FALSE. /
&DEVC XYZ = 15.00, 17.95, 6.35, ID = 'DETECT_12', QUANTITY = 'TEMPERATURE', SETPOINT = 100,
      INITIAL_STATE = .FALSE. /
&DEVC XYZ = 15.00, 23.95, 6.35, ID = 'DETECT_13', QUANTITY = 'TEMPERATURE', SETPOINT = 100,
      INITIAL_STATE = .FALSE. /
&DEVC XYZ = 15.00, 29.95, 6.35, ID = 'DETECT_14', QUANTITY = 'TEMPERATURE', SETPOINT = 100,
      INITIAL_STATE = .FALSE. /
&DEVC XYZ = 15.00, 35.95, 6.35, ID = 'DETECT_15', QUANTITY = 'TEMPERATURE', SETPOINT = 100,
      INITIAL_STATE = .FALSE. /
&DEVC XYZ = 15.00, 41.95, 6.35, ID = 'DETECT_16', QUANTITY = 'TEMPERATURE', SETPOINT = 100,
      INITIAL_STATE = .FALSE. /
&DEVC XYZ = 15.00, 47.95, 6.35, ID = 'DETECT_17', QUANTITY = 'TEMPERATURE', SETPOINT = 100,
      INITIAL_STATE = .FALSE. /
&DEVC XYZ = 15.00, 53.95, 6.35, ID = 'DETECT_18', QUANTITY = 'TEMPERATURE', SETPOINT = 100,
      INITIAL_STATE = .FALSE. /
&DEVC XYZ = 25.00, 05.95, 6.35, ID = 'DETECT_19', QUANTITY = 'TEMPERATURE', SETPOINT = 100,
      INITIAL_STATE = .FALSE. /
```

```
&DEVC XYZ = 25.00, 11.95, 6.35, ID = 'DETECT_20', QUANTITY = 'TEMPERATURE', SETPOINT = 100,
      INITIAL_STATE = .FALSE. /
&DEVC XYZ = 25.00, 17.95, 6.35, ID = 'DETECT_21', QUANTITY = 'TEMPERATURE', SETPOINT = 100,
      INITIAL_STATE = .FALSE. /
&DEVC XYZ = 25.00, 23.95, 6.35, ID = 'DETECT_22', QUANTITY = 'TEMPERATURE', SETPOINT = 100,
      INITIAL_STATE = .FALSE. /
&DEVC XYZ = 25.00, 29.95, 6.35, ID = 'DETECT_23', QUANTITY = 'TEMPERATURE', SETPOINT = 100,
      INITIAL_STATE = .FALSE. /
&DEVC XYZ = 25.00, 35.95, 6.35, ID = 'DETECT_24', QUANTITY = 'TEMPERATURE', SETPOINT = 100,
      INITIAL_STATE = .FALSE. /
&DEVC XYZ = 25.00, 41.95, 6.35, ID = 'DETECT_25', QUANTITY = 'TEMPERATURE', SETPOINT = 100,
      INITIAL_STATE = .FALSE. /
&DEVC XYZ = 25.00, 47.95, 6.35, ID = 'DETECT_26', QUANTITY = 'TEMPERATURE', SETPOINT = 100,
      INITIAL_STATE = .FALSE. /
&DEVC XYZ = 25.00, 53.95, 6.35, ID = 'DETECT_27', QUANTITY = 'TEMPERATURE', SETPOINT = 100,
      INITIAL_STATE = .FALSE. /

/-----------------------------------------------------------------------------------------------------------------------------------------
/ Creating make-up air equal to 50 % of the roof venting (which equates to 45 m².

&HOLE XB = 00.00, 30.00, 00.00, 00.05, 00.00, 00.25 /
&HOLE XB = 00.00, 00.05, 00.00, 60.00, 00.00, 00.25 /
&HOLE XB = 29.95, 30.00, 00.00, 60.00, 00.00, 00.25 /
&HOLE XB = 00.00, 30.00, 59.95, 60.00, 00.00, 00.25 /

/-----------------------------------------------------------------------------------------------------------------------------------------
/ Description of design fire.

&SURF ID ='FIRE', HRRPUA=1667., COLOR = 'ORCHID', RAMP_Q = 'Slow_t3'

&RAMP ID = 'Slow_t3', T =  00.0, F = 0.0 /
&RAMP ID = 'Slow_t3', T = 108.0, F = 0.1 /
&RAMP ID = 'Slow_t3', T = 155.0, F = 0.2 /
&RAMP ID = 'Slow_t3', T = 183.0, F = 0.3 /
&RAMP ID = 'Slow_t3', T = 205.0, F = 0.4 /
&RAMP ID = 'Slow_t3', T = 223.0, F = 0.5 /
&RAMP ID = 'Slow_t3', T = 238.0, F = 0.6 /
&RAMP ID = 'Slow_t3', T = 252.0, F = 0.7 /
&RAMP ID = 'Slow_t3', T = 264.0, F = 0.8 /
&RAMP ID = 'Slow_t3', T = 276.0, F = 0.9 /
&RAMP ID = 'Slow_t3', T = 286.0, F = 1.0 /

&REAC ID = 'VM2GENERICFUEL'
      C =1.
      H = 1.7
      O=0.6
      N=0.05
      HEAT_OF_COMBUSTION = 20000.
      CO_YIELD=0.04
      SOOT_YIELD=0.07
      IDEAL = .FALSE. / From Appendix B – Proposed Verification Method

/-----------------------------------------------------------------------------------------------------------------------------------------
/ Installing targets record radiation at height of 1.5 m.

&OBST XB = 04.75, 05.25, 09.75, 10.25, 01.50, 01.50, SURF_IDS = 'TARGET', 'INERT', 'INERT', THICKEN
      = .TRUE.  /
```

```
&OBST XB = 14.75, 15.25, 09.75, 10.25, 01.50, 01.50, SURF_IDS = 'TARGET', 'INERT', 'INERT', THICKEN
        = .TRUE.  /
&OBST XB = 24.75, 25.25, 09.75, 10.25, 01.50, 01.50, SURF_IDS = 'TARGET', 'INERT', 'INERT', THICKEN
        = .TRUE.  /
&OBST XB = 04.75, 05.25, 29.75, 30.25, 01.50, 01.50, SURF_IDS = 'TARGET', 'INERT', 'INERT', THICKEN
        = .TRUE.  /
&OBST XB = 14.75, 15.25, 29.75, 30.25, 01.50, 01.50, SURF_IDS = 'TARGET', 'INERT', 'INERT', THICKEN
        = .TRUE.  /
&OBST XB = 24.75, 25.25, 29.75, 30.25, 01.50, 01.50, SURF_IDS = 'TARGET', 'INERT', 'INERT', THICKEN
        = .TRUE.  /
&OBST XB = 04.75, 05.25, 49.75, 50.25, 01.50, 01.50, SURF_IDS = 'TARGET', 'INERT', 'INERT', THICKEN
        = .TRUE.  /
&OBST XB = 14.75, 15.25, 49.75, 50.25, 01.50, 01.50, SURF_IDS = 'TARGET', 'INERT', 'INERT', THICKEN
        = .TRUE.  /
&OBST XB = 24.75, 25.25, 49.75, 50.25, 01.50, 01.50, SURF_IDS = 'TARGET', 'INERT', 'INERT', THICKEN
        = .TRUE.  /

/----------------------------------------------------------------------------------------------------------------------------
/ Devices to record radiative heat flux at height of 1.5 m, orientated to receive radiation from ceiling.

&DEVC XYZ = 05.00, 10.00, 01.50, QUANTITY = 'RADIATIVE HEAT FLUX', IOR = 3, ID = 'RHF_FL_1.5' /
&DEVC XYZ = 15.00, 10.00, 01.50, QUANTITY = 'RADIATIVE HEAT FLUX', IOR = 3, ID = 'RHF_FC_1.5' /
&DEVC XYZ = 25.00, 10.00, 01.50, QUANTITY = 'RADIATIVE HEAT FLUX', IOR = 3, ID = 'RHF_FR_1.5' /
&DEVC XYZ = 05.00, 30.00, 01.50, QUANTITY = 'RADIATIVE HEAT FLUX', IOR = 3, ID = 'RHF_ML_1.5' /
&DEVC XYZ = 15.00, 30.00, 01.50, QUANTITY = 'RADIATIVE HEAT FLUX', IOR = 3, ID = 'RHF_MC_1.5' /
&DEVC XYZ = 25.00, 30.00, 01.50, QUANTITY = 'RADIATIVE HEAT FLUX', IOR = 3, ID = 'RHF_MR_1.5' /
&DEVC XYZ = 05.00, 50.00, 01.50, QUANTITY = 'RADIATIVE HEAT FLUX', IOR = 3, ID = 'RHF_BL_1.5' /
&DEVC XYZ = 15.00, 50.00, 01.50, QUANTITY = 'RADIATIVE HEAT FLUX', IOR = 3, ID = 'RHF_BC_1.5' /
&DEVC XYZ = 25.00, 50.00, 01.50, QUANTITY = 'RADIATIVE HEAT FLUX', IOR = 3, ID = 'RHF_BR_1.5' /

/----------------------------------------------------------------------------------------------------------------------------
/ Devices to record visibility at height of 1.5 m.

&DEVC XYZ = 05.00, 10.00, 01.50, QUANTITY = 'VISIBILITY', ID = 'VIS_FL_1.5' /
&DEVC XYZ = 15.00, 10.00, 01.50, QUANTITY = 'VISIBILITY', ID = 'VIS_FC_1.5' /
&DEVC XYZ = 25.00, 10.00, 01.50, QUANTITY = 'VISIBILITY', ID = 'VIS_FR_1.5' /
&DEVC XYZ = 05.00, 30.00, 01.50, QUANTITY = 'VISIBILITY', ID = 'VIS_ML_1.5' /
&DEVC XYZ = 15.00, 30.00, 01.50, QUANTITY = 'VISIBILITY', ID = 'VIS_MC_1.5' /
&DEVC XYZ = 25.00, 30.00, 01.50, QUANTITY = 'VISIBILITY', ID = 'VIS_MR_1.5' /
&DEVC XYZ = 05.00, 50.00, 01.50, QUANTITY = 'VISIBILITY', ID = 'VIS_BL_1.5' /
&DEVC XYZ = 15.00, 50.00, 01.50, QUANTITY = 'VISIBILITY', ID = 'VIS_BC_1.5' /
&DEVC XYZ = 25.00, 50.00, 01.50, QUANTITY = 'VISIBILITY', ID = 'VIS_BR_1.5' /

/----------------------------------------------------------------------------------------------------------------------------
/ Temperature devices at 9 evenly spaced points in warehouse to record temperature every 0.5 m.

&DEVC XYZ = 05.00, 10.00, 00.50, QUANTITY = 'TEMPERATURE', ID = 'TMP_FL_0.5' /
&DEVC XYZ = 15.00, 10.00, 00.50, QUANTITY = 'TEMPERATURE', ID = 'TMP_FC_0.5' /
&DEVC XYZ = 25.00, 10.00, 00.50, QUANTITY = 'TEMPERATURE', ID = 'TMP_FR_0.5' /
&DEVC XYZ = 05.00, 30.00, 00.50, QUANTITY = 'TEMPERATURE', ID = 'TMP_ML_0.5' /
&DEVC XYZ = 15.00, 30.00, 00.50, QUANTITY = 'TEMPERATURE', ID = 'TMP_MC_0.5' /
&DEVC XYZ = 25.00, 30.00, 00.50, QUANTITY = 'TEMPERATURE', ID = 'TMP_MR_0.5' /
&DEVC XYZ = 05.00, 50.00, 00.50, QUANTITY = 'TEMPERATURE', ID = 'TMP_BL_0.5' /
&DEVC XYZ = 15.00, 50.00, 00.50, QUANTITY = 'TEMPERATURE', ID = 'TMP_BC_0.5' /
&DEVC XYZ = 25.00, 50.00, 00.50, QUANTITY = 'TEMPERATURE', ID = 'TMP_BR_0.5' /

&DEVC XYZ = 05.00, 10.00, 01.00, QUANTITY = 'TEMPERATURE', ID = 'TMP_FL_1.0' /
```

```
&DEVC XYZ = 15.00, 10.00, 01.00, QUANTITY = 'TEMPERATURE', ID = 'TMP_FC_1.0' /
&DEVC XYZ = 25.00, 10.00, 01.00, QUANTITY = 'TEMPERATURE', ID = 'TMP_FR_1.0' /
&DEVC XYZ = 05.00, 30.00, 01.00, QUANTITY = 'TEMPERATURE', ID = 'TMP_ML_1.0' /
&DEVC XYZ = 15.00, 30.00, 01.00, QUANTITY = 'TEMPERATURE', ID = 'TMP_MC_1.0' /
&DEVC XYZ = 25.00, 30.00, 01.00, QUANTITY = 'TEMPERATURE', ID = 'TMP_MR_1.0' /
&DEVC XYZ = 05.00, 50.00, 01.00, QUANTITY = 'TEMPERATURE', ID = 'TMP_BL_1.0' /
&DEVC XYZ = 15.00, 50.00, 01.00, QUANTITY = 'TEMPERATURE', ID = 'TMP_BC_1.0' /
&DEVC XYZ = 25.00, 50.00, 01.00, QUANTITY = 'TEMPERATURE', ID = 'TMP_BR_1.0' /

&DEVC XYZ = 05.00, 10.00, 01.50, QUANTITY = 'TEMPERATURE', ID = 'TMP_FL_1.5' /
&DEVC XYZ = 15.00, 10.00, 01.50, QUANTITY = 'TEMPERATURE', ID = 'TMP_FC_1.5' /
&DEVC XYZ = 25.00, 10.00, 01.50, QUANTITY = 'TEMPERATURE', ID = 'TMP_FR_1.5' /
&DEVC XYZ = 05.00, 30.00, 01.50, QUANTITY = 'TEMPERATURE', ID = 'TMP_ML_1.5' /
&DEVC XYZ = 15.00, 30.00, 01.50, QUANTITY = 'TEMPERATURE', ID = 'TMP_MC_1.5' /
&DEVC XYZ = 25.00, 30.00, 01.50, QUANTITY = 'TEMPERATURE', ID = 'TMP_MR_1.5' /
&DEVC XYZ = 05.00, 50.00, 01.50, QUANTITY = 'TEMPERATURE', ID = 'TMP_BL_1.5' /
&DEVC XYZ = 15.00, 50.00, 01.50, QUANTITY = 'TEMPERATURE', ID = 'TMP_BC_1.5' /
&DEVC XYZ = 25.00, 50.00, 01.50, QUANTITY = 'TEMPERATURE', ID = 'TMP_BR_1.5' /

&DEVC XYZ = 05.00, 10.00, 02.00, QUANTITY = 'TEMPERATURE', ID = 'TMP_FL_2.0' /
&DEVC XYZ = 15.00, 10.00, 02.00, QUANTITY = 'TEMPERATURE', ID = 'TMP_FC_2.0' /
&DEVC XYZ = 25.00, 10.00, 02.00, QUANTITY = 'TEMPERATURE', ID = 'TMP_FR_2.0' /
&DEVC XYZ = 05.00, 30.00, 02.00, QUANTITY = 'TEMPERATURE', ID = 'TMP_ML_2.0' /
&DEVC XYZ = 15.00, 30.00, 02.00, QUANTITY = 'TEMPERATURE', ID = 'TMP_MC_2.0' /
&DEVC XYZ = 25.00, 30.00, 02.00, QUANTITY = 'TEMPERATURE', ID = 'TMP_MR_2.0' /
&DEVC XYZ = 05.00, 50.00, 02.00, QUANTITY = 'TEMPERATURE', ID = 'TMP_BL_2.0' /
&DEVC XYZ = 15.00, 50.00, 02.00, QUANTITY = 'TEMPERATURE', ID = 'TMP_BC_2.0' /
&DEVC XYZ = 25.00, 50.00, 02.00, QUANTITY = 'TEMPERATURE', ID = 'TMP_BR_2.0' /

&DEVC XYZ = 05.00, 10.00, 02.50, QUANTITY = 'TEMPERATURE', ID = 'TMP_FL_2.5' /
&DEVC XYZ = 15.00, 10.00, 02.50, QUANTITY = 'TEMPERATURE', ID = 'TMP_FC_2.5' /
&DEVC XYZ = 25.00, 10.00, 02.50, QUANTITY = 'TEMPERATURE', ID = 'TMP_FR_2.5' /
&DEVC XYZ = 05.00, 30.00, 02.50, QUANTITY = 'TEMPERATURE', ID = 'TMP_ML_2.5' /
&DEVC XYZ = 15.00, 30.00, 02.50, QUANTITY = 'TEMPERATURE', ID = 'TMP_MC_2.5' /
&DEVC XYZ = 25.00, 30.00, 02.50, QUANTITY = 'TEMPERATURE', ID = 'TMP_MR_2.5' /
&DEVC XYZ = 05.00, 50.00, 02.50, QUANTITY = 'TEMPERATURE', ID = 'TMP_BL_2.5' /
&DEVC XYZ = 15.00, 50.00, 02.50, QUANTITY = 'TEMPERATURE', ID = 'TMP_BC_2.5' /
&DEVC XYZ = 25.00, 50.00, 02.50, QUANTITY = 'TEMPERATURE', ID = 'TMP_BR_2.5' /

&DEVC XYZ = 05.00, 10.00, 03.00, QUANTITY = 'TEMPERATURE', ID = 'TMP_FL_3.0' /
&DEVC XYZ = 15.00, 10.00, 03.00, QUANTITY = 'TEMPERATURE', ID = 'TMP_FC_3.0' /
&DEVC XYZ = 25.00, 10.00, 03.00, QUANTITY = 'TEMPERATURE', ID = 'TMP_FR_3.0' /
&DEVC XYZ = 05.00, 30.00, 03.00, QUANTITY = 'TEMPERATURE', ID = 'TMP_ML_3.0' /
&DEVC XYZ = 15.00, 30.00, 03.00, QUANTITY = 'TEMPERATURE', ID = 'TMP_MC_3.0' /
&DEVC XYZ = 25.00, 30.00, 03.00, QUANTITY = 'TEMPERATURE', ID = 'TMP_MR_3.0' /
&DEVC XYZ = 05.00, 50.00, 03.00, QUANTITY = 'TEMPERATURE', ID = 'TMP_BL_3.0' /
&DEVC XYZ = 15.00, 50.00, 03.00, QUANTITY = 'TEMPERATURE', ID = 'TMP_BC_3.0' /
&DEVC XYZ = 25.00, 50.00, 03.00, QUANTITY = 'TEMPERATURE', ID = 'TMP_BR_3.0' /

&DEVC XYZ = 05.00, 10.00, 03.50, QUANTITY = 'TEMPERATURE', ID = 'TMP_FL_3.5' /
&DEVC XYZ = 15.00, 10.00, 03.50, QUANTITY = 'TEMPERATURE', ID = 'TMP_FC_3.5' /
&DEVC XYZ = 25.00, 10.00, 03.50, QUANTITY = 'TEMPERATURE', ID = 'TMP_FR_3.5' /
&DEVC XYZ = 05.00, 30.00, 03.50, QUANTITY = 'TEMPERATURE', ID = 'TMP_ML_3.5' /
&DEVC XYZ = 15.00, 30.00, 03.50, QUANTITY = 'TEMPERATURE', ID = 'TMP_MC_3.5' /
&DEVC XYZ = 25.00, 30.00, 03.50, QUANTITY = 'TEMPERATURE', ID = 'TMP_MR_3.5' /
```

```
&DEVC XYZ = 05.00, 50.00, 03.50, QUANTITY = 'TEMPERATURE', ID = 'TMP_BL_3.5' /
&DEVC XYZ = 15.00, 50.00, 03.50, QUANTITY = 'TEMPERATURE', ID = 'TMP_BC_3.5' /
&DEVC XYZ = 25.00, 50.00, 03.50, QUANTITY = 'TEMPERATURE', ID = 'TMP_BR_3.5' /

&DEVC XYZ = 05.00, 10.00, 04.00, QUANTITY = 'TEMPERATURE', ID = 'TMP_FL_4.0' /
&DEVC XYZ = 15.00, 10.00, 04.00, QUANTITY = 'TEMPERATURE', ID = 'TMP_FC_4.0' /
&DEVC XYZ = 25.00, 10.00, 04.00, QUANTITY = 'TEMPERATURE', ID = 'TMP_FR_4.0' /
&DEVC XYZ = 05.00, 30.00, 04.00, QUANTITY = 'TEMPERATURE', ID = 'TMP_ML_4.0' /
&DEVC XYZ = 15.00, 30.00, 04.00, QUANTITY = 'TEMPERATURE', ID = 'TMP_MC_4.0' /
&DEVC XYZ = 25.00, 30.00, 04.00, QUANTITY = 'TEMPERATURE', ID = 'TMP_MR_4.0' /
&DEVC XYZ = 05.00, 50.00, 04.00, QUANTITY = 'TEMPERATURE', ID = 'TMP_BL_4.0' /
&DEVC XYZ = 15.00, 50.00, 04.00, QUANTITY = 'TEMPERATURE', ID = 'TMP_BC_4.0' /
&DEVC XYZ = 25.00, 50.00, 04.00, QUANTITY = 'TEMPERATURE', ID = 'TMP_BR_4.0' /

&DEVC XYZ = 05.00, 10.00, 04.50, QUANTITY = 'TEMPERATURE', ID = 'TMP_FL_4.5' /
&DEVC XYZ = 15.00, 10.00, 04.50, QUANTITY = 'TEMPERATURE', ID = 'TMP_FC_4.5' /
&DEVC XYZ = 25.00, 10.00, 04.50, QUANTITY = 'TEMPERATURE', ID = 'TMP_FR_4.5' /
&DEVC XYZ = 05.00, 30.00, 04.50, QUANTITY = 'TEMPERATURE', ID = 'TMP_ML_4.5' /
&DEVC XYZ = 15.00, 30.00, 04.50, QUANTITY = 'TEMPERATURE', ID = 'TMP_MC_4.5' /
&DEVC XYZ = 25.00, 30.00, 04.50, QUANTITY = 'TEMPERATURE', ID = 'TMP_MR_4.5' /
&DEVC XYZ = 05.00, 50.00, 04.50, QUANTITY = 'TEMPERATURE', ID = 'TMP_BL_4.5' /
&DEVC XYZ = 15.00, 50.00, 04.50, QUANTITY = 'TEMPERATURE', ID = 'TMP_BC_4.5' /
&DEVC XYZ = 25.00, 50.00, 04.50, QUANTITY = 'TEMPERATURE', ID = 'TMP_BR_4.5' /

&DEVC XYZ = 05.00, 10.00, 05.00, QUANTITY = 'TEMPERATURE', ID = 'TMP_FL_5.0' /
&DEVC XYZ = 15.00, 10.00, 05.00, QUANTITY = 'TEMPERATURE', ID = 'TMP_FC_5.0' /
&DEVC XYZ = 25.00, 10.00, 05.00, QUANTITY = 'TEMPERATURE', ID = 'TMP_FR_5.0' /
&DEVC XYZ = 05.00, 30.00, 05.00, QUANTITY = 'TEMPERATURE', ID = 'TMP_ML_5.0' /
&DEVC XYZ = 15.00, 30.00, 05.00, QUANTITY = 'TEMPERATURE', ID = 'TMP_MC_5.0' /
&DEVC XYZ = 25.00, 30.00, 05.00, QUANTITY = 'TEMPERATURE', ID = 'TMP_MR_5.0' /
&DEVC XYZ = 05.00, 50.00, 05.00, QUANTITY = 'TEMPERATURE', ID = 'TMP_BL_5.0' /
&DEVC XYZ = 15.00, 50.00, 05.00, QUANTITY = 'TEMPERATURE', ID = 'TMP_BC_5.0' /
&DEVC XYZ = 25.00, 50.00, 05.00, QUANTITY = 'TEMPERATURE', ID = 'TMP_BR_5.0' /

&DEVC XYZ = 05.00, 10.00, 05.50, QUANTITY = 'TEMPERATURE', ID = 'TMP_FL_5.5' /
&DEVC XYZ = 15.00, 10.00, 05.50, QUANTITY = 'TEMPERATURE', ID = 'TMP_FC_5.5' /
&DEVC XYZ = 25.00, 10.00, 05.50, QUANTITY = 'TEMPERATURE', ID = 'TMP_FR_5.5' /
&DEVC XYZ = 05.00, 30.00, 05.50, QUANTITY = 'TEMPERATURE', ID = 'TMP_ML_5.5' /
&DEVC XYZ = 15.00, 30.00, 05.50, QUANTITY = 'TEMPERATURE', ID = 'TMP_MC_5.5' /
&DEVC XYZ = 25.00, 30.00, 05.50, QUANTITY = 'TEMPERATURE', ID = 'TMP_MR_5.5' /
&DEVC XYZ = 05.00, 50.00, 05.50, QUANTITY = 'TEMPERATURE', ID = 'TMP_BL_5.5' /
&DEVC XYZ = 15.00, 50.00, 05.50, QUANTITY = 'TEMPERATURE', ID = 'TMP_BC_5.5' /
&DEVC XYZ = 25.00, 50.00, 05.50, QUANTITY = 'TEMPERATURE', ID = 'TMP_BR_5.5' /

&DEVC XYZ = 05.00, 10.00, 06.00, QUANTITY = 'TEMPERATURE', ID = 'TMP_FL_6.0' /
&DEVC XYZ = 15.00, 10.00, 06.00, QUANTITY = 'TEMPERATURE', ID = 'TMP_FC_6.0' /
&DEVC XYZ = 25.00, 10.00, 06.00, QUANTITY = 'TEMPERATURE', ID = 'TMP_FR_6.0' /
&DEVC XYZ = 05.00, 30.00, 06.00, QUANTITY = 'TEMPERATURE', ID = 'TMP_ML_6.0' /
&DEVC XYZ = 15.00, 30.00, 06.00, QUANTITY = 'TEMPERATURE', ID = 'TMP_MC_6.0' /
&DEVC XYZ = 25.00, 30.00, 06.00, QUANTITY = 'TEMPERATURE', ID = 'TMP_MR_6.0' /
&DEVC XYZ = 05.00, 50.00, 06.00, QUANTITY = 'TEMPERATURE', ID = 'TMP_BL_6.0' /
&DEVC XYZ = 15.00, 50.00, 06.00, QUANTITY = 'TEMPERATURE', ID = 'TMP_BC_6.0' /
&DEVC XYZ = 25.00, 50.00, 06.00, QUANTITY = 'TEMPERATURE', ID = 'TMP_BR_6.0' /

&DEVC XYZ = 05.00, 10.00, 06.50, QUANTITY = 'TEMPERATURE', ID = 'TMP_FL_6.5' /
&DEVC XYZ = 15.00, 10.00, 06.50, QUANTITY = 'TEMPERATURE', ID = 'TMP_FC_6.5' /
```

```
&DEVC XYZ = 25.00, 10.00, 06.50, QUANTITY = 'TEMPERATURE', ID = 'TMP_FR_6.5' /
&DEVC XYZ = 05.00, 30.00, 06.50, QUANTITY = 'TEMPERATURE', ID = 'TMP_ML_6.5' /
&DEVC XYZ = 15.00, 30.00, 06.50, QUANTITY = 'TEMPERATURE', ID = 'TMP_MC_6.5' /
&DEVC XYZ = 25.00, 30.00, 06.50, QUANTITY = 'TEMPERATURE', ID = 'TMP_MR_6.5' /
&DEVC XYZ = 05.00, 50.00, 06.50, QUANTITY = 'TEMPERATURE', ID = 'TMP_BL_6.5' /
&DEVC XYZ = 15.00, 50.00, 06.50, QUANTITY = 'TEMPERATURE', ID = 'TMP_BC_6.5' /
&DEVC XYZ = 25.00, 50.00, 06.50, QUANTITY = 'TEMPERATURE', ID = 'TMP_BR_6.5' /

/----------------------------------------------------------------------------------------------------------------------------
/ Devices to measure mass flow across each vent opening

&DEVC XB = 04.05, 05.95, 05.00, 06.90, 06.50, 06.50, QUANTITY = 'MASS FLOW', ID = 'MF_L1' /
&DEVC XB = 04.05, 05.95, 11.00, 12.90, 06.50, 06.50, QUANTITY = 'MASS FLOW', ID = 'MF_L2' /
&DEVC XB = 04.05, 05.95, 17.00, 18.90, 06.50, 06.50, QUANTITY = 'MASS FLOW', ID = 'MF_L3' /
&DEVC XB = 04.05, 05.95, 23.00, 24.90, 06.50, 06.50, QUANTITY = 'MASS FLOW', ID = 'MF_L4' /
&DEVC XB = 04.05, 05.95, 29.00, 30.90, 06.50, 06.50, QUANTITY = 'MASS FLOW', ID = 'MF_L5' /
&DEVC XB = 04.05, 05.95, 35.00, 36.90, 06.50, 06.50, QUANTITY = 'MASS FLOW', ID = 'MF_L6' /
&DEVC XB = 04.05, 05.95, 41.00, 42.90, 06.50, 06.50, QUANTITY = 'MASS FLOW', ID = 'MF_L7' /
&DEVC XB = 04.05, 05.95, 47.00, 48.90, 06.50, 06.50, QUANTITY = 'MASS FLOW', ID = 'MF_L8' /
&DEVC XB = 04.05, 05.95, 53.00, 54.90, 06.50, 06.50, QUANTITY = 'MASS FLOW', ID = 'MF_L9' /

&DEVC XB = 14.05, 15.95, 05.00, 06.90, 06.50, 06.50, QUANTITY = 'MASS FLOW', ID = 'MF_C1' /
&DEVC XB = 14.05, 15.95, 11.00, 12.90, 06.50, 06.50, QUANTITY = 'MASS FLOW', ID = 'MF_C2' /
&DEVC XB = 14.05, 15.95, 17.00, 18.90, 06.50, 06.50, QUANTITY = 'MASS FLOW', ID = 'MF_C3' /
&DEVC XB = 14.05, 15.95, 23.00, 24.90, 06.50, 06.50, QUANTITY = 'MASS FLOW', ID = 'MF_C4' /
&DEVC XB = 14.05, 15.95, 29.00, 30.90, 06.50, 06.50, QUANTITY = 'MASS FLOW', ID = 'MF_C5' /
&DEVC XB = 14.05, 15.95, 35.00, 36.90, 06.50, 06.50, QUANTITY = 'MASS FLOW', ID = 'MF_C6' /
&DEVC XB = 14.05, 15.95, 41.00, 42.90, 06.50, 06.50, QUANTITY = 'MASS FLOW', ID = 'MF_C7' /
&DEVC XB = 14.05, 15.95, 47.00, 48.90, 06.50, 06.50, QUANTITY = 'MASS FLOW', ID = 'MF_C8' /
&DEVC XB = 14.05, 15.95, 53.00, 54.90, 06.50, 06.50, QUANTITY = 'MASS FLOW', ID = 'MF_C9' /

&DEVC XB = 24.05, 25.95, 05.00, 06.90, 06.50, 06.50, QUANTITY = 'MASS FLOW', ID = 'MF_R1' /
&DEVC XB = 24.05, 25.95, 11.00, 12.90, 06.50, 06.50, QUANTITY = 'MASS FLOW', ID = 'MF_R2' /
&DEVC XB = 24.05, 25.95, 17.00, 18.90, 06.50, 06.50, QUANTITY = 'MASS FLOW', ID = 'MF_R3' /
&DEVC XB = 24.05, 25.95, 23.00, 24.90, 06.50, 06.50, QUANTITY = 'MASS FLOW', ID = 'MF_R4' /
&DEVC XB = 24.05, 25.95, 29.00, 30.90, 06.50, 06.50, QUANTITY = 'MASS FLOW', ID = 'MF_R5' /
&DEVC XB = 24.05, 25.95, 35.00, 36.90, 06.50, 06.50, QUANTITY = 'MASS FLOW', ID = 'MF_R6' /
&DEVC XB = 24.05, 25.95, 41.00, 42.90, 06.50, 06.50, QUANTITY = 'MASS FLOW', ID = 'MF_R7' /
&DEVC XB = 24.05, 25.95, 47.00, 48.90, 06.50, 06.50, QUANTITY = 'MASS FLOW', ID = 'MF_R8' /
&DEVC XB = 24.05, 25.95, 53.00, 54.90, 06.50, 06.50, QUANTITY = 'MASS FLOW', ID = 'MF_R9' /

/----------------------------------------------------------------------------------------------------------------------------
/ Adding horizontal slice files

&SLCF PBZ = 01.50, QUANTITY = 'TEMPERATURE', VECTOR = .TRUE. /
&SLCF PBZ = 05.50, QUANTITY = 'TEMPERATURE', VECTOR = .TRUE. /
&SLCF PBZ = 01.50, QUANTITY = 'VISIBILITY', VECTOR = .TRUE. /

/----------------------------------------------------------------------------------------------------------------------------
/ Adding vertical slice files

&SLCF PBX = 10.00, QUANTITY = 'TEMPERATURE', VECTOR = .TRUE. /
&SLCF PBX = 20.00, QUANTITY = 'TEMPERATURE', VECTOR = .TRUE. /
&SLCF PBY = 20.00, QUANTITY = 'TEMPERATURE', VECTOR = .TRUE. /
&SLCF PBY = 40.00, QUANTITY = 'TEMPERATURE', VECTOR = .TRUE. /
&SLCF PBX = 10.00, QUANTITY = 'VISIBILITY', VECTOR = .TRUE. /
&SLCF PBX = 20.00, QUANTITY = 'VISIBILITY', VECTOR = .TRUE. /
```

```
&SLCF PBY = 20.00, QUANTITY = 'VISIBILITY', VECTOR = .TRUE. /
&SLCF PBY = 40.00, QUANTITY = 'VISIBILITY', VECTOR = .TRUE. /

/----------------------------------------------------------------------------------------------------------------------------
/ Adding plot3D static data dumps

&DUMP PLOT3D_QUANTITY(1:5) = 'TEMPERATURE', 'U-VELOCITY', 'V-VELOCITY', 'W-VELOCITY',
        'VISIBILITY', COLUMN_DUMP_LIMIT = .FALSE./

/----------------------------------------------------------------------------------------------------------------------------
/ End of file

&TAIL /
```

APPENDIX C1 – RADIATIVE HEAT FLUXES & TEMPERATURES IN SMALL WAREHOUSE – 15 % ROOF VENTING & RAPID FIRE

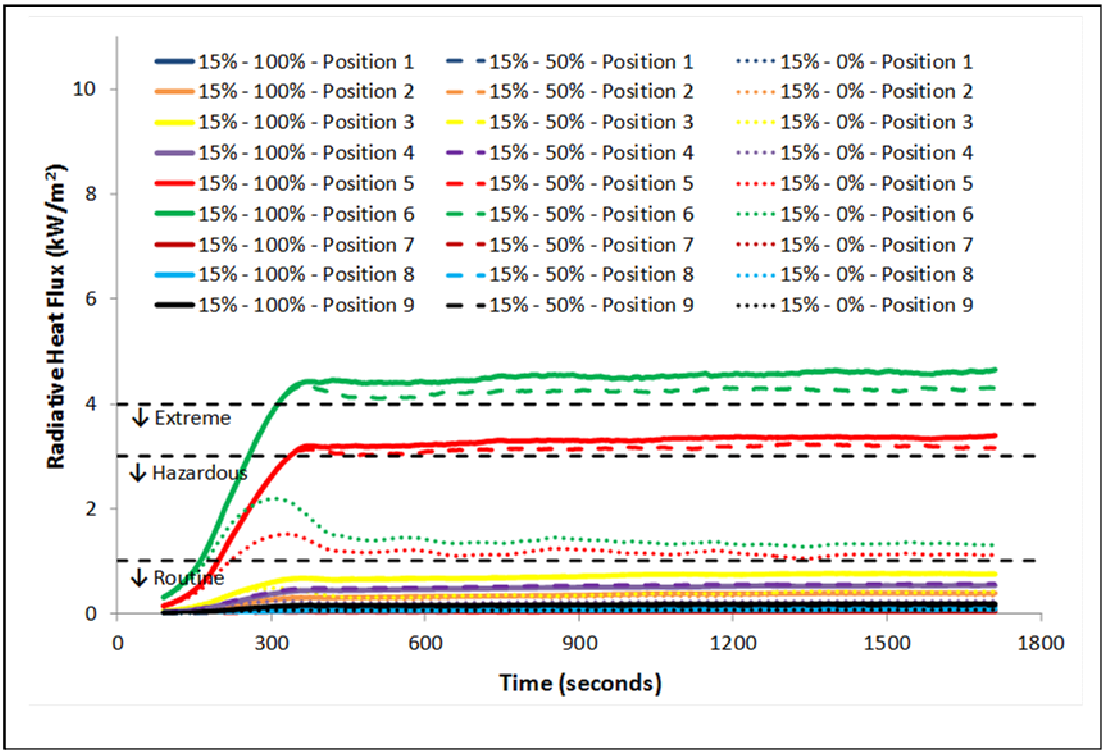

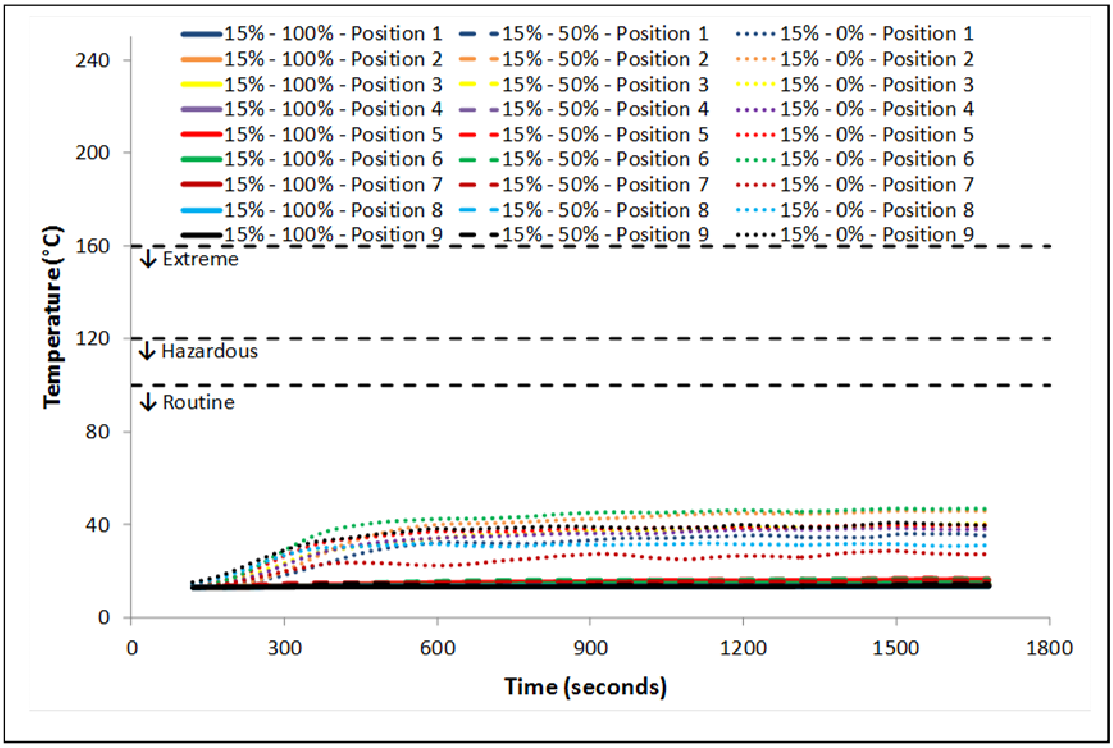

APPENDIX C2 – RADIATIVE HEAT FLUXES & TEMPERATURES IN SMALL WAREHOUSE – 10 % ROOF VENTING & RAPID FIRE

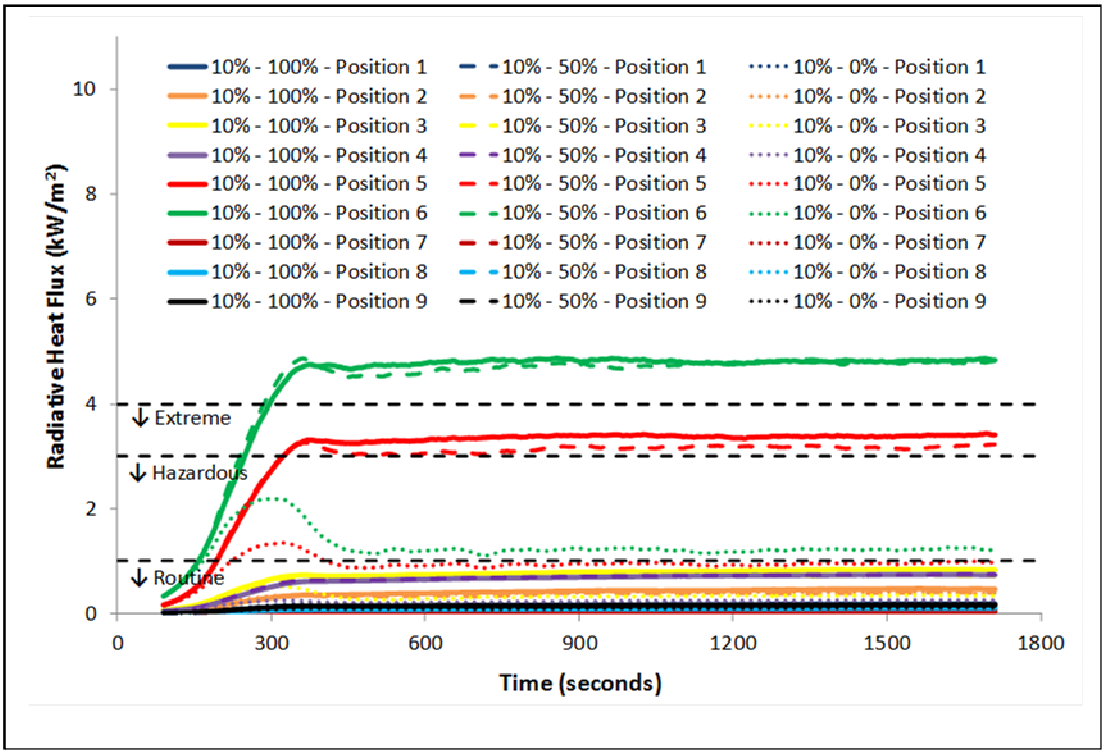

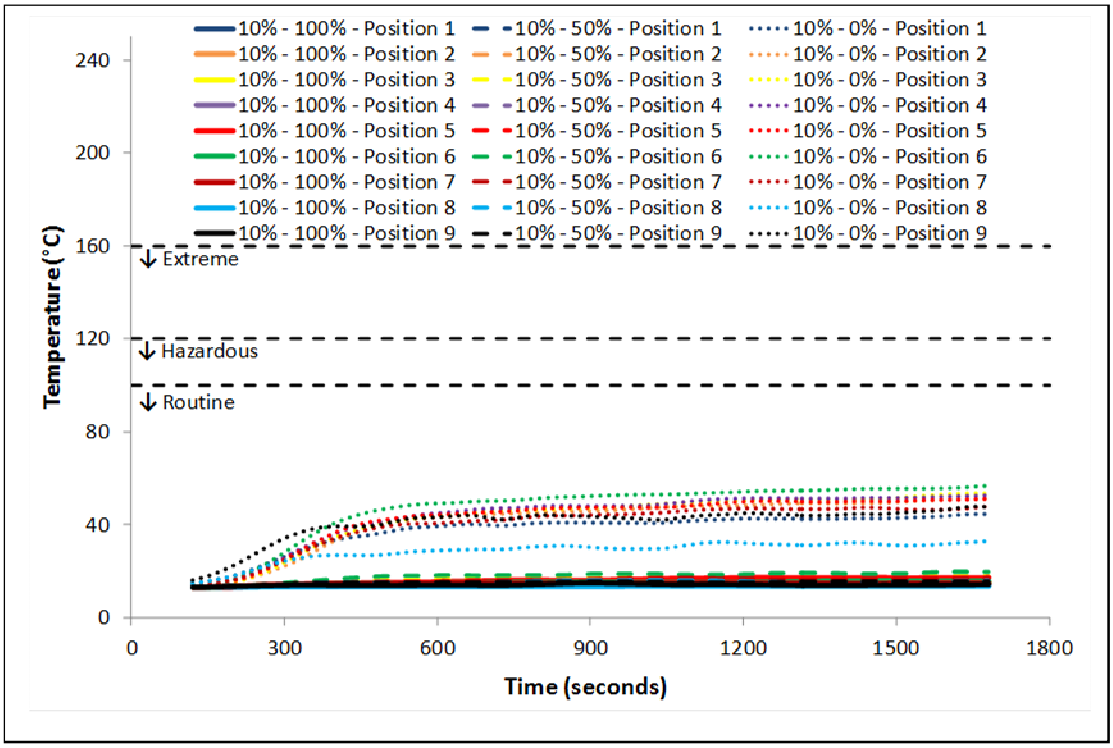

APPENDIX C3 – RADIATIVE HEAT FLUXES & TEMPERATURES IN SMALL WAREHOUSE – 5 % ROOF VENTING & RAPID FIRE

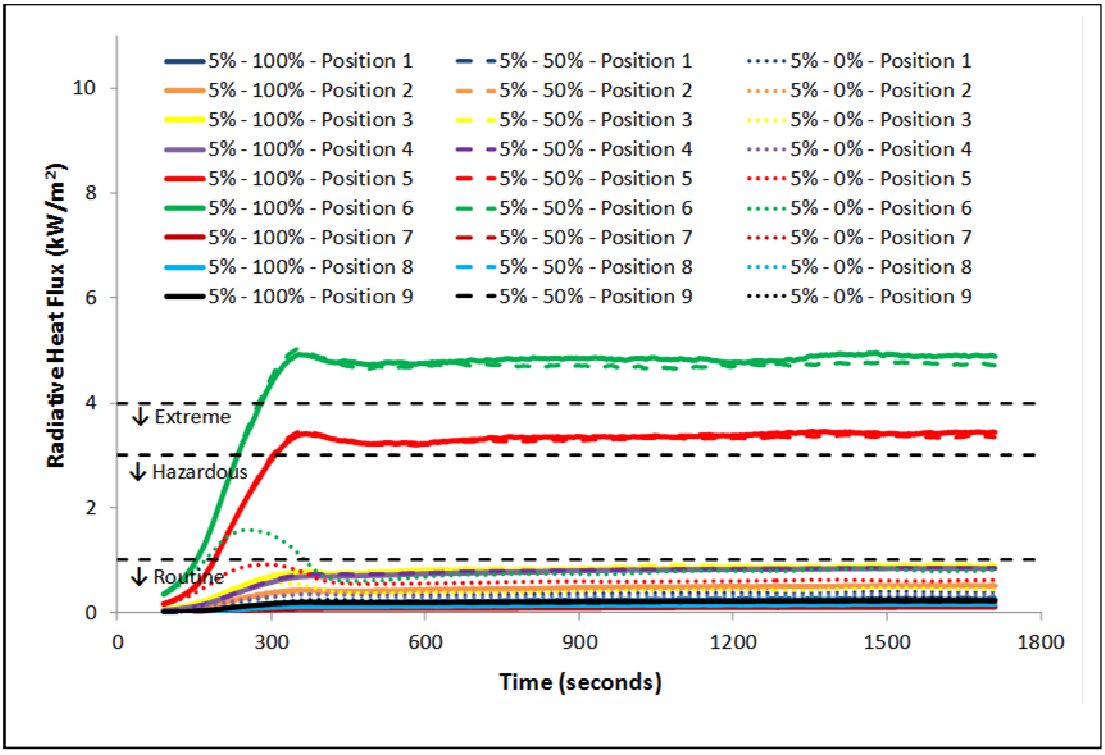

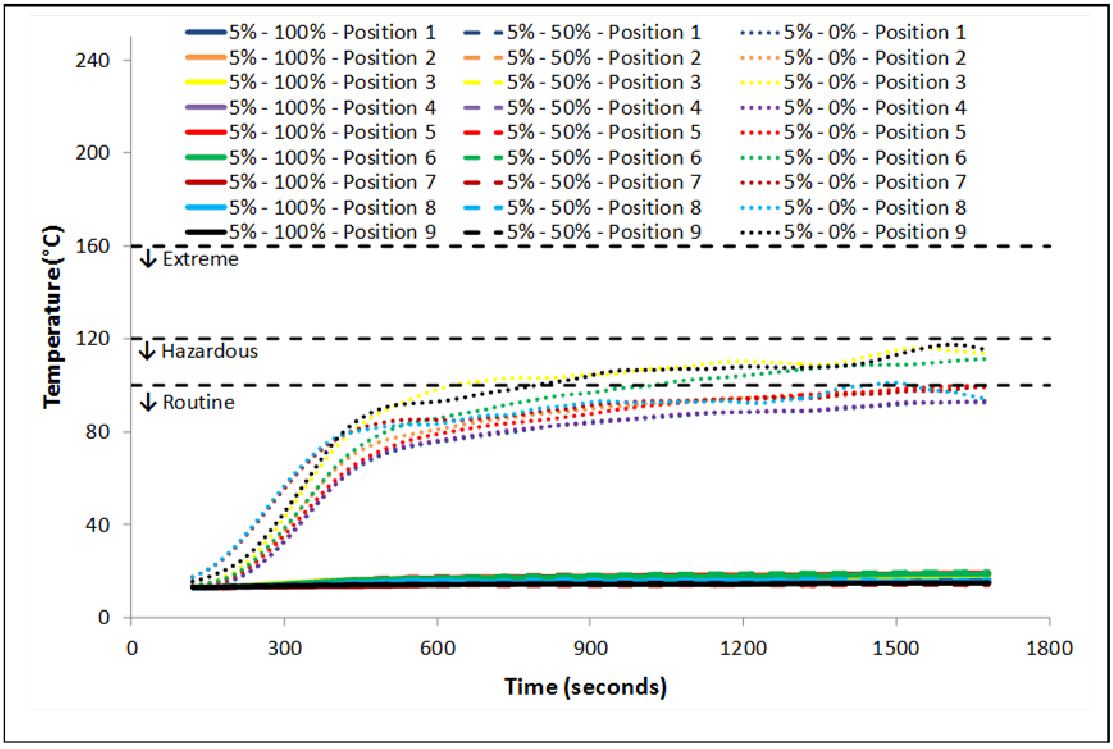

APPENDIX D1 – RADIATIVE HEAT FLUXES & TEMPERATURES IN SMALL WAREHOUSE – 15 % ROOF VENTING & EXTREME FIRE

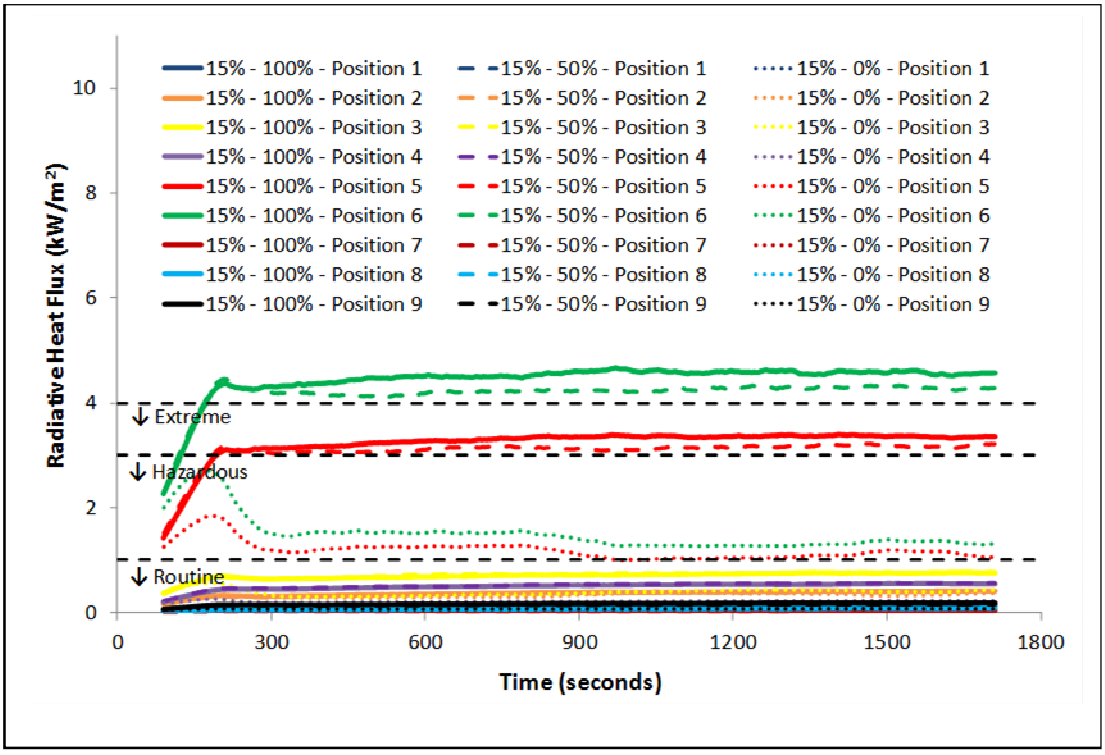

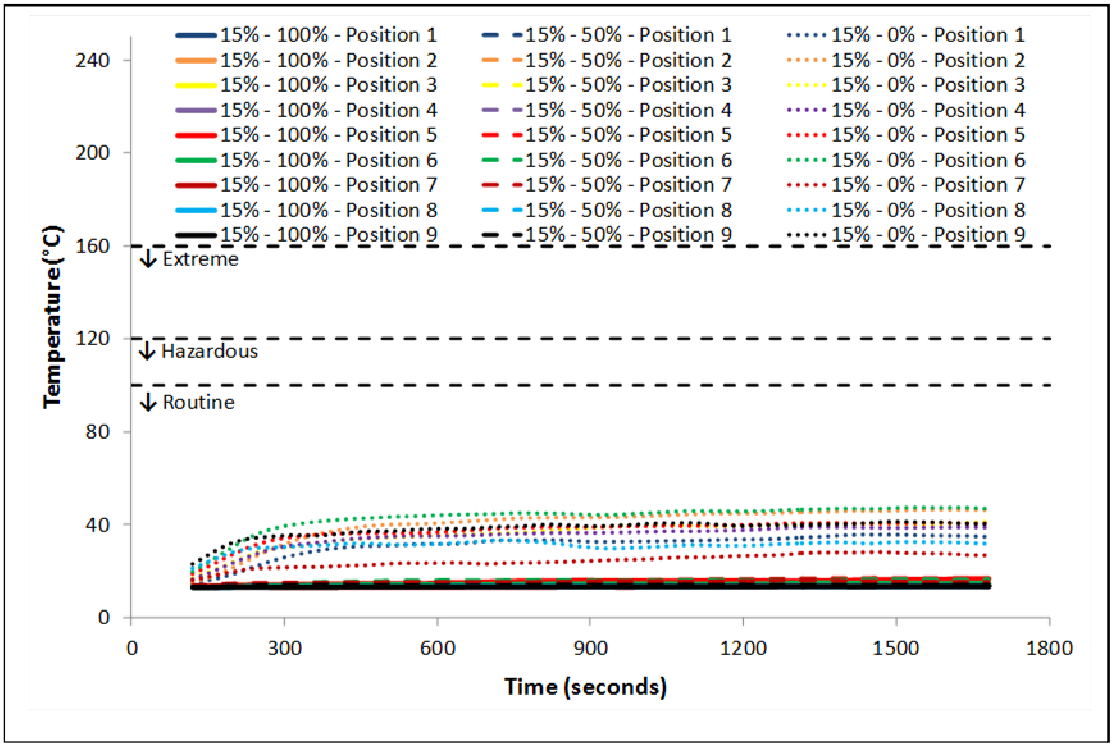

APPENDIX D2 – RADIATIVE HEAT FLUXES & TEMPERATURES IN SMALL WAREHOUSE – 10 % ROOF VENTING & EXTREME FIRE

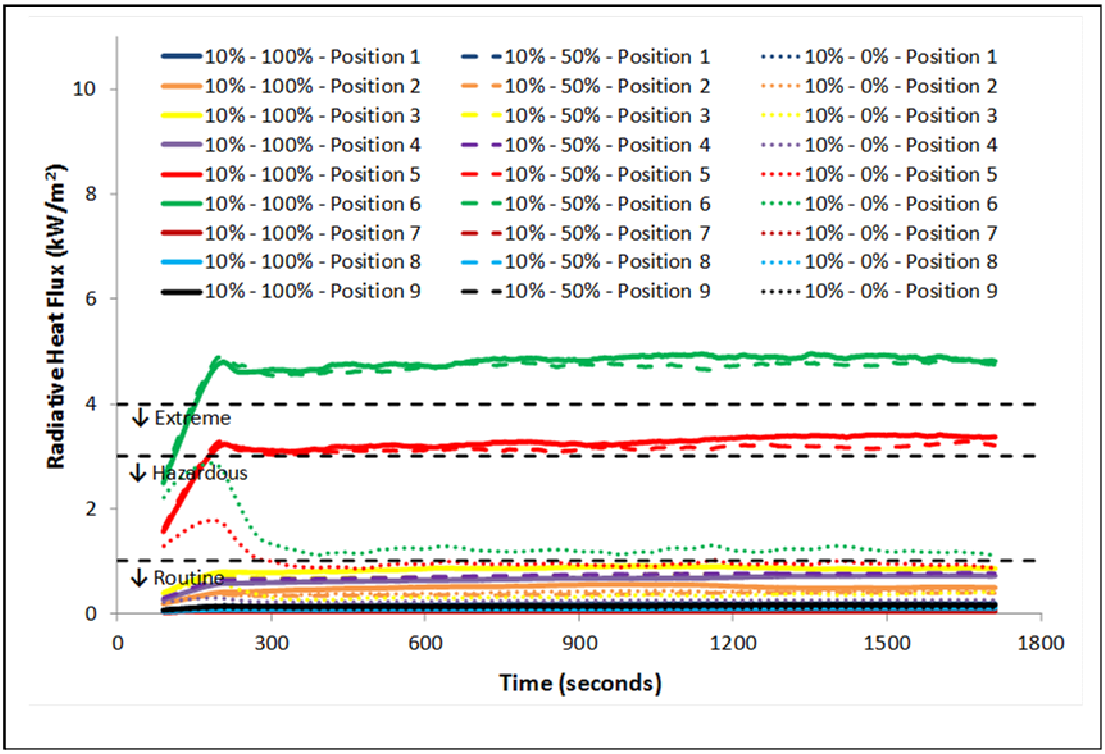

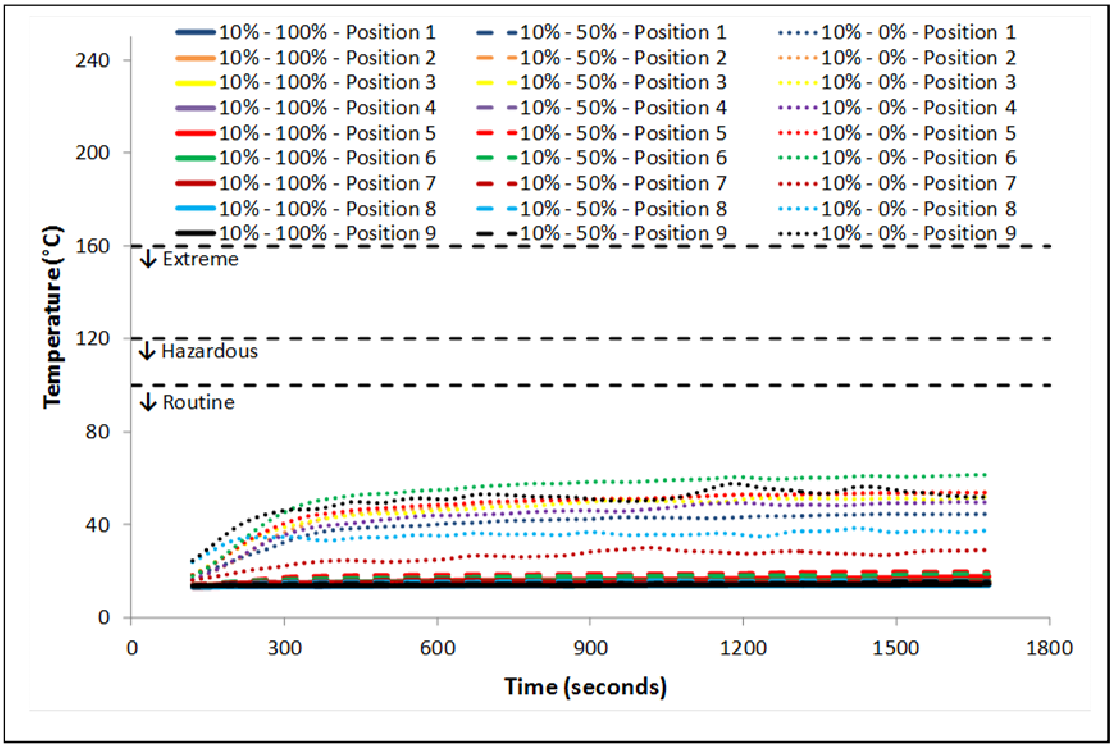

APPENDIX D3 – RADIATIVE HEAT FLUXES & TEMPERATURES IN SMALL WAREHOUSE – 5 % ROOF VENTING & EXTREME FIRE

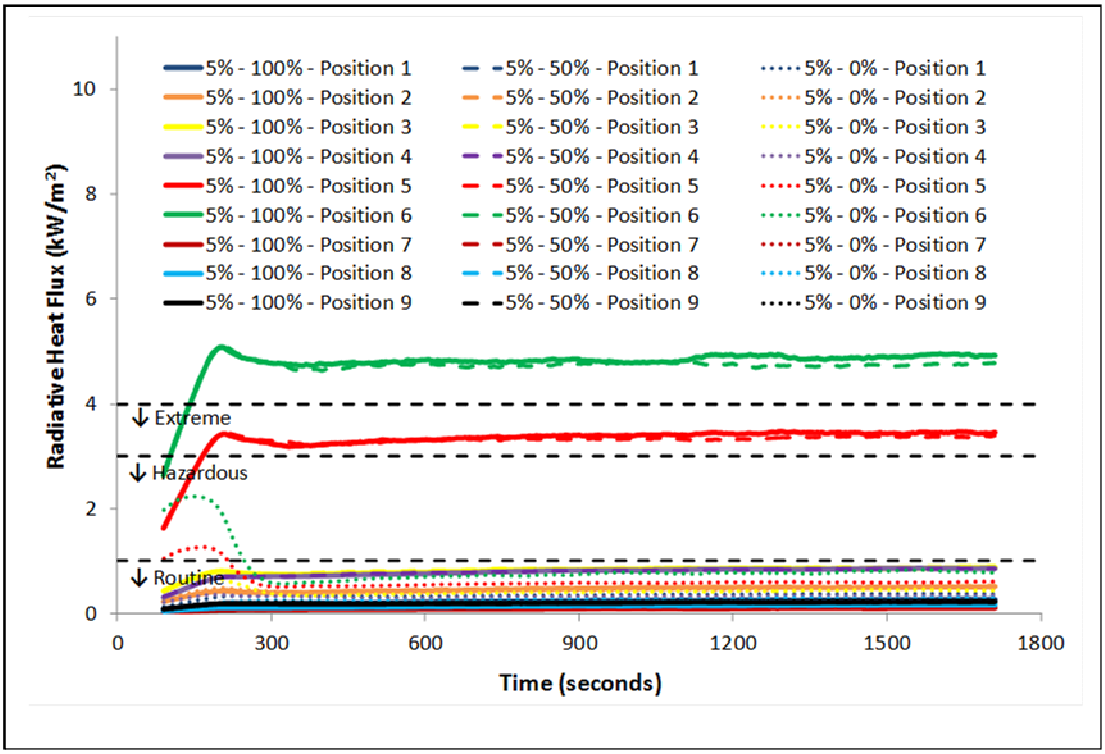

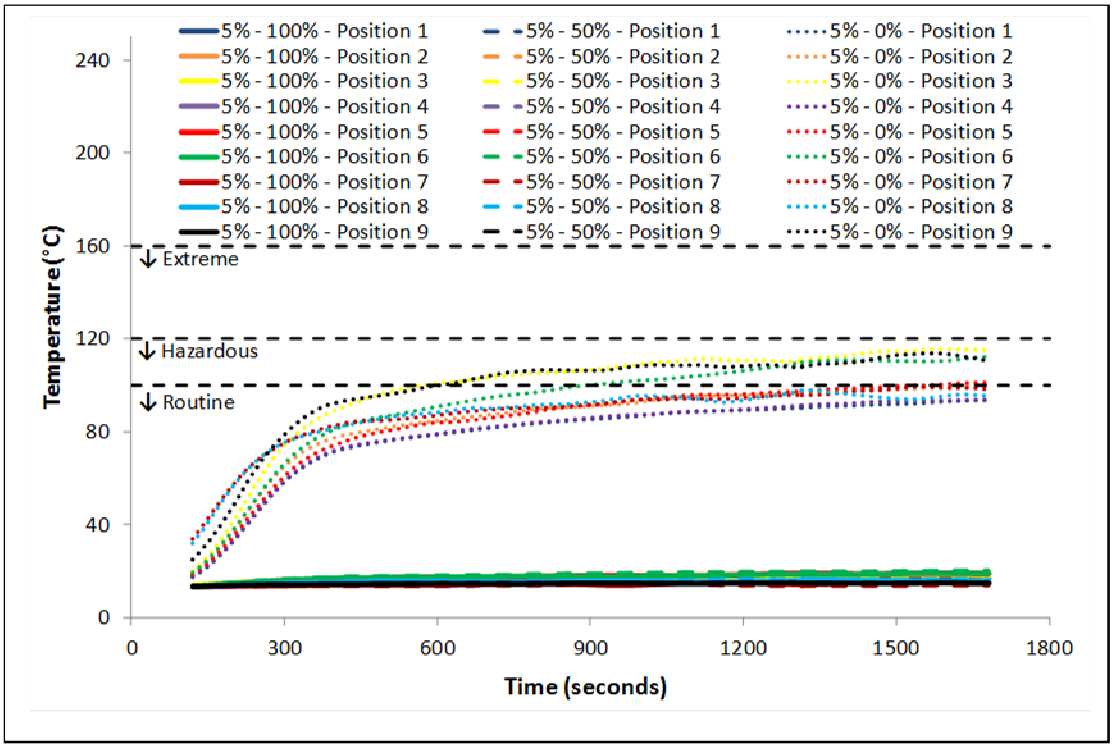

APPENDIX E1 – RADIATIVE HEAT FLUXES & TEMPERATURES IN LARGE WAREHOUSE – 15 % ROOF VENTING & RAPID FIRE

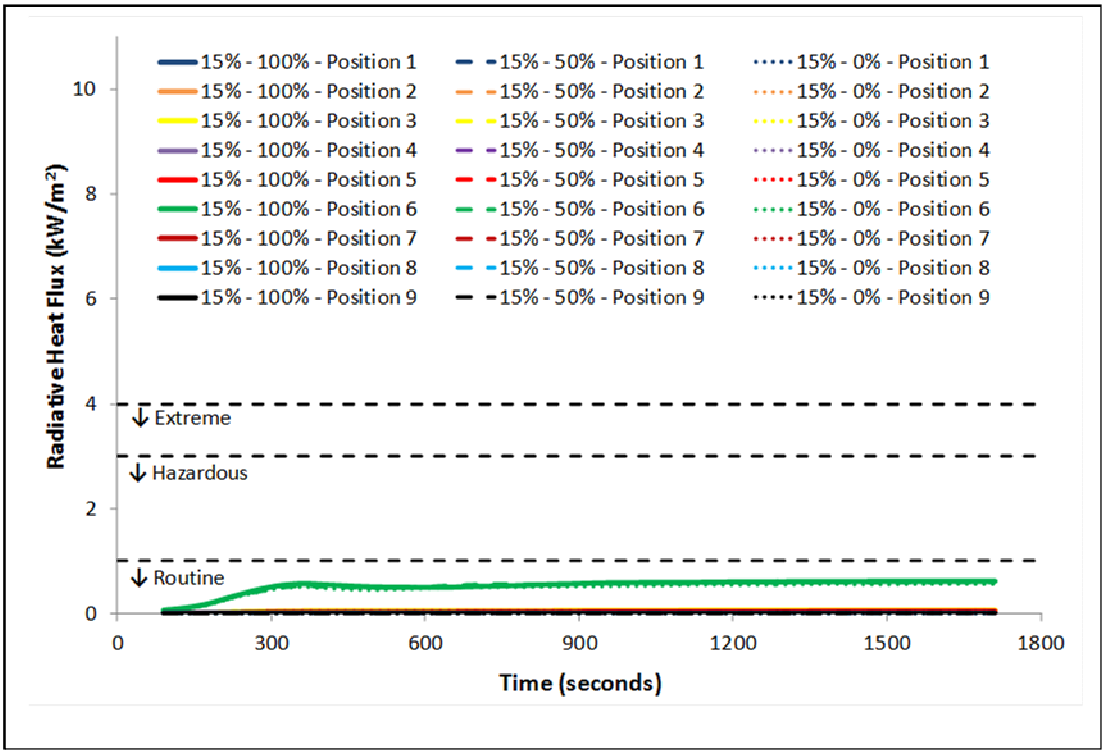

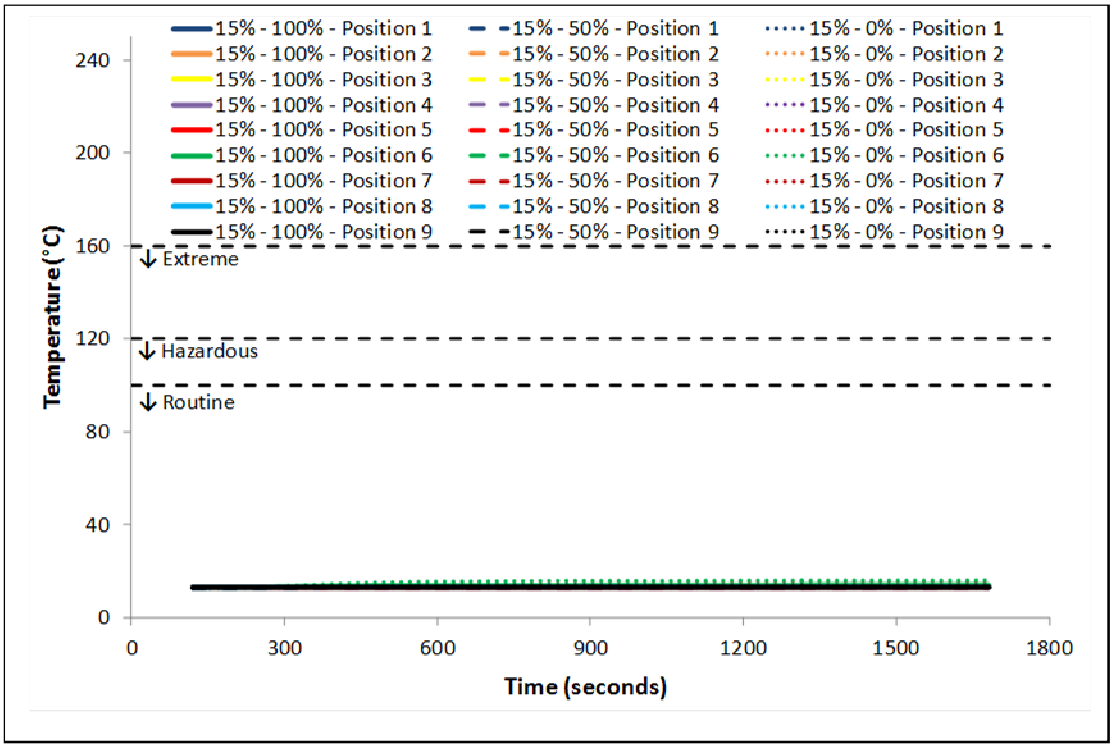

APPENDIX E2 – RADIATIVE HEAT FLUXES & TEMPERATURES IN LARGE WAREHOUSE – 10 % ROOF VENTING & RAPID FIRE

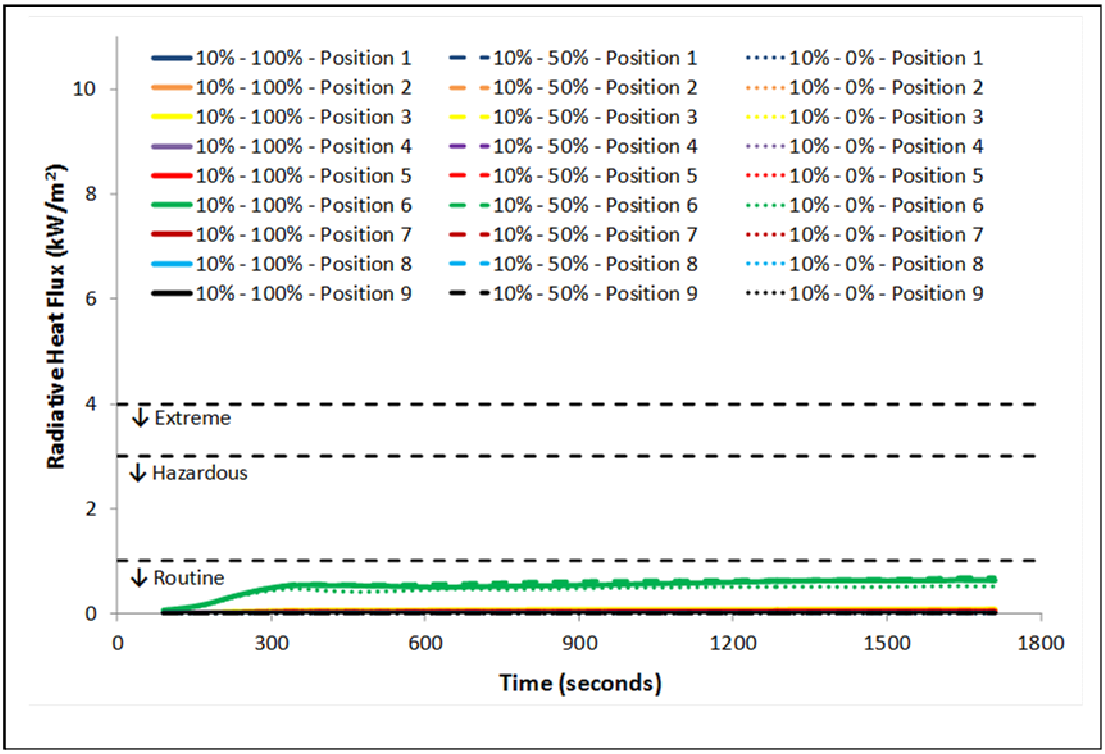

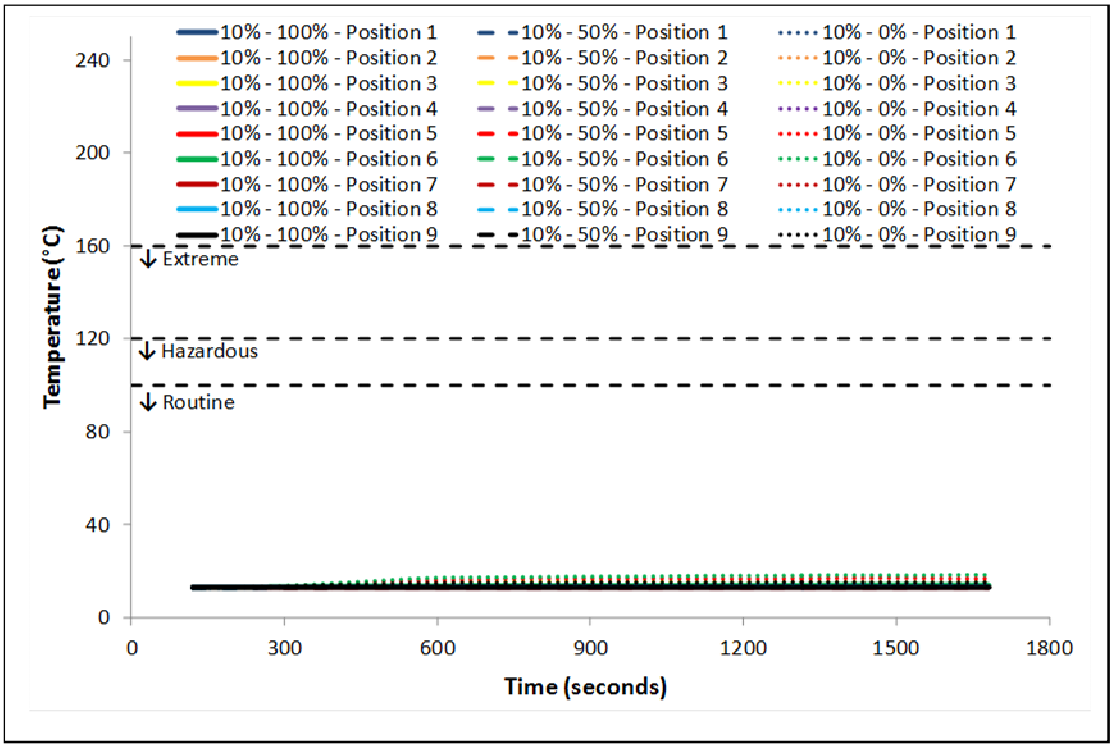

APPENDIX E3 – RADIATIVE HEAT FLUXES & TEMPERATURES IN LARGE WAREHOUSE – 5 % ROOF VENTING & RAPID FIRE

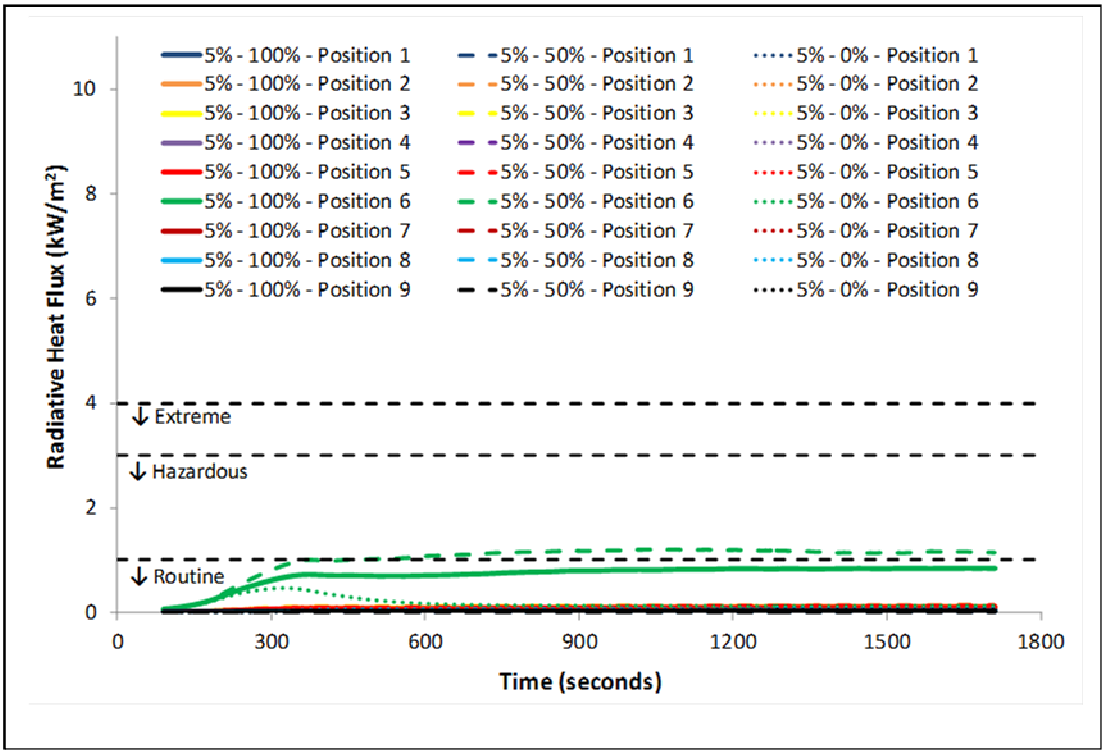

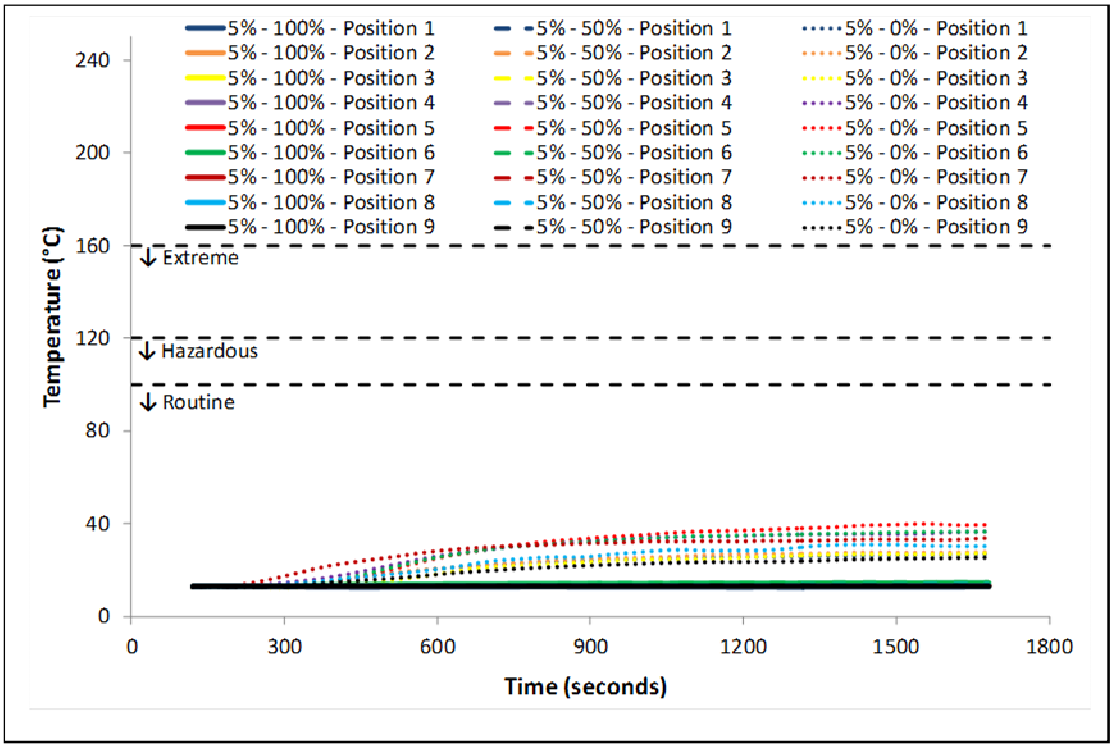

APPENDIX F1 – RADIATIVE HEAT FLUXES & TEMPERATURES IN LARGE WAREHOUSE – 15 % ROOF VENTING & EXTREME FIRE

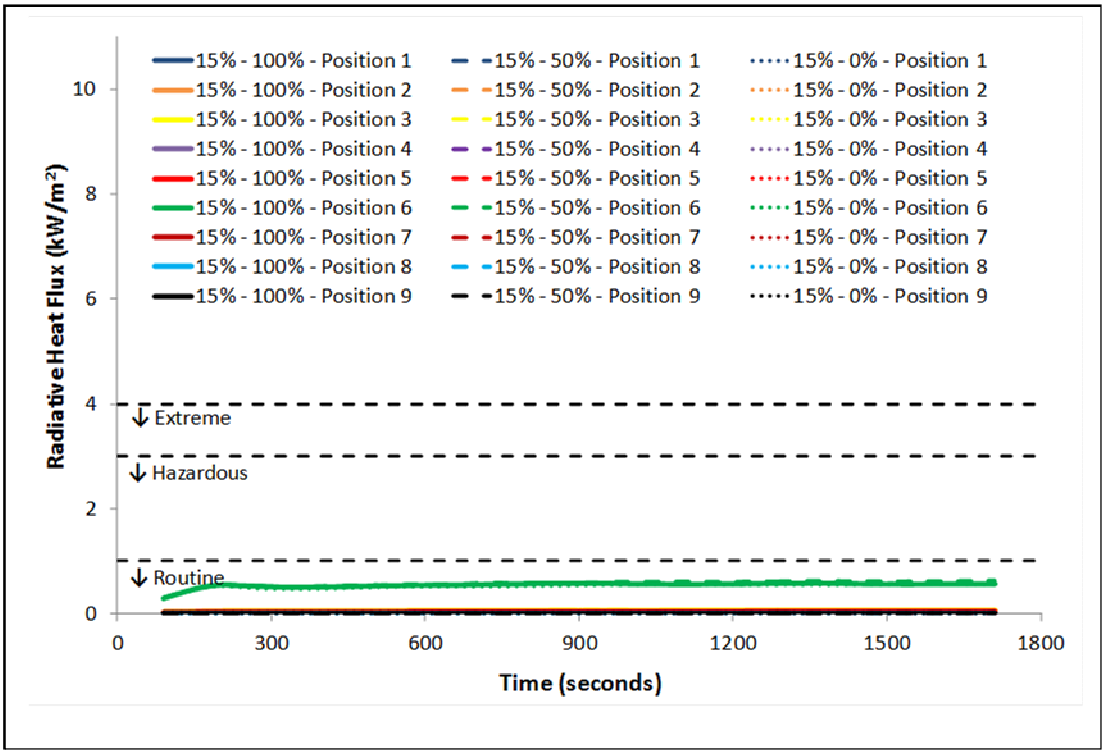

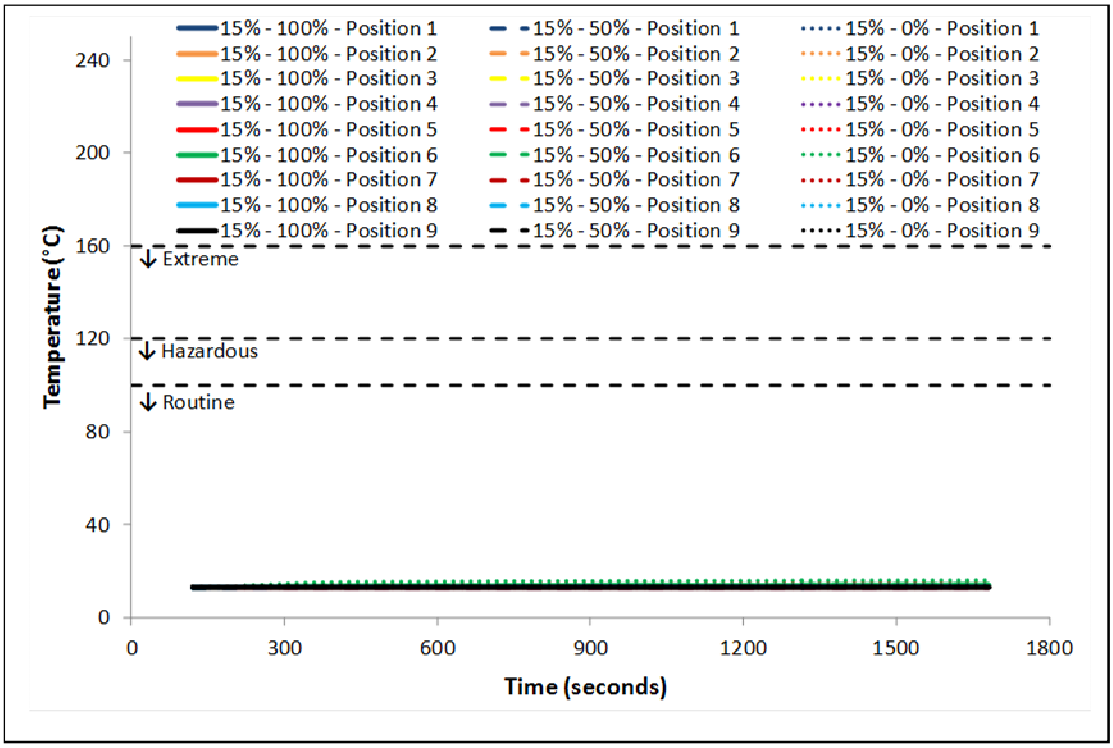

APPENDIX F2 – RADIATIVE HEAT FLUXES & TEMPERATURES IN LARGE WAREHOUSE – 10 % ROOF VENTING & EXTREME FIRE

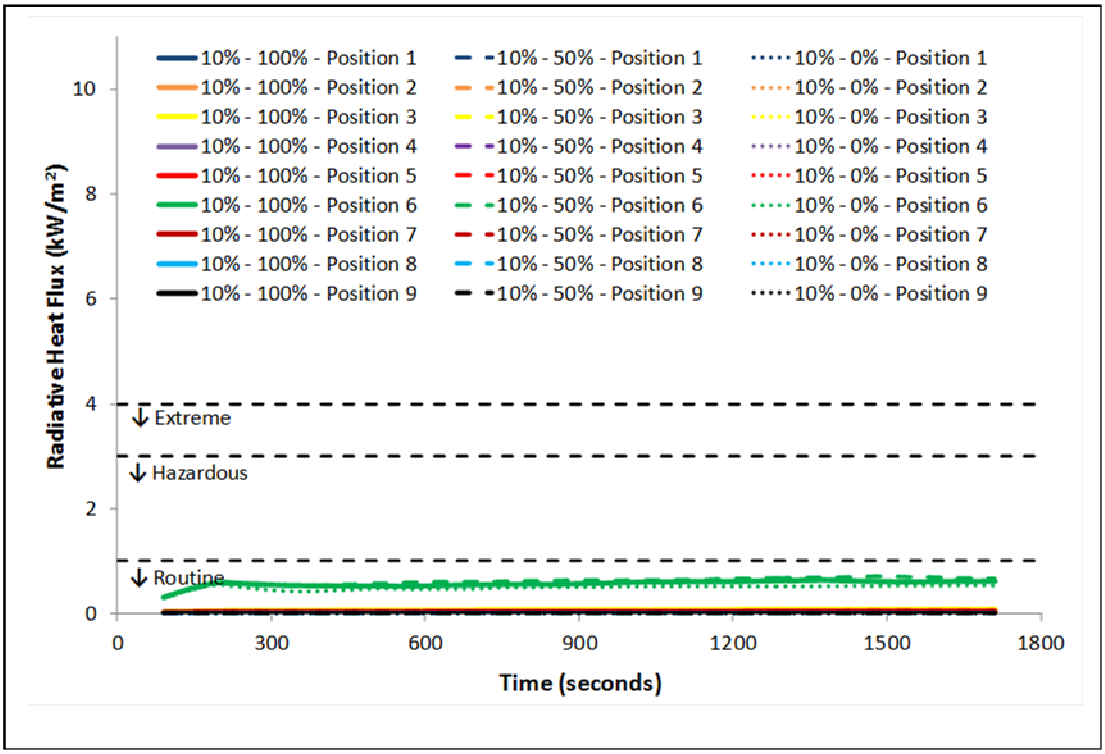

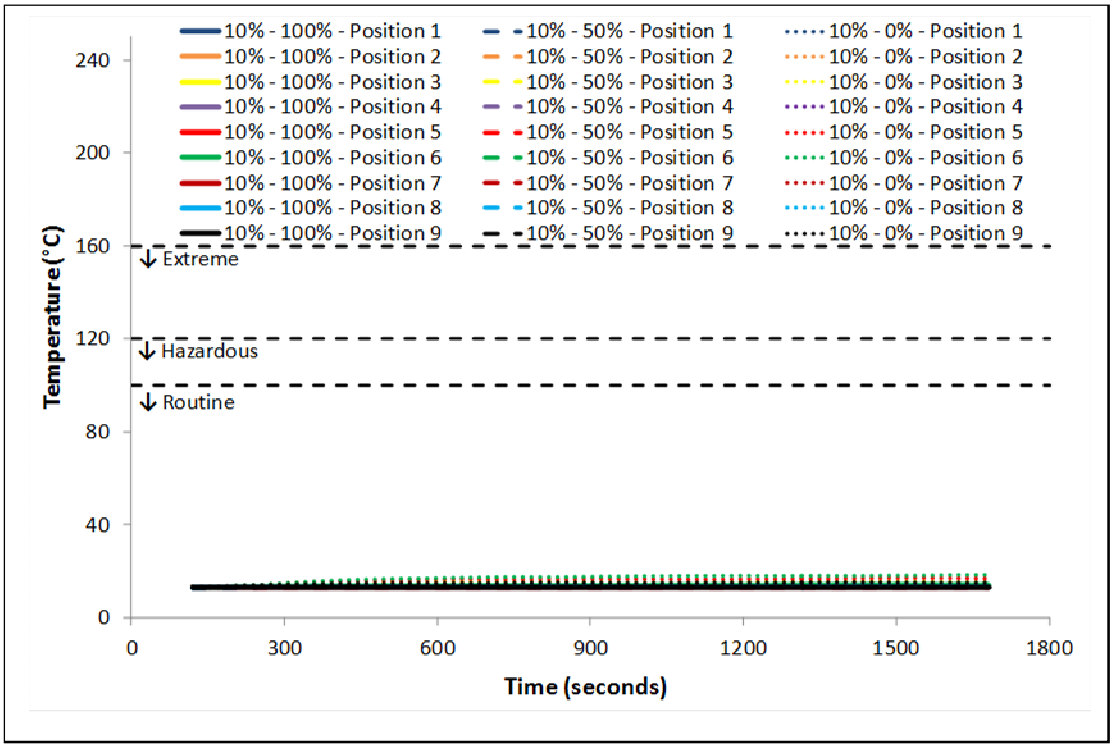

APPENDIX F3 – RADIATIVE HEAT FLUXES & TEMPERATURES IN LARGE WAREHOUSE – 5 % ROOF VENTING & EXTREME FIRE

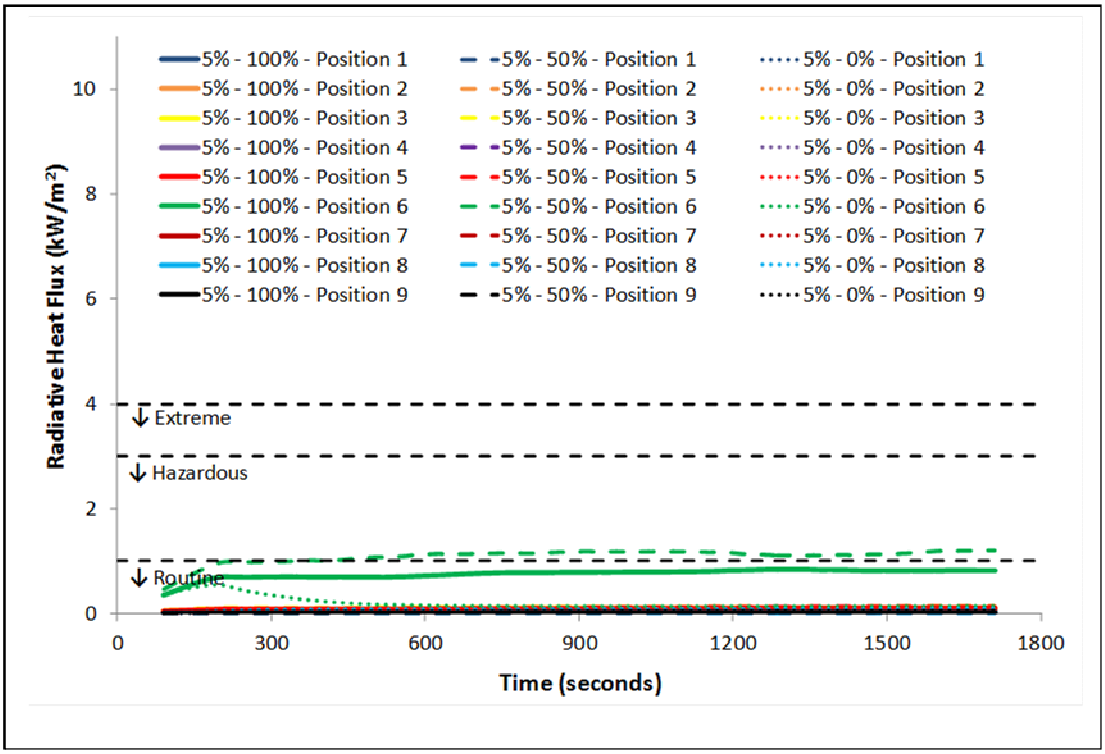

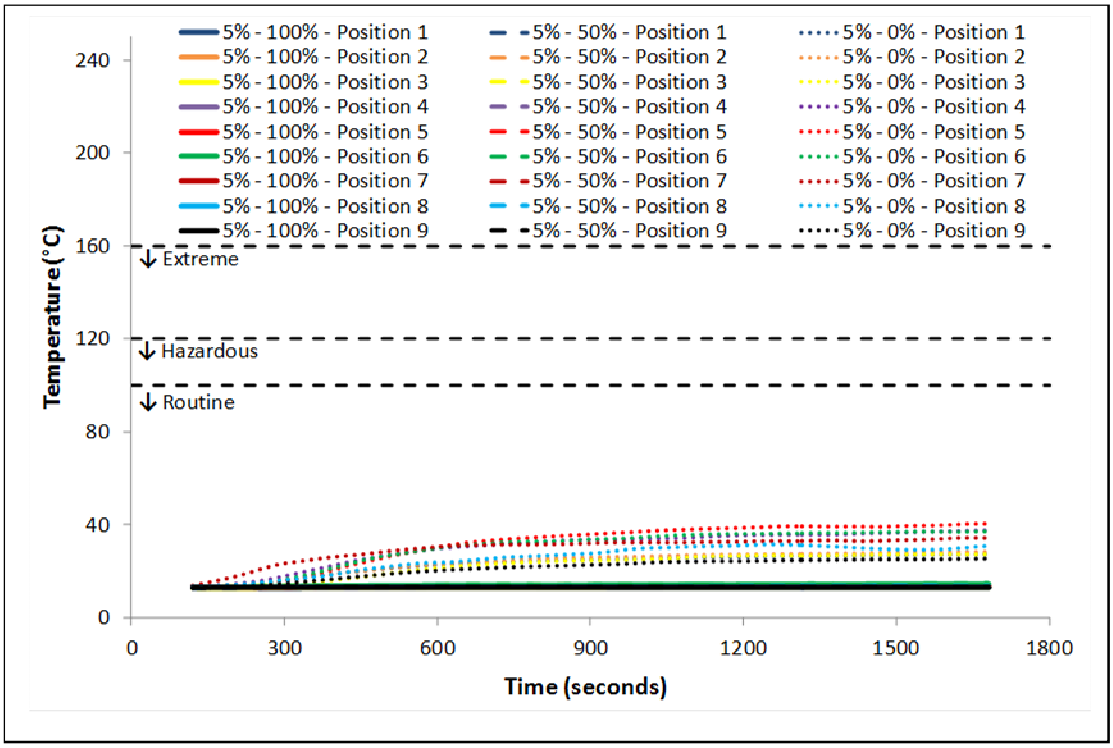

APPENDIX G1 – RADIATIVE HEAT FLUXES & TEMPERATURES IN SMALL WAREHOUSE – RAPID FIRE & SEQUENTIAL SQUARES

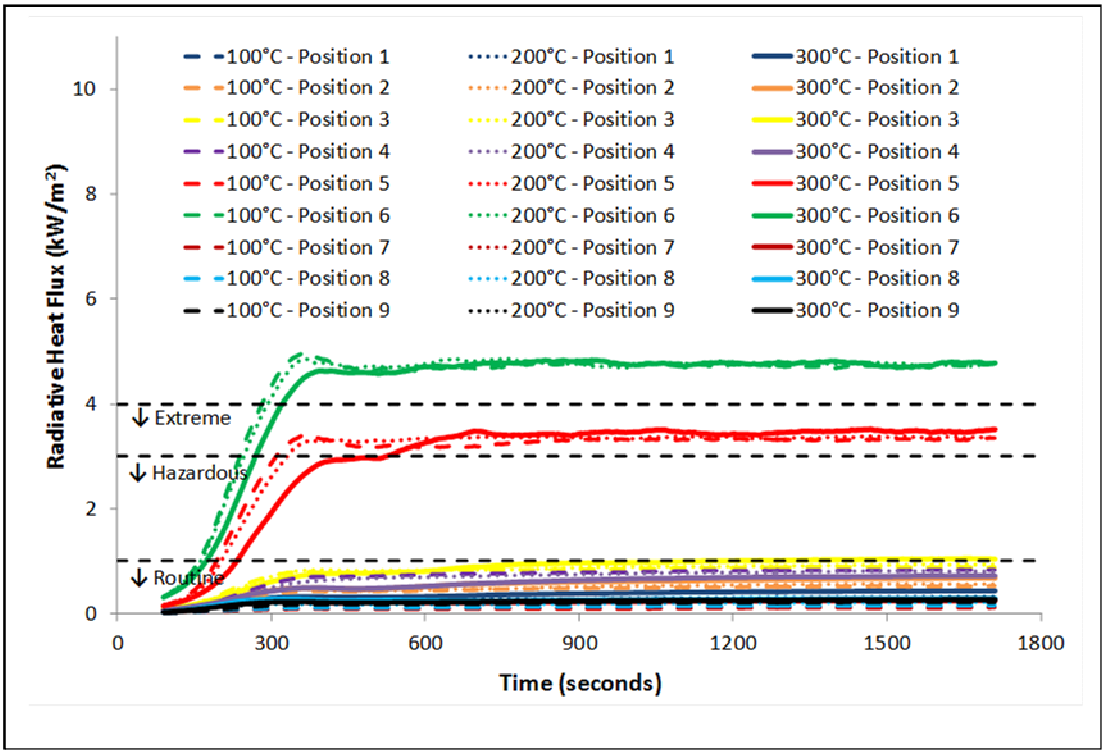

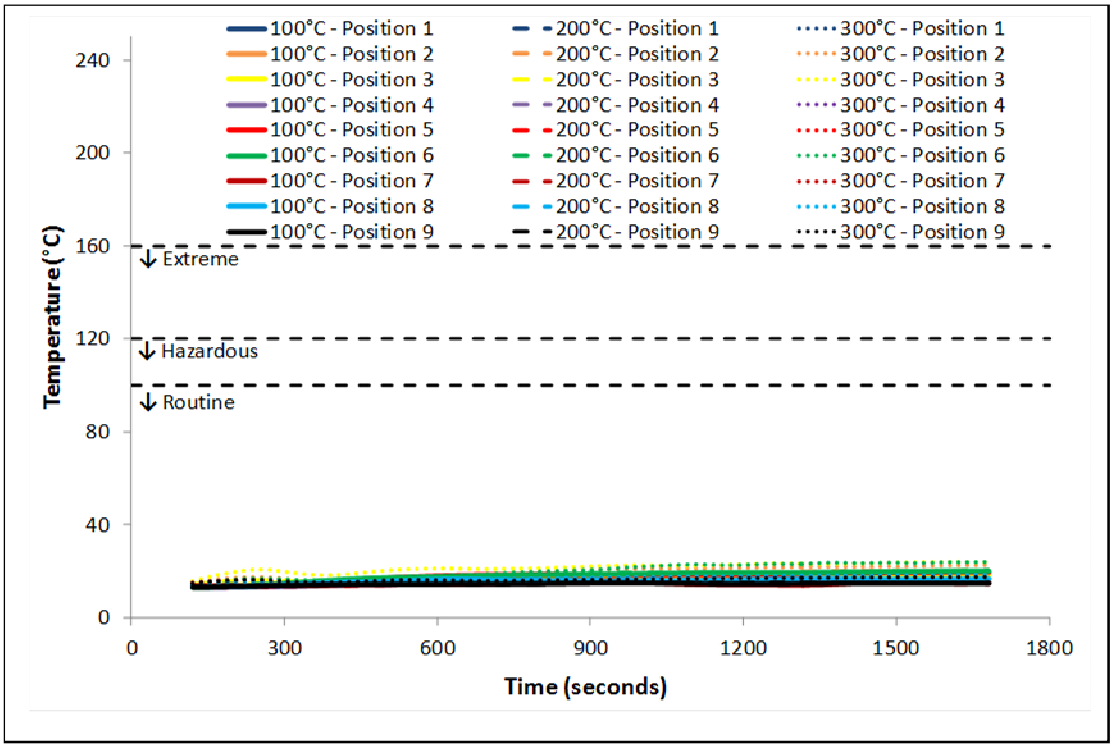

APPENDIX G2 – RADIATIVE HEAT FLUXES & TEMPERATURES IN SMALL WAREHOUSE – RAPID FIRE & SEQUENTIAL STRIPS

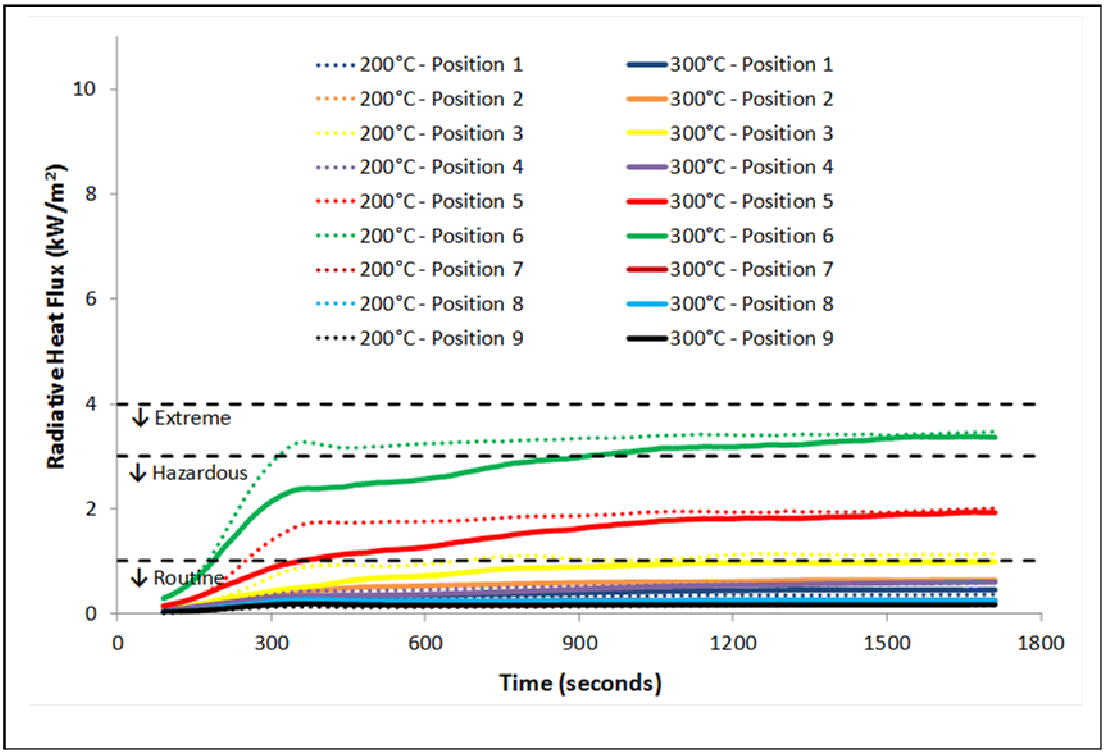

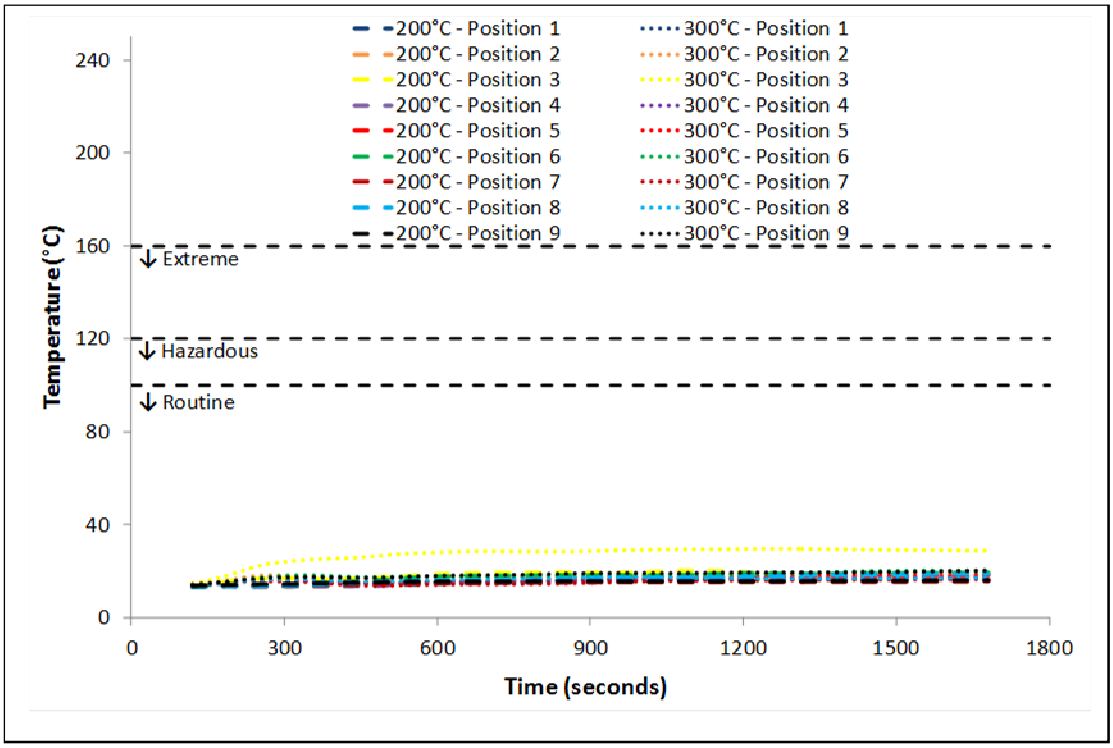

APPENDIX H1 – RADIATIVE HEAT FLUXES & TEMPERATURES IN SMALL WAREHOUSE – EXTREME FIRE & SIMULTANEOUS SQUARES

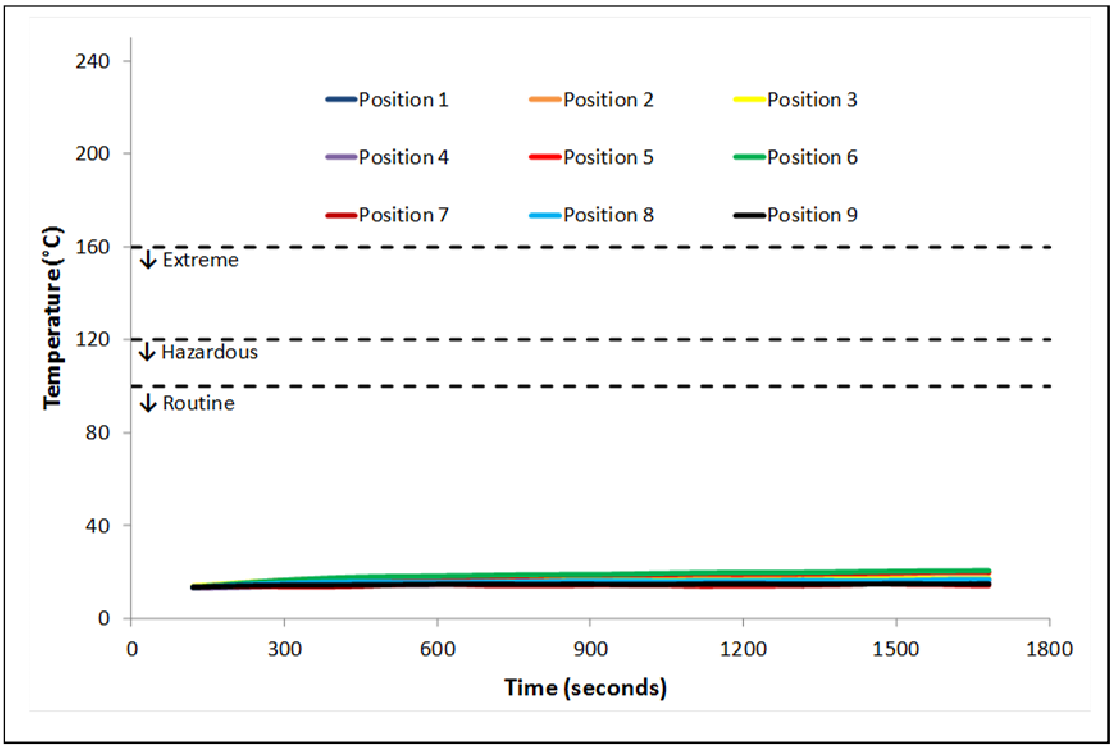

APPENDIX H2 – RADIATIVE HEAT FLUXES & TEMPERATURES IN SMALL WAREHOUSE – EXTREME FIRE & SEQUENTIAL SQUARES

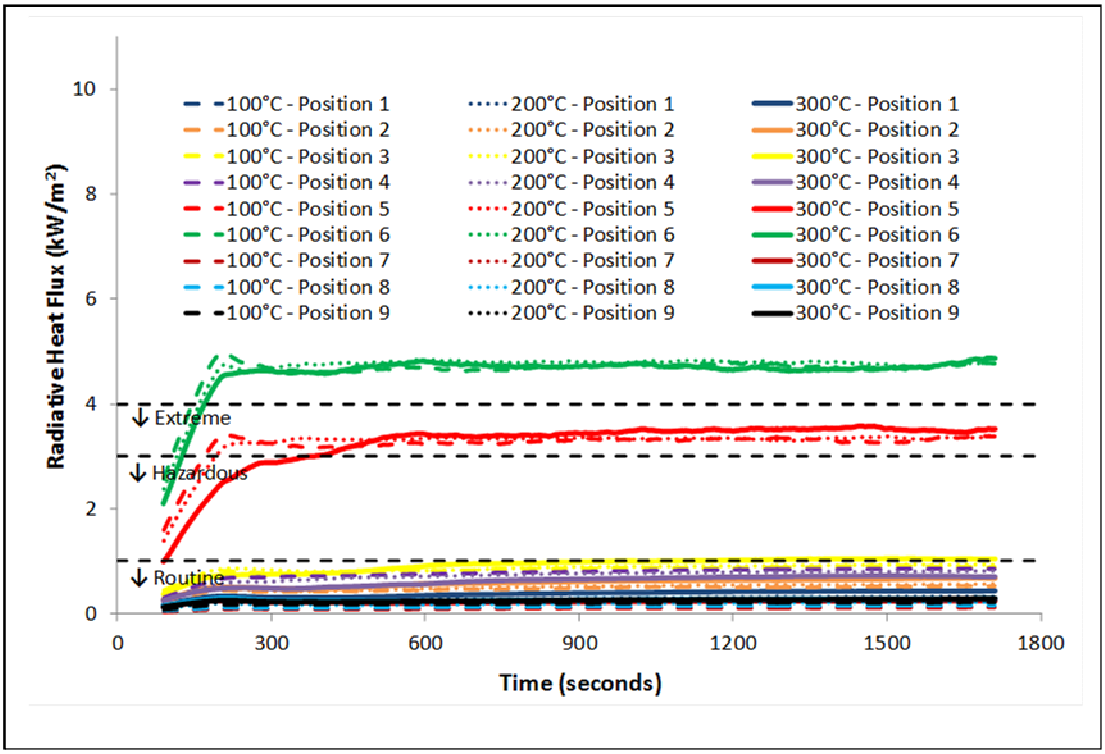

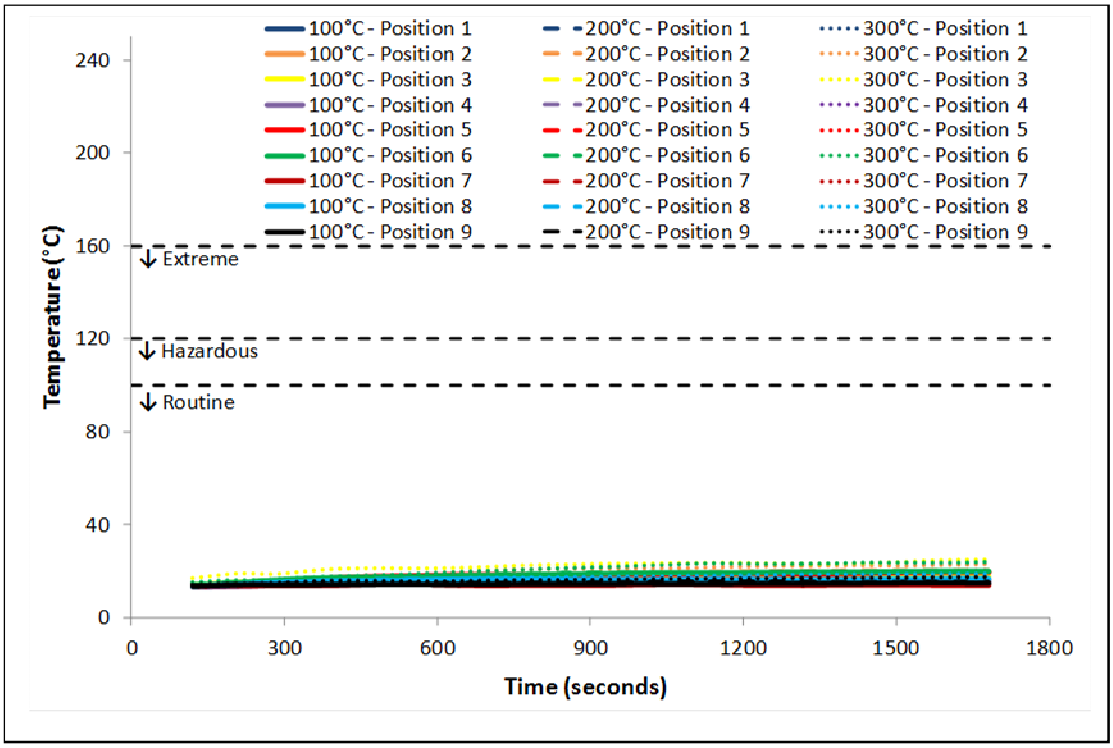

APPENDIX H3 – RADIATIVE HEAT FLUXES & TEMPERATURES IN SMALL WAREHOUSE – EXTREME FIRE & SEQUENTIAL STRIPS

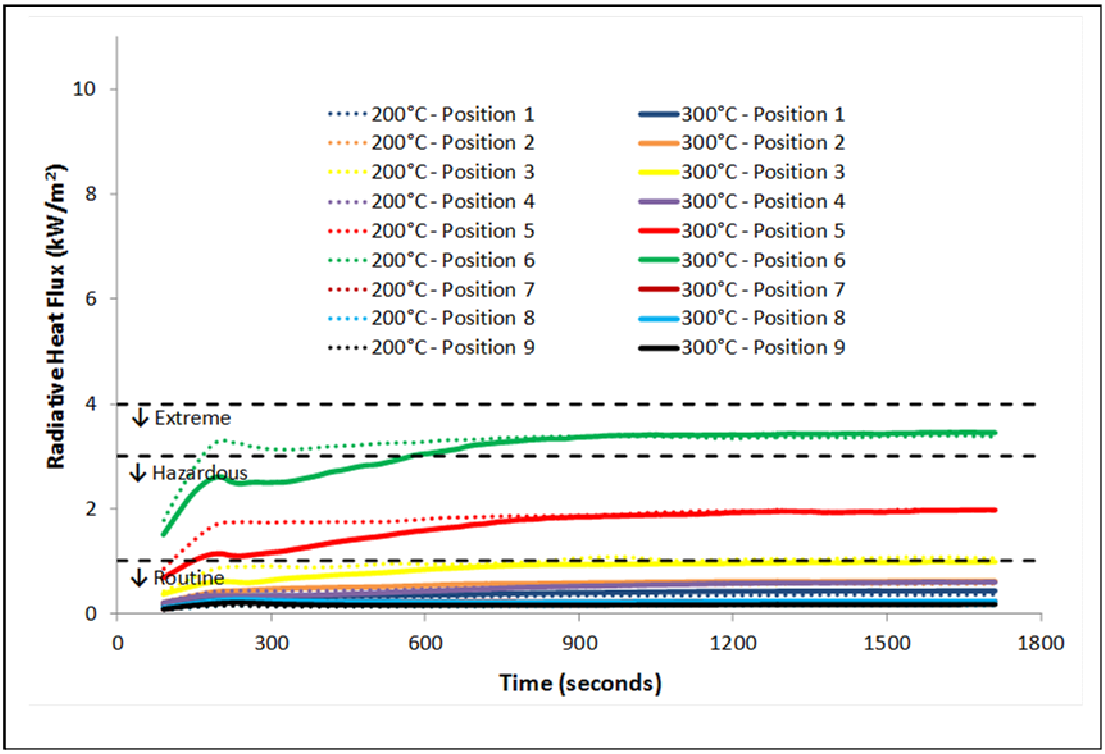

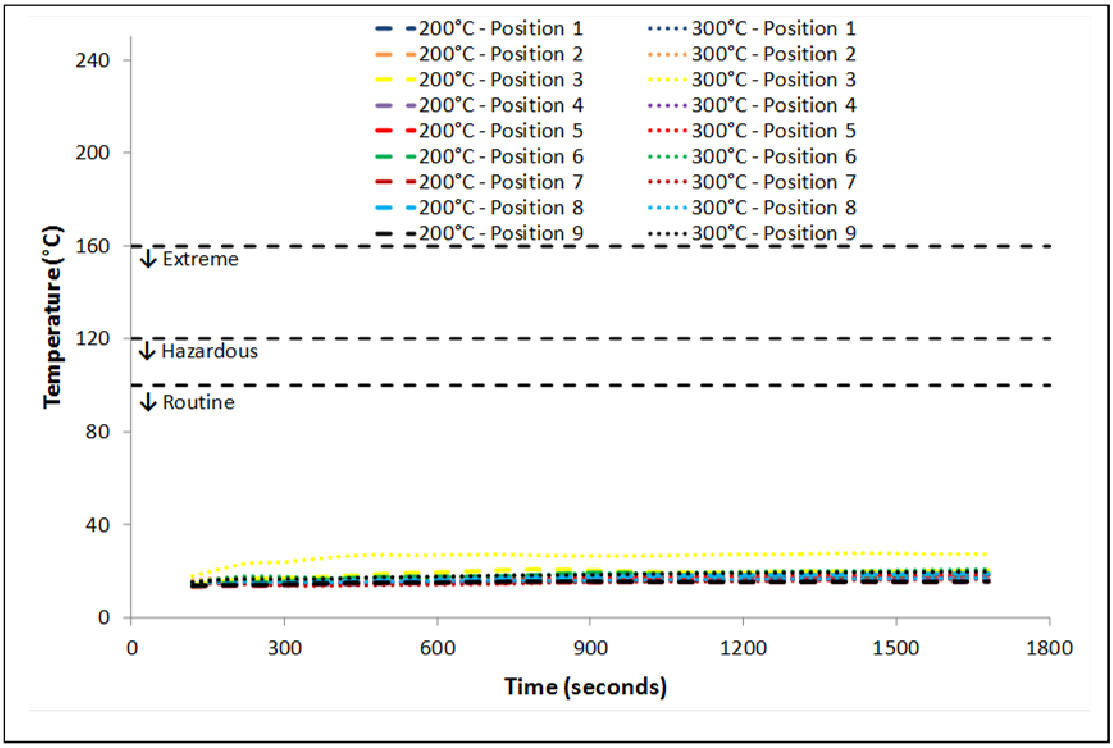

APPENDIX I1 – RADIATIVE HEAT FLUXES & TEMPERATURES IN LARGE WAREHOUSE – RAPID FIRE & SEQUENTIAL SQUARES

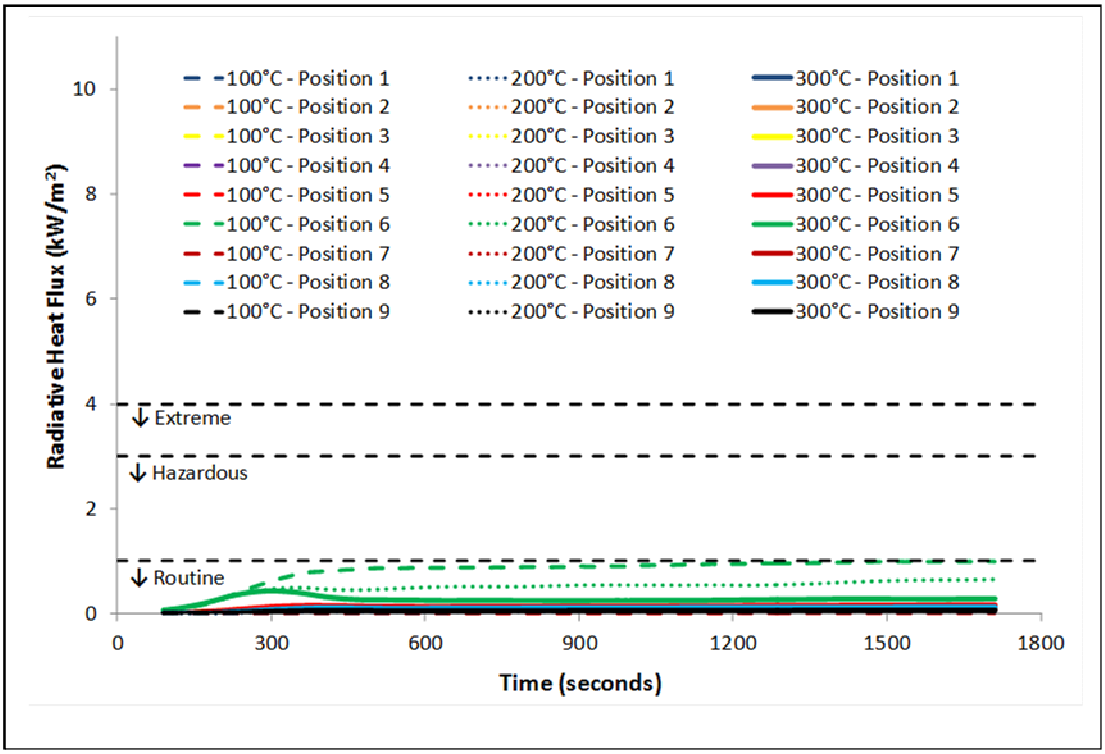

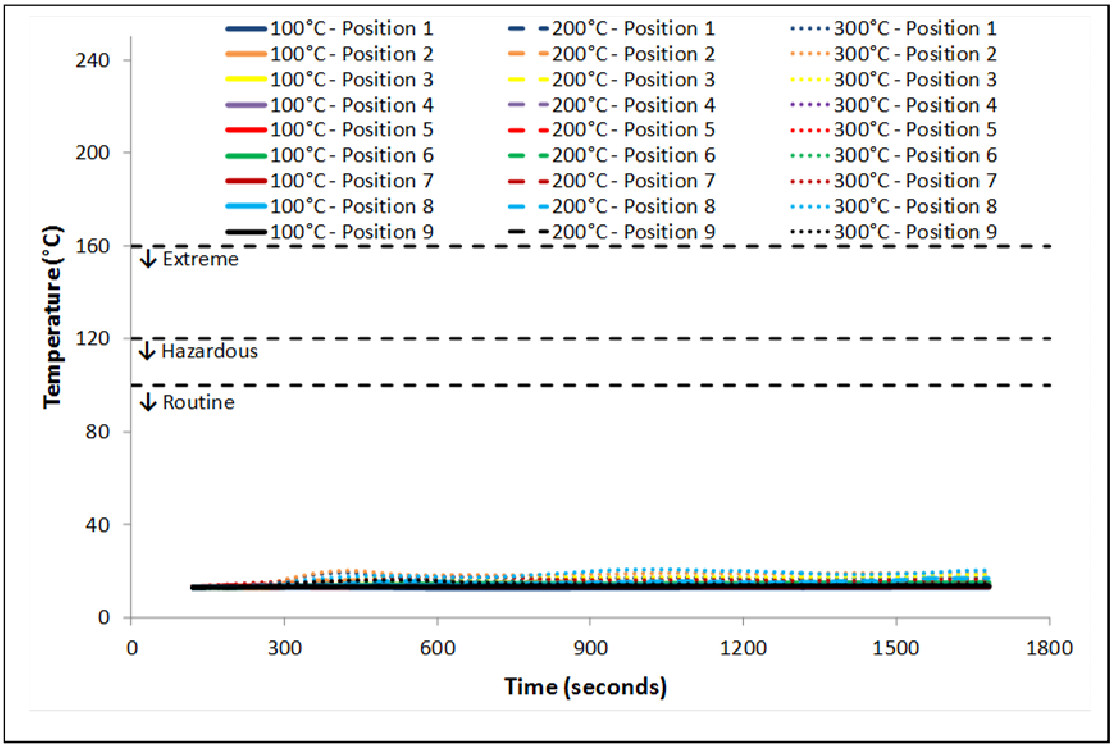

APPENDIX I2 – RADIATIVE HEAT FLUXES & TEMPERATURES IN LARGE WAREHOUSE – RAPID FIRE & SEQUENTIAL STRIPS

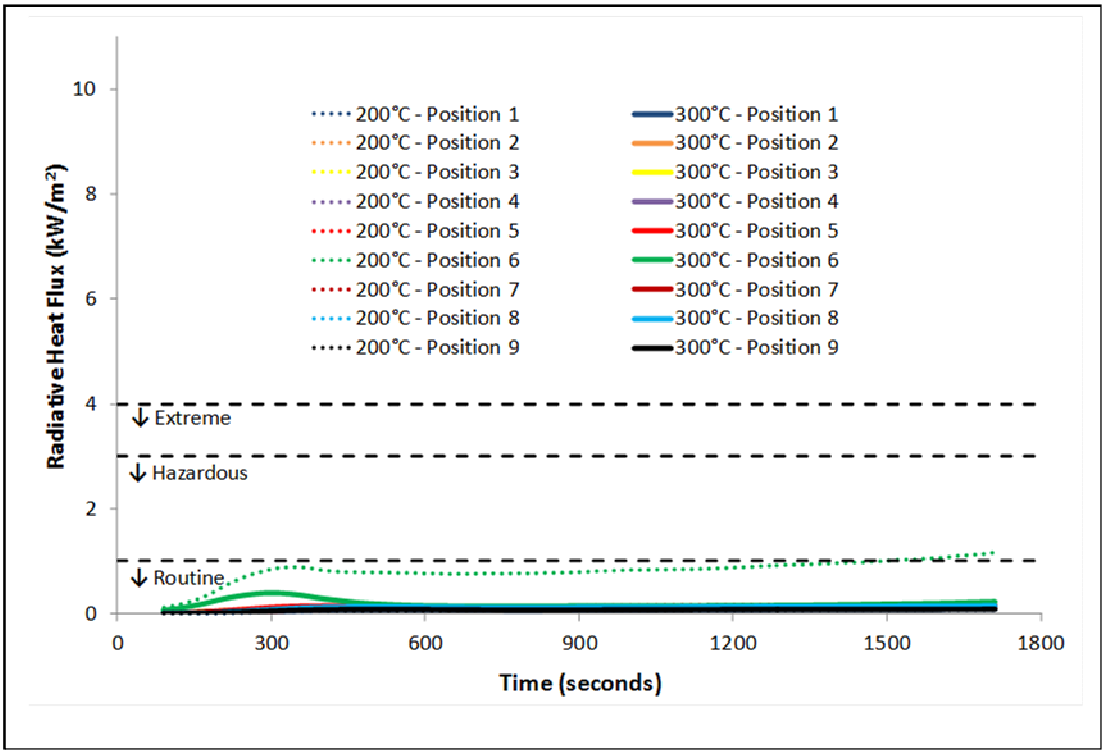

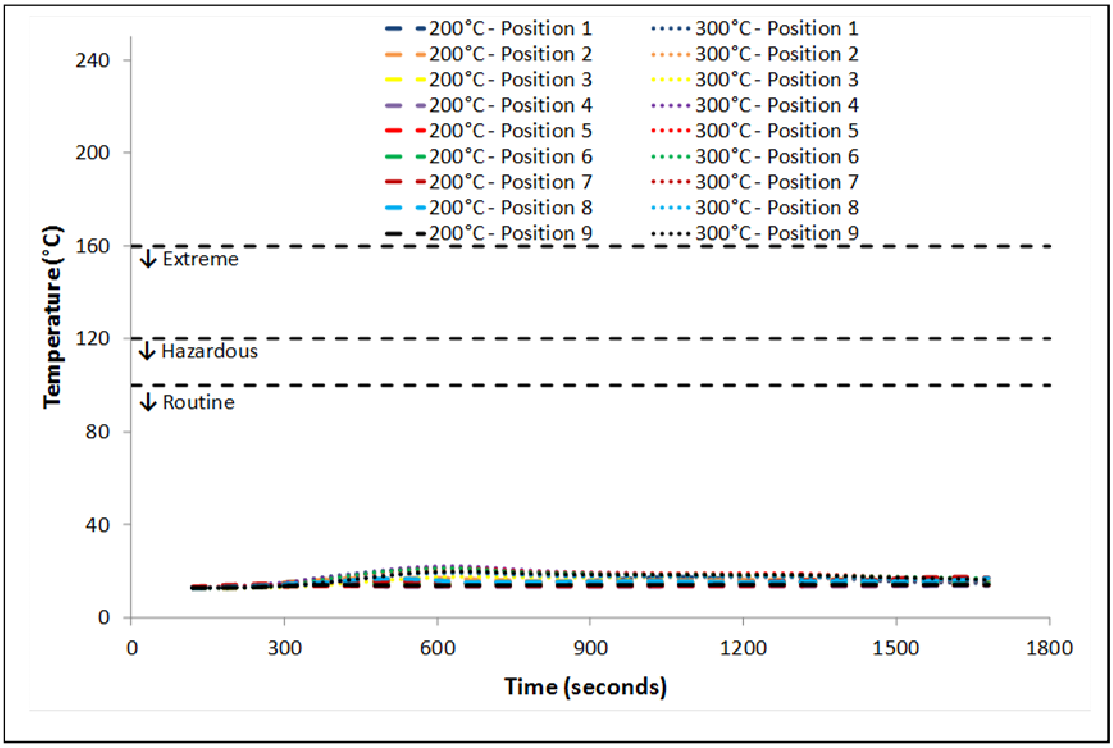

APPENDIX J1 – RADIATIVE HEAT FLUXES & TEMPERATURES IN LARGE WAREHOUSE – EXTREME FIRE & SIMULTANEOUS SQUARES

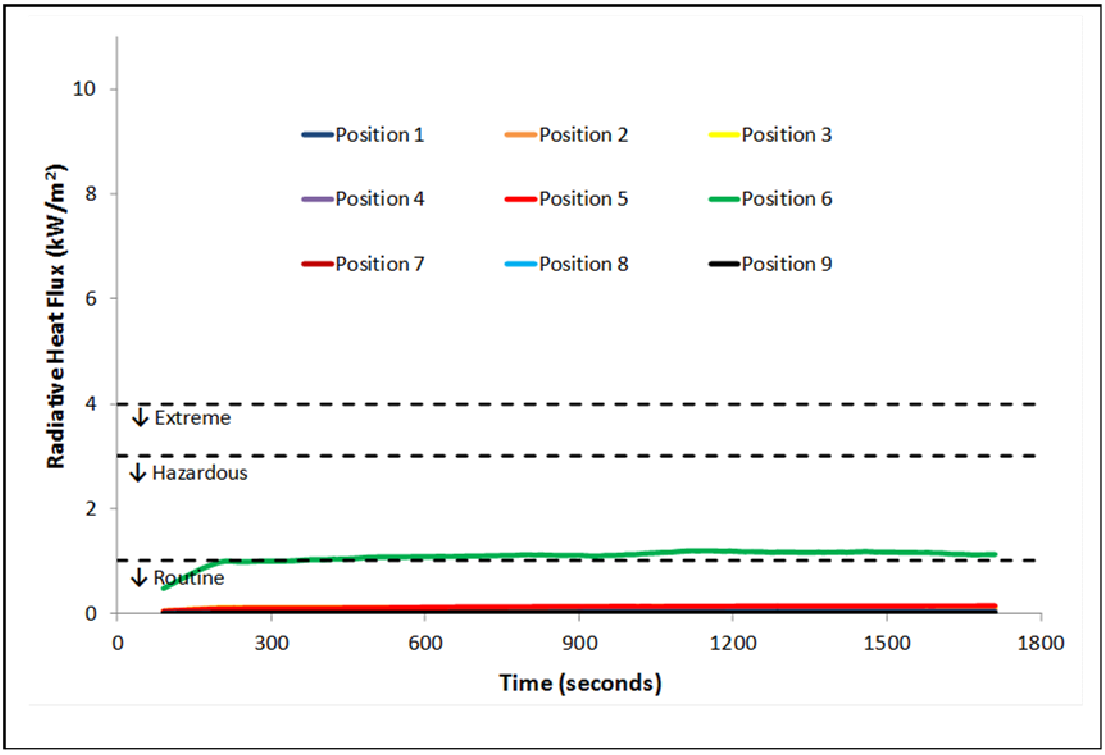

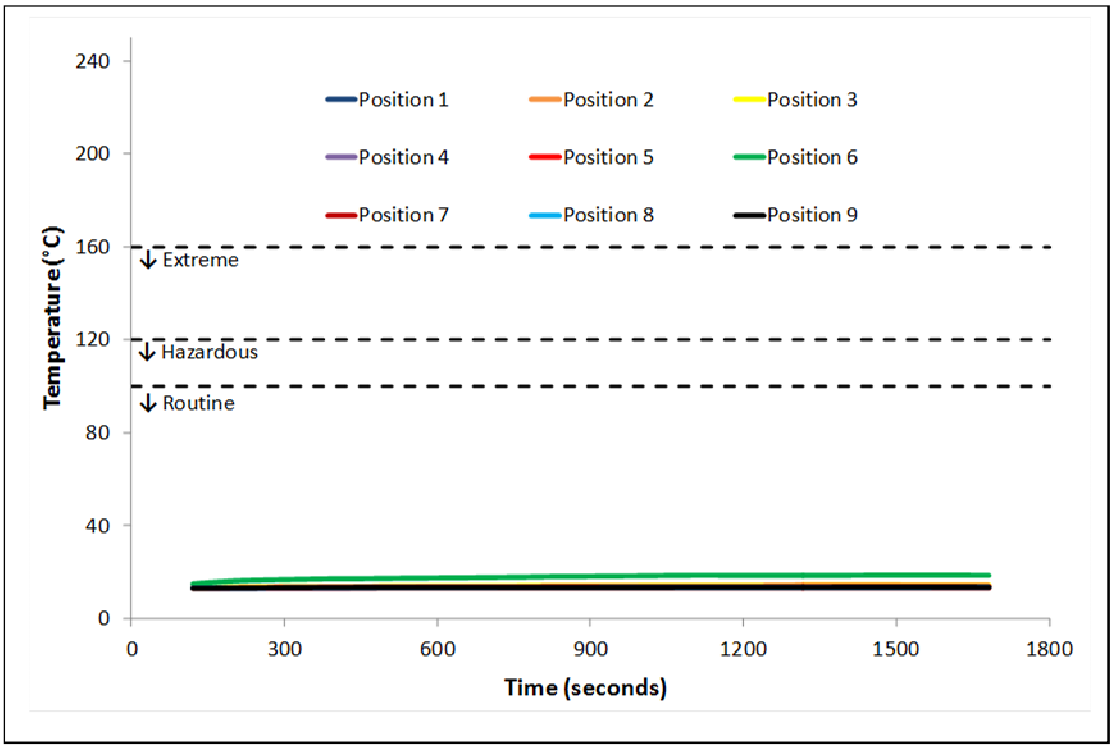

APPENDIX J2 – RADIATIVE HEAT FLUXES & TEMPERATURES IN LARGE WAREHOUSE – EXTREME FIRE & SEQUENTIAL SQUARES

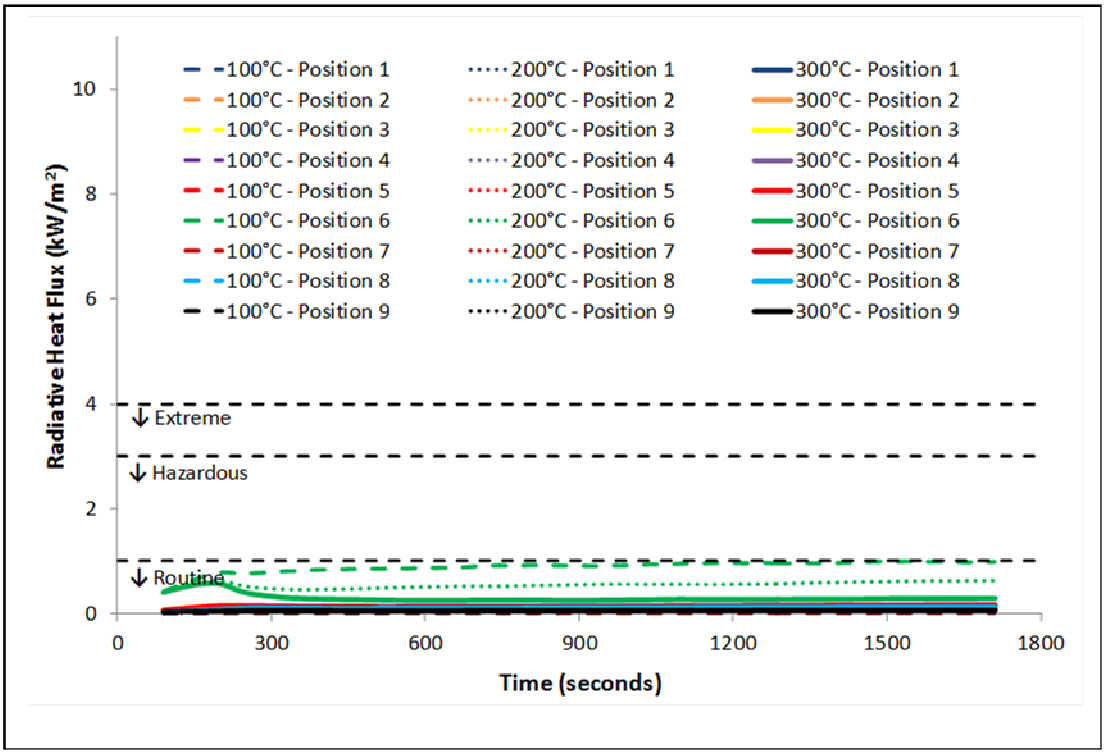

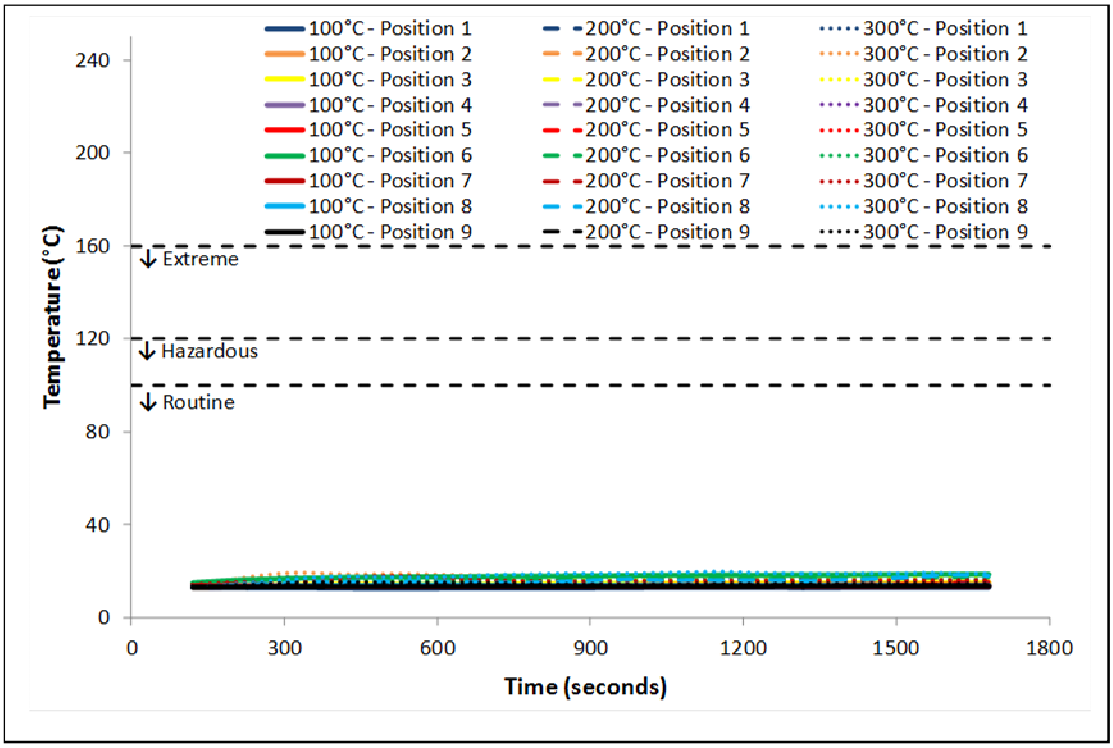

APPENDIX J3 – RADIATIVE HEAT FLUXES & TEMPERATURES IN LARGE WAREHOUSE – EXTREME FIRE & SEQUENTIAL STRIPS

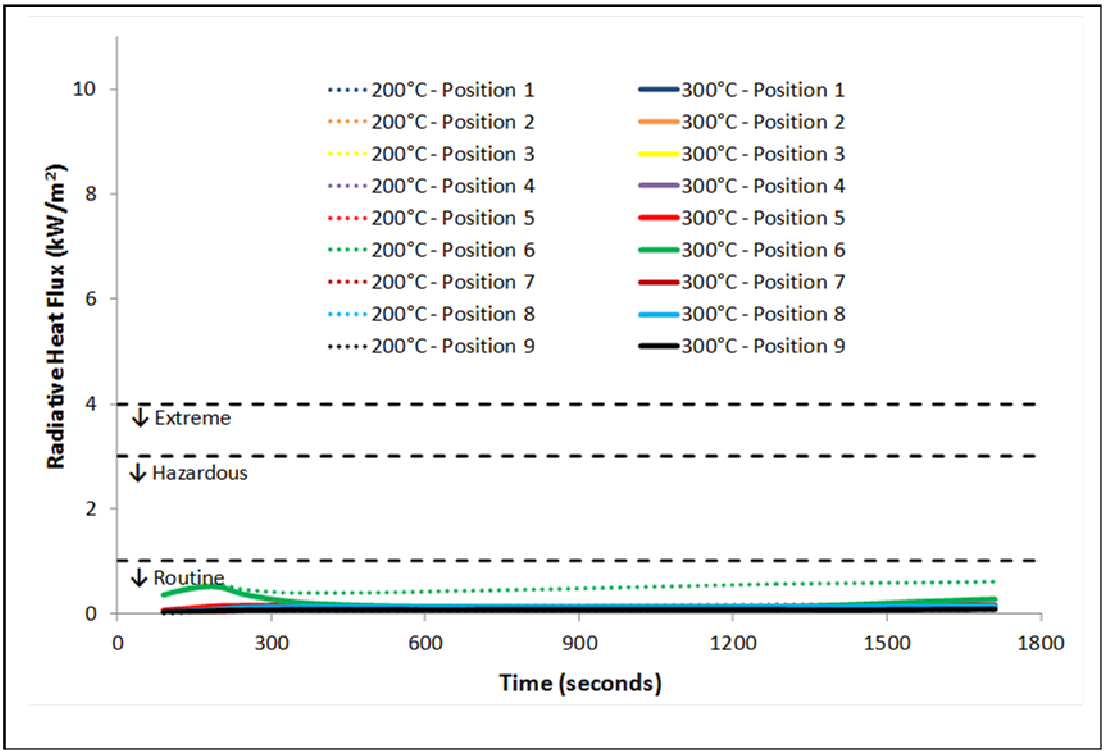

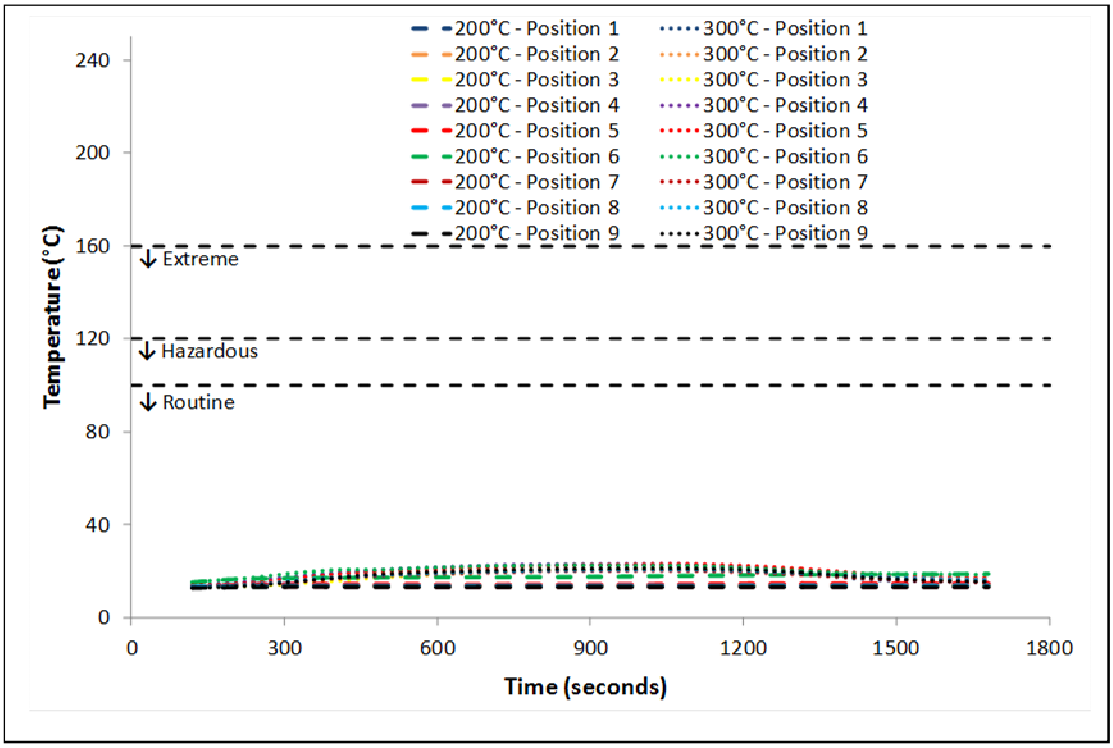

APPENDIX K1 – RADIATIVE HEAT FLUXES & TEMPERATURES IN SMALL WAREHOUSE – RAPID FIRE, SIMULTANEOUS SQUARES WITH 100°C ACTIVATION, & 3 DOWNSTAND DEPTHS

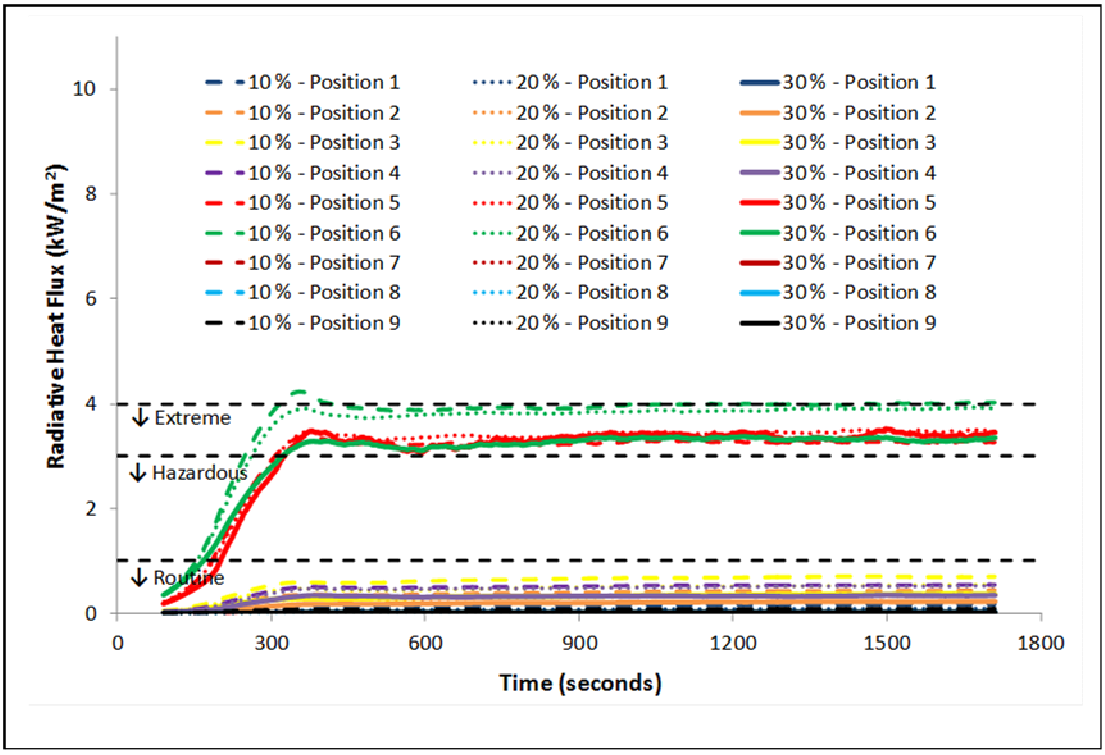

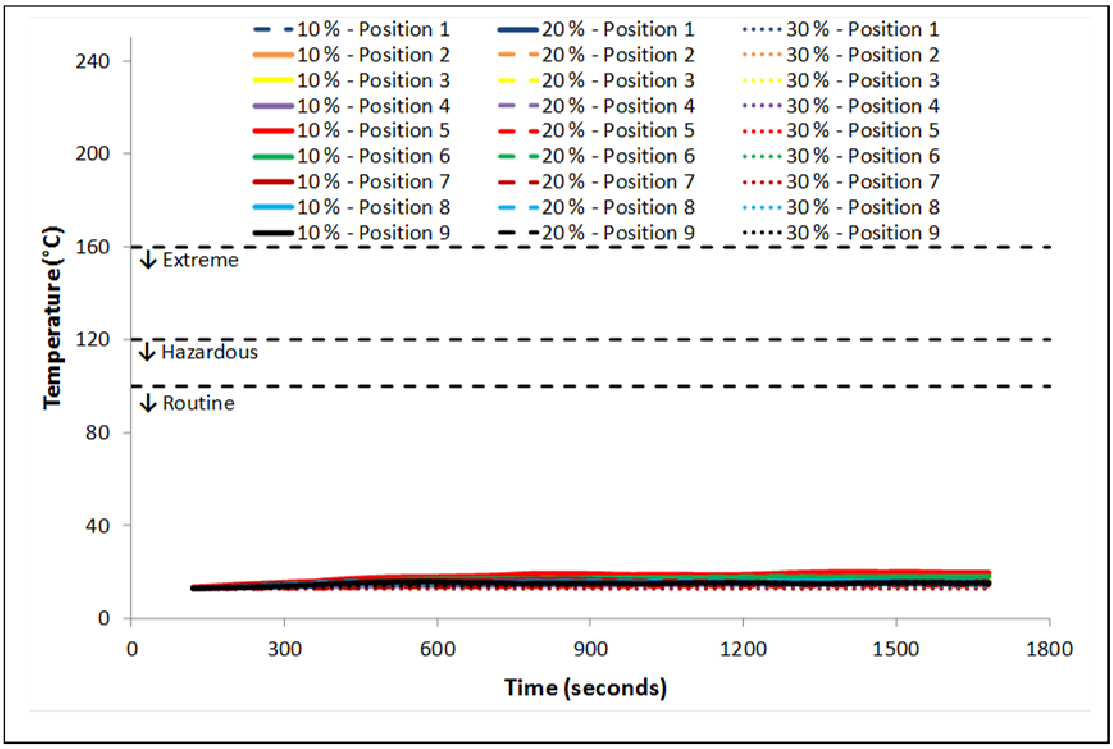

APPENDIX K2 – RADIATIVE HEAT FLUXES & TEMPERATURES IN SMALL WAREHOUSE – RAPID FIRE, SEQUENTIAL SQUARES WITH 100°C ACTIVATION, & 3 DOWNSTAND DEPTHS

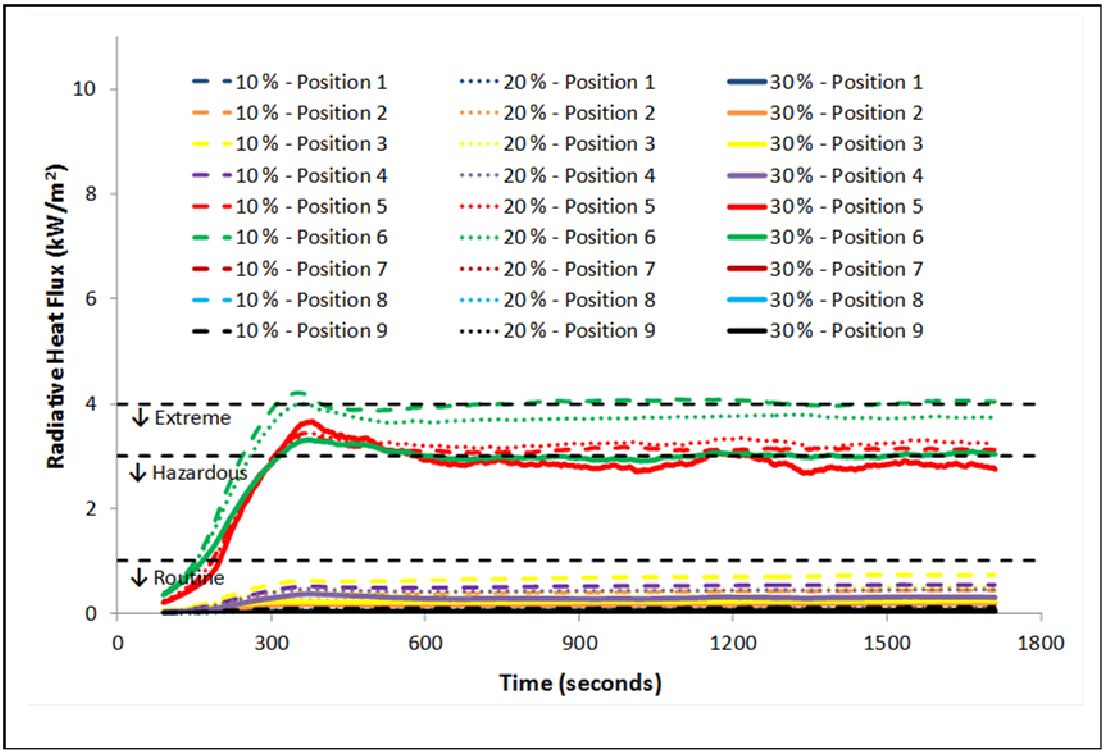

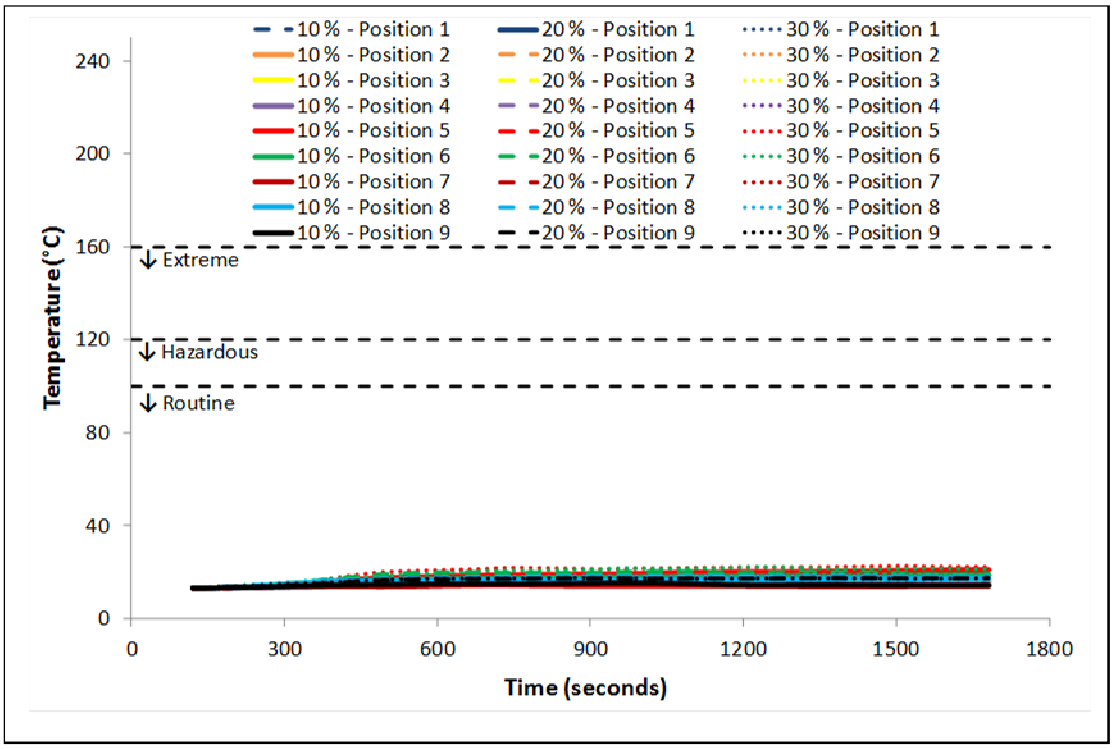

APPENDIX K3 – RADIATIVE HEAT FLUXES & TEMPERATURES IN SMALL WAREHOUSE – RAPID FIRE, SEQUENTIAL SQUARES WITH 300°C ACTIVATION, & 3 DOWNSTAND DEPTHS

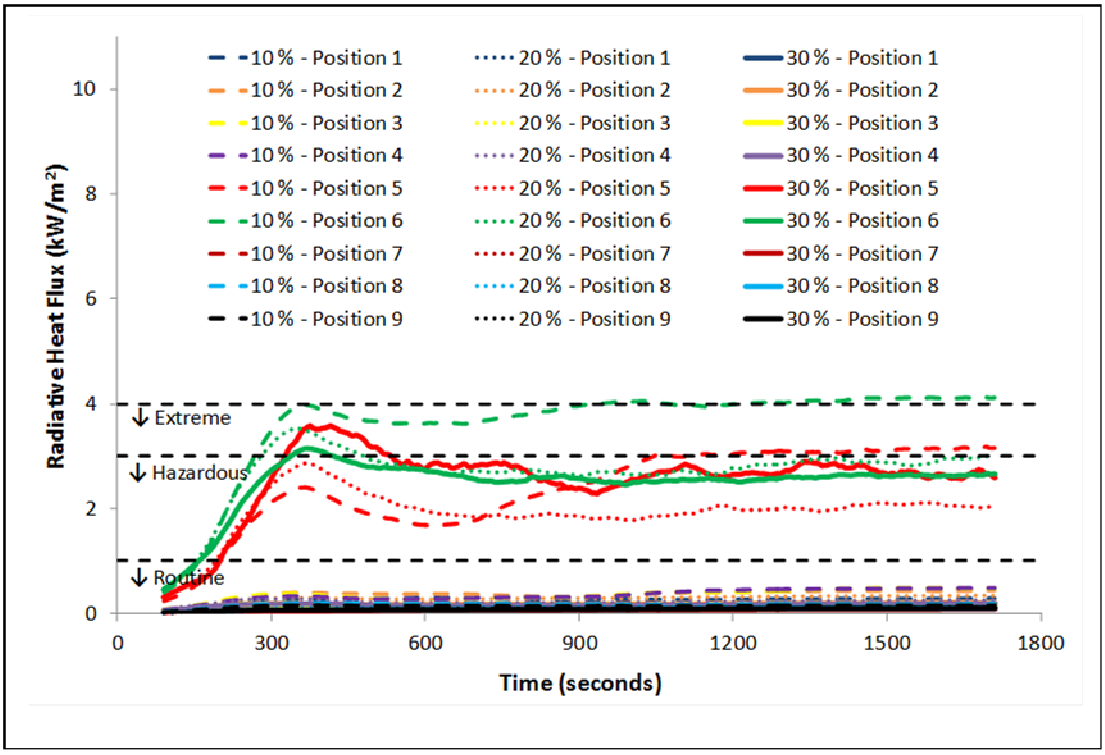

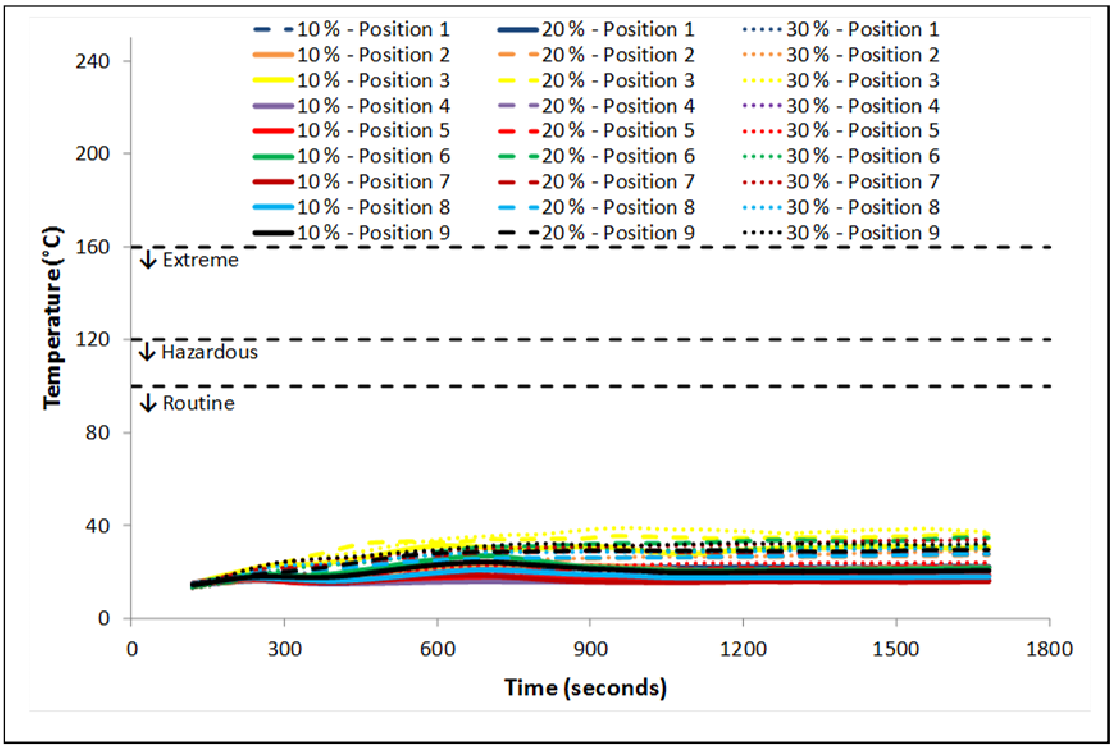

APPENDIX K4 – RADIATIVE HEAT FLUXES & TEMPERATURES IN SMALL WAREHOUSE – RAPID FIRE, SEQUENTIAL STRIPS WITH 300°C ACTIVATION, & 3 DOWNSTAND DEPTHS

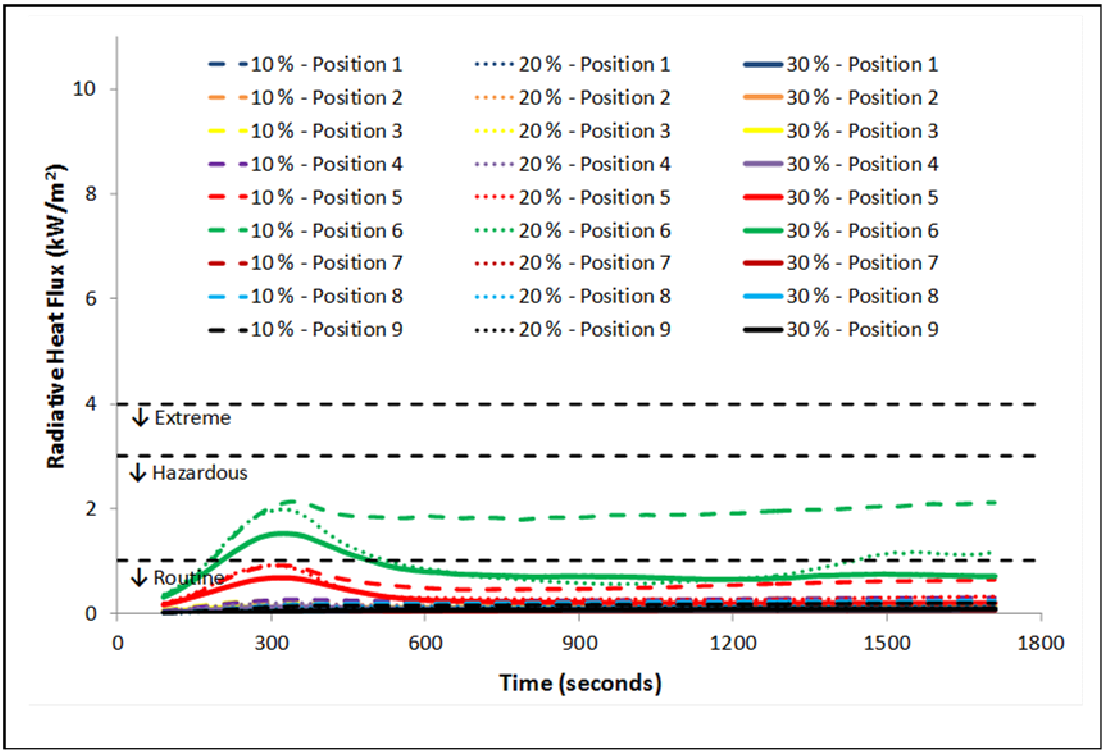

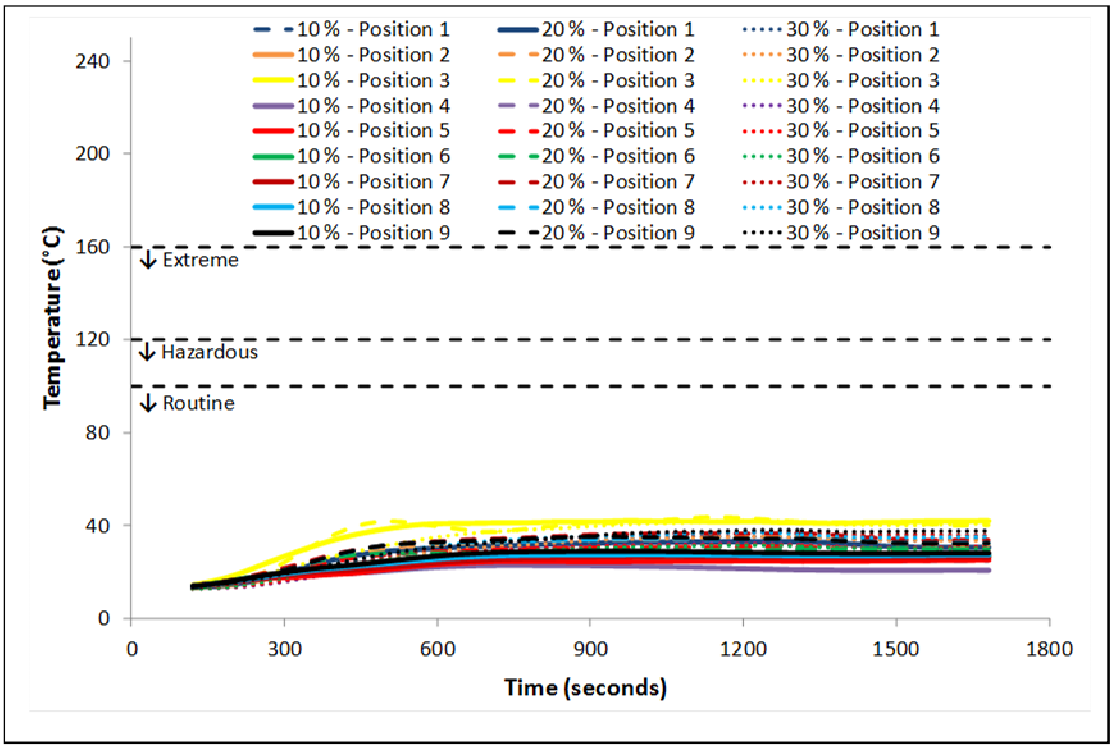

APPENDIX L1 – RADIATIVE HEAT FLUXES & TEMPERATURES IN SMALL WAREHOUSE – EXTREME FIRE, SIMULTANEOUS SQUARES WITH 100°C ACTIVATION, & 3 DOWNSTAND DEPTHS

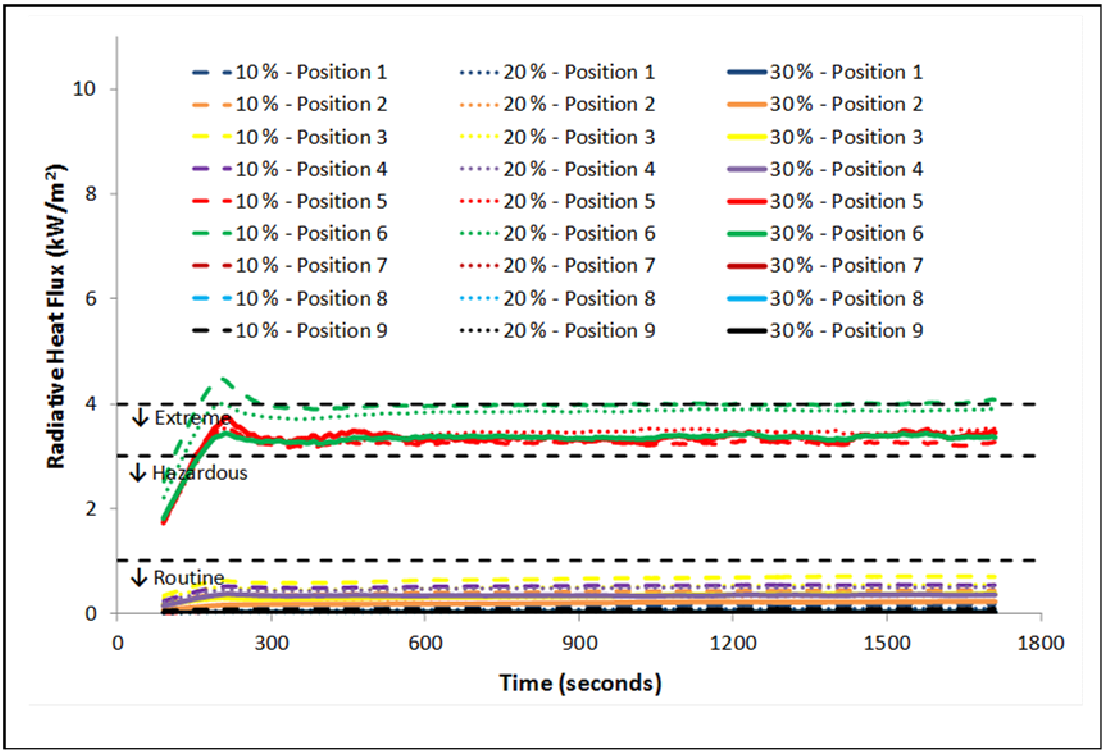

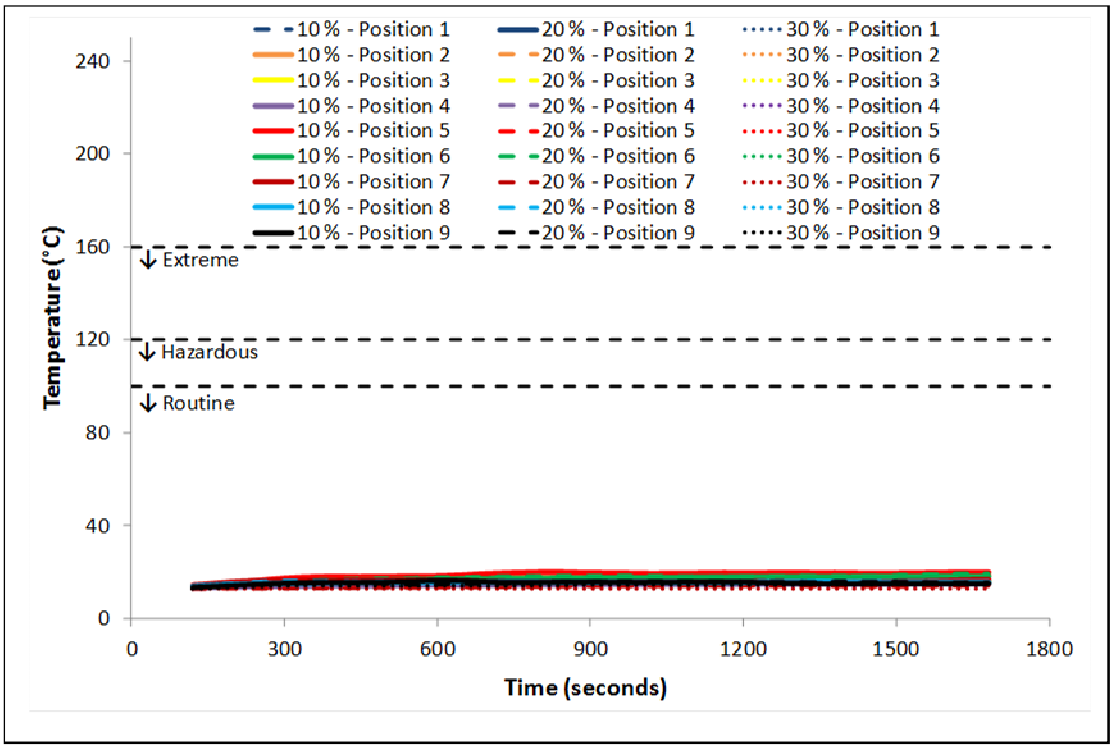

APPENDIX L2 – RADIATIVE HEAT FLUXES & TEMPERATURES IN SMALL WAREHOUSE – EXTREME FIRE, SEQUENTIAL SQUARES WITH 100°C ACTIVATION, & 3 DOWNSTAND DEPTHS

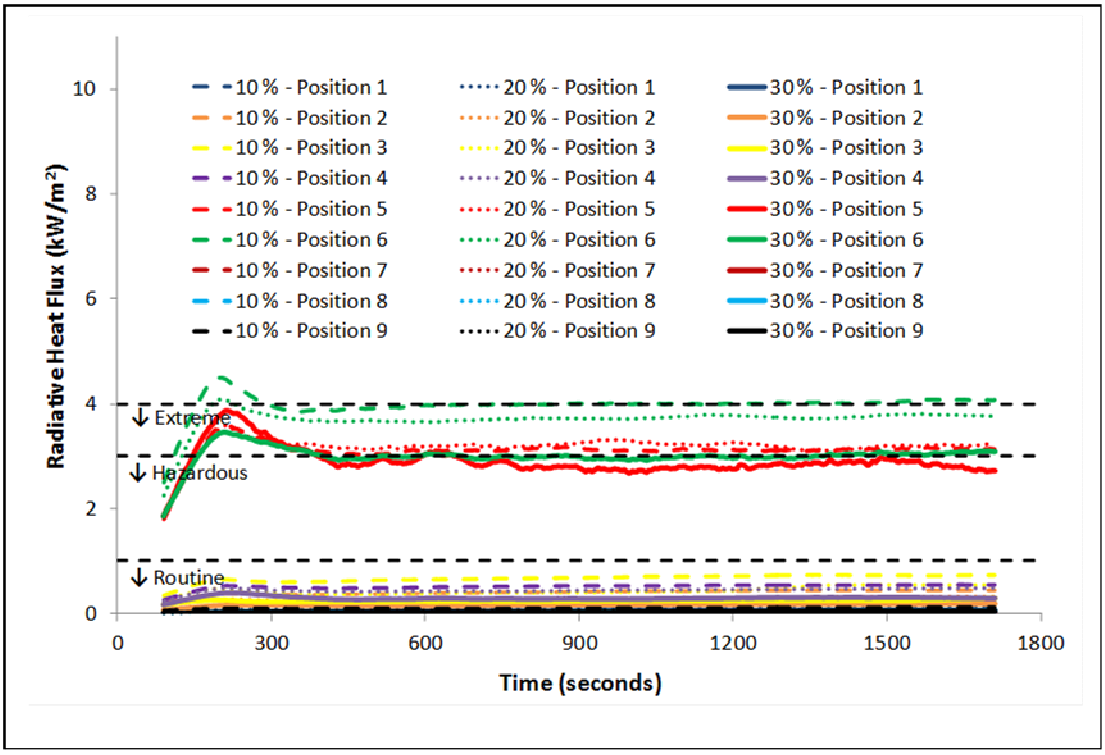

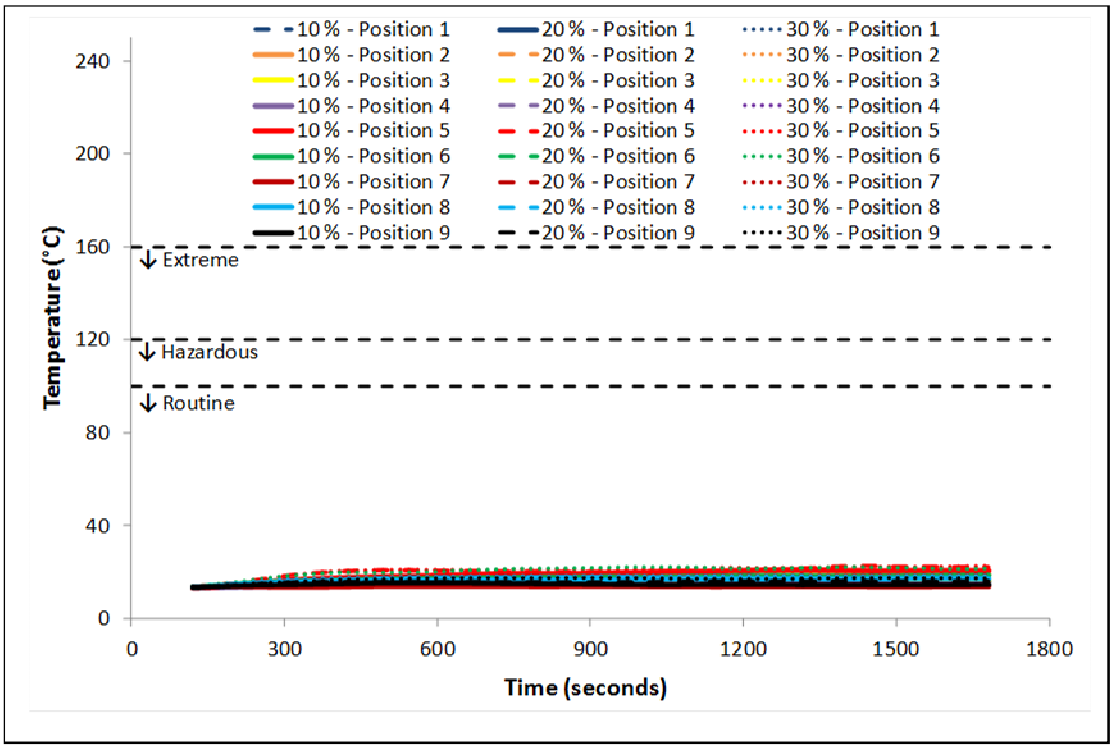

APPENDIX L3 – RADIATIVE HEAT FLUXES & TEMPERATURES IN SMALL WAREHOUSE – EXTREME FIRE, SEQUENTIAL SQUARES WITH 300°C ACTIVATION, & 3 DOWNSTAND DEPTHS

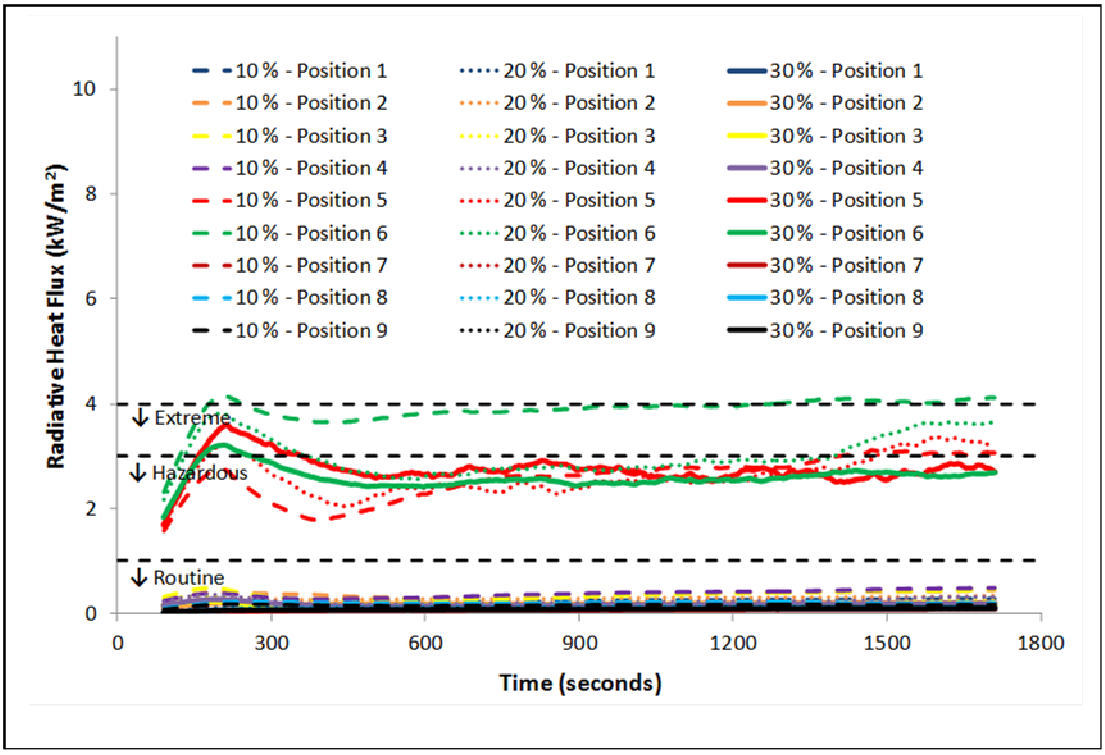

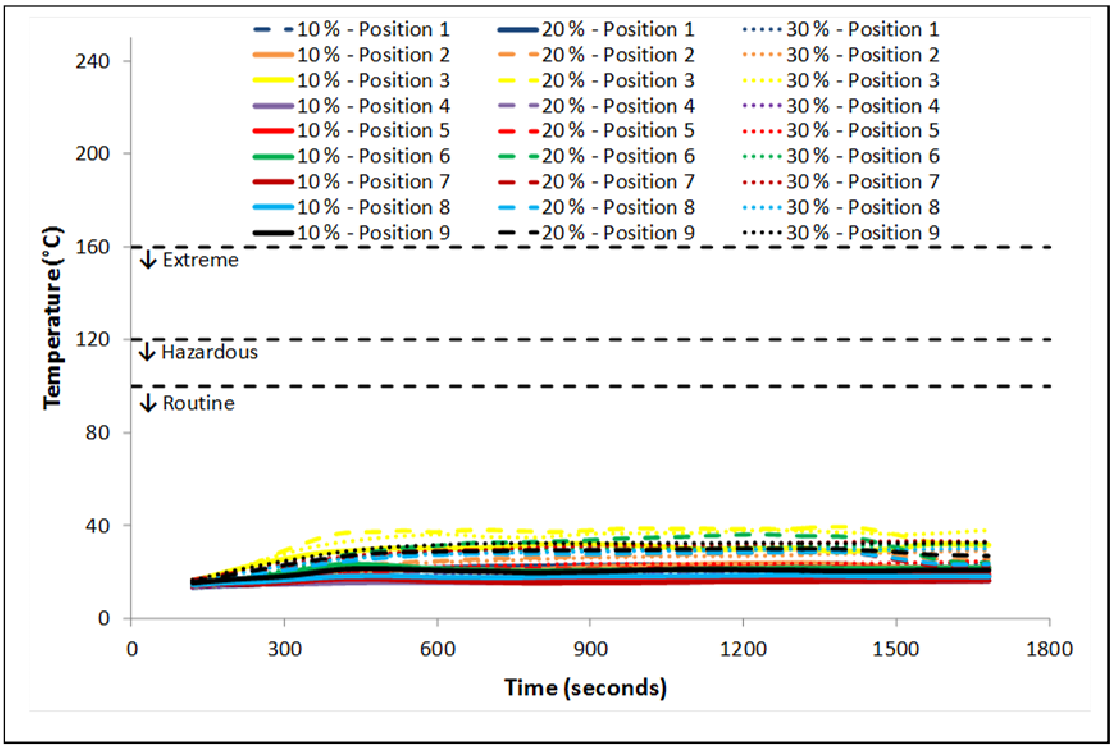

APPENDIX L4 – RADIATIVE HEAT FLUXES & TEMPERATURES IN SMALL WAREHOUSE – EXTREME FIRE, SEQUENTIAL STRIPS WITH 300°C ACTIVATION, & 3 DOWNSTAND DEPTHS

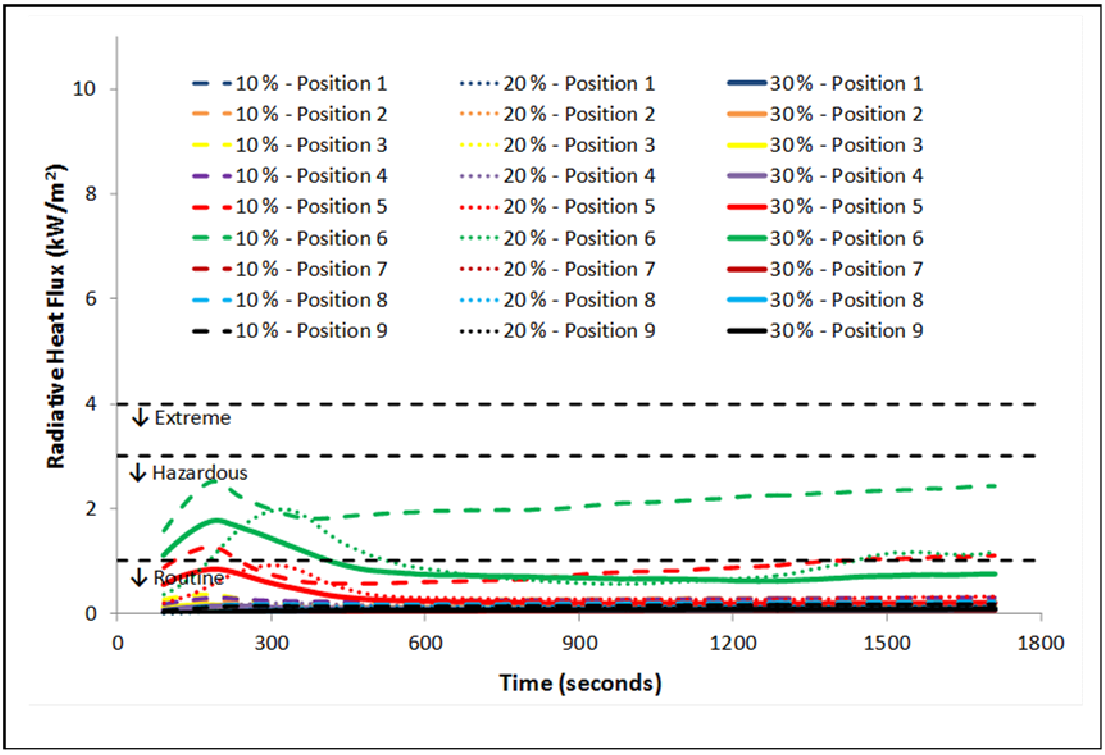

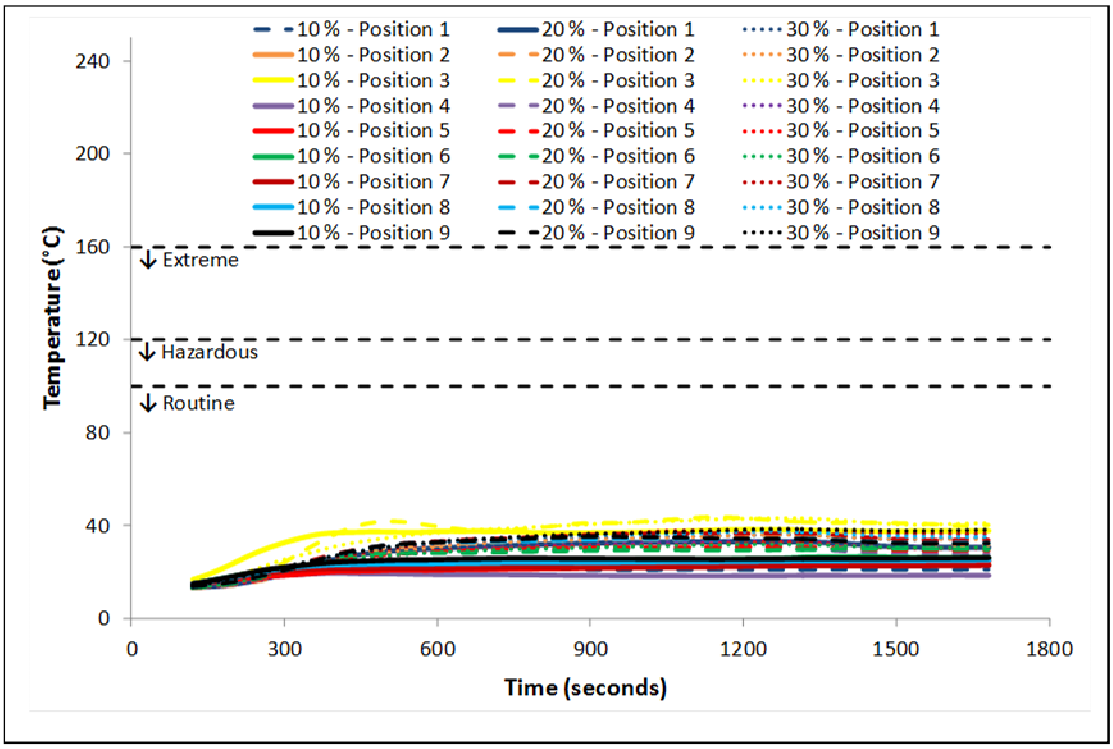

APPENDIX M1 – RADIATIVE HEAT FLUXES & TEMPERATURES IN LARGE WAREHOUSE – RAPID FIRE, SIMULTANEOUS SQUARES WITH 100°C ACTIVATION, & 3 DOWNSTAND DEPTHS

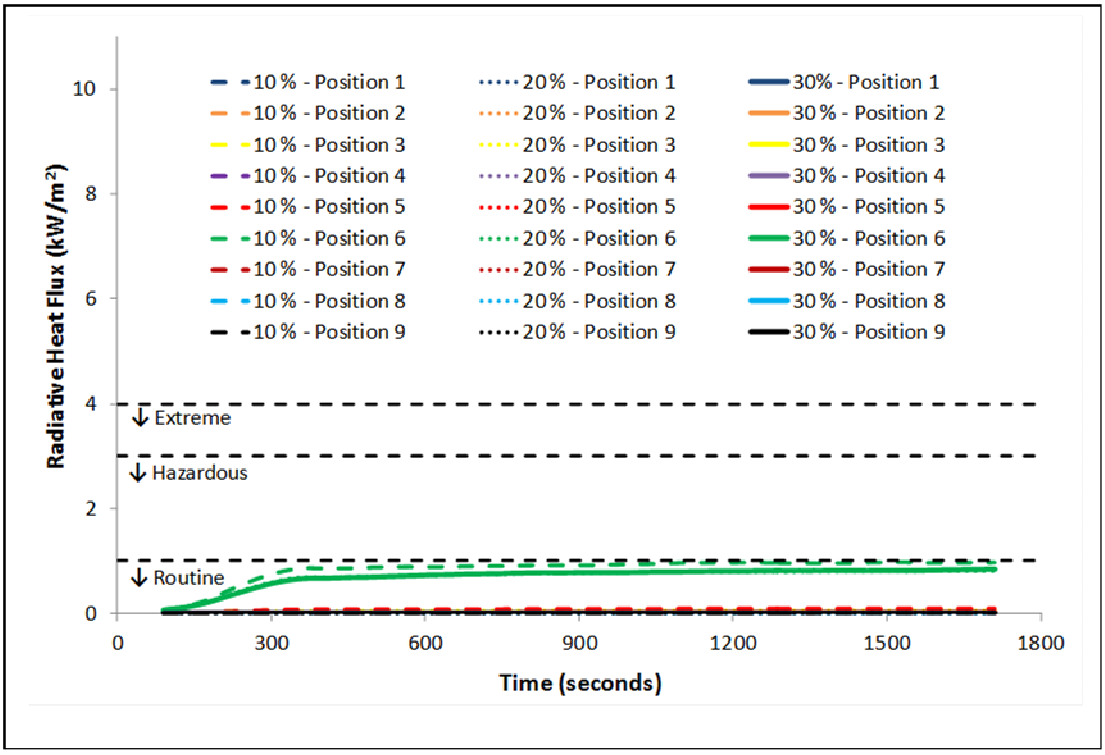

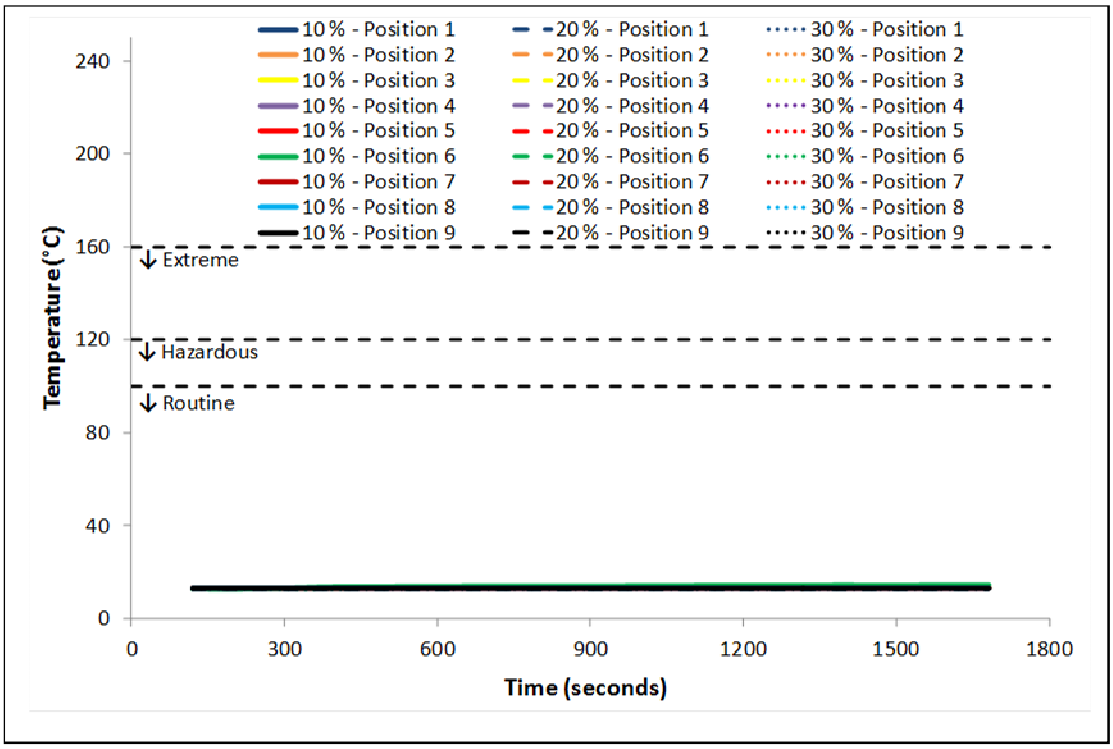

APPENDIX M2 – RADIATIVE HEAT FLUXES & TEMPERATURES IN LARGE WAREHOUSE – RAPID FIRE, SEQUENTIAL SQUARES WITH 100°C ACTIVATION, & 3 DOWNSTAND DEPTHS

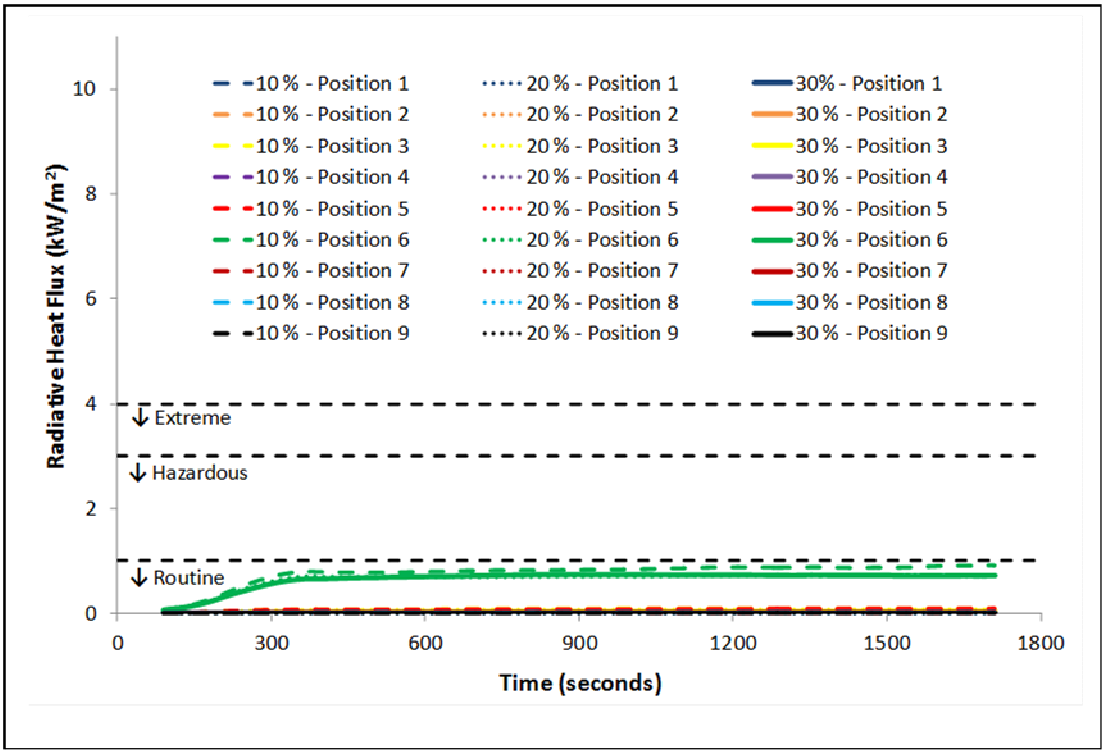

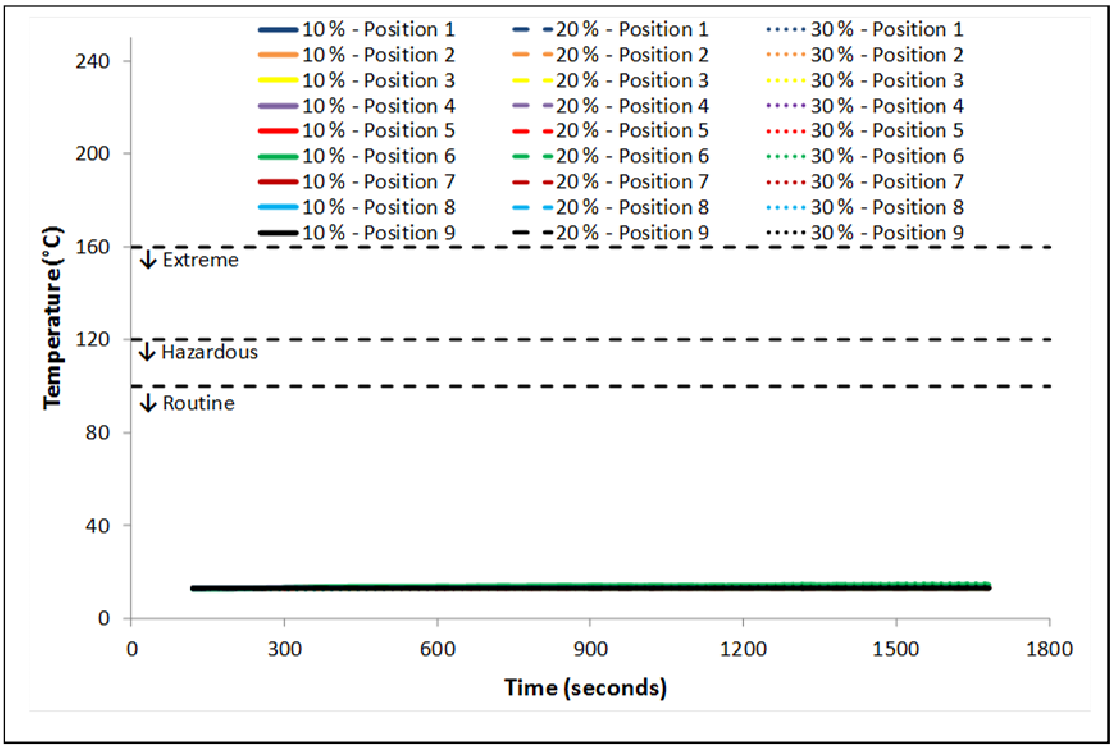

APPENDIX M3 – RADIATIVE HEAT FLUXES & TEMPERATURES IN LARGE WAREHOUSE – RAPID FIRE, SEQUENTIAL SQUARES WITH 300°C ACTIVATION, & 3 DOWNSTAND DEPTHS

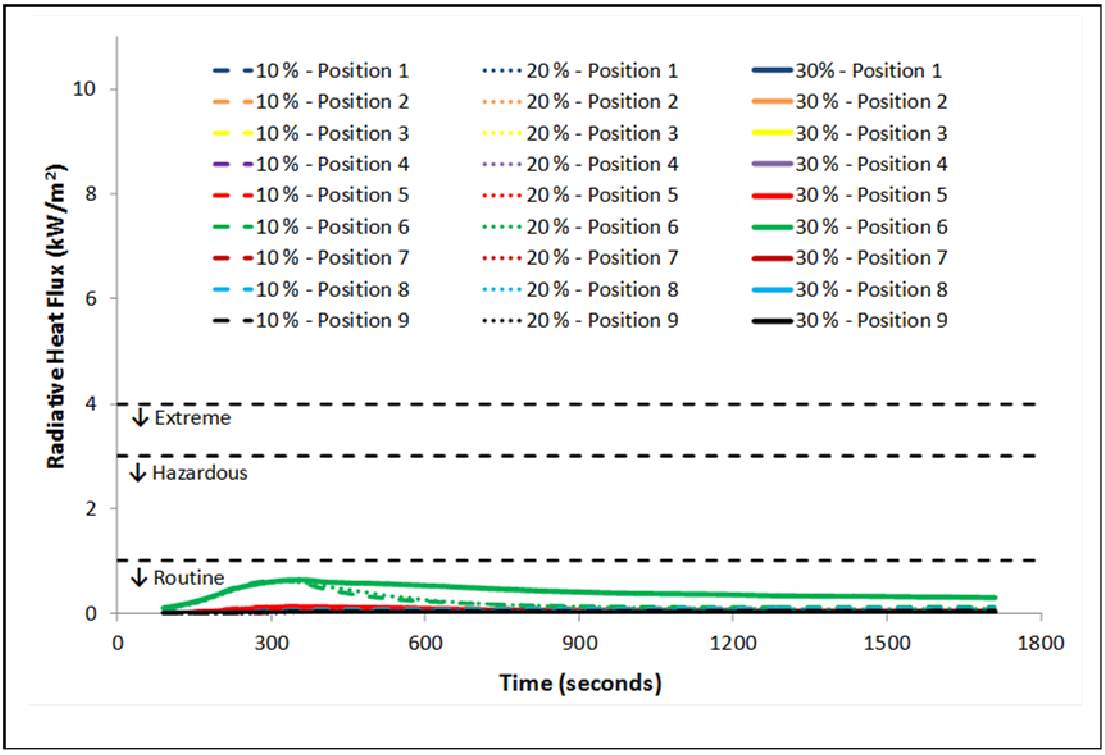

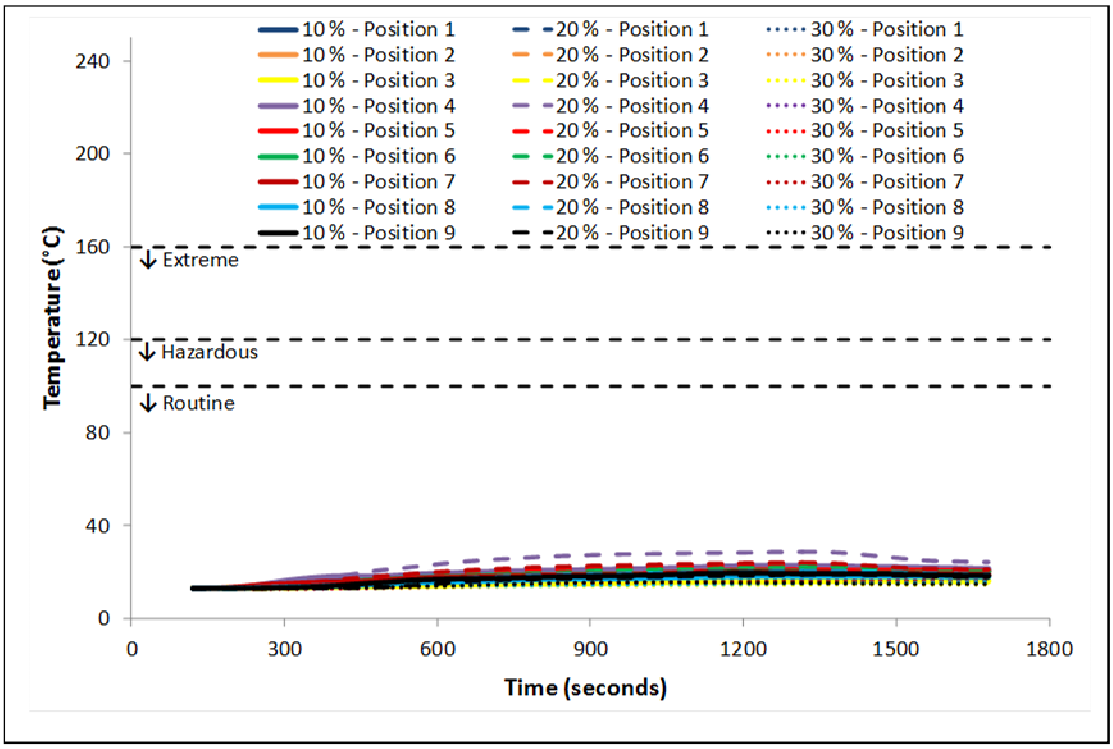

APPENDIX M4 – RADIATIVE HEAT FLUXES & TEMPERATURES IN LARGE WAREHOUSE – RAPID FIRE, SEQUENTIAL STRIPS WITH 300°C ACTIVATION, & 3 DOWNSTAND DEPTHS

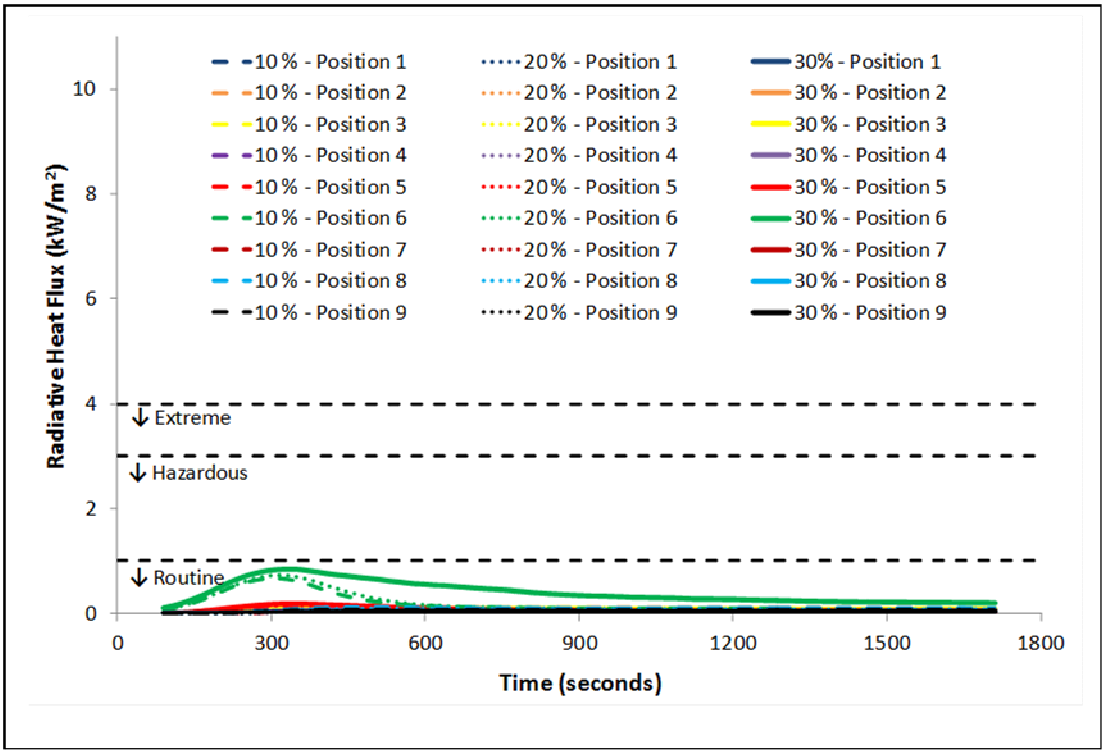

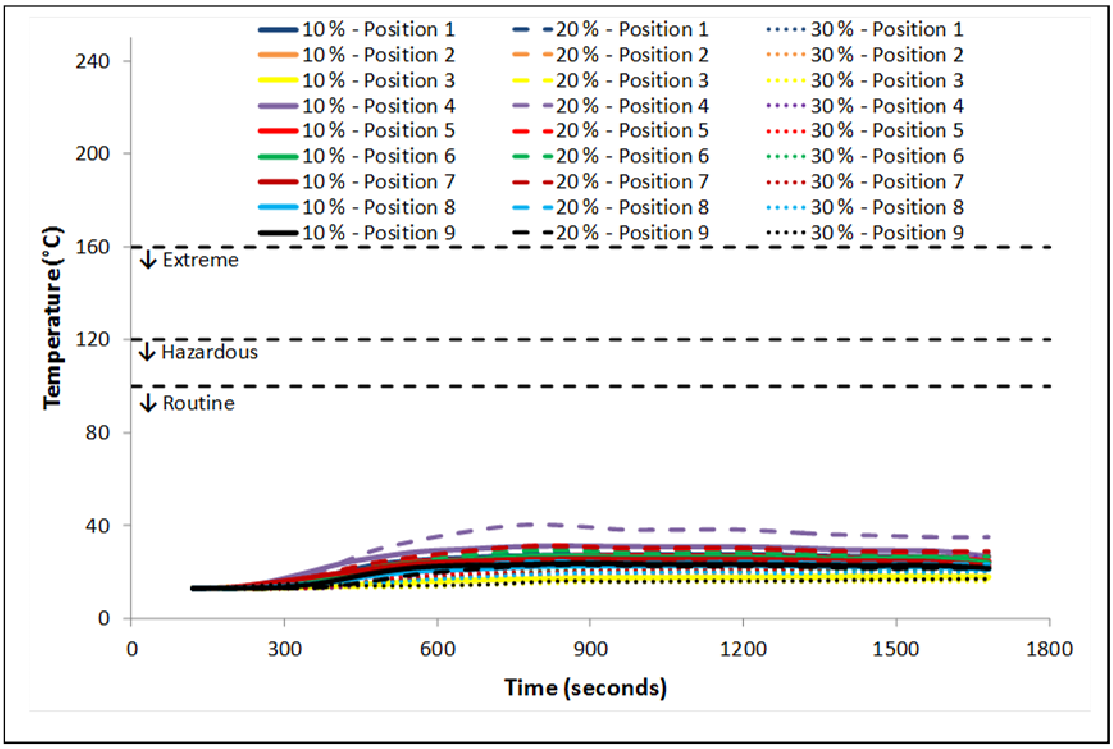

APPENDIX N1 – RADIATIVE HEAT FLUXES & TEMPERATURES IN LARGE WAREHOUSE – EXTREME FIRE, SIMULTANEOUS SQUARES WITH 100°C ACTIVATION, & 3 DOWNSTAND DEPTHS

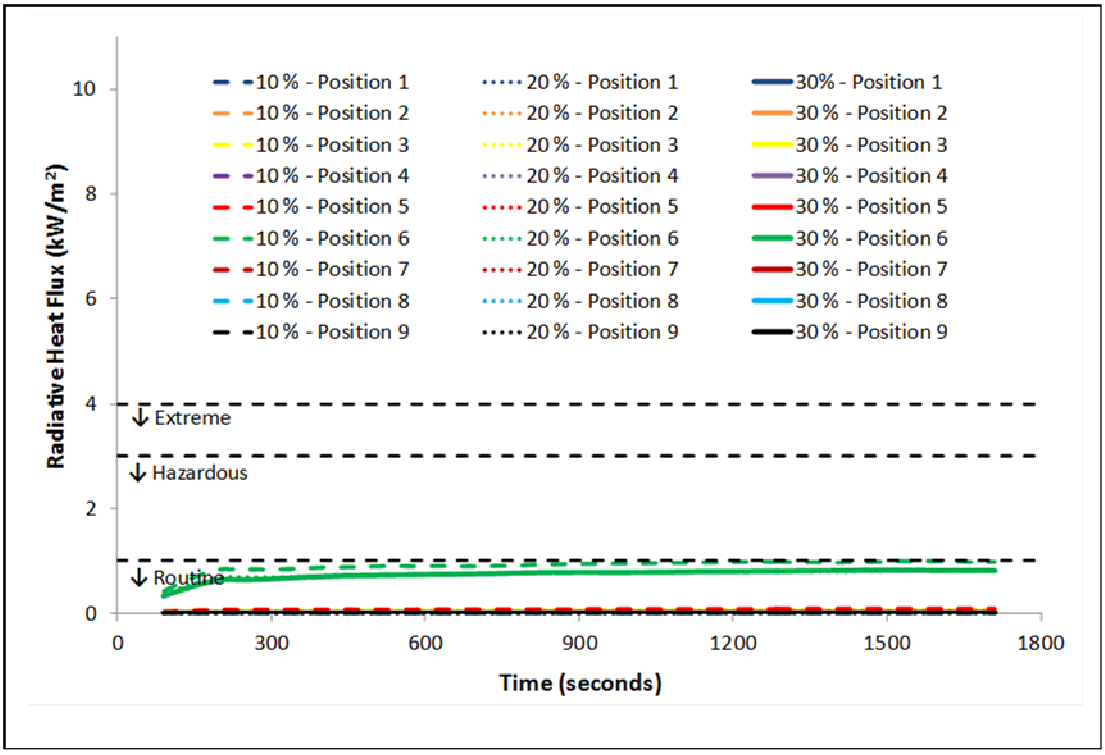

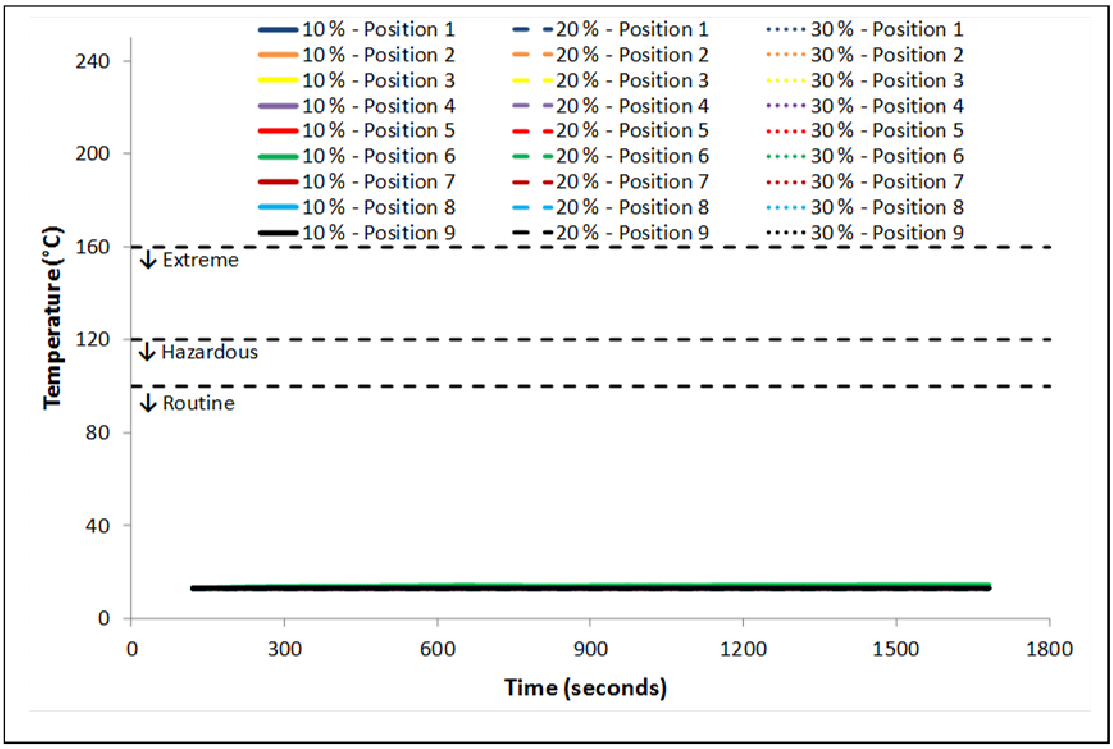

APPENDIX N2 – RADIATIVE HEAT FLUXES & TEMPERATURES IN LARGE WAREHOUSE – EXTREME FIRE, SEQUENTIAL SQUARES WITH 100°C ACTIVATION, & 3 DOWNSTAND DEPTHS

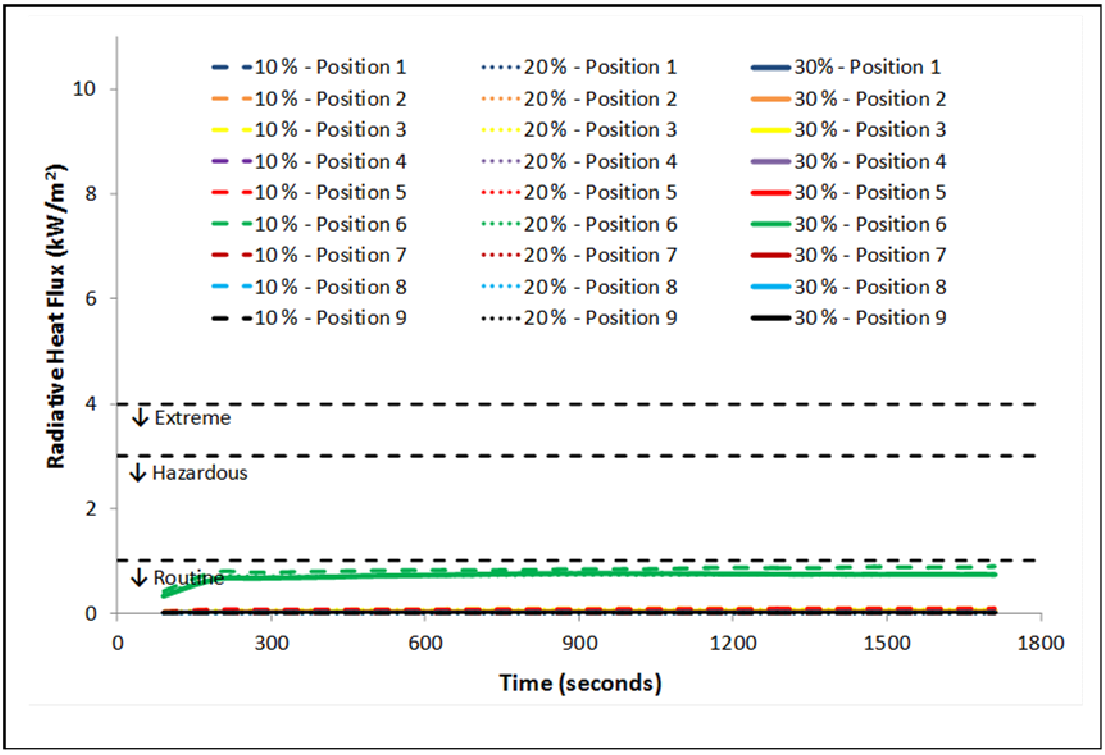

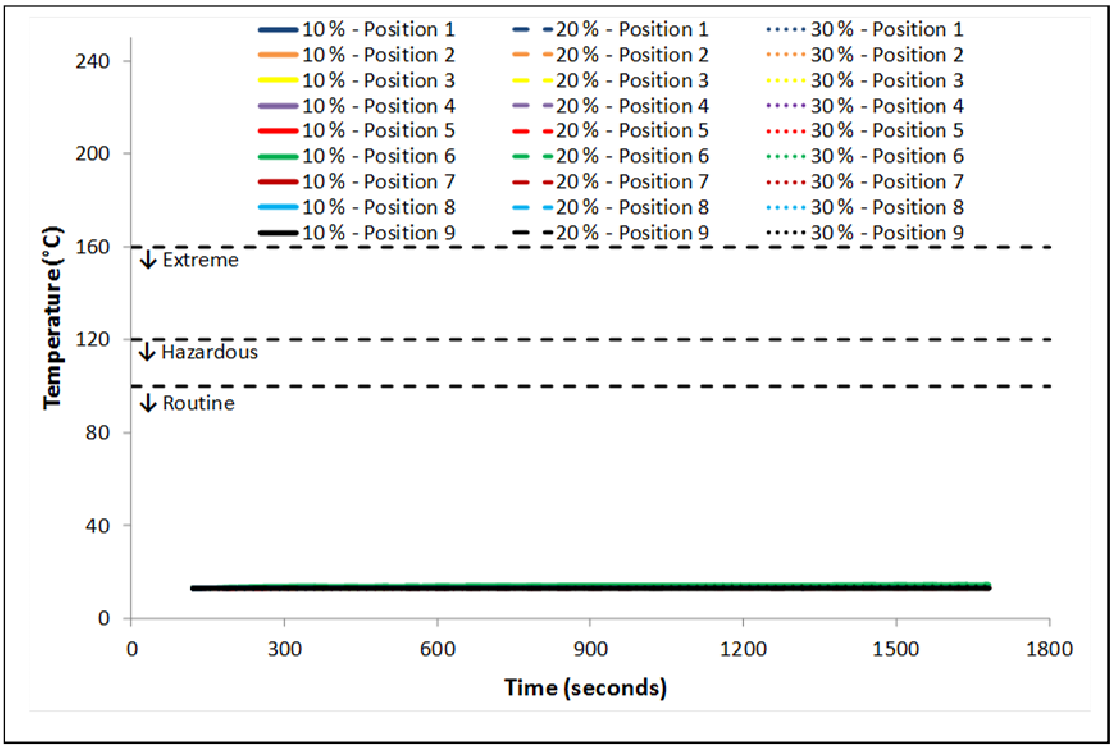

APPENDIX N3 – RADIATIVE HEAT FLUXES & TEMPERATURES IN LARGE WAREHOUSE – EXTREME FIRE, SEQUENTIAL SQUARES WITH 300°C ACTIVATION, & 3 DOWNSTAND DEPTHS

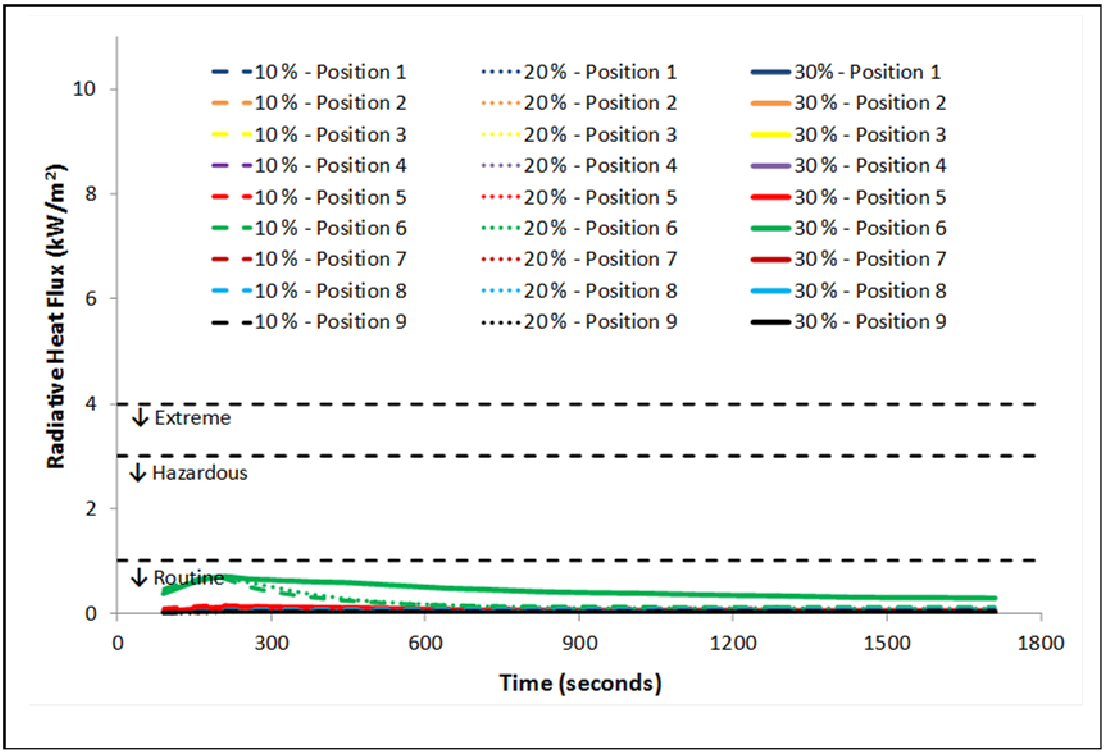

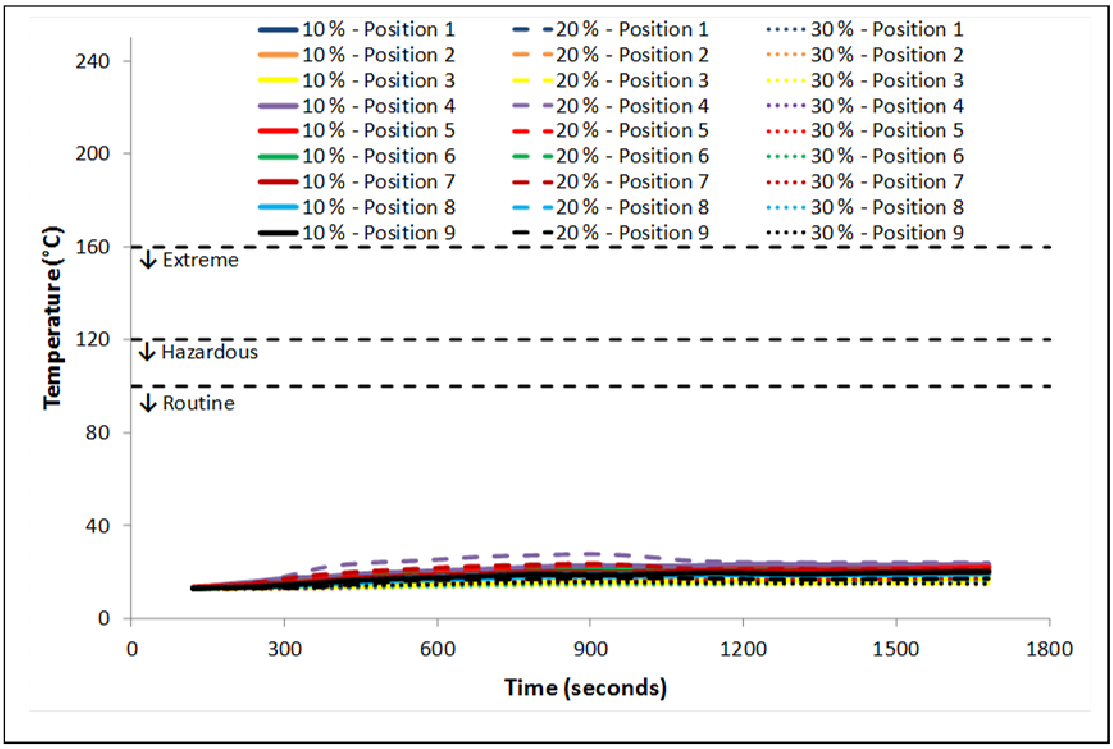

APPENDIX N4 – RADIATIVE HEAT FLUXES & TEMPERATURES IN LARGE WAREHOUSE – EXTREME FIRE, SEQUENTIAL STRIPS WITH 300°C ACTIVATION, & 3 DOWNSTAND DEPTHS